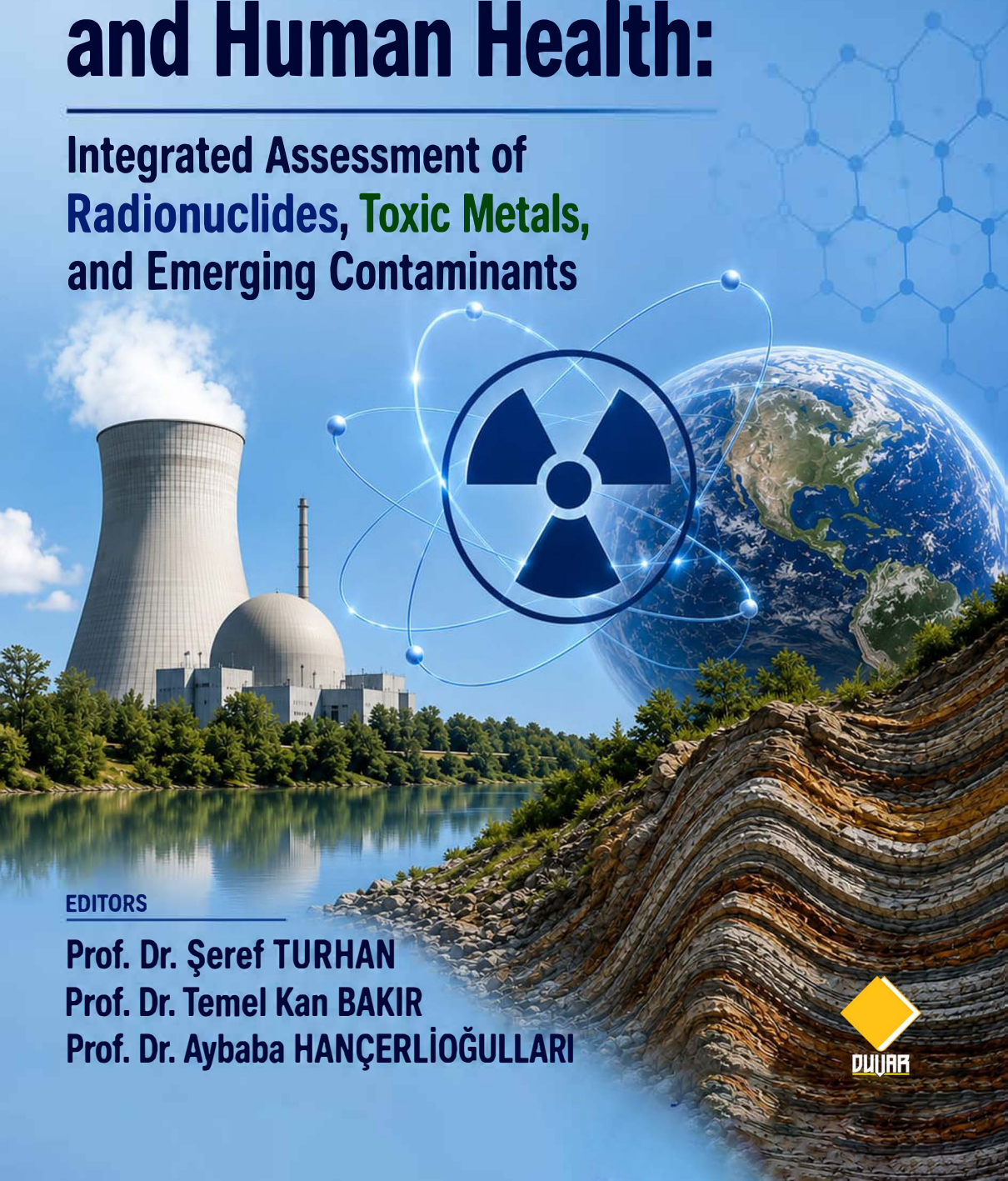
Environmental Pollutants, Radiation Exposure, and Human Health:

Integrated Assessment of Radionuclides, Toxic Metals, and Emerging Contaminants



EDITORS

Prof. Dr. Şeref TURHAN
Prof. Dr. Temel Kan BAKIR
Prof. Dr. Aybaba HANÇERLİOĞULLARI

DUVAR

Environmental Pollutants, Radiation Exposure, and Human Health:

Integrated Assessment of Radionuclides, Toxic Metals, and Emerging Contaminants

Editors

Prof. Dr. Şeref TURHAN

Prof. Dr. Temel Kan BAKIR

Prof. Dr. Aybaba HANÇERLİOĞULLARI (Editor in Chief)



Environmental Pollutants, Radiation Exposure, and Human Health: Integrated Assessment of Radionuclides, Toxic Metals, and Emerging Contaminants
Editors: Prof. Dr. Şeref TURHAN,
Prof. Dr. Temel Kan BAKIR
Prof. Dr. Aybaba HANÇERLİOĞULLARI (Editor in Chief)

General Director: Berkan Balpetek
Cover and Page Design: Duvar Design
Printing : October-2026
Publisher Certificate No: 49837
E-ISBN: 978-625-8936-81-0

© Duvar Yayınları
853 Sokak No:13 P.10 Kemeraltı-Konak/İzmir
Tel: 0 232 484 88 68
www.duvaryayinlari.com
duvarkitabevi@gmail.com

*"The authors bear full responsibility for the sources, opinions, findings, results, tables, figures, images, and all other content presented in the chapters of this book. They are solely accountable for any financial or legal obligations that may arise in connection with national or inter*national copyright regulations.The publisher and editors shall not be held liable under any circumstances"

TABLE OF CONTENTS

Chapter 1 ..... **1**
Assessment Of Health Risks Due to Heavy Metals in Some Commercially Operated Mineral Quarries in Türkiye
Onur METİN

Chapter 2 ..... **14**
Bentonite Minerals and Mining: Mineralogical Structure, Applications, Heavy Metal Concentrations, and Naturally Occurring Radioactive Material (NORM) Content
Onur METİN

Chapter 3 ..... **28**
Molasses Alleviates $Caco_3$-Induced Alkalinity Stress in Spinach: Implications for Sustainable Agriculture
Nezahat TURFAN, Yahya TUNÇAY, Veysel ORTAÇ, Burak TOMAÇOĞLU

Chapter 4 ..... **43**
Cadmium Sulfide (CdS) Cathode for Advanced Plasma Conversion Process
Hatice Hilal YÜCEL

Chapter 5 ..... **54**
Eco-Friendly Micro-Plasma Systems with High-Sensitivity Infrared Znse Photodetectors
Hatice Hilal YÜCEL, Seren Elifcan KIZIŞAR AKSIN

Chapter 6 ..... **66**
Environmental Health Literacy and Radiation Awareness: The Role of Stem Education In Building Community Resilience
Ahmet YALKIN

Chapter 7 ..... **80**
Sediment Quality and Ecological Risk Assessment Methods in Aquatic Ecosystems
Ayşegül EMİN GÜZEL, Ekrem MUTLU

Chapter 8 99
Monitoring Water Quality and Pollution in Inland Waters: Integrated Physicochemical, Toxic-Metal, and Microbial Assessment for Human and Environmental Health
Nuray EMİN, Ayşegül EMİN GÜZEL

Chapter 9 120
Forest Fungi, Environmental Chemistry, and Forest Pathology Responses to Toxic Metals, Radionuclides, and Emerging Pollutants
Mertcan KARADENİZ,Temel Kan BAKIR

Chapter 10 141
Post-Earthquake Microbiological Hazards:Integrating Environmental Microbiology, Multi-Omics Technologies, and Public Health Perspectives
Kübra TEKŞEN, Eda ALTINÖZ, Ergin Murat ALTUNER

Chapter 11.....181
Computational Modeling and Machine Learning for Toxic Metal Transport, Exposure, and Human Health Risk Assessment
Ekrem GÜLSEVİNÇLER, Hakan US

Chapter 12 198
Microplastic-Mediated Radionuclide Transport in Nuclear And Radiological Environments: A Screening-Level Computational Case Study
Hakan US, Ekrem GÜLSEVİNÇLER

Chapter 13 216
Radionuclide And Heavy Metal Contamination in Ecosystems: Environmental Risk Assessment
Almusa ATAMALIYEV, Temel KAN BAKIR, Malahat BAGİYEVA, Elsevar ATAMALİYEV, Bikakhanim YUZBASHYEVA

Chapter 14 232
Single-Atom Catalysts for Pem Fuel Cells: From Catalyst Design to Reaction Mechanisms
Alpaslan GÜRBÜZ, Bülent KUTLU

Chapter 15 247
Artificial Intelligence for Education for Sustainable Development: An Integrative Review of Environmental Sustainability, Resource Management, And Future Green Competencies
Meltem KAYGUSUZ

Chapter 16 266
Assessment of Radinucluide (Radon, Radium, Thorium and Potassium) Activity Concentration and Exhalation Rates in Building Materials Utilized in Türkiye
Aslı KURNAZ, Şeref TURHAN, Aybaba HANÇERLİOĞULLARI

Chapter 17 276
Analysing Naturally Occurring Radioactive Materials (NORM) in Structural Building Materials Used in Türkiye and Radiological Health Risk Evaluation
Şeref TURHAN, Aybaba HANÇERLİOĞULLARI, Aslı KURNAZ

Chapter 18 294
Applications of Radon In Earthquake Forecasting and Geohazard Assessment
Mehmet ERDOĞAN

Chapter 19 305
Natural Radiation: Sources and Human Exposure
Fatih ÖZDEMİR, Mehmet ERDOĞAN

Chapter 20 318
Examining The Integration of Environmental Physics and Radiation Health into the Physics Curriculum
Mehmet Altan KURNAZ

Chapter 21 334
Mapping The Thematic Evolution of Radionuclides, Toxic Metals, and Emerging Contaminants: A Bibliometric Study of the Last Decade
Mehmet Altan KURNAZ

Chapter 22 357
Radioactivity Levels in Mushroom Samples
Aydan ALTIKULAÇ

Chapter 23 367
Radiological Assessment of Coal-Fired Thermal Power Plants
Aydan ALTIKULAÇ

Chapter 24 378
Radiation Dosimetry and Environmental Monitoring: Modern Approaches for Assesing Population Exposure
Celal Tuğrul ZEYREK

Chapter 25 401
Optoelectronic and Vibrational Properties of Half-Heusler Libaas Compounds
Yasemin O. CIFTCI

Chapter 26 420
Hydrogen Storage, Mechanic, Electronic, and Vibrtional Properties of Novel TI2XH4 (X=LI, SC, NI) Hydrides
Yasemin O. CIFTCI

Chapter 1

Assessment Of Health Risks Due to Heavy Metals in Some Commercially Operated Mineral Quarries in Türkiye

Onur METİN[1]

1. INTRODUCTION

The mining sector is one of the strategic sectors that forms the basis of industrialization and economic development, providing raw materials needed by the construction, energy, metallurgy, ceramics, glass, chemical, agricultural, and advanced technology industries. While the mining and mineral processing industries make significant contributions to economic development, they also pose serious risks to the environment and public health [1]. In particular, dust generated during crushing, screening, transportation, and storage operations in commercially operated mineral quarries poses a chemical threat not only due to its particulate load but also to its heavy metal content. This situation can affect workers in the work area as well as communities living near the quarry sites, agricultural production areas, and water resources [2]. Mining activities pose a threat to human health in terms of chemical exposure. The effects of heavy metals on human health vary by metal type. Common heavy metals such as mercury, lead, chromium, cadmium, and arsenic cause problems such as oxidative stress, weakening of antioxidant defenses, enzyme inactivation, and DNA damage. Some metals can also cause genomic instability and may exhibit carcinogenic effects[3-4]. Studies examining occupational diseases in the mining sector indicate that it has a distinct risk profile in occupational health and safety [5-6]. Dusts generated during mining activities may contain not only silica minerals but also potentially toxic elements naturally present in rocks, such as arsenic (As), cadmium (Cd), chromium (Cr), lead (Pb), nickel (Ni), cobalt (Co), copper (Cu), zinc (Zn), manganese (Mn), and mercury (Hg). These elements are often referred to as "heavy metals" or "potentially toxic elements (PTEs)". Because heavy metals are not biodegradable, they can remain in the environment for a long time, accumulate in soil and sediments, be transported to groundwater and surface water, and enter the food chain through plants. Due to these characteristics, heavy metals are considered among the most important environmental pollutants resulting from mining activities [4-8]. Research conducted in bentonite, cement, perlite,

[1] Asst. Prof. Dr., Department of Electrıcıty and Energy, Kastamonu University, Turkey, ometin@kastamonu.edu.tr, (ORCID: 000-0001-6711-6452)

zeolite, marble, boron minerals, and other industrial mineral quarries in Türkiye reveals that heavy metal concentrations can vary depending on the geological structure of the region, mineralization characteristics, and mining methods. In particular, it has been noted that in some mining areas, toxic elements such as arsenic, lead, cadmium, and chromium can be found above natural background values, posing a health risk to both workers and the surrounding community. Therefore, regular environmental monitoring studies in mining areas, effective implementation of dust control systems, use of personal protective equipment, and monitoring of workers through biological monitoring programs are among the fundamental components of sustainable mining [9-12]. Critical pollution sources include dust emissions, greenhouse gases, especially carbon dioxide, heavy metals (HM), and particulate matter. Many studies have confirmed heavy metal pollution in soils near mines [13-15].

2. GENERAL PROPERTIES OF HEAVY METALS

Heavy metals are defined as metallic elements with high atomic weights and generally densities greater than 5 g/cm³. However, today, this definition is increasingly being replaced by the concept of potentially toxic elements (PTEs). The main reason is that some low-density elements can also exhibit high toxicity; conversely, some high-density metals are vital to biological systems [2]. Heavy metals are classified into two categories based on their roles in biological systems: essential (necessary) and non-essential. Essential heavy metals (such as iron, copper, zinc, and manganese) act as cofactors in important physiological processes and perform vital functions at low concentrations; however, when these metals exceed a certain threshold, they can become toxic. Non-essential heavy metals (such as cadmium, lead, mercury, arsenic) do not perform any biological functions in the organism and can exhibit toxic effects even at low concentrations [16]. Because these two groups of metals can have chemically similar properties and bind to the same biological ligands, the entry of non-essential metals into the organism can also disrupt the normal physiological functions of essential metals [17]. Among the potential toxic elements most frequently evaluated in mining activities are arsenic (As), cadmium (Cd), chromium (Cr), lead (Pb), nickel (Ni), cobalt (Co), copper (Cu), zinc (Zn), manganese (Mn), iron (Fe), and mercury (Hg). The main characteristics are given in Table 1. A significant portion of these elements are a natural component of the Earth's crust and are found in varying concentrations. Most heavy metal concentrations detected in mining sites are of geogenic origin. However, mining activities such as ore extraction, crushing, grinding, and transportation can accelerate the release of these elements into the environment, posing significant risks to human and environmental health [9]. The release of heavy metals into the environment

originates from two processes: natural and anthropogenic (human-made). Rock and soil erosion and volcanic activity are natural sources of erosion and volcanic activity. Mining, metal processing and smelting operations, industrial wastewater, agricultural inputs (mineral fertilizers, pesticides, fertilizers), atmospheric deposition, transportation, and domestic waste constitute human-made sources [18]. The contribution of natural processes to environmental heavy metal loads is relatively less compared to anthropogenic sources. In agricultural lands, especially in industrialized countries, atmospheric deposition is the primary source of heavy metal input [19].

Table 1. Heavy metals commonly found in ore mines and their basic characteristics [18,20]

Heavy Metal	Natural Resource	Main Toxic Effects	IARC Classification
As	sulfur minerals	Cancer, skin lesions	Group 1
Cd	Zn ores	Kidney damage	Group 1
Cr(VI)	Ultrabasic rocks	Lung cancer	Group 1
Pb	Galen	Neurotoxicity	2A
Ni	ultramafic rocks	Respiratory system	Group 1
Co	mafic rocks	Cardiovascular effects	2D
Cu	sulfur minerals	Liver	-
Zn	sphalerite	Low toxicity	-
Mn	mafic rocks	Nervous system	-
Hg	cinnaba	Neurotoxicity	Group 2B

Heavy metals are not biodegradable and do not completely disappear even when undergoing chemical transformations in the environment. Depending on environmental conditions, they can remain in soil, sediment, and water for years, transforming between different chemical forms. In particular, pH, oxidation-reduction potential, organic matter content, and the presence of clay minerals are key factors determining the mobility of heavy metals. Minerals with high cation exchange capacity, such as bentonite and zeolite, can adsorb some heavy metals. However, these metals can become free again if environmental conditions change. This necessitates long-term monitoring of heavy metal pollution [2, 9-19].

2.1 Sources of Heavy Metals in Mining Ovens

The sources and concentrations of heavy metals at mining sites and mineral processing facilities are shaped by the combined effects of natural geological processes and human activities. Therefore, the sources of heavy metals are generally classified into two main groups: geogenic (natural) and anthropogenic (human-made). Geogenic sources consist of elements naturally present in rocks and minerals,

formed by geological processes that produce mineral deposits. In contrast, anthropogenic sources include heavy metals released into the environment during mining activities, ore preparation, transportation, storage, and industrial production [18]. The contamination of soils in mining areas with heavy metals is largely due to anthropogenic sources, including ore extraction, crushing and grinding, on-site disposal of waste rock and slag, and inadequate waste management practices. Risk assessment studies in such sites show that mining activities can lead to the accumulation of heavy metals at levels that pose both carcinogenic and non-carcinogenic health risks to surrounding soils and residential areas [21]. Additionally, the potential sources of airborne metal and metalloid pollutants are primarily two mechanisms: emissions from smelting processes and the transportation of mine waste through wind erosion. The fine particles formed during the melting process disperse more readily into the environment than larger slag dust particles [22].As shown in Table 2, the heavy metal concentrations detected in bentonite, perlite, and zeolite quarries, as well as in cement factories, are influenced by factors such as geological structure, raw materials used, production technology, and operational activities. Naturally occurring heavy metals are more likely to enter the environment through mining activities; meanwhile, anthropogenic processes accelerate their spread into the atmosphere, soil, and water. Therefore, effective management of heavy metal pollution requires the combined assessment of both geogenic and anthropogenic sources [6,9,15,18].

Table 2. Bentonite, perlite, zeolite quarries, and cement factories are the main sources of heavy metals. [6,9,15,18]

Business	Geogenic resources	Anthropogenic resources	Common heavy metals
Bentonite quarry	Volcanic ash, montmorillonite, hydrothermal alteration	Excavation, drying, grinding, transportation	Cr, Ni, Co, As, Pb
Perlite quarry	Hydrated volcanic glass	Crushing, screening, and expansion	Pb, Cr, Ni, Zn
Zeolite quarry	Volcanic tuff, clinoptilolite	Crushing, grinding, transportation	Fe, Mn, Cu, Ni
Cement factory	Limestone, clay, iron ore, gypsum	Rotary kiln, grinding, alternative fuels, flue gases	Pb, Cd, Cr, Hg, Ni, Zn

2.2 Environmental Spread of Heavy Metals

Many factors influence the environmental distribution of heavy metals, including geological structure, mineralogical characteristics, climate, land use, hydrological processes, and mining activities. Environmental distribution occurs through a reciprocal exchange between soil and atmosphere. Both soil and atmosphere can

serve as sources and reservoirs for heavy metals. The transport of heavy metals from soil to atmosphere via wind erosion occurs in three ways: direct mixing of airborne aggregates into the air, fragmentation of jump and creep-sized aggregates through collision and abrasion, and fracture or disintegration of creep-sized aggregates [23]. Soil is both a natural reservoir and the most important medium for the environmental transport of heavy metals. The mobility of heavy metals in soil is controlled by factors such as pH, organic matter content, clay mineral type, cation exchange capacity, and oxidation-reduction conditions [18-23].Heavy metals released by mining and mineral processing are pollutants that move among environmental components through a complex transport cycle involving the atmosphere, soil, water, and biological systems. Studies around mining sites and similar emission sources show that dust accumulation decreases with distance from the source, exhibiting a clear distance-decay pattern; this is considered strong evidence that the examined emission source is the primary contributor to environmental pollution. Fine particulate matter generated during drilling, blasting, crushing, screening, grinding, and transportation in bentonite, perlite, and zeolite quarries, as well as in cement factories, is the primary mechanism for the release of heavy metals into the environment. Since these elements are biologically non-degradable, they can remain in the environment for long periods and be transported among environmental media, and accumulate in living organisms over time, thereby adversely affecting ecological balance and human health [6,9,15,18]. Heavy metals originating from a mine or processing facility are not limited to the immediate vicinity of the site; they can spread over a wider region, including agricultural areas and residential zones, through atmospheric transport, deposition, and resuspension cycles. This necessitates that both environmental monitoring studies and health risk assessments be designed to encompass not only the emission source itself but also the broader impact area surrounding it [23].

3. HUMAN HEALTH RISK ASSESSMENT METHODS

Human health risk assessment is the process of identifying the hazards posed by environmental pollutants and evaluating overall human exposure to these pollutants. It determines the severity of the harm that exposed individuals may experience and aims to identify potential negative health effects that may occur in the short or long term. The most commonly used approach to assess heavy metal risks is the human health risk assessment methodology developed by the United States Environmental Protection Agency (USEPA). This method calculates individual exposure doses using heavy metal concentrations measured in environmental settings. It quantitatively assesses non-carcinogenic and carcinogenic risks. In addition, heavy metals enter the human body mainly through three routes: oral ingestion, inhalation,

and skin contact (absorption). The importance of these exposure routes varies with factors such as the characteristics of the work environment, the physical and chemical properties of the pollutant, the age of the exposed individual, and daily habits [25-26].When assessing non-carcinogenic health effects, the first quantitative step is to calculate an individual's daily exposure to a specific heavy metal. For this purpose, the Average Daily Dose (ADD) is used. ADD is calculated separately for oral, inhalation, and dermal exposures, depending on the route by which the contaminant enters the body. The hazard quotient (HQ) is then calculated by dividing the daily intake for the relevant exposure route by the reference dose (for ingestion and dermal contact) or the reference concentration (for inhalation) established for that metal. In cases of simultaneous exposure to multiple metals or exposure routes, the hazard index (HI) is calculated by summing the individual HQ values, assuming dose addition [26-27]. For metals with carcinogenic potential (such as arsenic, cadmium, hexavalent chromium, and nickel), risk assessment is performed using the cancer slope factor (CSF); multiplying the daily intake amount for the relevant exposure route by the CSF yields the carcinogenic risk (CR), which indicates the probability of developing cancer over a lifetime due to excess exposure. The total carcinogenic risk (TCR/TKR) is calculated by summing the individual carcinogenic risk values for multiple metals or exposure routes [25].

4. EXPERIMENTAL MESUREMENT AND EVALUATION

Sample collection and preparation procedures include mining sites operated commercially in Turkey (bentonite, zeolite, cement factory). The collected samples were dried in an oven at 105°C, sieved to a depth of 100 μm, and homogenized. Analyses of heavy metals (Cr, Mn, Fe, Co, Ni, Cu, Zn, As, and Pb) were performed using Energy Dispersive X-ray Fluorescence (ED-XRF) [2,9-12]. The hazard quotient and hazard index values estimated to assess the non-carcinogenic human health risks associated with each heavy metal analyzed in samples from bentonite mines are presented in Table 3. From Table 3, the average total HQ ranks Zn < Cu < Pb < Ni < As < Co < Cr < Mn < Fe. The average values of HIi are 0.01 (HIInh), 0.09 (HIIng), and 0.01 (HIDerm). The estimated HI value is 0.01, which is below the risk threshold of 1 [28].

Table 3. Hazard index and hazard coefficient values[28].

HM	HQi		
	Inhalation	Ingestion	Dermal
Cr	$9.0x10^{-5}$	$5.8x10^{-3}$	$3.83x10^{-4}$
Mn	$1.0x10^{-2}$	$6.9x10^{-3}$	$3.45x10^{-6}$
Fe	$9.8x10^{-6}$	$6.7x10^{-3}$	$4.41x10^{-3}$
Co	$6.3x10^{-7}$	$4.8x10^{-3}$	$3.96x10^{-6}$
Ni	$1.6x10^{-7}$	$1.2x10^{-3}$	$1.91x10^{-3}$
Cu	$1.4x10^{-7}$	$9.5x10^{-4}$	$2.08x10^{-5}$
Zn	$4.7x10^{-8}$	$3.3x10^{-3}$	$1.09x10^{-5}$
As	$5.4x10^{-7}$	$3.7x10^{-3}$	$5.91x10^{-4}$
Pb	$1.5x10^{-7}$	$9.9x10^{-4}$	$4.38x10^{-4}$
HIi=ΣHQi	$1.0x10^{-2}$	$9.1x10^{-2}$	$1.1x10^{-2}$
HI=ΣHIi		0.11	

Estimated carcinogenic risk and total carcinogenic risk values for workers in bentonite quarries to assess the carcinogenic human health risks of Pb, As, Ni, and Cr analyzed in bentonite samples are given in Table 4. The average total CR was ranked as Pb < As < Cr < Ni [28].

Table 4. Values of carcinogenic risk and total carcinogenic risk [28].

HM	CRi		
	Inhalation	Ingestion	Dermal
Cr	1.1×10^{-7}	8.7×10^{-6}	2.3×10^{-5}
Ni	2.9×10^{-9}	3.9×10^{-5}	3.5×10^{-5}
As	2.4×10^{-9}	1.7×10^{-5}	2.7×10^{-7}
Pb	2.1×10^{-11}	3.0×10^{-5}	6.5×10^{-9}
TCRi=ΣCRi	1.1×10^{-7}	5.0×10^{-5}	5.8×10^{-5}
TCR=ΣTCRi		1.1×10^{-4}	

The average values of TCRi were 1.1×10^{-7} (TCRInh), 5.0×10^{-5} (TCRIng), and 5.8×10^{-5} (TCRDerm). The estimated TCR value for these four heavy metals and three exposure pathways is 1.1×10^{-4}, which is close to the carcinogenic risk limit of 1.0×10^{-4} [28].Descriptive statistical information regarding the concentrations of trace heavy metals, which are primarily toxic to human and environmental health, in

zeolite samples is given in Table 5. The average toxic heavy metal levels in zeolite samples are Zr: 87.8 mg/kg, Zn: 55.5 mg/kg, Pb: 47.8 mg/kg, As: 24.8 mg/kg, Ni: 9.9 mg/kg, Co: 8.8 mg/kg, Cr: 7.3 mg/kg, Cu: 4.3 mg/kg and Cd: 2.1 mg/kg, which are below the averages of the earth's crust. The heavy metals in the analyzed zeolite samples are ranked according to their average concentration values as Ta > Nb > Ga > Hf > Te > Sn > Ag > V > W [29].

Table 5. Descriptive information about toxic heavy metals contained in the zeolite mineral [29].

Heavy metal	Toxic heavy metal concentration (mg/kg)							
	Average	SH	Median	SS	Skewness	Kurtosis	Minimum	Maximum
Cr	7,3	0,4	5,9	3,7	-0,9	0,6	1,5	15,1
Co	8,8	0,3	7,9	2,3	1,9	1,4	6,0	17,2
Ni	9,9	0,2	9,3	2,2	-0,9	0,4	6,2	14,5
Cu	4,3	0,1	4,2	1,0	0,1	0,3	2,1	6,9
Zn	55,5	2,6	48,1	23,2	1,6	1,2	25,6	140,3
As	24,8	4,4	11,8	39,5	3,5	2,2	0,8	148,5
Zr	87,8	2,2	87,7	19,6	-0,7	-0,4	43,1	122,5
Cd	2,1	0,1	1,7	0,8	2,5	1,9	1,2	4,6
Pb	47,8	1,1	49,4	10,2	1,0	-0,4	22,8	78,6

The concentrations of heavy metals analyzed in cement samples are given in Table 5. The mean Ti content of cement samples was 4500 mg/kg, the mean Fe content was 46500 mg/kg, and the mean Zr content was 170 mg/kg, all of which were below the average of the Earth's crust [30-31].The average contents of Cr, Mn, Ni, and Pb in the CEM I, CEM II, and CEM VI cement samples were 83 mg/kg, 1000 mg/kg, 58 mg/kg, and 16 mg/kg, respectively, which are higher than the average levels of the Earth's crust. The average contents of V (90 mg/kg) and As (1.7 mg/kg) in the cement samples (excluding CEM VI) are also higher than the average of the Earth's crust [30-31].

Table 5. Heavy metals analyzed in cement samples [31].

Heavy metal	Concentration (mg/kg)					
	Cement type					
	CEM I	CEM II	CEM VI	SS	WP	SSW
Ti	1773 ± 18	2334 ± 20	4063 ± 25	177 ± 8	244 ± 9	138 ± 6
V	158 ± 8	137 ± 9	180 ± 10	239 ± 6	129 ± 5	101 ± 4
Cr	279 ± 5	254 ± 4	161 ± 4	< 1.0	< 1.0	< 1.0
Mn	1111 ± 8	2019 ± 10	4928 ± 15	65 ± 2	113 ± 3	36 ± 2
Fe	23970 ± 50	22120 ± 50	17530 ± 40	1883 ± 13	1894 ± 14	1307 ± 10
Ni	133 ± 4	116 ± 3	82 ± 3	57 ± 3	51 ± 3	32 ± 2
Cu	55 ± 2	53 ± 2	31 ± 2	< 0.5	< 0.5	< 0.5
Zn	126 ± 2	119 ± 2	67 ± 2	11 ± 1	12 ± 1	9 ± 1
As	8 ± 1	6 ± 1	< 0.5	7 ± 1	8 ± 1	5 ± 1
Zr	79 ± 5	88 ± 5	126 ± 5	46 ± 3	41 ± 3	28 ± 2
Pb	24 ± 1	23 ± 1	20 ± 1	16 ± 1	12 ± 1	10 ± 1

5. CONCLUSION

Turkey is among the countries with significant reserves of industrial minerals such as bentonite, perlite, and zeolite, and the economic utilization of these resources contributes significantly to the mining sector. However, dust emissions generated during open-pit mining, ore preparation, and mineral processing, along with naturally occurring heavy metals in the rocks, can be released into the environment, posing potential health risks to workers and residents in the surrounding area. Similarly, the mineralogical structure of raw materials used in cement production and high-temperature production processes can also contribute to the transport of heavy metals into the environment. Evaluating the potential effects of exposure to toxic heavy metals among workers in bentonite quarries and individuals who use bentonite as an additive is an important approach to protecting human health. As a result of the health risk assessment conducted within the scope of this study, it was determined that all calculated hazard quotient (HQ), hazard index (HI), cancer risk (CR), and total cancer risk (TCR) values were within internationally accepted safe limits. These findings indicate that current heavy metal levels do not pose a significant health risk to bentonite quarry workers and individuals using bentonite-containing products. However, the fact that risk indicators are within acceptable limits does not mean that occupational exposure can be completely disregarded. To minimize the potential negative effects of long-term exposure, particularly from inhalation of bentonite dust, implementing effective dust control systems, ensuring appropriate use of personal protective equipment, and regularly monitoring work

environments are of paramount importance. These measures will significantly contribute to protecting worker health and to the sustainability of occupational health and safety practices. This study reveals that the heavy metal content of materials produced by commercially operated mineral quarries in Türkiye should be regularly monitored to ensure final product quality and to protect the health of workers involved in the production process. While cement factory data provide a product-based chemical characterization, the risk assessment conducted for bentonite quarries serves as an example that quantifies the extent of occupational exposure. Presenting these two approaches together contributes to the limited number of studies in the literature that address both environmental and occupational health risks within the same framework.

REFERENCES

1- Bărbulescu, A., & Hosen, K. (2025). Cement industry pollution and its impact on the environment and population health: A review. Toxics, 13(7), Article 587. https://doi.org/10.3390/toxics13070587

2- Altıkulaç, A., & Turhan, Ş. (2023). Assessment of the levels of potentially toxic elements contained in natural bentonites collected from quarries in Turkey. ACS Omega, 8(23), 20979–20986. https://doi.org/10.1021/acsomega.3c01773

3- Martins, F. P., Botelho Junior, A. B., Batalhão, A. C. S., Paschoalotto, M. A. C., & Veras, M. M. (2025). Mining chemical exposures on health & environment impact: A global scoping review. Journal of Sustainability, 1(2), 1–31. https://doi.org/10.55845/jos-2025-1211

4- Balali-Mood, M., Naseri, K., Tahergorabi, Z., Khazdair, M. R., & Sadeghi, M. (2021). Toxic mechanisms of five heavy metals: Mercury, lead, chromium, cadmium, and arsenic. Frontiers in Pharmacology, 12, Article 643972. https://doi.org/10.3389/fphar.2021.643972

5- Erol, İ. (2020). Ülkemiz madencilik sektöründe görülen meslek hastalıklarının incelenmesi. Çukurova Üniversitesi Mühendislik-Mimarlık Fakültesi Dergisi, 35(4), 859–872. https://doi.org/10.21605/cukurovaummfd.867378

6- Turhan Ş. ,Duran C.at al..(2023). Impact of toxic metal pollution on surface water pollution: a case study of Tohma Stream in Sivas, Turkey, International Journal of Environmental Analytical Chemistry, 103(14)3224-3234 https://doi.org/10.1080/03067319.2021.1904916.

7- Donoghue, A. M. (2004). Occupational health hazards in mining: An overview. Occupational Medicine, 54(5), 283–289. https://doi.org/10.1093/occmed/kqh072

8- Parlak, M., Tunçay, T., & Özaslan Parlak, A. (2024). Heavy metals in tailings and soils in the Pb–Zn mining areas of North-west Türkiye and health risk evaluations. International Journal of Agriculture, Environment and Food Sciences, 8(1), 131–148. https://doi.org/10.31015/jaefs.2024.1.14

9-Turhan, Ş., Tokat, S., Kurnaz, A., & Altıkulaç, A. (2022). Distribution of elemental compositions of zeolite quarries and calculation of radiogenic heat generation. International Journal of Environmental Analytical Chemistry, 102(19), 7851–7862. https://doi.org/10.1080/03067319.2020.1844225

10-Metin, 0. (2023). Türkiye'de farklı sektörlerde katkı hammaddesi olarak kullanılan bentonit mineralinin kimyasal ve radyometrik karakterizasyonu. Doktora Tezi, Kastamonu Üniversitesi Fen Bilimleri Enstitüsü. Kastamonu.

11-Altıkulaç, A., & Turhan, Ş. (2024). Evaluation of some potentially toxic elements and associated ecological and health risks in topsoil samples adjacent to an industrial zone in Turkey. ACS Omega, 9(42), 42668–42678. https://doi.org/10.1021/acsomega.3c07638

12- Turhan, Ş., Türkdoğan, S., Altuner, E. M., Kurnaz, A., & Hançerlioğulları, A. (2026). Heavy metals in perlite quarries and exposure of worker. Environmental Earth Sciences, 85(2), Article 58. https://doi.org/10.1007/s12665-025-12654-x

13- Adekola, F. A., Inyinbor, A. A., & Abdul Raheem, A. M. O. (2012). Heavy metals distribution and speciation in soils around a mega cement factory in North-Central Nigeria. Ethiopian Journal of Environmental Studies and Management, 5(1), 11–19. https://doi.org/10.4314/ejesm.v5i1.2

14- Awos, A., Thompson, S., Adedeji, O., Zvomuya, F., & Zhang, Q. (2024). Monitoring of air quality for particulate matter (PM2.5, PM10) and heavy metals proximate to a cement factory in Ewekoro, Nigeria. Journal of Geoscience and Environment Protection, 12(10), 152–180. https://doi.org/10.4236/gep.2024.1210009

15- Ismail, Z., Ali, S., Zulfiqar, A., & El-Serehy, H. A. (2023). Impact of cement industries on potentially toxic elements' contamination and other characteristics of topsoil: A case study. Environmental Pollutants and Bioavailability, 35(1), Article 2271664. https://doi.org/10.1080/26395940.2023.2271664

16-Nucera, S., Serra, M., Caminiti, R., Ruga, S., Passacatini, L. C., Macrì, R., Scarano, F., Maiuolo, J., Bulotta, R., Mollace, R., Bosco, F., Guarnieri, L., Oppedisano, F., Ilari, S., Muscoli, C., Palma, E., & Mollace, V. (2024). Non-essential heavy metal effects in cardiovascular diseases: An overview of systematic reviews. Frontiers in Cardiovascular Medicine, 11, Article 1332339. https://doi.org/10.3389/fcvm.2024.1332339

17- Aprile, A., & De Bellis, L. (2020). Editorial for Special Issue "Heavy Metals Accumulation, Toxicity, and Detoxification in Plants". International Journal of Molecular Sciences, 21(11), Article 4103. https://doi.org/10.3390/ijms21114103

18-Martínez-Guijarro, R., Paches, M., Romero, I., & Aguado, D. (2021). Sources, mobility, reactivity, and remediation of heavy metal(loid) pollution: A review. Advances in Environmental and Engineering Research, 2(4), Article 033. https://doi.org/10.21926/aeer.2104033

19-Wan, Y., Liu, J., Zhuang, Z., Wang, Q., & Li, H. (2024). Heavy metals in agricultural soils: Sources, influencing factors, and remediation strategies. Toxics, 12(1), Article 63. https://doi.org/10.3390/toxics12010063

20- International Agency for Research on Cancer. (2023). Agents classified by the IARC Monographs, Volumes 1–136. IARC. https://monographs.iarc.who.int/agents-classified-by-the-iarc/

21- Baah, D. S., Gikunoo, E., Arthur, E. K., Agyemang, F. O., Foli, G., Koomson, B., & Opoku, P. (2023). Anthropogenic sources and risk assessment of heavy metals in mine soils: A case study of Bontesso in Amansie West District of Ghana. Journal of Chemistry, 2023, Article 6760154. https://doi.org/10.1155/2023/6760154

22-Csavina, J., Field, J., Taylor, M. P., Gao, S., Landázuri, A., Betterton, E. A., & Sáez, A. E. (2012). A review on the importance of metals and metalloids in atmospheric dust and aerosol from mining operations. Science of the Total Environment, 433, 58–73. https://doi.org/10.1016/j.scitotenv.2012.06.013

23-Zhang, Q., Liu, H., Li, X., & Liu, F. (2025). Process of heavy metal transport between soil and the atmosphere: A review. PeerJ, 13, Article e20381. https://doi.org/10.7717/peerj.20381

24- Matei, E., Râpă, M., Mateş, I. M., Popescu, A.-F., Bădiceanu, A., Balint, A. I., & Covaliu-Mierlă, C. I. (2025). Heavy metals in particulate matter—Trends and impacts on environment. Molecules, 30(7), Article 1455. https://doi.org/10.3390/molecules30071455

25- United States Environmental Protection Agency. (2024). Conducting a human health risk assessment. https://www.epa.gov/risk/conducting-human-health-risk-assessment

26- United States Environmental Protection Agency. (1989). Risk assessment guidance for Superfund, Volume I: Human health evaluation manual (Part A), Interim final (EPA/540/1-89/002). Office of Emergency and Remedial Response.

27- Miletić, A., Lučić, M., & Onjia, A. (2023). Exposure factors in health risk assessment of heavy metal(loid)s in soil and sediment. Metals, 13(7), Article 1266. https://doi.org/10.3390/met13071266

28- Turhan, Ş., & Metin, O. (2025, March 15–16). Evaluation of health risks that may arise from heavy metals contained in bentonite mineral for quarry workers. In Proceedings of the 8th International Dicle Scientific Research and Innovation Congress (pp. 187–199). Diyarbakır, Türkiye.

29- Tokat, S. (2019). Gördes (Manisa) zeolit ocaklarının kimyasal bileşenlerinin XRF spektrometrik yöntem ile belirlenmesi. Yüksek Lisans Tezi, Kastamonu Üniversitesi Fen Bilimleri Enstitüsü. Kastamonu.

30- Yaroshevsky, A. A. (2006). Abundances of chemical elements in the Earth's crust. Geochemistry International, 44(1), 48–55. https://doi.org/10.1134/S001670290601006X

31- Metin, O., & Turhan, Ş. (2026, April 16–19). Determination of oxide and heavy metal contents of some cement samples used as building materials in Türkiye. In Proceedings of the International Cairo Congress on Scientific Research and Innovation(pp. 162–169).. Cairo, Egypt.

Chapter 2

Bentonite Minerals and Mining: Mineralogical Structure, Applications, Heavy Metal Concentrations, and Naturally Occurring Radioactive Material (NORM) Content

Onur METİN[1]

1. INTRODUCTION

Minerals are generally defined as naturally occurring, inorganic substances formed through geological processes. They are solid, homogeneous materials characterized by a distinctive crystal structure (e.g., cubic, tetragonal, rhombohedral), specific yet variable physical properties (e.g., luster, hardness, and color), and a defined yet non-fixed chemical composition [1]. More than 4,000 mineral species have been identified and named through various classification methods. Industrial minerals and rocks have played a significant role in human life and in the economic and cultural development of nations for centuries, serving as fundamental components of modern lifestyles. Therefore, minerals are of great importance to both societies and national development [1,2]. Industrial mineral and rock sectors operating worldwide provide raw materials used in the manufacturing of a wide range of products, from ceramics and plastics to automobiles, refractory materials, and paper. Consequently, the availability, extraction, and distribution of economically valuable minerals continue to play a crucial role today, as they have throughout history [3]. Due to its geological setting and location within the Tethyan Metallogenic Belt, Türkiye is among the world's most mineral-rich countries. The country possesses commercially exploitable reserves of approximately fifty different minerals [1,2]. In 2019, Türkiye, with an annual production of 1.5 million tons, ranked behind China, the United States, and India, and by the end of 2024, its bentonite production reached approximately 2.5 million tons [4,5]. Annual per capita mineral consumption is around 16 tons in European Union countries and 21 tons in the United States, whereas in Türkiye it is only about 5 tons. [1]. Bentonite is a clay rock primarily composed of montmorillonite, a member of the smectite group, formed through the chemical alteration of volcanic ash in aqueous environments [6]. The

[1] Asst. Prof. Dr., Department of Electrıcıty and Energy, Kastamonu University, Turkey, ometin@kastamonu.edu.tr, (ORCID: 000-0001-6711-6452)

geological characteristics of bentonite vary from region to region, depending on whether the dominant montmorillonite is calcium (Ca), sodium (Na), or mixed Ca–Na type. Owing to its remarkable physical and chemical properties, including high cation adsorption capacity, cation exchange capacity, large specific surface area, small crystal size, chemical composition, swelling behavior, and hydration characteristics, bentonite is generally classified into two major types: (1) calcium bentonite (non-swelling), which is the most abundant variety, and (2) sodium bentonite (swelling), which is of greater industrial significance [5,6]. Due to these important physical and chemical properties, bentonites are widely used in numerous industrial applications, including the petroleum, paint, rubber, food, ceramics, paper, plastics, pharmaceutical, and civil engineering industries. Applications include foundry processes, drilling muds, iron ore pelletizing, filtration, adsorption, purification, and bleaching processes [5,6]. Humans are exposed to ionizing radiation emitted by naturally occurring radionuclides present in Earth-derived materials and products manufactured from such materials through two primary pathways: internal (inhalation or ingestion) and external exposure. Individuals are directly exposed to gamma radiation emitted by these radionuclides in indoor environments such as homes, schools, factories, and workplaces, as well as in outdoor environments. This type of exposure is called external irradiation. Individuals are also exposed to alpha and beta radiation emitted by radon (^{222}Rn) and its short-lived decay products, which are released from building materials, tap water, soils, and rocks beneath buildings, as well as from soils, rocks, and minerals in outdoor environments, and subsequently inhaled into the respiratory system. This exposure pathway, which increases the risk of lung cancer, is referred to as internal irradiation. Approximately 50% of the average annual radiation dose from natural sources is from radon gas inhalation, while about 12% is from gamma radiation emitted by naturally occurring radionuclides. The primary source of indoor radon gas in buildings and workplaces is the soil and rock underlying the structure, together with the building materials used in walls and foundations. Approximately 30% of indoor radon concentration originates from Earth-derived building materials. The annual radiation doses individuals receive may increase if they live or work in buildings constructed with materials that exhibit elevated levels of natural radioactivity. Therefore, determining the activity concentrations of naturally occurring radionuclides in Earth-derived materials and additive raw materials is of considerable importance for assessing the annual radiation doses received by individuals and workers exposed to environmental radioactivity [7–9].

2. DEFINITION, FORMATION, AND APPLICATIONS OF BENTONITE

Bentonites are formed through the chemical weathering and alteration of magnesium- and aluminum-rich volcanic ash, tuff, and lava deposits. Bentonite is a commercial and industrial mineral composed predominantly of smectite-group clay minerals and is characterized by its ability to absorb water, form thixotropic gels, and exhibit high cation exchange capacity, depending on the dominant exchangeable cation present in its structure (sodium or calcium). Clays formed by the weathering of magnesium- and aluminum-rich volcanic lavas and ashes, and consisting predominantly of montmorillonite, are referred to as bentonite. In commercial terms, bentonite is a clay mineral with superior liquid-absorption and colloidal properties. The geological properties of bentonite vary regionally, mainly depending on its processing from calcium, sodium, or mixed calcium-sodium montmorillonite [10–14]. Although bentonite does not have a fixed chemical formula, its general chemical composition can be represented as $(Na, Ca)_{0.33}(Al, Mg)_2Si_4O_{10}(OH)_2 \cdot nH_2O$, depending on its elemental composition. Table 1 presents the chemical composition of raw and modified bentonite clay reported in a previous study [15].

Table 1. Chemical composition of raw and modified bentonite clay.

% Composition	Bentonite clay	Alum-bent
SiO2	66.51	66.01
TiO2	0.14	0.14
Al2O3	16.81	17.22
Fe2O3	3.26	3.28
MnO	0.13	0.12
MgO	3.12	3.03
CaO	1.43	1.30
Na2	1.17	0.46
K2O	0.54	0.51
P2O5	0.03	0.03
LOI	7.19	7.55
TOTAL	100	99.68

2.1 Applications of Bentonite

Bentonite is a multifunctional raw material that has found widespread application across nearly all industrial sectors due to its unique crystal structure and high cation exchange capacity. Its ability to swell several times its original volume upon contact with water, form thixotropic gels, and retain contaminants within its pore structure has significantly expanded its range of applications.

These distinctive physicochemical properties make bentonite an indispensable material in numerous fields, including drilling operations, foundry processes, environmental remediation, wastewater treatment, construction engineering, pharmaceuticals, cosmetics, food processing, and pet litter production.

2.1.1 Foundry Industry

Bentonite is one of the most commonly used binders in the preparation of molding sands in the casting industry due to its high binding properties, plasticity capacity, and colloidal structure. In particular, the casting ratios of iron, steel, and non-ferrous metals ensure that the molds acquire sufficient strength, fluidity, compressibility, and resistance to high temperatures. Thanks to these properties, it helps maintain the mold's shape during casting, enabling the production of high-quality surfaces and dimensional accuracy without cutting. Engine blocks, body shells, brake drums, maintenance hole parts, rainwater drainage elements, brass plumbing parts, cast kitchenware, and numerous industrial casting products are produced using bentonite-modified molding sands [11,13,16].

2.1.2 Fertilizer and Animal Feed Industry

Both sodium and calcium bentonites are used in the pelletization of animal feed. In addition to their binding properties, these minerals act as adsorbents for bacteria and certain enzymes, thereby supporting animal growth and health. Bentonite is also incorporated into the feed of poultry such as chickens, turkeys, geese, and quails to enhance egg production and growth performance. Consequently, it is widely utilized in the animal feed industry [17–18].

2.1.3 Drilling Industry

Due to its fine size, large surface area and high layer load, sodium bentonite exhibits very high viscosity and thixotropic behavior when dispersed in water. These properties, together with its high swelling capacity, make sodium bentonite one of the most important and indispensable ingredients in freshwater drilling muds. It is widely used as a basic introducer in fluids used in oil and gas exploration, water wells, boreholes and environmental monitoring wells, as well as in drilling small holes [6,18].

2.1.4 Paper Industry

Bentonite used in paper distribution is intended to cause the deterioration of thin documents within the paper matrix, increase the flocculation of polymers, and thus determine drainage and layer formation. In addition, bentonite acts as an effective adsorbent in the removal process-related particles found in wood pulp during the

paper production process. Acid-activated bentonites, in particular, have an important application area in the production of carbon photocopy papers. These types of papers generally have a three-layered structure, with the upper surfaces of the middle and lower layers coated with bentonite exhibiting acidic properties. Bentonite acts as a solid acid, chemically reacting with colorless dyes in microcapsules similar to those on the lower surfaces of the two upper layers. When pressure temperature is applied to the upper layer, the microcapsules break down, and the released dye interacts with the acid-activated bentonite, creating a permanent colored trace [19,20].

2.1.5 Paint and Coatings Industry

Due to its adsorption properties, bentonite forms stable suspensions with raw materials used in paint formulations. As a result, it prevents pigment settling during storage and minimizes paint sagging after application. The incorporation of bentonite as an additive offers significant advantages to paint manufacturers by improving the stability and performance of their products. Therefore, bentonite is widely used as an additive in both solvent-based and water-based paints [17,21].

2.1.6 Cat Litter Industry

Bentonite is widely used in cat litter because it absorbs waste and forms compact clumps, leaving the remaining litter intact and suitable for continued use. Sodium bentonite clumps and traps pet waste thanks to its high absorption capacity. This feature allows the waste to be easily and completely removed from the cat litter. This property reduces litter consumption, facilitates cleaning, and helps maintain litter boxes in a clean and odor-free condition [17,21].

2.1.7 Pelletizing Industry

Sodium bentonite is widely used in the pelletization of iron ore concentrates due to its superior dry strength properties. This process improves handling during transportation and produces high-quality furnace feed materials. In some applications, iron ore concentrates to which bentonite is added are kept under high pressure to obtain briquettes. Bentonite is a commonly used preservative in iron ore pelleting, and approximately 20% of world bentonite production is consumed in this way [17,22].

2.1.8 Oil and Food Industry

Bentonite removes phospholipids, trace metals, free fatty acids and their degradation, which are undesirable substances in vegetable oils. In addition, bentonite removes oxidation such as glycerides and hydroperoxides during the bleaching process and improves the preservation of the oil [13,23].

2.1.9 Pharmaceutical, Cosmetic, and Medical Industry

In the pharmaceutical industry, bentonite is valued as a filler and contributes to the preparation of paste-like preparations thanks to its high adsorption and absorption capacity. In medical applications, its adsorbent properties have been particularly utilized against heavy metal poisoning. Thanks to its negatively charged surface, bentonite can adsorb excess oil, dirt, dead skin cells and some heavy metals that accumulate on the skin. Due to these properties, it is widely preferred in the production of clay masks, sunburn products, baby and face powders and various cosmetic creams [16–21].

2.2. Bentonite Reserves in the World and in Türkiye

Among the world's bentonite reserves, the most significant deposits are located in the United States, China, India, Greece, and Russia. Approximately 20% of the global bentonite reserves, corresponding to about 370 million tons, are located in Türkiye, particularly in the provinces of Ankara, Çankırı, Edirne, Artvin, Çorum, Giresun, Konya, Ordu, Tokat, and Trabzon. As shown in Table 2, global bentonite production over the last two years has ranged between 20.3 and 21.0 million tons. An examination of bentonite production by country shows that the United States, which holds one of the largest bentonite reserves in the world, ranks first globally. India, Türkiye, and China follow the United States in terms of bentonite production. These countries play a leading role in meeting the growing global demand for bentonite across various industrial sectors [24].

Table 2. World Bentonite Production ($\times 10^3$ tonnes) [24]

Countrıes	2023	2024
ABD	4360	4800
Brazil	386	390
China	2100	2100
Czechia	196	200
Denmark	925	930
Greece	1110	1100
India	3700	3700
Iran	850	850
Mexico	79	80
Turkiye	2490	2500
Uzbekistan	60	20
Other countries	3870	3900
World total	20300	21000

3. HEAVY METAL CONTENT IN BENTONITE

Heavy metals are naturally occurring elements characterized by relatively high atomic density and atomic weight compared with many other elements. Bentonite deposits may contain varying concentrations of heavy metals depending on their geological origin, mineralogical composition, and depositional environment. Elements such as Cr, Mn, Fe, Co, Ni, Cu, Zn, As, and Pb are among the most commonly encountered heavy metals in bentonite deposits. The presence of these elements is important not only for environmental and human health, but also for evaluating the suitability of bentonite for industrial, pharmaceutical, cosmetic, and environmental applications. Their extensive use in industry, agriculture, medicine, and technology has led to widespread environmental distribution, posing potential risks to human health and ecosystems [25–28].Thirty-seven bentonite samples were collected from bentonite quarries located in the Turkish provinces of Ankara (BNTQ1), Çankırı (BNTQ2), Çorum (BNTQ3), Edirne (BNTQ4), Konya (BNTQ5), Ordu (BNTQ6), and Tokat (BNTQ7). The collected samples were prepared and analyzed for heavy metals (Cr, Mn, Fe, Co, Ni, Cu, Zn, As, and Pb) using Energy-Dispersive X-ray Fluorescence (ED-XRF). The heavy metal concentrations obtained from these analyses are presented in Table 3 [7].

Table 3. Concentrations of heavy metals in bentonite samples [7].

Sample code	Location quarry	Concentration of heavy metal (mg/kg)								
		Cr	Mn	Fe	Co	Ni	Cu	Zn	As	Pb
BNTQ1	Ankara	169.6	1248.0	42070.0	71.7	214.1	22.2	72.7	4.3	26.8
BNTQ2		227.9	1131.0	43790.0	87.8	314.4	53.3	76.1	1.7	19.4
BNTQ3		203.3	189.3	29880.0	61.1	168.9	34.8	46.4	1.5	14.8
BNTQ4		143.8	120.4	26240.0	63.9	180.4	15.4	64.9	6.1	38.6
BNTQ5		172.1	615.1	40880.0	70.2	212.4	29.9	102.6	6.9	29.7
BNTQ6		247.6	2624.0	51200.0	84.1	259.5	46.6	76.7	2.4	21.8
BNTQ7		221.5	1086.0	49280.0	77.3	231.7	34.4	65.6	6.4	19.6
BNTQ8	Çankırı	175.2	555.6	46050.0	73.3	192.1	37.5	81.1	52.9	19.7
BNTQ9		423.2	1356.0	41780.0	79.5	285.7	36.5	67.1	12.3	20.6
BNTQ10		408.2	971.3	38520.0	74.2	242.9	31.7	73.3	19.4	19.7
BNTQ11		397.5	1004.0	30350.0	74.5	211.7	30.8	55.7	14.7	19.8
BNTQ12		206.3	601.9	53890.0	76.4	244.3	45.7	96.8	18.2	28.9
BNTQ13		310.3	853.1	39310.0	67.0	265.2	31.9	68.7	10.3	23.9
BNTQ14		206.6	733.3	53170.0	64.2	246.1	38.3	97.3	15.4	28.1

BNTQ15		45.6	268.0	51890.0	80.6	184.3	50.3	104.1	2.7	12.3
BNTQ16		26.2	349.8	21160.0	51.4	136.4	19.1	48.3	4.9	16.3
BNTQ17	Çorum	60.2	843.6	34750.0	62.0	154.2	26.6	64.5	3.2	19.5
BNTQ18		416.1	400.1	32000.0	74.8	165.7	29.5	52.4	1.1	19.9
BNTQ19		204.6	669.8	34640.0	81.0	194.3	33.0	56.7	2.1	19.5
BNTQ20		6.4	1180.0	41410.0	61.7	113.8	49.2	75.8	1.1	41.5
BNTQ21		77.5	681.3	40890.0	67.6	148.6	21.8	82.0	8.5	35.3
BNTQ22	Edirne	79.2	591.7	32950.0	80.1	148.8	21.0	63.3	8.6	31.8
BNTQ23		53.4	402.1	24890.0	53.2	107.3	11.7	44.0	1.4	20.8
BNTQ24	Konya	53.8	858.0	45670.0	60.2	160.9	23.4	62.7	13.2	30.2
BNTQ25		101.4	624.1	33700.0	63.4	207.3	33.6	72.2	25.4	23.1
BNTQ26		117.5	567.5	42450.0	73.0	205.5	31.3	91.3	16.8	21.6
BNTQ27		66.4	254.3	34750.0	50.8	122.9	37.0	198.4	18.5	66.0
BNTQ28		8.0	155.1	8699.0	49.1	96.1	7.8	32.1	2.3	23.5
BNTQ29		8.5	209.6	10020.0	52.2	97.8	11.0	91.4	1.2	27.1
BNTQ30	Ordu	3.8	265.5	3968.0	43.0	79.5	3.3	14.4	2.9	13.5
BNTQ31		7.6	159.5	8257.0	62.4	112.7	7.1	38.5	5.1	13.5
BNTQ32		3.5	314.9	7600.0	48.6	98.5	5.2	27.5	1.2	15.9
BNTQ33		14.4	330.8	9317.0	57.4	117.2	6.5	30.6	4.0	31.5
BNTQ34		3.8	1178.0	18690.0	85.0	163.7	19.3	44.9	3.6	36.9
BNTQ35	Tokat	11.6	215.3	27510.0	75.2	148.2	16.6	84.7	6.2	45.4
BNTQ36		2.8	533.4	23910.0	55.7	112.6	12.6	63.7	1.2	33.0
BNTQ37		3.0	774.8	35190.0	74.6	135.6	15.9	78.2	1.1	46.4

4. ASSESSMENT OF NATURAL RADIOACTIVITY IN BENTONITE

Radioactivity can be defined as the nuclear transformation of unstable atomic nuclei into more stable configurations through spontaneous and random radioactive decay, resulting in the formation of new elements or isotopes. Radioactivity is independent of the chemical and physical state of a radionuclide and is determined solely by nuclear properties; therefore, it is an intrinsic characteristic specific to each radionuclide [7, 29].While a certain degree of mineralogical impurities can be tolerated when bentonite is used in heavy industrial applications such as foundry operations and drilling fluids, the increasing utilization of bentonite in applications involving direct human and animal exposure, including food products, feed additives, cosmetics, and pharmaceuticals, necessitates stringent monitoring of both heavy metal

concentrations and Naturally Occurring Radioactive Materials (NORM) in accordance with international standards and regulations, such as those established by the U.S. Food and Drug Administration (FDA), European Union (EU) legislation, and Turkish Standards (TS EN) [7, 12, 28].The most widely used methods for determining natural radioactivity in bentonite include high-purity germanium (HPGe) gamma-ray spectrometry, sodium iodide scintillation gamma spectrometry [NaI(Tl)], and, more recently, energy-dispersive X-ray fluorescence (EDXRF) spectrometry for determining elemental concentrations, followed by their conversion into activity concentrations. Among these techniques, gamma-ray spectrometry is internationally recognized as the standard method for the radiological characterization of environmental samples and industrial raw materials due to its high sensitivity, accuracy, and ability to simultaneously determine naturally occurring radionuclides.

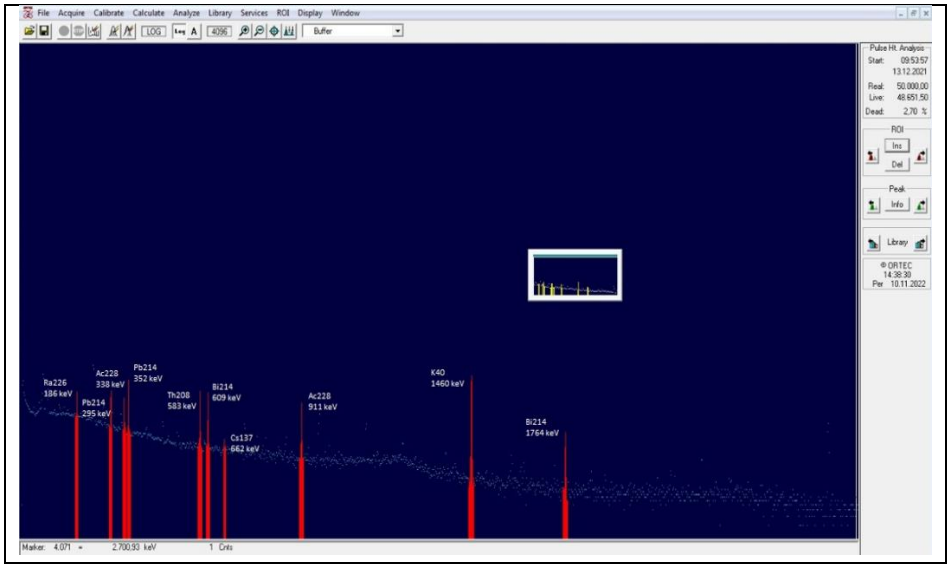


Figure 1. Gamma-ray spectrum of the bentonite sample [7].

In a study of samples collected from bentonite deposits, the gamma-ray spectrum of a representative bentonite sample is shown in Figure 1. In the recorded gamma-ray spectra, the photopeaks at 351.9, 609.3, and 1764.5 keV corresponding to 226Ra; 583.2 and 911.2 keV corresponding to 232Th; and 1460.8 keV corresponding to 40K were selected for analysis. The net photopeak areas (counts) of these gamma rays were determined by subtracting the corresponding background photopeak areas obtained from periodic laboratory background measurements from those measured in the bentonite sample spectra.

These net count rates were subsequently used to determine the activity concentrations of the respective radionuclides [7].The activity concentrations (A) of the radionuclides present in the bentonite samples were calculated using Equation (1) [29].

$$A = \frac{C}{\varepsilon(E_\gamma) \cdot P_\gamma \cdot M \cdot t} \quad (1)$$

where C is the net gamma-ray count obtained from the gamma-ray spectrum; ε(Eγ) is the full-energy peak efficiency of the detector at the gamma-ray energy Eγ; Pγ is the gamma-ray emission probability; t is the counting time; and M is the mass of the sample. The full-energy peak efficiency (ε) of the gamma-ray spectrometry system was calibrated using the certified reference materials RGU-1, RGTh-1, and RGK-1 prepared by the International Atomic Energy Agency (IAEA) [29].Descriptive statistical data for the activity concentrations of ^{226}Ra, ^{232}Th, and ^{40}K in the bentonite samples are presented in Table [29].

Table. 4 Some descriptive consistency data regarding the activity concentrations of radionuclides [7].

	Activity concentration (Bq/kg)		
	^{226}Ra	^{232}Th	^{40}K
Mean	50	76	373
Standard error	5	4	19
Median	32	67	353
Standard deviation	44	30	177
Collision	1.9	0.6	0.7
Kurtosis	3.5	–0.8	0.7
Minimum	7	19	26
Maximum	232	175	953
Sample size	100	100	100

As shown in Table 4, the measured ^{226}Ra values in bentonite samples ranged from 7–232 Bq/kg with an average of 50 ± 5 Bq/kg, ^{232}Th values ranged from 19–175 Bq/kg with an average of 76 ± 4 Bq/kg, and ^{40}K values ranged from 26–953 Bq/kg with an average of 373 ± 19 Bq/kg.

5. CONCLUSION AND DISCUSSION

Bentonite is among the most important industrial clay minerals due to its unique physicochemical properties, such as its high swelling capacity and adsorption performance. These properties have led to its widespread use in drilling fluids, foundry sands, iron ore pelletizing, civil engineering, environmental remediation, pharmaceuticals, cosmetics, food processing, and radioactive waste disposal, and the comprehensive evaluation of its elemental composition and natural radioactivity has become increasingly important [10–16]. From an environmental perspective, bentonite may naturally contain radionuclides and heavy metals due to its geological origin. Owing to its adsorption capacity, bentonite is an effective material for immobilizing heavy metals and radionuclides in contaminated environments. Therefore, it is widely used as an engineered barrier material in deep geological repositories for radioactive waste. The mean activity concentration of ^{226}Ra was higher than the world average (Earth's crust) value of 32 Bq/kg, while the mean activity concentration of ^{232}Th exceeded the world average value of 45 Bq/kg [30]. However, the mean activity concentration of ^{40}K was lower than the world average value of 412 Bq/kg [30]. The activity concentration of ^{226}Ra measured in 51% of the bentonite samples, the activity concentration of ^{232}Th measured in 74% of the samples, and the activity concentration of ^{40}K measured in 24% of the samples were higher than the corresponding world average values for each radionuclide [7]. In the analysis of heavy metal (HM) contents (Cr, Mn, Fe, Co, Ni, Cu, Zn, As, and Pb) in bentonite samples produced in Türkiye, it was observed that the concentrations of Cr, Co, Ni, As, and Pb were enriched compared with their average concentrations in the Earth's crust. In addition, the highest HM concentrations were determined in the samples collected from the mine coded BQ2, whereas the lowest HM concentrations were observed in the samples collected from the mine coded BQ6. These findings provide valuable information that may increase awareness regarding the utilization areas of bentonite and the occupational health of workers in bentonite mines. Furthermore, the distribution of potentially toxic elements in bentonite quarries can serve as a database for future studies. To eliminate potential risks that may threaten workers' health, necessary precautions, such as preventing dust inhalation by workers, should be implemented [26, 7].

REFERENCES

1- Krista E.M.A. (2021). Manisa (Yatağan) mika mineral ocaklarının elemental dağılımlarının belirlenmesi ve radyojenik isi üretiminin hesaplanması. Yüksek Lisans Tezi. Kastamonu Üniversitesi, Fen Bilimleri Enstitüsü. Kastamonu.

2- Tokat, S. (2020). Gördes (Manisa) zeolit ocaklarının kimyasal bileşenlerinin XRF spektrometrik yöntem ile belirlenmesi. Yüksek Lisans Tezi, Kastamonu Üniversitesi Fen Bilimleri Enstitüsü. Kastamonu.

3- Jeffrey, K., (2006). In Industrial Minerals & Rocks: Commodities, Markets, and Uses, 7th edition. Kogel, J.E., Trivedi, N.C., Barker, J.M. & Krukowski, S.T. (Eds.), Society for Mining, Metallurgy, and Exploration, (pp. 3–6). Littleton, Colorado.

4- Reichl, C. & Schatz, M. (2021). World Mining Data 2021. Mineral Production. Federal Ministry of Agriculture, Regions and Tourism, 36, Vienna.

5- U.S. Geological Survey. (2025). Clays. Mineral Commodity Summaries 2025. U.S. Department of the Interior.

6- Eisenhour, D., & Reisch, F. (2006). Bentonite, in Industrial minerals and rocks 7th edition. Kogel, J.E., Trivedi, N.C., Barker, J.M., & Krukowski, S.T. (eds.) Society for Mining, Metallurgy, and Exploration Inc, (pp 357-368). Littleton, Colorado.

7- Metin, 0. (2023). Türkiye'de farklı sektörlerde katkı ham maddesi olarak kullanılan bentonit mineralinin kimyasal ve radyometrik karakterizasyonu. Doktora Tezi, Kastamonu Üniversitesi Fen Bilimleri Enstitüsü. Kastamonu.

8- Kurnaz A, Turhan Ş, Hançerlioğulları A, Gören E, Karataşlı M, Altıkulaç A, Erer AM, Metin O(2020). Natural radioactivity, radon emanating power and mass exhalation rate of environmental soil samples from Karabük province, Turkey. Radiochim Acta 108(7):573–579.

9- Chen, C., Zhou, W., Yang, Q., Zhu, L., & Zhu, L. (2014). Sorption characteristics of nitrosodiphenylamine (NDPhA) and diphenylamine (DPhA) onto organo-bentonite from aqueous solution. Chemical Engineering Journal, 240, 487-493.

10- Mitchell, J.K. & Soga, K. (2005). Fundamantals of Soil Behavior Third Edition. John Wiley & Sons, 577, New York

11- Eisenhour, D. D., & Brown, R. K. (2009). Bentonite and its impacts on modern life. Elements, 5(2), 83-88. https://doi.org/10.2113/gselements.5.2.83

12- Ait, H.H., Akodad, M., Baghour, M., Moumen, A., Skalli, A., Azizi, G., Gueddari, H. Maach, M., Aalaoul, M., Anjjar, A., & Daoudi, L. (2021). Valorization of Moroccan bentonite deposits: purification and treatment of margin by the adsorption process. Molecules, 26(18). 1-20. https://doi.org/10.3390/molecules26185528

13- Akbulut, A. (1996). Bentonit. MTA Eğitim Serisi, 78, Ankara.
14- (DPT), (2001). Sekizinci Beş Yıllık Kalkınma Planı.
15- Masindi, V., Gitari, W. M., Mugera, W., & Ngulube, T. (2014). Defluoridation of drinking water using Al3+-modified bentonite clay: Optimization of fluoride adsorption conditions. Toxicological & Environmental Chemistry, 96(9), 1293–1306. https://doi.org/10.1080/02772248.2014.977289
16-Çinku, K. (2008). Aktivasyon Yöntemleri ile Bentonitten Su Bazlı Kıvamlaştırıcı Üretiminin Araştırılması. Doktora Tezi. İstanbul Üniversitesi Fen Bilimleri Enstitüsü. İstanbul
17- Murray, H. H. (2000). Traditional and new applications for kaolin, smectite, and palygorskite: a general overview. Applied Clay Science, 17(5-6), 207–221. https://doi.org/10.1016/S0169-1317(00)00016-8
18- Jalil, H., Rehman, A., & Jehangir, M. (1996). Study on the effect of sodium bentonite supplementation on the performance of the brolier chicks. Poultry Research Enstitute. Shamasabad.
19- Asselman, T., & Garnier, G. (2000). Adsorption of model wood polymers and colloids on bentonites. Colloids and Surfaces A: Physicochemical and Engineering Aspects, 168(2), 175–182. https://doi.org/10.1016/S0927-7757(00)00430-1
20- Avcı, S.B. (2009). Soda ve MgO ile Aktifleştirilmiş Ara Tip Bentonitlerin Sondaj ve Döküm Bentoniti Karakteristiklerinin İncelenmesi. Yüksek Lisans Tezi, İstanbul Üniversitesi Fen Bilimleri Enstitüsü. İstanbul.
21- Fındıkçı, B. (2020). Bentonit Kilinin Cam Fiber İle İyileştirilmesi. Yüksek Lisans Tezi, Kocaeli Üniversitesi Fen Bilimleri Enstitüsü. Kocaeli.
22-İpekoğlu B., Kurşun. İ., Bilge. Y., & Barut A. (1997). Türkiye Bentonit Potansiyeline Genel Bir Bakış. 2.Endüstriyel Hammaddeler Sempozyumu, 51-57, İzmir.
23-Christidis, G. E., Scott, P. W., & Dunham, A. C. (1997). Acid activation of bentonite clays for the bleaching of vegetable oils. Applied Clay Science, 12(4), 329–347. https://doi.org/10.1016/S0169-1317(97)00016-1
24- U.S. Geological Survey. (2025). Mineral commodity summaries 2025. U.S. Department of the Interior. https://doi.org/10.3133/mcs2025
25-Tchounwou, P. B., Yedjou, C. G., Patlolla, A. K., & Sutton, D. J. (2012). Heavy metal toxicity and the environment. Experientia Supplementum, 101, 133–164. https://doi.org/10.1007/978-3-7643-8340-4_6
26-Altıkulaç, A., & Turhan, Ş. (2023). Assessment of the levels of potentially toxic elements contained in natural bentonites collected from quarries in Turkey. ACS Omega, 8(23), 20979–20986. https://doi.org/10.1021/acsomega.3c01773

27-Kurnaz, A., Turhan, Ş., Metin, O., Altıkulaç, A., & Duran, C. (2023). Evaluation of terrestrial radionuclide levels and concomitant radiological risks of bentonites used in many industries. International Journal of Environmental Health Research, 33(12), 1706–1715. https://doi.org/10.1080/09603123.2022.2120190

28-Turhan, Ş., Metin, O., Hançerlioğulları, A., Kurnaz, A., & Duran, C. (2024). Determination of elemental concentrations of radionuclides in Turkish bentonite and calculation of radiogenic heat generation. International Journal of Environmental Analytical Chemistry, 104(18), 6286–6295. https://doi.org/10.1080/03067319.2022.2140419

29- Sultan, D.A.O. (2020). Kastamonu'da yetiştirilen siyez (Triticum monococcum L.) buğdayının radyonüklit, esansiyel ve ağır metal içeriklerinin tahribatsız analiz yöntemi ile belirlenmesi. Yüksek Lisans Tezi, Kastamonu Üniversitesi, Fen Bilimleri Enstitüsü. Kastamonu.

30-UNSCEAR (2008). Sources and effects of ionizing radiation. United Nations Scientific Committee on the Effects of Atomic Radiation, United Nations Publication, New York, USA.

Chapter 3

Molasses Alleviates Caco₃-Induced Alkalinity Stress in Spinach: Implications for Sustainable Agriculture

Nezahat TURFAN[1], Yahya TUNÇAY[2], Veysel ORTAÇ[3], Burak TOMAÇOĞLU[4]

1. INTRODUCTION

This study aimed to investigate whether molasses supplementation enhances tolerance to $CaCO_3$-induced alkalinity stress. Six-week-old seedlings were subjected to soil-applied $CaCO_3$ and molasses treatments. Pigment contents, oxidative stress markers, and mineral status were evaluated as indicators of alkalinity stress tolerance. $CaCO_3$-induced stress severely disrupted the physiological and biochemical status of spinach, whereas molasses supplementation mitigated these adverse effects. $CaCO_3$ stress decreased SPAD, lutein, total phenolic content, total flavonoid content, and protein levels, while enhancing proline relative to the control. Conversely, molasses supplementation promoted SPAD, lutein, phenolic compounds, flavonoids, and protein content. The combined $CaCO_3$ + MOL treatment largely restored these parameters and produced the highest lutein and flavonoid levels. $CaCO_3$ stress also markedly enhanced oxidative stress, increasing MDA, H_2O_2, and LOX activity. $CaCO_3$ additionally invoked nitrate accumulation and caused pronounced mineral imbalance, characterised by increased Na and Cl and reduced Mg, P, S, K, Ca, Mn, Zn, Cu, Ni, and Fe. Molasses substantially mitigated these alterations and improved mineral nutrient accumulation under alkalinity stress. In conclusion, molasses mitigated $CaCO_3$-induced damage in spinach by improving physiological performance, reducing oxidative damage, and regulating mineral status, highlighting its potential as a sustainable strategy for spinach cultivation in alkaline soils.Spinach (*Spinacia oleracea* L.) is a dark green leafy vegetable belonging to the Chenopodiaceae family and is extensively consumed worldwide

[1] Assoc.Prof. Dr., Department of Biology/Faculty of Science, Kastamonu University, Turkey, nturfan@kastamonu.edu.tr, (ORCID: 0000-0002-5753-0390)
[2] Student, Department of Biology/Faculty of Science, Kastamonu University, Turkey, tuncayyahya656@gmail.com, (ORCID:0009-0009-3824-0732)
[3] Student, Department of Biology/Faculty of Science, Kastamonu University, Turkey, veyselortac127@gmail.com, (ORCID: 0009-0005-1994-7960)
[4] Student, Department of Biology/Faculty of Science, Kastamonu University, Turkey, tomacogluburak@gmail.com, (ORCID: 0009-0009-9308-1113)

owing to its distinctive nutritional profile. Rich in pigments, secondary metabolites, vitamins, amino acids, and essential minerals such as iron, calcium, magnesium, and potassium, spinach is considered one of the most nutrient-dense vegetables [1]. Its diverse phytonutrients and bioactive compounds, including chlorophyll, lutein, ascorbic acid, flavonoids, and polyphenols, together with high levels of K, Mg, and P, contribute to its nutritional value. Moreover, its low caloric content and high water and dietary fibre contents provide important dietary benefits for managing obesity, hypertension, cardiovascular diseases, and gastrointestinal disorders [2,3]. Spinach can be cultivated under diverse environmental conditions as both summer and winter cultivars, exhibits rapid growth, and has moderate tolerance to low temperatures, salinity, and calcareous conditions. These characteristics make it a promising crop for sustainable food production amid climate change and resource constraints [4]. Furthermore, its affordability, economic viability, and broad accessibility reinforce its importance in meeting the growing food demands of a rapidly expanding global population, now surpassing 8.2 billion [2]. Beyond these attributes, spinach's moderate salinity tolerance and high ecological plasticity make it suitable for the reclamation and productive use of alkaline, calcareous, and degraded soils [3,4]. However, spinach production is increasingly threatened by abiotic stresses, particularly salinity, calcareousness, and alkalinity, driven by inappropriate irrigation and fertilisation, soil degradation, and climatic fluctuations [5,6,7]. According to FAO (2024), approximately 750 million people experience hunger and malnutrition, highlighting the urgent need for sustainable agricultural practices to ensure food security [1,5]. Within this context, calcareous soils constitute a major constraint to sustainable crop production because their alkaline conditions profoundly affect nutrient availability and plant performance [6,8]. Calcareous soils occupy approximately 30% of the global land area and are generally defined as soils containing more than 15% $CaCO_3$ [7,9]. In these soils, where pH values may reach 8.5, carbonate precipitation and associated physicochemical constraints can suppress microbial activity and restrict the availability of nitrogen (N), iron (Fe), phosphorus (P), and organic matter [8,10]. Furthermore, their high albedo increases exposure to direct and reflected solar radiation, potentially intensifying thermal stress and limiting plant establishment [7–11]. High $CaCO_3$ levels can induce osmotic stress in the soil solution, suppressing seed germination and seedling development while restricting water and nutrient acquisition and impairing root and shoot growth [11,12]. Moreover, $CaCO_3$-induced stress can disrupt photosynthesis, respiration, and carbohydrate and nitrogen metabolism [12, 13], while promoting oxidative stress and cellular damage that may ultimately cause severe growth inhibition or plant death [15,16].

The deleterious effects of calcareous stress have been documented in several crops, including cucumber, spinach, blackberry, tomato, and sugar beet [11-11-17]. These attributes, together with its renewable origin, organic nature, and low cost, highlight molasses as an environmentally friendly and sustainable biostimulant/organic amendment. Nevertheless, studies examining the effects of molasses on plant growth, photosynthetic pigments, lutein, phenolic and flavonoid compounds, proline and protein metabolism, nitrate accumulation, oxidative stress markers, and mineral composition of spinach under $CaCO_3$-induced alkalinity stress in Türkiye remain limited. Therefore, a significant knowledge gap exists regarding its potential to alleviate physiological and biochemical impairments associated with alkalinity stress. Hence, this study investigated the effects of $CaCO_3$-induced alkalinity stress and molasses application, applied individually and in combination, on the growth, photosynthetic pigments, lutein, total phenolic and flavonoid contents, protein, proline and nitrate contents, oxidative stress markers including MDA, H_2O_2 and LOX, and mineral element composition of spinach (*Spinacia oleracea* L. cv. 'Matador'). The potential of molasses application to mitigate the adverse effects of $CaCO_3$-induced alkalinity stress was also evaluated. We hypothesised that molasses application would enhance the tolerance of spinach to alkalinity stress by supporting plant growth and mineral nutrition, promoting the accumulation of protective metabolites, and limiting oxidative damage.

2. MATERIAL METHOD

2.1. Plant Material and Experimental Conditions

Seeds of spinach (*Spinacia oleracea* L.) cv. 'Matador', obtained from Intfa Seed Company, were used in the experiment (Figure 1). Before sowing, the seeds were surface-sterilised with 5% sodium hypochlorite (NaOCl) for 5 min to remove potential microbial contaminants. Following sterilisation, the seeds were thoroughly rinsed several times with sterile distilled water to remove residual NaOCl and sown in 500-mL pots filled with peat substrate. The pots were placed on a roofed, open-sided balcony under natural environmental conditions.



Figure 1. Phenotypic responses of spinach (*Spinacia oleracea* L. cv. 'Matador') plants to $CaCO_3$ stress and molasses application.

During germination and early seedling stages, irrigation was performed with 75 mL of tap water per pot until the seedlings reached the 5–6-leaf stage. At this stage, the stress applications were initiated through soil application.

The $CaCO_3$ solution was prepared at a concentration of 20% (w/v) by dissolving $CaCO_3$ in tap water, whereas the molasses (MOL) solution was made as a 2% (v/v) solution by thoroughly mixing molasses with tap water. For the combined treatment, $CaCO_3$ was formulated directly in the 2% molasses solution. The control plants received tap water only. Each treatment solution was applied directly to the soil at a volume of 75 mL per pot, twice weekly for six consecutive weeks. In the seventh week, the plants were harvested for biochemical and mineral element analyses.

1-Element Analysis

For mineral element determination, leaves together with their petioles were collected at harvest and dried in a forced-air oven at 65 °C until a constant weight was achieved. The dried plant material was subsequently ground to a fine,

homogeneous powder using a laboratory blender. The powdered samples were transferred into polyethene bags and submitted to the Central Research Laboratory of Kastamonu University for elemental analysis. Element concentrations were determined using an X-ray fluorescence (XRF) spectrometer. The results were expressed on a dry-weight basis, with Na, Cl, Mg, K, P, S, and Ca reported in mg g^{-1}, whereas Mn, Fe, Zn, and Cu were expressed in mg kg^{-1}.

2-Chemical Analyses

SPAD values were measured on the upper surface of spinach leaves at three different points, avoiding the midrib, using a SPAD-502Plus chlorophyll meter (Konica Minolta, Japan), and the mean value was recorded as the SPAD value. Lutein content in the samples was determined according to the method described by Kukrić et al. [18]. Xanthophyll (lutein) content was calculated according to the equations and expressed as mg g^{-1} fresh weight.

$$Xanthophyll\ (lutein)(mg\ g^{-1}) = Sample\ mass 11.51A480 - 20.51A495 \times 200$$

Total phenolic content (TPC) was employed using the Folin–Ciocalteu colourimetric method [19]. Plant extracts were mixed with Folin–Ciocalteu reagent and sodium carbonate solution, and the reaction mixture was incubated under dark conditions for colour development. Absorbance was noted at 765 nm. TPC was calculated from the corresponding standard curve prepared with gallic acid and expressed as mg gallic acid equivalents (GAE) g^{-1} fresh weight. Total flavonoid content (TFC) was determined using the aluminium chloride colourimetric method described by Zhishen et al. [20] (1999). Briefly, plant extracts were mixed with AlC2 and the appropriate reagents and absorbance was taken spectrophotometrically at 510 nm. Quercetin was used as the calibration standard, and the results were expressed as mg quercetin equivalents (QE) g^{-1} fresh weight.Free proline content was determined using the method of Bates et al. [21]. Fresh leaf tissue (0.5 g) was homogenised in 3% sulfosalicylic acid and filtered. The extract was combined with acid ninhydrin and glacial acetic acid at 90 °C for 1 h. After cooling, toluene was added, and absorbance was recorded at 520 nm. Proline concentration was calculated using a standard curve prepared with L-proline and expressed as µmol g^{-1} fresh weight. Total soluble protein content was determined using the Bradford [22] assay. Fresh leaf tissue was homogenised in 50 mM phosphate buffer (pH 7.4) and centrifuged at 10,000 ×g for 10 min. The extract was mixed with Coomassie Brilliant Blue G-250 reagent, and absorbance was noted at 595 nm. Bovine serum albumin was used as the calibration standard, and protein concentration was given as mg g^{-1} fresh weight. Total nitrate (NO_3^-) content was examined following the salicylic acid nitration

method [23]. Fresh leaf samples were extracted in distilled water, and the extract was combined with salicylic acid under acidic conditions. Following neutralisation with NaOH, absorbance was measured spectrophotometrically at 410 nm. Nitrate concentration was calculated using a potassium nitrate standard curve and expressed as mg NO_3^- g^{-1} fresh weight. Malondialdehyde (MDA) content was determined with the thiobarbituric acid-reactive substances assay according to the method described by Lutts et al. [24]. Fresh leaf tissue was homogenised in cold trichloroacetic acid, and the homogenate was centrifuged to obtain the supernatant. The supernatant was reacted with thiobarbituric acid and heated at 95 °C. After cooling and centrifugation, absorbance was measured at 532 and 600 nm, and MDA content was expressed as μmol g^{-1} fresh weight. Hydrogen peroxide (H_2O_2) content was quantified using the residual extracts obtained after MDA determination [25]. The absorbance was measured spectrophotometrically at 355 nm. Lipoxygenase (LOX) activity was determined spectrophotometrically according to Pinto et al. [26]. Fresh leaf tissue was homogenised in an appropriate extraction buffer, and the homogenate was centrifuged to obtain the enzyme extract. The enzyme activity was determined based on the formation of lipid hydroperoxides and expressed as U mg^{-1} soluble protein. All statistical analyses were performed using IBM SPSS Statistics (version 2016; IBM Corp., Armonk, NY, USA). The data were subjected to one-way analysis of variance (ANOVA) to reveal the effects of the experimental applications on the measured biochemical and mineral parameters. When significant differences among treatment means were detected, Tukey's honestly significant difference (HSD) test was used for post hoc multiple comparisons. Statistical significance was considered at $P<0.05$. Data are presented as means ± standard deviation (SD) of the experimental replicates.

3. RESULTS AND DISCUSSION

3.1Effects of the Treatments on Secondary Metabolite and Osmolyte Contents

Despite being a rich source of phytochemicals with antioxidant and health-promoting properties, including chlorophyll, lutein, phenolic compounds, and flavonoids, the concentrations of these molecules in spinach can vary considerably in response to environmental stresses, such as calcareous/alkaline conditions, salinity, and heavy metal contamination [1-5].

In this study, the impacts of the treatments on chlorophyll (SPAD), lutein (LUT), total phenolic content (TPC), total flavonoid content (TFC), protein, and proline contents are presented in Figures 2 and 3. The values of the measured parameters in the control group were 12.36, 0.74, 19.49, 16.46, 13.31, and 18.30, respectively. $CaCO_3$ stress significantly declined SPAD, LUT, TPC, TFC, and protein contents, whereas it

increased proline accumulation (P<0.001). In contrast, molasses application increased SPAD, LUT, TPC, TFC, and protein levels compared with the control. Furthermore, the $CaCO_3$ + MOL combination clearly compensated for the reductions triggered by $CaCO_3$ stress, resulting in particularly high TFC and LUT levels.

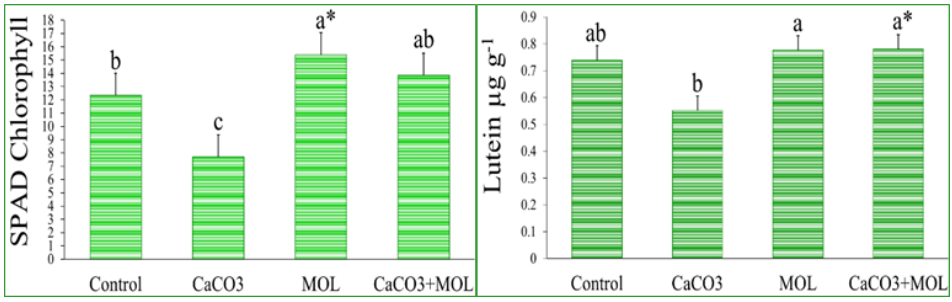


Figure 2. Effects of $CaCO_3$ stress and molasses application on SPAD chlorophyll index and lutein content in spinach (*Spinacia oleracea* L. cv. 'Matador'). Values are means ± SE (n =3). Different lowercase letters indicate significant differences among treatments (Duncan's test, $p < 0.05$), while asterisks (*) denote significant differences from the control ($p < 0.05$).

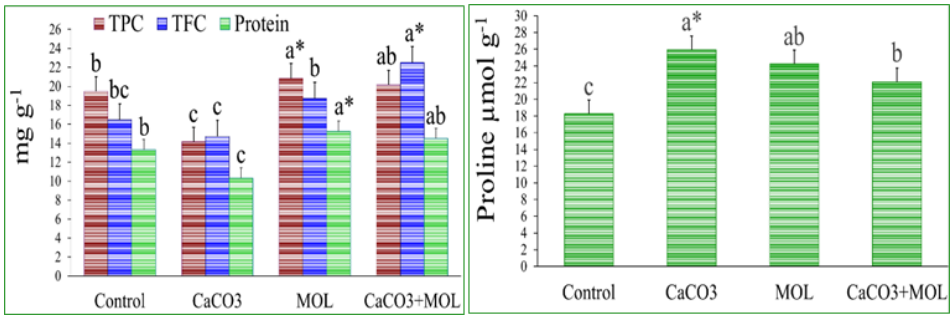


Figure 3. Effects of $CaCO_3$-induced alkalinity stress and molasses (MOL) application on total phenolic content (TPC), total flavonoid content (TFC), protein, and proline contents in spinach (*Spinacia oleracea* L. cv. 'Matador'). Values are means ± SE (n =3). Different lowercase letters indicate significant differences among treatments ($p < 0.05$).

Proline content, however, was promoted by $CaCO_3$, whereas MOL supplementation partially restrained this stress-induced accumulation (Figure 3). The findings obtained are consistent with the existing literature, demonstrating that alkalinity/calcareous conditions suppress phytochemical biosynthesis in spinach [1, 5, 9,10], whereas this suppression can be substantially alleviated through the application of plant-derived biostimulants [5, 27, 28].

3.2Effects of the Treatments on Oxidative Stress Indicators

Calcareous/alkaline conditions impair the productivity and quality of plants by evoking osmotic stress, nutrient deficiency, and ionic toxicity, thereby disrupting photosynthesis, respiration, and nitrogen and carbon metabolism, while simultaneously promoting ROS accumulation and lipid peroxidation [1, 11, 12, 14]. However, numerous studies have confirmed that the adverse effects of calcareous stress can be greatly reversed through the application of organic biostimulants, as reported by Desoky et al. [17], Kózmińska et al. [27], and Wise et al. [29]. The effects of the treatments on MDA, H_2O_2, and LOX activity are shown in Figure 4.The control values for MDA, H_2O_2, and LOX were 14.89 µmol g^{-1}, 18.34 µmol g^{-1}, and 24.04 U mg^{-1} protein**,** respectively. $CaCO_3$ stress notably evoked all oxidative stress-related parameters**,** with MDA, H_2O_2, and LOX activity reaching 23.67 µmol g^{-1}, 26.33 µmol g^{-1}, and 31.93 U mg^{-1} protein (Figure 4). In contrast, MOL alone sustained these parameters close to the control levels. Remarkably, the $CaCO_3$ + MOL considerably mitigated MDA, H_2O_2, and LOX activity to 11.92 µmol g^{-1}, 14.41 µmol g^{-1}, and 19.19 U mg^{-1} protein, respectively. In this study, the alleviation of oxidative stress following molasses supplementation can be explained by its ability to activate antioxidant defence mechanisms while improving water uptake and osmolyte accumulation in spinach [5, 14, 16, 31]. Similarly, Turfan et al. [30] demonstrated that alkaline stress increased MDA and H_2O_2 accumulation in spinach, whereas exogenous tyrosine supplementation substantially suppressed this increase.

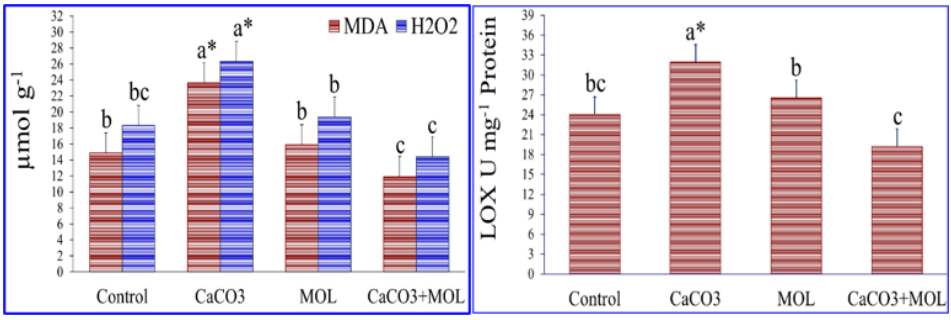


Figure 4. Effects of $CaCO_3$-induced alkalinity stress and molasses (MOL) application on malondialdehyde (MDA) and hydrogen peroxide (H_2O_2) concentration and lipoxygenase activity (LOX) in spinach (*Spinacia oleracea* L. cv. 'Matador'). Values are means ± SE (n =3). Different lowercase letters indicate significant differences among treatments ($p < 0.05$).

3.3 Effects of The Treatments on Mineral Status in Spinach Seedlings

Nitrate (NO_3^-) is a vital precursor for the biosynthesis of chlorophyll, amino acids, proteins, and enzymes in crops. However, under stress conditions, inhibition of nitrate reductase (NR), the key enzyme responsible for NO_3^- assimilation, can disrupt nitrate metabolism and lead to excessive NO_3^- accumulation in spinach tissues, posing a potential health risk to consumers, particularly infants aged 0–6 months and young children [1, 30]. In this current study, the influence of the treatments on NO_3^- content is summarised in Table 1. The nitrate content in the control group was 1.84 μg g^{-1}**.** $CaCO_3$ stress markedly increased nitrate accumulation**,** reaching 2.88 μg g^{-1}. In contrast, molasses application reduced nitrate content to 1.55 μg g^{-1}**,** below the control level ($P<0.001$). Notably, the $CaCO_3$ + MOL combination substantially attenuated the $CaCO_3$-induced increase in nitrate accumulation**,** reducing its content to 1.97 μg g^{-1}.

Table 1. Effects of $CaCO_3$-induced alkalinity stress and molasses application on Mg, P, S, K and Ca accumulation in seedlings (in mg g^{-1})

Group	NO_3	Na	Cl	Mg	P	S	K	Ca
Control	1.84±0.05c*	0.87±0.5d	1.58±1.3d	1.42±1.3ab	7.57±	8.36±7.2b	12.33±1.4b	1.56±1.4b
$CaCO_3$	2.88±0.12a	5.44±4.3a	9.88±7.6a	0.93±0.8c	5.54±	6.48±5.8c	9.56±8.4c	1.06±0.8c
MOL	1.55±0.06d	1.22±0.8c	2.22±1.5c	1.49±1.3a	8.23±	9.58±8.2a	14.78±112.6a	2.42±2.3aa
$CaCO_3$+MOL	1.97±0.06b	3.25±1.5b	5.66±4.7b	1.35±1.2b	7.85±	9.26±7.8ab	11.55±9.8b	2.12±0.8ab
F	54.15	1773.99	4356.59	1898.75	423.92	1398.13	773.21	433.79
P	<0.001	<0.001	<0.001	<0.001	<0.001	<0.001	<0.001	<0.001

*****_Different lowercase letters indicate significant differences among treatments (p < 0.05). MOL:Molasses_

In the present study, the stimulation of NO_3^- accumulation under $CaCO_3$ stress was associated with the inhibition of nitrogen utilisation through the inactivation of NR [1, 5, 30, 32], whereas the mitigating effect of molasses was attributed to the amelioration of this reduction, thereby facilitating more efficient nitrogen metabolism [21-30].The effects of the treatments on Mg, P, S, K, and Ca contents are illustrated in Table 1. The mean values of these elements in the control group were 1.42, 7.57, 8.36, 12.33, and 1.56 mg g^{-1}**,** respectively. Under $CaCO_3$ stress, Na and Cl accumulation was promoted, whereas Mg, P, S, K, and Ca contents were lowered compared with the control. In contrast, MOL application enriched the contents of all measured mineral elements, particularly P, S, K, and Ca, relative to the control (Table 1). The $CaCO_3$ + MOL treatment substantially alleviated the $CaCO_3$-induced alterations in mineral composition, reducing Na and Cl accumulation while restoring Mg, P, S, K, and Ca contents toward the control levels. Notably, molasses application under $CaCO_3$ stress markedly improved P, S, K, and Ca accumulation**,** indicating its potential to mitigate the

mineral nutritional imbalance induced by alkalinity stress [Table 1]. The outcomes regarding element status are also consistent with those reported by Kim et al. [1], Gunnarsson et al. [10], Kbibow et al. [12], and Nyström et al. [8], who exhibited that high alkalinity can induce ionic toxicity, thereby disrupting mineral homeostasis in spinach. A finding consistent with the present study was also cited by Wiise et al. [29], Kózmińska et al. [27], and Turfan [30], who revealed that exogenous molasses supplementation improved nutrient and water uptake from the soil and alleviated the restrictive effects of $CaCO_3$ stress. Accumulating evidence highlights spinach as a valuable dietary source of Fe, Mn, Ni, and Cu, while also supporting its contribution to immune function and overall health as part of a nutritious and balanced diet [1, 2]. Spinach provides approximately 2.71 mg Fe, 0.90 mg Mn, 0.53 mg Zn, and 0.13 mg Cu per 100 g fresh weight, contributing to daily dietary intake [31, 33]. The effects of the treatments on Mn, Zn, Cu, Ni, and Fe contents are summarised in Table 2. The values of the measured micronutrients in the control group were 86, 95, 42, 14, and 578**,** respectively.

Table 2. Effects of $CaCO_3$-induced alkalinity stress and molasses application on trace element contents of spinach (*Spinacia oleracea* l. cv. 'Matador ') (in mg kg^{-1}).

Group	Mn	Fe	Zn	Cu	Ni
Control	86±5.6b*	578±14.6bc	95±8.4a	42±3.5bc	14±0.8b
$CaCO_3$	65±4.8c	308±12.6c	78±6.7c	28±2.2c	11±0.4c
MOL	100±8.6a	624±18.6a	92±8.8ab	44±3.7b	14±0.5b
$CaCO_3$+MOL	88±6.5b	594±16.8b	86±7.8b	47±4.3a	16±0.6a
F	846	68718	242.8	12.75	658.75
P	<0.001	<0.001	<0.001	<0.001	<0.001

*: Different lowercase letters indicate significant differences among treatments ($p < 0.05$). MOL: Molasses

Under $CaCO_3$ stress, the contents of Mn, Zn, Cu, Ni, and Fe were repressed compared with the control, with the greatest decline recorded in Fe content. Conversely, molasses supplementation promoted Mn, Cu, and Fe contents relative to the control, while Zn and Ni remained relatively close to the control levels. The $CaCO_3$ + MOL combination remarkably alleviated the $CaCO_3$-induced reductions in micronutrient accumulation, particularly for Cu, Ni, and Fe**,** which reached 47, 16, and 594 mg g^{-1}, respectively (Table 2). Notably, molasses application under $CaCO_3$ stress markedly improved Fe and Cu accumulation**,** indicating its potential to alleviate the micronutrient imbalance associated with alkalinity stress. The fluctuations in trace element contents observed between stressed and non-stressed seedlings have also been

documented by Turfan [30], Turfan et al. [5], and Kim et al. [1]. Nevertheless, fluctuations in elemental contents may also have been influenced by factors such as antagonistic interactions among elements, the concentrations of the applied biostimulants, and the duration of treatment [5, 16, 18, 25].

4.CONCLUSION

Overall, the findings demonstrate that molasses application can effectively counteract $CaCO_3$-induced alkalinity stress in spinach by simultaneously improving photosynthetic pigments, secondary metabolite accumulation, protein metabolism, mineral nutrition, and oxidative stress regulation**.** The particularly strong response of lutein and flavonoids, together with the marked suppression of MDA, H_2O_2, and LOX under combined treatment, suggests that molasses promotes a coordinated protective response rather than acting through a single physiological pathway. Moreover, the attenuation of Na and Cl accumulation and the recovery of essential macro- and micronutrients indicate that molasses contributes to the restoration of mineral homeostasis under alkalinity stress. These findings support the potential use of molasses as a low-cost, organic, and sustainable biostimulant for improving spinach performance under alkaline conditions. Further field-scale studies are warranted to determine the optimal application rate and to clarify the molecular mechanisms underlying molasses-mediated stress tolerance.

REFERENCES

[1] Kim, B. M., Lee, H. J., Song, Y. H., & Kim, H. J. (2021). Effect of salt stress on the growth, mineral contents, and metabolite profiles of spinach. *Journal of the Science of Food and Agriculture, 101*(9), 3787–3794. https://doi.org/10.1002/jsfa.11011

[2] Kal, Ü. (2026). Comparative analysis of leaf characteristics and yield components in some spinach varieties. *Akademik Ziraat Dergisi, 15*. https://doi.org/10.29278/azd.1899155

[3] Turfan, N., Tekşen, K., Altuner, E. M., Yıldız, F., & Kaya, O. (2026). Divergent biochemical strategies and organ-specific metabolic adjustments in spinach mediated by exogenous amino acids under salt stress. *Physiologia Plantarum, 178*(2), e70845. https://doi.org/10.1111/ppl.70845

[4] Gayretli, G. (2025). *Determination of population structure of the qualified spinach gene pool and obtaining of F1 spinach variety candidates resistant to Peronospora effusa (Pe)* [Doctoral dissertation, Selcuk University].

[5] Turfan, N., Dovletov, A., & Kaya, O. (2026). Organ-specific some physiological, biochemical, and metabolic responses of spinach to foliar and soil-applied Aminosol under salt stress. *Journal of Plant Growth Regulation*. https://doi.org/10.1007/s00344-026-12357-y

[6] Schad, P. (2023). World Reference Base for Soil Resources—Its fourth edition and its history. *Journal of Plant Nutrition and Soil Science, 186*, 151–163.

[7] Sun, Z., Meng, F., & Zhu, B. (2023). Influencing factors and partitioning methods of carbonate contribution to CO_2 emissions from calcareous soils. *Soil Ecology Letters, 5*, 6–20. https://doi.org/10.1007/s42832-022-0139-1

[8] Nyström, A. O., Blomquist, J., Persson, L., Gunnarsson, A., & Berglund, K. (2023). Long-term effects of liming on crop yield, plant diseases, soil structure and risk of phosphorus leaching. *Agricultural and Food Science, 32*, 139–153. https://doi.org/10.23986/afsci.130983

[9] Turfan, N. (2017). Effect of some abiotic stress factors on Savrun spinach (*Spinacea oleracea* L.). *Turkish Journal of Agriculture - Food Science and Technology, 5*(6), 660–667. https://doi.org/10.24925/turjaf.v5i6.660-667.1138

[10] Gunnarsson, A., Blomquist, J., Persson, L., Olsson, Å., Hamnér, K., & Berglund, K. (2022). Liming alkaline clay soils: Effects on soil structure, nutrients, barley growth and yield. *Acta Agriculturae Scandinavica, Section B—Soil & Plant Science, 72*, 803–817. https://doi.org/10.1080/09064710.2022.2089590

[11] İpek, M., & Eşitken, A. (2024). Regulation of the negative effects of lime-induced stress on plant hormone balance in blackberry by plant growth-promoting rhizobacteria. *Applied Fruit Science, 66*, 1221–1227. https://doi.org/10.1007/s10341-024-01107-7

[12] Kbibow, I. K., Khalil, N., Ashram, M., & Mkhies, S. (2024). Effect of soil content of calcium carbonate on some growth and productivity indicators of sweet corn (*Zea mays* L. saccharata). *The Arab Journal for Arid Environments, 17*(1).

[13] Pyakurel, A., Dahal, B. R., & Rijal, S. (2019). Effect of molasses and organic fertilizer in soil fertility and yield of spinach in Khotang, Nepal. *International Journal of Applied Sciences and Biotechnology, 7*(1), 49–53. https://doi.org/10.3126/ijasbt.v7i1.23301

[14] Sediqui, N., Amin, M. W., Dawlatzai, N., Gulab, G., Poyesh, D. S., Terada, N., Sanada, A., Kamata, A., & Koshio, K. (2024). Elucidation of shoot and root growth, physiological responses, and quality traits of tomato (*Solanum lycopersicon* L.) exposed to elevated calcium carbonate concentrations. *Horticulturae, 10*, 573.

[15] Olsson, Å., Persson, L., & Olsson, S. (2019). Influence of soil characteristics on yield response to lime in sugar beet. *Geoderma, 337*, 1208–1217. https://doi.org/10.1016/j.geoderma.2018.11.020

[16] Elayaraj, B. (2014). Impact of sugar factory effluent on germination, biochemical and antioxidant enzyme activity of black gram (*Vigna mungo* (L.) Hepper) variety Vamban-3. *International Journal of Current Research, 3*, 84–89.

[17] Desoky, E. S. M., Elrys, A. S., Mansour, E., Eid, R. S., Selem, E., Rady, M. M., Ali, E. F., Mersal, G. A., & Semida, W. M. (2021). Application of biostimulants promotes growth and productivity by fortifying the antioxidant machinery and suppressing oxidative stress in faba bean under various abiotic stresses. *Scientia Horticulturae, 288*, 110340.

[18] Kukrić, Z. Z., Topalić-Trivunović, L. N., Kukavica, B. M., Matoš, S. B., Pavičić, S. S., Boroja, M. M., & Savić, A. V. (2012). Characterisation of antioxidant and antimicrobial activities of nettle leaves (*Urtica dioica* L.). *Acta Periodica Technologica, 43*, 257–272. https://doi.org/10.2298/APT1243257K

[19] Singleton, V. L., & Rossi, J. A. (1965). Colorimetry of total phenolics with phosphomolybdic-phosphotungstic acid reagents. *American Journal of Enology and Viticulture, 16*, 144–158.

[20] Zhishen, J., Mengcheng, T., & Jianming, W. (1999). The determination of flavonoid content in mulberry and their scavenging effects on superoxide radicals. *Food Chemistry, 64*, 555–559.

[21] Bates, L. S., Waldren, R. P., & Teare, I. D. (1973). Rapid determination of free proline for water-stress studies. *Plant and Soil, 39*, 205–207. https://doi.org/10.1007/BF00018060

[22] Bradford, M. M. (1976). A rapid and sensitive method for the quantitation of microgram quantities of protein utilizing the principle of protein-dye binding. *Analytical Biochemistry, 72*, 248–254. https://doi.org/10.1016/0003-2697(76)90527-3

[23] Cataldo, D. A., Haroon, M., Schrader, L. E., & Youngs, V. L. (1975). Rapid colorimetric determination of nitrate in plant tissue by nitration of salicylic acid. *Communications in Soil Science and Plant Analysis, 6*, 71–80. https://doi.org/10.1080/00103627509366547

[24] Lutts, S., Kinet, J. M., & Bouharmont, J. (1996). NaCl-induced senescence in leaves of rice (*Oryza sativa* L.) cultivars differing in salinity resistance. *Annals of Botany, 78*(3), 389–398.

[25] Velikova, V., Yordanov, I., & Edreva, A. (2000). Oxidative stress and some antioxidant systems in acid rain-treated bean plants: Protective role of exogenous polyamines. *Plant Science, 151*, 59–66. https://doi.org/10.1016/S0168-9452(99)00197-1

[26] Pinto, M. C., Tejeda, A., Duque, A. L., & Macías, P. (2007). Determination of lipoxygenase activity in plant extracts using a modified ferrous oxidation–xylenol orange assay. *Journal of Agricultural and Food Chemistry, 55*. https://doi.org/10.1021/jf070537x

[27] Kózmińska, A., Hanus-Fajerska, E., Halecki, W., & Ciarkowska, K. (2021). Beet molasses enhance salinity tolerance in *Thymus serpyllum*—A study under greenhouse condition. *Plants, 10*(9), 1819. https://doi.org/10.3390/plants10091819

[28] Samavat, S., & Samavat, S. (2014). Effects of fulvic acid and sugarcane molasses on yield and qualities of tomato. *International Research Journal of Applied and Basic Sciences, 8*(3), 266–268.

[29] Wise, K., Williams, L. B., Selby-Pham, S., Wright, P. F. A., Simovich, T., Gill, H., Gupta, A., Puri, M., & Selby-Pham, J. (2024). Supplementation of fertiliser with the biostimulant molasses enhances hemp (*Cannabis sativa*) seed functional food antioxidant capacity by induction of stress responses. *Scientia Horticulturae, 334*, 113299. https://doi.org/10.1016/j.scienta.2024.113299

[30] Turfan, N. (2023). The effects of exogenous tyrosine supplement on spinach (*Spinacia oleracea* L.) cultivation under lithium stress. *Mediterranean Agricultural Sciences, 36*(3), 101–108. https://doi.org/10.29136/mediterranean.1300307

[31] Gaafar, M. S., El-Shimi, N. M., & Helmy, M. (2019). Effect of foliar and soil application of some residuals of sugar cane products (molasses and vinasses) with mineral fertilizer levels on growth, yield and quality of sweet pepper. *Minoufia Journal of Plant Production, 4*, 353–373.

[32] Han, K., Wang, C., Gao, Y., et al. (2025). Response of amino acids, phenolic acids, organic acids, and mineral elements to fulvic acid in spinach (*Spinacia oleracea* L.) under nitrate stress. *Scientific Reports, 15*, 9444. https://doi.org/10.1038/s41598-025-93974-7

Chapter 4

Cadmium Sulfide (CdS) Cathode for Advanced Plasma Conversion Process

Hatice Hilal YÜCEL[1]

1. INTRODUCTION

In recent decades, semiconductor chalcogenide-based materials (sulfides, selenides, and tellurides) have gained increasing importance [1,2]. CdS is a direct-bandgap, n-type chalcogenide (Group II-VI) semiconductor with an optical bandgap of 2.42 eV and a refractive index of 2.5 at room temperature [3]. Notable for its structural, optical, electrical, magnetic, and dielectric properties, CdS is also of interest due to its optoelectronic and photoconductive characteristics [4–6]; consequently, it is utilized in applications such as light detectors, display panels, photoconductors [6], photodetectors, multilayer light-emitting diodes [3], radiation detectors, laser materials [7], DNA sensors, photosensors [8], IR detectors [9,10], photovoltaic cells [3,11], and gas sensors [3,12,13].In electronics, CdS refers to Cadmium Sulfide. It is primarily known for its use in photoresistors, also frequently called Light-Dependent Resistors (LDRs) or CdS cells. A CdS sensor is a passive component that functions based on the photoelectric effect. The resistance of a CdS cell decreases as the intensity of incident light increases. In total darkness, the device exhibits very high resistance (often in the mega-ohm range). In bright light, its resistance drops significantly (down to a few hundred or thousand ohms). One notable feature of CdS cells is that their spectral sensitivity is very similar to that of the human eye, making them useful for applications where you want to measure "visible" light as a person would perceive it. Because they are inexpensive and easy to interface with circuits, CdS sensors are widely used in;

- Automatic Lighting: Streetlights that turn on at dusk and off at dawn.
- Light Meters: Used in photography or environmental monitoring to gauge ambient light levels.
- Automation & Toys: Triggering actions based on shadows or changes in light intensity (e.g., security sensors or line-following robots).
- Circuit Design: Often placed in a voltage divider configuration to convert the change in resistance into a voltage signal that can be read by a microcontroller (like an Arduino or similar platform).

[1] Prof. Dr., Department of Physics/Faculty of Science, Gazi University, Turkey, hkurt@gazi.edu.tr, (ORCID: 0000-0002-1277-5204)

These materials CdS, InP, GaAs, and ZnSe—are all semiconductors, but they serve very different roles in optics and infrared (IR) technology. While some are foundational materials for IR windows and lenses, others are primarily used for their electronic properties in devices like sensors or lasers.

Table1 Comparision of the Optic Materials

Comparison Summary

Material	Primary Role in IR/Optics	Notable Characteristics
ZnSe	Optical Window/Lens	Wide transparency (0.6–21 µm); low absorption at 10.6 µm (CO_2 lasers).
GaAs	Optical Window/Electronic	Wide transmission (0.9–16 µm); high-speed electronics; robust/hard.
InP	Optoelectronic Device	Telecommunications (1.3–1.55 µm); high-speed photodetectors/lasers.
CdS	Photoconductive/Research	Often used in visible/near-IR; frequently studied in research/plasma cells.

CdS is less of an "infrared material" in the industrial sense and more of a research-oriented semiconductor:

- *Best For: Photoconductive sensors and experimental plasma-semiconductor cells.*
- *Key Advantage: It is widely studied for its electrical and optical behaviors. While it shows sensitivity to infrared in laboratory experiments, it is not a standard material for IR optical windows or high-speed telecommunications in the same way as the others listed.*

Cadmium Sulfide (CdS): Primarily recognized as a window or buffer layer in thin-film solar cell heterojunctions. Its wide bandgap allows the majority of incident light to pass through to the narrow-bandgap absorber layer, while its electrical properties facilitate effective charge collection.Semiconductor manufacturing is the bedrock of modern electronics (computers, mobile phones). Plasma processing is not just a secondary step; it involves roughly 50% of the production steps and constitutes

the majority of equipment costs in a fabrication plant. Because modern chips contain millions of transistors that must be etched with extreme accuracy, the reliability of plasma equipment is paramount. Any deviation can result in catastrophic yield loss. For decades, low-temperature plasma physics was an elusive science. Today, it is evolving rapidly due to:

Computational Advancement: The ability to simulate radiofrequency plasmas allows engineers to peek inside the discharge, accounting for complex collisions between electrons and neutral atoms

- **Fusion Synergy:** The cross-pollination of data from fusion energy research (which studied "miniature suns") is now providing the fundamental physical framework needed to optimize manufacturing-grade plasmas.
- **The Bottom Line:** As the physical limits of transistor size continue to shrink, the ability to control plasma behavior is no longer just a manufacturing convenience; it is the defining technical bottleneck that will dictate the next generation of computing power.

2. THEORETICAL

Cadmium sulfide (CdS) predominantly crystallizes into two distinct polymorphs that govern its characteristic optoelectronic and physical properties: the thermodynamically stable hexagonal wurtzite phase (commonly occurring as the mineral greenockite) and the metastable cubic zincblende phase, which typically precipitates under specific thin-film deposition conditions. As a direct bandgap semiconductor ($E_g \approx 2.42$ eV), CdS exhibits highly efficient optical absorption and emission characteristics, manifest in its distinct yellow to orange-red pigmentation resulting from the absorption of blue wavelengths.

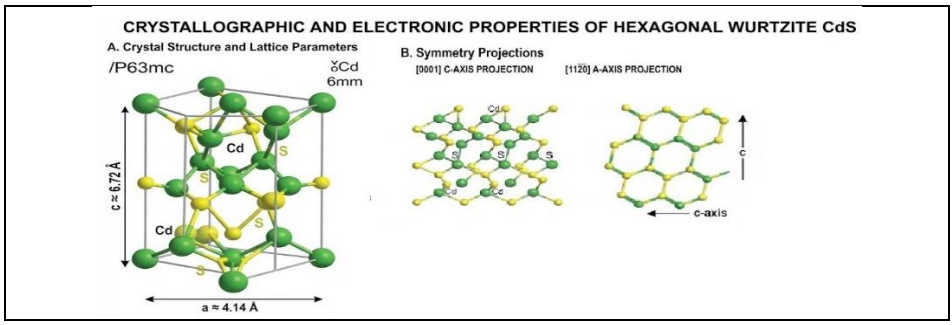


Figure 1. The crystallographic structure of CdS [17-19]

Beyond the gaseous state lies plasma, a phase of matter characterized by high thermal energy sufficient to detach outer electrons from their parent atoms. This creates a plasma composed of positive ions immersed in a sea of electrons. It is

important to note that the degree of ionization varies significantly: low-temperature processing plasmas typically exhibit low ionization fractions (1–10%), whereas fusion-grade plasmas achieve complete ionization. When classifying plasmas as "hot" or "cold," one must evaluate their thermal state. In standard fluids, particles reach thermal equilibrium, characterized by the following Maxwell-Boltzmann distribution [12];

$$f(v) = Ae^{-(½mv^2/KT)}$$

The normalization factor A and Boltzmann constant k define the Maxwellian velocity distribution, where T serves as the scaling factor for distribution width. Unlike atmospheric gases, plasmas typically function as multi-temperature systems ($T_i \neq T_e \neq T_n$). Due to the relatively low particle densities characteristic of plasmas, the lack of sufficient inter-species thermalization prevents a uniform temperature across components [12]. While each species typically maintains a Maxwellian profile through self-collision, extreme thermal conditions may lead to non-Maxwellian distributions, requiring more rigorous treatment via kinetic theory. Beyond industrial material processing, plasmas are essential to the generation of coherent electromagnetic radiation, finding application in microwave tubes, gas lasers, and free-electron lasers. Furthermore, contemporary research in high-energy physics is increasingly focused on the development of plasma-based particle acceleration technologies [12].The applications of plasma science range from the experimental exploration of inertial confinement fusion to the practical demands of large-scale manufacturing. Beyond the development of ultra-fast diagnostic tools using femtosecond lasers, plasma science is central to modern materials engineering, facilitating processes such as the corrosion-resistant nitriding of turbine components and the surface modification of polymers. Perhaps most vital is the reliance of the semiconductor industry on plasma processing technologies, which are essential to produce advanced microprocessors. This technological dependency has highlighted a notable deficit in the global workforce of qualified plasma scientists, identifying a significant gap between industrial requirements and available technical expertise [12].

3. RESULTS AND DISCUSSION

In our experiment, the cycle that occurs when an IR light beam strikes the CdS—used here as the cathode is illustrated in figure- 2. When light falls on the CdS, electrons released via the photoconductivity mechanism undergo ionizing collisions with gas atoms; consequently, upon reaching the breakdown voltage,

emission in the visible region is observed. Characterizing the structural properties of cadmium sulfide (CdS) is fundamental to the development of high-performance optoelectronic devices. Given that the material's crystalline configuration specifically the transition between hexagonal wurtzite and cubic zincblendeis highly sensitive to the chosen synthesis methodology, rigorous verification of phase purity, grain size, and overall crystallinity is required.

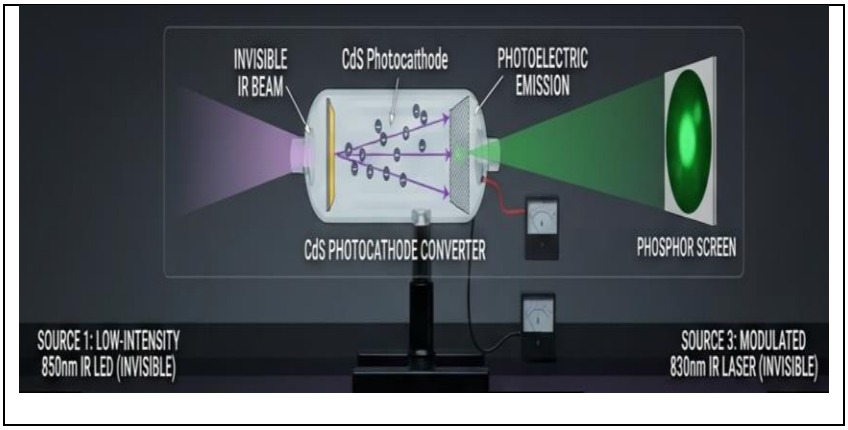


Figure 2. IR conversion process [20]

Since CdS was used as the cathode, its surface characterization was first examined at the Bilkent UNAM center. AFM, SEM, and phase images were analyzed to determine the surface's morphological properties. The image reveals the presence of some superficial scratches, marks, and small particle-like structures (possibly contaminants or crystal defects) on a relatively smooth surface. Such SEM images are commonly used in materials science studies to examine surface morphology in Figure 3. Figure -4 is a Scanning Electron Microscope (SEM) image of the sample captured at a high magnification. The technical details are as follows;Magnification (Mag): 20,000x (Surface details have become more distinct). Scale bar: 2 µm (Confirms that microscopic scratches and irregularities on the surface are visible in greater detail due to the higher resolution).Other Parameters: Accelerating voltage (5.00 kV), working distance (14.2 mm), and detectors (ETD) were kept constant.

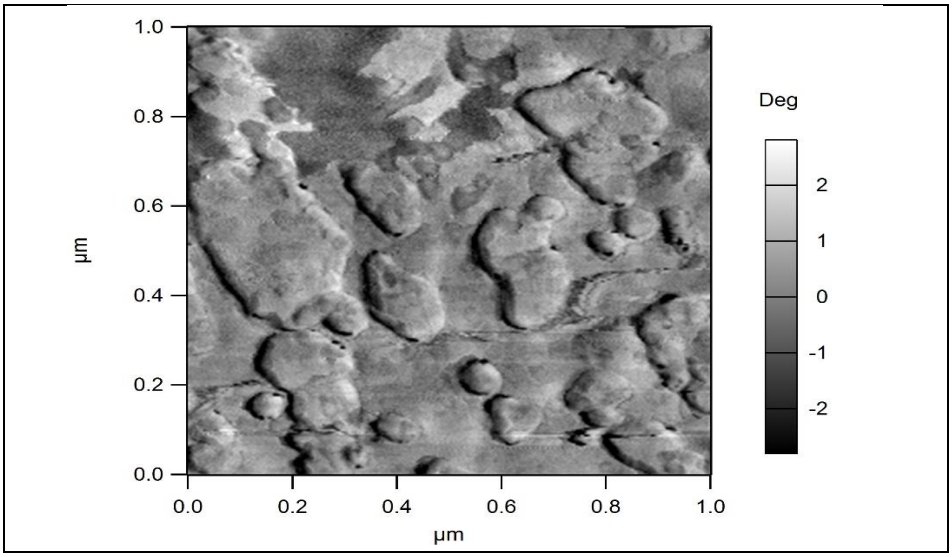


Figure 3. AFM Micrograph and Profile of CdS (Bilkent Unam)

Image0001HeightRetraceMod0
RoughnessData:

Parameter	Full Image Values:	Mask Image Values:
Number Of Points:	65536	
Average:	0.000 m	nan m
Standard Deviation:	2.061 nm	nan m
Max:	38.164 nm	nan m
Min:	-49.238 nm	nan m
RMS:	2.061 nm	nan m
Average Deviation:	1.520 nm	nan m
Skew:	-1.05	nan
Kurtosis:	52.9	nan
Percent XY:	100 %	0 %
Surface Area:	1.0 µm²	nan µm²
Area Percent:	1.426 %	nan %
Volume	0.0 µm³	nan µm³

Table 1. Roughness parameters (Bilkent Unam)

At this magnification, very fine "nanoscale" scratches and textural variations—which may have originated from the polishing or manufacturing process—can be distinguished much more clearly. At figure -5 shows the structural characteristics of the CdS thin film, which were investigated using a GNR APD Pro 2000 X-ray diffractometer (Bragg-Brentano geometry) with CuKα radiation ($\lambda = 1.5406$ Å). The diffraction pattern exhibits high phase purity with no detectable impurities, matching the standard ICDD PDF 041-1049 for the hexagonal wurtzite structure. The

observed peaks at 2θ values of 26,5°, 50.7°, and 54.5° correspond to the (002), (103), and (004) crystalline planes, respectively.

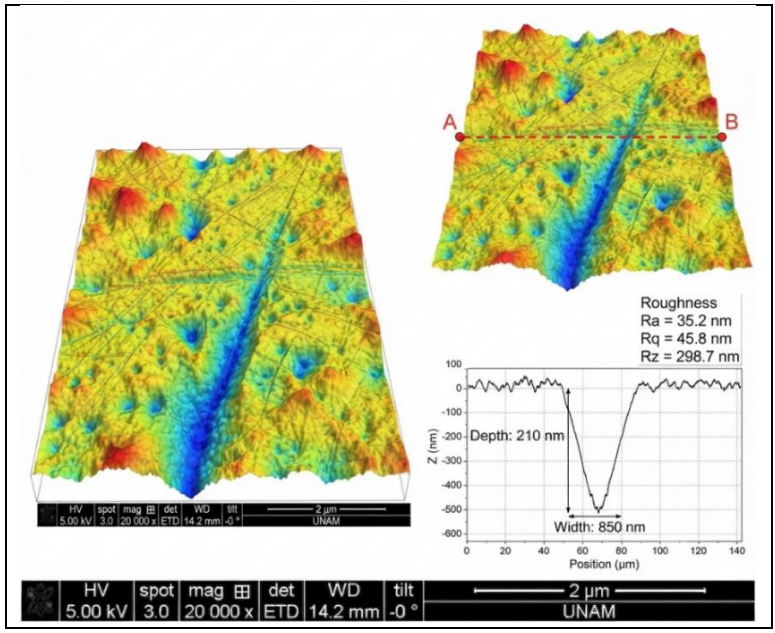


Figure 4. Reconstruction and Line Profile Analysis of CdS (*Bilkent UNAM*)

The dominance of the (002) and (004) reflections indicates a strong c-axis preferential orientation. The crystallinity of the sample is further confirmed by the Full Width at Half Maximum (FWHM) of 0.286° for the (002) peak. Lattice parameters were derived using standard hexagonal geometric relations, yielding values of $a = 4.14$ Å and $c = 6.71$ Å.

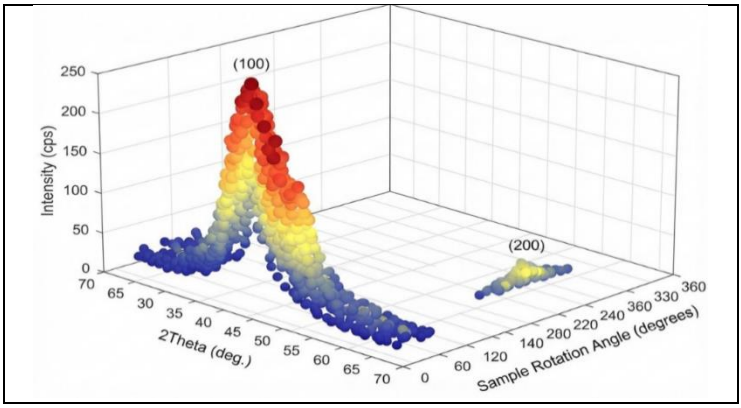


Figure 5. CdS Hexagonal 3D XRD Analysis [*Gazi University XRD Laboratory*]

$$c = \frac{\lambda l}{2 \sin\theta \cos\tau}$$

$$a = \frac{\lambda \sqrt{(4/3)(h^2 + hk + k^2}}{2 \sin\theta \sin\tau}$$

Phase identification and structural parameters determined via X-ray diffraction (XRD) analysis using a GNR APD Pro 2000 diffractometer in Bragg-Brentano configuration, utilizing CuKα radiation ($\lambda = 1.5406$ Å). The diffraction data, indexed according to ICDD PDF 041-1049, confirms the successful synthesis of a high-purity hexagonal wurtzite CdS phase. The diffraction pattern is dominated by the (002) and (004) reflections, indicative of a strong c-axis preferential orientation. Crystalline quality was further assessed through the Full Width at Half Maximum (FWHM) of the (002) peak, recorded at 0.286°. Lattice constants a and c were derived by applying the hexagonal geometric relation, incorporating sample tilt τ to account for geometric corrections.Unlike corona discharge or diffuse discharge (which is spread out and uniform), filamentary discharges are characterized by constricted, bright current channels as shown in Figure- 6.

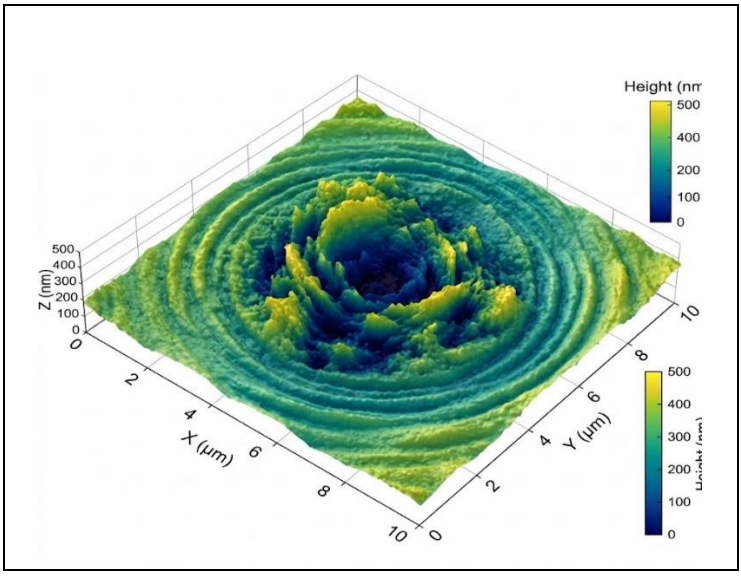


Figure 6 a) 3D Topographical Reconstruction of CdS Surface Defect Under Filamentary Discharge (Image Pro Plus Programme)

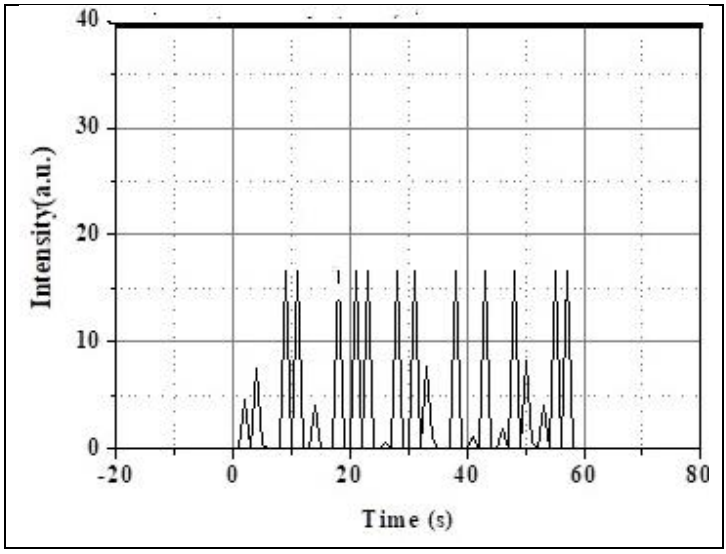


Figure 6b) Experimental Filamentary DLE Graph as a Function of the Time

Cadmium sulfide (CdS) is an important and widely used semiconductor due to its promising applications in the UV-Visible (UV-VIS) and infrared (IR) regions [1,16-18]. CdS is a significant semiconductor material owing to its distinct advantages in numerous light-sensitive and photovoltaic devices, including gas sensors and optoelectronic devices. However, CdS cannot withstand high voltages to the same extent as materials like GaAs or ZnSe [14-18]. Although it is currently widely used—particularly in batteries and solar panelsour experiments revealed that it degrades rapidly, causing a transition from a stable mode to an unstable, filamentary structure within the plasma (Figure 6b). As shown in Figure -6a, this resulted in the formation of a pit on the CdS surface. CdS is a material that operates efficiently primarily at low voltages.

4. CONCLUSION

Since CdS was used as the cathode in the plasma system, experimental methods specifically AFM, SEM, and X-ray diffraction (XRD)were employed to examine its surface and morphological characteristics. These measurements were conducted at the Bilkent UNAM center. The 3D phase pattern reveals that the image is relatively smooth, while also showing the presence of some superficial scratches, marks, and small particle-like structures on the surface—likely contaminants or crystal defects. The XRD results confirm the successful synthesis of a high-purity CdS phase with a hexagonal wurtzite structure, based on diffraction data indexed according to ICDD PDF 041-1049. Furthermore, the diffraction pattern reveals the dominance of the (002) and (004) reflections,

indicating a strong c-axis preferred orientation. Following the examination of all these structural and morphological characteristics, our experiments revealed that when the CdS material was used as the cathode in our plasma cell, an unstable filamentary discharge occurred at high currentsspecifically above 10^{-3} A—accompanied by surface degradation of the CdS. It was concluded that CdS, a material widely used in modern battery technology and solar panels, should be operated at low voltages and currents.

REFERENCES

1. Mukherjee, N., Ahmed, S.F., Mukherjee, D., Chattopadhyay, K.K., Mondal A. (2008) *Phys. Status Solidi C,* 5, 3458–3462.
2. Ghosh, P.K, Maiti, U.N., Ahmed, S.F., Chattopadhyay, K.K., *Opt. Mater.* 29 (2007) 1584–1590.
3. Pushpalatha, H.L. Bellappa, S., Narayanaswamy, T.N., Ganesha, R. (2014*) Indian J. Pure Appl. Phys*, 52, 545–549.
4. Okorie, O., Buba, A.D.A., Ramalan, A.M., IOSR (2017) *J. Appl. Phys*, 9, 82-89.
5. Xavier, R.J., Prema, A.A., Sahayaraj, P.A., Pragathiswaran, C., Dharmalingam, V. (2016) *Adv. Appl. Sci. Res*, 7, 178–182.
6. Amiri, O., Mashkani, S.M.H., Rad, M.M., Abdvali, F. (2014) *Superlattices Microstruc*., 66, 67–75.
7. Mandawade, A.S., More, A.A., J.A. Borse, A.V. Patil, J. Emerg. Tech. Innov. Res. 5 (2018) 361–365.
8. Yang, X., Yang, Y., Wang, B., Wang, T., Wang, Y., Meng, D. (2019) *Solid State Sci*, 92, 31–35.
9. Sagadevan, S., Chowdhury, Z.Z., Johan, M.R.B., Aziz, F.A., L.S. Roselin, H.L. Hsu, Selvin, R. (2019) *Res. Phys*, 12, 878–885.
10. Kavitha P., Suseela S., Mathelane, R.M. (2013) *Int. J. Eng. Sci*, 2, 108–110.
11. Kumar, B.R., Meher, D.S.R., IOSR (2016) *J. Appl. Phys*, 8, 47–55.
12. An, B.G., Kim, H.R., Chang, Y.W. *et al.* (2021). Photosensor-based on cadmium sulfide (CdS) nanostructures: a review. *J. Korean Ceram. Soc.,* 58, 631–644. https://doi.org/10.1007/s43207-021-00141-5
13. Francis, F., Chen, Jane, P. Chang, Lecture Notes on PRINCIPLES OF PLASMA PROCESSING, Electrical Engineering Department, Chemical Engineering Department, University of California, Los Angeles, Plenum/Kluwer Publishers 2002.
14. Kurt. H, Çetin, S, Salamov, B.G. (2011) *IEEE Transactions on Plasma Science,* 39 (4), 1086-1091.
15Kurt. H, Inalöz, A, Salamov, B.G. (2010) *Optoelectronics and Advanced Materials-Rapid Communications,*4*, 205-210.*
16. Kurt, H., Hilal, Tanrıverdi, E., Salamov, B.G (2019) *JOM*, 71 (2), 644-650.
17. Chang Cheng, Linxi Wang, Jiaguo Yu. (2023) Chapter 5 - CdS- based S-scheme photocatalyst*. Interface Science and Technology*, 35, 175-199.
18. Byung-Gi, An (2021) "Photosensors based on cadmium sulfide (CdS) nanostructures: a review. *Journal of The Korean Ceramic Society* 81, 631–644.

Chapter 5

Eco-Friendly Micro-Plasma Systems with High-Sensitivity Infrared Znse Photodetectors

Hatice Hilal YÜCEL[1], Seren Elifcan KIZIŞAR AKSIN[2]

1. INTRODUCTION

With the advancement of technology, there is a growing need for semiconductor detector-based electronic systems at the nano and micro scales. Consequently, efforts to develop nano- and microelectronic systems have gained momentum, and the search for solutions to various technical challenges in this field has become increasingly important. Although numerous studies have focused on these issues, the situation is complicated by the fact that semiconductors can be doped with various impurities, which in turn give rise to distinct physical mechanisms. Coordinated efforts are being carried out across various fields to achieve access to clean energy. In this context, plasma-based systems have recently garnered significant interest within the scientific community, as they represent an area attracting global research attention as an alternative to renewable energy sources. The rise in energy consumptionparalleling global population growth combined with the inadequacy of existing energy sources, has brought plasma technology to the forefront. However, the nascent nature of this field complicates the task of unraveling the many unknown physical and chemical processes that lie beyond basic plasma technology. The eco-friendly nature of plasma-based systems facilitates the use of particularly room-temperature cold plasmas in industrial and medical fields. Plasma systems are employed across a wide spectrum of applications, ranging from semiconductor growth to fusion energy. However, as is the case in every field, maintaining plasma stability over extended periods remains the most significant challenge for technological products based on plasma systems. This challenge necessitates a thorough understanding of numerous complex physical and chemical processes, as well as the achievement of optimal plasma conditions. Plasma equations necessitate both an understanding of the numerous chain reactions involved in gas discharge and the careful selection of materials used as cathodes in plasma cells. In this context, a plasma system must be viewed as a

[1] Prof. Dr., Department of Physics/Faculty of Science, Gazi University, Turkey, hkurt@gazi.edu.tr (ORCID: 0000-000-1277-5204)
[2] (ORCID: 0000-0003-2250-9142), serenelifkizisar@gmail.com

combination of gas and semiconductor systems. Determining which semiconductor offers efficiency in energy generation and storage is a subject that requires careful investigation. Fortunately, ZnSe photodetectorsw hich operate excellently at room temperature and atmospheric pressure have emerged in this field. These detectors exhibit superior conductivity and infrared absorption at high pressures. ZnSe is an II-VI group IR detector. Its direct bandgap enables the optical signal to be captured and converted into energy very rapidly. It also possesses structurally superior morphological characteristics that ensure plasma stability. The ZnSe detector offers an alternative to the GaAs detector used in satellite systems. Zinc Selenide (ZnSe) has established itself as a cornerstone material in modern optics and optoelectronics, primarily due to its unique combination of thermal, optical, and electronic properties. The utility of ZnSe stem substrates for lenses and windows stems from their ability to maintain performance under demanding conditions:

- *Broad Transmission Range: It is one of the few materials that offers high transparency from the visible spectrum through the mid-infrared (mid-IR) and well into the far-infrared (far-IR) regions.*

The generation of radiation in the mid-infrared region is of great interest, as it enables a wide range of applications across various fields. The mid-IR region is particularly significant because both organic and inorganic materials exhibit strong absorption within it. This part of the electromagnetic spectrum is valuable due to the presence of numerous distinctive absorption lines [1, 2]; these lines offer immense spectroscopic potential and provide crucial information for applications such as studying complex biological systems [3], identifying atmospheric pollutants [4], and conducting other environmental analyses. Furthermore, this region is utilized in night-vision technology, the defense industry, and free-space optics. This range is also employed in communications that are vital for civilian use [5, 6] and is essential for night-vision technologies [7]. Zinc Selenide (ZnSe) is widely used in infrared optics, FTIR spectroscopy, and CO_2 laser systems. Additionally, the scattering of laser emission by small atmospheric particles described by Mie and Rayleigh scattering modelsdiminishes at longer wavelengths. This reduction is a key factor driving the development of lasers for mid-IR LIDAR applications [8]. When discussing plasma, three types of plasma modes must be recognized: Townsend discharge, glow discharge, and arc discharge. Among these, glow discharge is one of the simplest and most effective methods for generating plasma in industrial and laboratory settings; the process is characterized by a transition of the gas from an insulating to a conductive state once the applied voltage exceeds a critical threshold, resulting in a structure with distinct regions forming between the

cathode and anodedetermined by the applied voltage, the type of gas, and the inter-electrode distance. In figure- 1 show that application areas of cold plasma.

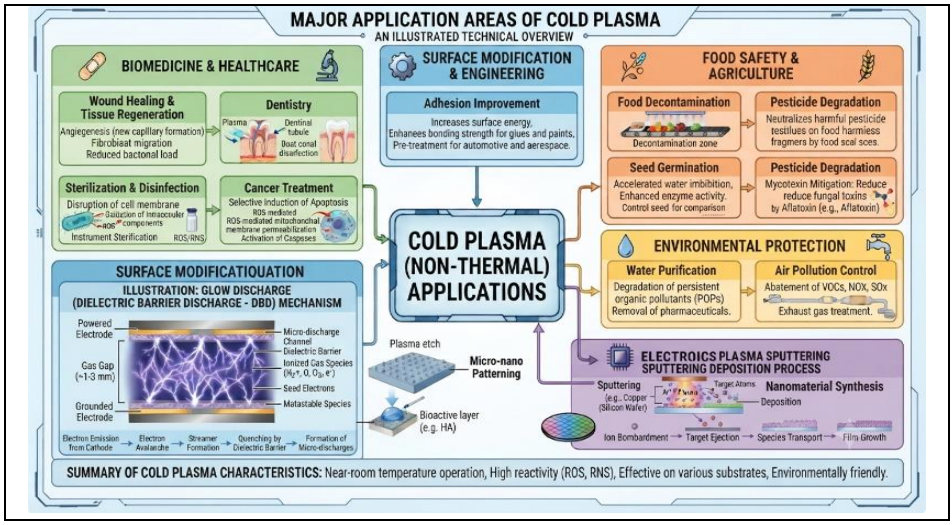


Figure 1. Major application areas of cold plasma discharge [18].

Glow discharge is a type of electrical discharge in a gas that occurs between two electrodes placed in a low-pressure environment or at atmospheric pressure. It is a fundamental process in plasma physics and is used extensively in materials science, manufacturing, and lighting. Key applications are as follows;1-Materials Analysis (Spectroscopy): Techniques like GD-OES (Glow Discharge Optical Emission Spectroscopy) or GD-MS (Glow Discharge Mass Spectrometry) use the plasma to sputter atoms from a solid sample, allowing for precise chemical composition analysis and depth profiling. 2- Surface Treatment and Thin Film Deposition: It is a core mechanism in physical vapor deposition (PVD) and plasma-enhanced chemical vapor deposition (PECVD), which are used to apply coatings or modify the surface properties of materials.3-Lighting: Classical examples include neon signs and fluorescent lighting, where the plasma discharge through the gas mixture produces visible or ultraviolet light.

2. STRUCTURE OF THE PLASMA SYSTEM (EXPERIMENTAL)

While ZnSe is traditionally recognized for IR applications, its potential in the ultraviolet (UV) regime is significant, especially when compared to legacy semiconductor materials like Silicon (Si) and Gallium Arsenide (GaAs).

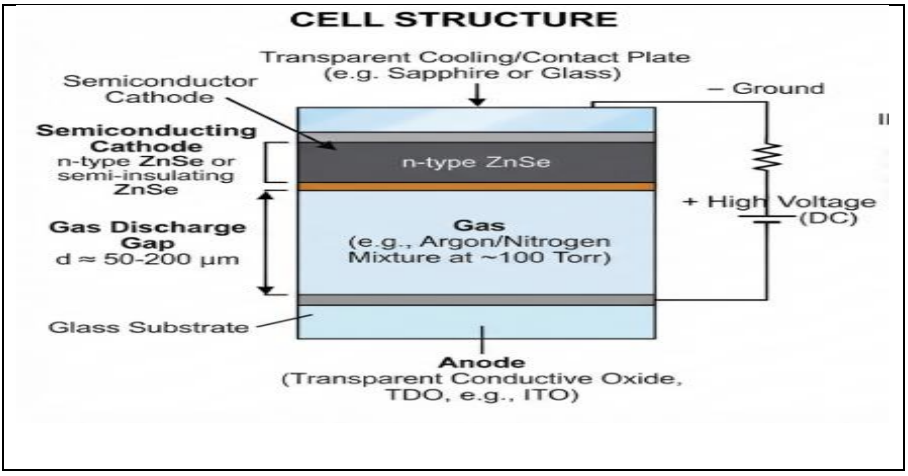


Figure 2. The cell structure of the Plasma system

The plasma-generating system features an anode nozzle with an output aperture diameter of 50 mm. To maintain consistent performance, the system is configured so that the distance from the cathode apex to the edge of the anode aperture is precisely between 50 mm and 1 mm. Plasma production occurs just beyond the nozzle, where the argon working gas fills the cell. The system is powered by a DC voltage source, starting at an open-circuit voltage of 2500 V, which drops to 200 V once the discharge ignites. 1-kΩ ballast resistor is used to account for the difference between the supply and discharge voltages.

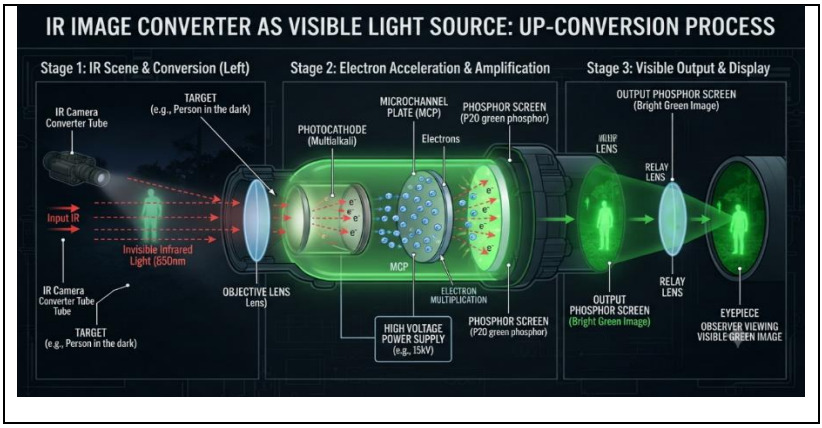


Figure 3. (a,b) Experimental setup. It shows the conversion process of the IR light beam to a visible one [18].

Standard semiconductors often suffer from structural or electronic degradation when exposed to high-intensity UV radiation over prolonged periods.

ZnSe provides a robust alternative because;Wide Bandgap: This property inherently allows for selective detection of UV light while remaining blind to lower-energy photons.Electric Field Resilience: ZnSe exhibits a high threshold for electrical breakdown. Even under intense UV flux, it maintains structural integrity and performance stability where other materials would begin to fail.This resilience makes ZnSe an ideal candidate for harsh-environment monitoring, flame detection, and space-based UV sensing applications where device longevity is non-negotiable

3. RESULTS AND DISCUSSION

Its high resistance to thermal shock allows it to withstand significant temperature gradients, which is critical for high-power laser systems. With a high refractive index and low dispersion, ZnSe allows for the design of thin, high-performance optics that minimize chromatic aberration.Low absorption coefficients ensure that minimal energy is lost as heat, which is essential for maintaining beam quality and preventing damage to the optical elements themselves. Scanning Electron Microscopy (SEM) is a powerful imaging technique that uses a focused beam of high-energy electrons to scan the surface of a sample. Unlike optical microscopes that use light, SEM uses electrons to achieve significantly higher magnification and resolution, allowing for the observation of microscopic features that would otherwise be invisible. Atomic Force Microscopy (AFM) topology refers to the process of mapping the physical surface featuresthe "landscape"of a sample at the nanoscale. By scanning a sharp probe across a surface, AFM builds a high-resolution representation of the sample’s topography, revealing features like height, roughness, and grain structure. The provided image is a 2D Phase map generated by Atomic Force Microscopy (AFM) of a zinc selenide (ZnSe) surface (Figure 4b). In AFM, the "topography" image represents the actual height (z-axis) of surface features. The phase image of ZnSe, on the other hand, measures the phase lag between the cantilever's driving oscillation and its actual oscillation as it interacts with the surface. Phase images are highly sensitive to variations in material properties such as stiffness, adhesion, viscoelasticity, and friction rather than height. 2D phase image would be physically incorrect and misleading, as the intensity values (levels of "brightness" or "darkness") do not represent height.

It is important to note that not every ionized gas is plasma; for an ionized gas to be classified as plasma, it must possess certain characteristics specific to plasmas. For instance, the ionized gas is expected to be collectively neutral while exhibiting conductive properties [9].

Furthermore, the charged particle density must exceed a certain threshold for these characteristic plasma properties to emerge. The density of charged particles is a crucial factor in the definition of plasma because it influences the system's statistical behavior. Neutral particles within the plasma structure also interact with one another through electromagnetic interactions, just as charged particles do. However, since the forces between neutral particles are short-range, in most cases, we assume that two neutral atoms do not interact until they collide. Consequently, one of the defining characteristics of plasma is that it consists of charged particles that exert forces on each other via Coulomb interactions. The density of charged particles within the plasma ensures that Coulomb forces dominate, giving rise to collective behavior [10].

Table 1 Roughness data (Figure 4a)

Image0004HeightRetraceMod0
RoughnessData:

Parameter	Full Image Values:	Mask Image Values:
Number Of Points:	65536	
Average:	0.000 m	nan m
Standard Deviation:	1.318 nm	nan m
Max:	4.578 nm	nan m
Min:	-5.449 nm	nan m
RMS:	1.318 nm	nan m
Average Deviation:	1.034 nm	nan m
Skew:	-0.111	nan
Kurtosis:	0.244	nan
Percent XY:	100 %	0 %
Surface Area:	1.0 µm²	nan µm²
Area Percent:	1.164 %	nan %
Volume	0.0 µm³	nan µm³

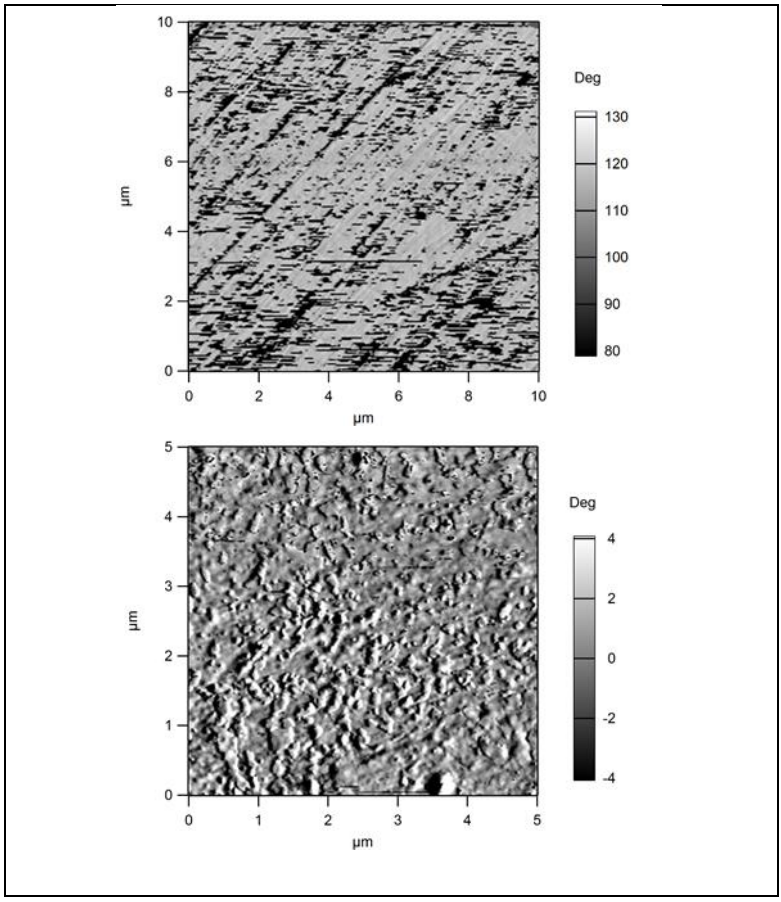


Figure 4. (a,b) Topographic analysis of ZnSe: a) 2D SEM image, b) phase image

Ultimately, collective effects are essential for a gas composed of charged particles to be classified as plasma [11]. As can be seen from figure -5, increasing the active plasma cathode diameter enhances the response of the ZnSe photodetector, thereby yielding a higher plasma current.Figure 5 suggests that if the system is to be utilized as a light or energy source, a larger diameter is more optimal for the non-toxic and eco-friendly ZnSe detector. Today, ZnSe possesses highly advantageous properties for numerous optical systems, particularly in the infrared (IR) range and is consequently utilized for optical lenses and windows. Some of these properties include [12, 13].Low absorption, Wide bandgap, High resistance to thermal shock, Transmission ranging from the visible spectrum to mid-IR and far-IR wavelengths, High refractive index, Low dispersion. These characteristics also pave the way for the use of ZnSe semiconductors as UV photodetectors. While the degradation of Si and GaAs semiconductors—commonly used for UV photodetectors—under intense UV radiation poses a disadvantage, ZnSe significantly mitigates this effect, as it is

subject to electrical breakdown only under high electric field strengths [14-16]. In Figure -6 show that current-voltage characteristics (*CVC*) and *DE* (discharge emission) graphs with strong IR illumination A_3 and without IR illumination for various gap distances *d*.

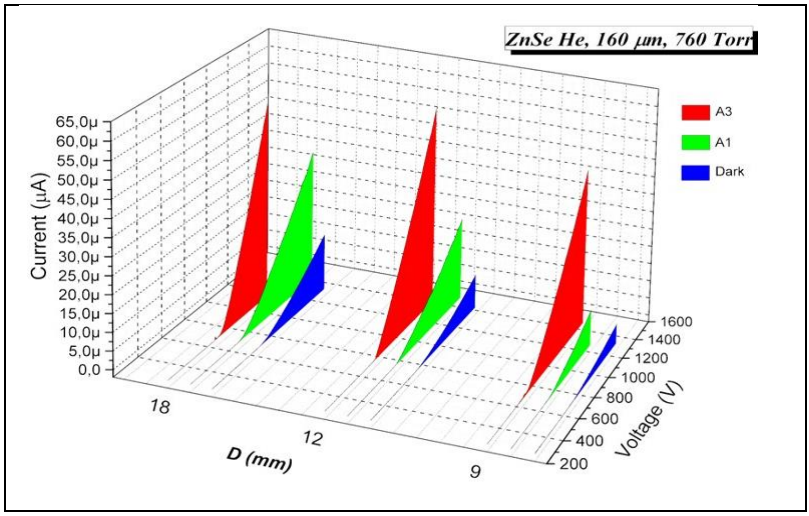


Figure 5. Plasma Current-Voltage Characteristic under different Infrared stimulation. A_1 shows the weak IR and A_3 shows the strong IR stimulation in the case of various cathode diameters *D* [17].

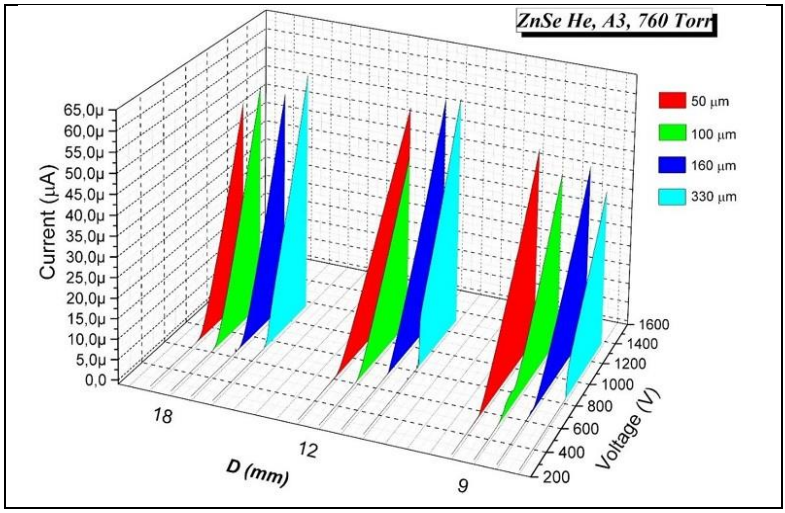


Figure 6. CVCs as a function of cathode diameter D under different d [17].

To better understand the relationship between gap length *d*, gas pressure *p*, and breakdown voltage, we can reframe the core principles of Paschen's Law and

its implications for DC plasma in Argon. The Scaling Law of Gas Breakdown, that is, Paschen's Law, dictates that the breakdown voltage (V_b) is not merely a product of the gap distance (d), but of the product of pressure (p) and distance (d). The requirement for a much higher electric field at smaller gaps (e.g., our 50 μm examples) exists because the electrons have less space to gain kinetic energy.

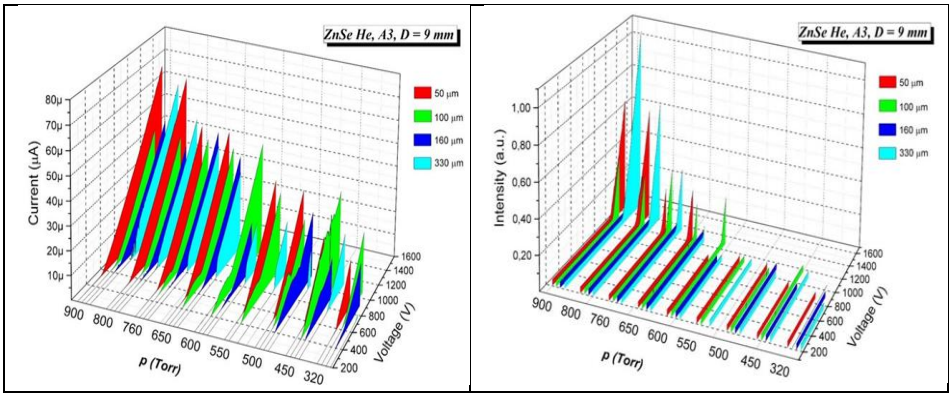


Figure 7 (a,b) a) *CVC* and b) *DLE* graphs for various pressure values under strong IR stimulation A_3 [17].

To compensate for the lack of ionization collisions, the field strength must be intensified to ensure an electron avalanche occurs before the electron hits the anode. Pressure can be used as a Control Variable shown in Figure -7. By adjusting pressure, we are modifying the mean free path of electrons. Increasing pressure from 320 Torr to 900 Torr reduces the average distance an electron travels between collisions, which shifts the discharge mode and alters how quickly the current pulse forms and decays.In our specific investigation (320 Torr to 900 Torr) in Figure 7 (a,b), we are manipulating the discharge through two primary mechanisms;Ionization Rate: Increasing the pressure increases the density of neutral atoms. This affects the number of ionizing collisions per unit of length, which dictates the rate of rise for your current peak.Quenching Dynamics: The "width" of the current formation is defined by the speed at which charge accumulates on the ZnSe photodetector to cancel out the external electric field. This pressure-dependent control allows us to "tune" the discharge, making it a critical parameter for optimizing the current values in our parameter set.

4.CONCLUSION

The analysis of the data obtained from the study indicates that the measured current in the system is directly proportional to the cathode radius *D*. This is an expected result, as an increase in the cathode surface area facilitates higher

electron emission into the medium, naturally leading to an increase in current. It was observed that the current value decreases as the distance between the electrodes increases. This decline can be interpreted as the result of a decrease in the ionization rate; as the distance increases, electrons require a longer path to sustain sufficient ionization, and their energy becomes insufficient for this process.In this study, the current-voltage characteristics of the ZnSe semiconductor were investigated under various conditions to evaluate the resistance change of ZnSe under illumination. By examining the radiation intensities in the gas discharge region, it was demonstrated that at high voltage and pressure values, this gas discharge chamber has the capacity to be utilized as UV light source.he energy band gaps and refractive indices of semiconductors directly determine their optical and electronic behaviors. Accordingly, the data obtained show that as pressure values increase, the current value also rises, dependent upon electron density. The characteristic features of ZnSe pave the way for the use of ZnSe semiconductors as UV photodetectors. While the degradation of Si and GaAs semiconductors—commonly used for UV photodetectors—under intense UV radiation poses a disadvantage, ZnSe significantly mitigates this effect, as it is subject to electrical breakdown only under high electric field strengths. Unlike other semiconductors, ZnSe generates higher plasma current and emission at high pressures; the higher value obtained in our experiments at 900 Torr serves as evidence of this. It is a material that withstands high pressure and is highly sensitive to infrared radiation. For these reasons, it offers advantages as an optical light source. Furthermore, being less toxic and more environmentally friendly than GaAs, ZnSe can be integrated into a wide range of systems for optoelectronic applications.Based on these results, the ZnSe cathode plasma cell shows excellent light sensitivity compared with other semiconductor cathode cells at atmospheric pressure and even at higher pressures; therefore, it can be used as a light source. Moreover, we conclude that ZnSe exhibits high-performance photodetector characteristics by storing infrared energy in the ZnSe cathode and subsequently generating visible light via a plasma process. Furthermore, based on these properties, we propose a plasma system utilizing ZnSe that is suitable for the design of photo-charged capacitors. This structure enables the charging of the plasma capacitor by collecting light and allowing active ions to generate surface charges on the ZnSe detector. Consequently, it offers superior long-term stability and a reversible, high charge-storage capacity with minimal loss. Therefore, the design of the ZnSe photodetector holds promise for the development of energy-efficient and Eco-friendly photocathodes intended for future photo-accelerated energy storage applications.

REFERENCES

1. Gordon, I.E., Rothman, L.S., Hargreaves, R.J., Hashemi, R., Karlovets, E.V., Skinner, F.M., Conway, E.K., C. Hill, Kochanov, R.V, Tan, Y., Wcisło, P., Finenko, A.A., Nelson, K., Bernath, P.F., Birk, M., Boudon, V., Campargue, A., Chance, K.V., Coustenis, A. (2022). The HITRAN2020 molecular spectroscopic database. *J Quant Spectrosc Radiat Transfer*, 277, 107949. https:// doi. org/ 10. 1016/j. jqsrt. 2021. 107949.

2. Tittel, F.K., Richter, D., Fried, A. Mid-Infrared Laser Applications in Spectroscopy. In: Sorokina, I.T., Vodopyanov, K.L. (eds.) (2003). Solid-state mid-infrared laser sources. *Topics in applied physics*, 458–529. Springer, Berlin, Heidelberg. https:// doi. org/ 10. 1007/3- 540- 36491-9_ 11

3. Nagl, N. (2021). A new generation of ultrafast oscillators for mid-infrared applications (Springer, Berlin, https:// doi. org/ 10. 1007/ 978-3- 030-89754-3

4. Gong, Y., Bu, L., Yang, B., Mustafa, F. (2020). High repetition rate mid-infrared differential absorption lidar for atmospheric pollution detection. *Sensors*, 20(8), 2211 https:// doi. org/ 10. 3390/ s2008 2211

5. Willner, A.E., Zou, K., Pang, K., Song, H., Zhou, H., Minoofar, A., X. Su (2023). Free-space mid-IR communications using wavelength and mode division multiplexing. *Opt. Commun*, 541, 129518. https:// doi. org/ 10. 1016/j. optcom. 2023. 129518

6. Soibel, A., Wright, M., Farr, W., Keo, S., Hill, C., Yang, R.Q., Liu, H.C. (2010). Free-space optical communication utilizing mid-infrared interband cascade laser. *In: Free-Space Laser Communication Technologies XXII*, 7587, 241–250. SPIE, https://doi. org/ 10. 1117/ 12. 845788

7. Bekman, H.H.P.T., Heuvel, J.C.v.d., Putten, F.J.M.V., Schlei jpen, R. (2004) Development of a mid-infrared laser for study of infrared countermeasures techniques. *In: Technologies for Optical Countermeasures*, vol. 5615, pp. 27–38. SPIE, https://doi. org/ 10. 1117/ 12. 578214

8. Kurt, H., Hilal, Tanrıverdi, E., Salamov, B.G (2019) *JOM*, 71 (2), 644-650.

9. Wiesemann, K. (2013). A Short Introduction to Plasma Physics. In Bailey, R (Ed.). Proceedings of CAS- CERN Accelerator School, Ion Sources (p. 586). European Organization for Nuclear Research (CERN)

10. Krall, N. A.; Trivelpiece, A. W. (1973). Principles of plasma physics, New York: McGraw-Hill

11. Gedalin, M. (2017). Introduction to Plasma Physics. 10. Hazeltine, R.; Waelbroeck, F. (2004). The Framework of Plasma Physics, CRC Press

12. Zhang, F., Qing, Y., Bian, H., Liu, F., Li, M., Hou, X., and Chen, F. (2020). Fabrication of ZnSe Microlens Array for a Wide Infrared Spectral Region. *IEEE Photonics Technology Letters*, 32(20), 1327-1330.

13. Zhao Y-Y, Sheng S-Y (2024) First-principles calculation of interface interactions and photoelectric properties of ZnSe/SnSe heterostructure. *PLoS ONE*, 19(5): e0304032. https://doi.org/10.1371/journal.pone.0304032.

14. Kurt. H, Çetin, S, Salamov, B.G. (2011) *IEEE Transactions on Plasma Science,* 39 (4), 1086-1091.

15. Kurt. H, Inalöz, A, Salamov, B.G. (2010) *Optoelectronics and Advanced Materials-Rapid Communications,*4*, 205-210.*

16. Kurt, H., Hilal, Tanrıverdi, E., Salamov, B.G (2019) *JOM*, 71 (2), 644-650.

17. Helyum plazma etkisi altında ZnSe detektörünün optoelektronik özelliklerinin incelenmesi, Yücel H. H. (Advisor) S. Elifcan, master's thesis, 2023

18. https://gemini.google.com

Chapter 6

Environmental Health Literacy and Radiation Awareness: The Role of Stem Education In Building Community Resilience

Ahmet YALKIN[1]

1. INTRODUCTION

Environmental degradation is seen in contemporary societies as a multi-dimensional problem area directly related to public health, risk communication, environmental justice, and education policies, not limited to ecological systems. Factors such as air and water pollution, health risks related to climate change, technology-related accidents, waste management, and environmental exposures are making issues related to individual and public health increasingly complex. It is necessary to understand the relationships between these concepts. Much of the scientific knowledge related to environmental risks is often emphasized as being technical, measurement-based, and interdisciplinary. However, the societal response to these risks is closely related to trust, experience, and local understanding. Therefore, environmental health education processes should not be limited to a model based solely on information transfer.

Environmental Health Literacy (EHL) offers an interdisciplinary framework focusing on revealing the relationship between environmental and health terms, explaining knowledge about environmental exposures, and transforming this knowledge into preventive health actions. Environmental health literacy has recently coalesced as a new subdiscipline combining key principles and procedural elements from the fields of health literacy, risk communication, environmental health sciences, communications research, and safety culture. With this definition, EHL is presented as a topic too important to be limited to individuals recognizing environmental hazards. Individuals are expected to understand the relationship between environmental exposure and health outcomes, evaluate evidence, and use it in decision-making processes. This framework conceptualises EHL as a continuum that connects an understanding of how environmental exposures influence health with individual and community action, while explicitly incorporating self-efficacy and skill development [1].

Environmental health education integrates environmental, health, and risk education and is most effective when combined with local knowledge to support

1 Dr., Project Office, Tarsus University, Türkiye, ahmetyalkin@tarsus.edu.tr, ORCID: 0000-0002-1914-4608

health promotion, behaviour change, and social action [2]. Participants who lacked baseline environmental science knowledge showed significant gains following training; those with low initial self-efficacy also demonstrated increased self-efficacy [3]. An extensive report-back process provided individuals and communities with the information and tools needed to exert greater control over environmental exposures that may lead to adverse health outcomes [4]. The findings indicate that EHL constitutes a competency area encompassing the entire spectrum from information acquisition to health-protective action. As radiation is not directly perceptible to the human senses, the concept of radiation awareness is regarded as a technically challenging and distinctive area within EHL.

The comprehension of radiation risk may be contingent upon the utilisation of measuring instruments, the evaluation of dose amounts, the interpretation of expert opinions, and the provision of reliable risk communication. Education on radiation issues is likely to be more effective when it explicitly targets dose- and exposure-based reasoning, systematically distinguishes hazard from risk, and treats uncertainty as a natural component of environmental and health decision-making. A public survey identified a difference between the perceived and actual health risks associated with radiation exposure [5]. High school students' attitudes and behaviours toward radiation can be positively influenced by radiation education, which can provide fundamental and useful knowledge [6]. The contextually rich example of the Semipalatinsk Nuclear Test Site has also been used to study radiation literacy, demonstrating how interdisciplinary education that integrates physical mechanisms, spatial distribution, and historical factors can improve risk-based thinking [7].

The STEM (Science, Technology, Engineering, and Mathematics) education paradigm proposes a multidisciplinary approach with the capacity to construct a pedagogical bridge between environmental health literacy and radiation awareness. Furthermore, STEM education has emerged as a promising framework for developing sustainability and environmental health literacy [8]. It is commonly understood that if education were to address the growing environmental, social and economic challenges facing societies worldwide, then frameworks such as education for sustainable development and climate change education would become centre stage. In order to comprehend the consequences of radiation exposure, it is necessary to take into account a number of factors including those pertaining to physical dose, chemical degradation processes, biological health effects, geographical pollution models, mathematical data interpretation, and societal risk communication.

Ultimately, STEM education can have an important role on students' understandings and engineering design process about environmental issues since it engages students in real-world environmental problem-solving that integrates science, technology, engineering, and math.

A positive relationship has been identified between environmental education and STEM education: environmental education can improve students' perceptions of environmental problems, while STEM education can strengthen engineering design processes [9]. A problem-solving-based STEM model in environmental sustainability can also improve students' understanding of environmental issues and collaborative problem-solving skills [10]. This section conceptually addresses how STEM education can support community resilience through environmental health literacy, radiation awareness, and community-based environmental monitoring practices. In this context, community resilience is not limited to post-disaster recovery capacity; it is a multidimensional structure that includes recognising risks in advance, using evidence-based decision-making processes, establishing trust-based communication networks, and developing post-crisis learning capacity. Community resilience therefore involves recognising vulnerabilities and developing capabilities to prevent, withstand, and mitigate the stress of an incident [11]. Educational processes can further strengthen socio-ecological resilience through systems thinking and participatory environmental monitoring [12]. Within this framework, STEM education can help learners understand, measure, and interpret environmental health risks and translate evidence into community action.

2. ENVIRONMENTAL HEALTH LITERACY AND RADIATION AWARENESS

Environmental health literacy is defined as an interdisciplinary concept encompassing the knowledge, skills, and competencies required to understand the effects of environmental exposures on human health, evaluate environmental risk information, and transform this information into health-protective behaviours. EHL begins with an understanding of the link between environmental exposures and health and incorporates principles and procedures from health literacy and risk communication [13]. It should therefore be considered not only at the level of awareness but also in terms of interpreting environmental information, evaluating its reliability, and using it in individual or collective decision-making. Awareness and knowledge are important starting points; when combined with information-seeking and decision-making skills and self-efficacy for specific behaviours, they can inform collective action [1]. EHL is thus a developmental construct that includes awareness, knowledge, skills, self-efficacy, and community-level change. Environmental health education should not be reduced to the transfer of information. Knowing the name

of an environmental pollutant does not necessarily mean that an individual can correctly interpret its exposure pathway, health impact, measurement value, or protection strategy. The crucial element is the functionality of this knowledge in risk assessment and action development. Contextual learning can improve EHL [3]. In training conducted with communities at risk, participants' prior knowledge and personal experiences were incorporated into the co-creation of training content. This approach increased environmental health knowledge, self-efficacy, and specific environmental health skills.

This result implies that local experience in environmental health education is a resource that makes learning meaningful rather than a barrier to scientific learning. Environmental justice and environmental health literacy can be supported by sharing environmental exposure results with communities [4]. Communicating individual or household exposure data can help participants better understand their circumstances, change household behaviours, and develop strategies to reduce exposure. An exploratory study of public awareness and perceptions of ionising radiation risk identified inconsistencies in knowledge, underscoring the need for targeted education and communication in public health practice [5]. Studies conducted after Fukushima further highlight the importance of educational intervention. Radiation education can provide high school students with relevant basic and practical knowledge and positively influence their attitudes and behaviours toward radiation [6]. These classes covered the scientific foundations of radiation, local radiation measurements, and everyday protective measures. Radiation literacy has also been examined using the Semipalatinsk Nuclear Test Site as a context-rich example that integrates historical dimensions, physical mechanisms, and spatial distribution [7].



Figure 1. The multidimensional continuum of Environmental Health Literacy (EHL), adapted [1]

3. CONTRIBUTION OF STEM EDUCATION TO ENVIRONMENTAL HEALTH LITERACY

One significant pedagogical approach that brings the multidisciplinary nature of environmental health issues into the classroom is STEM education. Environmental health risks may be too complex to be addressed within a single discipline. Water pollution may require chemical analysis and microbiology; air pollution may involve atmospheric events, chemical processes, and respiratory health; radiation risk may require an understanding of physical dose concepts, biological effects, and environmental transport pathways; and climate change may involve atmospheric science, ecology, health, and social policy.Considering these reasons together, EHL-focused STEM education can position scientific knowledge as an integrated tool used in solving environmental health problems.

By integrating environmental education with STEM education, the E-STEM approach can enhance students' understanding of environmental issues and strengthen their engineering design processes [9]. This approach treats environmental issues as real-world situations that students analyse, model, and address by developing possible solutions.Topics such as plant growth, acid rain, pollution, and sustainable agriculture can be examined through observation, data collection, design, testing, and revision. This process can transform students from passive recipients of information into active problem solvers [9]. A problem-solving-based STEM model used in environmental sustainability programmes increased students' understanding of environmental problems and supported collaborative problem-solving attitudes [10]. Project-based STEM applications have also shown positive effects on scientific literacy and environmental attitudes [14], while STEM project-based learning has demonstrated the potential to improve environmental literacy [15]. Taken together, these studies suggest that environmental health issues should be approached not merely as topics within STEM education but as learning contexts involving research, design, decision-making, and communication. Research on climate literacy provides further evidence for environmental health-focused STEM education. STEM-based physics teaching materials can improve climate literacy among high school students [16]. An i-STEM intervention examining the role of trees in climate regulation also produced positive changes in interdisciplinary conceptual knowledge, scientific self-perception, and epistemic feelings [17]. Complex environmental health phenomena can therefore be taught more meaningfully through data, models, measurement, and context.

To raise awareness about radiation, STEM education can address conceptual, methodological, and socio-scientific dimensions together. Conceptually, attention should be given to radiation categories and sources, dose, exposure duration, protective measures, radioactive decay, biological effects, and environmental

transport pathways. Methodologically, learners should consider measurement instruments and units, mapping, data quality, sampling strategy, and the interpretation of uncertainty. From a socio-scientific perspective, discussion should encompass risk perception, ethical responsibility, public awareness, trust, decision-making, and collective memory. Radiation education can produce more robust learning outcomes when it is connected to local measurements, historical context, and everyday applications [6,7].

4. CITIZEN SCIENCE, RADIATION DATA, AND COMMUNITY PARTICIPATION

Citizen science provides a notable means of combining environmental health literacy with usable data production and community participation. In this context, individuals move from being recipients of scientific information to active participants who collect data, take measurements, interpret findings, and communicate results. Citizen science can function as a complementary knowledge-production mechanism, particularly when communities perceive official environmental health data as inadequate, delayed, or unreliable. Community and citizen science initiatives have produced progress across a range of environmental education outcomes [18]. These projects can improve scientific content knowledge, research skills, attitudes toward the environment and science, self-efficacy, environmental behaviour, responsibility for environmental protection, and community commitment. These outcomes correspond to the awareness, self-efficacy, and community-change dimensions of EHL [1]. Citizen science can therefore be understood as an applied pedagogy of environmental health literacy. Participatory environmental health research ranges from basic data collection to more advanced forms of citizen science [19]. Low-cost sensors, mobile devices, open-data platforms, and mapping technologies can make environmental monitoring more accessible. Participation in data production, however, does not automatically constitute scientific literacy. Participants need to understand what instruments can and cannot measure, how sampling patterns affect results, and how data quality shapes interpretation. Data literacy is therefore a fundamental component of environmental health literacy. The post-Fukushima Safecast initiative is one of the most prominent examples of citizen science in radiation monitoring. This international volunteer-based organisation, created immediately after the accident, monitors environmental radiation and openly shares the resulting information [20]. Beyond producing data, Safecast operates as a participatory infrastructure connecting measurement, mapping, communication, and public interpretation. Actionable scientific information for disasters and emergencies may also be derived from non-traditional citizen-generated data, although such data are not always

formally vetted [21]. Their reliability must therefore be assessed in relation to measurement units, instrument calibration, location and timing, sampling patterns, and the transparency of data-processing procedures. Citizen science can make radiological contamination publicly visible and draw attention to hazards that cannot be perceived directly [22]. Independent monitoring can help make imperceptible hazards such as radiation observable and publicly recognisable. Numerical data alone, however, may not acquire public meaning unless they are communicated clearly, uncertainty is conveyed accurately, and trust is established. Risk and safety communication should therefore account for public misconceptions, literacy levels, plain language, and actionable safety information [23].

5. ENHANCING COMMUNITY RESILIENCE THROUGH STEM EDUCATION

Community resilience should not be understood merely as a community's ability to overcome a crisis or return to its previous state after an environmental or technological disruption. A resilient community must be able to recognise potential risks before they escalate, prepare for possible scenarios, interpret scientific information accurately, coordinate institutional responses, involve local actors in decision-making, and transform crisis experience into collective learning. This process includes public health preparedness, disaster-management capacity, civil-society participation, and locally based action planning [11]. Environmental health literacy strengthens resilience by enabling individuals and communities to interpret environmental risk information and use it in practical decisions. Inadequate understanding of exposure data can make communities more vulnerable to misinformation, anxiety-driven reactions, delayed protective measures, or fatalistic interpretations of risk. Communities with stronger EHL are more likely to ask relevant questions, evaluate the credibility of risk communication, identify appropriate protective measures, and participate in local risk-management processes. Context-based learning can improve environmental health knowledge and self-efficacy in communities exposed to environmental risks [3]. Communicating exposure results to participants can also promote household-level behavioural change and support strategies to reduce exposure [4]. Evidence-based reasoning under conditions of uncertainty is a central component of STEM education and contributes to the development of resilience. Environmental crises rarely arise from a single cause or within a single system.

Pollutants can move among air, water, soil, and food systems. Climate-related risks may interact with infrastructure, health, and economic vulnerability. Although radiation is governed by physical principles, it can also influence public trust, collective memory, and risk perception. Resilience education therefore requires a

broad pedagogical repertoire that includes systems thinking, metacognition, scenario-based reasoning, citizen science, environmental responsibility, and place-based learning [12]. These approaches demonstrate the value of environmental health literacy-focused STEM education. Citizen science also clarifies how the resilience cycle operates in practice and can support both learning outcomes and community engagement [18]. Participation in environmental monitoring moves citizens from passively receiving expert knowledge toward contributing to a shared evidence base, allowing environmental risks to be discussed, interpreted, and managed more collectively.

6. EDUCATIONAL IMPLICATIONS AND FUTURE DIRECTIONS

In view of the information provided, it is evident that the relationships between environmental health literacy, radiation awareness, STEM education, and citizen science hold considerable implications for the design of educational curricula. It is imperative that environmental health issues are incorporated into STEM programmes, not as an additional or supplementary topic, but as a fundamental component of the learning environment. Key learning areas include water quality, air pollution, climate-related health risks, radiation monitoring, waste management and environmental justice. These subjects require a synthesis of scientific knowledge and civic reasoning skills. It is imperative that data interpretation, sensor use, mapping, modelling, uncertainty analysis and risk communication are integrated into these learning processes.

Radiation awareness is particularly important in STEM programmes because it combines conceptual complexity, public concern, and policy dimensions. A well-designed radiation education module can cover the fundamental principles of radiation physics, environmental transport pathways, health implications, dose estimation, measurement technologies, risk perception, and ethical decision-making. The Fukushima and Semipalatinsk cases illustrate how historical and local contexts can enhance learning [6,7]. Teacher training is pivotal to this process. Teaching environmental health issues requires pedagogical competence in areas such as uncertainty, controversial socio-scientific issues, community engagement, and risk communication. EHL-focused STEM teaching should therefore develop competence in guiding inquiry, evaluating data, facilitating socio-scientific discussion, and communicating risk responsibly. Both pre-service and in-service teacher education should incorporate environmental health science, risk communication, citizen science methods, and local partnership design. Assessment approaches must also be reconsidered. If EHL includes awareness, skills, self-efficacy, and community engagement, multiple-choice knowledge tests alone are insufficient. Broader assessment tools are therefore needed [1], including interpretation of real datasets,

scenario-based risk reasoning, performance tasks, reflective writing, risk-communication products, and evidence of collaborative problem solving. Research focused on defining and measuring EHL has consequently increased [24,25].

7. CONCLUSION

Environmental health literacy and radiation awareness are closely connected competencies in societies facing complex environmental risks. Pollution, climate-related health threats, technological accidents, and radiation exposure often create situations in which scientific uncertainty becomes part of everyday public life. In such contexts, individuals need more than general awareness of science. They need to recognise environmental problems, understand possible exposure pathways, interpret risk-related information, communicate responsibly under uncertainty, and participate in decisions that may affect public health. Environmental health literacy offers a broad foundation for these competencies, while radiation awareness represents one of its most demanding fields of application because radiation risk is technically complex, difficult to perceive directly, and socially sensitive.

STEM education can support the development of these competencies when it is connected to real environmental and health-related problems. Instead of presenting science as a set of abstract facts, a problem-based STEM approach allows students to work with measurement, data analysis, modelling, design, and evidence-informed decision-making. Studies on e-STEM, project-based STEM, climate literacy, and interdisciplinary scientific literacy indicate that students can develop a deeper understanding of environmental issues when they examine real-world problems through collaborative inquiry. The discussions addressed in this section reveal that the development of resilient communities capable of coping with environmental risks cannot be reduced to a single discipline or learning approach. Furthermore, resilience is defined as the product of an integrated effort where the processes of understanding, interpreting, and translating scientific knowledge into action reinforce each other. At this juncture, students' aptitude to transcend the mere memorisation of scientific concepts and employ this knowledge in practical, local, and socially significant scenarios constitutes a fundamental tenet of this process. It can be argued that radiation education offers the most illustrative example of this integrated approach. Radiation may be a powerful educational environment for creating a connection between environmental health literacy and STEM-based learning by combining unseen risks, quantitative data, public concern, ethical reasoning, and risk communication into a cohesive

framework. Radiation-related education could provide a bridge between scientific knowledge and public decision-making if students are able to analyse data, question the interpretation of measurements, consider the limits of certainty, and evaluate the social implications of risk communication.

One idea that is thought to help strengthen this relationship is citizen science. Initiatives like Safecast, which was created in the wake of the Fukushima nuclear accident, for example, show how the general public can significantly contribute to the creation of environmental knowledge if they are equipped with the right tools, data sources, and participatory research techniques [20]. A parallel viewpoint is offered by the findings concerning the wider environmental citizen science applications. It has been shown that taking part in monitoring studies improves learning processes, boosts self-efficacy beliefs, raises knowledge of environmental responsibility, promotes community involvement, and strengthens trust in public institutions [18]. It is clear that these activities are worth more than just gathering data. These settings have the ability to support the cooperative creation of scientific knowledge, evaluate it critically, and share it with pertinent stakeholders. These settings can also establish connections with community-level actions.

It is possible to propose that community resilience is a comprehensive result shaped by interacting processes in light of the findings outlined above. STEM education promotes the growth of evidence-based reasoning, but environmental health literacy is critical to people's capacity to translate knowledge into protective action. Radiation awareness will further support the interpretation of uncertain and invisible risks. On the other hand, citizen science can improve these procedures by providing opportunities for collective community participation, which adds a social component. Communities can become more resilient, critical, and prepared for environmental uncertainty through educational models that incorporate these aspects.It is crucial to stress that these models do not claim to completely remove environmental risks. However, these approaches could enable communities to improve their understanding of risk. When informed public decision-making is needed, they can support the use of evidence, lay the groundwork for successfully conveying ambiguity, and promote responsible behaviour. From this perspective, one of the most promising methods for building resilient communities in a world full of environmental hazards is an integrated approach that incorporates literacy, education, and engagement.

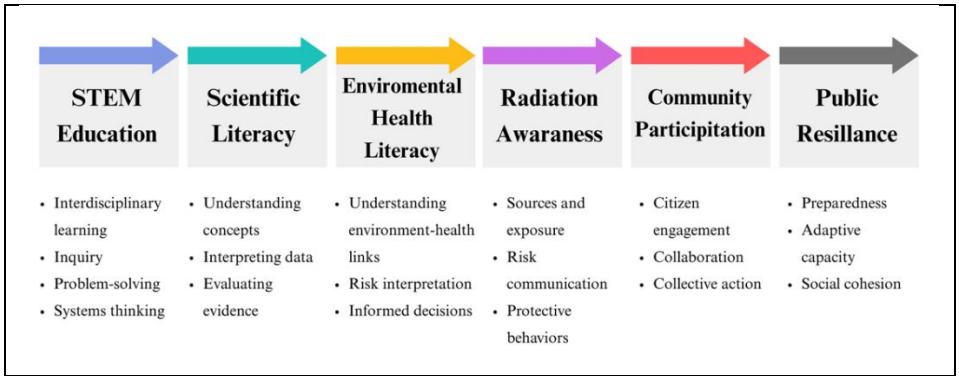


Figure 2. Conceptual pathway linking STEM education, environmental health literacy, radiation awareness, and public resilience. Developed by the author based on related literature [1,11,13]

REFERENCES

[1] Gray, K. M. (2018). From content knowledge to community change: A review of representations of environmental health literacy. *International Journal of Environmental Research and Public Health*, *15*(3), 466. https://doi.org/10.3390/ijerph15030466

[2] White, B. M., Hall, E. S., & Johnson, C. (2014). Environmental health literacy in support of social action: An environmental justice perspective. *Journal of Environmental Health*, *77*(1), 24–29.

[3] Davis, L. F., Ramirez-Andreotta, M. D., McLain, J. E. T., Kilungo, A., Abrell, L., & Buxner, S. (2018). Increasing environmental health literacy through contextual learning in communities at risk. *International Journal of Environmental Research and Public Health*, *15*(10), 2203. https://doi.org/10.3390/ijerph15102203

[4] Ramirez-Andreotta, M. D., Brody, J. G., Lothrop, N., Loh, M., Beamer, P. I., & Brown, P. (2016). Improving environmental health literacy and justice through environmental exposure results communication. *International Journal of Environmental Research and Public Health*, *13*(7), 690. https://doi.org/10.3390/ijerph13070690

[5] Evans, K. M., Bodmer, J., Edwards, B., Levins, J., O'Meara, A., Ruhotina, M., Smith, R., Delaney, T., Hoffman-Contois, R., Boccuzzo, L., Hales, H., & Carney, J. K. (2015). An exploratory analysis of public awareness and perception of ionizing radiation and guide to public health practice in Vermont. *Journal of Environmental and Public Health*, *2015*, Article 476495. https://doi.org/10.1155/2015/476495

[6] Tsubokura, M., Kato, S., Nihei, M., Sakuma, Y., Furutani, T., Nomura, S., Kami, M., & Oikawa, T. (2018). Post-Fukushima radiation education for Japanese high school students in affected areas and its positive effects on their radiation literacy. *Journal of Radiation Research*, *59*(4), 471–477. https://doi.org/10.1093/jrr/rry010

[7] Zhanibek, M., Mamyrbekov, A., & Ospanova, B. (2026). Developing radiation literacy through interdisciplinary education: A case study of the Semipalatinsk nuclear test site. *Qubahan Academic Journal*, *6*(1), 781–808. https://doi.org/10.48161/qaj.v6n1a2346

[8] Helmi, M. H., & Herliani, E. (2021). Developing sustainability literacy through STEM learning: A review. *SEAQIS Journal of Science Education*, *1*(1), 36–43. https://doi.org/10.58249/sjse.v1i1.23

[9] Koculu, A., & Girgin, S. (2022). The effect of E-STEM education on students' perceptions and engineering design process about environmental issues.

World Journal of Education, *12*(6), 49–55. https://doi.org/10.5430/wje.v12n6p49

[10] Alkair, S., Ali, R., Abouhashem, A., Aledamat, R., Bhadra, J., Ahmad, Z., Sellami, A., & Al-Thani, N. J. (2023). A STEM model for engaging students in environmental sustainability programs through a problem-solving approach. *Applied Environmental Education & Communication*, *22*(1), 13–26. https://doi.org/10.1080/1533015X.2023.2179556

[11] Chandra, A., Acosta, J., Stern, S., Uscher-Pines, L., Williams, M. V., Yeung, D., Garnett, J., & Meredith, L. S. (2013). Getting actionable about community resilience: The Los Angeles County Community Disaster Resilience Project. *American Journal of Public Health*, *103*(7), 1181–1189. https://doi.org/10.2105/AJPH.2013.301270

[12] Spellman, K. V. (2015). Educating for resilience in the North: Building a toolbox for teachers. *Ecology and Society*, *20*(1), Article 46. https://doi.org/10.5751/ES-07243-200146

[13] Finn, S., & O'Fallon, L. (2017). The emergence of environmental health literacy: From its roots to its future potential. *Environmental Health Perspectives*, *125*(4), 495–501. https://doi.org/10.1289/EHP1409337

[14] Winarni, E. W., Hambali, D., & Purwandari, E. P. (2022). Integrated PjBL-STEM in scientific literacy and environment attitude for elementary school. *International Journal of Education and Practice*, *10*(4), 303–315. https://doi.org/10.20448/edu.v8i2.3873

[15] Pertiwi, T. U., Oetomo, D., & Sugiharto, B. (2024). The effectiveness of STEM project-based learning in improving students' environmental literacy abilities. *Journal of Biological Education Indonesia (Jurnal Pendidikan Biologi Indonesia)*, *10*(2), 476–485. https://doi.org/10.22219/jpbi.v10i2.33562

[16] Hakim, A., Efwinda, S., Damayanti, P., Syam, M., Mutmainah, O., & Norsaputra, A. (2023). Improving climate literacy of high school students through physics teaching materials based on STEM. *Jurnal Pendidikan IPA Indonesia*, *12*(4), 526–536. https://doi.org/10.15294/jpii.v12i4.43188

[17] Nagele, F., Hof, A., Auer, V., & Gimenez-Maranges, M. (2024). Investigating trees as an interdisciplinary phenomenon in climate regulation: An intervention study on iSTEM education and scientific literacy in secondary schools. *International Journal of Science Education*, *47*(4), 475–493. https://doi.org/10.1080/09500693.2024.2334295

[18] Ballard, H. L., Lindell, A. J., & Jadallah, C. C. (2024). Environmental education outcomes of community and citizen science: A systematic review of empirical research. *Environmental Education Research*, *30*(6), 1007–1040. https://doi.org/10.1080/13504622.2024.2348702

[19] English, P. B., Richardson, M. J., & Garzón-Galvis, C. (2018). From crowdsourcing to extreme citizen science: Participatory research for environmental health. *Annual Review of Public Health*, *39*, 335–350. https://doi.org/10.1146/annurev-publhealth-040617-013702

[20] Brown, A., Franken, P., Bonner, S., Dolezal, N., & Moross, J. (2016). Safecast: Successful citizen-science for radiation measurement and communication after Fukushima. *Journal of Radiological Protection*, *36*(2), S82–S95. https://doi.org/10.1088/0952-4746/36/2/S82

[21] Hultquist, C., & Cervone, G. (2018). Citizen monitoring during hazards: Validation of Fukushima radiation measurements. *GeoJournal*, *83*(2), 189–206. https://doi.org/10.1007/s10708-017-9767-x

[22] Kuchinskaya, O. (2019). Citizen science and the politics of environmental data. *Science, Technology, & Human Values*, *44*(5), 871–880. https://doi.org/10.1177/0162243919858669

[23] Lindsey, M., Richmond, B., Quintanar, D. R., Spradlin, J., & Halili, L. (2022). Insights into improving risk and safety communication through environmental health literacy. *International Journal of Environmental Research and Public Health*, *19*(9), 5330. https://doi.org/10.3390/ijerph19095330

[24] Bert, F., Gea, M., Previti, C., Massocco, G., Lo Moro, G., Scaioli, G., Schilirò, T., & Siliquini, R. (2023). The environmental health literacy of Italian general population: The SPeRA cross-sectional study. *International Journal of Environmental Research and Public Health*, *20*(5), 4486. https://doi.org/10.3390/ijerph20054486

[25] Buta, B. O., Manchineri, W. S. C. S., Froner, M. B., Ecija, M. B., Cardoso, D. H. R., & Tabak, B. M. (2025). Environmental health literacy of Brazilian Indigenous people. *International Journal of Environmental Research and Public Health*, *22*(4), 625. https://doi.org/10.3390/ijerph22040625

Chapter 7

Sediment Quality and Ecological Risk Assessment Methods in Aquatic Ecosystems

Ayşegül EMİN GÜZEL[1], Ekrem MUTLU[2]

1. INTRODUCTION

Sediment is defined as the sedimentary layer formed over time on the bottoms of water bodies, such as rivers, lakes, reservoirs, lagoons, and seas, created by the breakdown of rocks, minerals, and organic matter through physical, chemical, and biological processes, and by their transport by water. Also referred to as "tortul" or "çökel" in Turkish, sediment is a naturally occurring formation in nature [1].Sediment formation is a highly dynamic cycle that begins with erosion and weathering on land surfaces, followed by transport to aquatic environments, deposition, and eventual lithification (diagenesis). This process fundamentally begins with the physical and chemical breakdown of rocks by atmospheric factors such as temperature changes, freeze-thaw cycles, rain, wind, and chemical reactions. Weathered particles are transported across the basin via rivers, winds, glaciers, or ocean currents. In areas where the kinetic energy of the transporting medium decreases (for example, in riverbeds where river flow slows down or in stagnant areas where water bodies reach the sea/lake), these particles begin to settle to the bottom and accumulate under the influence of gravity [2].In addition to river and wind movements, natural geomorphological processes such as basin-wide soil erosion, rock weathering, and coastal erosion, along with primary and secondary biological production residues in aquatic systems, and settled solid discharges from domestic, agricultural, and industrial wastewater, constitute the other primary mechanisms leading to sediment accumulation [3]. Over time, these heterogeneous sediment layers stacked on top of one another consolidate under increasing lithostatic pressure; as water within their pores is expelled, they undergo cementation and transform into sedimentary rocks [4, 5].In rivers, particles are transported in different sizes; while the largest particles are transported by rolling along the riverbed (bed load), smaller particles are carried in suspension (suspended load). Fast-flowing waters can pick up and transport larger particles more easily than slow-flowing

[1] Dr., Materials Science and Engineering / Institute of Science, Kastamonu University, Türkiye, eminguzel.a@gmail.com (ORCID: 0000-0003-1600-368X)
[2] Prof. Dr., Geography / Faculty of Humanities and Social Sciences, Kastamonu University, Türkiye, emutlu@kastamonu.edu.tr (ORCID: 0000-0002-6000-245X)

waters. Complete clarity does not exist in natural waters. Surface waters, such as rivers and lakes, in particular, contain dissolved and suspended substances that affect the color or turbidity of the water [2].

Although sediment formation is a natural part of freshwater ecosystem functioning, human activities such as dam and road construction, and changes in land use (forest/pasture) can greatly increase the amount of sediment entering the system and alter sediment quality. Sediment quality refers to the evaluation of the risks that pollutants within the sediment pose to ecosystem health; in particular, this assessment focuses on potential adverse effects on benthic (bottom-dwelling) organism populations [6].Due to their dynamic nature, rivers have high transport capacities. Both bed load and suspended load move together along the current. When the current slows down or reaches the sea, these loads begin to settle relatively more rapidly. Likewise, river water entering lakes slows down, bedload transport stops, and suspended load begins to settle to the bottom, starting with the largest particle sizes. Therefore, lakes function as natural "sediment traps" [7, 8].Lake sediments mostly consist of clastic material (clay, silt, and sand-sized sediment), organic debris, chemical precipitates, or a combination thereof [9]. These proportions vary depending on the drainage basin's structure, climate, and the lake's age. In addition, wave and current action along the shoreline leads to further erosion and sediment accumulation. A small amount of material may also be transported into the lake by wind action [10].In lakes connected to rivers, pronounced fluctuations are observed between water and sediment factors and water quality because these two systems are not isolated. Water and sediment factors play a critical role in regulating water quality in river-connected lakes. For example, in a study based on a 31-year dataset, the contribution of these factors to water quality ranged from 9% to 21% [11].

Reflecting the geological, hydrological, and ecological status of the river basin, this critical indicator layer is a fundamental dynamic component shaping the physical, chemical, and biological structure of aquatic ecosystems [3]. Ecologically located at the center of the aquatic ecosystem, sediment plays a vital role in maintaining aquatic biodiversity and trophic balance by providing habitat, shelter, and nutrient sources for an exceptionally wide group of organisms, particularly macroinvertebrates, benthic bacteria, and microalgal communities in the benthic zone [12].In addition to these ecological functions, sediment is in continuous and dynamic interaction with the overlying water body; the chemical and physical exchange of matter between these two phases directly influences the overall quality and chemical equilibrium of the aquatic ecosystem [13]. However, in basins under anthropogenic influence, particularly where industrial activities and urban settlements are intensive, sediment with an increasing pollutant load shifts away from its vital habitat role and becomes a hazardous sink that poses severe

ecotoxicological risks and chronic environmental problems for the aquatic environment [14].

In aquatic ecosystems, sediments serve as more than mere mechanical deposition areas; they act as vast reservoirs and sinks for inorganic and organic pollutants entering the system. Heavy metals, metalloids, pesticides, polycyclic aromatic hydrocarbons (PAHs), polychlorinated biphenyls (PCBs), and nutrient elements such as nitrogen and phosphorus introduced into the aquatic environment tend to rapidly precipitate by adsorbing onto suspended solids rather than remaining in the dissolved phase in the water column. Indeed, in the hydrogeological cycle, less than 1% of inorganic pollutants that threaten water quality by mass are dissolved in the water column, whereas more than 99% are stored in bottom sediment [3,15]. This immense storage capacity makes the sediment layer a powerful environmental indicator for determining the historical evolution of water quality and the pollution pressure to which the basin has been exposed, constituting a geochemical memory of anthropogenic impacts from the past to the present.The impacts of this geochemical memory layer on water quality and aquatic life occur through two fundamental mechanisms:

a) **Direct Physical Effect (Suspended Sediment Dynamics):** Fine-grained sediment particles suspended in the water column reduce light penetration, shading submerged macrophytes (aquatic plants) and disrupting primary production. Settling sediments directly inflict physical damage on biological communities by covering spawning beds and microhabitats in the benthic zone. Ecological assessments conducted across the United States have revealed that excessive sediment accumulation is the leading cause of qualitative water degradation; rivers and streams are the most heavily impacted by this physical stress, followed by lakes, reservoirs, ponds, and estuaries [16].
b) **Pollutant Carrier and Secondary Source Role (Indirect Chemical and Ecotoxicological Effect):** Sediment is not merely an element that causes physical turbidity in the water column; it functions both as a permanent sink and as a dynamic secondary source for pollutants. Heavy metals and other toxic compounds bound in bottom sediment through physicochemical processes (adsorption, precipitation, and complexation) can be remobilized and released back into the water phase, increasing their bioavailability, as environmental conditions such as pH balance, redox potential, and organic matter content change [17]. Triggered by changes in external and internal conditions, this release dynamic poses chronic threats to aquatic organisms and human welfare, particularly following acute pollution events [18].One of the clearest pieces of scientific evidence illustrating this hidden

ecotoxicological effect of sediment emerged from studies conducted in the Nidda River basin in Germany. In the study, no negative effects were observed in trials where fish embryos were exposed solely to the river's surface water, whereas marked toxic effects on embryonic development were detected in natural samples exposed to both river water and bottom sediment. As a result of this exposure, developmental delays of up to 100% and partial malformations (deformities) ranging from 10% to 25% were observed in the embryos [19]. These experimental findings clearly demonstrate that focusing solely on the water column in conventional water quality monitoring studies is inadequate for assessing ecological risks and that bottom sediments must be integrated into ecotoxicological evaluation processes.

2. Dynamic Effects of Sediment Quality on Water Quality

Sediments in aquatic ecosystems are not static, inert, or permanently locked storage areas. On the contrary, continuous, dynamic, and bidirectional physical, chemical, and biological exchanges of matter occur between the water column and the sediment layer [20]. Even microscopic changes in environmental conditions can alter the chemical form of toxic substances stored in sediment, releasing them into the water. This interaction leaves deep imprints on the sustainability of water quality and biodiversity through three primary mechanisms.

2.1. Secondary Pollution Source Mechanism

Even if external, domestic, and industrial discharges are completely cut off, or treatment plants operate perfectly, the expected improvement in water quality may be delayed or may not occur at all due to sediment. Metals and other toxic pollutants accumulated in sediment over many years dissolve and are re-released into the water column when environmental physicochemical conditions change (e.g., drops in pH, reductions in dissolved oxygen concentration, shifts in redox potential, increases in temperature and salinity). This release process is termed a 'secondary pollution source' [3,21]. Furthermore, physical impacts such as wind-induced wave action, currents, bottom-feeding activities of benthic fish, and dredging operations lead to sediment resuspension, mechanically reintroducing pollutants into the water column and triggering severe water quality problems.

2.2. Internal Nutrient Loading and Eutrophication

Particularly in shallow lakes, dam reservoirs, and slow-flowing streams, phosphorus and nitrogen dynamics are the most critical parameters directly dictating water quality [22]. Phosphorus entering the water column is adsorbed and accumulates in sediment in organic and inorganic forms. However, this

accumulation is not permanent; a continuous adsorption and desorption (release) equilibrium exists at the sediment-water interface [20]. Especially during the summer months, as water temperatures rise and anoxic (oxygen-depleted) conditions develop at the bottom, iron-phosphate complexes are reduced, and iron-bound phosphorus dissolves and is released. This situation leads to "internal phosphorus loading", which represents one of the major obstacles in lake restoration [20]. High amounts of phosphate released from sediment into the water trigger eutrophication, causing excessive proliferation of harmful blue-green algae (cyanobacteria) (algal blooms), loss of water clarity, oxygen depletion, mass fish kills, and dramatic deterioration of water quality [20].

2.3. Heavy Metal Toxicity, Bioaccumulation, and Biomagnification

Heavy metals (mercury, cadmium, lead, nickel, copper, zinc, chromium, etc.) cannot degrade in nature like organic matter, nor can they be biologically decomposed by microorganisms [23, 24, 25]. Due to their persistence and high potential for toxicity, they are among the most dangerous pollutants accumulating in sediments [12]. Organisms living in the benthic zone (benthic macroinvertebrates, crustaceans, larvae, etc.) feed by coming into direct contact with sediment or filtering sediment particles. During feeding, they ingest and accumulate heavy metals present in the sediment (bioaccumulation). When predatory fish at higher levels of the food web consume these benthic organisms, metals are transferred to higher trophic levels. During this transfer, metal concentrations increase exponentially with trophic level (biomagnification/biological accumulation) [3]. Ultimately, through human consumption of these fish, metals reach the human body, leading to neurological damage, kidney failure, organ destruction, and carcinogenic effects. Therefore, determining sediment quality is imperative for the direct protection of human and environmental health.

3. Sediment Quality Guidelines (SQGs)

To determine whether heavy metal concentrations detected in sediment will exhibit acute or chronic adverse effects on living organisms in aquatic ecosystems, international sediment quality guidelines and benchmark values have been developed. These guidelines are numerical limits derived by matching chemical concentrations with extensive databases of biological toxicity tests and benthic community structures. The four most widely used guideline limit concepts, developed by the U.S. National Oceanic and Atmospheric Administration (NOAA) and Environment Canada and broadly accepted in the literature, are as follows [26, 27, 3];

- **TEL (Threshold Effects Level):** Represents the lower threshold effect level. When the metal concentration in sediment is below the TEL, no biological or toxic effects are expected to occur in aquatic biota. It represents the biological safety zone.
- **PEL (Probable Effects Level):** The probable upper effect level. When concentrations exceed the PEL, toxic effects on aquatic organisms are expected to occur frequently and distinctly. It is the toxic danger zone.
- **ERL (Effects Range Low):** The lowest concentration threshold at which adverse biological effects are observed rarely or only in very sensitive species.
- **ERM (Effects Range Median):** Represents the mid-to-upper critical threshold at which adverse biological effects occur frequently in at least half of the tested biota.

Table 1. Most Commonly Used Sediment Quality Guidelines in Literature (mg/kg dry weight) and Pre-Industrial Reference Geochemical Background Values

Metal / Element	TEL	PEL	ERL	ERM	Ref (Background)
Copper (Cu)	35	197	70	390	45
Lead (Pb)	35	91	35	110	20
Zinc (Zn)	123	315	120	270	95
Nickel (Ni)	18	36	30	50	68
Chromium (Cr)	37.3	90	80	145	90
Cadmium (Cd)	0.6	3.53	5.0	9.0	0.3
Mercury (Hg)	0.17	0.49	0.15	1.3	0.4
Arsenic (As)	5.9	17	33	85	13
Manganese (Mn)	--	--	--	--	850
Iron (Fe)	--	--	--	--	47200
Aluminum (Al)	--	--	--	--	80000

Note: Data in the table were compiled from Smith et al. [27], Long and Morgan [26], and Earth's crust average shale values from Turekian and Wedepohl [28] for reference background values. The '--' sign indicates that no established standard limit value exists for the respective element [3].

4. Pollution and Risk Indices Evaluating Individual Metals

Various geochemical indices have been developed to measure the intensity of heavy metal accumulation in sediments, whether it originates from human activities or natural geogenic processes, and the pressure of individual pollutants on the ecosystem. These methods produce standardized mathematical outputs by comparing sediment chemical analysis results with pre-industrial reference background values [29, 30].

4.1. Contamination Factor (CF)

The Contamination Factor (CF), developed by Hakanson [29], is one of the most fundamental and widely used indices, calculated as the ratio of the metal concentration measured in sediment to the pre-industrial reference background value for that metal [3]. It is formulated as Equation 1:

$$CF = \frac{C_{HE}}{C_{HEB}} \quad (1)$$

In the equation 1, C_{HE} represents the analytically measured concentration of the respective heavy metal in the sediment sample (mg/kg), and C_{HEB} denotes the pre-industrial reference value (shale) for that metal [28] [12]. The resulting CF value is classified as follows;CF < 1: Low contamination level,1 ≤ CF < 3: Moderate contamination level,3 ≤ CF < 6: Considerable contamination level,CF ≥ 6: Very high contamination level [29]

4.2. Enrichment Factor (EF)

The Enrichment Factor (EF) is a robust method applying geochemical normalization to distinguish whether metal accumulation in sediment originates from natural geological sources (geogenic) or human-induced activities (anthropogenic) [31, 32]. To eliminate naturally occurring variations, reference elements that are highly stable in the Earth's crust and unaffected by anthropogenic inputs are utilized. Aluminum (Al) and iron (Fe) are the most commonly used reference elements. It is formulated as Equation 2 [3]:

$$EF = \frac{\frac{C_{HE}}{C_{HEB}}sample}{\frac{B_n}{B_{ref}}background} \quad (2)$$

In equation 2: $(C_{HE} / C_{ref})_{sample}$ indicates the ratio of the target metal concentration to the reference element (Al or Fe) concentration in the sample, and $(B_n / B_{ref})_{background}$ represents the ratio of background metal concentration to reference element concentration in the reference environment (Earth's crust). When the EF value is below 1.5, the metal is considered to originate entirely from natural mineral weathering. An EF > 1.5 indicates anthropogenic pollution input [12]. The classification is as follows:EF < 2: Minimal enrichment (natural origin),2 ≤ EF < 5: Moderate enrichment,5 ≤ EF < 20: Significant enrichment,20 ≤ EF < 40: Very high enrichment,EF ≥ 40: Extremely high enrichment

4.3. Index of Geoaccumulation (I_{geo})

The Index of Geoaccumulation (I_{geo}) was first introduced by Müller [30] to evaluate metal contamination in river sediments and monitor historical accumulation. The method was designed to account for fluctuations in natural rock formations and lithogenic effects. It is calculated using the following mathematical equation 3 [30]:

$$I_{geo} = \log 2 \left[\frac{C_n}{1.5 \times B_n}\right] \quad (3)$$

In the equation, C_n is the measured metal content in the sample; B_n is the geochemical background reference value for that metal. The factor '1.5' in the formula is a correction coefficient used to compensate for natural fluctuations in rock composition, lithogenic variations, and potential natural variability during analysis [3, 33]. The Index of Geoaccumulation is one of the most sensitive indices for determining land/sediment pollution and was divided by Müller into seven classes:

- $\boldsymbol{I_{geo} \leq 0}$**:** Uncontaminated (Class 0 - Practically uncontaminated)
- $\boldsymbol{0 < I_{geo} < 1}$**:** Uncontaminated to moderately contaminated (Class 1)
- $\boldsymbol{1 < I_{geo} < 2}$**:** Moderately contaminated (Class 2)
- $\boldsymbol{2 < I_{geo} < 3}$**:** Moderately to strongly contaminated (Class 3)
- $\boldsymbol{3 < I_{geo} < 4}$**:** Strongly contaminated (Class 4)
- $\boldsymbol{4 < I_{geo} < 5}$**:** Strongly to extremely contaminated (Class 5)
- $\boldsymbol{I_{geo} \geq 5}$**:** Extremely contaminated (Class 6)

4.4. Potential Ecological Risk Factor (E_r^i)

Introduced to the literature by Hakanson [29], the Potential Ecological Risk Factor (E_r^i) evaluates metal accumulation in sediment not merely as a physical quantity but also by weighting it according to the degree of biological toxicity it poses to aquatic organisms. It is calculated using the following Equation 4:

$$\boldsymbol{E_r^i = T_r^i \times C_f^i} \quad \textbf{(4)}$$

Here, T_r^i is the toxic response factor of the respective metal. The toxic response factor represents the coefficient of biological damage caused by metals to aquatic biota and humans, defined by Hakanson as follows: Mercury (Hg): 40, Cadmium (Cd): 30, Arsenic (As): 10, Lead (Pb): 5, Copper (Cu): 5, Nickel (Ni): 5, Chromium

(Cr): 2, and Zinc (Zn): 1. C_f^i is the contamination factor of the respective metal [12, 33]. The calculated E_r^i value is evaluated within the following risk categories:

- $E_r^i < 40$: Low ecological risk level
- $40 \leq E_r^i < 80$: Moderate ecological risk level
- $80 \leq E_r^i < 160$: Considerable ecological risk level
- $160 \leq E_r^i < 320$: High ecological risk level
- $E_r^i \geq 320$: Very high ecological risk level

5. Investigating Combined Ecological Effects of Multiple Metals

In aquatic ecosystems, sediments are rarely contaminated by a single metal. Agricultural, domestic, and industrial effluents generally discharge mixtures of multiple heavy metals into the environment. Therefore, it is essential to use multi-parameter indices that holistically (in an integrated manner) reveal the combined and synergistic ecological risk status created by all metals on the sediment [3].

5.1. Contamination (C_d) and Modified Degree of Contamination (mC_d)

The Degree of Contamination (C_d), developed by Hakanson [29], is an index expressing the algebraic sum of the contamination factors of all studied metals:

$$C_d = \sum_{i=1}^{n} C_f^i \quad \textbf{(5)}$$

However, this formula has a serious drawback in practical application: as the number of metals analyzed increases, the total C_d value becomes artificially inflated even when the actual pollution level is low. To resolve this issue, which rendered comparisons between studies involving different numbers of metals impossible, Abrahim and Parker [34] modified the formula by dividing it by the number of analyzed metals and proposed the Modified Degree of Contamination (mC_d) using Equation 6:

$$mC_d = \frac{\sum_{i=1}^{n} C_f^i}{n} \quad \textbf{(6)}$$

Here, C_f^i represents the contamination factor of each metal, and n is the total number of studied metals. Thanks to this formula, the contamination effect of metals is normalized. The pollution classes established for mCd are as follows:

- $mC_d < 1.5$: Very low/negligible contamination
- $1.5 \leq mC_d < 2$: Low contamination
- $2 \leq mC_d < 4$: Moderate contamination

- $4 \leq mC_d < 8$: High contamination
- $8 \leq mC_d < 16$: Very high contamination
- $16 \leq mC_d < 32$: Extremely high contamination
- $mC_d \geq 32$: Ultra-high degree of contamination

5.2. Pollution Load Index (PLI)

Developed by Tomlinson et al. [35], the Pollution Load Index (PLI) is a widely used index that quantifies the overall heavy metal load at a sampling station or across the entire study area using the geometric mean method. Its equation is as follows at Equation 7:

$$PLI = (C_{f1} \times C_{f2} \times C_{f3} \times \ldots \times C_{fn})^{(1/n)} \quad (7)$$

- The resulting PLI value is interpreted as follows:
- PLI = 0: Represents perfection.
- PLI ≤ 1: Indicates that metal levels are at natural background or reference levels, with no pollution present.
- PLI > 1: Provides conclusive proof that anthropogenic contamination and sediment quality deterioration have commenced.

5.3. Potential Ecological Risk Index (RI)

Developed by Hakanson [29], this integrated index determines the total ecological risk created by all evaluated heavy metals in the sediment ecosystem. It is calculated by summing the individual risk factors (E_r^i) using Equation 8:

$$\boldsymbol{RI = \sum_{i=1}^{n} E_r^i} \quad \textbf{(8)}$$

The RI value combines the accumulation levels and biological sensitivity coefficients of all metals into a single score. Its classification is as follows:

- **RI < 150:** Low potential ecological risk
- **150 ≤ RI < 300:** Moderate potential ecological risk
- **300 ≤ RI < 600:** Considerable potential ecological risk
- **RI ≥ 600:** Very high potential ecological risk

5.4. Mean ERM Quotient (m-ERM-Q) and Mean PEL Quotient (m-PEL-Q) Models

The Mean ERM Quotient (m-ERM-Q) and Mean PEL Quotient (m-PEL-Q) are advanced probabilistic toxicity models that mathematically estimate the probability that complex metal mixtures accumulated in sediment will exhibit acute or chronic

biological toxicity to living organisms [36, 37]. Their formulas are as follows at Equation 9:

$$\mathrm{m-ERM-Q} = \frac{\sum_{i=1}^{n} \frac{C_i}{\mathrm{ERM_i}}}{n} \quad ; \quad \mathrm{m-PEL-Q} = \frac{\sum_{i=1}^{n} \frac{C_i}{\mathrm{PEL_i}}}{n} \tag{9}$$

In the formulas, C_i represents the concentration of the target metal in the sample; ERM_i and PEL_i represent the standard benchmark values in the guidelines. Based on database matching of toxicological tests, the biological toxicity prediction scale of m-ERM-Q values is as follows [3]:

- m-ERM-Q < 0.1: 9% toxicity probability (low biological risk)
- 0.11 < m-ERM-Q < 0.5: 21% toxicity probability (moderate-low biological risk)
- 0.51 < m-ERM-Q < 1.5: 49% toxicity probability (moderate-high biological risk)
- m-ERM-Q > 1.5: 76% toxicity probability (very high biological risk)

5.5. Total Toxic Units ($\sum TUs$) and Toxic Unit Ratio

Total Toxic Units ($\sum$ TUs) is calculated by summing the ratios of measured metal concentrations in sediment to their probable effect levels (PELs). The Toxic Unit Ratio represents the percentage contribution of each metal to this total risk [3]. Their formulas are as follows at Equation 10:

$$\sum TUs = \sum_{i=1}^{n} \frac{C_i}{PEL_i} \quad ; \quad Proportional\ TU\ (\%) = \left[\frac{\frac{C_i}{PEL_i}}{\sum TUs}\right] \times 100 \tag{10}$$

This method provides critical data for researchers to diagnose which element is primarily responsible for the ecological threat (the one with the highest percentage) in sediment metal contamination.

Table 2. Numerical Evaluation and Classification Scales of Sediment Pollution and Risk Indices

Index Name	Value Range	Pollution / Risk Classification Definition
Contamination Factor (CF_i)	$CF_i < 1$ $1 \leq CF_i < 3$ $3 \leq CF_i < 6$ $CF_i \geq 6$	Low Contamination Moderate Contamination Considerable Contamination Very High Contamination
Enrichment Factor (EF)	$EF < 2$ $2 \leq EF < 5$ $5 \leq EF < 20$ $20 \leq EF < 40$ $EF \geq 40$	Minimal Enrichment Moderate Enrichment Significant Enrichment Very High Enrichment Extremely High Enrichment
Index of Geoaccumulation (I_{geo})	$I_{geo} \leq 0$ $0 < I_{geo} < 1$ $1 < I_{geo} < 2$ $2 < I_{geo} < 3$ $3 < I_{geo} < 4$ $4 < I_{geo} < 5$ $I_{geo} \geq 5$	Uncontaminated Uncontaminated to Moderately Contaminated Moderately Contaminated Moderately to Strongly Contaminated Strongly Contaminated Strongly to Extremely Contaminated Extremely Contaminated
Modified Degree of Contamination (mCd)	$mC_d < 1.5$ $1.5 \leq mC_d < 2$ $2 \leq mC_d < 4$ $4 \leq mC_d < 8$ $8 \leq mC_d < 16$ $mC_d \geq 16$	Very Low / Negligible Contamination Low Contamination Moderate Contamination High Contamination Very High Contamination Extremely / Ultra-High Contamination
Pollution Load Index (PLI)	$PLI \leq 1$ $PLI > 1$	Background Level (No Pollution) Quality Deterioration Present
Potential Ecological Risk Index (RI)	$RI < 150$ $150 \leq RI < 300$ $300 \leq RI < 600$ $RI \geq 600$	Low Ecological Risk Moderate Ecological Risk Considerable Ecological Risk Very High Ecological Risk

6. Academic Case Studies and Applications from Türkiye

To monitor sediment quality and assess ecological risk status in inland waters and coastal areas of Türkiye, Turkish scientists have conducted successful field and laboratory studies that adhere to international standards in recent years. These studies provide excellent examples of how indices can be applied in real ecosystems and how they can supply data for basin management:

6.1. Heavy Metal Accumulation and Ecological Risk Analysis in the Munzur Stream

The research titled 'Contamination and Ecological Risk Assessment of Heavy Metals in Surface Sediments of the Munzur Stream, Türkiye,' conducted by Kutlu [12], investigated the sediment quality of the Munzur Stream over 12 months with monthly sampling across 9 different stations. The Munzur Stream holds immense ecological sensitivity, as it is one of Türkiye's largest and cleanest drinking water sources, is used for drinking water supply, and hosts a gold mining site near its headwaters. Surface sediment samples (0–10 cm depth) collected in the study were dried and analyzed using an ICP-MS device, yielding an average metal accumulation ranking of Fe > Mn > Ni > Cr > Pb > Zn > Cu > Cd > Hg [12].When index results were examined, sediments of the Munzur Stream were generally found to fall within the uncontaminated class. However, in enrichment factor (EF) analyses, nickel (Ni) and manganese (Mn) exhibited a distinct behavior from other elements, reaching significant enrichment levels indicative of anthropogenic input. Particularly at Station 5, the nickel concentration reached up to 555 mg/kg dry weight, severely exceeding the probable effect level (PEL: 36 mg/kg). The study revealed that nickel enrichment stemmed from local geological rock formations, coal, and mining activities, while manganese enrichment originated from agricultural fertilizer use and domestic wastewater. In the potential ecological risk (PER) index, high chromium (Cr) concentrations significantly elevated ecological risk values; excluding chromium, the entire area remained in the low-risk category. Pearson correlation and principal component analysis (PCA) demonstrated that Cu, Cr, Ni, and Fe originated from a common source or exhibited similar geochemical behavior [12].

Table 3. Station-Based Comparison of Mean Heavy Metal Concentrations Measured in Munzur Stream Sediments and Corresponding Index Results

St. No	Cu (mg/kg)	Pb (mg/kg)	Ni (mg/kg)	Mn (mg/kg)	Fe (mg/kg)	PLI	Mean Risk Score
St. 1	33.25	50.75	116.20	982.50	179471.00	0.01	507.40 (High)
St. 2	22.75	27.25	71.25	542.50	125858.00	0.00	331.90 (Considerable)
St. 3	31.00	108.25	97.75	657.50	111178.00	0.00	319.60 (Considerable)
St. 4	32.50	15.75	243.50	555.00	126132.00	0.02	227.50 (Moderate)
St. 5	18.75	19.75	555.00	717.50	76949.00	0.01	307.50 (Considerable)
St. 6	21.25	20.25	62.00	607.50	131182.00	0.00	209.00 (Moderate)
St. 7	21.25	19.00	376.50	527.50	169703.00	0.00	248.90 (Moderate)
St. 8	4.50	9.75	21.50	133.00	22973.00	0.01	151.00 (Low)
St. 9	23.00	17.00	462.50	607.70	71006.00	0.01	247.20 (Moderate)

Note: Concentrations and risk scores in the table were directly compiled from Kutlu [12]. The average risk score was elevated by the dominant effect of chromium, and the highest value at Station 1 was associated with untreated domestic discharges and source rock composition.

6.2. Tigris (Dicle) River Sediment Quality Monitoring Study

In the study conducted by Varol [38], metal contamination in Tigris River sediments was comprehensively examined using the Index of Geoaccumulation (I_{geo}), Enrichment Factor (EF), Pollution Load Index (PLI), and multivariate statistical techniques. As a result of the research, it was determined that copper mine wastes and untreated domestic and industrial wastewater located in the Tigris River basin locally degraded sediment quality in the riverbed and posed serious risks to aquatic organisms. This study played a pioneering role in integrating geochemical normalization and multivariate statistical analysis into sediment pollution monitoring programs in Türkiye.

6.3. Method Selection and Planning Approaches in Turkish Aquatic Systems

In the most comprehensive methodological review conducted by Balık and Tunca [3], an integrated methodology was proposed for scientists investigating sediment pollution in lakes and rivers across Türkiye. The researchers emphasized that sediment studies must not only utilize physical indices measuring pollution quantity

(CF_i, I_{geo}, EF, PLI) but also incorporate biological benchmark models (RI, m-ERM-Q, m-PEL-Q) that estimate the probability of toxicity associated with this accumulation on aquatic ecosystems. This dual approach both identifies pollution levels and reveals the actual risk of this contamination on organisms, thereby providing the most scientifically accurate decisions in river basin management plans.

7. Conclusion and Sustainable Basin Management Strategies

Monitoring and managing sediment quality is critical to protecting aquatic ecosystems, maintaining biodiversity, and ensuring the safety of drinking water resources. The sediment layer acts both as a memory, reflecting the historical development of pollution in the system, and as a dynamic ticking time bomb that re-releases pollutants into the water in response to changing environmental conditions. Even if external pollutant inputs are completely halted, internal loadings originating from sediment (especially phosphorus and toxic heavy metals) can continue to degrade the quality of aquatic systems for many years.In future effective basin management planning, the implementation of the following strategic measures is recommended;

- **Holistic Monitoring Programs:** Regular sediment quality and benthic ecotoxicological monitoring tests should be conducted at the basin scale, rather than relying solely on water quality analyses.
- **Source Control and Treatment:** Discharges originating from domestic, industrial, and mining sources must be prevented from being released into water bodies without being treated to meet limit values in treatment plants. The use of chemical fertilizers and pesticides in agricultural areas should be controlled to minimize sediment transport via erosion.
- **Dredging and Remediation Activities:** In ports, lakes, and reservoirs where pollution has reached critical levels, ecological risk analyses should be conducted to execute controlled bottom sediment dredging and phosphorus inactivation techniques (e.g., aluminum sulfate applications).
- **Integrated Decision Support Systems:** Decision-makers should implement scientifically integrated decision support systems that combine pollution quantity indices with biological toxicity probability models (m-ERM-Q, m-PEL-Q, etc.).

REFERENCES

[1] Bortone, G. (2007). Sediment treatment—A general introduction. In Sustainable management of sediment resources (Vol. 2, pp. 1-10). Elsevier. https://doi.org/10.1016/S1872-1990(07)80013-4

[2] Hajigholizadeh, M., Melesse, A. M., & Fuentes, H. R. (2018). Erosion and sediment transport modelling in shallow waters: A review on approaches, models and applications. International Journal of Environmental Research and Public Health, 15(3), Article 518. https://doi.org/10.3390/ijerph15030518

[3] Balık, İ., & Tunca, E. (2015). Sedimentteki Metal Kirliliğini Değerlendiren Yöntemler Üzerine Bir Derleme [A Review of Sediment Contamination Assessment Methods]. Turkish Journal of Maritime and Marine Sciences, 1(1), 37-47.

[4] Friedman, G. M. (1964). Early diagenesis and lithification in carbonate sediments. Journal of Sedimentary Research, 34(4), 777–813. https://doi.org/10.1306/74D71195-2B21-11D7-8648000102C1865D

[5] Karahanli, E. (2026). The role of early diagenesis in shaping marine sediment records: A review. Arabian Journal of Geosciences, 19, Article 144. https://doi.org/10.1007/s12517-026-12557-6

[6] Birch, G. F. (2018). A review of chemical-based sediment quality assessment methodologies for the marine environment. Marine Pollution Bulletin, 133, 218–232. https://doi.org/10.1016/j.marpolbul.2018.05.039

[7] Brune, G. M. (1953). Trap efficiency of reservoirs. Transactions, American Geophysical Union, 34(3), 407–418. https://doi.org/10.1029/TR034i003p00407

[8] Apolinarska, K., Pleskot, K., Pełechata, A., Migdałek, M., Siepak, M., & Pełechaty, M. (2020). The recent deposition of laminated sediments in highly eutrophic Lake Kierskie, western Poland: 1 year pilot study of limnological monitoring and sediment traps. Journal of Paleolimnology, 63(4), 283-304. https://doi.org/10.1007/s10933-020-00116-2

[9] Cruz Guevara, L. E., Cruz-Ceballos, L. F., & Avendaño-Sanchez, G. M. (2024). General classification and nomenclature of sedimentary deposits and rocks, a review. Earth Sciences Research Journal, 28(2), 183–204.

[10] Sack, D. (2009). Evidence for climate change from desert basin palaeolakes. In A. J. Parsons & A. D. Abrahams (Eds.), Geomorphology of desert environments (pp. 621–636). Springer. https://doi.org/10.1007/978-1-4020-5719-9_25

[11] Geng, M., Qian, Z., Jiang, H., Huang, B., Huang, S., Deng, B., Peng, Y., Xie, Y., Li, F., Zou, Y., & Deng, Z. (2024). Assessing the impact of water-sediment factors on water quality to guide river-connected lake water environment

improvement. Science of the Total Environment, 912, Article 168866. https://doi.org/10.1016/j.scitotenv.2023.168866

[12] Kutlu, B. (2023). Contamination and Ecological Risk Assessment of Heavy Metals in Surface Sediments of the Munzur Stream, Turkey. Polish Journal of Environmental Studies, 32(1), 587-597. https://doi.org/10.15244/pjoes/154734

[13] Yang, H., Feng, Q., Zhu, J. Y., Liu, G. L., Dai, Y. R., Zhou, Q. H., Xia, S. B., Wu, Z. B., & Zhang, Y. (2024). Towards sustainable futures: A review of sediment remediation and resource valorization techniques. Journal of Cleaner Production, 435, Article 140529. https://doi.org/10.1016/j.jclepro.2023.140529

[14] Maqsood, A., & Łobos-Moysa, E. (2025). Bottom sediments as dynamic arenas for anthropogenic pollutants: Profiling sources, unraveling fate mechanisms, and assessing ecological consequences. International Journal of Molecular Sciences, 26(20), Article 10219. https://doi.org/10.3390/ijms262010219

[15] Salomons, W., & Stigliani, W. M. (Eds.). (2012). Biogeodynamics of pollutants in soils and sediments: risk assessment of delayed and non-linear responses. Springer Science & Business Media.

[16] U.S. Environmental Protection Agency. (2003). Developing water quality criteria for suspended and bedded sediments (SABS): Potential approaches [Draft]. Office of Water, Office of Science and Technology. https://archive.epa.gov/epa/sites/production/files/2015-10/documents/sediment-report.pdf

[17] Osae, R., Hayford, O., Owusu, F., & Aidoo, P. (2026). A literature review on heavy metal pollution in aquatic environments: Assessment methods, ecotoxicological impacts, and health risk implications. Marine Pollution Bulletin, 224, 119045. https://doi.org/10.1016/j.marpolbul.2025.119045

[18] He, L., Chen, G., Wang, X., Shen, J., Zhang, H., Lin, Y., Shen, Y., Lang, F. & Gong, C. (2024). Pollution characteristics and risk assessment of heavy metals in the sediments of the inflow rivers of Dianchi Lake, China. Toxics, 12(5), 322. https://doi.org/10.3390/toxics12050322

[19] Schweizer, M., Dieterich, A., Corral Morillas, N., Dewald, C., Miksch, L., Nelson, S., Wick, A., Triebskorn, R. & Köhler, H. R. (2018). The importance of sediments in ecological quality assessment of stream headwaters: embryotoxicity along the Nidda River and its tributaries in Central Hesse,

Germany. Environmental Sciences Europe, 30(1), 22. https://doi.org/10.1186/s12302-018-0150-4

[20] Topçu, A., & Pulatsü, S. (2018). Göl Ekosistemlerinde Sedimentte Fosfor Sorpsiyon Mekanizması. Ziraat Mühendisliği, (365), 45-52. https://doi.org/10.33724/zm.476134

[21] Yuan, Z., Taoran, S., Yan, Z., & Tao, Y. (2014). Spatial distribution and risk assessment of heavy metals in sediments from a hypertrophic plateau lake Dianchi, China. Environmental Monitoring and Assessment, 186, 1219-1234. https://doi.org/10.1007/s10661-013-3451-5

[22] Emin, N., & Mutlu, E. (2024). Akgöl Gölet Havzasının (Sinop-Ayancık) Su Kalitesinin Yerinde Analizlerle Tespiti ve Ağır Metal Kirliliğinin Araştırılması. Memba Kastamonu Üniversitesi Su Ürünleri Fakültesi Dergisi, 10(3), 243-252. https://doi.org/10.58626/menba.1575325

[23] Emin, N., Mutlu, E., & Emin Güzel, A. (2020). Determination the effectiveness of the cytotoxic analysis on the water quality assessments. Turkish Journal of Agriculture-Food Science and Technology, 8(2), 478-483. https://doi.org/10.24925/turjaf.v8i2.478-483.3221

[24] Mutlu, E., & Emin Güzel, A. (2019). Evaluation of some physicochemical water quality parameters of Gümüşsuyu Pond (Sinop-Erfelek). Turkish Journal of Agriculture-Food Science and Technology, 7(3), 72-77. https://doi.org/10.24925/turjaf.v7isp3.72-77.3220

[25] Mutlu, E., & Emin Güzel, A. (2024). Tekirler Baraj Gölü (Nallıhan–Ankara)'Nün Su Kalitesi Parametreleri Üzerine Araştırma. Memba Kastamonu Üniversitesi Su Ürünleri Fakültesi Dergisi, 10(2), 105-114. https://doi.org/10.58626/menba.1527460

[26] Long, E. R., & Morgan, L. G. (1991). The potential for biological effects of sediment-sorbed contaminants tested in the National Status and Trends Program. NOAA Technical Memorandum NOS OMA 52, National Oceanic and Atmospheric Administration, Seattle, WA.

[27] Smith, S. L., Macdonald, D. D., Keenleyside, K. A., Ingersoll, C. G., & Field, L. J. (1996). A preliminary evaluation of sediment quality assessment values for freshwater ecosystems. Journal of Great Lakes Research, 22(3), 624-638. https://doi.org/10.1016/S0380-1330(96)70985-1

[28] Turekian, K. K., & Wedepohl, K. H. (1961). Distribution of the Elements in some major units of the Earth's crust. Geological Society of America Bulletin,

72, 175-192. https://doi.org/10.1130/0016-7606(1961)72[175:DOTEIS]2.0.CO;2

[29] Hakanson, L. (1980). An ecological risk index for aquatic pollution control: A sedimentological approach. Water Research, 14, 975-1001. https://doi.org/10.1016/0043-1354(80)90143-8

[30] Müller, G. (1969). Index of geoaccumulation in sediments of the Rhine River. GeoJournal, 2, 108-118.

[31] Almasoud, F. I., Usman, A. R., & Al-Farraj, A. S. (2015). Heavy metals in the soils of the Arabian Gulf coast affected by industrial activities: analysis and assessment using enrichment factor and multivariate analysis. Arabian Journal of Geosciences, 8(3), 1691-1703. https://doi.org/10.1007/s12517-014-1298-x

[32] Ustaoğlu, F., Islam, M. S., & Tokatli, C. (2022). Ecological and probabilistic human health hazard assessment of heavy metals in Sera Lake Nature Park sediments (Trabzon, Turkey). Arabian Journal of Geosciences, 15(7), 597. https://doi.org/10.1007/s12517-022-09838-1

[33] Emin Güzel, A. (2023). Karadere Baraj Göleti (Taşköprü-Kastamonu) Su Kalitesinin Ve Canlılar Üzerine Etkisinin Belirlenmesinde Sediment Ve Sitotoksik Analizin Kullanımı. (Doctoral Dissertation, Kastamonu University). https://hdl.handle.net/20.500.12597/18168

[34] Abrahim, G. M. S., & Parker, R. J. (2008). Assessment of heavy metal enrichment factors and the degree of contamination in marine sediments from Tamaki Estuary, Auckland, New Zealand. Environmental Monitoring and Assessment, 136, 227-238. https://doi.org/10.1007/s10661-007-9678-2

[35] Tomlinson, D. L., Wilson, J. G., Harris, C. R., & Jeffrey, D. W. (1980). Problems in the assessment of heavy-metal levels in estuaries and the formation of a pollution index. Helgoländer Meeresuntersuchungen, 33, 566-575. https://doi.org/10.1007/BF02414780

[36] Carr, S. R., Chapman, D. C., Long, E. R., Windom, H. L., Thursby, G., Sloane, G. M., & Wolfe, D. A. (1996). Sediment quality assessment studies of Tampa Bay, Florida. Environmental Toxicology and Chemistry, 15(7), 1218-1231. https://doi.org/10.1002/etc.5620150730

[37] Long, E. R., Field, L. J., & Macdonald, D. D. (1998). Predicting toxicity in marine sediments with numerical sediment quality guidelines. Environmental Toxicology and Chemistry, 17(4), 714-727. https://doi.org/10.1002/etc.5620170428

[38] Varol, M. (2011). Assessment of heavy metal contamination in sediments of the Tigris River (Turkey) using pollution indices and multivariate statistical techniques. Journal of Hazardous Materials, 195, 355-364. https://doi.org/10.1016/j.jhazmat.2011.08.051

Chapter 8

Monitoring Water Quality and Pollution in Inland Waters: Integrated Physicochemical, Toxic-Metal, and Microbial Assessment for Human and Environmental Health

Nuray EMİN[1], Ayşegül EMİN GÜZEL[2]

1. INTRODUCTION

Water is a fundamental resource that, in general, has the capacity to self-purify over time and, in addition to its biological and ecological aspects, holds natural potential in many fields such as agriculture, energy, recreation, and transportation [1,2]. On the one hand, in parallel with the changing conditions of a rapidly developing world, demands for the use of water resources for different purposes are steadily increasing; on the other hand, more sensitive attitudes have begun to be adopted toward problems related to water, which has for many years been one of the essential elements of the natural environment. This awareness has led to a growing emphasis on the systematic re-examination and improvement of all activities that are directly or indirectly linked to the development of water resources. In this context, studies and practices aimed at the rational and planned use and protection of water resources are required [1, 3, 4, 5].Ecosystems serve humankind through the assets and quality they contain [6]. However, advancing technology, rapid population growth, global climate change, and domestic, industrial, and agricultural pollution sources exert significant pressure on water bodies, leading to water pollution and water quality problems, which are among the most important issues of our age [7, 8, 9]. They disrupt the balance of ecosystems that serve humankind, leading to rapid water pollution and environmental degradation [10].Water quality expresses the physical, chemical, and biological properties of water and is essential for ecosystems, human health, and all life forms [11]. High-quality water is considered free of pollutants and clean, whereas low-quality water is considered polluted and can be harmful [12]. Critical water quality indicators include pH, dissolved oxygen (DO), nutrients, and pollutants [9,12]. Physicochemical characterization of a water source is

[1]Assoc. Prof. Dr., Kastamonu University, Faculty of Engineering and Architecture, Department of Biomedical Engineering, Kastamonu/Türkiye, nurayemin@kastamonu.edu.tr (ORCID: 0000-0002-0859-2536)

[2]Dr., Kastamonu University, Institute of Science, Materials Science and Engineering, Kastamonu/Türkiye, eminguzel.a@gmail.com (ORCID: 0000-0003-1600-368X)

useful for identifying the basin's potential for use [10]. At the same time, determining the direct or indirect effects of water on agricultural lands or on organisms that benefit from the water source can provide information about where the water can be used.Water bodies provide habitat for a wide diversity of flora and fauna; perform important functions in hydrological and chemical cycles; and are important ecosystems in terms of groundwater storage, tourism, recreation, fisheries, and natural beauty, as well as being the most important freshwater reserves [1, 4, 5, 8]. For this reason, systematic monitoring of water quality and pollution to protect, monitor, and improve water resources is critical to the sustainability of aquatic ecosystems.This chapter defines the concept of inland water and its types; addresses the ecological, agricultural, and animal-husbandry importance of lakes, ponds, and rivers; and systematically examines water sampling methods, the physicochemical, heavy-metal, and microbial analyses used to determine water quality and pollution, the use of biological indicators, national and international standards, water quality indices, and fish farming types associated with water quality.

2. WHAT IS INLAND WATER?

Inland waters is a general term for all freshwater bodies on land or underground, lying outside seas and oceans. Lakes, ponds, dam reservoirs, rivers (river, stream, brook), marshes, wetlands, springs, and groundwater are considered within the scope of inland waters. Freshwater, which constitutes only a small portion of the total amount of water on Earth, is the most fundamental resource that organisms can use to sustain their lives [10].Inland waters constitute the terrestrial component of the hydrological cycle. Water carried to the atmosphere by evaporation returns to the surface as precipitation and, through surface runoff and infiltration, feeds rivers, lakes, and groundwater reserves. Only about 2.5% of the total water on Earth is freshwater, and most of it is held in glaciers and permanent snow cover. While a significant part of usable freshwater is in the groundwater, surface waters such as lakes and rivers—despite occupying a relatively small volume are of disproportionate ecological and economic importance.Lakes and artificial ponds, which are among the most important freshwater basins, are significant water bodies owing to the biological species richness they contain, aquaculture, cultural and nature tourism, and their role in the hydrogeological cycle [13]. Artificial ponds are constructed to meet human needs, generally within or near settlement areas; through their water surfaces and natural and cultural features, they are also of great importance as recreational resources [8]. The protection and appropriate use of water resources vary with societies' awareness of this issue and individuals' sensitivity [7, 8].

As a concrete example at the national scale, Türkiye, although rich in inland water assets, is among the countries experiencing water scarcity. There are approximately 320 natural lakes across the country; Lake Van (3,713 km²), Lake Tuz (1,300 km²), Lake Beyşehir (656 km²), and Lake Eğirdir (482 km²) are the largest natural lakes. Among the principal rivers are the Kızılırmak (1,355 km), Yeşilırmak (519 km), and Ceyhan (509 km), while transboundary rivers such as the Euphrates, Tigris, Çoruh, Aras, and Meriç also hold significant potential. Türkiye is divided into 25 main river basins. The country's average annual precipitation is approximately 574 mm, and its technically and economically usable water potential is approximately 112 billion m³; a significant part of this potential is used in agricultural irrigation [14, 15]. This situation makes monitoring the quality and ensuring the sustainable use of inland water resources a strategic priority at the national scale.

3. DIFFERENCES AMONG INLAND WATER TYPES

Inland waters are generally classified into two main groups based on water movement: still waters (lentic systems) and flowing waters (lotic systems). Still-water ecosystems such as lakes, ponds, dam reservoirs, and marshes are called lentic; flowing-water ecosystems such as rivers, streams, and brooks are called lotic systems. The main differences between these two groups lie in the speed of water movement, stratification of the water column, distribution of dissolved oxygen, temperature regime, nutrient and sediment transport, and the characteristics of the biological communities they host.

In still (lentic) waters, water movement is limited, and the water column can stratify seasonally. Especially in deep lakes, a three-layered structure forms during the summer months: the upper layer, the epilimnion, where the temperature is relatively high and uniform; the transition layer, the metalimnion (thermocline), where temperature falls rapidly with depth; and the cold bottom layer, the hypolimnion, where the temperature is fixed at about +4 °C. Overturning events in spring and autumn bring nutrient-rich bottom waters to the surface, thereby affecting productivity. In rivers (lotic systems), because the water mass flows continuously in a certain direction, the water is well mixed, stratification does not occur, oxygenation is generally high, and nutrient and sediment transport are dominant [16]. While artificial ponds constitute an example of lentic systems, the streams and brooks feeding the pond show lotic-system characteristics [17].Wetlands (marshes, peatlands, floodplains), where the soil is saturated with water or occasionally submerged, are considered a third group with transitional characteristics between lentic and lotic systems. The main differences between lentic and lotic systems are summarized in Table 1.

Table 1. Main differences between lentic and lotic inland water systems (adapted from [16]).

Feature	Lentic systems (still waters)	Lotic systems (flowing waters)
Examples	Lake, pond, reservoir, marsh	River, stream, brook, spring
Water movement	Slow or stagnant; non-directional	Continuous and unidirectional flow
Stratification	Seasonal stratification occurs (epi-/meta-/hypolimnion)	Generally absent; water well mixed
Dissolved oxygen	Varies with depth and season; may decrease near the bottom	Generally high and uniform
Nutrients/sediment	Tendency to accumulate in the basin	Transport by flow is dominant
Dominant organisms	Plankton, macrophytes, still-water fish	Benthic macroinvertebrates, rheophilic fish

4. IMPORTANCE OF LAKES AND PONDS

Lakes and ponds are vital to both ecosystems and human communities through their multifunctional roles, including water storage, climate regulation, biodiversity conservation, agricultural irrigation, animal husbandry, fisheries, drinking-water supply, recreation, and tourism. Artificial pond areas provide a new living environment for organisms [7, 8].

4.1Ecological Importance

Lakes and ponds provide habitat for a wide diversity of flora and fauna and undertake important functions in hydrological and chemical cycles. They are important ecosystems for groundwater recharge, regulation of the water table, carbon and nutrient cycles, and their effects on the microclimate [1, 4, 5, 8]. Being among the most important freshwater reserves and providing shelter and breeding grounds for aquatic organisms increases their ecological value.

4.2Importance for Agriculture

Lakes, especially artificial ponds, are important water resources for irrigating agricultural lands and gardens. A large part of Türkiye's land area is semi-arid, and irrigation is required in areas outside regions that receive sufficient and regular precipitation [18]. From this perspective, dams and ponds built to irrigate agricultural lands are of vital importance. Indeed, ponds used to irrigate agricultural lands and gardens play a fundamental role in the sustainability of regional agricultural production [19].

4.3Animal Husbandry

Lakes and ponds are important resources in animal husbandry for meeting animals' water needs and for irrigating pastures. The streams feeding the pond and the surrounding wooded areas also provide water for wildlife; wild animals such as wild boar, bear, wolf, jackal, and hare can be encountered around lakes and ponds [17]. For this reason, the quality of lake and pond waters must remain within appropriate limits for the health of both domestic and wild animals.Lakes and ponds also host a wide range of organisms from phytoplankton and macrophytes to benthic invertebrates, fish, and waterbirds whose differing sensitivities to changes in water quality make them useful biological indicators of ecological status. In particular, excessive nutrient loads of nitrogen and phosphorus from domestic, industrial, and agricultural sources drive eutrophication: algal blooms block light, and their subsequent decomposition depletes dissolved oxygen, forming oxygen-poor bottom zones. Eutrophication is therefore one of the principal pollution-driven pressures that degrade lake water quality, and it is routinely tracked through these biological and physicochemical responses.

5. IMPORTANCE OF RIVERS AND STREAMS

Rivers and streams are lotic water systems that flow continuously from land toward the seas. They play a vital role in providing the natural drainage of basins, transporting sediment and nutrients, feeding lakes and dam reservoirs, supplying drinking and irrigation water, and supporting fisheries.

5.1Ecological Importance

Rivers are corridors that provide the transport of matter and energy within basins; by carrying water, sediment, and nutrients from source areas to lower basins, they feed wetlands, lakes, and coastal ecosystems. Owing to their high oxygenation capacity and their flow-dependent self-purification (self-cleaning) properties, they are ecologically dynamic systems [1]. As in the example of an artificial lake formed by the confluence of two streams feeding a pond, rivers constitute the fundamental water source of lakes and ponds [17].

5.2Importance for Agriculture

Rivers are among the principal water resources used directly to irrigate agricultural lands along their banks. However, chemicals used on agricultural lands and domestic and industrial waste can be transported by the river and affect water quality [20]. For this reason, monitoring the quality of irrigation rivers is important for agricultural sustainability.

5.3Animal Husbandry

Rivers are an accessible water source for watering animals and feeding livestock in rural areas. The quality of river water is decisive for animal health and, indirectly, for the safety of milk and meat production; for this reason, the pollutant sources transported along the river (point and non-point) must be monitored.Rivers and streams host benthic macroinvertebrates, diatoms, fish, and riparian communities; among these, benthic macroinvertebrates hold a special place as biological indicators of river water quality, because they occur in most river environments, have limited mobility and so cannot escape pollution events, differ in their pollution tolerance among taxa, and can accumulate toxic substances that may be undetectable in the water itself [21]. The EPT groupsEphemeroptera (mayflies), Plecoptera (stoneflies), and Trichoptera (caddisflies) require high dissolved oxygen and are sensitive to organic pollution, so their high diversity indicates good water quality, whereas dominance by pollution-tolerant taxa signals degradation. Biotic indices based on taxa tolerance (e.g., BMWP and the EPT index) and diatom indices are widely used to classify river water quality; in Türkiye, for example, the effect of trout farms on benthic macroinvertebrate communities in the Değirmen Stream (Kastamonu) illustrates how pollution alters these communities [22].

6. WATER SAMPLING METHODS

The reliability of the results obtained in water quality studies largely depends on the accuracy of the sampling stage. For example, determining the study area, correctly selecting the sampling points (stations), using appropriate sample containers, transporting the samples to the laboratory without deterioration, and storing them under appropriate conditions until analysis are critical stages that determine the representativeness of the results.

6.1 Selection and Quantity of Sample Containers

The sample containers used for water sampling are washed by passing them, in order, through an acid bath (1% HCl) and pure water before going into the field. The sample containers, then rinsed with pure water, are left to dry in an oven [23]. Sample containers are immersed approximately 15 cm below the water surface and filled by the water's own gravity; water samples are collected in this way. To prevent deterioration, the collected water samples are transported to the laboratory within 3 hours in thermally insulated transport boxes and stored at +4 °C [24]. For samples set aside for heavy-metal analysis, it is important to use acid-washed containers to prevent metal ions from adhering to the container surface and to preserve the samples appropriately.

6.2 Sampling Points and Station Layout

Sampling stations are selected to represent the entire water body under study. In a pond study, in addition to stations representing the different parts of the lake, stations are also established on the streams feeding the pond. For example, in the Akgöl Pond study, in situ water quality analyses and sampling for heavy-metal pollution were carried out seasonally at four (4) stations representing the lake and on two (2) streams feeding the pond [17]. Similarly, in the İncesu Pond study, surface-water samples were collected from three (3) stations identified in the study area [19].Sampling is repeated to cover the spring, summer, autumn, and winter periods and monitor seasonal variation. When the findings obtained across the stations are close to one another, the results can be evaluated as the pond average [17]. In station layout, criteria such as proximity to pollutant sources (stream inlets, agricultural lands, settlements), water depth, and accessibility are considered.

7. ANALYSES USED TO DETERMINE WATER QUALITY AND POLLUTION

In determining water quality and pollution, in situ (field) measurements, physicochemical analyses performed in the laboratory, heavy-metal analyses, microbial analyses, and supporting (e.g., cytotoxic) analyses are used together. The holistic evaluation of these analyses enables the determination of the quality class of the water source and of possible pollutant pressures.

7.1 In-Situ Field Analyses

Some water quality parameters are measured in the field (in situ) because they may change during transport of the sample to the laboratory. Among the water quality parameters, dissolved oxygen (DO), temperature, pH, salinity, and electrical conductivity (EC) are measured in the field using a portable field-type multiparameter device (e.g., Hach Lange HQ40D) [17]. These parameters reflect the instantaneous physicochemical status of the water body and are fundamental indicators in monitoring seasonal variation.

7.2 Physicochemical Analyses

Physicochemical analyses cover the measurements that reveal the physical and chemical properties of water. The total amount of dissolved salt ions in the water determines its salinity; chemicals used on agricultural lands and domestic and industrial wastes carried into the water by precipitation can increase the concentration of salt ions [20]. Electrical conductivity is related to the concentration of ions in the water, and it increases with increasing ion

concentration [25]. The pH of water is an important parameter that affects the biological composition of ecosystems; most aquatic organisms prefer a pH between 6.5 and 8.5 for life [12]. Dissolved oxygen is essential for the survival of fish and other aquatic organisms; low DO levels may indicate pollution in the basin. Turbidity indicates how clear the water is; high turbidity can block sunlight, affect aquatic plants, and increase due to organic waste and algae [12].

7.3 The Link Between Field and Laboratory Physicochemical Analyses

The parameters measured in the field and the physicochemical parameters determined in the laboratory are not two independent categories; they are two stages of the same physicochemical characterization. Physicochemical evaluation actually begins in the field. Quantities read in the field, such as temperature, pH, conductivity, salinity, and dissolved oxygen, are both a precursor to and an interpretive framework for parameters such as ion concentrations, hardness, nutrients, and heavy metals measured in the laboratory. For this reason, field measurements should not be evaluated individually but collectively, through the physicochemical relationships among them.

One of the most striking of these relationships is that between ionic load and electrical conductivity. Because the ions formed by the dissociation of salts dissolved in water carry an electric charge, conductivity is a direct indicator of the total amount of dissolved ions (and hence of total dissolved solids and salinity); as ion concentration increases, conductivity also increases [25]. Indeed, in the Akgöl Pond data, a strong positive correlation ($r \approx 0.75$) was observed between conductivity and salinity, with conductivity reaching its highest value in autumn, when agricultural return waters were influential [17]. This relationship allows a rapid preliminary estimate of mineralization level to be obtained from the conductivity measurement before detailed ion analysis is carried out in the laboratory. In practice, total dissolved solids (TDS) are estimated approximately from conductivity by the following relationship:

$$TDS\ (mg/L) \approx k_e \times EC\ (\mu S/cm)$$

Here, k_e is an empirical coefficient that depends on the ionic composition of the water and typically ranges from approximately 0.55 to 0.75 for most natural waters. This approximate relationship allows a TDS estimate to be obtained from the field conductivity reading before the laboratory step; the exact value is determined in the laboratory by ion chromatography or gravimetric methods.The second fundamental relationship expresses the relationship between dissolved oxygen and temperature (and salinity/conductivity). Because the solubility of

gases in water decreases as temperature and ion concentration increase, the equilibrium (saturation) solubility of oxygen decreases in warm and more mineralized waters. For this reason, the DO measured in the field varies inversely with temperature and conductivity. For example, in the Akgöl Pond water-analysis data, negative correlations were found between DO and temperature ($r \approx -0.53$) and between DO and conductivity ($r \approx -0.64$) [17]. At this point, the distinction between the raw DO concentration (mg/L) and oxygen saturation (%) becomes important: oxygen saturation is the ratio of the measured DO to the equilibrium solubility calculated for the temperature, pressure (altitude), and salinity conditions at that moment. In this way, the temperature-dependent solubility effect is eliminated, and values clearly below 100% may indicate organic pollution and decomposition, while values above 100% may indicate intense photosynthetic production (supersaturation). Oxygen saturation is defined as the ratio of the measured concentration to the equilibrium (saturation) solubility (Equation 1).

$$DO\% = (C / C^*) \times 100 \tag{1}$$

Here, C is the measured dissolved-oxygen concentration (mg/L), and C* is the equilibrium oxygen solubility of the water with the atmosphere at the temperature, salinity, and pressure at that moment (mg/L). The equilibrium solubility C* is calculated for fresh and saline waters by the semi-empirical equations derived by Benson and Krause, which are accepted as standard today [26, 27]. Its form at sea level (1 atm), as a function of temperature (T, Kelvin) and salinity (S), is given in Equation 2.

$$\ln C^* = \left(-139.34411 + \frac{1.575701\times10^5}{T} - \frac{6.642308\times10^7}{T^2} + \frac{1.243800\times10^{10}}{T^3} - \frac{8.621949\times10^{11}}{T^4}\right) - S\left(0.017674 - \frac{10.754}{T} + \frac{2140.7}{T^2}\right) \tag{2}$$

This equation quantitatively expresses that the solubility of oxygen decreases with increasing temperature and salinity. However, this form of the equation is valid for sea-level pressure (1 atm); the altitude of the water basin above sea level also directly affects oxygen saturation. Because atmospheric (barometric) pressure decreases as altitude increases, the equilibrium oxygen solubility of the water with the atmosphere also decreases proportionally. This effect is taken into account through a correction factor based on the ratio of the local barometric pressure (P) to sea-level pressure (P_0 = 760 mmHg) (Equation 3).

$$C^*_P = C^* \times (P / P_0) \quad (3)$$

In more precise calculations, a full pressure correction that also includes the water-vapor pressure is used [27]. If the altitude correction is ignored, saturation percentages measured in high-altitude basins may appear systematically higher. For example, in a basin such as Akgöl Pond, located at an altitude of approximately 1,200 m above sea level [17], because barometric pressure is markedly lower than at sea level, the equilibrium oxygen solubility (C*) and hence the saturation reference for water at the same temperature are lower; for this reason, a pressure correction according to the altitude of the basin must be applied in the oxygen-saturation assessment.PH is also part of this network; because the consumption of carbon dioxide during photosynthesis makes the water more alkaline, pH varies with temperature and biological productivity and, in the Akgöl data, shows a very strong positive correlation with temperature ($r \approx 0.93$) [17]. Consequently, temperature is a central variable that simultaneously affects gas solubility, ionic equilibria, and biological activity. Interpreting these field-measured parameters in relation to one another and to the laboratory results provides a far more reliable water quality assessment than any single parameter could provide on its own; this integrated interpretation also forms the basis of the correlation analyses (Pearson, Spearman) addressed in the following section.

7.4 Heavy Metal Analyses

The heavy-metal content that determines water quality covers the analysis of elements such as iron, lead, copper, cadmium, mercury, nickel, and zinc. These analyses are carried out on appropriately collected and preserved samples using sensitive instruments such as ICP-OES (Inductively Coupled Plasma – Optical Emission Spectrometry) [17]. Heavy metals can accumulate in the bodies of aquatic organisms and, through the food chain, threaten ecosystems and human health; for this reason, they are of great importance for determining the pollution of water resources [24, 28]. For example, lead is a heavy metal with high toxicity and can affect neurological, cardiovascular and renal functions; cadmium and mercury, even at low concentrations, can pose health risks through bioaccumulation [29, 28].

7.5 Microbial Analyses

Microbial analyses assess the suitability of water for drinking, domestic use, irrigation, and recreation by determining the microorganism load in the water. Because it is not practical to search for every pathogenic microorganism in water individually, indicator organisms present in large numbers in human and animal

feces that signal possible fecal pollution are used [30]. In this way, the hygienic status of lake, pond, and river water can be evaluated indirectly but reliably.The main indicator groups are total coliforms, fecal (thermotolerant) coliforms, Escherichia coli, enterococci, and the heterotrophic plate count (HPC). Total coliforms are Gram-negative, non-spore-forming rod bacteria that produce acid and gas from lactose at 37 °C; however, because they can also be found in nature, they are weak as a stand-alone indicator of fecal pollution. Fecal coliforms are feces-derived coliforms, and their most typical member is E. coli, found only in the intestines of warm-blooded animals. For this reason, E. coli is accepted as the most reliable indicator of fresh fecal pollution [31, 30]. The heterotrophic plate count, rather than being a direct health indicator, is used as a warning parameter signaling general deterioration in water quality.After sampling, microorganisms in water samples are determined mainly by three approaches: in the membrane filtration method, usually 100 mL of sample is passed through a membrane filter containing a selective medium and the retained colonies are counted (this method is often accepted as the gold standard); in the most probable number (MPN) method, serial dilutions are inoculated into liquid media to obtain a statistical estimate; and enzyme-substrate-based presence/absence tests rapidly provide presence–absence information without giving a concentration. On media such as chromogenic coliform agar (CCA), coliforms and E. coli form colonies of distinguishing colors [30]. In Türkiye, coliform and E. coli analysis of waters is largely carried out according to the TS EN ISO 9308-1 standard.It should be remembered that a negative result does not guarantee absolute safety; some pathogens, such as viruses and Cryptosporidium, are more resistant to disinfection than indicator bacteria [30]. In addition, whether or not water has been freed of microorganisms can also be checked by sterilization procedures applied before advanced tests, such as in vitro cytotoxicity and bioavailability analyses [19].

7.6 Other Analyses

Although conventional physicochemical and microbial analyses largely reveal the quality characteristics of water, they can be limited in evaluating water's direct effects on living organisms. To address this shortcoming, in vitro cytotoxic assays have been developed to directly assess the effects of water on organisms [19]. In this approach, water samples are tested as reactive agents on mammalian cell cultures (e.g., mesenchymal stem cells and endothelial cell lines), and the IC50 value and bioavailability are determined using methods such as the MTT assay, which measures mitochondrial dehydrogenase activity in the cells. The results obtained can reveal direct tissue-level effects that conventional methods may

overlook and can make an important contribution to routine water quality analyses [19]. In addition, bioaccumulation and health-risk assessments conducted on aquatic organisms (e.g., fish) are used to evaluate the effects of water on living organisms [24].

8. NATIONAL AND INTERNATIONAL STANDARDS USED IN WATER QUALITY ANALYSES

The findings obtained from water quality analyses are interpreted by comparison with national and international standards. In Türkiye, the primary national regulation governing the evaluation of surface water resources is the Surface Water Quality Regulation (SWQR). According to the classification scheme in the relevant annex of the regulation (Quality Criteria for Inland Surface Water Resources by Class), water resources are classified as Classes I, II, III, and IV; Class I waters represent the highest quality [32]. The measured physicochemical parameters and heavy-metal concentrations are compared with these criteria to determine the water body's quality class [17, 33].A water source is evaluated in a given class only if it meets all parameter values specified for that class; exceeding the limit of any parameter lowers the water to a lower quality class. For example, in the Akgöl Pond study, the measured parameters and heavy-metal contents were compared with the SWQR criteria, and the pond water was found to fall within the Class I water category [17].At the international level, the World Health Organization (WHO) Drinking-water Quality Guidelines, the United States Environmental Protection Agency (US-EPA) criteria, and the European Union Water Framework Directive (2000/60/EC) are common references. The WHO guideline defines guideline values for chemicals of health significance [34]. Some national (SWQR) and international (WHO) limit/guideline values are compared in Table 2. In cytotoxic analyses evaluating the effects of water on living organisms in vitro, the international ISO-EN 10993 standard, used in the biocompatibility assessment of medical devices and materials, is used as the basis [19].

Table 2. Some SWQR Class I surface-water and WHO drinking-water guideline values for selected parameters [32, 17, 34]. It should be noted that drinking-water and surface-water criteria serve different purposes.

Parameter	SWQR Class I (surface water)	WHO drinking-water guideline value
pH	6.5 – 8.5	~6.5 – 8.5 for potability
Dissolved oxygen	≥ 8 mg/L	—
Iron (Fe)	0.3 mg/L	No health-based value (aesthetic ~0.3 mg/L)
Lead (Pb)	10 µg/L	10 µg/L
Copper (Cu)	20 µg/L	2000 µg/L
Nickel (Ni)	20 µg/L	70 µg/L
Zinc (Zn)	200 µg/L	No health-based value
Cadmium (Cd)	—	3 µg/L
Mercury (Hg)	—	6 µg/L (inorganic)
Arsenic (As)	—	10 µg/L
Nitrate (NO_3)	—	50 mg/L

9. WATER QUALITY PARAMETERS AND CALCULATION OF INDICES

Water quality indices (Water Quality Index, WQI) have been developed to summarize the many parameters that constitute water quality in a single numerical value and to allow different water bodies to be compared. Indices are calculated by combining selected parameters (e.g., DO, pH, turbidity, nutrients, conductivity, heavy metals) using weights and expressing the overall quality of the water as a single score [35, 36].Among the indices widely used in the literature is the National Sanitation Foundation Water Quality Index (NSF-WQI) [35]. In addition, WQI applications based on key parameters in systems with high sediment loads [36] and spatial assessments that combine index calculations with Geographic Information Systems (GIS) [25] enable interpretation of water quality at the basin scale. When index results are evaluated alongside classification systems such as the SWQR, the water source's quality status can be assessed holistically.One of the most widely used approaches is the weighted arithmetic water quality index. This method consists of four basic steps [37, 38]:

- Unit (relative) weight: For each parameter, $W_i = K / S_i$ is calculated, where S_i is the standard (permissible) value of the parameter and $K = 1 / \Sigma(1/S_i)$ is a proportionality constant. Thus, parameters with a small standard (i.e., a stricter limit) receive a larger weight, and the sum of the weights equals 1.

- Quality rating: For each parameter, $q_i = |(V_i - V_o) / (S_i - V_o)| \times 100$ is calculated. V_i is the measured value, and V_o is the ideal value ($V_o = 0$ for parameters other than pH; $V_o = 7$ for pH).
- Sub-index: The contribution of each parameter is found by $SI_i = W_i \times q_i$.
- Aggregation: All parameters are converted into a single score by $WQI = \Sigma SI_i$.

The resulting WQI value is matched to quality classes. According to a commonly used classification, 0–25 indicates excellent, 26–50 good, 51–75 poor, 76–100 very poor, and above 100 water quality unsuitable for drinking; however, the class ranges and the selected parameters may vary from study to study [38].An example calculation is shown in Table 3. Using the standard and measured values for three parameters (pH, nitrate, and lead), the unit weights, quality ratings, and sub-indices were calculated; the sum of the sub-indices was WQI ≈ 50. This value places the example water at the upper limit of the "good" class. The example also shows that the lead parameter, whose standard is very small (S_i = 0.01 mg/L), makes a disproportionately large contribution to the index.

Table 3. Example calculation for the weighted arithmetic WQI [37, 38]. S_i: standard value, V_i: measured value.

Parameter (S_i; V_i)	W_i / q_i	Sub-index SI_i
pH (8.5; 8.0)	0.0012 / 66.7	0.08
Nitrate (50; 20 mg/L)	0.0002 / 40.0	0.01
Lead (0.01; 0.005 mg/L)	0.9986 / 50.0	49.93
Total (WQI)	$\Sigma W_i \approx 1.00$	≈ 50.0 (good)

Statistical methods are also used in determining the relationships among parameters. The Pearson correlation, which measures the linear relationship between variables, and the non-parametric Spearman's rho correlation are widely used in interpreting the relationships among water quality and pollution parameters (e.g., the relationships among DO, pH, salinity, temperature, and conductivity with heavy metals) [39, 40, 41].

9.1 Statistical Analyses and Selection of the Appropriate Test

The correct interpretation of water quality data depends on selecting the statistical test appropriate to each analysis objective. The first step in test selection is to determine the distribution of the data: whether the data conform to a normal distribution should be tested with the Shapiro–Wilk test for small sample groups ($n < 50$) and with the Kolmogorov–Smirnov test for large groups

($n \geq 50$) [42]. This result determines whether parametric or non-parametric tests will be used in subsequent steps. Analyses are usually carried out in statistical programs such as SPSS, and a significance level of $p < 0.05$ is taken as the basis [17].The following pairings summarize which test is appropriate for which analysis:

- For descriptive summaries, the central tendency and variability of each parameter should be reported as the mean ± standard deviation, along with the minimum and maximum values.
- For comparing more than two groups (e.g., stations or seasons): if the data are normally distributed, one-way analysis of variance (ANOVA) should be applied, followed by the Tukey HSD multiple-comparison test to determine which pairs the differences among groups arise from; if the data are not normally distributed, the non-parametric Kruskal–Wallis test should be used, followed by the Dunn multiple-comparison test.
- For comparing only two groups, the independent-samples t-test should be preferred for a normal distribution and the Mann–Whitney U test for a non-normal distribution.
- To determine the relationship between two parameters, the Pearson correlation coefficient should be used if both variables are normally distributed and the relationship is linear; Spearman's rho should be used if the variables are not normally distributed, are ordinal, or the relationship is monotonic [41].
- To distinguish pollutant sources and evaluate multiple parameters together, multivariate methods such as principal component analysis (PCA) / factor analysis, and cluster analysis (CA) for grouping sampling stations according to their similarities, should be employed [40].

For example, in the Akgöl Pond study, differences among seasons and stations were evaluated using one-way ANOVA with Tukey's test ($p < 0.05$), while relationships among parameters were examined using both Pearson and Spearman correlation analyses [17]. This approach shows that, rather than relying on a single test, using tests appropriate to the data's distributional characteristics together increases the reliability of the water quality assessment.

10. FISH FARMING TYPES ACCORDING TO WATER QUALITY

Fish farming (aquaculture) is directly related to water quality characteristics; temperature, dissolved oxygen, pH, salinity, and pollutant levels determine which species can be farmed in which water source. Cold-water species that require high dissolved oxygen and low temperature (e.g., trout) and warm-water species

tolerant of higher temperatures require different water quality conditions.In general, a pH range of 6.5–8.5 is suitable for most farmed fish species; dissolved oxygen is expected to be kept at least at 4 mg/L, preferably at 5–10 mg/L, toxic ammonia below 0.5 mg/L, and nitrite below approximately 0.75 mg/L [43]. The main factor distinguishing the species is temperature and, accordingly, oxygen demand. While cold-water species require clear waters with low temperatures and high oxygen levels, warm-water species are tolerant of higher temperatures and relatively low oxygen levels. The water quality requirements of the main species groups are summarized in Table 4.

Table 4. Requirements of the main fish-farming species groups by water quality [43].

Species group / example species	Optimum temperature	Dissolved oxygen and pH
Cold-water — rainbow trout (O. mykiss)	10–16 °C (5–20 °C); critical upper ~22–26 °C	Requires high O_2 (preferably above 7 mg/L); pH 6.5–8.5
Warm-water — common carp	~20–30 °C	More tolerant of low O_2 (min ~4 mg/L); pH 6.5–8.5
Warm-water — tilapia (O. niloticus)	28–32 °C (18–34 °C); critical lower ~10–14 °C	Tolerant of low O_2; pH 6.5–8.5

For example, in Akgöl Pond, most dissolved-oxygen values were measured above 8 mg/L; the pond water was classified as Class I according to the SWQR, and, owing to the low-temperature and high-oxygen conditions, the water was assessed as suitable for trout (rainbow trout) farming [17]. In contrast, in warmer waters with relatively low oxygen, warm-water species such as common carp and tilapia are preferred. This example demonstrates the decisive role of monitoring water quality parameters in determining which fish species a water source is suitable for farming. In addition, heavy metal and microbial pollution levels are critical criteria that must be monitored to ensure the food safety of the farmed product [24].

11. CONCLUSION

Inland waters, lakes, ponds, and rivers in particular, are ecosystems of vital importance in terms of freshwater reserves, biodiversity, agriculture, animal husbandry, fisheries, and recreation. However, developing technology, rapid population growth, climate change, and domestic, industrial, and agricultural pollution sources exert increasing pressure on these resources [7, 8].Water

pollution occurs when harmful substances contaminate water bodies and damage ecosystems; depending on their source, it is classified as point-source or non-point-source pollution. Monitoring these pressures requires the holistic use of accurate sampling, field and laboratory measurements, heavy-metal and microbial analyses, and supporting cytotoxic assessments. Comparing the measured parameters with national (SWQR) and international standards and summarizing them using water quality indices enables determination of the water source's quality status and usage potential. Thus, the systematic monitoring of water quality and pollution required to sustain inland aquatic ecosystems can be carried out. Beyond their physicochemical and chemical characterization, aquatic organisms from phytoplankton to benthic macroinvertebrates and fish—also function as biological indicators of water quality. Integrating physicochemical, heavy-metal, and microbial analyses with these biological indicators reveals not only the instantaneous quality of the water source but also its health and its trend over time. The information thus obtained provides a basis for many usage decisions, from drinking-water supply to irrigation, and from animal husbandry to the farming of the appropriate fish species. In conclusion, protecting inland water resources and human health requires a systematic, continuous monitoring approach in which accurate sampling, multifaceted analysis (physicochemical, heavy-metal, and microbial), comparison with standards, index-based summarization, and biological indicators are conducted in tandem.

REFERENCES

[1] Daigger, G. T. (2009). Evolving urban water and residuals management paradigms: Water reclamation and reuse, decentralization, and resource recovery. Water Environment Research, 81(8), 809–823.

[2] De Groot, R. S., Wilson, M. A. & Boumans, R. M. J. (2002). A typology for the classification, description and valuation of ecosystem functions, goods and services. Ecological Economics, 41(3), 393–408.

[3] Hajkowicz, S. & Collins, K. (2007). A review of multiple criteria analysis for water resource planning and management. Water Resources Management, 21, 1553–1566.

[4] Hu, F., Liu, J., Zhou, S. & Han, S. (2018). Research and exploration on rational utilization of urban water resources and environment. Desalination and Water Treatment, 122, 165–169.

[5] Kosolapova, N. A., Matveeva, L. G., Nikitaeva, A. Y. & Molapisi, L. (2021). The rational use of water resources in the strategy of Industry 4.0. Water Resources Management, 35(9), 3023–3041.

[6] Kocataş, A. (1997). Ekoloji ve Çevre Biyolojisi [Ecology and Environmental Biology]. Ege University Press.

[7] Emin Güzel, A. & Mutlu, E. (2023). Su kalitesi ve kirliliğinin iyonik bileşen içeriği tespiti ile değerlendirilmesi. Journal of Anatolian Environmental and Animal Sciences, 8(4), 707–713.

[8] Meyerhoff, J., Klefoth, T. & Arlinghaus, R. (2019). The value artificial lake ecosystems provide to recreational anglers: Implications for management of biodiversity and outdoor recreation. Journal of Environmental Management, 252, 109580.

[9] Mutlu, E. & Emin Güzel, A. (2019). Gümüşsuyu Göleti (Erfelek-Sinop)'nin bazı fizikokimyasal su kalitesi parametrelerinin değerlendirilmesi. Turkish Journal of Agriculture - Food Science and Technology, 7, 72–77.

[10] Yılmaz, M. L. & Peker, H. S. (2013). Su kaynaklarının Türkiye açısından ekono-politik önemi ekseninde olası bir tehlike: Su savaşları. Çankırı Karatekin University Journal of the Faculty of Economics and Administrative Sciences, 3(1), 57–74.

[11] Şimşek, A. & Mutlu, E. (2023). Assessment of the water quality of Bartın Kışla (Kozcağız) Dam by using geographical information system (GIS) and water quality indices (WQI). Environmental Science and Pollution Research, 30(20), 58796–58812.

[12] Sagan, V., Peterson, K. T., Maimaitijiang, M., Sidike, P., Sloan, J., Greeling, B. A., Maalouf, S. & Adams, C. (2020). Monitoring inland water quality using remote sensing: Potential and limitations of spectral indices, bio-

optical simulations, machine learning, and cloud computing. Earth-Science Reviews, 205, 103187.
[13] Mutlu, E., Demir, T., Kutlu, B. & Yanık, T. (2013). Determination of water quality parameters in Sivas - Kurugöl Lake. Iğdır University Journal of the Institute of Science and Technology, 3(1).
[14] Ministry of Agriculture and Forestry (2023). Türkiye water resources and water availability data (SYGM). https://www.tarimorman.gov.tr (Accessed August 2026).
[15] WWF-Türkiye (2023). Current status of water resources in Türkiye. https://www.wwf.org.tr (Accessed August 2026).
[16] Wetzel, R. G. (2001). Limnology: Lake and River Ecosystems (3rd ed.). Academic Press, San Diego.
[17] Emin, N. & Mutlu, E. (2024). Akgöl Gölet Havzasının (Sinop-Ayancık) su kalitesinin yerinde analizlerle tespiti ve ağır metal kirliliğinin araştırılması. Menba Journal of Kastamonu University Faculty of Fisheries, 10(3), 243–252.
[18] Kapluhan, E. (2013). Türkiye'de kuraklık ve kuraklığın tarıma etkisi. Marmara Coğrafya Dergisi, (27), 487-510.
[19] Emin, N., Mutlu, E. & Emin Güzel, A. (2020). Determination the effectiveness of the cytotoxic analysis on the water quality assessments. Turkish Journal of Agriculture - Food Science and Technology, 8(2), 478–483.
[20] Mutlu, E. & Paruğ, Ş. Ş. (2018). Dereköy Göleti'nin (Kilimli-Zonguldak) bazı su kalitesi parametrelerinin incelenmesi. Menba Journal of Fisheries Faculty, 4(2), 20–28.
[21] Bonada, N., Prat, N., Resh, V. H. & Statzner, B. (2006). Developments in aquatic insect biomonitoring: A comparative analysis of recent approaches. Annual Review of Entomology, 51, 495–523.
[22] Yaman, H. & Uzbilek, M. (2020). Değirmen Deresinin (Kastamonu) üzerindeki alabalık işletmelerinin bentik makroomurgasızlara etkisi. Menba Journal of Kastamonu University Faculty of Fisheries, 6(2), 74–85.
[23] Boyd, C. E. & Tucker, C. S. (1992). Water Quality and Pond Soil Analyses for Aquaculture. Alabama Agricultural Experiment Station, Auburn University.
[24] Demir, T., Mutlu, E. & Gültepe, N. (2024). Bioaccumulation of heavy metals in Capoeta tinca fish and health risk assessment. Revista Científica de la Facultad de Veterinaria, 34(2).
[25] İpek, G. G., Aras, S., Arslan, N. & Mutlu, E. (2024). Evaluation of freshwater water quality with indexes and GIS-based: A case study, Güren

Stream, Küre Mountains National Park, Western Black Sea Basin, Turkey. Water Resources, 51(3), 332–343.

[26] Benson, B. B. & Krause, D. (1980). The concentration and isotopic fractionation of gases dissolved in freshwater in equilibrium with the atmosphere. 1. Oxygen. Limnology and Oceanography, 25(4), 662–671.

[27] Benson, B. B. & Krause, D. (1984). The concentration and isotopic fractionation of oxygen dissolved in freshwater and seawater in equilibrium with the atmosphere. Limnology and Oceanography, 29(3), 620–632.

[28] Tokatlı, C., Mutlu, E., Ustaoğlu, F., Islam, A. R. T. & Muhammad, S. (2024). Spatiotemporal variations, health risk assessment, and sources of potentially toxic elements in potamic water of the Anday Stream Basin (Türkiye), Black Sea Region. Environmental Monitoring and Assessment, 196(5), 1–12.

[29] Güzel, A. E. (2023). Karadere Baraj Göleti (Taşköprü-Kastamonu) su kalitesinin canlılar üzerine etkisinin belirlenmesinde sediment ve sitotoksik analizin kullanımı [PhD Thesis]. Kastamonu University.

[30] Cabral, J. P. S. (2010). Water microbiology. Bacterial pathogens and water. International Journal of Environmental Research and Public Health, 7(10), 3657–3703.

[31] Edberg, S. C., Rice, E. W., Karlin, R. J. & Allen, M. J. (2000). Escherichia coli: The best biological drinking water indicator for public health protection. Journal of Applied Microbiology, 88(S1), 106S–116S.

[32] Re-Ga (2012). Surface Water Quality Regulation (Yerüstü Su Kalitesi Yönetmeliği). Annex-5 (Amended: OG-10/8/2016-29797), environmental quality standards and intended-use criteria for certain parameters in surface water bodies. Official Gazette, 28483 (repeated).

[33] Kutlu, B. & Mutlu, E. (2024). Evaluation of the Şerefiye (Zara-Sivas) Dam according to water quality indexes. Menba Journal of Kastamonu University Faculty of Fisheries, 10(2), 1–12.

[34] WHO – World Health Organization (2022). Guidelines for Drinking-water Quality: Fourth Edition Incorporating the First and Second Addenda. WHO, Geneva.

[35] Noori, R., Berndtsson, R., Hosseinzadeh, M., Adamowski, J. F. & Abyaneh, M. R. (2019). A critical review on the application of the National Sanitation Foundation Water Quality Index. Environmental Pollution, 244, 575–587.

[36] Pan, B., Han, X., Chen, Y., Wang, L. & Zheng, X. (2022). Determination of key parameters in water quality monitoring of the most sediment-laden

Yellow River based on water quality index. Process Safety and Environmental Protection, 164, 249–259.

[37] Brown, R. M., McClelland, N. I., Deininger, R. A. & Tozer, R. G. (1970). A water quality index — Do we dare? Water and Sewage Works, 117(10), 339–343.

[38] Chatterjee, C. & Raziuddin, M. (2002). Determination of water quality index (WQI) of a degraded river in Asansol industrial area, Raniganj, Burdwan, West Bengal. Nature, Environment and Pollution Technology, 1(2), 181–189.

[39] Lettenmaier, D. P. (1976). Detection of trends in water quality data from records with dependent observations. Water Resources Research, 12(5), 1037–1046.

[40] Mutlu, E., Tokatlı, C., Islam, A. R. M. T., Islam, M. S. & Muhammad, S. (2023). Water quality assessment of Şehriban stream (Kastamonu, Türkiye) from a multi-statistical perspective. International Journal of Environmental Analytical Chemistry.

[41] Zhao, G., Ding, W., Tian, J., Liu, J., Gu, Y., Shi, S., Wang, R. & Sun, N. (2022). Spearman rank correlations analysis of the elemental, mineral concentrations, and mechanical parameters of the Lower Cambrian Niutitang shale. Journal of Petroleum Science and Engineering, 208, 109550.

[42] Shapiro, S. S. & Wilk, M. B. (1965). An analysis of variance test for normality (complete samples). Biometrika, 52(3–4), 591–611.

[43] Boyd, C. E. & Tucker, C. S. (1998). Pond Aquaculture Water Quality Management. Kluwer Academic Publishers, Boston.

Chapter 9

Forest Fungi, Environmental Chemistry, and Forest Pathology Responses to Toxic Metals, Radionuclides, and Emerging Pollutants

Mertcan KARADENİZ[1],Temel Kan BAKIR[2]

1. INTRODUCTION

Heavy metals are extensively released into the environment through various anthropogenic sources, such as mining activities, industrial emissions, fossil fuel consumption, and the application of phosphate fertilizers, as well as natural mechanisms including the weathering of metal-bearing rocks and volcanic eruptions [1]. The global increase in industrialization and urbanization rates has accelerated the mobility of these hazardous inorganic compounds, resulting in severe disruptions of biogeochemical cycles within the biosphere [1]. Forest ecosystems act as natural sinks for these global pollutants, which can be transported over long distances via dry and wet atmospheric deposition, industrial effluents, and agricultural runoff [1]. As non-biodegradable substances, these inorganic pollutants tend to accumulate continuously within the ecosystem, adversely affecting the microbiological balance and soil fertility of terrestrial ecosystems by suppressing the activities of soil microorganisms [1-3]. Furthermore, within forest environments, radionuclide fallout released into the atmosphere as a result of nuclear industry accidents or nuclear weapon tests also possesses the potential to accumulate in the soil [4,5]. Upon entering the food chain via soil or water, these toxic elements undergo a process of bioaccumulation across trophic levels, reaching hazardous concentrations in ultimate consumers, primarily wildlife and humans [1]. The toxicity of non-essential heavy metals, such as cadmium (Cd), lead (Pb), mercury (Hg), and arsenic (As), induces oxidative stress at both environmental and cellular levels, thereby causing carcinogenic, mutagenic, and teratogenic effects in organisms [1,2].

Fungi are among the most important biological factors in determining the cycling of matter, nutrient transfer, and the environmental fate of radionuclides in forest ecosystems [6]. Fungal mycelial networks, which cover extensive

[1] Assist. Prof. Dr., Department of Nature Conservation and Biodiversity Management, Faculty of Forestry, Kastamonu University, Türkiye, mkaradeniz@kastamonu.edu.tr, (ORCID: 0000-0002-3627-9424)
[2] Prof. Dr., Department of Chemistry, Faculty of Science, Kastamonu University, Türkiye, temelkan@kastamonu.edu.tr, (ORCID: 0000-0002-7447-1468)

surface areas on the forest floor, interact directly with inorganic elements and heavy metals in the soil matrix through both physicochemical and biological pathways [5]. Chitin, melanin, various polysaccharides, and proteins present in the structure of the fungal cell wall possess a high binding affinity for heavy metals and radionuclides, playing an active role in the immobilization of these pollutants via biosorption [5]. In the context of their ecological functions, mycorrhizal fungi, which establish symbiotic relationships with tree roots, protect plants from toxicity stress by regulating the transport of heavy metals and radionuclides from the soil into plant tissues [6]. Additionally, saprotrophic species such as white-rot fungi are important for the bioremediation of complex xenobiotics, as they release extracellular enzymes and low molecular weight organic acids [7]. In stressful conditions with high pollutant concentrations, fungi contribute to the buffering capacity of the ecosystem, absorbing toxic ions inside their own biomass by means of biosorption and bioaccumulation mechanisms [8]. However, the presence of nanoparticle pollution in the environment such as silver and copper can directly affect growth rates of forest pathogens causing damping-off disease and wood-decay fungi [9].The study of the effects of toxic elements on environmental biogeochemistry and forest pathology calls for a comprehensive strategy due to the complex interactions between microbial communities, pathogens and inorganic pollutants in forest ecosystems [10]. In particular, the high-affinity binding of heavy metals and radionuclides via the mycelial networks of commonly consumed saprotrophic wild mushrooms, such as *Pleurotus ostreatus* and *Coprinus comatus*, presents environmental remediation potential on the one hand, while posing a risk of pollutant accumulation within the food chain on the other [11,12]. Furthermore, the fact that environmental pollutants alter not only plant and fungal physiology but also host-pathogen interactions at the cellular level, thereby increasing the susceptibility of forest trees to diseases, deepens the ecological dimension of the problem [9]. The primary objective of this chapter is to comprehensively analyze the impacts of toxic metals, radionuclides, and emerging pollutants in forest ecosystems within the framework of the physiological adaptations, mycoremediation capacities, and pathological processes of forest fungi [8]. Consequently, it aims to elucidate, throughscientific evidence, the shifting ecosystem balances under pollution-induced stress, the molecular foundations of fungus-metal interactions, and the implications of toxic elements on human health via trophic transfer [1].

2. TOXIC METALS AND FUNGI

2.1. Bioaccumulation and Biosorption Mechanisms

In forest ecosystems, the cellular uptake and retention of heavy metals by fungi occur primarily through two distinct biological mechanisms: biosorption and bioaccumulation [3,13] (Figure 1). Biosorption is a quick passive process, independent of metabolic energy (ATP), characterized by the binding of heavy metal ions to functional groups on the fungal cell wall by physical and chemical means [8]. The main components of the fungal cell wall are polysaccharides, lipids and proteins, which are extremely rich in reactive functional groups such as carboxylate, hydroxyl, amino, sulfhydryl, and phosphate that are capable of forming direct complexes with the surrounding heavy metal ions [12]. These structural functional groups enable the high-affinity adsorption of toxic metals, particularly lead (Pb), cadmium (Cd), and mercury (Hg), onto the cell surface by hyphal networks [13]. The cell wall of the fungi is considered the most important structural element that enhances the fungi biosorption capacity by precipitating heavy metals or binding them through ion exchange and contains chitin and chitosan polymers, as well as melanin pigments. These fungal mycelia develop a tremendously large surface area on the forest floor due to their biological filter characteristics, which helps in the immobilization of heavy metals in the ecosystem by avoiding leaching into the lower strata of the soil profile and groundwater [5]. The biosorption process does not depend on the viability of the cells and can be carried out efficiently by dead fungal biomass, while bioaccumulation requires continuous growth and active enzymatic functions of living mycelia [8].

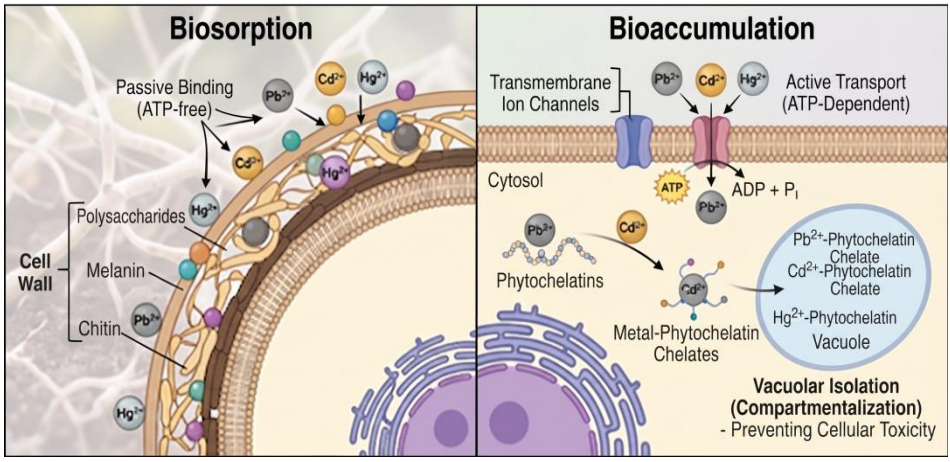


Figure 1. Mechanisms of biosorption and bioaccumulation of toxic metals in fungal cells.

In contrast, bioaccumulation is a dynamic cellular process in living fungal cells that requires expenditure of metabolic energy. It involves active transportation of heavy metals across the cell membrane into the cytoplasm, followed by their storage in intracellular compartments [13]. In this active transport process, transmembrane ion channels and carrier proteins, normally responsible for the transport of essential elements like calcium, magnesium or zinc, also facilitate the intracellular influx of non-essential toxic metals like lead, arsenic and cadmium due to their chemical and structural similarities [1]. The kinetics of cellular heavy metal uptake by fungi is strongly dependent on genetic characteristics of the specific fungal species and on environmental factors such as pH of the soil, content of organic matter, redox potential, and bioavailability of the metals in the soil [14]. Fungi also synthesize sulfur-rich peptides such as metallothioneins and phytochelatins to bind metal ions and to prevent actively transported toxic metals from damaging cellular metabolism and inducing oxidative stress by the formation of free radicals. These bound inorganic pollutants are shuttled to vacuoles, the safest storage compartments at the cellular level, for compartmentalization and thus separated from cytosolic enzyme systems and risks of cytotoxicity are minimized [15]. In the field it has been shown that edible mushroom species, such as *Pleurotus ostreatus* and *Coprinus comatus*, which grow naturally in the forests, take up these toxic metals from the soil through their hyphae and transfer them from the mycelium to the sporocarps, leading to a significant bioaccumulation in the fruiting bodies [12,16]. Although these bioaccumulation mechanisms offer a unique advantage for the ecological remediation of contaminated forest soils viamycoremediation, they concomitantly pose a risk of foodborne heavy metal toxicity for humans and ultimate consumers at the highest trophic levels of the food chain [1].

2.2. Protective Role of Mycorrhizal Fungi

In forest ecosystems, the survival and development of vegetation are directly dependent upon the presence of mycorrhizal fungi, which establish mutualistic symbiotic relationships with tree roots [15]. By forming a critical interface between the soil matrix and the plant root system, these mycorrhizal networks act as a dynamic "biological shield" that mitigates the toxic effects of heavy metal pollution on the plant [17]. Ectomycorrhizal fungi, commonly observed in

forest trees, form a dense hyphal mantle around the root tips and penetrate between the root cortical cells to form the Hartig net [5]. Generating an immense biomass in the soil and around the roots, these ectomycorrhizal structures sequester toxic heavy metals within their extraradical hyphae and the mantle

layer, thereby physically and chemically preventing the translocation of these elements into the vascular system of the host tree [5] (Figure 2).

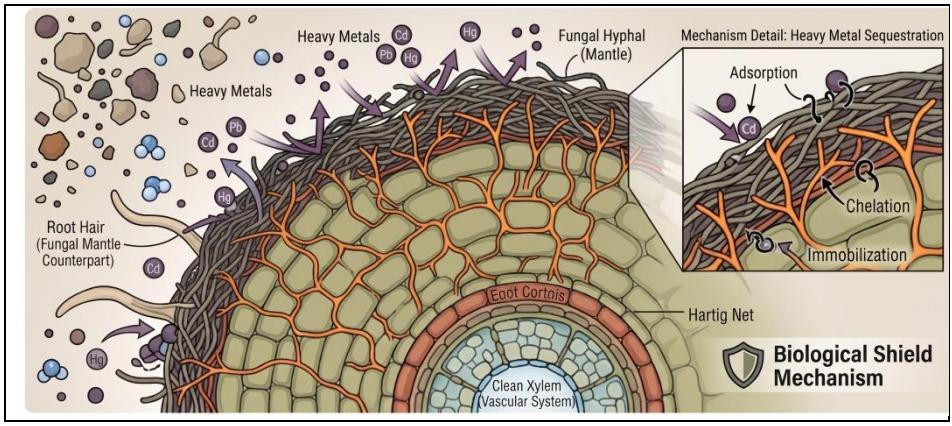


Figure 2. "The biological shield" function of the hyphal mantle and Hartig net formed by ectomycorrhizal fungi, protecting the host tree from toxicity by blocking heavy metals.

In contrast, endomycorrhizal fungi, which invade the plant root cells, play an important ecological role in the survival of plants and their development of metal tolerance even in the soils under heavy metal stress [15]. Arbuscular mycorrhizal fungi significantly restrict the translocation of these toxic ions to the shoot tissues, where photosynthetic activity occurs, by binding andimmobilizing heavy metals within the plant root system [17]. These protective mechanisms provided to host trees by mycorrhizal fungi involve specific cellular processes, such as the adsorption of heavy metals onto chitin polymers in the fungal cell wall, their binding in the rhizosphere via extracellular glycoprotein secretions like glomalin, and the sequestration of toxic ions within fungal vacuoles [5]. Consequently, the integrated functioning of ectomycorrhizal and endomycorrhizal networks protects host trees from acute metal toxicity by reducing the bioavailability of heavy metals in the soil, thereby significantly supporting the ecological rehabilitation of forested areas severely degraded by pollution [15,17].

2.3. Effect of Heavy Metal Stress on Host-Pathogen Interactions

The abiotic stress induced by heavy metal pollution on plants in forest ecosystems disrupts fundamental physiological processes by suppressing the cellular defense mechanisms of trees [1].Toxic metals accumulated in the soil lead to the overproduction of reactive oxygen species and severe oxidative stress; consequently, cell membrane integrity and physiological viability in tree roots

are severely impaired [2]. This pollution-induced cellular damage in the innate immune systems of trees renders them much more vulnerable to biotic stress factors, particularly secondary forest pathogens[1].Forest seedlings physiologically weakened due to heavy metal toxicity become highly susceptible to infections by soil-borne fungal and oomycete pathogens causing damping-off disease, such as *Rhizoctonia solani*, *Fusarium oxysporum*, and *Phytophthora cactorum* [9]. Similarly, in mature forest trees under chronic pollution stress, the colonization dynamics of wood-decay fungi that specifically cause root and butt rot, such as *Fistulina hepatica*, *Grifola frondosa*, and *Meripilus giganteus*, can be altered within the forest ecosystem [9]. Consequently, while high levels of environmental pollution compromise the disease resistance of forest trees, they pave the way for certain pathogenic fungal strains capable of developing tolerance to inorganic toxicities to gain a competitive advantage in the ecosystem, thereby modifying the microbial community structure and facilitating the spread of secondary pathological syndromes [13].

3. RADIONUCLIDES AND FUNGAL INTERACTIONS

3.1. Radioecology and Fungi: Accumulation of Radioactive Fallout by Fungi

Forest ecosystems represent one of the most significant terrestrial sinks for the accumulation of radionuclides, particularly radiocesium (^{137}Cs) and radiostrontium (^{90}Sr), released into the atmosphere following major nuclear power plant accidents such as Chernobyl and Fukushima [5]. Upon reaching the forest floor post-nuclear fallout, these radionuclides are retained with high affinity by fungal mycelial networks densely distributed in the upper organic horizons of the soil [5,18]. After the Chernobyl accident radioecological investigations have clearly shown the key role of forest fungi as radionuclide accumulators in the ecosystem. Fungi have a much higher competitive capacity for cesium isotopes in the soil matrix than plants and can accumulate this element in their biomass up to 10 to 150 times higher than plants [5].Ectomycorrhizal fungi, the symbiotic partners of forest trees, uptake radionuclides like ^{137}Cs and ^{90}Sr from the soil into their cellular frameworks via extraradical hyphae and transfer these ions from the substrate to the mycelium and subsequently to their sporocarps at high rates . This active transport from the mycelium to the sporocarps results in a long term sequestration of radioactive contamination from the forest floor in the fungal biomass and thus a considerable reduction of the leaching of radionuclides to the groundwater [4,5]. Numerous investigations of different fungal species collected from locations severely impacted by the Chernobyl accident have confirmed that the concentrations of radiocesium in the

sporocarps of ectomycorrhizal fungi are significantly increased as compared with those in saprotropic species [5]. This spectacular bioaccumulation capacity offered by fungi opens up great potential for the remediation of contaminated lands after nuclear accidents by means of mycoremediation strategies. However, one of the most important hazards that should be taken into account in the radioecological management of forest ecosystems is that of the radionuclides entering the food chain by the consumption of these highly radioactive wild mushrooms, and their subsequent direct transfer to humans due to the trophic transfer processes [5,10].

3.2. Fungal Radiotolerance: Protective Role of Melanin Pigmentation and Radiotrophic Adaptation

In forest ecosystems, especially in regions affected by major nuclear accidents, certain fungal species exposed to high doses of ionizing radiation have evolved extraordinary cellular adaptation mechanisms that allow them to survive such extreme conditions. Another important aspect of the outstanding resistance of fungi to environmental radiation stress is that melanin, a complex polymeric macromolecule with a high level of production and storage in the fungal cell walls, fulfills an essential protective role [5]. Acting almost as a physical shield, this dark-colored phenolic pigment helps preserve cellular integrity by absorbing the direct destructive impacts of ionizing radiation on intracellular nucleic acids (DNA/RNA) and other vital organelles [19]. From a biochemical perspective, the melanin pigment possesses the capacity to capture and neutralize, with high binding affinity, the harmful free radicals generated by the radiolysis of water molecules by high-energy radiation; thus, it successfully insulates the fungal cell from secondary damages potentially induced by lethal oxidative stress [19].

Going a step beyond radiotolerance, it has been determined that certain dark-pigmented fungal strains, which can be isolated even in the most severe extreme environments such as the walls of the Chernobyl nuclear reactor, not only tolerate radiation but also directly utilize this energy as a source for their metabolic activities [19]. In this extraordinary adaptation strategy, termed radiotrophism, the melanin network in the cell wall captures the ionizing energy from gamma rays—analogous to how chlorophyll in plants harvests light—triggering cellular electron transfer processes and converting it into metabolic energy that supports the increase in fungal biomass [5] (Figure 3). This unique evolutionary capability enables radiotrophic fungi to emerge as dominant colonizers in forest ecosystems subjected to nuclear fallout and in areas with high radioactive contamination; simultaneously, it presents groundbreaking biotechnological prospects for

scenarios involving the safe removal of radionuclides from the environment via mycoremediation processes [5,10].

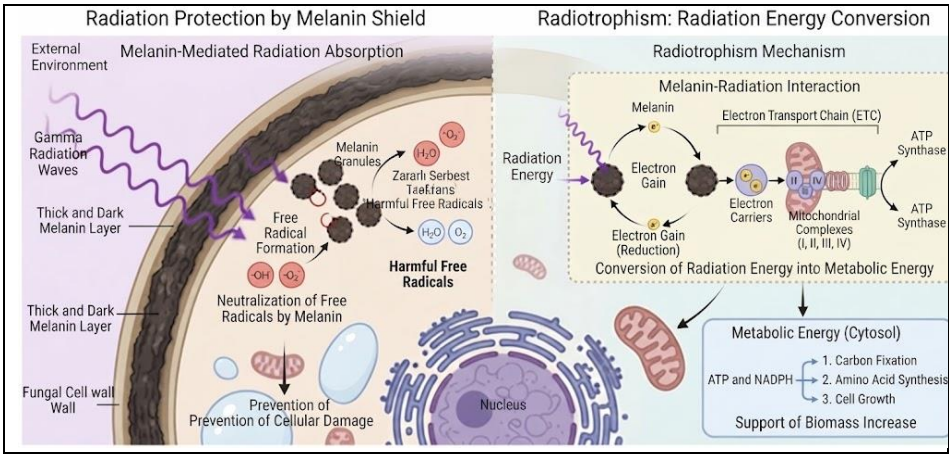


Figure 3. The protective shield role of melanin pigment against ionizing radiation and the radiotrophism mechanism by which energy is incorporated into cellular metabolism.

3.3. Effect of Chronic Radiation on Host-Pathogen Interactions

A long-term contact with ionizing radiation because of radionuclide accumulation in forest ecosystems causes a serious change in cellular repair processes and morphological stability of trees and, consequently, a weakening of their natural defense mechanisms [20]. Radiation causes long-lasting oxidative stress and DNA damage in cells that hinder the immune response of host trees and the production of phytochemicals that fight pathogens [5]. Such a large decrease in the biological defense mechanisms of the tree allows for the quicker invasion of living plant tissues by secondary forest pathogens, permanently altering host-pathogen interactions in favor of the pathogen. Studies in forests with heavy radioactive contamination from Chernobyl and Fukushima show that the stress caused by radiation gives some wood- and root-decaying fungi a unique ecological advantage over their rivals [5,6]. In particular, pathogenic fungi that rapidly acquire radioresistance by increasing melanin content infect physiologically weakened trees, thus increasing disease prevalence in forest ecosystems [10]. Thus, persistent radiation pressure causes not only direct cellular injury to forest trees, but also broad secondary ecological damage in forest pathology by enhancing the virulence and dissemination of secondary fungi [20].

4. EMERGING POLLUTANTS

4.1. Physical and Chemical Pressures of Micro- and Nanoplastics on the Forest Soil Microbiome and Mycelial Networks

Microplastics and nanoplastics are a significant concern for forest ecosystems and are described as novel xenobiotic pollutants with rapid accumulation in the terrestrial biosphere [21]. Atmospheric movement and precipitation driven by wind can transport microplastics, which are less than 5 millimeters in diameter, and nanoplastics, which measure less than 100 nanometers, into the soil layers of even the most isolated forest regions [22]. The build-up of these synthetic polymers within the soil matrix changes key physical properties of forest soils such as aeration, water retention and aggregate stability, and therefore constitutes a significant abiotic stress for the microbiome [23].Fungal mycelia grow in a wide and complex network on the forest floor, and as they grow in search of a substrate, they are forced to make direct physical contact with micro- and nano-sized plastic particles [24]. The dainty and thin hyphal tips of mycelial networks experience cellular mechanical stress upon encountering nanoplastic particles in soil pores, adversely influencing the fungi's growth kinetics and colonization rate [25]. In addition to physical stresses, microplastics contain toxic chemical additives such as phthalates, bisphenol A (BPA), flame retardants, which are slowly leaching into the soil solution through abiotic degradation, leading to xenobiotic contamination and cytotoxic effects on forest microbiota [7]. At the same time, the huge surface area and hydrophobic nature of microplastics make them a dangerous carrier of toxic metals by adsorbing heavy metals and a variety of inorganic contaminants from the environment onto their surfaces [14].The application of these microplastic complexes enriched with heavy metals and changed physicochemical properties challenged the cellular antioxidant defense systems of fungal populations in the rhizosphere and forest soil and inhibited the essential enzymatic functions of the fungi [26]. The potent extracellular ligninolytic enzyme systems of saprotrophic organisms, notably white-rot fungi, are capable of degrading these novel xenobiotics. However, the bioremediation is significantly hampered by the large steric hindrance of microplastics and the toxicity of the heavy metals present [7]. Therefore, micro- and nanoplastic pollution threaten fungal biodiversity, and the functional integrity of mycelial networks in forest soils, imposing severe, dynamic and complex pressures on essential ecosystem functions such as the carbon cycle, organic matter decomposition and plant-microorganism symbiosis [24].

4.2. Pharmaceuticals and Forever Chemicals: Effects of Emerging Pollutants on Fungal Enzyme Systems

Forests are becoming more and more as sinks for pharmaceuticals and persistent chemicals including per- and polyfluoroalkyl substances (PFAS) transported through pathways such as the use of domestic wastewater for irrigating agriculture, flooding, and atmospheric deposition. [14]. These xenobiotics, novel, persistent and resistant to chemical degradation, are accumulated in forest soils and exert major chemical stress on microbial communities, in particular on saprotrophic fungi, which are responsible for the decomposition of organic matter. White-rot fungi degrade complex polymeric compounds and resistant environmental contaminants at cellular level by oxidative extracellular enzyme systems such as laccase, lignin peroxidase (LiP) and manganese peroxidase (MnP). [7]. Pharmaceutical residues and PFAS substances that reach the forest floor directly contact with the specific ligninolytic enzyme systems of fungi, modifying their enzyme kinetics and catalytic efficiencies [8]. In some cases, low concentrations of pharmaceutical wastes create a stimulatory effect that promotes the transcription of enzymes like laccase; whereas the highly stable molecular structures of forever chemicals, such as fluorocarbon bonds, can block the active sites of enzymes, leading to competitive or non-competitive inhibition [7]. In particular, the mycelial networks of macrofungi with high bioremediation potential, such as *Pleurotus ostreatus* and *Coprinus comatus*, are forced to alter their enzyme production profiles and secretion mechanisms as a cellular stress response when encountering these recalcitrant pollutants [12]. However, this disruptive effect of pharmaceuticals and PFAS on fungal enzyme systems not only hinders the mycoremediation of xenobiotics but also severely decelerates fundamental biogeochemical processes concerning forest health—such as humus formation, carbon cycling, and enzymatic defense against pathogens—which are the primary functions of laccase and lignin peroxidase [7]. Consequently, this physiological damage caused by emerging pollutants via enzyme inhibition is considered a latent pathological threat that weakens the resilience and biodiversity of forest ecosystems in the long term [14].

4.3. Disruption of the Disease Triangle: Emerging Pollutants Altering the Plant-Pathogen Balance as an Environmental Stress Factor

In forest ecosystems, the occurrence and severity of plant diseases are explained by the concept of the "disease triangle," which is formed by the convergence of a susceptible host tree, a virulent pathogen, and favorable environmental conditions that support this interaction [14]. Emerging xenobiotic

pollutants, such as microplastics, pharmaceuticals, forever chemicals (PFAS), and heavy metals, fundamentally disrupt plant-pathogen dynamics by dramatically altering the environmental parameters of this triangle [7] (Figure 4). Accumulating in the soil matrix and groundwater resources, these emerging recalcitrant pollutants cause chronic oxidative stress, cellular membrane damage, and metabolic deceleration in forest trees, thereby significantly weakening the innate immune barriers of the host [1]. Simultaneously, these continuous pollution-induced abiotic pressures increase the susceptibility of trees to secondary pathogens by inhibiting the protective and nutritional functions provided to the plant by beneficial mycorrhizal fungal networks in the soil [27].

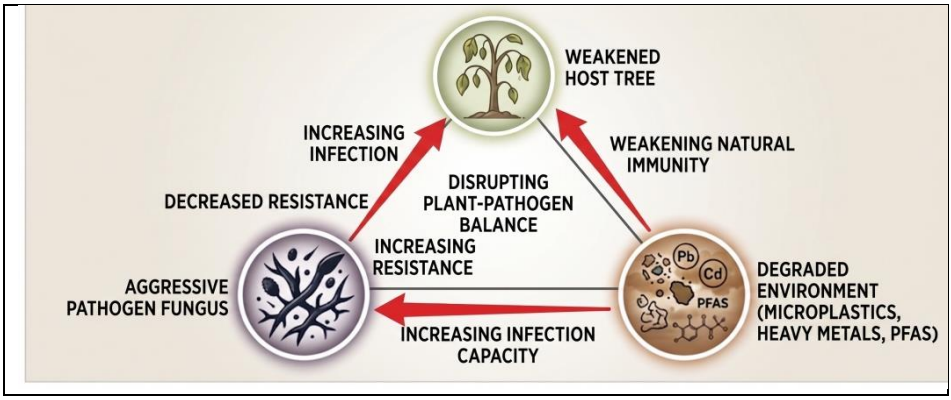


Figure 4. Disruption of the Disease Triangle dynamics by emerging pollutants as an abiotic stress factor, shifting the plant-pathogen balance in favor of the pathogen.

On the other hand, certain soil-borne pathogenic fungi exhibiting a high cellular adaptive capacity to environmental toxicity can tolerate the abiotic stress induced by these emerging pollutants and enhance their pathogenicity by exploiting the environment of reduced microbial competition [9]. For example, on forest floors characterized by intense silver and copper nanoparticle pollution or heavy metal accumulation, while host trees become physiologically exhausted, a marked increase is observed in the growth rates and infection capacities of certain opportunistic wood-decay and root-infecting fungi [9]. This demonstrates that environmental pollution is not merely an issue of toxicity, but simultaneously acts as a selective pressure operating in favor of the pathogen [8]. Consequently, by breaking down host resistance within the disease triangle and stimulating pathogen activity, these emerging pollutants introduced into the ecosystem pave the way for severe infection outbreaks and mass tree mortalities that are difficult to reverse in forest pathology [13].

5. IMPLICATIONS OF FOREST POLLUTION ON HUMAN HEALTH AND ECOTOXICOLOGICAL RISK ANALYSIS

5.1. Food Chain and Toxicity: Risks Posed by Heavy Metal and Radionuclide Accumulation in Edible Wild Mushrooms Through Human Consumption

The most important and immediate consequences for human health of microbial bioaccumulation in forest ecosystems are related to the transfer through the food chain via consumption of foraged edible wild mushrooms [1]. Macrofungi growing in their natural habitat, which can efficiently obtain nutrients from the substrate through their extensive mycelial networks, are simultaneously capable of accumulating toxic heavy metals and radionuclides from the surrounding environment in their fruiting bodies at high concentrations [12]. Elemental evaluations of selected, heavily consumed and nutritionally important saprotrophic fungi such as *Pleurotus ostreatus* and *Coprinus comatus* demonstrate that these fungi can accumulate heavy metals such as Pb, Cd and Hg at levels that greatly exceed permissible levels for foodstuffs [11]. In the fruit bodies of these wild mushrooms collected from polluted or mineral-rich forest soils, the concentrations of heavy metals can reach bioconcentration factors several hundred times greater than those found in the neighboring flora and the underlying soil [16].In addition to heavy metals, persistent radionuclides such as radiocesium (^{137}Cs) and radiostrontium (^{90}Sr) deposited on the forest floor after major nuclear accidents are rapidly taken up by the extraradical hyphae of fungi, which concentrate them into the edible parts for human consumption [5]. The consumption of these contaminated wild mushrooms entering the food chain by humans causes the absorption of inorganic toxins and radionuclides through the gastrointestinal tract and their accumulation in vital organs such as kidneys and liver, causing cellular oxidative stress [1] (Figure 5). In cases of long-term exposure, this biomagnification process paves the way for an exceptionally broad spectrum of chronic and fatal health issues, including neurotoxic, hepatotoxic, mutagenic, and carcinogenic diseases [1]. Consequently, this latent mycotoxicity risk—arising from forest ecosystems functioning as sinks—necessitates the creation of regional pollution maps and the implementation of stringent biomonitoring programs prior to the consumption of edible wild mushrooms (e.g., *Pleurotus* and *Coprinus*) gathered from forests, in order to ensure food safety [11].

5.2. Respiratory Health of Forestry Workers Exposed to Increased Pathogens and Spores in Weakened Forest Ecosystems

Forest ecosystems, whose defense systems are weakened under the influence of abiotic stress factors such as environmental pollutants and heavy metals, pave the way for the rapid and aggressive colonization of host trees by opportunistic fungal pathogens [9]. This abnormal increase in the populations of wood-decay fungi and secondary forest pathogens elevates the biological aerosol density and microbial spore load in the forest atmosphere to hazardous levels [7]. Forestry workers conducting routine silvicultural activities such as logging, pruning, and forest monitoring in these pathologically degraded habitats are continuously exposed to these dense, airborne pathogenic fungal spores and mycelial fragments [28].

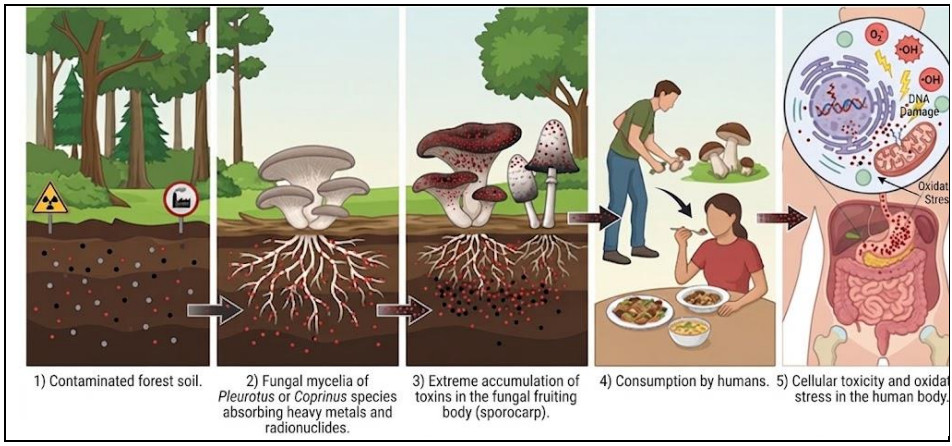


Figure 5. Transfer of toxic metals and radionuclides accumulated in edible wild mushrooms to humans via the food chain

Reaching directly into the pulmonary alveoli via the respiratory tract, these bioaerosols trigger severe inflammatory reactions in the bronchial epithelium due to the mycotoxins and allergenic glycoproteins they contain, as well as the toxic heavy metals physicochemically adsorbed onto their surfaces [1]. As a result of long-term occupational exposure in these contaminated ecosystems, a significant increase is observed in the incidence of hypersensitivity pneumonitis also known as "woodworker's lung"—occupational asthma, allergic rhinitis, and chronic obstructive respiratory diseases among forestry workers [8]. Particularly in areas with intense heavy metal and radionuclide accumulation, the inhalation of fungal spores not only causes immunological damage but also paves the way for airborne environmental pollutants, carried via spores, to enter the human bloodstream directly through the respiratory system [5]. Accordingly, protecting the

respiratory health of workers operating in forest ecosystems weakened under pollution pressure is an urgent public health issue that requires environmental toxicology and occupational health and safety disciplines to be addressed through an integrated approach [28].

5.3. Degradation of Ecosystem Services and Public Health

Forest ecosystems constitute one of the fundamental pillars of global public health and sustainability by providing critical ecosystem services such as the natural purification of water resources, the enhancement of air quality, and the conservation of terrestrial biodiversity [27]. Forest soils are characterized by high accumulation of industrial pollutants such as heavy metals, inorganic substances and xenobiotics, which result in rapid loss of forest vitality and swift deterioration of crucial ecosystem services [14]. Polluted and stressed by more pathogens, forest trees are diminished in biomass, impaired, and diseased and much of their ability to filter particulates and atmospheric contaminants from the air with their foliage is lost. This drastic decline in air filtration efficiency allows airborne toxic particulates to directly enter urban and rural areas causing a surge in respiratory and cardiovascular diseases in humans[1].The contamination of heavy metal also leads to a decline in the natural water purification and phyto-filtration systems performed by forest soil, plant roots, and mycorrhizal fungi. The loss of the ability to purify and retain water in the ecosystem puts the quality of groundwater and surface water resources at risk [13]. Biological components of soil are ineffective in sequestering toxic metals, which leach into drinking water sources via precipitation, contributing to cumulative cellular toxicity, chronic anemia, and irreversible organ damage including renal failure in humans via the hydrological cycle [2]. The ‘One Health’ paradigm in this framework clearly indicates that human health cannot be protected without environmental and forest health. Hence the urgent need to restore ecologically degraded and polluted forest landscapes by techniques of ecological restoration, bioremediation and phytoremediation is not only an ecological necessity but also a necessary step to ensure the public health of modern societies [8].

6. BIOREMEDIATION AND SOLUTION APPROACHES

6.1. Mycoremediation: The Use of Saprophytic and Mycorrhizal Fungi in the Rehabilitation of Contaminated Forest Areas

Mycoremediation is an innovative and environmentally friendly biological remediation method that exploits the impressive metabolic capabilities of fungi to decompose, immobilize or neutralize environmental contaminants in polluted forest ecosystems. [13, 29]. Particularly, saprophytic white-rot fungi, such as

Pleurotus ostreatus and *Coprinus comatus*, produce highly efficient extracellular enzymes, such as laccase and lignin peroxidase, that can degrade pesticides, pharmaceuticals and persistent industrial xenobiotics that accumulate on the forest floor at the molecular scale [7] (Figure 6). In addition to their capacity to degrade organic pollutants, these large saprophytic networks act as effective ecological filters by removing toxic heavy metals and radionuclides from the soil matrix into their cellular frameworks, locking them in their biomass [12]. Moreover, mycorrhizal fungi, which establish symbiosis with the roots of forest trees, play a key role in the rehabilitation of polluted sites, being an important phytostabilization factor by trapping heavy metals within the rhizosphere, thus preventing their translocation to the photosynthetic tissues [8]. The use of entomopathogenic fungi as biological control agents in these large-scale rehabilitation programs ensures the control of secondary forest pests that threaten forest trees weakened by heavy metal stress, while also increasing the overall ecological resilience of the ecosystem due to the high environmental tolerance of these pathogenic fungi to inorganic pollution [30]. Therefore, an integrated use of saprophytic decomposers, mycorrhizal partners and biological control agents provides a holistic nature-based restoration strategy to rehabilitate disrupted biogeochemical cycles, rejuvenate soil fertility and restore ecological equilibrium in critically degraded forest ecosystems [10].

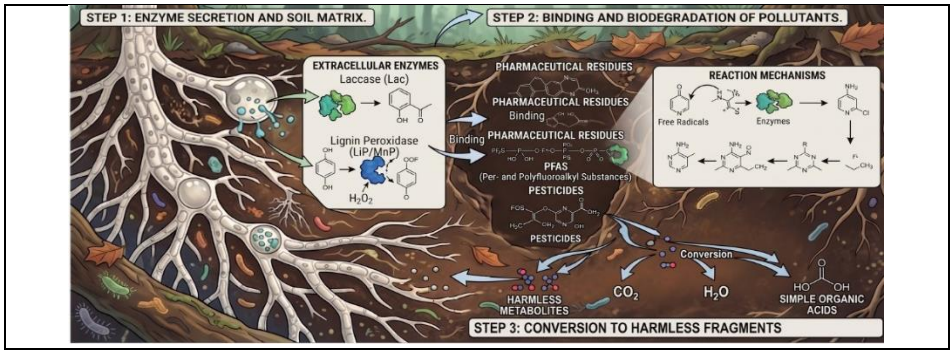


Figure 6. The process of saprophytic fungi degrading xenobiotic pollutants and rehabilitating the ecosystem via extracellular enzymes (laccase and lignin peroxidase).

6.2. Forest Management and Policy Recommendations: Silvicultural Interventions to Minimize Pathogen Outbreaks and Toxin Accumulation

Sustainable forest management strategies and proactive policies that take ecosystem dynamics into account are urgently needed to control heavy metal pollution and associated pathogen outbreaks in forest ecosystems [17]. Phyto-

management approaches implemented to minimize toxin accumulation in contaminated forest areas not only reduce environmental risks but also enable the ecological and economically viable reclamation of contaminated lands [17]. Within the scope of silvicultural interventions, cultivating native tree species with high heavy metal tolerance and deep root systems directly supports the immobilization of toxic elements in the soil and restricts their environmental mobility [8, 18]. At the same time, inoculating the root zone of these resilient tree species with specific mycorrhizal fungi and plant growth-promoting rhizobacteria (PGPR) enhances the physiological resistance of plants against heavy metal stress while competitively suppressing the root colonization of secondary forest pathogens targeting weakened trees [27]. For decision-makers, making mycoremediation and phytoremediation processes a legal ecosystem protection standard to reduce the inorganic pollution load on the forest floor is a critical step for the success of long-term ecological restoration [30]. Among silvicultural interventions aimed at preventing pathogen outbreaks, the controlled removal of physiologically collapsed and diseased individuals due to toxicity from the site and eliminating the vulnerability of monoculture plantations to pathogens by increasing tree species diversity stand out [14]. To prevent toxin accumulation, it is recommended to integrate short-rotation forestry practices and plant harvesting strategies into forest management plans in a way that limits the recycling of heavy metals returning to the upper soil layers via leaf litter [17]. In summary, establishing forest ecosystems resilient to environmental stress factors and secondary pathogen pressures will be possible through the full synergy of modern forestry policies with innovative biotechnological rehabilitation methods and ecosystem-based silvicultural practices [31, 32].

6.3. Future Research Needs: Gaps in the Literature on the Effects of Climate Change and Pollution Synergy on Forest Pathology

When examining the multifaceted environmental crises facing forest ecosystems, the consequences of synergistic effects formed by climate change-triggered abiotic stress factors and anthropogenic pollution (heavy metals, radionuclides, and emerging xenobiotics) on forest pathology constitute one of the critical knowledge gaps that remain insufficiently investigated in today's scientific world [17]. Climatic shifts such as global temperature increases, prolonged drought periods, and irregular precipitation regimes directly alter the physicochemical properties and hydrological balance of forest soils, thereby triggering the mobility of inorganic pollutants and their rates of bioavailability to plants and fungi [17]. The cumulative effects of this complex climate-pollution synergy on the physiological resistance mechanisms of trees and the soil microbiome have not

yet been fully elucidated [15]. Particularly at the ecosystem level, there is an urgent need for empirical field studies and long-term ecological models regarding how chronic pollution pressure shapes the virulence, dissemination dynamics, and host-pathogen interactions of forest pathogens under climatic variables [17]. It is of vital importance that future research moves beyond laboratory-scale studies to address combinations of multiple pollutant and climate stresses under real ecosystem conditions, examining the adaptation capacities of the forest microbiota, ectomycorrhizal networks, and saprophytic communities in this process through genomic, proteomic, and metabolomic tools [8, 17]. Shedding light on these gaps in the literature will serve as a guide both for the protection of weakened forest ecosystems and for the development of holistic bioremediation and forest health management strategies resilient to the climate crisis [17].

7. CONCLUSION

Forest ecosystems are under the threat of intensive anthropogenic impacts, such as industrialization, mining, and agricultural activities, by heavy metals, radionuclides, and emerging xenobiotic pollutants such as microplastics and pharmaceuticals [1]. The synthesis of the primary findings discussed in this study clearly demonstrates that fungi operating in the forest floor and rhizosphere play a central role in determining the mobility, transformation, and ecological fate of inorganic and organic pollutants in the ecosystem [6]. The high surface area and cell wall components possessed by fungal mycelial networks enable the immobilization of toxic metals and radionuclides via biosorption and bioaccumulation, thereby preventing these pollutants from leaching into groundwater [5, 29]. In contrast, the chronic abiotic stress created by environmental pollution on forest trees weakens the plants' immune systems, increases their susceptibility to secondary forest pathogens, and disrupts the disease triangle balance, leading to widespread destruction in the ecosystem [7]. This detrimental degradation of forest ecosystems and reduced ability of forest ecosystems to filter pollutants leads to the accumulation of toxic substances in wild mushrooms that then enter the human food chain, posing a cumulative threat to public health in the “One Health” paradigm [1].

In this regard, the importance of mycological studies in the rehabilitation and protection of the fragile balance between nature and human welfare has emerged as an important aspect [17]. Additional research should study in detail the impacts of climate change and the interaction of several pollutants on forest diseases using omics approaches, incorporate mycological information into forestry management strategies and continuously monitor pollution trends through biomonitoring [13]. Future scientific studies must thoroughly investigate the

effects of climate change and multi-pollution synergy on forest pathology using omics technologies, integrate mycological data into silvicultural management plans, and continuously monitor pollution dynamics via biomonitoring [8, 17]. Therefore, a thorough understanding of the ecological roles of forest microbiota and the pioneering biotechnological advances based on this knowledge will contribute to resilience in forest ecosystems, ensuring ecosystem stability and public health for future generations [17, 31].

REFERENCES

1. Ali, H., Khan, E., & Ilahi, I. (2019). Environmental Chemistry and Ecotoxicology of Hazardous Heavy Metals: Environmental Persistence, Toxicity, and Bioaccumulation. *Journal of Chemistry*, 2019, 6730305.

2. Ali, H., Khan, E., & Sajad, M.A. (2013). Phytoremediation of heavy metals-Concepts and applications. *Chemosphere*, 91, 869-881.

3. Jacob, J. M., Karthik, C., Saratale, R.G., Kumar, S.S., Prabakar, D., Kadirvelu, K., & Pugazhendhi, A. (2018). Biological approaches to tackle heavy metal pollution: a survey of literature. *Journal of environmental management*, *217*, 56-70.

4. Tabak, H.H., Lens, P., Van Hullebusch, E.D., & Dejonghe, W. (2005). Developments in bioremediation of soils and sediments polluted with metals and radionuclides–1. Microbial processes and mechanisms affecting bioremediation of metal contamination and influencing metal toxicity and transport. *Reviews in Environmental Science and Bio/Technology*, *4*(3), 115-156.

5. Dighton, J. (2019). Fungi and Remediation of Radionuclide Pollution. *Fungal Bioremediation: Fundamentals and Applications*, pp.238-263

6. Steiner, M., Linkov, I., & Yoshida, S. (2002). The role of fungi in the transfer and cycling of radionuclides in forest ecosystems. *Journal of Environmental Radioactivity*, 58(2-3), 217-241.

7. Magan, N., Fragoeiro, S., & Bastos, C. (2010). Environmental Factors and Bioremediation of Xenobiotics Using White Rot Fungi. *Mycobiology*, 38(4), 238-248.

8. Mani, D., & Kumar, C. (2014). Biotechnological advances in bioremediation of heavy metals contaminated ecosystems: an overview with special reference to phytoremediation. *International Journal of Environmental Science and Technology*, 11, 843-872.

9. Aleksandrowicz-Trzcińska, M., Szaniawski, A., Olchowik, J., & Drozdowski, S. (2018). Effects of copper and silver nanoparticles on growth of selected species of pathogenic and wood-decay fungi in vitro. *The Forestry Chronicle*, 94(2), 109-116.

10. Barkay, T., & Schaefer, J. (2001). Metal and radionuclide bioremediation: issues, considerations and potentials. Current Opinion in Microbiology, 4(3), 318-323.

11. Zhu, F., Qu, L., Fan, W., Qiao, M., Hao, H., & Wang, X. (2011). Assessment of heavy metals in some wild edible mushrooms collected from Yunnan Province, China. *Environmental Monitoring and Assessment*, 179, 191-199.

12. Ab Rhaman, S.M.S., Naher, L., & Siddiquee, S. (2021). Mushroom Quality Related with Various Substrates' Bioaccumulation and Translocation of Heavy Metals. *Journal of Fungi*, 8, 42.

13. Dixit, R., Wasiullah, Malaviya, D., Pandiyan, K., Singh, U.B., Sahu, A., Shukla, R., Singh, B.P., Rai, J.P., Sharma, P.K., Lade, H. & Paul, D. (2015). Bioremediation of Heavy Metals from Soil and Aquatic Environment: An Overview of Principles and Criteria of Fundamental Processes. *Sustainability*, 7, 2189-2212.

14. Kumar, D., Malik, S., Rani, R., Kumar, R., & Duhan, J.S. (2023). Behavior, risk, and bioremediation potential of heavy metals/metalloids in the soil system. *Rendiconti Lincei. Scienze Fisiche e Naturali*, 34, 809-831.

15. Bhargava, A., Carmona, F.F., Bhargava, M., & Srivastava, S. (2012). Approaches for enhanced phytoextraction of heavy metals. *Journal of Environmental Management*, 105, 103-120.

16. Isildak, O., Turkekul, I., Elmastas, M., & Aboul-Enein, H.Y. (2007). Bioaccumulation of Heavy Metals in Some Wild-Grown Edible Mushrooms. *Analytical Letters*, 40(6), 1099-1116.

17. DalCorso, G., Fasani, E., Manara, A., Visioli, G., & Furini, A. (2019). Heavy Metal Pollutions: State of the Art and Innovation in Phytoremediation. *International Journal of Molecular Sciences*, 20(14), 3412.

18. Lloyd, J. R., & Lovley, D. R. (2001). Microbial detoxification of metals and radionuclides. Current opinion in biotechnology, 12(3), 248-253.

19. Dadachova, E., Bryan, R.A., Huang, X., Moadel, T., Schweitzer, A.D., Aisen, P., Nosanchuk, J.D. & Casadevall, A. (2007). Ionizing radiation changes the electronic properties of melanin and enhances the growth of melanized fungi. *PLoS One*, 2(5), e457.

20. Mousseau, T.A., & Møller, A.P. (2020). Plants in the light of ionizing radiation: What have we learned from Chernobyl, Fukushima, and other "hot" places?. *Frontiers in Plant Science*, 11, 552505.

21. Rillig, M.C. (2012). Microplastic in terrestrial ecosystems and the soil?. *Environmental Science & Technology*, 46(16), 6453-6454.

22. Allen, S., Allen, D., Phoenix, V.R., Le Roux, G., Durantez Jimenez, P., Simonneau, A., Binet, S., & Galop, D. (2019). Atmospheric transport and deposition of microplastics in a remote mountain catchment. *Nature Geoscience*, 12(5), 339-344.

23. de Souza Machado, A.A., Kloas, W., Zarfl, C., Hempel, S., & Rillig, M.C. (2018). Microplastics as an emerging threat to terrestrial ecosystems. *Global Change Biology*, 11(2), 71-75.

24. Rillig, M. C., Ziersch, L., & Hempel, S. (2017). Microplastic transport in soil by earthworms. *Scientific Reports*, 7(1), 1362.

25. Büks, F., van Schaik, N.L., & Kaupenjohann, M. (2020). What do we know about how the terrestrial multicellular soil fauna reacts to microplastic?. *Soil*, 6(2), 245-267.

26. Neenu, G., Ceasar, S.A., & Krishnakumar, N.M. (2026). Harnessing mushrooms as bioindicators to monitor heavy metal pollution. *Environmental Quality Management*, 35(4), e70348.

27. Ojuederie, O.B., & Babalola, O.O. (2017). Microbial and Plant-Assisted Bioremediation of Heavy Metal Polluted Environments: A Review. *International Journal of Environmental Research and Public Health*, 14(12), 1504.

28. van der Schalie, W.H., Gardner, H.S., Bantle, J.A., De Rosa, C.T., Finch, R.A., Reif, J.S., Reuter, R.H., Backer, L.C., Burger, J., Folmar, L.C., & Stokes, W.S. (1999). Animals as sentinels of human health hazards of environmental chemicals. *Environmental Health Perspectives*, 107(4), 309-315.

29. Karaman, M., Novakovic, M., & Matavuly, M. (2012). Fundamental fungal strategies in restoration of natural environment. Fungi: Types, environmental impact and role in disease. New York: Nova Science Publishers Inc.

30. Patra, D.K., Pradhan, C., & Patra, H.K. (2020). Toxic metal decontamination by phytoremediation approach: Concept, challenges, opportunities and future perspectives. *Environmental Technology & Innovation*, 21, 101271.

31. Misra, C.S., Appukuttan, D., Kantamreddi, V.S.S., Rao, A.S., & Apte, S.K. (2012). Recombinant *D. radiodurans* cells for bioremediation of heavy metals from acidic/neutral aqueous wastes. *Bioengineered*, 3(1), 44-48.

32. Yan, A., Wang, Y., Tan, S.N., Mohd Yusof, M.L., Ghosh, S., & Chen, Z. (2020). Phytoremediation: A Promising Approach for Revegetation of Heavy Metal-Polluted Land. *Frontiers in Plant Science*, 11, 359.

Chapter 10

Post-Earthquake Microbiological Hazards: Integrating Environmental Microbiology, Multi-Omics Technologies, and Public Health Perspectives

Kübra TEKŞEN[1], Eda ALTINÖZ[2], Ergin Murat ALTUNER[3]

1. INTRODUCTION

Earthquakes are among the most devastating natural disasters, causing extensive destruction to human settlements, critical infrastructure, and environmental systems. Beyond their immediate physical impact, earthquakes frequently trigger complex crises that extend far beyond the initial shock. Widespread infrastructure failure including systemic failure of water and sanitation infrastructure poses a significant threat to public health [1]. Consequently, earthquakes should require coordinated multidisciplinary responses involving disaster management, epidemiology, environmental microbiology, and healthcare systems. The majority of earthquake-related fatalities occur during the acute phase of the disaster caused by traumatic injuries, crush syndrome, asphyxiation, severe hemorrhage, and exposure to harsh environmental conditions [1-3]. With an estimated 95% of deaths taking place within the first hours and days following the event, which is dominated by physical trauma [1-3]. Nevertheless, the health consequences of earthquakes extend far beyond this immediate period. In the subsequent days and weeks, delayed morbidity and mortality may arise from dehydration, thermal stress, wound infections, sepsis, and compromised access to healthcare services [1]. These complications create a critical window for the emergence and transmission of infectious diseases. A common misconception is that human corpses are major sources of epidemic outbreaks. However, studies proved that the bodies of earthquake victims do not pose a significant risk of infectious disease transmission unless the deceased had been infected with specific communicable diseases prior to death [2,4,5]. The decomposition process itself does not generate epidemic diseases. For instance, following the 2023 earthquake in İslahiye, Türkiye, no increase in infectious disease incidence was linked to the presence of decomposing bodies [2]. Thus, there is a

[1] Department of Biology, Faculty of Science, Kastamonu University, Türkiye, kubrateksen@kastamonu.edu.tr, (ORCID: 0009-0009-5010-4290)
[2] Department of Biology, Institute of Science, Kastamonu University, Türkiye, altinozedaa@gmail.com, (ORCID: 0000-0003-1277-2019)
[3] Department of Biology, Faculty of Science, Kastamonu University, Türkiye, ergin.murat.altuner@ gmail.com, (ORCID: 0000-0001-5351-8071)

growing consensus that post-disaster microbiological risks are primarily driven by environmental and infrastructural failure, such as the collapse of water systems, population displacement, and overcrowding [2,4,5]. These conditions create conducive environments for the transmission of waterborne, foodborne, respiratory, and vector-borne pathogens. The destruction of healthcare infrastructure further increases the risks by limiting access to medical care and interrupting vaccination programs. Following the 2015 Nepal earthquake, 392 healthcare facilities were completely destroyed [6]. Similar challenges were observed after the 2023 Türkiye-Syria earthquakes, creating unprecedented hurdles for infectious disease prevention and management [3,7,8]. The epidemiology of post-earthquake infectious diseases is classified into distinct temporal phases. During the impact phase, typically encompassing the first three days, increases in communicable diseases are rarely documented [1,2,9]. In contrast, the post-impact phase is often associated with a marked upsurge in acute gastrointestinal, respiratory, and wound-related infections [1,2,6]. Subsequently, during the recovery phase, infections with longer incubation periods or the reactivation of latent pathogens, including tuberculosis, parasitic diseases, and viral hepatitis, may manifest more frequently [1,2,10]. Understanding these dynamics is fundamental for designing surveillance and evidence-based intervention strategies. Recent experiences from earthquakes have demonstrated the severity of post-disaster infectious disease risks. Lessons from the 1999 Marmara earthquake in Türkiye, the 2005 Kashmir earthquake, the 2010 Haiti earthquake, the 2011 Great East Japan earthquake and tsunami, and the 2023 Türkiye-Syria earthquakes have collectively underscored the vital necessity of rapid surveillance systems, safe water provision, sanitation management, vaccination programs, and healthcare accessibility in mitigating secondary public health crises [2,3,6,7]. Beyond the immediate physical destruction, earthquakes alter environmental conditions that substantially transform the physical and biological characteristics of affected ecosystems [2,4,5]. These shifts led to microbial proliferation and pathogen dissemination. From this perspective, the disaster environment becomes a dynamic landscape where the stability of natural microflora is disrupted, allowing for the emergence of opportunistic and pathogenic microorganisms. The structural failure of drinking water pipelines and wastewater treatment facilities frequently leads to the cross-contamination [2,11,12], which introduces enteric pathogens into previously controlled aquatic environments. Beyond the immediate epidemiological risks, this contamination fundamentally alters the composition of aquatic microbial communities by introducing fecal-associated microorganisms into pristine or uncontaminated ecosystems [2,11,12]. The extent of this microbial transformation is governed by several ecological and anthropogenic determinants [4]. Post-earthquake longitudinal studies demonstrate that these factors cause gastrointestinal outbreaks

following environmental contamination [12,13]. For instance, in the 2023 Türkiye earthquakes, the structural failure and the resulting interruptions in clean water supply facilitated the increased circulation of *Noroviruses*, *Rotaviruses*, *Cryptosporidium* spp., and *Giardia intestinalis* within affected communities [2]. These observations underscore how seismic disturbances can rapidly trigger the proliferation and transmission of specific enteric pathogens. Earthquake-induced disturbances extend beyond aquatic systems to profoundly impact terrestrial environments. Soil ecosystems experience substantial structural disruption due to ground displacement, liquefaction, and landslides, as well as the widespread accumulation of anthropogenic debris. Air quality and atmospheric microbial composition are similarly altered by seismic events. The collapse of infrastructure generates vast loads of particulate matter, which serve as vehicles for soil-dwelling microorganisms, fungal spores, and various environmental contaminants [7,14]. A hallmark example of this pathway is the aerosolization of *Coccidioides immitis* and *Coccidioides posadasii*. Following significant soil disturbance, their arthroconidia may lead to outbreaks of coccidioidomycosis (Valley Fever) [15]. Seismic events further perturb the complex ecological interactions between humans, animals, and microorganisms. The widespread destruction frequently triggers the displacement of synanthropic rodents and other wildlife species into human settlements, heightening the frequency of contact and the risk of zoonotic pathogen spillover [5,6,16,17]. Consequently, post-disaster landscapes frequently exhibit an elevated risk of zoonotic and vector-borne diseases, most notably tularemia and leishmaniasis [4,17-19]. From an environmental microbiology perspective, these seismic disturbances represent unprecedented, large-scale ecological perturbations that reshape microbial community assembly across soil, water, air, and the built environment. The lethality of communicable disease outbreaks in post-disaster settings can rival that of the initial seismic impact, making the maintenance of food safety, water quality, and hygiene standards imperative for population survival [20,21]. Traditional surveillance systems have historically been instrumental in detecting post-earthquake outbreaks and informing emergency interventions. However, these conventional approaches possess intrinsic limitations; they primarily focus on a narrow spectrum of predefined pathogens, often failing to capture the full complexity of microbial communities reshaped by environmental upheaval. The primary objective of this chapter is to provide a comprehensive synthesis of the microbiological hazards that emerge following seismic disasters, integrating the perspectives of environmental microbiology, molecular epidemiology, and public health. Furthermore, this chapter evaluates the transition from conventional surveillance to high-resolution technologies, highlighting the transformative role of multi-omics, such as metagenomics, metatranscriptomics, metaproteomics, and

metabolomics, alongside artificial intelligence in monitoring microbial dynamics and antimicrobial resistance.

2. EARTHQUAKE-INDUCED ENVIRONMENTAL CHANGES AND MICROBIAL DYNAMICS

2.1 Physical and Chemical Alterations in Affected Ecosystems

Seismic events reshape the Earth's crust, fracturing rock matrices to create hydraulic connections between deep reservoirs and shallow aquifers [22-24]. This mechanical process accelerates water-rock interactions by exposing reactive surfaces and generating reactive oxygen species (ROS), such as H_2O_2, which shift groundwater redox chemistry and mobilize metals [22, 25-27]. Increased permeability further triggers the ascent and mixing of deep fluids, causing anomalies in dissolved gases and isotopes [22].

Table 1. Summary of Geochemical and Hydrological Anomalies in Various Seismic Contexts

System	Primary Anomalies	Hydrological Mechanism	Consequence	Sources
Yellowstone Geothermal	Elevated H_2, sulfide, and DOC; depleted $\delta^{13}C$-DOC	Mechanical comminution and crushing of rhyolitic bedrock.	Generation of chemical disequilibria fueling chemolithoautotrophy.	[25].
Kumamoto Dual-Layer	Dilution of Ca^{2+}, Na^{+}, Cl^{-}; elevation of NO_3^{-}, SO_4^{2-}	Normal faulting crosscutting flow paths; mountain water release.	Water table fluctuations; mixing of soil water and deep confined waters.	[26, 28].
Gyeongju & Pohang	Surges in dissolved Rn, Thoron, and He isotopes.	Volumetric strain change and fault shearing; seawater intrusion.	Gaseous anomalies acting as indicators of deep fault activity.	[34-36].
Tibetan Alpine Grassland	Depletion of TC, TN, TP, and SOC; soil acidification.	Landslides, slope collapse, and soil profile disruption.	Loss of agricultural fertility; inhibition of plant root nutrient uptake.	[29-31].

Case studies illustrate these impacts: the 2016 Kumamoto earthquake caused significant water-table shifts and ion fluctuations [26, 28], while Yellowstone's 2021 swarm demonstrated that rock crushing abiotically generates H_2 and releases carbon

[25]. Beyond hydrology, seismic activity induces landslides and soil failures that deplete essential nutrients (C, N, P) and trigger acidification [29, 30]. This leaches toxic metals and alters stoichiometric ratios, hindering long-term vegetation restoration and ecosystem stability [29, 31-33].

2.2 Disruption of Soil, Water, and Waste Management Systems

Seismic energy causes widespread failure of water, sewage, and waste infrastructure, acting as a primary vector for post-earthquake contamination [11, 37-39]. In municipal networks, ground deformation and liquefaction fracture pipelines, leading to raw sewage exfiltration and increased infiltration/inflow (I/I) that floods surface waters with fecal pathogens [37, 39-42]. Similarly, damaged decentralized systems (e.g., septic tanks, Johkasou) allow pathogens to bypass natural soil filters [37, 38, 43].

These structural failures facilitate the rapid migration of stable viruses and bacteria through new fractures into drinking wells, triggering outbreaks of Rotavirus, Hepatitis, Cholera, and wound-associated infections [10, 11, 39, 44, 45]. Furthermore, seismic hazards compromise landfill liners and covers, allowing toxic leachate to reach aquifers [46-49]. The accumulation of demolition debris containing hazardous materials, often saturated with fecal pathogens from damaged lines, further intensifies environmental toxicity [1].

Finally, socio-economic impacts include wastewater injection-induced seismicity; high-pressure brine disposal triggers earthquakes that heighten public contamination fears and depress property values near injection wells [50, 51].

2.3 Effects on Indigenous Microbial Communities

Seismic activity triggers profound taxonomic and functional shifts in microbial communities through physical restructuring and chemical release [11, 34, 35, 37, 38]. Enhanced permeability transports deep-crustal consortia to shallow aquifers via advection [11, 37, 52], while geogenic substrates (e.g., H_2, reduced sulfur) stimulate chemolithoautotrophs like Dethiobacteraceae and shift sulfate-reducing populations [38, 53]. These microbial responses, alongside markers like Peregrinibacteria or ROS-induced stress, serve as sensitive bio-indicators of tectonic events [34-36, 40].

Long-term, seismic turbidites transport microbes and carbon to hadal zones, accelerating deep-sea carbon cycling [34, 54–56]. Additionally, geotechnical engineering utilizes native bacteria for Microbially-Induced Desaturation (MID) and Calcite Precipitation (MICP), which stabilize liquefiable soils and mitigate structural damage [57-60].

3. MAJOR MICROBIOLOGICAL HAZARDS FOLLOWING EARTHQUAKES

Seismic disasters rapidly disrupt ecological and structural systems, altering interactions among populations, pathogen reservoirs, and environmental barriers [61,62]. The epidemiologic triad is fundamentally altered within hours, shifting the crisis from acute trauma to an escalating infectious disease threat [10,62-65].

The impact phase (first four days) is dominated by trauma, wound contamination, and tissue necrosis. The post-impact phase (4 days-4 weeks) brings increased enteric, foodborne, and respiratory infections due to disrupted sanitation, limited clean water, and crowding. The recovery phase (>4 weeks) is characterized by pathogens with prolonged incubation, chronic or latent infections, and vector-borne outbreaks [10,62,64-66]. Quantitative meta-analyses show that gastrointestinal and hepatic infections are the most common post-disaster illnesses (163.4 cases/100,000), followed by dermal and ectoparasitic infections (84.5/100,000), respiratory infections (9.9/100,000), and central nervous system infections (0.5/100,000) [4,10,12]. In contrast, under normal conditions in the United States, waterborne pathogens cause an estimated 7.15 million illnesses, 118,000 hospitalizations, and 6,630 deaths annually, largely involving biofilm-associated pathogens such as *Legionella* and non-tuberculous mycobacteria [67]. Earthquake-related infrastructure collapse shifts this baseline toward highly transmissible enteric and pyogenic pathogens [11,62,63].

3.1 Waterborne diseases

Earthquake damage to subterranean water and sewage networks can cause fecal and chemical contamination of drinking water [10,11,62,63,68]. Displaced populations may then rely on unsafe surface water, wells, or shared tanks, increasing diarrheal disease risk, which can account for up to 40% of deaths in temporary shelters [11,61]. Loss of residual chlorine and water stagnation also promote biofilm release of opportunistic pathogens such as *Legionella* spp. and non-tuberculous mycobacteria, increasing gastrointestinal and respiratory outbreaks [63,67].

3.1.1 *Vibrio* spp.

Among waterborne pathogens, *Vibrio cholerae* O1 and O139 pose a major rapid-onset threat after disasters, particularly under warm, alkaline aquatic conditions [4,11,69]. The M7.0 2010 Haiti earthquake illustrates this risk displaced over 1 million people and severely damaged sanitation infrastructure. Nine months later, *V. cholerae* O1 was introduced into the Artibonite River and rapidly spread through compromised watersheds [70,71].

3.1.2 *Escherichia coli*

Disruptions to municipal water networks and filtration barriers can cause *Escherichia coli* outbreaks [2,17]. Pathogenic serotypes such as Enterotoxigenic *E. coli* (ETEC) and Shiga toxin-producing *E. coli* (STEC) pose major post-disaster threats [72,73]. ETEC is a principal cause of acute watery diarrhea in children under five and often co-circulates with other enteric pathogens in displaced populations [72,74]. Ground liquefaction and subterranean shifts can rupture sewage lines, allowing human waste to contaminate drinking wells and groundwater [11,62,68]. Agricultural runoff may also introduce animal-derived STEC into domestic water supplies, causing hemorrhagic colitis and Hemolytic-Uremic Syndrome (HUS) [62,69,73].

3.1.3 *Salmonella* spp.

Post-earthquake salmonellosis involves both non-typhoidal *Salmonella* causing gastroenteritis and typhoidal serotypes such as *S. enterica* serotype Paratyphi A causing potentially severe enteric fever [11,63,73]. Poor sanitation contributed to transmission after the 2005 Kashmir and 2015 Gorkha earthquakes [11,74]. Earthquake-induced hydrogeological changes may also allow surface contamination to reach protected water sources; after the 2009 L'Aquila earthquake, a later *Salmonella* outbreak was linked to an earthquake-affected spring contaminated by agricultural runoff [4].

3.1.4 *Shigella* spp.

Shigella flexneri and *S. sonnei* pose a high epidemic risk in crowded settlements due to their very low infectious dose; as few as 10-100 bacilli can cause severe shigellosis and facilitate person-to-person transmission [4,10,75]. Following the 1999 Marmara earthquake, *Shigella* spp. was the leading bacterial cause of diarrheal outbreaks in Turkish tent cities [11]. After the 1999 Chi-Chi earthquake, 90% of isolates in Nantou were *S. flexneri* 2a, with highest incidence among children and older adults, highlighting the role of population movement in regional spread [75].

3.2 Foodborne Microbial Risks

Foodborne microbial risks increase rapidly after earthquakes due to power loss, kitchen damage, and disruption of food supply chains [10]. Humanitarian responses may further increase these risks, as mass catering for rescue workers, volunteers, and displaced populations involves preparing large volumes of food under makeshift conditions. Disaster response therefore follows the priority hierarchy: Food Security → Food Safety → Food Suitability → Food Quality. While ensuring adequate caloric intake is the primary goal, it must be balanced with strict food hygiene to

prevent outbreaks from overwhelming field hospitals and disrupting rescue operations [68].

3.3 Airborne Microorganisms and Dust-Associated Pathogens

Seismic activity and landslides release soil-dwelling and environmental pathogens into the atmosphere, while collapsing structures generate dust plumes that disperse microorganisms over large areas [76-79]. The primary fungal hazard is coccidioidomycosis (Valley Fever) [76, 77]. After the 1994 Northridge earthquake, >11,000 landslides released *Coccidioides immitis* spores, resulting in 203 cases, 55 hospitalizations, six disseminated infections, and three deaths within eight weeks [77-79]. Airborne dust facilitates long-range spore transport [76].

3.4 Wound Infections

Structural injuries cause severe wound contamination, while impaired perfusion, necrosis, and delayed care promote invasive infections [10,64,66,80,81]. Fasciotomy wounds are particularly vulnerable, with infection rates up to 81% and wound sepsis associated with threefold higher mortality [10]. MDR Gram-negative bacteria, especially carbapenem-resistant *Acinetobacter baumannii*, are major late-stage pathogens. After the February 6, 2023 Kahramanmaraş earthquakes, MDR pathogens were detected in 57.4% of wound cultures; *A. baumannii* comprised 53.6% of isolates and showed 100% carbapenem resistance [66]. These infections are largely nosocomial and reflect infection-control breakdown in mass-casualty settings [66, 82]. Anaerobic pathogens, particularly *Clostridium tetani*, also pose major risks [11,81,83]. The 2005 Kashmir earthquake caused 139 tetanus cases and 41 deaths, while the 2004 Aceh tsunami caused 106 cases with an 18.9% case-fatality rate [83]. Management requires debridement, antibiotics, and TIG [81,83]. Gas gangrene, mainly caused by *C. perfringens*, can rapidly cause necrosis, gas formation, and septic shock [62,84].

3.5 Respiratory Infections

Acute respiratory infections (ARIs) are a major post-disaster public health concern [11,12,65,]. Crowded, poorly ventilated, and under-heated shelters promote respiratory transmission, while cold weather, poor hygiene, indoor smoke, and stress-related immunosuppression further increase risk [12,63,65,78,85-87]. Following the 2003 Bam earthquake, 792 respiratory infections were reported within one month, with an attack rate of 68.6 per 10,000 residents [65]. Earthquake-triggered tsunamis can cause “tsunami lung,” a severe necrotizing pneumonia caused by aspiration of contaminated seawater, introducing polymicrobial environmental pathogens into the lower respiratory tract [10,12,65]. Major pathogens include

Pseudomonas aeruginosa, *Legionella pneumophila*, *Scedosporium* spp., *Stenotrophomonas maltophilia*, *Burkholderia* spp., and *Aspergillus* spp. [88-91]. Tsunami lung can rapidly progress to necrotizing pneumonia, lung destruction, and cavitation due to environmental fungi and MDR bacteria. Pulmonary damage may enable systemic dissemination, causing brain abscesses, septic spondylodiscitis, and mycotic intracranial aneurysms, with high mortality [88-91].

3.6 Vector-borne Diseases

Seismic disasters alter vector-borne disease risks through environmental changes and population displacement [61,92]. Although earthquakes may initially destroy breeding sites, damaged water infrastructure and prolonged camp conditions can promote vector proliferation [92,93]. Water-system failures force displaced populations to store water in open containers, creating breeding sites for *Aedes aegypti*, the main vector of Dengue, Yellow fever, Chikungunya, and Zika virus (ZIKV) [92,93]. Inadequate window screens and mosquito nets further increase exposure [92].

3.7 Opportunistic and Nosocomial Infections in Temporary Shelters

Communal living in post-earthquake shelters promotes infectious disease transmission through overcrowding, poor hygiene, and disrupted infection control [11,86]. Scabies, caused by *Sarcoptes scabiei* var. *hominis* and transmitted through prolonged skin-to-skin contact, is a major dermatological concern [12,94]. Following the February 6, 2023 earthquakes in Turkey and Syria, scabies was the second most common diagnosis in Hatay tent cities (9.7% of consultations), while studies in tent and container cities reported a prevalence of at least 0.54% [95]. Displaced and malnourished populations are also vulnerable to opportunistic fungal infections such as invasive candidiasis, particularly where healthcare and hygiene systems have collapsed [96]. Meanwhile, MDR Gram-negative bacteria, especially carbapenem-resistant *A. baumannii*, can contaminate surgical tables, ventilator tubing, and medical carts, contributing to nosocomial bloodstream infections and postoperative sepsis [66,82].

3.8 Emerging and Re-Emerging Infectious Diseases

Earthquakes can trigger the emergence or re-emergence of endemic infections by disrupting infrastructure, ecosystems, and populations [61,16]. Post-earthquake contamination and rainfall may also increase leptospirosis, particularly through rodent exposure [10,11]. In Haiti, persistent water-infrastructure damage after the 2010 earthquake contributed to cholera re-emergence in 2022, highlighting the long-term risk of disease resurgence [71].

3.9 Epidemiological Conclusions and Actionable Recommendations

Post-earthquake public health management requires a shift from reactive clinical care to a proactive, multisectoral prevention framework [3,4,9]. Structural collapse can initiate complex biological cascades by disrupting environments and facilitating pathogen transmission [62]. Effective risk reduction therefore requires several critical public health control measures [63,64,66,68].

4. PUBLIC HEALTH IMPLICATIONS OF POST-EARTHQUAKE MICROBIAL HAZARDS

The immediate aftermath of a catastrophic earthquake initiates a multi-phase public health crisis extending beyond acute trauma [1]. While rescue efforts focus on physical extraction and surgical triage, a prolonged biological threat emerges as geological, physical, and municipal structures collapse [97]. Earthquakes and cascading phenomena such as landslides, tsunamis, and soil liquefaction rapidly alter the local ecological and microbial landscape [1]. This disruption exposes displaced, injured, and immunocompromised survivors to high pathogen densities under conditions that compromise host defenses [98,80].

Epidemiological evaluations confirm a statistically significant and predictable rise in infectious diseases following destructive seismic events [99]. This increase is driven by host susceptibility, environmental contamination, and the collapse of sanitary and healthcare systems [11,97]. Understanding these dynamics requires examining specific outbreak risks, vulnerable populations, emergency sanitation challenges, and infection-control constraints within damaged healthcare infrastructure [12,66,97].

4.1 Disease Outbreak Risks

Earthquake-related disruption of physical and social infrastructure creates multiple transmission pathways for opportunistic pathogens [12,97]. Infectious diseases typically peak within 4-30 days after a disaster, while some subacute or latent infections may emerge months later [1,11]. Major clinical domains include traumatic wound, waterborne enteric, respiratory, and ectoparasitic infections [1,12].

Traumatic Wound and Soft-Tissue Infections

Traumatic wound infections are an immediate complication, with mortality of 19.0%-35.0% [5]. Crush injuries, prolonged entrapment, and contaminated wounds promote ischemia and bacterial colonization [100, 11]. Early infections commonly involve *S. aureus*, *E. coli*, *E. faecalis*, and *E. cloacae*, while later infections increasingly involve MDR Gram-negative bacteria, particularly *A. baumannii*, *P. aeruginosa*, and *K. pneumoniae* [11,101]. Tsunamis may introduce aquatic pathogens into wounds and the respiratory tract, including *A. baumannii*,

Pseudomonas, *S. maltophilia*, and *E. faecium*, while aspiration can cause *S. apiospermum* infections and necrotizing pneumonia due to *B. pseudomallei* and *Nocardia* spp. [1,98].

Waterborne and Enteric Outbreaks

Seismic damage to water and sewer networks contaminates drinking water, forcing displaced populations to use unsafe sources and increasing enteric disease outbreaks [11, 101,102]. Earthquakes affecting >10,000 people were associated with 2.26-fold higher odds of above-average cholera rates, although not statistically significant [97,103]. Major risks include ETEC, *Salmonella enterica* serotype Paratyphi A, *Cryptosporidium parvum*, hepatitis E, and leptospirosis, with flooding and liquefaction further increasing transmission [102].

Airborne and Respiratory Pathogens

Respiratory infections are major post-disaster causes of morbidity, driven by dust exposure and displacement [98,104]. Earthquake-induced dust and landslides can aerosolize fungal spores; after the 1994 Northridge earthquake, 203 coccidioidomycosis cases and three deaths were reported within eight weeks [1,105]. Crowded, poorly ventilated shelters further facilitate transmission of influenza, RSV, Mycoplasma pneumoniae, measles, Neisseria meningitidis, varicella-zoster virus, and Mycobacterium tuberculosis [11,12,98].

Dermatological and Parasitic Infestations

Overcrowding, limited water access, and poor hygiene in displacement camps increase ectoparasitic infestations, particularly scabies caused by *Sarcoptes scabiei* var. hominis [12, 11, 106]. Following the 2023 Kahramanmaraş earthquakes, scabies prevalence in tent and container cities was at least 0.54%, with pruritus (99.0%) and rash (97.9%) as the predominant symptoms [106].

4.2 Vulnerable Populations

Post-earthquake microbial hazards disproportionately affect vulnerable populations, including pregnant and postpartum women, infants and children, older adults, and displaced low-income groups, who face greater exposure and disease severity due to physiological and social vulnerabilities [1,107].

Pregnant and Postpartum Women

Pregnancy involves immunological adaptation that shifts immunity from Th1- to Th2-dominance and reduces CD4+ lymphocyte counts, potentially impairing clearance of intracellular pathogens. Increased innate immunity provides partial compensation but may not prevent severe infections [108,109]. Physiological Vulnerability: Pregnancy-related cardiopulmonary changes reduce physiological reserve and increase the risk of hypoxemia and respiratory complications. During the 2009 H1N1 pandemic, pregnant women accounted for 5% of U.S. pandemic

deaths despite representing only 1% of the population [109]. Pathogen Susceptibility and Severity: Pregnancy increases susceptibility to severe malaria, listeriosis, toxoplasmosis, and Hepatitis E, which may cause maternal complications, fetal loss, or congenital disease [102,108,109]. Measles and varicella can also cause severe maternal morbidity [108,109].

Pediatric Populations

Infants and young children are highly vulnerable to post-earthquake infections due to immature immunity and dependence on caregivers. Preventable respiratory infections, gastroenteritis, and skin diseases account for over 75% of pediatric deaths in disaster settings. Disrupted breastfeeding and unsafe formula preparation can cause diarrhea, dehydration, and malnutrition, further weakening immunity [110].

Geriatric Populations

Poor oral hygiene and dysphagia promote respiratory pathogen colonization and aspiration pneumonia, a major cause of mortality among elderly evacuees. Prevention requires integrated dental, nutritional, and supportive care [107].

Displaced, Low-Income, and Refugee Populations

Displaced refugees, low-income individuals, and marginalized minorities face disproportionate microbial risks due to overcrowding, poor living conditions, and limited healthcare and vaccination access [97,107]. Earthquakes can further exacerbate existing health disparities and associated physical and mental health burdens [107].

5. ENVIRONMENTAL MICROBIOLOGY APPROACHES FOR POST-EARTHQUAKE ASSESSMENT

Seismic events disrupt water and sanitation infrastructure, pushing displaced populations into crowded camps where poor hygiene sharply raises biological loads in water, soil, and air [3,92,111]. The scale of what is at stake is illustrated by two contrasting earthquakes: the 2010 Haiti earthquake, whose collapsed sanitation system triggered a cholera epidemic causing roughly 8,534 deaths, and the 2016 Ecuador earthquake, where standing water in building debris created breeding sites that fueled a Zika virus surge [69,92,112]. Neither outbreak was inevitable, both reflect a diagnostic gap: by the time conventional surveillance flagged the contamination, transmission was already underway. This gap is visible in real time. In Nepal, 16S rRNA gene sequencing of Kathmandu's drinking water sources after the 2015 earthquake tracked fecal-indicator bacteria spiking immediately post-quake and only normalizing eight months later-a recovery timeline that routine testing alone would have missed, since it samples too coarsely and too late to capture the trajectory [111]. The practical question this chapter asks for each available technology is not how it works, but when, in the weeks after an earthquake, it actually

changes what responders do. Conventional culture-based methods, PCR-based molecular techniques, and multi-omics technologies are evaluated according to their ability to provide timely and actionable information for post-earthquake response, drawing on evidence from documented responses in Haiti, Nepal, Türkiye, and Japan [3,69,92,111,113-115].

5.1 Conventional Microbiological Monitoring

Conventional monitoring is the regulatory backbone of water safety - WHO drinking-water guidelines and the U.S. EPA Safe Drinking Water Act set the Maximum Contaminant Levels that agencies still default to during a disaster. In the acute phase this is simplified further: WHO and Oxfam protocols assume every source is contaminated, chlorinate centrally rather than test first, and treat a free residual chlorine reading as sufficient evidence of safety without waiting for lab confirmation [112,115-120].

Table 2. Regulatory and Emergency Water Quality Monitoring Frameworks

Parameter / Indicator	Routine Regulatory Standard (US EPA NPDWR)	Post-Disaster Emergency Target (Oxfam / WHO / Sphere)	Operational Significance in Seismic Response
Escherichia coli / Fecal Coliforms	Zero CFU/100 mL [119, 121].	Zero CFU/100 mL; 95% of camp samples must meet this [115, 120].	Marks acute fecal contamination from fractured sewers [115, 120].
Turbidity	≤1.0 NTU (≤0.3 NTU in 95% of samples) [119].	<5 TU before chlorination [120].	Shields pathogens from disinfectants; signals soil collapse or runoff [119, 120].
Free Residual Chlorine	No fixed cap; residual monitored network-wide [2, 119].	0.5–1.0 mg/L at delivery (min. 0.2 mg/L after 30 min contact) [115, 120].	Chemical barrier against pathogens in vulnerable lines [115, 120].
Heterotrophic Plate Count (HPC)	Triggers Treatment Technique if >500 CFU/mL [119].	Not prioritized during acute phase; monitored during stabilization [115, 120].	Tracks biofilm regrowth in repaired piping [119].

This is close to the sequence followed in most post-earthquake responses, including after the 2023 Kahramanmaraş earthquakes in Türkiye, where compromised water and sewage networks across a wide affected area forced authorities to prioritize blanket chlorination and syndromic surveillance over source-

by-source testing in the first weeks [111]. The approach works for its purpose - fast, cheap, and effective against the most common exposure route - but it is also why conventional monitoring under-detects: a 24-to-48-hour incubation delay means water is already in use before contamination is confirmed, and standard indicator tests miss viruses, protozoan cysts, and as the next section details pathogens that survive without growing at all [119,122-127].

5.2 Culture-Based Identification Techniques

Culture remains the reference method for confirming that a pathogen is alive, and it is still the only route to antibiotic susceptibility testing - which matters directly for post-disaster wound infections, where multidrug-resistant strains are common [3, 122, 128-134]. Standard protocols exist for the pathogens that dominate post-earthquake outbreaks: *Vibrio cholerae* is enriched and streaked onto TCBS agar and confirmed by serotyping, while thermotolerant *E. coli* is enumerated via EPA Method 1603's single-step chromogenic assay [132, 134-138].

Table 3. Decision Comparison of Post-Earthquake Pathogen Detection Methods

Method	Turnaround Time	Sensitivity	Detects VBNC?	Field-Deployable?	Relative Cost
Conventional Culture	24-48 h	Low (culturable fraction only)	No	Limited	Low
Qualitative PCR	6-8 h	Moderate (targeted genes)	Yes	Yes	Low-Moderate
qPCR	2-6 h	High (quantitative)	Yes	Yes	Moderate
Digital PCR (dPCR/ddPCR)	Hours	Very high (single-copy)	Yes	Yes	High
Metagenomics	12-48 h	Very high, non-targeted	Yes	Emerging	High

The gap the table makes visible is the “Detects VBNC?” column. Under post-earthquake stressors - chlorination, starvation, UV exposure-many gram-negative pathogens enter a Viable But Non-Culturable (VBNC) state: they keep an intact membrane and stay infectious, but stop forming colonies. Standard cultivation typically recovers less than 0.1% of the bacteria actually present in an environmental sample, and *V. cholerae* culturability can fall by 90% within a day even as VBNC

cells remain fully capable of causing disease once ingested [69,120,122,130]. This is the limitation that recurs through the rest of this chapter: every molecular and multi-omics method that follows exists, in large part, to close this specific blind spot.

5.3 Molecular Detection Methods

Molecular methods sidestep the VBNC blind spot entirely: they detect a pathogen's DNA or RNA directly, whether or not the organism can still form a colony, and return a result the same day [123-130]. The tradeoff is sample chemistry - post-earthquake water and soil are loaded with clay, humic acids, and metals that inhibit the PCR reaction itself, so every field protocol below depends on getting extraction right before amplification ever begins [124,139-144].

5.3.1 PCR

Conventional (qualitative) PCR amplifies a specific DNA target using sequence-matched primers, returning a yes/no answer rather than a quantity [127,141,145-147]. Application in post-earthquake surveillance: in the days after an earthquake, field teams use portable thermocyclers to screen wastewater and soil for a short list of markers ctxA for toxigenic *V. cholerae*, uidA for *E. coli*, stx1/stx2 for Shiga-toxin-producing strains, or antimicrobial-resistance genes and get a presence/absence answer within 6 to 8 hours, without shipping samples to a central lab [3,125,132,141, 142,145,146,148-150]. This is the method's real value: not diagnostic depth, but speed at the point of collapse. Its limitations are practical rather than fundamental: post-amplification handling risks contaminating later batches, the assay only answers “present or absent” with no quantification, and the same humic-acid inhibition noted above can produce false negatives in turbid water without careful extraction [124,139,141,146,151,152].

5.3.2 qPCR

Real-time quantitative PCR (qPCR) adds fluorescent signal tracking during amplification, so instead of a yes/no answer it returns an estimated pathogen concentration via the Cycle Threshold (CT) [127,140,141,146,151-153].Application in post-earthquake surveillance: this quantification is what makes wastewater-based epidemiology possible - tracking CT values across a sewershed lets responders estimate community level transmission trends days before clinical cases peak, turning sewage into an early-warning signal rather than just a hazard [127,149,154,155].Its accuracy depends on stable standard curves, which is exactly what post-earthquake matrices undermine: degraded reference material or environmental inhibitors distort the CT-to-concentration relationship, and multiplexing several targets in one reaction sacrifices sensitivity, the same matrix-

inhibition problem that limits conventional PCR, just harder to notice because the assay still returns a number [124,140,152,156].

5.3.3 Digital PCR

Digital PCR (dPCR/ddPCR) partitions a single reaction into thousands of separate microreactions, each independently scored positive or negative, then uses Poisson statistics to back-calculate an absolute pathogen concentration-no standard curve required [139,140,152,156,157]. Application in post-earthquake surveillance: because inhibitors get diluted into a handful of partitions rather than poisoning the whole reaction, dPCR tolerates the humic acids and clay in turbid post-earthquake water at concentrations that would defeat qPCR outright, and it detects pathogens at 2-to-5-fold lower concentrations-the difference between catching a contamination event early and only confirming it after an outbreak is already visible clinically [126,139,140,152,157-158]. It also multiplexes cleanly: a single turbid sample can be screened simultaneously for *Vibrio*, *Salmonella*, and *Shigella* without cross-reactivity [152, 157].

Table 4. Analytical Sensitivity and Genetic Targets of Multiplexed Digital PCR Assays

Target Pathogen	**Conserved Genetic Target**	**dPCR Limit of Detection (LOD) in Spiked Wastewater**	**Post-Disaster Epidemiological Significance**
Vibrio cholerae	*ctxA* (Cholera Toxin A subunit gene) [125].	660 CFU / 100 mL [157].	Specific genetic marker for toxigenic epidemic cholera 125, 150].
Shigella spp.	*ipaH* (Invasion plasmid antigen H gene)	11 CFU / 100 mL [157].	Flags highly infectious dysentery in crowded camps [119, 159].
Salmonella spp.	*invA* (Invasion protein A gene) [160].	390 CFU / 100 mL [159].	Flags salmonellosis/typhoid risk from wastewater runoff [160, 159].
Escherichia coli	*uidA* (*β*-D-glucuronidase gene) [125].	Variable (highly sensitive indicator)	Quantifies fecal pollution directly from complex matrices [161, 125].

5.4 Operational Paradigm Integration

Put together, no single method covers the full response. Conventional culture remains indispensable for confirming that a pathogen is alive and for antibiotic susceptibility testing - but its blind spot to VBNC cells and its 24-to-48-hour delay

make it a poor tool for real-time containment. PCR and qPCR close the speed gap and, in qPCR's case, add quantification for wastewater surveillance, but both remain vulnerable to the matrix inhibition that defines post-earthquake water and soil. Digital PCR resolves that specific tension - absolute quantification without a standard curve, and meaningful tolerance for the same inhibitors that defeat qPCR - which is why it is increasingly the method of choice for trace detection in turbid, post-disaster matrices.

Even dPCR, however, only answers questions its primers were designed to ask. It cannot tell responders whether an unanticipated pathogen is present, whether resistance genes are circulating, or whether a detected organism is metabolically active rather than degraded DNA fragments - questions that matter as much for post-earthquake preparedness as for rapid outbreak detection. That gap is where the multi-omics technologies covered next take over.

6. MULTI-OMICS TECHNOLOGIES IN POST-EARTHQUAKE MICROBIAL RISK ASSESSMENT

As outlined earlier, molecular methods solve speed and the VBNC blind spot but only answer targeted questions. Multi-omics technologies remove that constraint: metagenomics, metatranscriptomics, metaproteomics, metabolomics, and resistomics profile a microbial community without deciding in advance what to look for, at the cost of needing more sequencing capacity and computational infrastructure than a field lab typically has [161,162,164]. The five layers answer five different questions about the same sample, and the real power comes from reading them together, not any one in isolation.

6.1 Metagenomics for Pathogen Surveillance

Shotgun metagenomic sequencing answers metagenomics' foundational question “what is actually there?” by sequencing all DNA in a sample rather than amplifying pre-selected targets. That is what let it catch what targeted assays would have missed after the 2015 Nepal earthquake: 16S rRNA sequencing of Kathmandu's groundwater documented a sharp spike in fecal-contamination markers that gradually reverted to baseline only after eight months, tracking recovery in a way no single targeted assay was built to do [111,165,166]. This same untargeted approach is what wastewater-based networks such as CASPER rely on to track community-level infection dynamics non-invasively valuable for slow-growing or opportunistic pathogens like *Acinetobacter baumannii*, which dominated post-earthquake wound infections after both the 1999 Marmara and 2023 Kahramanmaraş earthquakes in Türkiye, and which conventional wound cultures often catch too late to guide empirical antibiotic choice [3,80,111, 160,166,167].

6.2 Metatranscriptomics for Functional Activity Analysis

Metagenomics answers whether a pathogen's DNA is present; metatranscriptomics answers whether it is doing anything - sequencing active messenger RNA instead of DNA reveals which genes a community is actually expressing right now, which matters because a large fraction of the DNA in any environmental sample belongs to dormant or dead cells [165,168-171].

After a 2008 earthquake in Iceland created new geothermal soil-warming gradients, metatranscriptomics showed soil bacteria down-regulating protein synthesis to conserve energy under sustained heat stress - the kind of active physiological response that DNA sequencing alone cannot see, and that post-earthquake soil and water monitoring increasingly needs, since seismic disturbance itself can alter microbial activity independent of any single pathogen's presence [172].

This sensitivity is also metatranscriptomics' weakness: RNA degrades within minutes once a sample leaves cold storage, so results depend heavily on field preservation protocols that are hard to guarantee in a disaster zone, and because expression varies with time of day and temperature, a single sampling snapshot can be misread as a change in community activity when it is really just normal fluctuation [168,171,173-176].

6.3 Metaproteomics for Community-Level Functional Insights

Metaproteomics goes one step further, using mass spectrometry to identify the actual proteins a community is producing - because gene expression does not always translate into functional protein, this is the layer that confirms an active gene is really doing biological work [177-181].

In practice, its use is limited by extraction chemistry - humic and phenolic compounds common in post-disaster soil interfere with the mass spectrometry itself - and by the same reference-database gap noted for metagenomics, though purpose-built tools such as Kaiko, which build sample-specific protein databases directly from the spectrometry data, are starting to close it [177,179,181].

6.4 Metabolomics for Environmental Health Assessment

Metabolomics profiles the small molecules - the actual chemical output of gene expression and protein activity - making it the layer closest to physiological effect: the mobilized heavy metals, PAHs, and PFAS that seismic damage releases from ruptured storage and disturbed soil produce a measurable oxidative-stress and lipid-disruption signature well before any clinical symptom appears [182-188].

Linking that signature to real health outcomes is the goal of frameworks like “Meet-in-the-Middle,” which pairs biomarker discovery with retrospective

exposure-pathway analysis, relevant post-earthquake because soil ingestion, especially by young children playing in contaminated debris, is a major route for exactly these compounds [184,185,188,189].

Its main constraint is causal, not technical: a metabolic shift confirms exposure occurred, but disentangling which specific contaminant caused it, in a post-disaster environment where multiple pollutants are elevated simultaneously, usually requires combining metabolomics with the exposure and genomic layers above rather than reading it alone [184,185].

6.5 Resistomics

The environmental "resistome" - resistance genes carried across pathogenic, commensal, and environmental microorganisms - matters most where crush injuries, overcrowded shelters, and empirical antibiotic use collide, which is exactly the post-earthquake wound-care environment: a meta-analysis of post-earthquake wound cultures found *E. coli*, *Acinetobacter baumannii, Pseudomonas aeruginosa*, *Enterobacter cloacae*, and *Staphylococcus aureus* as the dominant isolates, with high resistance to carbapenems, cephalosporins, and aminoglycosides (Table 6.1) [190,191,192].

Table 5: Detection Rates and Antibiotic Resistance of Prevalent Post-Earthquake Pathogens

Prevalent Post-Earthquake Pathogen	Detection Rate [95% CI]. [22].	Frontline Antibiotic Resistance Rates [95% CI]. [22].
Escherichia coli	14.5% [10.8%,18.9%].	Imipenem: 79.8% [29.6%,99.5%]. Piperacillin: 70.8% [28.7%,98.2%].
Acinetobacter baumannii	12.1% [6.4%,19.7%].	Cefazolin: 85.1% [30.0%,95.9%]. Ceftriaxone: 62.3% [7.9%,99.9%].
Pseudomonas aeruginosa	10.5% [7.6%,13.8%].	Piperacillin: 45.5% [25.1%,66.2%]. Piperacillin/Tazobactam: 42.0% [14.8%,71.7%].
Enterobacter cloacae	9.6% [4.6%,16.3%].	Cefazolin: 85.8% [30.0%,95.5%].
Staphylococcus aureus	7.4% [5.2%,9.9%].	Ceftriaxone: 87.9% [55.0%,99.9%].

Resistomics also reveals drivers that wound cultures alone cannot: after the 2010 Chile earthquake and tsunami mobilized mercury and arsenic into coastal aquifers, MRSA carrying a heavy-metal-resistance plasmid rose to 88% prevalence in the tsunami-affected area versus 29% elsewhere - heavy-metal pollution had co-selected for the resistant lineage, a mechanism invisible to standard susceptibility testing

[186]. Mobile genetic elements - transposases and class 1 integrons - are what let such resistance spread horizontally between unrelated species in contaminated soil and water [186, 192].

The VBNC blind spot has a resistome-specific consequence: dormant *Acinetobacter baumannii* in cold, nutrient-depleted aquifers keeps actively transcribing most of its resistance genes even while evading filtration and culture, then rapidly regains full phenotypic resistance once mixed with nutrient-rich post-disaster runoff - metagenomics has confirmed hundreds of resistance genes shared between such rural drinking water and the gut microbiomes of nearby residents [193].

This is not a localized problem: a survey of over 4,000 seawater samples across 140 sites found resistance genes in every major ocean basin, and rising global temperatures are linked to a measurable climate-driven increase in *Salmonella* resistance worldwide - a reminder that post-earthquake hotspots feed into, and draw from, a much larger global reservoir [159,194].

6.6 Integrated Multi-Omics Strategies

Each omics layer answers a different question about the same sample, and none of them alone is conclusive. A pathogen's DNA can be present in metagenomic data without the organism being alive or dangerous; its genes can be transcribed without the corresponding protein being made; a protein can be made without producing a measurable physiological effect; and a measurable effect can occur without any resistance genes being clinically relevant. Reading the layers in sequence turns that ambiguity into a decision chain (Figure -1).

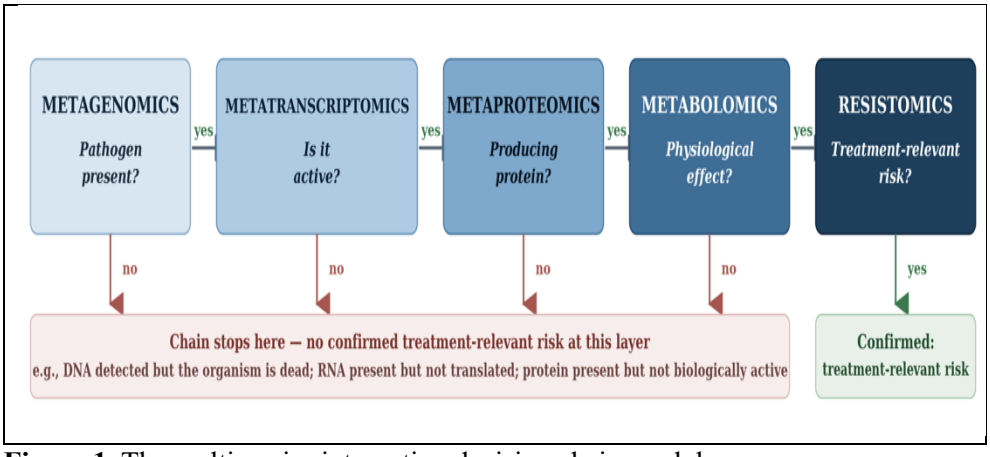


Figure 1. The multi-omics integration decision chain: each layer answers a narrower question than the last.

A “yes” at every step is what separates a genuine, treatment-relevant risk from a sequencing artifact, which is also why single-omics surveillance, however sophisticated, tends to overstate risk (detecting DNA that reflects no living threat) or understate it (missing an active, resistant organism that a targeted assay was never designed to look for) [161,163,165,169].

Turning this chain into a single risk score requires computational fusion across layers: approaches such as Similarity Network Fusion, Hypergraph-induced Orthogonal Non-negative Matrix Factorization (HONMF), and Graph Convolutional Networks (e.g., SynOmics) each merge omics layers differently, and a river-sediment pollution study found that fusing metagenomics and metatranscriptomics this way outperformed any single-omics model at predicting community resilience to chemical mixtures [195, 196].

6.7 Actionable Biosecurity Recommendations

Conventional monitoring remains indispensable for immediate public health decisions , it is fast to deploy and it is what most emergency responders already know how to run, but its inability to detect VBNC organisms and emerging antimicrobial resistance limits its predictive capacity. Integrating molecular and multi-omics technologies does not replace conventional monitoring; it enables environmental surveillance to move from reactive monitoring toward predictive biosecurity, answering not just what is contaminating this water today but what is likely to emerge next.

Translating that shift into practice points to six concrete priorities:

- Deploy Mobile Sequencing Units: field-deployable sequencing for untargeted surveillance within 12 to 24 hours of a disaster [160].
- Standardize Sample Preparation: common extraction protocols for low-biomass, contaminated matrices [177,179].
- Use AI-Assisted Proteomics: tools such as Kaiko to profile uncultured organisms without reference genomes [40].
- Monitor Resistome and Heavy Metals Together: track ARGs alongside metal contamination, given their co-selection [186].
- Deploy Integrated Computational Platforms: fuse environmental, clinical, and omics data [195,196].
- Monitor Dormant Aquifer Reservoirs: continuously sample VBNC bacterial fractions in rural and municipal groundwater [193].

7. CONCLUSIONS

This chapter has traced post-earthquake microbiological risk from the moment seismic energy ruptures water, sanitation, and soil systems to the point where that risk becomes detectable and actionable. Three conclusions follow. First, infectious disease risk after an earthquake is not incidental but phase-dependent and predictable: acute trauma gives way to enteric, respiratory, and wound-related infections within days, and then to latent and vector-borne disease over the following weeks and months [1,2,62]. Anticipating which pathogens dominate each phase allows surveillance and clinical resources to be positioned ahead of, rather than behind, an outbreak. Second, the environmental microbiology perspective adopted throughout this chapter matters because seismic disturbance itself reshapes microbial communities in soil, water, and air, independent of any single pathogen [11,34,37]. Treating water, soil, and air quality only as vectors for known organisms, rather than as disrupted ecosystems in their own right, leaves responders unprepared for what actually emerges. Third, the progression from conventional culture to molecular diagnostics to integrated multi-omics is best read as a set of complementary tools rather than competing ones: culture remains the fastest first response, molecular methods close the VBNC blind spot, and multi-omics enables the untargeted, forward-looking biosecurity needed to anticipate the next threat rather than merely confirm the last one [111,161,195,196]. Realizing this potential depends on resourcing the operational priorities outlined previously before the next disaster, not during it - integrating environmental microbiology, molecular epidemiology, and public health practice into one coordinated response, and turning post-disaster surveillance from a reactive account of what already happened into a predictive system for what is about to.

Declaration of Generative AI:

During the preparation of this work the authors used AI in order to improve the readability and language.

REFERENCES

1- Mavrouli, M., Mavroulis, S., Lekkas, E., & Tsakris, A. (2023). The impact of earthquakes on public health: A narrative review of infectious diseases in the post-disaster period aiming to disaster risk reduction. *Microorganisms*, *11*(2), 419.

2- Korkmaz, H. A. (2023). Public health emergencies and disaster risk management: A rural experience following the earthquake. *Turkish archives of pediatrics*, *58*(3), 353.

3- Orak, Y., Orak, F., Göçer, S., & Doğanay, M. (2023). Earthquake in Türkiye: impact on health services and infection threats. *Journal of Clinical Practice and Research*, *45*(6), 549.

4- Beşli, Y., & Sancak, B. (2023). Gastrointestinal infections after earthquake. *Microbiology Australia*, *44*(4), 193-196.

5- Aryal, S. (2022, August 10). *How to protect yourself from infectious diseases like diarrhoea, swine flu, etc. after an earthquake*. Microbiology Info. https://microbiologyinfo.com/how-to-protect-yourself-from-infectious-diseases-like-diarrhoea-swine-flu-etc-after-an-earthquake/

6- Marahatta, S. B. (2015). Control of the outbreak of disease aftermath earthquake: an overview. *Nepal Journal of Epidemiology*, *5*(2), 468.

7- Jabbour, E., Mouawad, Y., Abou Khater, D., & Helou, M. (2024). Lessons from the February 2023 Turkish earthquake. *Cureus*, *16*(10), e71042.

8- Manirambona, E., Obnial, J. C., Musa, S. S., Miranda, A. V., Haruna, U. A., & Shomuyiwa, D. O. (2023). The need for health system strengthening in the wake of natural disasters: Lessons from the 2023 Türkiye–Syria earthquake. *Public health challenges*, *2*(4), e131.

9- Akın, L. (2023, February 09). *Deprem Sonrası Bulaşıcı Hastalık Kontrolü*. Türkiye Milli Pediatri Derneği. https://millipediatri.org.tr/Custom/Upload/files/depremde_bulasici_hastalik. hacettepe_halk_ sagligi.pdf

10- Tuna, A. (2023). Infectious diseases that can occur after an earthquake: a review. *Intercont. J. Emerg. Med.*, *1*(1), 4-8.

11- Avcu, G. (2023). Infections after the earthquake disaster. *The Journal of Pediatric Research*, 10(4):235-237.

12- Baran, A., & Özer, A. (2023). Prevention of Infectious Diseases after an Earthquake. *Cam ve Sakura Medical Journal*, 3 (Suppl 1):42-47.

13- Najafi, S., Rezayat, A. A., Beyzaei, S. F., Shahriari, Z., Nour, M. G., Mosaed, R., ... & Farahani, R. H. (2022). Incidence of infectious diseases after earthquakes: a systematic review and meta-analysis. *Public Health, 202*, 131-138.

14- Ahmed, S. K., Chandran, D., Hussein, S., Sv, P., Chakraborty, S., Islam, M. R., & Dhama, K. (2023). Environmental health risks after the 2023 Turkey-Syria earthquake and salient mitigating strategies: a critical appraisal. *Environmental Health Insights*, *17*, 11786302231200865.

15- Herrick, K. R., Trondle, M. E., & Febles, T. T. (2020). Coccidioidomycosis (valley fever) in primary care. *American Family Physician*, *101*(4), 221-228.

16- Topluoglu, S., Taylan-Ozkan, A., & Alp, E. (2023). Impact of wars and natural disasters on emerging and re-emerging infectious diseases. *Frontiers in public health*, *11*, 1215929.

17- Shahsavari, S., Baghi, H. B., Kafil, H. S., & Leylabadlo, H. E. (2018). Re-emerging tularemia in some Middle East countries: what are the reasons?. *Iranian journal of public health*, *47*(2), 305.

18- Gürcan, Ş. (2014). Epidemiology of tularemia. *Balkan medical journal*, *2014*(1), 3-10.

19- Ardic, I. N., & Ardic, N. (2023). A minor emphasis on the outbreak of cutaneous leishmaniasis after devastating earthquakes in Turkey. *Asian Pacific Journal of Tropical Medicine*, *16*(3), 97-98.

20- Yates, T., Vujcic, J. A., Joseph, M. L., Gallandat, K., & Lantagne, D. (2018). Efficacy and effectiveness of water, sanitation, and hygiene interventions in emergencies in low-and middle-income countries: a systematic review. *Waterlines*, 31-65.

21- International Food Safety Authorities Network. (2005, February 09). *Food Safety in Natural Disasters*. INFOSAN. https://www.paho.org/sites/default/files/2022-07/FoodSafetyinDisasters.pdf

22- Jung, H., & Lee, J. (2026). Geochemical responses of groundwater to earthquakes: a review. *Journal of Hazard Literacy*, *2*(1), e19.

23- Moriarty, E., Dumbleton, B., & Gregor, J. (2012, June). *Summary of Literature Impacts of Earthquakes on Groundwater Quality*. ESR. https://www.phfscience.nz/media/cpvdgn0n/summary-of-literature-impacts-of-earthquakes-on-groundwater-quality.pdf

24- Zhang, Y., Horne, R. N., Hawkins, A. J., Primo, J. C., Gorbatenko, O., & Dekas, A. E. (2022). Geological activity shapes the microbiome in deep-subsurface aquifers by advection. *Proceedings of the National Academy of Sciences*, *119*(25), e2113985119.

25- Boyd, E. S., Colman, D. R., Menchaca, A., Spietz, R. L., Shoemaker, A., Finn, C., ... & Onstott, T. C. (2025). Seismic shifts in the geochemical and microbial composition of a Yellowstone aquifer. *PNAS nexus*, *4*(11), pgaf344.

26- Nakagawa, K., Shimada, J., Yu, Z. Q., Ide, K., & Berndtsson, R. (2020). Effects of the Japanese 2016 Kumamoto earthquake on nitrate content in groundwater supply. *Minerals*, *11*(1), 43.

27- Baniya, S., Paudel, S. R., Angove, M. J., Acharya, G., Wagle, A., Khatri, M., ... & Mainali, B. (2024). Theoretical and earthquake-induced groundwater chemistry changes: A perspective. *Journal of Hydrology*, *643*, 131917.

28- Hosono, T., Yamada, C., Manga, M., Wang, C. Y., & Tanimizu, M. (2020). Stable isotopes show that earthquakes enhance permeability and release water from mountains. *Nature Communications*, *11*(1), 2776.

29- Huang, X., Xian, T., Long, T., He, L., Donald, M. L., Deng, D., & Dong, T. (2024). Impacts of vegetation restoration strategies on soil nutrients and stoichiometry of the earthquake-induced landslides in Jiuzhaigou, eastern Qinghai-Tibet Plateau. *Frontiers in Environmental Science*, *11*, 1296187.

30- Zuo, H., Shen, H., Dong, S., Wu, S., He, F., Zhang, R., ... & Xiao, J. (2023). Potential short-term effects of earthquake on the plant–soil interface in alpine grassland of the Qinghai–Tibetan Plateau. *Frontiers in Plant Science*, *14*, 1240719.

31- Hore, S., Alim, M. A., & Hore, R. (2025). Impact of Earthquakes on Soil Chemical Properties: A Review of Mechanisms, Changes, and Implications for Environmental and Structural Resilience. *Earthquake*, *3*(1), 8575.

32- Huang, X., Xian, T., Long, T., He, L., Donald, M. L., Deng, D., & Dong, T. (2024). Impacts of vegetation restoration strategies on soil nutrients and stoichiometry of the earthquake-induced landslides in Jiuzhaigou, eastern Qinghai-Tibet Plateau. *Frontiers in Environmental Science*, *11*, 1296187.

33- Liu, R., & Wang, D. (2020). Soil C, N, P and K stoichiometry affected by vegetation restoration patterns in the alpine region of the Loess Plateau, Northwest China. *PloS one*, *15*(11), e0241859.

34- Kim, H., Kaown, D., Kim, J., Park, I. W., Joun, W. T., & Lee, K. K. (2020). Impact of earthquake on the communities of bacteria and archaea in groundwater ecosystems. *Journal of Hydrology*, *583*, 124563.

35- Kim, J., Kim, H., Kaown, D., & Lee, K. K. (2024). Thoron, radon and microbial community as supportive indicators of seismic activity in groundwater. *Scientific Reports*, *14*(1), 25955.

36- Kim, H. (2021). Need for seismic hydrology research with a geomicrobiological focus. *Sustainability*, *13*(16), 8704.

37- Toprak, S., Wham, B. P., Nacaroglu, E., Sakamoto, M., Tunc, S. C., Davis, C. A., ... & Ince, M. B. (2026). Assessment of Infrastructure Failures in the 2023 Kahramanmaras Earthquakes. *ASCE OPEN: Multidisciplinary Journal of Civil Engineering*, *4*(1), 04026001.

38- EPA. (2024, December). *Safeguarding Against Natural Hazards and Extreme Weather Events: A Resource Guide for Onsite Wastewater Treatment Systems*. EPA. https://www.epa.gov/system/files/documents/2024-12/septic-tanks-and-natural-hazards-resource-guide.pdf

39- Rusiñol, M. (2023). Waterborne viruses in urban groundwater environments. *PLoS Water*, *2*(8), e0000168.

40- National Science Foundation. (1981, September). *Earthquake Design Criteria for Water Supply and Wastewater Systems*. https://nehrpsearch.nist.gov/static/files/NSF/PB82189291.pdf

41- Biswas, R. R., & Biswas, T. R. (2017). Modelling earthquake effects on wastewater overflow pollutants. *Research Journal of Science and Technology*, *9*(4), 663-667.

42- Villafani, Y., Apel, H., Oostwegel, L. J., Huynh, T. T. N., Nguyen, H. Q., Downes, N. K., ... & Sairam, N. (2026). Quantifying Compounded Economic Impacts and Disease Burden of Flooding in Can Tho, Vietnam. *EGUsphere*, *2026*, 1-27.

43- Ebie, Y. (2015, August). *Johkasou: Earthquake-Resistant Wastewater Treatment System*. National Institute for Environmental Studies. https://www-cycle.nies.go.jp/eng/column/page/202103_01.html

44- Okoh, A. I., Sibanda, T., & Gusha, S. S. (2010). Inadequately treated wastewater as a source of human enteric viruses in the environment. *International journal of environmental research and public health*, *7*(6), 2620-2637.

45- Chowdhari, S., Rana, S., Rana, S., Morrison, C. M., Abney, S. E., Singh, R., ... & Vivekanandan, P. (2022). Quantitative assessment of microbial pathogens and indicators of wastewater treatment performance for safe and sustainable water reuse in India. *Microbiology spectrum*, *10*(6), e01720-22.

46- Lee, G. F., & Jones-Lee, A. (2015, January). *Flawed technology of subtitle D landfilling of municipal solid waste*. NSWAI. https://www.nswai.org/docs/Flawed Technology of Subtitle D Landfilling of MSW.pdf

47- Lee, G. F., & Jones-Lee, A. (2022, June). *Municipal Solid Waste Landfills – Water Quality Issues*. GFREDLEE. https://www.gfredlee.com/Landfills/WileyLandfills.pdf

48- Karslı, H., Babacan, A. E., Sayıl, N., Çoban, K. H., & Akın, Ö. (2024). An assessment of seismicity and near surface geophysical characteristics of potential solid waste landfill sites in the Eastern Black Sea Region of Türkiye. *Environmental Science and Pollution Research*, *31*(9), 14156-14177.

49- Nascimento, V. F., Yesiller, N., Clarke, K. C., Ometto, J. P. H. B., Andrade, P. R., & Sobral, A. C. (2017). Modeling the environmental susceptibility of landfill sites in California. *GIScience & Remote Sensing*, *54*(5), 657-677.

50- Virginia Tech. (2021, May 10). *Geoscientists find that shallow wastewater injection drives deep earthquakes in Texas*. ScienceDaily. https://www.sciencedaily.com/releases/2021/05/210510161428. htm

51- Ferreira, S., Liu, H., & Brewer, B. (2018). The housing market impacts of wastewater injection induced seismicity risk. *Journal of Environmental Economics and Management*, *92*, 251-269.

52- Merino, N., Jackson, T. R., Campbell, J. H., Kersting, A. B., Sackett, J., Fisher, J. C., ... & Moser, D. P. (2022). Subsurface microbial communities as a tool for characterizing regional-scale groundwater flow. *Science of The Total Environment*, *842*, 156768.

53- Lipus, D., Jia, Z., Sondermann, M., Bussert, R., Bartholomäus, A., Yang, S., ... & Kallmeyer, J. (2024). Microbial diversity and biogeochemical interactions in the seismically active and CO2-rich Eger Rift ecosystem. *Environmental Microbiome*, *19*(1), 113.

54- Chu, M., Liu, J., Li, H., Zhou, Y., Wang, N., Xia, C., ... & Bao, R. (2023). Earthquake-induced redistribution and reburial of microbes in the hadal trenches. *Innov. Geosci*, *1*(2), 100027.

55- Peoples, L. M., Grammatopoulou, E., Pombrol, M., Xu, X., Osuntokun, O., Blanton, J., ... & Bartlett, D. H. (2019). Microbial community diversity within sediments from two geographically separated hadal trenches. *Frontiers in microbiology*, *10*, 347.

56- Chu, M., Bao, R., Strasser, M., Ikehara, K., Ding, Y., Liu, K., ... & Druffel, E. (2025). Removal of dissolved organic carbon in the West Pacific hadal zones. *Nature Communications*, *16*(1), 733.

57- Sukel, K. (2026, January 5). *Soil-strengthening techniques are gaining momentum*. American Society of Civil Engineers. https://www.asce.org/publications-and-news/civil-engineering-source/civil-engineering-magazine/issues/magazine-issue/article/2026/05/soil-strengthening-techniques-are-gaining-momentum

58- Hall, C. A., Van Turnhout, A., Kavazanjian Jr, E., Van Paassen, L. A., & Rittmann, B. (2023). A multi-phase biogeochemical model for mitigating earthquake-induced liquefaction via microbially induced desaturation and calcium carbonate precipitation. *Biogeosciences*, *20*(14), 2903-2917.

59- Kullman, J. (2023, February 27). *Boosting seismic resilience*. ASU News. https://news.asu.edu/20230227-boosting-seismic-resilience

60- Dejong, J. (2007, February 21). *Bacteria can help prevent earthquake damage*. Mongabay. https://news.mongabay.com/2007/02/bacteria-can-help-prevent-earthquake-damage/

61- Kouadio, I. K., Aljunid, S., Kamigaki, T., Hammad, K., & Oshitani, H. (2012). Infectious diseases following natural disasters: prevention and control measures. *Expert review of anti-infective therapy*, *10*(1), 95-104.

62- Liang, S. Y., & Messenger, N. (2018). Infectious diseases after hydrologic disasters. *Emergency Medicine Clinics*, *36*(4), 835-851.

63- Akova, M. (2023). In the Aftermath of a Natural Disaster: The Infectious Diseases may Strike Back. *Infectious Diseases & Clinical Microbiology*, *5*(1), 1.

64- Mavrouli, M., Mavroulis, S., Lekkas, E., & Tsakris, A. (2023). The impact of earthquakes on public health: A narrative review of infectious diseases in the post-disaster period aiming to disaster risk reduction. *Microorganisms, 11*(2), 419.

65-Mohite, P., Rajput, T., Pangeni, P., Shah, S., Bhandari, S., Mehta, R., ... & Mohanty, A. (2024). Reviewing History of Earthquake in 21 st Century and Possible Infectious Diseases. *Journal of Pure & Applied Microbiology, 18*(4), 2218.

66-Törüyenler-Coşkunpınar, M., Gülten, E., Akdemir, İ., Çınar, G., Sarıcaoğlu, E. M., & Yörük, F. (2026). Evaluation of Wound Infections after the 2023 Kahramanmaraş Earthquakes. *Infectious Diseases & Clinical Microbiology, 8*(1), 45.

67-Kunz, J. M. et al. (2024). Surveillance of waterborne disease outbreaks associated with drinking water-United States, 2015–2020. MMWR. Surveillance Summaries, 73.

68-Johnston, S. (2012). “Shake, Rattle and Roll”: risk assessment and management for food safety during two Christchurch earthquakes. *Western Pacific Surveillance and Response Journal: WPSAR, 3*(2), e1.

69-Ramírez-Castillo, F. Y., Loera-Muro, A., Jacques, M., Garneau, P., Avelar-González, F. J., Harel, J., & Guerrero-Barrera, A. L. (2015). Waterborne pathogens: detection methods and challenges. *Pathogens, 4*(2), 307-334.

70-Orata, F. D., Keim, P. S., & Boucher, Y. (2014). The 2010 cholera outbreak in Haiti: how science solved a controversy. *PLoS pathogens, 10*(4), e1003967.

71-Ocasio, D. V.; et al. (2023). Cholera Outbreak-Haiti, September 2022-January 2023. *Morbidity and mortality weekly report, 72*.

72-Charles, M., Delva, G. G., Boutin, J., Severe, K., Peck, M., Mabou, M. M., ... & Pape, J. W. (2014). Importance of cholera and other etiologies of acute

diarrhea in post-earthquake Port-au-Prince, Haiti. *The American journal of tropical medicine and hygiene, 90*(3), 511.

73-Stein, R. A., & Chirilã, M. (2017). Routes of transmission in the food chain. In Foodborne diseases (pp. 65-103). Academic Press.

74-Shakya, G., Marasini, B., Karki, K. B., Upadhaya, B. P., Acharya, J., Adhikari, S., ... & Dhimal, M. (2018). Outbreak investigation following the 2015 earthquake disaster in Nepal.

75-Chiu, C. S., Chen, U. M., Yang, L. C., Wei, C. L., & Liao, C. L. (2001). Shigellosis infections in nantou county: 1995-1999. *Epidemiology Bulletin, 17*(7), 159-178.

76-Gorris, M. E., & Barker, B. M. (2026). Hypothesis on the dust-borne atmospheric transport of Coccidioides, causative fungal pathogen for coccidioidomycosis (Valley fever). *Medical Mycology, 64*(3), myag012.

77-Jibson, R. W., Harp, E. L., Schneider, E., Hajjeh, R. A., & Spiegel, R. A. (1998). An outbreak of coccidioidomycosis (valley fever) caused by landslides triggered by the 1994 Northridge, California, earthquake.

78-Jibson, R. W. (2002). A public health issue related to collateral seismic hazards: the valley fever outbreak triggered by the 1994 Northridge, California earthquake. *Surveys in Geophysics, 23*(6), 511-528.

79-Keefer, D., & Wilson, R. (2013). Effects from earthquake-triggered landslides [Online]. USGS.

80-Xue, W., Chen, W., Wang, J., Cao, K., & Liu, H. (2025). Distribution and antibiotic resistance of pathogens in post-earthquake traumatic infections: a systematic review and meta-analysis. *BMC Infectious Diseases, 25*(1), 1449.

81-Mardani, M. (2018). Tetanus in Area Affected by Earthquake: Risk, Prevention and Management. *Archives of Clinical Infectious Diseases, 13*(13), e87049.

82-Scott, P., Deye, G., Srinivasan, A., Murray, C., Moran, K., Hulten, E., ... & Petruccelli, B. (2007). An outbreak of multidrug-resistant Acinetobacter baumannii-calcoaceticus complex infection in the US military health care system associated with military operations in Iraq. *Clinical infectious diseases, 44*(12), 1577-1584.

83-Afshar, M., Raju, M., Ansell, D., & Bleck, T. P. (2011). Narrative review: tetanus—a health threat after natural disasters in developing countries. Annals of internal medicine, 154(5), 329-335.

84-Leiblein, M., Wagner, N., Adam, E. H., Frank, J., Marzi, I., & Nau, C. (2020). Clostridial gas gangrene-a rare but deadly infection: case series and comparison to other necrotizing soft tissue infections. *Orthopaedic surgery, 12*(6), 1733-1747.

85-Hadzhiminev, V., & Kalacheva, K. (2026). A case report of gas gangrene caused by rare type of clostridium-clostridium limosum. Medis. *International Journal of Medical Sciences and Research, 5*(2), 69-73.

86-Mavrouli, M., Mavroulis, S., Lekkas, E., & Tsakris, A. (2023, April). An emerging health crisis in Turkey and Syria after the earthquake disaster on 6 February 2023: risk factors, prevention and management of infectious diseases. In Healthcare. *MDPI, 11*(7), 1022.

87-Watson, J., Connolly, M., & Gayer, M. (2006). Communicable diseases following natural disasters: Risk assessmnt and priority interventions. In Communicable diseases following natural disasters: Risk assessmnt and priority interventions (pp. 19-19).

88-Oda, N., Hirahara, T., Fujioka, Y., Mitani, R., & Takata, I. (2019). Legionella pneumonia following the heavy rain event of July 2018 in Japan. *Internal Medicine, 58*(19), 2831-2834.

89-Allworth, A. M. (2005). Tsunami lung: a necrotising pneumonia in survivors of the Asian tsunami. *The Medical Journal of Australia, 182*(7), 364.

90-Nakadate, T., Nakamura, Y., Yamauchii, K., & Endo, S. (2012). Two cases of severe pneumonia after the 2011 Great East Japan Earthquake. *Western Pacific Surveillance and Response Journal: WPSAR, 3*(4), 67.

91-Mavrouli, M., Mavroulis, S., Lekkas, E., & Tsakris, A. (2021). Respiratory infections following earthquake-induced tsunamis: transmission risk factors and lessons learned for disaster risk management. *International Journal of Environmental Research and Public Health, 18*(9), 4952.

92-Reina Ortiz, M., Le, N. K., Sharma, V., Hoare, I., Quizhpe, E., Teran, E., ... & Izurieta, R. (2017). Post-earthquake Zika virus surge: Disaster and public health threat amid climatic conduciveness. *Scientific reports, 7*(1), 15408.

93-Quintanilla, N. (2022). Outbreaks of vector-borne infectious disease following a natural disaster. *Georgetown Medical Review, 6*(1).

94-Demir, B., Şahin, L., Kaya, K., & Akın, M. A. (2025). Itchy skin diseases in the emergency department before and after the earthquakes. *Signa Vitae, 21*(9), 35.

95-Froeschl, G., Zagli, B., Erucar, E., Alaaeddin, K., Othman, M. E., & Hatunoglu, C. (2025). Needs and early response towards internally displaced people in Hatay Province in the aftermath of the 2023 earthquake in Turkey. *BMC Public Health, 25*(1), 1706.

96-Rivas-Pinedo, P., Motta, J. C., & Gutierrez, J. M. O. (2025). Invasive candidiasis in contexts of armed conflict, high violence, and forced displacement in latin america and the caribbean (2005–2025). *Journal of Fungi, 11*(8), 583.

97-Charnley, G. E., Kelman, I., Gaythorpe, K. A., & Murray, K. A. (2021). Traits and risk factors of post-disaster infectious disease outbreaks: a systematic review. *Scientific reports, 11*(1), 5616.

98-Mavrouli, M., Mavroulis, S., Lekkas, E., & Tsakris, A. (2021). Respiratory infections following earthquake-induced tsunamis: transmission risk factors and lessons learned for disaster risk management. *International Journal of Environmental Research and Public Health, 18*(9), 4952.

99-Najafi, S., Rezayat, A. A., Beyzaei, S. F., Shahriari, Z., Nour, M. G., Mosaed, R., ... & Farahani, R. H. (2022). Incidence of infectious diseases after earthquakes: a systematic review and meta-analysis. *Public Health, 202*, 131-138.

100-Xue, W., Chen, W., Wang, J., Cao, K., & Liu, H. (2025). Distribution and antibiotic resistance of pathogens in post-earthquake traumatic infections: a systematic review and meta-analysis. *BMC Infectious Diseases, 25*(1), 1449.

101-Sekine, K., & Roskosky, M. (2018). Emergency response in water, sanitation and hygiene to control cholera in post-earthquake Nepal in 2016. *Journal of Water, Sanitation and Hygiene for Development, 8*(4), 799-802.

102-Watson, J. T., Gayer, M., & Connolly, M. A. (2007). Epidemics after natural disasters. *Emerging infectious diseases, 13*(1), 1.

103-Sumner, S. A., Turner, E. L., & Thielman, N. M. (2013). Association between earthquake events and cholera outbreaks: a cross-country 15-year longitudinal analysis. *Prehospital and Disaster Medicine, 28*(6), 567-572.

104-Kojima, K., Nakakuki, K., Tsuboyama-Kasaoka, N., Ueda, N., Yamamoto, M., Takasugi, T., ... & Ojima, T. (2025). Qualitative analysis of the relationship between oral health and nutritional care during the 2024 Noto Peninsula Earthquake disaster in Japan. *Preventive Medicine Research, 3*(2), 58-67.

105-Jibson, R. W. (2002). A public health issue related to collateral seismic hazards: the valley fever outbreak triggered by the 1994 Northridge, California earthquake. *Surveys in Geophysics, 23*(6), 511-528.

106-Demir, B., Şahin, L., Kaya, K., & Akın, M. A. (2025). Itchy skin diseases in the emergency department before and after the earthquakes. *Signa Vitae, 21*(9), 35.

107-Marshall, J., Wiltshire, J., Delva, J., Bello, T., & Masys, A. J. (2020). Natural and manmade disasters: vulnerable populations. In Global health security: Recognizing vulnerabilities, creating opportunities (pp. 143-161). Cham: Springer International Publishing.

108-Jamieson, D. J., Theiler, R. N., & Rasmussen, S. A. (2006). Emerging infections and pregnancy. *Emerging infectious diseases, 12*(11), 1638.

109-Sappenfield, E., Jamieson, D. J., & Kourtis, A. P. (2013). Pregnancy and susceptibility to infectious diseases. *Infectious diseases in obstetrics and gynecology, 2013*(1), 752852

110-Gülistan Çakar, E., & Demir, E. (2026). Field study on the health status of children aged 0–18 in container cities after the 2023 Türkiye earthquake-Hatay example. *BMC Public Health, 26*(1), 1367.

111- Uprety, S., Hong, P.-Y., Sadik, N., Dangol, B., Adhikari, R., Jutla, A., Shisler, J. L., Degnan, P., & Nguyen, T. H. (2017). The effect of the 2015 earthquake on the bacterial community compositions in water in Nepal. *Frontiers in Microbiology, 8*, Article 2380. https://doi.org/10.3389/fmicb.2017.02380

112- American Academy of Microbiology. (2025). Water, waterborne pathogens, and public health: Environmental drivers. *American Society for Microbiology*. https://www.ncbi.nlm.nih.gov/books/NBK621436/

113- Association of Public Health Laboratories. (n.d.). Environmental microbiology outbreak response. https://aphl.org/focus-areas/environmental-health/readiness-and-response/EMOR

114- Khant, N. A., Lumongsod, R. M., San, A., Moon, J., Namkoong, S., & Kim, H. (2025). Navigating the complex landscape of waterborne disease research. *Journal of Water and Health, 23*(2), 168–189. https://doi.org/10.2166/wh.2025.280

115- U.S. Agency for International Development. (2024). A guide to resources on emergency drinking water quality. Programme Solidarité Eau. https://bdd.pseau.org/outils/ouvrages/usaid_a_guide_to_resources_on_emergency_drinking_water_quality_2024.pdf

116- U.S. Environmental Protection Agency. (n.d.). Drinking water regulations. https://www.epa.gov/dwreginfo/drinking-water-regulations

117- Microbac Laboratories. (2026). 2026 EPA drinking water compliance guide. https://www.microbac.com/2026-epa-drinking-water-compliance-guide/

118- World Health Organization. (2023, September 13). Drinking-water. https://www.who.int/news-room/fact-sheets/detail/drinking-water

119- U.S. Environmental Protection Agency. (n.d.). National primary drinking water regulations. https://www.epa.gov/ground-water-and-drinking-water/national-primary-drinking-water-regulations

120- Oxfam. (n.d.). Water quality analysis in emergency situations. Oxfam WASH. https://www.oxfamwash.org/water-quality-analysis-in-emergency-situations/

121- World Health Organization. (2018). Table 8.3, WHO guideline values for drinking-water quality: Bacteria. In WHO housing and health guidelines. National Center for Biotechnology Information (US). https://www.ncbi.nlm.nih.gov/books/NBK535301/table/ch8.tab3/

122- Foddai, A. C. G., & Grant, I. R. (2020). Methods for detection of viable foodborne pathogens: Current state-of-art and future prospects. *Applied Microbiology and Biotechnology, 104*(10), 4281–4288. https://doi.org/10.1007/s00253-020-10542-x

123- Feleni, U., Morare, R., Masunga, G. S., Magwaza, N., Saasa, V., Madito, M. J., & Managa, M. (2025). Recent developments in waterborne pathogen detection technologies. *Environmental Monitoring and Assessment, 197*(3), Article 233. https://doi.org/10.1007/s10661-025-13644-z

124- Nappier, S. P., Ichida, A., Jaglo, K., Haugland, R., & Jones, K. R. (2019). Advancements in mitigating interference in quantitative polymerase chain reaction (qPCR) for microbial water quality monitoring. *Science of the Total Environment, 671*, 776–785.

125- Pandey, S. K., Khan, A. B., & Puri, S. (2025). Waterborne pathogen surveillance in flood-prone regions using qPCR. *International Journal of Environmental Sciences, 11*(2), 674–679.

126- Nema, R. K., Singh, S., Singh, A. K., Sarma, D. K., Diwan, V., Tiwari, R. R., Mondal, R. K., & Mishra, P. K. (2024). Protocol for detection of pathogenic enteric RNA viruses by regular monitoring of environmental samples from wastewater treatment plants using droplet digital PCR. *Science in One Health, 3*, Article 100080.

127- Botes, M., de Kwaadsteniet, M., & Cloete, T. E. (2013). Application of quantitative PCR for the detection of microorganisms in water. *Analytical and Bioanalytical Chemistry, 405*(1), 91–108. https://doi.org/10.1007/s00216-012-6399-3

128- Oon, Y.-L., Oon, Y.-S., Ayaz, M., Deng, M., Li, L., & Song, K. (2023). Waterborne pathogens detection technologies: Advances, challenges, and future perspectives. *Frontiers in Microbiology, 14*, Article 1286923. https://doi.org/10.3389/fmicb.2023.1286923

129- U.S. Environmental Protection Agency. (n.d.). SAM pathogen methods. https://www.epa.gov/esam/sam-pathogen-methods

130- Huq, A., Haley, B. J., Taviani, E., Chen, A., Hasan, N. A., & Colwell, R. R. (2012). Detection, isolation, and identification of Vibrio cholerae from the environment. *Current Protocols in Microbiology, 26*(1), 6A.5.1–6A.5.51.

131- U.S. Environmental Protection Agency. (2021, January 19). SAM pathogen methods [Archived snapshot]. Environmental Sampling and Analytical Methods (ESAM) Program. https://19january2021snapshot.epa.gov/esam/sam-pathogen-methods_.html

132-. Centers for Disease Control and Prevention. (2024). Chapter 6: Isolation and identification of Vibrio cholerae. In Laboratory methods for the diagnosis of

epidemic dysentery and cholera. https://www.cdc.gov/cholera/media/pdfs/2024/07/Chapter-6-Laboratory-methods-for-the-diagnosis-of-epidemic-dysentery-and-cholera_ENG-6.pdf

133- Centers for Disease Control and Prevention. (2024). Isolation of Vibrio cholerae from fecal specimens. In Laboratory methods for the diagnosis of Vibrio cholerae. https://www.cdc.gov/cholera/media/pdfs/2024/07/4-Isolation-of-Vibrio-cholerae-from-Fecal-Specimens-Laboratory-methods-for-the-diagnosis-of-Vibrio-cholerae_ENG-4.pdf

134- U.S. Environmental Protection Agency. (2009). Method 1603: Escherichia coli (E. coli) in water by membrane filtration using modified membrane-thermotolerant Escherichia coli agar (modified mTEC). https://19january2017snapshot.epa.gov/sites/production/files/2015-08/documents/method_16 03_2009.pdf

135- BioTrading. (n.d.). m-TEC agar, product information. https://biotrading.com/assets/productinformatie/acumedia/tds/7421.pdf

136- Difco. (n.d.). mTEC agar, modified [Manual]. https://cdn.media.interlabdist.com.br/uploads/2021/01/MTEC-Agar-Modified.pdf

137- Centers for Disease Control and Prevention. (2024). Preparation of media and reagents. In Laboratory methods for the diagnosis of Vibrio cholerae. https://www.cdc.gov/cholera/media/pdfs/2024/07/11-Preparation-of-Media-and-Reagents-Laboratory-methods-for-the-diagnosis-of-Vibrio-cholerae_ENG-11.pdf

138- National Environmental Methods Index. (n.d.). EPA-MICRO: 1103.1 (modified): Membrane filtration plating of E. coli on modified mTEC agar. https://www.nemi.gov/methods/method_summary/5575/

139- Separation Science. (n.d.). Next-generation pathogen detection methods for food and water. https://www.sepscience.com/next-generation-pathogen-detection-methods-for-food-and-water-12226

140- Ahmed, W., Smith, W. J. M., Metcalfe, S., Jackson, G., Choi, P. M., Morrison, M., Field, D., Gyawali, P., Bivins, A., Bibby, K., & Simpson, S. L. (2022). Comparison of RT-qPCR and RT-dPCR platforms for the trace detection of SARS-CoV-2 RNA in wastewater. *ACS ES&T Water, 2*(11), 1871–1880. https://doi.org/10.1021/acsestwater.1c00387

141- MyBioSource. (n.d.). Environmental applications of PCR: Microbial ecology and pollution monitoring. MyBioSource Learning Center. https://www.mybiosource.com/learn/environmental-applications-of-pcr-microbial-ecology-and-pollution-monitoring/

142- JoVE (Journal of Visualized Experiments). (n.d.). PCR system to detect phytopathogens: Protocol preview [Video]. YouTube. https://www.youtube.com/watch?v=b0EmE6hlwQI

143- Akello, J. O., Bellekom, B., Shaw, A. G., & Grassly, N. C. (2026). Principles and performance of wastewater concentration methods for environmental surveillance of viruses: A systematic review and meta-analysis. medRxiv. https://doi.org/10.64898/2026.03.19.26348821

144- Borchardt, M. A., Boehm, A. B., Salit, M., Spencer, S. K., Wigginton, K. R., & Noble, R. T. (2021). The Environmental Microbiology Minimum Information (EMMI) guidelines: qPCR and dPCR quality and reporting for environmental microbiology. *Environmental Science & Technology, 55*(15), 10210–10223. https://doi.org/10.1021/acs.est.1c01767

145- Duhachek Muggy, S., Avriette, M., Roberts, D., & Leuschner, K. J. (2024). Modern biosurveillance methods: A lay introduction to effective use of nucleic acid methods. RAND Corporation. https://www.rand.org/content/dam/rand/pubs/research_reports/RRA3200/RRA3263-1/RAND_RRA3263-1.pdf

146- Sibley, C. D., Peirano, G., & Church, D. L. (2012). Molecular methods for pathogen and microbial community detection and characterization: Current and potential application in diagnostic microbiology. *Infection, Genetics and Evolution, 12*(3), 505–521. https://doi.org/10.1016/j.meegid.2012.01.011

147- Orlikowska, T. (2025). Diagnostic sensitivity of Phytophthora ×alni from environmental samples using conventional and real-time PCR. *Forests, 16*(1), Article 68. https://doi.org/10.3390/f16010068

148- GT Molecular. (n.d.). Wastewater surveillance PCR kits — Multiplex. https://www.gtmolecular.com/wastewater-and-water-pathogen-pcr-detection-kits/ (148)

149- Siko, J. E. E., Dahmer, K. J., Manoharan, Z. Z., Muthukumar, A., Amato, H. K., LeBoa, C., Harris, M., Janagaraj, V., Manuel, M., Varghese, T., Houngbegnon, P., Pilotte, N., Bouko, B., Saïdou, S., Luty, A. J. F., Ramesh, R. M., Ibikounlé, M., Ajjampur, S. S. R., & Pickering, A. J. (2025). Environmental surveillance of soil-transmitted helminths and other enteric pathogens in settings without networked wastewater infrastructure. *PLOS Water, 4*(1), Article e0000337. https://doi.org/10.1371/journal.pwat.0000337

150- Centers for Disease Control and Prevention. (n.d.). Cholera clinical detection. https://www.cdc.gov/cholera/php/laboratories/cholera-clinical-detection.html

151- Engstrom-Melnyk, J., Rodriguez, P. L., Peraud, O., & Hein, R. C. (2015). Clinical applications of quantitative real-time PCR in virology. In Methods in

Microbiology (Vol. 42, pp. 161–197). Elsevier. https://doi.org/10.1016/bs.mim.2015.04.005

152- U.S. Environmental Protection Agency. (2016). The next generation PCR-based quantification method for ambient water. https://19january2017snapshot.epa.gov/sites/production/files/2016-06/documents/next-generation-pcrbased.pdf

153- Bonacorsi, S., Visseaux, B., Bouzid, D., Pareja, J., Rao, S. N., Manissero, D., Hansen, G., & Vila, J. (2021). Systematic review on the correlation of quantitative PCR cycle threshold values of gastrointestinal pathogens with patient clinical presentation and outcomes. *Frontiers in Medicine, 8*, Article 711809. https://doi.org/10.3389/fmed.2021.711809

154- Lin, Y., Hay, J. A., Meng, Y., Cowling, B. J., & Yang, B. (2025). Generalizing population RT-qPCR cycle threshold values-informed estimation of epidemiological dynamics: Impact of surveillance practices and pathogen variability. *PLOS Computational Biology, 21*(9), Article e1013527. https://doi.org/10.1371/journal.pcbi.1013527

155- Zhang, S., Li, X., Wu, J., Coin, L., O'Brien, J., Hai, F., & Jiang, G. (2021). Molecular methods for pathogenic bacteria detection and recent advances in wastewater analysis. *Water, 13*(24), Article 3551. https://doi.org/10.3390/w13243551

156- Thermo Fisher Scientific. (n.d.). Digital PCR applications: Environmental pathogen quantification. https://www.thermofisher.com/us/en/home/life-science/pcr/digital-pcr/education/basic-research/environmental-pathogen-quantification.html

157-. Sun, H., Yao, Q., Zhao, X., Li, X., Deng, F., Han, J., Zhang, L., Yao, X., Kan, B., Zhang, J., & Tang, S. (2025). A quadruplex digital PCR assay for the simultaneous detection of four intestinal bacterial pathogens and its application in wastewater samples. *China CDC Weekly, 7*(12), 393–399. https://doi.org/10.46234/ccdcw2025.065

158- Bio-Rad Laboratories. (n.d.). Wastewater SARS-CoV-2 testing with droplet digital PCR (ddPCR) technology. Bioradiations. https://www.bioradiations.com/wastewater-sars-cov-2-testing-with-ddpcr-422/

159- Cyprus Mail. (2026, June 13). Antibiotic resistance genes found across world oceans, Italian study shows. https://cyprus-mail.com/2026/06/13/antibiotic-resistance-genes-found-across-world-oceans-italian-study-shows

160- Gauthier, J., Mohammadi, N., Kukavica-Ibrulj, I., Boyle, B., Landgraff, C., Goodridge, L., White, A. P., Chapman, B., & Levesque, R. C. (2025). Leveraging artificial intelligence community analytics and nanopore

metagenomic surveillance to monitor early enteropathogen outbreaks. *Frontiers in Public Health, 13*, Article 1675080. https://doi.org/10.3389/fpubh.2025.1675080

161- Arıkan, M., & Muth, T. (2023). Integrated multi-omics analyses of microbial communities: A review of the current state and future directions. *Molecular Omics, 19*(8), 607–623. https://doi.org/10.1039/D3MO00089C

162- Nabila Haddad, Nick Johnson, Sophia Kathariou, Aline Métris, Trevor Phister, Annemarie Pielaat, Chrysoula Tassou, Marjon H.J. Wells-Bennik, Marcel H. Zwietering, Next generation microbiological risk assessment-Potential of omics data for hazard characterisation, *International Journal of Food Microbiology*, Volume 287, 2018, Pages 28-39, ISSN 0168-1605, https://doi.org/10.1016/j.ijfoodmicro.2018.04.015.

163- McElhinney, J. M. W. R., Catacutan, M. K., Mawart, A., Hasan, A., & Dias, J. (2022). Interfacing machine learning and microbial omics: A promising means to address environmental challenges. *Frontiers in Microbiology, 13*, Article 851450. https://doi.org/10.3389/fmicb.2022.851450

164- Smith, K. F., Pochon, X., Melvin, S. D., Wheeler, T. T., & Tremblay, L. A. (2025). Integration of "omics"-based approaches in environmental risk assessment to establish cause and effect relationships: A review. *Toxics, 13*(9), Article 714. https://doi.org/10.3390/toxics13090714

165- Hong, P.-Y., Mantilla-Calderon, D., & Wang, C. (2020). Metagenomics as a tool to monitor reclaimed-water quality. *Applied and Environmental Microbiology, 86*(16), Article e00724-20. https://doi.org/10.1128/AEM.00724-20

166- Hong, P.-Y., Julian, T. R., & Jumat, M. R. (2018). Editorial: Microbial safety in water resources. *Frontiers in Microbiology, 9*, Article 3064. https://doi.org/10.3389/fmicb.2018.03064

167- Justen, A., et al. (2026). Deep untargeted wastewater metagenomic sequencing from sewersheds across the United States. medRxiv. https://doi.org/10.64898/2026.03.05.26345726

168- Helbling, D. E., Ackermann, M., Fenner, K., Kohler, H.-P. E., & Johnson, D. R. (2012). The activity level of a microbial community function can be predicted from its metatranscriptome. *The ISME Journal, 6*(4), 902–904. https://doi.org/10.1038/ismej.2011.158

169- Wu, J., Gao, W., Johnson, R. H., Zhang, W., & Meldrum, D. (2013). Integrated metagenomic and metatranscriptomic analyses of microbial communities in the meso- and bathypelagic realm of North Pacific Ocean. *Marine Drugs, 11*(10), 3777–3801. https://doi.org/10.3390/md11103777

170- Huang, Y., Hu, H., Zhang, T., Wang, W., Liu, W., & Tang, H. (2024). Meta-omics assisted microbial gene and strain resources mining in contaminant environment. *Engineering in Life Sciences, 24*(5). https://doi.org/10.1002/elsc.202300207

171- Sadeghi, J., Hashemi Shahraki, A., Chaganti, S. R., & Heath, D. (2023). Functional gene transcription variation in bacterial metatranscriptomes in large freshwater lake ecosystems: Implications for ecosystem and human health. *Environmental Research, 231*, Article 116298. https://doi.org/10.1016/j.envres.2023.116298

172- Söllinger, A., et al. (2022). Down-regulation of the bacterial protein biosynthesis machinery in response to weeks, years, and decades of soil warming. *Science Advances, 8*(13), Article eabm3230. https://doi.org/10.1126/sciadv.abm3230

173- Kibambe, M. G., Keshri, J., & Momba, M. N. B. (2026). Metatranscriptomic insights into microbial responses of a bacterial consortium from activated sludge at the Zeekoegat Wastewater Treatment Plant to perfluorooctane sulfonate and perfluorooctanoic acid. *Water, 18*(11), Article 1367. https://doi.org/10.3390/w18111367

174- Chowdhury, S. F., Sarkar, M. M. H., Al Sium, S. M., & Khan, M. S. (2025). Metatranscriptomic analysis uncovers microbial and immune signatures underlying COVID-19 severity. Briefings in Bioinformatics. https://doi.org/10.1093/bib/bbaf631.015

175- Rajagopala, S. V., Bakhoum, N. G., Pakala, S. B., et al. (2021). Metatranscriptomics to characterize respiratory virome, microbiome, and host response directly from clinical samples. *Cell Reports Methods, 1*(6), Article 100091. https://doi.org/10.1016/j.crmeth.2021.100091

176- Chowdhury, S. F., Sarkar, M. M. H., Al Sium, S. M., Naser, S. R., Hossain, M. S., Habib, M. A., Akter, S., Banu, T. A., Goswami, B., Jahan, I., Chakrovarty, T., Molla, M. M. A., Nafisa, T., Yeasmin, M., Ghosh, A. K., & Khan, M. S. (2026). Metatranscriptomic insights into host-microbiome interactions underlying asymptomatic COVID-19 cases. *Scientific Reports, 16*, Article 11916. https://doi.org/10.1038/s41598-026-40563-x

177- Williams, M. A., Taylor, E. B., & Mula, H. P. (2010). Metaproteomic characterization of a soil microbial community following carbon amendment. *Soil Biology and Biochemistry, 42*(7), 1148–1156. https://doi.org/10.1016/j.soilbio.2010.03.021

178- Wang, D.-Z., Kong, L.-F., Li, Y.-Y., & Xie, Z.-X. (2016). Environmental microbial community proteomics: Status, challenges and perspectives.

International Journal of Molecular Sciences, 17(8), Article 1275. https://doi.org/10.3390/ijms17081275

179- Pan, H., Wattiez, R., & Gillan, D. (2024). Soil metaproteomics for microbial community profiling: Methodologies and challenges. *Current Microbiology, 81*, Article 257. https://doi.org/10.1007/s00284-024-03781-y

180- Zhang, B., Feng, S., Parajuli, M., Xiong, Y., Pan, C., & Guo, X. (2024). SEMQuant: Extending Sipros-Ensemble with match-between-runs for comprehensive quantitative metaproteomics. In Bioinformatics Research and Applications (ISBRA 2024). Springer. https://doi.org/10.1007/978-981-97-5087-0_9

181- Pacific Northwest National Laboratory. (n.d.). Unparalleled resolution of how microbes and viruses impact biogeochemistry in rivers. https://www.pnnl.gov/publications/unparalleled-resolution-how-microbes-and-viruses-impact-biogeochemistry-rivers

182- MetwareBio. (n.d.). Metabolomics: Environmental exposure impact on health hazards. https://www.metwarebio.com/metabolomics-environmental-exposure-impact-on-health-hazards/

183- Chen, M. (2024). Environmental chemical exposomics and metabolomics in toxicology: The latest updates. *Toxics, 12*(9), Article 647. https://doi.org/10.3390/toxics12090647

184- Deng, P., Li, X., Petriello, M. C., Wang, C., Morris, A. J., & Hennig, B. (2019). Application of metabolomics to characterize environmental pollutant toxicity and disease risks. *Reviews on Environmental Health, 34*(3), 251–259. https://doi.org/10.1515/reveh-2019-0030

185- MDPI. (n.d.). Metabolites: Special issue on environmental metabolomics. https://www.mdpi.com/journal/metabolites/special_issues/environmental_metabolomics

186- Martínez, J. R. W., Alcalde-Rico, M., Jara-Videla, E., Reyes, J., Carvajal, L. P., Rincon, S., Ríos, R., Diaz, L., Quesille-Villalobos, A., Riquelme-Neira, R., Rivas, L., Moustafa, A. M., Hanson, B., Undurraga, E. A., Olivares-Pacheco, J., García, P., Araos, R., Planet, P. J., Arias, C. A., & Munita, J. M. (2025). Geographic divergence of methicillin-resistant Staphylococcus aureus ST5-SCCmecI in the aftermath of a major earthquake and tsunami: Impact of a plasmid harboring heavy metal resistance genes. *mBio, 16*(4), Article e03669-24. https://doi.org/10.1128/mbio.03669-24

187- Geological Survey. (n.d.). Comprehensive research on PFAS exposomics and risk assessment. https://www.usgs.gov/centers/columbia-environmental-research-center/science/comprehensive-research-pfas-exposomics-and

188- Shetty, S. S., D., D., S., H., Sonkusare, S., Naik, P. B., Kumari N., S., & Madhyastha, H. (2023). Environmental pollutants and their effects on human health. *Heliyon, 9*(9), Article e19496. https://doi.org/10.1016/j.heliyon.2023.e19496

189- Song, Y., Yao, S., Li, X., Wang, T., Jiang, X., Bolan, N., Warren, C. R., Northen, T. R., & Chang, S. X. (2024). Soil metabolomics: Deciphering underground metabolic webs in terrestrial ecosystems. *Eco-Environment & Health, 3*(2), 227–237. https://doi.org/10.1016/j.eehl.2024.03.001

190- Berger, F. (2025). Exploring the nexus of antimicrobial resistance and natural hazards and associated disasters: A scoping approach [Master's thesis, Lund University]. Lund University Student Papers. https://lup.lub.lu.se/student-papers/record/9196937/file/9196944.pdf

191- Han, B., Ma, L., Yu, Q., Yang, J., Su, W., Hilal, M. G., Li, X., Zhang, S., & Li, H. (2022). The source, fate and prospect of antibiotic resistance genes in soil: A review. *Frontiers in Microbiology, 13*, Article 976657. https://doi.org/10.3389/fmicb.2022.976657

192- von Wintersdorff, C. J. H., Penders, J., van Niekerk, J. M., Mills, N. D., Majumder, S., van Alphen, L. B., Savelkoul, P. H. M., & Wolffs, P. F. G. (2016). Dissemination of antimicrobial resistance in microbial ecosystems through horizontal gene transfer. *Frontiers in Microbiology, 7*, Article 173. https://doi.org/10.3389/fmicb.2016.00173 (192)

193- Earth.com. (n.d.). Rural groundwater may be hiding antibiotic resistant microbes, a new study links them to human gut genes. https://www.earth.com/news/rural-groundwater-may-be-hiding-antibiotic-resistant-microbes-a-new-study-links-them-to-human-gut-genes/

194- Kan, K. (2026, May 27). Climate change fueling growth of antibiotic-resistant salmonella. The Japan Times. https://www.japantimes.co.jp/environment/2026/05/27/climate-change/climate-change-antibiotic-salmonella/

195- Alif, M. N., & Zhang, W. (2025). SynOmics: Integrating multi-omics data through feature interaction networks. bioRxiv. https://doi.org/10.1101/2025.09.17.676954

196- Ma, Y., Liu, L., Ma, Y., & Zhang, S. (2023). HONMF: Integration analysis of multi-omics microbiome data via matrix factorization and hypergraph. *Bioinformatics, 39*(6), Article btad335. https://doi.org/10.1093/bioinformatics/btad335

Chapter 11

Computational Modeling and Machine Learning for Toxic Metal Transport, Exposure, and Human Health Risk Assessment

Ekrem GÜLSEVİNÇLER[1], Hakan US[2]

1. INTRODUCTION

Nuclear-fuel-cycle and legacy-waste environments may contain chemically toxic metal(loid)s together with radionuclides, yet transport calculations, exposure assumptions, toxicity values, and machine-learning models are often evaluated separately. This chapter develops a traceable source–transport–exposure–risk framework and demonstrates it with a documented MATLAB benchmark for dissolved inorganic arsenic in a generic saturated aquifer. A retarded one-dimensional Ogata–Banks solution generated 12,000 Latin-hypercube cases. Feedforward artificial neural networks (ANNs), bagged regression trees, and a linear model estimated relative concentration, while a deterministic layer calculated source concentration, exposure, and risk. The models were selected using training and validation data, then assessed on a locked test set and a boundary-focused stress set. The selected 30–15 ANN achieved a mean test RMSE of 0.169 $\log_{10}$ units, compared with 0.285 for bagged trees and 2.603 for the linear model. Its mean stress-set RMSE rose to 0.266. ANN accuracy was 99.78% for the hazard-quotient decision and 99.72% for three cancer-risk bands, with no end-to-end monotonicity violation for source concentration or ingestion rate; this result was structural because these variables bypassed the learner. The analytical generator remained faster than the ANN. The reported results support physics-structured surrogates as verification and uncertainty-analysis tools, but not as substitutes for site characterization, reactive transport, independent monitoring, or expert risk interpretation.Chemical toxicity is part of the safety problem at many nuclear-fuel-cycle and legacy-waste sites. Uranium mines, mills, tailings impoundments, process-water systems, and historic disposal trenches can contain radionuclides together with arsenic and other metals. Acidic or alkaline process residues may also modify metal

[1] Asst. Prof. Dr., Department of Nuclear Energy Engineering, Faculty of Engineering and Architecture, Sinop University, Sinop, Turkey. E-mail: egulsevincler@sinop.edu.tr. ORCID: 0000-0002-4787-6275.
[2] Asst. Prof. Dr., Department of Nuclear Energy Engineering, Faculty of Engineering and Architecture, Sinop University, Sinop, Turkey. E-mail: hakanus@sinop.edu.tr. ORCID: 0000-0003-0111-685X.

speciation and mobility. International Atomic Energy Agency guidance therefore treats effluent management and legacy remediation as source-characterization problems that include both radiological and chemically hazardous constituents [1,2]. The relevant question is site-specific: a nuclear label does not prove that a particular metal is present, but it also does not justify excluding chemical hazards before characterization.Useful assessment preserves a traceable release-to-consequence chain: source terms define mass and chemical form; flow and geochemistry determine receptor concentrations; exposure converts concentration into intake; and toxicity data produce screening indicators. Studies near uranium facilities demonstrate water, soil, food-chain, radiological, and toxicological linkages [3,4], while fracture channeling shows how homogeneous models can fail [5]. Source terms, coupled processes, uncertainty, monitoring, and defense-in-depth therefore make toxic-metal transport a nuclear-engineering concern.Machine learning (ML) can emulate costly transport simulations for Monte Carlo analysis, inversion, optimization, or screening. Groundwater studies use ANNs, Kriging, and other nonlinear learners [6,7]. Yet a surrogate learns its generator only within a sampled domain; high random-test R^2 does not establish site validity, unseen-geology coverage, or threshold fidelity.This chapter connects toxic-metal sources and pathways to an auditable transport–exposure–risk model. A MATLAB experiment compares an ANN, bagged trees, and a linear baseline on one physics-generated arsenic dataset using locked-test, boundary-stress, threshold, monotonicity, importance, and runtime checks. It evaluates a declared computational benchmark, not a field site or an individual's health outcome.

2. TOXIC METALS IN NUCLEAR-FUEL-CYCLE AND LEGACY ENVIRONMENTS

Source inventories vary across the fuel cycle. Mining and milling can expose sulfides and generate U, As, Mo, or Se bearing seepage; hydrometallurgy adds acids, bases, oxidants, and ligands; tailings retain water and fines; and historic trenches may contain uncertain radioactive–chemical mixtures [1,2]. Measured soil–water–rice transfer near one uranium mine produced pathway-dependent risks [3], supporting pathway identification but not transfer of its concentrations to other sites.Mobility depends on chemical form as much as total concentration. pH, redox, mineral surfaces, organic matter, competing ions, and colloids govern speciation, solubility, precipitation, and adsorption. Arsenic species behave differently from Cd or Pb cations, while uranium has chemical and radiological dimensions. Toxicity likewise varies by element, dose, route, and duration [8], one “heavy-metal” category cannot supply universal transport or toxicity

parameters.Hydrogeology adds another source of model-form uncertainty. Matrix flow may dominate in one aquifer, whereas fractures or preferential channels control travel time in another [5]. Consequently, the conceptual model should be revised against borehole data, hydraulic tests, mineralogy, water chemistry, tracer information, and monitoring trends. Table 1 summarizes the source–pathway structure used to organize that work.

Table 1. Source–process–pathway matrix for chemically toxic constituents in nuclear environments[1–5,8,26–31,34,35,39].

Source setting	Representative constituents	Dominant controls to examine	Potential receptor pathways
Uranium mine and mill drainage	As, Cd, Cr, Mo, Ni, Pb, Se, U	Oxidation, acidity, mineral dissolution, neutralization	Groundwater and surface-water ingestion; irrigation
Tailings and process-water systems	As, Mo, Se, U and site-specific reagents	Seepage, saturation, redox fronts, sorption, precipitation	Wells, streams, sediment, food-chain transfer
Hydrometallurgical residues	Process-specific metals and complexants	pH, competing ligands, solids aging, leachability	Leachate, soil contact, water reuse
Historic waste trenches	Mixed radioactive and chemical wastes	Inventory uncertainty, container degradation, interactions, preferential flow	Groundwater, vapor or dust where relevant, surface discharge

The matrix is a scoping device rather than a universal inventory. Sampling must establish which rows and constituents apply. Once the source and receptor pathways are defined, the next task is to represent transport and risk with equations whose assumptions can be inspected.

2.1 Generalization to other toxic metals

The arsenic benchmark developed later is one case study, not a generic metal model. Transfer to another constituent requires metal-specific speciation, reaction, exposure, and validation choices. Table 2 provides a compact synthesis for six priority elements; the listed ML methods are candidate tools whose suitability still depends on data volume, spatial structure, and the decision context [8,26–28,30,31].

Table 2. Metal-specific controls for extending computational transport and exposure models [6-8,17–33, 26–31].

Metal	Dominant transport mechanism	Critical geochemical control	Principal exposure emphasis	Representative computational or ML approach
As	Redox-driven desorption/dissolution and sorption	Oxidation state, pH, Fe/Mn oxides, competing oxyanions	Drinking water; irrigated food	Reactive transport plus ANN/tree surrogate
Pb	Strong sorption and precipitation; colloid or dust transport	pH, organic matter, clay and Fe/Mn oxides	Soil/dust ingestion; occupational inhalation	Surface-complexation model plus boosted trees
Cd	Cation exchange and pH-dependent desorption	pH, ionic strength, oxides and organic matter	Food crops; tobacco or workplace inhalation	Geochemical speciation plus Gaussian process
Hg	Atmospheric–aquatic cycling and microbial methylation	Redox, sulfide, organic matter, microbial activity	Fish/shellfish; elemental-vapor inhalation	Multimedia food-web model plus spatiotemporal ML
Cr	Redox transformation between mobile Cr(VI) and sorbing Cr(III)	Eh–pH, Fe(II), organic reductants	Occupational inhalation; drinking water	Reactive-transport classifier or hybrid surrogate
U	Oxidized U(VI) complexation and reduction and precipitation	Redox, carbonate, pH, Ca and organic matter	Drinking water; mine/mill dust	Multispecies reactive transport plus PINN or emulator

These mappings guide model selection rather than supply universal parameter values. Site-specific mineralogy, water chemistry, source form, and exposure behavior remain essential, and predictions outside the training domain should trigger additional sampling or mechanistic simulation [26,27,28,29,30,31].

3. INTEGRATED TRANSPORT, EXPOSURE, AND RISK MODELING

3.1 Transport hierarchy and benchmark equations

For a conservative dissolved constituent in a homogeneous saturated porous medium, one-dimensional advection and hydrodynamic dispersion can be written with linear equilibrium retardation as [9,10]

$$R\frac{\partial C}{\partial t} = D\frac{\partial^2 C}{\partial x^2} - v\frac{\partial C}{\partial x} \tag{1}$$

Here, C is dissolved concentration, v is average pore-water velocity, and $D = \alpha_L v + D_m$ combines longitudinal mechanical dispersion with molecular diffusion. Linear equilibrium sorption gives

$$R = 1 + \frac{\rho_b K_d}{n_e}, v_R = \frac{v}{R}, D_R = \frac{D}{R} \tag{2}$$

The bulk density ρ_b, effective porosity n_e, and distribution coefficient K_d determine the retardation factor R. A constant K_d compresses several geochemical mechanisms into one empirical parameter. It cannot represent changing arsenic speciation, competitive adsorption, kinetic reactions, colloidal transport, or mineral transformation. Equation (2) is suitable for a transparent sensitivity benchmark only when that limitation is explicit.For a maintained inlet concentration C_0 in a semi-infinite domain, the Ogata–Banks solution provides a closed-form concentration ratio [9],

$$\frac{C}{C_0} = \frac{1}{2}\left[\operatorname{erfc}\left(\frac{x - v_R t}{2\sqrt{D_R t}}\right) + \exp\left(\frac{v_R x}{D_R}\right)\operatorname{erfc}\left(\frac{x + v_R t}{2\sqrt{D_R t}}\right)\right] \tag{3}$$

The solution is transparent for code verification and screening but is not a three-dimensional site model. MODFLOW 6 can represent advection, dispersion, sorption, mobile–immobile transfer, reactions, and source–sink mixing [10]. Analytical source approximations may be materially inaccurate [11], and fracture flow can invalidate homogeneity [5]. Model complexity should follow the decision and evidence.

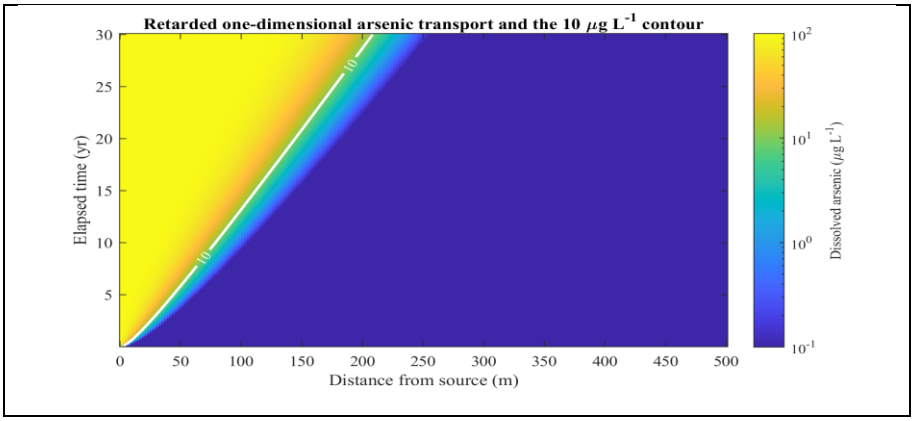


Figure 1. Representative retarded one-dimensional arsenic field for C_0 = 0.10 mg L^{-1}, v = 0.10 m day^{-1}, α_L = 2 m, K_d = 1 L kg^{-1}, n_e = 0.30, and ρ_b = 1.60 kg L^{-1}. The white line is the WHO provisional 10 μg L^{-1} drinking-water guideline contour. The figure is illustrative and not a site forecast.

3.2 Exposure and screening-risk equations

The transport model supplies concentration at a receptor; it does not by itself supply health risk. For chronic drinking-water ingestion, average daily dose (ADD) and lifetime average daily dose (LADD) were calculated using the structure of the U.S. EPA Risk Assessment Guidance for Superfund [12]:

$$\mathrm{ADD} = \frac{C \times \mathrm{IR} \times \mathrm{EF} \times \mathrm{ED}}{\mathrm{BW} \times \mathrm{AT_{nc}}}, \mathrm{AT_{nc}} = \mathrm{ED} \times 365 \quad (4)$$

$$\mathrm{LADD} = \frac{C \times \mathrm{IR} \times \mathrm{EF} \times \mathrm{ED}}{\mathrm{BW} \times \mathrm{AT_{ca}}}, \mathrm{AT_{ca}} = 70 \times 365 \quad (5)$$

C is expressed in mg L^{-1}, IR is ingestion rate, EF is exposure frequency, ED is exposure duration, and BW is body weight. Water ingestion varies among individuals and life stages, so exposure factors should be selected for the population and purpose of the assessment [13]. The present ranges are exploratory design bounds, not fitted population distributions.

Noncancer and cancer indicators were computed as

$$\mathrm{HQ} = \frac{\mathrm{ADD}}{\mathrm{RfD}}, \mathrm{Risk} = \mathrm{LADD} \times \mathrm{CSF} \quad (6)$$

The January 2025 EPA inorganic-arsenic assessment reports an oral reference dose (RfD) of 6 × 10^{-5} mg kg^{-1} day^{-1} and cancer slope factor (CSF) of 32 (mg kg^{-1} day^{-1})−1 [14]. Toxicity values require date stamps because revisions change

risk without changing concentration. The WHO provisional 10 μg L^{-1} drinking-water guideline is a management value [15], not HQ = 1 or a cancer-risk boundary.These indicators require careful language. HQ is a screening ratio, not the probability that disease will occur. Cancer risk from a slope factor is a model-based screening estimate rather than a patient-specific prediction. Uncertainty enters at three distinct layers: environmental concentration, exposure behavior, and toxicological dose response. Reporting only the surrogate's concentration error would omit the latter two.

4. MACHINE LEARNING AND PHYSICS-GUIDED SURROGATES

Surrogates are most useful when a process model is too expensive to evaluate thousands or millions of times. Published applications include Monte Carlo propagation, parameter inversion, remediation optimization, breakthrough-curve prediction, and emulation of spatial fields [6,7]. A deep-learning meta-model has, for example, accelerated Monte Carlo contaminant-transport calculations [16]. Bagged trees, Gaussian-process or Kriging models, ANNs, and convolutional networks offer different tradeoffs in smoothness, dimensionality, uncertainty representation, and training cost. There is no universally superior learner.

“Physics-informed” should specify where physics enters. Simulator outputs make a learner physics-generated; transport features make it physics-featured; and theory may shape architecture [17]. A PINN more narrowly places equation residuals, boundary conditions, and observations in its loss [18,19], with extensions such as pretraining [20]. Scientific ML spans these designs [21,22]. The ANN below is physics-generated, physics-featured, and coupled to deterministic output equations; it is not a PINN.Validation must match the claim. Random same-domain samples test interpolation, not new hydrostratigraphy, sources, or redox regimes; spatial, temporal, geological, and boundary tests are harder [36]. Leakage occurs if standardization, architecture selection, or dependent samples use test information [37]. Threshold fidelity must be assessed separately because small errors near HQ = 1 can change decisions.Interpretability has similar limits. Permutation importance measures how much predictive error rises after information in an input is disrupted. It is not a causal effect, and correlated or derived physical variables can redistribute the ranking [38]. Variance-based sensitivity indices offer a stronger global decomposition when their assumptions and sampling cost are acceptable [23]. The benchmark uses permutation importance as a diagnostic and recomputes all derived physics features after each base-input permutation.

Table 3. Comparative roles of common surrogate-model families in toxic-metal assessment. Sources by model family are ANN bagged trees , [6,7,17], [25], XGBoost [32], Gaussian processes [33], and PINNs [18,19].

Model	Main strength	Main limitation	Suitable application	Typical data requirement
ANN	Flexible high-dimensional nonlinear mapping	Calibration and extrapolation are difficult to interpret	Repeated emulation of large simulator ensembles	Moderate to large, domain-covering dataset
Bagged trees	Robust baseline; handles interactions with little preprocessing	Piecewise predictions and weak extrapolation	Tabular screening and variable-ranking checks	Moderate tabular dataset
XGBoost	Strong accuracy on structured data with nonlinear interactions	Tuning and leakage control are essential	Concentration or exceedance prediction from monitoring covariates	Moderate tabular dataset
Gaussian process	Predictive uncertainty and good small-data efficiency	Cubic scaling and kernel assumptions	Low-dimensional emulation and adaptive sampling	Small to moderate, well-designed dataset
PINN	Governing equations can constrain sparse-data learning	Optimization is difficult and uncertainty is not automatic	Forward/inverse PDE problems with explicit equations and boundaries	Collocation points plus boundary/observation data

This is a functional comparison, not a performance ranking. XGBoost extends tree boosting efficiently [32], Gaussian processes make smoothness and predictive uncertainty explicit [33], and PINNs embed differential-equation residuals [18,19]. Model choice should follow whether the evidence is tabular monitoring, simulator output, sparse observations, or a fully specified PDE.

5. MATLAB COMPUTATIONAL DEMONSTRATION

5.1 Design and reproducibility

The MATLAB R2020b experiment generated 12,000 Latin-hypercube combinations of the 12 inputs in Table 4 [24]. Molecular diffusion was fixed at 10^{-5} m² day^{-1}, and log-uniform sampling covered parameters spanning orders of

magnitude. These are broad verification bounds, not a site-specific aquifer or population distribution.

Table 4. The ranges are not empirical population distributions. Inputs to the mechanistic–ML benchmark. Transport ranges were chosen as broad verification bounds informed by [9,10,26–31], while exposure-variable definitions follow [12–14,34,35].

Input	Lower	Upper	Unit	Sampling
Source concentration, C_0	0.005	0.5	mg L^{-1}	Log-uniform
Receptor distance, x	10	500	m	Uniform
Elapsed time, t	0.25	30	yr	Log-uniform
Pore-water velocity, v	0.01	0.5	m day^{-1}	Log-uniform
Longitudinal dispersivity, α_L	0.1	20	m	Log-uniform
Distribution coefficient, K_d	0.05	10	L kg^{-1}	Log-uniform
Effective porosity, n_e	0.15	0.45	—	Uniform
Bulk density, ρ_b	1.3	1.9	kg L^{-1}	Uniform
Water ingestion rate, IR	0.8	3.0	L day^{-1}	Uniform
Body weight, BW	50	100	kg	Uniform
Exposure frequency, EF	250	365	day yr−1	Uniform
Exposure duration, ED	1	40	yr	Uniform

The analytical solution generated concentration, HQ, and a linear-slope-factor cancer-risk index. A fixed seed produced a 70/15/15% training/validation/locked-test split; a separate 2,000-case within-range stress set emphasized input boundaries. Neither evaluation set entered model selection.Broad-scale inputs were $\log_{10}$ transformed and standardized from training data only. The features $vt/(Rx)$ and x/α_L represented retarded travel and dispersion. Learners estimated $\log_{10}(C/C_0 + 10^{-12})$, while source concentration and exposure variables bypassed them; Equations (4)–(6) then preserved source and dose algebra.Four feedforward ANN architectures were compared using validation RMSE, with three seeded starts per architecture. A pseudoinverse linear model and 100-tree bagged ensembles were baselines [25]. For reproducibility, the architecture, early-stopping settings, tree settings, and random seed should be reported in the accompanying package. Evaluation covered log-error, R^2, factor-of-two accuracy, HQ > 1, three cancer-risk bands, 2% monotonicity probes for C_0 and IR, and runtime. No site measurements or human-subject data were used.

5.2 Results

The selected 30–15 ANN had validation RMSE 0.103 $\log_{10}$ units. On the locked test set, mean end-to-end RMSE was 2.603 for the linear model, 0.285 for bagged trees, and 0.169 for the ANN; stress values were 2.557, 0.558, and 0.266. In Table -5 adds screening metrics.

Table 5. Regression and locked-test screening performance.

Model	Mean test RMSE	Mean stress RMSE	Test C R^2	HQ acc. (%)	HQ sens. (%)	Risk-band acc. (%)
Linear	2.603	2.557	0.6599	86.67	10.11	83.50
Bagged trees	0.285	0.558	0.9960	99.67	97.75	99.61
ANN	0.169	0.266	0.9991	99.78	98.88	99.72

Note: RMSE is the mean across concentration, HQ, and cancer risk in $\log_{10}$ output space. Decision metrics use the locked test set. Stress cases remain within the declared ranges but concentrate near their boundaries. Outcome-specific metrics should be included in the reproducibility package.

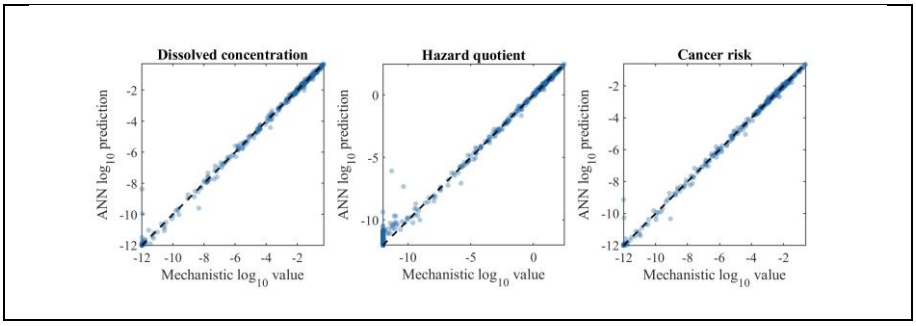


Figure 2. Selected ANN predictions against mechanistic values for 1,500 randomly displayed cases from the 1,800-case locked test set. The dashed line denotes equality; Table 5 uses all test cases.

For HQ > 1, the ANN achieved 99.93% specificity and F1 = 0.992 in addition to the metrics in Table 5. Its three-band cancer-risk macro-F1 was 0.981, versus 0.972 for bagged trees. The linear model's 10.11% HQ sensitivity shows why accuracy alone is unreliable for an imbalanced threshold. Within this sampled domain, the ANN preserved the selected screening thresholds well.The broad dynamic range explains part of the high R^2 values, so threshold metrics provide complementary evidence. Stress-set ANN RMSE was about 57% higher than locked-test RMSE although the stress samples stayed inside the stated bounds: “within range” does not guarantee uniform training support. Numerical-floor

behavior among very small non-arrival outputs affects global log-error summaries but has little influence on the HQ > 1 decision.

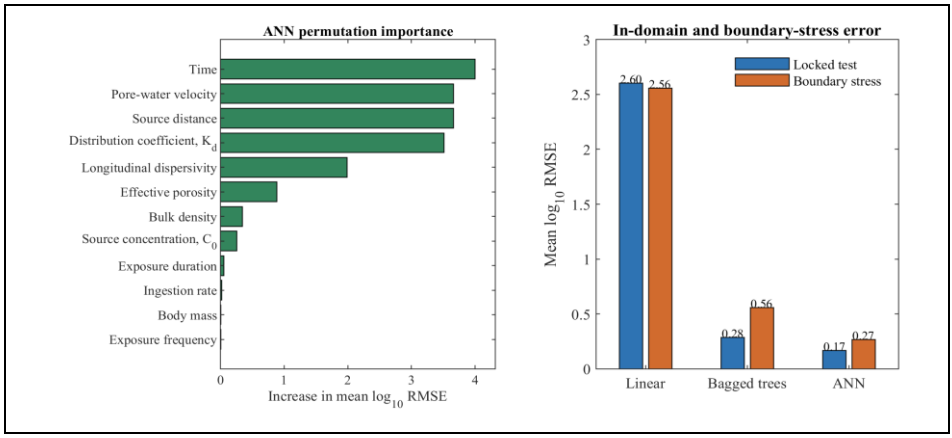


Figure 3. ANN base-input permutation importance (left) and mean locked/stress $\log_{10}$ RMSE (right). Importance is predictive sensitivity, not causal attribution; derived features were rebuilt after each base-input permutation.

Time, velocity, distance, and K_d accounted for 21.8%, 19.9%, 19.9%, and 19.1% of normalized positive permutation importance. Dispersivity contributed 10.8%. These rankings agree with the analytical travel and retardation structure, but the aggregation across all three outputs downweights exposure variables relative to inputs controlling many orders of concentration variation.The physical-consistency probe found no violation among 1,000 cases when source concentration or ingestion rate increased by 2%. This was structural: the learner estimated relative concentration while C_0 multiplication and exposure–risk equations remained deterministic; it does not prove unconstrained ANN monotonicity. In the reported run, 100,000 analytical evaluations took 0.006 s versus 0.052 s for feature construction, ANN prediction, and risk calculation.

6. IMPLICATIONS, LIMITATIONS, AND GOOD PRACTICE

The results support tiered use: analytical synthetic tests verify code at Tier 1; a surrogate emulates a calibrated site model at Tier 2; and Tier 3 decision support adds independent monitoring, change control, applicability checks, and expert review. Progression requires new evidence; Tier-1 accuracy does not authorize Tier-3 use.

Table 6. Evidence requirements and failure conditions for a deployable toxic-metal surrogate**.**

Component	Minimum evidence	Failure condition requiring revision or restricted use
Source and chemistry	Inventory, speciation, release history, pH/redox/mineralogy	Missing constituent or release mechanism
Flow and transport	Calibrated hydraulics, heterogeneity and pathway tests	Unmodeled preferential flow or boundary behavior
Exposure and toxicity	Defined receptor/pathway, dated factors and toxicity values	Unversioned toxicity or pathway change
ML verification	Leakage-free split, nonlinear comparator, threshold/stress tests	Claim based on a random split alone
Operational governance	Independent monitoring, domain alarm and audit trail	Out-of-domain or unreviewed prediction

The benchmark assumes one-dimensional homogeneous saturated flow, a maintained inlet, and instantaneous linear K_d sorption; it omits transient flow, reactions, speciation changes, competing ions, colloids, fractures, source depletion, and mixtures. Its synthetic data verify the generator, not environmental prediction, and boundary stress remains inside that model. Fracture-flow evidence [5], analytical-solution limits [11], and surrogate reviews [6] support using a calibrated simulator such as MODFLOW 6 [10], spatial or temporal holdouts, and measurements withheld from calibration.Surrogates inherit generator error. Equation-residual learning can reduce inconsistency [18–21] but cannot recover omitted processes. Monotonicity here was guaranteed only for relations outside the learner; ANN transport remained statistical. Reports should distinguish enforced, learned, and omitted constraints [22], check importance against physics or global sensitivity analysis [23], archive toxicity values, code, seeds, bounds, preprocessing, and versions, and block silent extrapolation with a domain alarm.

6.1 Beyond drinking-water exposure

A receptor-centered assessment maps contaminated air, water, soil, dust, sediment, crops, and animal foods to contact routes before combining only toxicologically compatible doses. EPA guidance provides age- and activity-dependent factors for ingestion, inhalation, dermal contact, diet, and body weight [12,34,35]; drinking-water results therefore cannot represent total risk.

Occupational scenarios require task resolution because mining, milling, residue handling, maintenance, and decommissioning can aerosolize metal-bearing dust or fumes. Inhalation, incidental hand-to-mouth ingestion, dermal uptake, air and surface monitoring, hygiene, protective equipment, and take-home controls may all matter [34,35,39]. Dermal uptake depends on species, solubility, adhered mass, skin condition, area, and duration and is not interchangeable with oral intake.Irrigation and deposition transfer metals to crops, while contaminated sediments transfer them to fish or livestock. Uranium-mine measurements show element-specific water–soil–rice transfer [3]; mercury methylation and biomagnification make fish consumption central [29]. Life stage also changes body mass, diet, soil/dust contact, sensitive windows, and occupational peaks [35]. A defensible extension would model sequential life stages, retain route-specific bioavailability and toxicity values, and report pathway contributions before aggregation. It requires new data and cannot be inferred from this arsenic case.

7. CONCLUSIONS

A defensible assessment links source, transport, exposure, and toxicity without hiding assumptions. This is important where chemical and radiological hazards coexist. Inside its declared domain, the reported benchmark indicated that the physics-generated, physics-featured ANN emulated relative arsenic concentration more accurately than bagged trees or a linear baseline, while a deterministic layer preserved source, exposure, and risk algebra.Boundary-focused error increased, ANN transport was not equation-constrained, and the analytical equation remained faster; high R^2 therefore established neither speed nor site validity. Application requires a calibrated multidimensional generator, site chemistry, independent measurements, transfer tests, current toxicity inputs, and oversight. ML is credible as an auditable mechanistic-workflow component, not a substitute for evidence.

DECLARATIONS

Ethics Statement: Formal ethics review was not required for this computational study because it involved no human participants, animals, clinical records, or identifiable personal data.

Ethics Statement: Ethics approval and informed consent were not applicable because this study was entirely computational and involved no human participants, animals, clinical records, or identifiable personal data.

Funding: This chapter received no specific grant from any funding agency in the public, commercial, or not-for-profit sectors.

Competing Interests: The authors declare that they have no competing financial or non-financial interests.

REFERENCES

1- International Atomic Energy Agency. (2002). *Technologies for the treatment of effluents from uranium mines, mills and tailings* (IAEA-TECDOC-1296). https://www-pub.iaea.org/MTCD/publications/PDF/te_1296_prn/t1296_part1.pdf

2- International Atomic Energy Agency. (2025). *Environmental remediation and management of trenches containing historic radioactive wastes: Legacy trench sites* (Nuclear Energy Series No. NW-G-3.3). https://doi.org/10.61092/iaea.rgwy-0qia

3- Wang, Z., Qin, H., & Liu, X. (2019). Health risk assessment of heavy metals in the soil–water–rice system around the Xiazhuang uranium mine, China. *Environmental Science and Pollution Research, 26*(6), 5904–5912. https://doi.org/10.1007/s11356-018-3955-1

4- Zanoz, B. Y., & Bugai, D. O. (2024). Modeling of long-term radiological and toxicological impacts of the uranium mill tailings on groundwater and surface water. *Nuclear Physics and Atomic Energy, 25*(3), 277–288. https://doi.org/10.15407/jnpae2024.03.277

5- Xie, T., Zhu, J., Liu, X., Hao, Y., Wang, R., Liang, P., Wang, Z., Zhang, A., Qian, T., & Zhao, D. (2025). Fissure channeling caused anomalous uranium concentration in groundwater downstream of a uranium mine tailings impoundment site. *Journal of Hazardous Materials, 488*, 137492. https://doi.org/10.1016/j.jhazmat.2025.137492

6- Luo, J., Ma, X., Ji, Y., Li, X., Song, Z., & Lu, W. (2023). Review of machine learning-based surrogate models of groundwater contaminant modeling. *Environmental Research, 238*, 117268. https://doi.org/10.1016/j.envres.2023.117268

7- Yu, X., Cui, T., Sreekanth, J., Mangeon, S., Doble, R., Xin, P., Rassam, D., & Gilfedder, M. (2020). Deep learning emulators for groundwater contaminant transport modelling. *Journal of Hydrology, 590*, 125351. https://doi.org/10.1016/j.jhydrol.2020.125351

8- Tchounwou, P. B., Yedjou, C. G., Patlolla, A. K., & Sutton, D. J. (2012). Heavy metal toxicity and the environment. In A. Luch (Ed.), *Molecular, clinical and environmental toxicology* (Experientia Supplementum, Vol. 101, pp. 133–164). Springer. https://doi.org/10.1007/978-3-7643-8340-4_6

9- Ogata, A., & Banks, R. B. (1961). *A solution of the differential equation of longitudinal dispersion in porous media* (USGS Professional Paper 411-A). https://doi.org/10.3133/pp411A

10- Langevin, C. D., Provost, A. M., Panday, S., & Hughes, J. D. (2022). *Documentation for the MODFLOW 6 Groundwater Transport Model* (USGS Techniques and Methods 6-A61). https://doi.org/10.3133/tm6A61

11- Sangani, J., & Srinivasan, V. (2021). Improved Domenico solution for three-dimensional contaminant transport. *Journal of Contaminant Hydrology, 243*, 103897. https://doi.org/10.1016/j.jconhyd.2021.103897

12- U.S. Environmental Protection Agency. (1989). *Risk assessment guidance for Superfund, Volume I: Human Health Evaluation Manual (Part A)* (EPA/540/1-89/002). https://www.epa.gov/sites/default/files/2015-09/documents/rags_a.pdf

13- U.S. Environmental Protection Agency. (2019). *Exposure Factors Handbook Chapter 3 (Update): Ingestion of Water and Other Select Liquids* (EPA/600/R-18/259F). https://assessments.epa.gov/risk/document/%26deid%3D343661

14- U.S. Environmental Protection Agency. (2025). *IRIS toxicological review of inorganic arsenic* (EPA/635/R-25/005). https://cfpub.epa.gov/ncea/risk/recordisplay.cfm?deid=363892

15- World Health Organization. (2022). *Arsenic* [Fact sheet]. https://www.who.int/news-room/fact-sheets/detail/arsenic

16- Špetlík, M., & Březina, J. (2022). Groundwater contaminant transport solved by Monte Carlo methods accelerated by deep learning meta-model. *Applied Sciences, 12*(15), 7382. https://doi.org/10.3390/app12157382

17- He, T., Wang, N., & Zhang, D. (2021). Theory-guided full convolutional neural network: An efficient surrogate model for inverse problems in subsurface contaminant transport. *Advances in Water Resources, 157*, 104051. https://doi.org/10.1016/j.advwatres.2021.104051

18- He, Q., & Tartakovsky, A. M. (2021). Physics-informed neural network method for forward and backward advection–dispersion equations. *Water Resources Research, 57*(7), e2020WR029479. https://doi.org/10.1029/2020WR029479

19- Raissi, M., Perdikaris, P., & Karniadakis, G. E. (2019). Physics-informed neural networks: A deep learning framework for solving forward and inverse problems involving nonlinear partial differential equations. *Journal of Computational Physics, 378*, 686–707. https://doi.org/10.1016/j.jcp.2018.10.045

20- Ke, Z.-W., Wei, S.-J., Yao, S.-Y., Chen, S., Chen, Y.-M., & Li, Y.-C. (2025). Pre-trained physics-informed neural networks for analysis of contaminant transport in soils. *Computers and Geotechnics, 180*, 107055. https://doi.org/10.1016/j.compgeo.2025.107055

21- Karniadakis, G. E., Kevrekidis, I. G., Lu, L., Perdikaris, P., Wang, S., & Yang, L. (2021). Physics-informed machine learning. *Nature Reviews Physics, 3*(6), 422–440. https://doi.org/10.1038/s42254-021-00314-5

22- Willard, J., Jia, X., Xu, S., Steinbach, M., & Kumar, V. (2023). Integrating scientific knowledge with machine learning for engineering and environmental systems. *ACM Computing Surveys, 55*(4), Article 66. https://doi.org/10.1145/3514228

23- Sobol′, I. M. (2001). Global sensitivity indices for nonlinear mathematical models and their Monte Carlo estimates. *Mathematics and Computers in Simulation, 55*(1–3), 271–280. https://doi.org/10.1016/S0378-4754(00)00270-6

24- McKay, M. D., Beckman, R. J., & Conover, W. J. (1979). A comparison of three methods for selecting values of input variables in the analysis of output from a computer code. *Technometrics, 21*(2), 239–245. https://doi.org/10.1080/00401706.1979.10489755

25- Breiman, L. (2001). Random forests. *Machine Learning, 45*(1), 5–32. https://doi.org/10.1023/A:1010933404324

26- Smedley, P. L., & Kinniburgh, D. G. (2002). A review of the source, behaviour and distribution of arsenic in natural waters. *Applied Geochemistry, 17*(5), 517–568. https://doi.org/10.1016/S0883-2927(02)00018-5

27- Bradl, H. B. (2004). Adsorption of heavy metal ions on soils and soils constituents. *Journal of Colloid and Interface Science, 277*(1), 1–18. https://doi.org/10.1016/j.jcis.2004.04.005

28- Kubier, A., Wilkin, R. T., & Pichler, T. (2019). Cadmium in soils and groundwater: A review. *Applied Geochemistry, 108*, 104388. https://doi.org/10.1016/j.apgeochem.2019.104388

29- Hsu-Kim, H., Kucharzyk, K. H., Zhang, T., & Deshusses, M. A. (2013). Mechanisms regulating mercury bioavailability for methylating microorganisms in the aquatic environment: A critical review. *Environmental Science & Technology, 47*(6), 2441–2456. https://doi.org/10.1021/es304370g

30- Richard, F. C., & Bourg, A. C. M. (1991). Aqueous geochemistry of chromium: A review. *Water Research, 25*(7), 807–816. https://doi.org/10.1016/0043-1354(91)90160-R

31- Cumberland, S. A., Douglas, G., Grice, K., & Moreau, J. W. (2016). Uranium mobility in organic matter-rich sediments: A review of geological and geochemical processes. *Earth-Science Reviews, 159*, 160–185. https://doi.org/10.1016/j.earscirev.2016.05.010

32- Chen, T., & Guestrin, C. (2016). XGBoost: A scalable tree boosting system. In *Proceedings of the 22nd ACM SIGKDD International Conference on Knowledge Discovery and Data Mining* (pp. 785–794). https://doi.org/10.1145/2939672.2939785

33- Rasmussen, C. E., & Williams, C. K. I. (2005). *Gaussian processes for machine learning*. MIT Press. https://doi.org/10.7551/mitpress/3206.001.0001

34- U.S. Environmental Protection Agency. (2019). *Guidelines for human exposure assessment* (EPA/100/B-19/001). https://www.epa.gov/risk/guidelines-human-exposure-assessment

35- U.S. Environmental Protection Agency. (2011). *Exposure Factors Handbook: 2011 Edition* (EPA/600/R-09/052F). https://www.epa.gov/expobox/exposure-factors-handbook

36- Roberts, D. R., Bahn, V., Ciuti, S., Boyce, M. S., Elith, J., Guillera-Arroita, G., Hauenstein, S., Lahoz-Monfort, J. J., Schröder, B., Thuiller, W., Warton, D. I., Wintle, B. A., Hartig, F., & Dormann, C. F. (2017). Cross-validation strategies for data with temporal, spatial, hierarchical, or phylogenetic structure. Ecography, 40(8), 913–929. https://doi.org/10.1111/ecog.02881

37- Kapoor, S., & Narayanan, A. (2023). Leakage and the reproducibility crisis in machine-learning-based science. Patterns, 4(9), 100804. https://doi.org/10.1016/j.patter.2023.100804

38- Strobl, C., Boulesteix, A.-L., Kneib, T., Augustin, T., & Zeileis, A. (2008). Conditional variable importance for random forests. BMC Bioinformatics, 9, Article 307. https://doi.org/10.1186/1471-2105-9-307

39- Occupational Safety and Health Administration. (n.d.). Toxic metals. Retrieved August 13, 2026, from https://www.osha.gov/toxic-metals

Chapter 12

Microplastic-Mediated Radionuclide Transport in Nuclear And Radiological Environments: A Screening-Level Computational Case Study

Hakan US[1], Ekrem GÜLSEVİNÇLER[2]

1. INTRODUCTION

This chapter reviews selected emerging contaminants in nuclear and radiological settings and presents an illustrative one-dimensional model of microplastic-mediated radionuclide transport. Literature-derived partition values and synthetic, literature-anchored isotherm datasets are coupled to aqueous, mobile-particle and immobile-matrix phases. Within the assumed scenario, slow desorption permits an early particle-associated signal for strongly retarded radionuclides, whereas rapid exchange produces little change. These results are hypothesis-generating and scenario-specific: the synthetic regressions do not constitute experimental validation, and the current peak-based health metrics must be replaced by integration of the transient concentration history before they are interpreted as lifetime risk. Code, model settings, synthetic-data generation details, uncertainty analysis and external validation are required for reproducibility and site-specific application.

Environmental protection around nuclear installations has traditionally been organised around a short list of well-characterised radionuclides whose behaviour is described by equilibrium distribution coefficients and whose consequences are expressed as effective dose. That framework was not designed for emerging contaminants: synthetic or anthropogenically mobilised species that are widely distributed, insufficiently regulated, and for which exposure and effect data remain incomplete [1,15]. Microplastics and nanoplastics, per- and polyfluoroalkyl substances (PFAS), engineered nanomaterials and technologically enhanced naturally occurring radioactive material (TENORM) all fall within this definition, and all are now ubiquitous in the water bodies, soils and sediments that receive licensed radioactive effluents. Where they share space with radiological sources, the relevant question is no longer how each family behaves alone but whether their interaction changes the exposure reaching a human receptor.

[1] Asst. Prof. Dr., Department of Nuclear Energy Engineering, Faculty of Engineering and Architecture, Sinop University, Sinop, Turkey. E-mail: hakanus@sinop.edu.tr. ORCID: 0000-0003-0111-685X.
[2] Asst. Prof. Dr., Department of Nuclear Energy Engineering, Faculty of Engineering and Architecture, Sinop University, Sinop, Turkey. E-mail: egulsevincler@sinop.edu.tr. ORCID: 0000-0002-4787-6275.

A polymer fragment suspended in groundwater is not chemically inert. Its surface carries oxidised functional groups produced by photo-ageing and it accumulates a biofilm within days of immersion, so it offers binding sites for hydrolysed metal cations and oxyanions [4,6]. Once a radionuclide is bound to a particle that travels with the water rather than with the aquifer matrix, the geochemical retardation on which most safety assessments rely is partially bypassed. The precedent is documented in the actinide literature: plutonium, whose measured distribution coefficients predict essentially no mobility, was detected 1.3 km from its underground source at the Nevada Test Site, associated almost entirely with the colloidal fraction [11,12]. The mass transported was minute, yet sufficient to invalidate a purely dissolved-phase model. Microplastics differ from natural colloids in that their concentrations are rising rather than stationary, their surface chemistry evolves with ageing, and they are themselves an ingestion vector.This chapter explores that gap through an illustrative, screening-level computational case study. Sections 2 and 3 review selected sources of emerging contaminants in nuclear environments and the surface-chemical mechanisms of radionuclide binding to polymer particles; Section 4 embeds literature-anchored, synthetic isotherm datasets in a three-phase advection-dispersion-reaction model; and Section 5 discusses screening-level radiological and chemical metrics. The calculations are scenario-specific and are not a validated site prediction. They support the hypothesis that desorption kinetics can control particle-facilitated transport and identify measurements needed for subsequent experimental and site-specific validation.

2. SOURCES AND CLASSIFICATION OF EMERGING CONTAMINANTS

Emerging contaminants reach nuclear and radiological environments through pathways that differ in scale, continuity and regulatory visibility. Three groups may be distinguished: species released by the fuel cycle itself, including the difficult-to-measure nuclides of legacy inventories; radioactive species concentrated by non-nuclear industry as NORM and TENORM; and non-radioactive contaminants simply co-located with radiological sources, principally microplastics, PFAS, engineered nanomaterials and inorganic colloids.

2.1. Fuel-cycle and accident-derived sources

Routine operation of light-water reactors releases tritium, carbon-14 and small activities of activation and fission products under authorised limits. The difficult-to-measure radionuclides iodine-129, technetium-99, strontium-90 and tritium are poorly constrained in legacy inventories because each is a pure beta emitter or has a very low specific activity, so quantification requires destructive radiochemical separation rather than gamma spectrometry [23]. Their mobility is high, since they

form anionic or neutral species that sorb weakly to negatively charged mineral surfaces.Accident and post-accident inventories add a second layer. At Fukushima Daiichi, the controlled discharge of ALPS-treated water is subject to site-specific radiological assessment and monitoring [14]. Its relevance here is conceptual: radiological releases may occur in coastal systems that also contain microplastics, but co-occurrence alone does not demonstrate enhanced exposure. Legacy and decommissioning settings require case-by-case assessment using source-term characteristics and site-specific data; quantitative source-zone concentrations must therefore be treated as scenario inputs rather than universal field values [19,24]. Uranium mill tailings constitute a major volume of radiologically contaminated material and require site-specific geochemical assessment [19].

2.2. NORM and TENORM from non-nuclear industry

Naturally occurring radioactive material becomes an environmental concern when industrial processes concentrate it. Phosphate fertiliser production, oil and gas extraction, rare-earth processing, coal combustion and metal smelting can generate residues enriched in uranium- and thorium-series radionuclides [17]. Phosphate rock and phosphogypsum from the Gabès fertiliser industry contain elevated natural radionuclide activities [18]. Management practices and co-disposal conditions vary among sites; therefore, radionuclide–microplastic association at TENORM locations should be evaluated with measured, site-specific data rather than assumed.

2.3. Co-located non-radioactive emerging contaminants

Microplastics are commonly operationally defined as polymer particles smaller than 5 mm. Polyethylene, polypropylene, polyvinyl chloride, polyamide and polystyrene are frequently reported in environmental samples. Their relevance to radionuclide transport derives from their mobile surface area, ageing state and biofilm, all of which can alter sorption and desorption [3]. Claims about occurrence in deep groundwater, particle-size scaling or radionuclide activity require matrix-specific sampling evidence and should not be generalised across compartments.PFAS are another relevant class. A global analysis of approximately 45,000 samples concluded that PFAS burdens in surface water and groundwater can be underestimated [15], and source types influence reported groundwater concentration ranges [16]. Co-occurrence with radiological contaminants is plausible at some facilities but must be demonstrated using site-specific monitoring rather than inferred from fire-suppression capacity. Natural colloids provide an established analogue: plutonium has been observed at unexpected distances from an underground source in association with colloidal material [11,12].

3. INTERACTION MECHANISMS AND SORPTION DESCRIPTIONS

3.1. Surface chemistry, ageing and biofilm

A pristine polyolefin surface is hydrophobic and largely unreactive towards hydrated metal cations. Ultraviolet irradiation and mechanical abrasion introduce carbonyl, carboxyl and hydroxyl functionalities, lowering the point of zero charge and creating deprotonated sites at circumneutral pH. Sorption of uranium(VI) onto polyethylene, polyamide-6 and polyvinyl chloride is consequently strongly pH dependent, following uranyl speciation [2], and polyamide, whose backbone carries amide nitrogen available for coordination, binds uranium far more strongly than polyolefins, with distribution coefficients reaching 2670 litres per kilogram [3].Biofilm colonisation is the second control and often the dominant one. Within days of immersion, polymer surfaces acquire extracellular polymeric substances rich in carboxyl and phosphoryl groups, together with iron and manganese oxide precipitates. Caesium and strontium uptake by biofilm-covered high-density polyethylene exceeds that by pristine material by roughly an order of magnitude [5], and radioiodine uptake correlates with biofilm biomass rather than polymer identity [6]. Natural organic matter acts similarly: humic-acid-coated polyethylene achieved close to complete uranium uptake at low pH where uncoated material achieved about 25 per cent [7]. Complementary batch experiments have also quantified U-232 and Am-241 sorption on polyurethane and polylactic-acid microplastics [8].Two consequences follow. First, the distribution coefficient of a polymer particle is not a universal material constant; it depends on polymer type, water chemistry, ageing and biofilm. Second, binding reversibility may also evolve, potentially producing hysteresis. Experiments on natural clays and fractured granite demonstrate time-dependent actinide sorption and rate-limited transport among dissolved and colloidal plutonium species [9,13]. Field observations further establish long-distance colloid-facilitated plutonium transport [11,12]. These findings motivate, but do not by themselves validate, the kinetic assumptions tested in Section 4.

3.2. Equilibrium descriptions

Batch sorption data are conventionally described by the Langmuir model [29], which assumes a fixed number of energetically equivalent sites and monolayer coverage, or by the Freundlich model [30], an empirical power law appropriate to energetically heterogeneous surfaces:

$$q_e = q_{max}\, K^{L}\, C_e / (1 + K^{L}\, C_e) \tag{1}$$

$$q_e = K_F\, C_e^{(1/n)} \tag{2}$$

Here q_e is the equilibrium loading on the polymer in milligrams per gram, C_e is the equilibrium aqueous concentration in milligrams per litre, q_{max} is the monolayer capacity, K^L is the Langmuir affinity constant, and KF is the Freundlich capacity parameter. The units of KF depend on the value of 1/n and are not dimensionless. The separation factor $R^L = 1/(1 + K^L C_0)$ is commonly used to describe Langmuir favourability; $0 < R^L < 1$ indicates favourable uptake under the fitted model but does not establish reversibility.

$$K_d\ (\mathrm{L\ kg^{-1}}) = 1000 \lim(C_e \to 0)\ q_e/C_e = 1000\ q_{max}\ K^L \quad (3)$$

The factor 1000 in Equation (3) converts litres per gram, obtained from q_e in mg g^{-1} divided by C_e in mg L^{-1}, to litres per kilogram. Use of the dilute-limit slope in transport calculations is a modelling assumption that requires confirmation over environmentally relevant concentrations and water chemistries. Table 1 compiles system-specific polymer values and representative aquifer-solid values used as scenario inputs.

Table 1. Reported distribution coefficients for radionuclide sorption onto polymer particles, with representative sandy-aquifer values for comparison.

Nuclide	Sorbent	K_d (L kg^{-1})	Note	Ref.
U(VI)	Polyamide-6 (PN6)	2670	Amide coordination; strongly pH dependent	[3]
Cs(I)	HDPE with biofilm	480	Approximately six-fold enhancement over pristine	[5]
U(VI)	Polyethylene	79	log K_d 1.9	[2,3]
Cs(I)	Polyethylene, pristine	80	Freshwater conditions	[4]
Am(III)	Polyurethane	79	log K_d 1.9	[8]
Sr(II)	Polyethylene, pristine	5	Estuarine conditions	[4]
Cs(I)	Sandy aquifer solid	2000	Representative value, range 500–5000	[28]
Am(III)	Sandy aquifer solid	1900	Representative value	[28]
U(VI)	Sandy aquifer solid	35	Strongly pH and carbonate dependent	[28]
Sr(II)	Sandy aquifer solid	15	Representative value	[28]

The values in Table 1 are system-specific and do not follow a uniform ordering between polymer and aquifer solids. For example, the listed U(VI)/polyamide-6 value (2670 L kg^{-1}) is approximately 76 times the listed sandy-aquifer value (35 L kg^{-1}), whereas the listed caesium/biofilm-coated HDPE value (480 L kg^{-1}) is about

four times lower than the sandy-aquifer value (2000 L kg^{-1}). Comparisons must therefore be made for each radionuclide, polymer, solution chemistry and porous medium; Table 1 does not support a general claim that all polymer Kd values are lower by one to three orders of magnitude.

4. COMPUTATIONAL CASE STUDY

4.1. Model formulation

The system considered is a shallow sandy aquifer downgradient of a legacy nuclear facility. A release of 30 days duration enters at x = 0, carrying suspended microplastic equilibrated with source-zone water, and is monitored at an abstraction point 100 m downgradient. Three phases are tracked, all per unit volume of pore water: the aqueous concentration C, the activity on mobile microplastic C_{MP}, and the activity bound to the immobile aquifer matrix C_S. The governing system is

$$\partial C/\partial t = D\,\partial^2 C/\partial x^2 - v\,\partial C/\partial x - k_{ads}\,C + k_{des}\,C_{MP} - k_{ads,S}\,C + k_{des,S}\,C_S - \lambda\,C \quad (4)$$

$$\partial C_{MP}/\partial t = D_{MP}\,\partial^2 C_{MP}/\partial x^2 - v_{MP}\,\partial C_{MP}/\partial x + k_{ads}\,C - k_{des}\,C_{MP} - \lambda\,C_{MP} \quad (5)$$

$$\partial C_S/\partial t = k_{ads,S}\,C - k_{des,S}\,C_S - \lambda\,C_S \quad (6)$$

Where; D is the aqueous longitudinal dispersion coefficient, DMP is the effective dispersion coefficient of the mobile microplastic phase, v is the pore-water velocity, vMP is the microplastic velocity, and $\lambda = \ln 2/t_{½}$ is the decay constant. For the present screening calculations, vMP = v and DMP = D are assumed. Equations (4)–(6) are the formulation used in this chapter; the aquifer-matrix term is informed by the general kinetic and multisite ion-exchange rationale used for caesium and strontium [10], rather than by a previously validated radionuclide–microplastic transport equation.

$$\beta_{MP} = K_{d,MP}\,c_{MP}, \quad \beta_S = \rho_b\,K_{d,S}/\theta$$

$$k_{ads} = \beta_{MP}\,k_{des}, \quad k_{ads,S} = \beta_S\,k_{des,S} \quad (7)$$

in which c_{MP} is the suspended microplastic mass concentration in kilograms per litre, ρ_b the dry bulk density and θ the porosity; the retardation factor of the fully equilibrated system is $R = 1 + \beta_{MP} + \beta_S$.

Writing the constants this way separates the thermodynamics, fixed by K_d, from the kinetics, fixed by k_{des}, so the two can be varied independently — the separation on which the results below depend.

The equations were discretised by a conservative finite-volume method on 401 cells with upwind advection and central dispersion, and integrated with an implicit backward-differentiation method using NumPy and SciPy [34,35]. The model uses a third-type inlet during the finite release and a zero-gradient outlet. For reproducibility, the exact initial and boundary-condition equations, solver tolerances, time-step controls, Jacobian implementation, non-negativity handling, mass-balance error and grid/time convergence results must accompany the code and input files. The dispersivity follows the field-scale compilation of Gelhar et al. [31]. Parameters are listed in Table 2.

Table 2. Parameters of the coupled sorption-transport model.

Parameter	Value	Parameter	Value
Flow-path length, L (m)	200	Release duration, t_{inj} (d)	30
Observation distance, x_{obs} (m)	100	Simulation horizon, t_{end} (d)	60 000
Pore-water velocity, v (m d^{-1})	0.50	Microplastic load, c_{MP} (mg L^{-1})	1.0
Longitudinal dispersivity, α_L (m)	2.0	Load sensitivity range (mg L^{-1})	0.01–100
Dispersion coefficient, D (m^2 d^{-1})	1.0	k_{des}, reversible case (d^{-1})	5.0
Porosity, θ (–)	0.30	k_{des}, hysteretic case (d^{-1})	1.0×10^{-3}
Dry bulk density, ρ_b (kg L^{-1})	1.60	k_{des} sensitivity range (d^{-1})	10^{-5}–0.3
Control volumes N; grid Peclet Pe	401; 0.249	Matrix constant, $k_{des,S}$ (d^{-1})	5.0×10^{-2}

4.2. Isotherm regression

Five radionuclide–polymer systems were represented over an equilibrium concentration range of 0.5–120 mg L^{-1}. These are synthetic, literature-anchored illustrative datasets, not new experimental observations. Affinity parameters were selected so that the dilute-limit relation in Equation (3) approximated the reported values in Table 1, after which log-normal perturbations were applied and both isotherms were fitted by nonlinear least squares. The random-number seed, perturbation distribution and scale, weighting scheme, parameter bounds, initial values and generated dataset must be reported to permit exact reproduction.

Table 3. Illustrative Langmuir and Freundlich regressions for synthetic, literature-anchored datasets; subscripts L and F denote the two fitted models.

System	q_{max} (mg g^{-1})	K_L (L mg^{-1})	R_L	R^2_L	K_F	1/n	R^2_F	K_d fit (L kg^{-1})	K_d rep. (L kg^{-1})
U(VI) / PA-6	38.56	0.0660	0.112	0.9933	5.453	0.405	0.9559	2545	2670
Cs(I) / HDPE-biofilm	11.51	0.0406	0.170	0.9971	1.102	0.469	0.9748	467	480
U(VI) / PE	6.50	0.0122	0.407	0.9983	0.176	0.654	0.9911	79.0	79
Cs(I) / PE	4.18	0.0182	0.314	0.9980	0.180	0.590	0.9882	76.0	80
Sr(II) / PE	1.71	0.0026	0.761	0.9982	0.007	0.864	0.9976	4.5	5

The high coefficients of determination and differences between fitted models primarily reflect how the synthetic datasets were generated; they cannot establish model superiority, adsorption mechanism or experimental traceability. Values of $0 < R^L < 1$ indicate favourable uptake under the Langmuir formulation, not reversibility. Likewise, differences in the Freundlich exponent should not be interpreted as a mechanistic ranking of surface heterogeneity without independently measured data and uncertainty analysis. The fitted parameters are therefore inputs to the illustrative transport exercise, not validated material constants.

4.3. Transport simulation

Each nuclide was simulated in three configurations: without microplastic; with microplastic at 1 mg per litre and reversible sorption (k_{des} = 5 per day, equilibration within hours); and with the same loading but hysteretic sorption (k_{des} = 10^{-3} per day, release half-time approximately 690 days). Results at the abstraction point are given in Table 4 and Figure 1.

Table 4. Simulated breakthrough at the abstraction point (x = 100 m); peak values are normalised to the source concentration C_0. The no-microplastic and reversible configurations are reported jointly because they differ by less than one per cent.

Nuclide	R matrix	Configuration	Peak C_{tot}/C_0	t peak (a)	First arrival (a)
^{137}Cs	10 668	No MP / reversible	no arrival	–	–
		MP hysteretic	1.12×10^{-4}	0.56	0.27
^{90}Sr	81.0	No MP / reversible	1.29×10^{-3}	40.7	18.5
		MP hysteretic	1.29×10^{-3}	40.7	0.39
^{238}U	188	No MP / reversible	1.53×10^{-3}	98.2	45.4
		MP hysteretic	1.53×10^{-3}	98.2	0.29
^{241}Am	10 134	No MP / reversible	no arrival	–	–
		MP hysteretic	1.86×10^{-5}	0.56	0.27

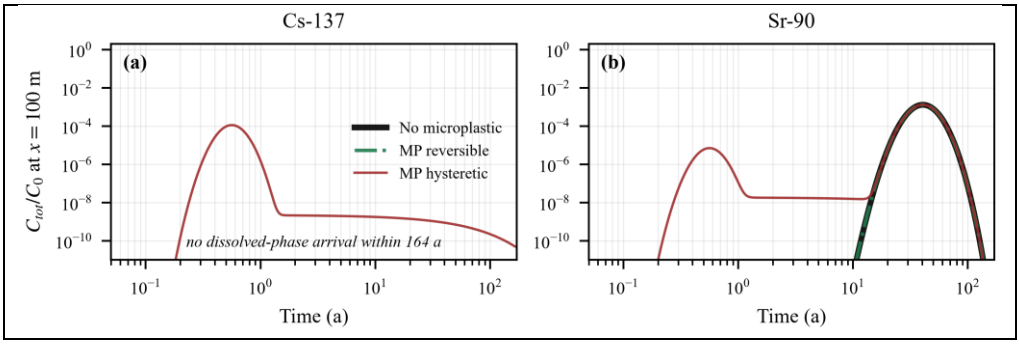


Figure 1. Breakthrough curves at x = 100 m for (a) caesium-137 and (b) strontium-90 in the three configurations. In (a) the no-microplastic and reversible curves are absent because no dissolved-phase arrival occurs within the 164-year simulation.

Within the tested parameter set, strontium-90 and uranium-238 produce later dissolved-phase peaks, while caesium-137 and americium-241 do not produce a dissolved-phase arrival within the stated simulation horizon. These outcomes are conditional on the selected matrix Kd values, exchange rates, flow properties, boundary conditions and simulation duration; they should not be interpreted as general behaviour of the four radionuclides.In the reversible configuration and under the selected exchange rates, the simulated polymer-bound fraction remains close to local equilibrium and provides little change in arrival at the observation point. This scenario result illustrates how rapid exchange can suppress a mobile-particle pathway when the aqueous phase is strongly coupled to the aquifer matrix; it is not evidence that reversible microplastic sorption is universally immobile.Under the assumed slow-desorption scenario, early particle-associated peaks occur for caesium-137 and americium-241.

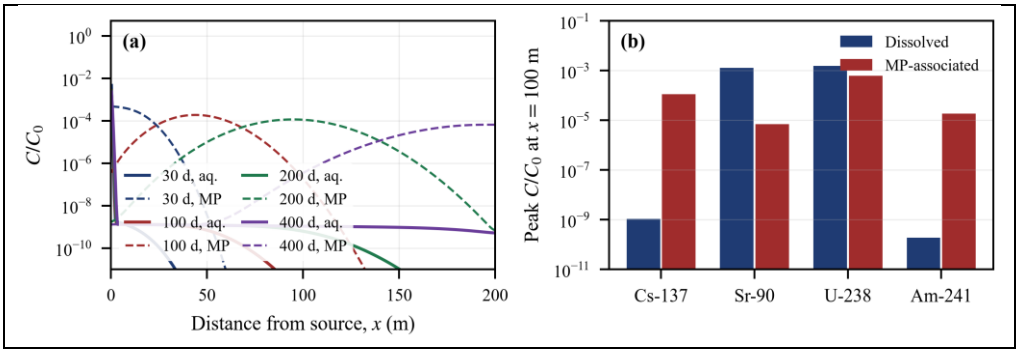


Figure 2. (a) Aqueous (solid) and microplastic-bound (dashed) concentration profiles for caesium-137 at four times under hysteretic kinetics. (b) Peak aqueous and peak microplastic-associated concentrations at x = 100 m for the four nuclides.

The reported peak times and magnitudes are model outputs for the stated parameter set and require code release, mass-balance verification, sensitivity analysis and comparison with column or field data before use in exposure assessment. Figure 2 illustrates the simulated phase separation; it does not demonstrate an observed environmental mechanism.

4.4. Vector efficiency and the kinetic threshold

To generalise, the simulated peak was normalised by the capacity ratio to define a vector efficiency, and the desorption rate constant scaled by the advective travel time $t_{adv} = x/v$ to give a Damkohler number:

$$\eta = (C_{tot}/C_0)_max / \beta_{MP}, \quad Da = k_{des}\, t_{adv} \tag{8}$$

Within the tested loading range and the stated linear-capacity formulation, the simulated peak is approximately proportional to cMP, so η is nearly constant with loading. Caesium-137 and americium-241 also show similar η values over the tested desorption-rate range. These numerical similarities are scenario-specific and do not establish independence from nuclide identity, half-life, polymer affinity or nonlinear effects outside the tested model domain.

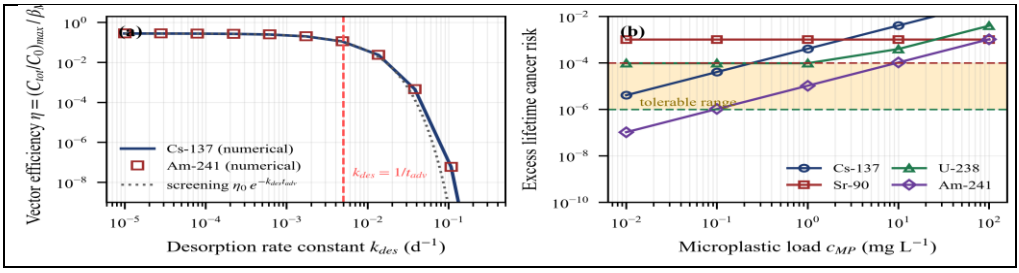


Figure 3. (a) Simulated vector efficiency as a function of desorption rate for caesium-137 and americium-241, with a first-order screening approximation. (b) Peak-concentration-based radiological screening metric versus microplastic loading; the shaded band is an illustrative decision band, not a universal ICRP or WHO risk limit.

Three response regions appear within the tested scenario. At low Da, efficiency approaches a plateau set by the modelled finite pulse and dispersion; at intermediate Da, progressive desorption increases transfer to the aqueous phase; and at higher Da, the particle-associated pathway declines sharply. The apparent transition near Da ≈ 1 (kdes ≈ 1/tadv) is a candidate screening relationship for this model and should be tested across alternative travel times, attachment/straining processes, parameter uncertainty and experimental datasets before being treated as a general threshold.A first-order ap-

proximation that treats desorption as irreversible loss reproduces the numerical output reasonably at low Da in this dataset but diverges at higher Da, where simulated resorption contributes to continued transport. The direction and magnitude of bias are conditional on the model formulation and parameter set; broader validation is required before the approximation is described as conservative or non-conservative in applications.

5. HUMAN HEALTH RISK IMPLICATIONS

5.1. Screening-level radiological metrics for drinking water

Radiological screening should account for the transient concentration history rather than applying a short-lived peak concentration continuously for 70 years. Using an adult water intake of 730 L y^{-1}, ingestion dose coefficients from ICRP Publication 119 [26] and the ICRP Publication 103 detriment-adjusted nominal risk coefficient [21,25], the appropriate expressions are

$$E_{annual} = \bar{C}w \cdot IR \cdot DCF; \quad ELCR = r \int Cw(t) \cdot IRd \cdot DCF\, dt \tag{9}$$

The source-zone concentrations used in the simulation—1×10^5 Bq L^{-1} for caesium-137, 1×10^4 Bq L^{-1} for strontium-90, 1×10^3 Bq L^{-1} for americium-241 and 5×10^2 Bq L^{-1} for uranium-238—are illustrative scenario assumptions, not established representative values for legacy sites. Consistent with IAEA guidance on site-specific source terms and uncertainty, these values require a traceable site-specific source or sensitivity distribution before publication [24]. Because the current table applies the simulated 30-day-release peak as though it were a constant annual concentration over 70 years, its ELCR column is retained only as a conservative peak-based screening bound; a defensible lifetime estimate requires numerical integration of Cw(t).

Table 5. Peak-concentration-based radiological screening metrics and a conditional chemical hazard quotient. WHO activity concentrations are screening levels used to determine whether further radionuclide-specific assessment is needed [27], not universal safe/unsafe boundaries.

Nuclide	Configuration	C peak (Bq L^{-1})	C / WHO	E (μSv a^{-1})	Peak-based risk bound
^{137}Cs	No MP / reversible	no arrival	–	–	–
	MP hysteretic	1.12×10^1	1.12	1.06×10^2	4.08×10^{-4}
^{90}Sr	All configurations	1.29×10^1	1.29	2.63×10^2	1.01×10^{-3}
^{238}U	All configurations	7.67×10^{-1}	0.077	2.52×10^1	9.70×10^{-5}
^{241}Am	No MP / reversible	no arrival	–	–	–
	MP hysteretic	1.86×10^{-2}	0.019	2.71×10^0	1.04×10^{-5}
^{238}U, chemical	All configurations	0.062 mg L^{-1}	–	HQ = 2.94	–

In the slow-desorption scenario, the modelled caesium-137 peak is 11.2 Bq L^{-1}. This is above the cited WHO screening level and therefore indicates a need for radionuclide-specific assessment; it does not by itself establish that the water is unsafe. The annual dose and lifetime-risk values currently shown are peak-concentration-based upper-bound calculations because the transient 30-day-release peak was treated as a constant exposure. They must be replaced with metrics integrated over Cw(t) before quantitative health-risk conclusions are made. The no-microplastic and reversible scenarios show no arrival within the chosen simulation horizon, not zero risk under all conditions.Americium-241, strontium-90 and uranium-238 results are likewise conditional on the stated scenario. Figure 3b currently depicts peak-based screening bounds rather than integrated lifetime risks. Any reported loading at which a risk band is crossed is therefore model- and exposure-assumption-specific and must be recalculated from the full concentration–time series with uncertainty bounds.

5.2. Chemical toxicity and combined endpoints

For uranium, chemical toxicity and radiological detriment should be assessed separately. Equation (10) follows the general hazard-quotient structure in risk-assessment guidance [33]. The oral reference dose of 6×10^{-4} mg kg^{-1} d^{-1} used here is a scenario input and requires a uranium-specific primary regulatory or toxicological source; Risk Assessment Guidance for Superfund [33] does not itself substantiate that value. With an intake of 2 L d^{-1} and body mass of 70 kg:

$$HQ = C_w \cdot IR_d / (BW \cdot RfD) \quad (10)$$

Under the stated conversion and reference-dose assumptions, the simulated uranium concentration of 0.767 Bq L^{-1} corresponds to 0.062 mg L^{-1} and yields HQ = 2.94. This conditional result suggests potential chemical concern and exceeds the WHO provisional uranium guideline value of 0.03 mg L^{-1} [20,27], but the conversion from activity to mass, isotopic composition, exposure assumptions and selected reference dose must be documented and uncertainty-tested. The radiological and chemical metrics should not be classified as mutually contradictory pass/fail decisions.

Radiological detriment and chemical toxicity use different endpoints, denominators and policy contexts. They may be reported side by side, but they should not be merged or placed on a common risk scale without a validated framework [22,25]. The present uranium calculation is best presented as a conditional illustration of why both endpoints require independent assessment.

5.3. The particle-ingestion vector pathway

A possible additional route is ingestion of radionuclide-bearing microplastic. Equation (11) is an upper-bound screening expression because it assumes that the equilibrium polymer loading applies to ingested particles and that 100% of particle-associated activity is released and systemically available in the gastrointestinal tract. A realistic assessment would require particle-size distributions, ingestion-rate uncertainty, gastrointestinal transit, desorption/bioaccessibility experiments and radionuclide-specific absorption fractions. Using an annual ingested microplastic mass of 0.25 g [32], the illustrative expression is

$$E_{ing} = K_{d,MP} \cdot C_w \cdot M_{MP} \cdot DCF \quad (11)$$

The resulting values should be interpreted only as upper-bound screening estimates under complete bioavailability. Comparisons at WHO activity screening levels do not establish general safety, and source-zone calculations do not demonstrate actual dose without evidence that the assumed polymer loading, Kd, ingestion rate and gastrointestinal release occur together. Near-field or accident scenarios therefore warrant targeted measurement rather than a categorical conclusion that the particle-ingestion pathway is significant.

6. CONCLUSION AND DISCUSSION

This focused review and screening case study supports four conditional conclusions. Polymer and aquifer-solid distribution coefficients are system-specific; Table 1 does not justify a universal ordering, and bulk capacity also depends on suspended mass. In the selected slow-desorption scenario, mobile particles produce earlier modelled arrival for strongly retarded radionuclides, but this hypothesis requires experimental and site-specific validation. The selected Damköhler metric is a sensitivity descriptor only within the tested formulation. Radiological and chemical uranium endpoints must remain separate, while peak concentrations are screening bounds rather than lifetime-risk estimates or universal thresholds.Interpretation is limited by the one-dimensional conservative-particle model, single-site matrix sorption, synthetic isotherms, incomplete numerical documentation, absent external validation and uncertainty analysis, and assumptions of constant peak exposure and complete gastrointestinal bioavailability. Size-dependent transport, attachment/straining, nanoplastics and decay-chain ingrowth are omitted, precluding site-specific or causal health claims. Priorities are long-duration desorption and labelled column experiments, facility-specific particle monitoring, transient dose integration, probabilistic uncertainty analysis, model benchmarking, mass-balance reporting, and release of code and synthetic-data inputs. PFAS extension

requires a defined interaction mechanism and supporting data; conclusions should remain calibrated to evidence and site context.

DECLARATIONS

Ethics Statement: Formal ethics review was not required for this computational study because it involved no human participants, animals, clinical records, or identifiable personal data.

Ethics Statement: Ethics approval and informed consent were not applicable because this study was entirely computational and involved no human participants, animals, clinical records, or identifiable personal data.

Funding: This chapter received no specific grant from any funding agency in the public, commercial, or not-for-profit sectors.

Competing Interests: The authors declare that they have no competing financial or non-financial interests.

REFERENCES

1- Adeola, A. O., Iwuozor, K. O., Akpomie, K. G., Adegoke, K. A., Oyedotun, K. O., Ighalo, J. O., Amaku, J. F., Olisah, C., & Conradie, J. (2023). Advances in the management of radioactive wastes and radionuclide contamination in environmental compartments: A review. Environmental Geochemistry and Health, 45(6), 2663–2689. https://doi.org/10.1007/s10653-022-01378-7

2- Ioannidis, I., Anastopoulos, I., & Pashalidis, I. (2022). Microplastics as radionuclide (U-232) carriers. Journal of Molecular Liquids, 351, 118641. https://doi.org/10.1016/j.molliq.2022.118641

3- Ioannidis, I., Kinigopoulou, V., Giannakoudakis, D. A., Arkas, M., Anastopoulos, I., Triantafyllidis, K. S., & Pashalidis, I. (2023). Microplastics and disposable face masks as "Trojan Horse" for radionuclides pollution in water bodies—A review with emphasis on the involved interactions. Sustainable Chemistry for the Environment, 1, 100005. https://doi.org/10.1016/j.scenv.2023.100005

4- Johansen, M. P., Prentice, E., Cresswell, T., & Howell, N. (2018). Initial data on adsorption of Cs and Sr to the surfaces of microplastics with biofilm. Journal of Environmental Radioactivity, 190–191, 130–133. https://doi.org/10.1016/j.jenvrad.2018.05.001

5- Johansen, M. P., Cresswell, T., Davis, J., Howard, D. L., Howell, N. R., & Prentice, E. (2019). Biofilm-enhanced adsorption of strong and weak cations onto different microplastic sample types: Use of spectroscopy, microscopy and radiotracer methods. Water Research, 158, 392–400. https://doi.org/10.1016/j.watres.2019.04.029

6- Rout, S., Yadav, S., Joshi, V., Karpe, R., Pulhani, V., & Kumar, A. V. (2022). Microplastics as vectors of radioiodine in the marine environment: A study on sorption and interaction mechanism. Environmental Pollution, 307, 119432. https://doi.org/10.1016/j.envpol.2022.119432

7- Ioannidis, I., Antoniou, A., & Pashalidis, I. (2025). Enhanced radionuclide (U-232) adsorption by humic acid-coated microplastics. Journal of Environmental Chemical Engineering, 13(1), 115064. https://doi.org/10.1016/j.jece.2024.115064

8- Ioannidis, I., Kinigopoulou, V., Anastopoulos, I., Giannakoudakis, D. A., & Pashalidis, I. (2024). The interaction of two emerging pollutants, microplastics and radionuclides, in the environment: Sorption of U-232 and Am-241 by polyurethane and polylactic-acid microplastics. Sustainable Chemistry for the Environment, 8, 100184. https://doi.org/10.1016/j.scenv.2024.100184

9- Lujanienė, G., Beneš, P., Štamberg, K., & Ščiglo, T. (2012). Kinetics of plutonium and americium sorption to natural clay. Journal of Environmental Radioactivity, 108, 41–49. https://doi.org/10.1016/j.jenvrad.2011.07.012

10- Siroux, B., Latrille, C., Beaucaire, C., Petcut, C., Tabarant, M., Benedetti, M. F., & Reiller, P. E. (2021). On the use of a multi-site ion-exchange model to predictively simulate the adsorption behaviour of strontium and caesium onto French agricultural soils. Applied Geochemistry, 132, 105052. https://doi.org/10.1016/j.apgeochem.2021.105052

11- Kersting, A. B., Efurd, D. W., Finnegan, D. L., Rokop, D. J., Smith, D. K., & Thompson, J. L. (1999). Migration of plutonium in ground water at the Nevada Test Site. Nature, 397(6714), 56–59. https://doi.org/10.1038/16231

12- Kersting, A. B. (2013). Plutonium transport in the environment. Inorganic Chemistry, 52(7), 3533–3546. https://doi.org/10.1021/ic3018908

13- Zhang, X., Wang, Z., Reimus, P. W., Ma, F., Soltanian, M. R., Xing, B., Zang, J., Wang, Y., & Dai, Z. (2022). Plutonium reactive transport in fractured granite: Multi-species experiments and simulations. Water Research, 224, 119068. https://doi.org/10.1016/j.watres.2022.119068

14- International Atomic Energy Agency. (2023). Comprehensive report on the safety review of the ALPS-treated water at the Fukushima Daiichi Nuclear Power Station. IAEA. https://www.iaea.org/sites/default/files/iaea_comprehensive_alps_report.pdf

15- Ackerman Grunfeld, D., Gilbert, D., Hou, J., Jones, A. M., Lee, M. J., Kibbey, T. C. G., & O'Carroll, D. M. (2024). Underestimated burden of per- and polyfluoroalkyl substances in global surface waters and groundwaters. Nature Geoscience, 17(4), 340–346. https://doi.org/10.1038/s41561-024-01402-8

16- Johnson, G. R., Brusseau, M. L., Carroll, K. C., Tick, G. R., & Duncan, C. M. (2022). Global distributions, source-type dependencies, and concentration ranges of per- and polyfluoroalkyl substances in groundwater. Science of the Total Environment, 841, 156602. https://doi.org/10.1016/j.scitotenv.2022.156602

17- Vearrier, D., Curtis, J. A., & Greenberg, M. I. (2009). Technologically enhanced naturally occurring radioactive materials. Clinical Toxicology, 47(5), 393–406. https://doi.org/10.1080/15563650902997849

18- El Zrelli, R., Rabaoui, L., Abda, H., Daghbouj, N., Pérez-López, R., Castet, S., Aigouy, T., Bejaoui, N., & Courjault-Radé, P. (2018). Characterization of phosphate rock and phosphogypsum from Gabès phosphate fertilizer factories (SE Tunisia): High mining potential and implications for environmental protection. Environmental Science and Pollution Research, 25(15), 14690–14702. https://doi.org/10.1007/s11356-018-1648-4

19- Abdelouas, A. (2006). Uranium mill tailings: Geochemistry, mineralogy, and environmental impact. Elements, 2(6), 335–341. https://doi.org/10.2113/gselements.2.6.335

20- World Health Organization. (2012). Uranium in drinking-water: Background document for development of WHO Guidelines for Drinking-water Quality (WHO/SDE/WSH/03.04/118/Rev/1). WHO. https://cdn.who.int/media/docs/default-source/wash-documents/wash-chemicals/background-uranium-rev-1.pdf
21- Cléro, E., Vaillant, L., Hamada, N., Zhang, W., Preston, D., Laurier, D., & Ban, N. (2019). History of radiation detriment and its calculation methodology used in ICRP Publication 103. Journal of Radiological Protection, 39(3), R19–R36. https://doi.org/10.1088/1361-6498/ab294a
22- Chen, J., Meyerhof, D. P., & Tracy, B. L. (2004). Model for assessing radiation and chemical toxicity of uranium in drinking water. Health Physics, 86(1), 3–11. https://doi.org/10.1097/00004032-200401000-00003
23- Croudace, I. W., Russell, B. C., & Warwick, P. E. (2017). Plasma source mass spectrometry for radioactive waste characterisation in support of nuclear decommissioning: A review. Journal of Analytical Atomic Spectrometry, 32, 494–526. https://doi.org/10.1039/C6JA00334F
24- International Atomic Energy Agency. (2018). Prospective radiological environmental impact assessment for facilities and activities (IAEA Safety Standards Series No. GSG-10). IAEA. https://www-pub.iaea.org/MTCD/Publications/PDF/PUB1819_web.pdf
25- ICRP (2007). The 2007 Recommendations of the International Commission on Radiological Protection. ICRP Publication 103. Annals of the ICRP, 37(2–4).
26- ICRP. (2012). ICRP Publication 119: Compendium of dose coefficients based on ICRP Publication 60. Annals of the ICRP, 41(Suppl.), 1–130. https://doi.org/10.1016/j.icrp.2012.06.038
27- WHO (2022). Guidelines for Drinking-water Quality: Fourth Edition Incorporating the First and Second Addenda. World Health Organization, Geneva.
28- IAEA (2010). Handbook of Parameter Values for the Prediction of Radionuclide Transfer in Terrestrial and Freshwater Environments. Technical Reports Series No. 472. International Atomic Energy Agency, Vienna.
29- Langmuir, I. (1918). The adsorption of gases on plane surfaces of glass, mica and platinum. Journal of the American Chemical Society, 40(9), 1361–1403. https://doi.org/10.1021/ja02242a004
30- Freundlich, H. (1907). Über die Adsorption in Lösungen. Zeitschrift für Physikalische Chemie, 57U(1), 385–470. https://doi.org/10.1515/zpch-1907-5723
31- Gelhar, L. W., Welty, C., & Rehfeldt, K. R. (1992). A critical review of data on field-scale dispersion in aquifers. Water Resources Research, 28(7), 1955–1974. https://doi.org/10.1029/92WR00607

32- Senathirajah, K., Attwood, S., Bhagwat, G., Carbery, M., Wilson, S., & Palanisami, T. (2021). Estimation of the mass of microplastics ingested—A pivotal first step towards human health risk assessment. Journal of Hazardous Materials, 404, 124004. https://doi.org/10.1016/j.jhazmat.2020.124004

33- USEPA (1989). Risk Assessment Guidance for Superfund, Volume I: Human Health Evaluation Manual (Part A). EPA/540/1-89/002. United States Environmental Protection Agency, Washington DC.

34- Harris, C. R., Millman, K. J., van der Walt, S. J., Gommers, R., Virtanen, P., Cournapeau, D., et al. (2020). Array programming with NumPy. Nature, 585(7825), 357–362. https://doi.org/10.1038/s41586-020-2649-2

35- Virtanen, P., Gommers, R., Oliphant, T. E., Haberland, M., Reddy, T., Cournapeau, D., et al. (2020). SciPy 1.0: Fundamental algorithms for scientific computing in Python. Nature Methods, 17(3), 261–272. https://doi.org/10.1038/s41592-019-0686-2

Chapter 13

Radionuclide And Heavy Metal Contamination in Ecosystems: Environmental Risk Assessment

Almusa ATAMALIYEV[1], Temel KAN BAKIR[2], Malahat BAGİYEVA[3]
Elsevar ATAMALİYEV[4], Bikakhanim YUZBASHYEVA[5]

INTRODUCTION

Rapid urban development, expanding energy production, and the intensive use of natural resources have substantially increased the environmental release of inorganic contaminants, particularly radionuclides and heavy metals. Owing to their persistence, toxicity, and potential to accumulate in biological systems, these contaminants can produce long-lasting effects on ecosystem structure and function and may also pose significant risks to human health. Although radionuclides are distinguished by their radioactive decay, heavy metals are generally characterized by their resistance to biological degradation. Consequently, understanding how these contaminants behave, move, and undergo transformation within environmental systems has become an important research focus in radioecology, ecotoxicology, and environmental science [1–4].Pollution associated with human activities originates from various sources, including nuclear energy and activities related to its production, uranium extraction, mining and the processing of ferrous and non-ferrous metals, the combustion of fossil fuels, chemicals used in agricultural activities, industrial waste, and electronic waste. Once released into the environment, radionuclides and heavy metals can rapidly spread between the atmospheric, hydrospheric, and lithospheric compartments through interacting physical, chemical, and biological processes. Their mobility in the environment and accessibility to living organisms are not constant; rather, they depend considerably on numerous site-specific conditions and factors, such as soil pH, redox potential, mineral composition, the

[1] Kastamonu University, Faculty of Science, Department of Chemistry, Almusa, TÜRKİYE, almusa.atamaliyev@adpu.edu.az orcid id: 0009-0009-8887-6149
[2] Prof. Dr., Department of Chemistry, Faculty of Science, Kastamonu University, Türkiye, temelkan@kastamonu.edu.tr, (ORCID: 0000-0002-7447-1468)
[3] Baku State University, Faculty of Chemistry, Malahat, AZERBAIJAN, malahatbagiyeva@bsu.edu.az orcid id : 0009-0001-8619-8059
[4] Azerbaijan Cooperation University, Faculty of Economics and Environmental Engineering, Elsavar, AZERBAIJAN, atamaliyev.elsever@aku.edu.az, orcid id : 0009-0005-4397-706X
[5] Baku State College of Communications and transport under Azerbaijan Technical University , Faculty of General Technical Subjects and Transport , Bikakhanim, AZERBAIJAN, bdrnk.yuzbasyevabikexanım@gmail.com orcid id : 0009-0004-8085-087X

amount of organic matter in water and soil, and climatic factors [2,5,6]. The ecological significance of radionuclide and heavy metal contamination cannot be evaluated solely on the basis of their total concentrations. Chemical speciation and bioavailability are equally important for this purpose, as these parameters determine the uptake of contaminants by all types of living organisms and their level of transfer through food webs. The accumulation of such harmful substances in organisms may cause oxidative stress, as well as genotoxicity, impairment of reproductive functions, and changes at the population level. This, in turn, may lead to a decline in biodiversity and disruption of ecosystem services. Furthermore, the transfer of contaminated substances through food chains is considered one of the main pathways through which harmful substances such as radionuclides and heavy metals can enter the human body, potentially resulting in chronic toxicological and radiological effects [3,7–9]. Any changes occurring in nature may affect the fate and behavior of these contaminants. These include climate change, soil erosion, extreme hydrological events, and increasing anthropogenic pressures, which may enhance the remobilization of radionuclides and heavy metals accumulated in previously stabilized environmental compartments. Consequently, these processes may alter their spatial distribution, mobility, and migration pathways within ecosystems. Therefore, the behavior of contaminants should be comprehensively investigated, ecological risk assessments should be conducted, the application of new monitoring methods should be tested, and sustainable remediation and management strategies should be continuously developed. These measures are of significant importance for maximizing the reduction of environmental hazards, maintaining ecosystem integrity, and protecting human health [1,4,10].



Figure1. Environmental Pathways Radionuclide and Heavy Metal Contamination [4,10]

2. RADIONUCLIDE AND HEAVY METAL POLLUTION

Radionuclides and heavy metals are considered major inorganic contaminants because of their potential to cause environmental pollution due to their ability to persist in the environment for extended periods. The presence and distribution of these contaminants are determined by the combined effects of natural geochemical processes and human activities. Therefore, identifying the sources of contaminants is of significant importance for observing their pathways of dispersion in the environment, tracking their subsequent migration, assessing associated risks, and planning appropriate management measures. The dispersion of radionuclides and heavy metals in the environment is influenced not only by the magnitude of their release into the environment but also by direct interactions among geological characteristics, soil and water properties, climatic variability, and anthropogenic factors [2,11]

2.1. Natural Sources

Radionuclides and heavy metals occur naturally in the Earth's crust and continuously enter ecosystems through geochemical cycles. Their background levels are generally determined by regional geological characteristics as well as mineralogical composition. Nevertheless, under certain geological and climatic conditions, these substances may accumulate at concentrations that can pose serious environmental hazards [5,12].Natural processes constitute one of the main pathways through which radionuclides and heavy metals enter the environment. Substances such as uranium and thorium, as well as their radioactive decay products, are naturally present in many igneous and metamorphic rocks and enter soil and water environments when these rocks undergo weathering processes. Heavy metals, including lead, cadmium, arsenic, and mercury, can also be mobilized from mineral-bearing geological formations through seismic and volcanic processes and subsequently enter the biosphere. The environmental behavior of these elements is highly dependent on their chemical speciation, redox conditions, and the surrounding geochemical environment. For example, under oxidizing conditions, uranium may exhibit greater mobility, whereas the environmental mobility of arsenic may vary considerably depending on its oxidation state. Such conditions can significantly increase the bioavailability, toxicity, and overall environmental significance of these elements [6,13].Volcanic activity is one of the major natural mechanisms contributing to the global cycling of radionuclides and heavy metals. Volcanic eruptions release gases and ash into the atmosphere, along with mercury, arsenic, lead, cadmium, and other elements. Once released into the atmosphere, these materials can be transported over considerable distances and subsequently deposited in soil and aquatic environments. Therefore, volcanic eruptions can cause temporary increases in regional background concentrations of heavy metals and alter the geochemical balance of affected ecosystems [5,14].

2.2. Weathering of Soils and Rocks

The physical and chemical weathering of rocks is one of the main natural mechanisms through which radionuclides and heavy metals enter the biosphere. Elements released through the decomposition of minerals enter soil and water and subsequently migrate between different ecosystems through rivers and groundwater. The intensity of weathering depends on climatic conditions; chemical weathering is generally predominant in humid areas, whereas physical weathering is more commonly observed in arid environments. Climate change intensifies erosion processes, which in turn accelerates the remobilization of radionuclides and heavy metals [7,12]. The extraction and processing of uranium ores are among the major sources of radionuclide contamination. During mining operations, radium, thorium, and other radioactive elements are also released into the environment along with uranium.Acid mine drainage can enhance the dissolution of radionuclides and accelerate their migration into groundwater. Waste materials generated at mining sites may remain sources of radioactive contamination for many years, even after mining operations have ceased [2,8,11]. The processing and smelting of ores in metallurgical facilities generate metal-containing gases, aerosols, and solid wastes. Lead, cadmium, arsenic, and nickel can be dispersed through the atmosphere and subsequently accumulate in soil and aquatic ecosystems. Because the bioavailability of these metals increases under acidic conditions, their uptake by plants and other organisms may be enhanced, consequently intensifying bioaccumulation and biomagnification processes [9,13].

2.3. Chemical Industry

Metal-containing catalysts and reagents used in the chemical industry are important sources of heavy-metal contamination. Processes involving chlor-alkali production, paints, pigments, pesticides, and fertilizers may release toxic elements such as mercury and hexavalent chromium into the environment. Since interactions among multiple contaminants can increase their combined toxicity, green chemistry technologies are considered an important strategy for reducing environmental risks [10,14]. Electronic waste is a rapidly expanding hazardous-waste stream. Computers, mobile devices, batteries, and other electronic equipment contain hazardous substances such as lead, cadmium, mercury, nickel, chromium, and arsenic. If the waste products generated from these devices are not properly disposed of and are burned in open conditions, these elements are released into the soil, water, and air, as a result of which they can persist in the environment for long periods and enter food chains. Therefore, waste management based on the circular economy is of great importance for ensuring sustainable environmental protection. [4,15].Soil plays an important role as a

geochemical barrier controlling the mobility and bioavailability of radionuclides and heavy metals. Their behavior is determined by soil mineralogy, organic matter content, pH, redox conditions, and cation-exchange capacity [5,13,16]. Adsorption on the surfaces of soil particles immobilizes contaminants and limits their mobility, whereas desorption may release them back into the soil solution and increase their mobility. Clay minerals, iron and manganese oxides, humic substances, and colloids play particularly important roles in these processes. For example, 137Cs is strongly retained by clay minerals, whereas 90Sr and cadmium generally exhibit higher mobility. Under acidic conditions, reduced adsorption may further increase the bioavailability of heavy metals [6, 13, 21]. Ion exchange also affects the retention of contaminants in soil; ^{137}Cs primarily interacts with potassium, whereas 90Sr interacts with calcium, thereby affecting their subsequent uptake by plants. Therefore, soil cation-exchange capacity is an important factor in assessing the immobilization of radionuclides and heavy metals [12,13,22]. In aquatic ecosystems, these contaminants exist mainly in dissolved or particle-associated forms. Dissolved species generally have greater mobility and bioavailability, whereas particle-bound contaminants are mainly associated with clay minerals, organic matter, and colloidal particles. The distribution between these forms depends on various environmental conditions, including pH, temperature, salinity, and the physicochemical properties of organic matter [17,18,23]. Particle-associated contaminants may settle as a result of sedimentation and accumulate in bottom sediments, which can function as long-term reservoirs. However, changes in hydrodynamic conditions, sediment resuspension, mixing of the water column, pH, and oxygen availability may cause the remobilization of previously deposited contaminants and their return to the water column. This behavior is particularly important in estuarine and deltaic environments, reservoirs, and other aquatic systems exposed to significant hydrological or climatic changes [19,20,24].

3. HEAVY METALS TO LIVING ORGANISMS AND HUMANS

Radionuclides and heavy metals can enter living organisms mainly through ingestion, inhalation, and dermal contact. The importance of each pathway depends on the properties of the contaminant, organism physiology, and environmental conditions [25,26]. Ingestion is generally the dominant route, allowing contaminants from soil, water, and sediments to enter plants and subsequently move through food chains to higher trophic levels. Radionuclides such as 137Cs and 90Sr, together with metals such as Cd and As, may accumulate in biological tissues depending on their chemical form, bioavailability, and metabolic behavior. Their similarity to essential elements, particularly the

resemblance of cesium to potassium and strontium to calcium, can facilitate their uptake by organisms [21,26]. Inhalation is also important for contaminants present in airborne particles, aerosols, or gaseous forms. Radon, plutonium-containing particles, and mercury vapor can enter the respiratory system and cause internal irradiation or toxic effects, with fine particles potentially reaching the alveolar region and entering systemic circulation [10,27]. Dermal uptake is especially relevant for aquatic organisms and amphibians and may also contribute to exposure under conditions of prolonged contamination [28,29]. Humans may ultimately be exposed through contaminated food, drinking water, and inhaled atmospheric particles. Cereals, vegetables, milk, fish, and seafood can serve as important pathways for contaminant transfer, while arsenic and uranium are of particular concern in contaminated drinking-water sources [7,10,21]. After entering the body, these substances may accumulate in specific tissues according to their chemical and physiological behavior. For example, 90Sr is mainly incorporated into bones, 137Cs is distributed largely in muscle tissue, mercury may accumulate in the nervous system, and cadmium is preferentially retained in the kidneys [8,26,30]. Consequently, bioaccumulation and biomagnification are important for understanding contaminant transfer through food webs and for evaluating environmental risks, supporting biomonitoring, and developing sustainable management strategies [9,25,31].

4.ECOTOXICOLOGICAL EFFECTS

Radionuclides and heavy metals are among the major contaminants posing serious risks to the environment due to their persistence, toxicity, and ability to accumulate in biological systems. Their effects can be observed at various levels of biological organization, ranging from molecular and cellular levels to individual organisms, populations, and entire ecosystems. Although the effects of radionuclides are primarily associated with ionizing radiation, while those of heavy metals are mainly related to chemical toxicity, both groups can cause oxidative stress, genetic alterations, metabolic disturbances, and impairment of essential physiological functions [8,9,33]. Ecotoxicological assessment enables the comprehensive characterization of the lethal and sublethal effects of these contaminants, including reproductive and developmental disturbances, as well as changes in key ecosystem functions [10,34].

4.1. Effects at the Cellular and Molecular Levels

The ionizing radiation emitted by radionuclides and the genotoxic effects of heavy metals can cause DNA damage, chromosomal alterations, and disruptions in gene expression. In particular, cadmium, arsenic, and hexavalent chromium

can adversely affect DNA repair processes, whereas radionuclides cause molecular damage as a result of high-energy radiation. The accumulation of such damage may lead to mutations, apoptosis, and disruption of cellular functions, thereby increasing long-term toxicological and genetic risks [8,32–36].

4.2. Effects at the Individual and Population Levels

Exposure can impair growth, development, reproduction, and immune function. Early developmental stages are particularly sensitive, while plants may show reduced root development, photosynthesis, and productivity [21,33,37]. Ionizing radiation can damage reproductive cells, and cadmium, mercury, and lead can disrupt hormonal regulation, reducing reproductive success and impairing embryonic development [8,34,38]. Immune suppression may increase disease susceptibility [35,36,38]. At the population level, these effects can increase mortality, reduce reproduction and genetic diversity, and lower population density; chronic exposure may select tolerant individuals while altering population genetic and ecological structure [34,39].

4.3. Effects at the Ecosystem Level

Contamination can reduce biodiversity, disrupt trophic interactions and nutrient cycling, and impair ecosystem services [9,10]. Bioaccumulation and biomagnification may increase contaminant burdens at higher trophic levels, reduce sensitive species, and trigger trophic cascades [9,31,40]. Disruption of energy flow, productivity, microbial activity, nutrient cycling, and self-purification can consequently affect food and water security and ecosystem functioning [10,39,40]. These interconnected effects require integrated risk assessment and biomonitoring to support effective management [8,9,40].

5. RISK ASSESSMENT METHODOLOGIES

Effective management requires scientifically robust assessment of contaminant distribution, exposure pathways, and toxicological effects. Modern methods evaluate current contamination, predict future environmental and health risks, identify vulnerable ecosystems, and prioritize mitigation [7,10,41].Ecological Risk Assessment (ERA) systematically evaluates potential adverse effects on ecosystem components and generally comprises problem formulation, exposure assessment, effects assessment, and risk characterization [41,42]. Problem formulation identifies sources, receptors, and exposure pathways and establishes a conceptual risk model. Exposure assessment estimates contaminant exposure using monitoring data, transport models, and bioaccumulation indicators. Effects assessment considers mortality, reproductive

impairment, genotoxicity, and other endpoints. Risk characterization integrates exposure and toxicity information to estimate risk and guide management [34,41,42].

Human health risk assessment is a scientific approach used to evaluate possible exposure to radionuclides and heavy metals through food, drinking water, soil, and air. The assessment typically encompasses four interconnected components: hazard identification, dose-response assessment, exposure assessment, and risk characterization. By integrating these elements, the approach facilitates the identification and characterization of potential health hazards associated with environmental contaminants and provides a scientific basis for developing appropriate preventive and risk-management measures [7, 41, 43]. Carcinogenic risk refers to the probability that prolonged or lifetime exposure to a contaminant may result in cancer development. Arsenic, cadmium, hexavalent chromium, and certain radionuclides are among the contaminants recognized for their carcinogenic potential. In quantitative risk assessment, carcinogenic risk is commonly estimated from the product of chronic daily intake (CDI) and the cancer slope factor (SF)

$$\mathbf{CR = CDI \times SF} \tag{1}$$

Where; CR ;denotes carcinogenic risk,CDI; chronic daily intake and SF; cancer slope factor. The resulting value provides an estimate of the incremental lifetime cancer risk associated with exposure to the contaminant [41,43]. Non-carcinogenic risks include functional impairments affecting the nervous system, liver, kidneys, reproductive system, and immune system. The Hazard Quotient (HQ) is one of the most widely used indicators for evaluating such risks:

$$\mathbf{HQ} = \frac{\mathbf{CDI}}{\mathbf{RfD}} \tag{2}$$

where ,**RfD;** reference dose. An **HQ < 1** generally indicates that significant adverse health effects are unlikely, whereas an **HQ > 1** suggests the potential for adverse effects. The combined effects of multiple contaminants or exposure pathways can be evaluated using the **Hazard Index (HI)**;

$$HI = \Sigma HQ_i \tag{3}$$

An **HI > 1** indicates the potential presence of an overall non-carcinogenic risk and may warrant additional monitoring and risk-control measures [41-46].

Radionuclide and heavy-metal contamination is expected to remain a major environmental concern in the coming decades, driven by continued industrialization, mining, energy production, urban expansion, and climate change. Their persistence, mobility, and capacity for bioaccumulation necessitate risk evaluation within local, regional, and global environmental-security frameworks. Particular attention should be given to the increasingly complex relationship between climate change and contaminant fate. Rising temperatures, changes in precipitation patterns, drought, flooding, wildfires, and permafrost thawing can remobilize contaminants retained in soils and sediments, while extreme hydrological events may enhance their transfer into aquatic environments. Consequently, climate projections need to be incorporated into geochemical and ecological models alongside long-term monitoring and multifactorial risk-assessment approaches [44-56, 57]. Advances in environmental monitoring are creating new opportunities for the rapid detection and spatial assessment of contamination. Nanoscale biosensors, electrochemical sensors, unmanned aerial vehicles (UAVs), and multispectral or hyperspectral satellite systems can facilitate high-resolution surveillance across extensive areas [58–60]. Future monitoring frameworks should integrate sensor networks with laboratory analyses, satellite observations, meteorological information, and biomonitoring within unified digital infrastructures capable of real-time assessment and early warning [58–60]. The increasing prevalence of mixed contamination also requires greater research attention, as radionuclides and heavy metals frequently occur alongside microplastics, pesticides, and other environmental pollutants. The synergistic, additive, or antagonistic interactions among these contaminants remain insufficiently characterized. Multipollutant models and multifactorial experimental designs can therefore provide more realistic estimates of ecological risks under environmentally relevant exposure conditions [56, 57,61]. At the molecular level, omics-based approaches-including genomics, transcriptomics, proteomics, metabolomics, and epigenomics-offer valuable tools for detecting early biomarkers, elucidating cellular responses, and identifying mechanisms underlying biological adaptation to chronic contaminant exposure [61,62]. New remediation approaches include nanoscale sorbents, magnetic nanoparticles, functionalized carbon materials, metal-organic frameworks, and bio-based nanocomposites. Although these technologies offer broad opportunities for more efficient contaminant removal, their long-term environmental safety, risk of secondary contamination, and impacts throughout their life cycle should also be considered together with remediation efficiency [58, 60, 65]. Phytoremediation, bioremediation, and other nature-based methods can also support the application of these technologies by providing more

sustainable solutions for ecosystem restoration [57,67]. At the same time, the One Health and Planetary Health approaches provide an integrated assessment of contaminant-related risks in terms of human, animal, and ecosystem health. These approaches are particularly important when exposure to contaminants occurs through different pathways associated with food, water, and the environment [64-67]. Overall, the future management of radionuclide and heavy-metal contamination will increasingly depend on the combined use of artificial intelligence, big-data analysis, remote sensing, omics technologies, climate modeling, and digital monitoring systems. The combined application of these technologies can help enable the early identification of contamination, improve the prediction of contaminant behavior, and support the implementation of more effective and preventive environmental management measures [58–67].

6. CONCLUSION

Radionuclide and heavy-metal contamination is a complex, persistent environmental challenge affecting ecosystem stability, biodiversity, and human health. In addition to natural geochemical processes, industrial activity, mining, metallurgy, energy production, nuclear operations, and urbanization have increased contaminant burdens [57–60,63]. Their persistence, movement among environmental compartments, and food-web transfer create long-term ecological risks [58,59,63].Environmental behavior depends not only on total concentrations but also on chemical speciation, bioavailability, adsorption–desorption, ion exchange, redox transformations, and biogeochemical cycling [57,58,63]. Bioaccumulation and biomagnification can increase contaminant burdens at higher trophic levels. Mercury, cadmium, arsenic, and cesium may be transferred through food webs, contributing to reproductive impairment, immune dysfunction, genotoxicity, population decline, biodiversity loss, and ecosystem disruption [57,59,60,63]. Risk-assessment tools such as HQ, HI, Pollution Load Index, Geoaccumulation Index , and radiological models, together with GIS, Monte Carlo simulations, and artificial intelligence, improve risk characterization [58,59,64]. Gamma and alpha spectrometry, ICP-MS, ICP-OES, AAS, and XRF remain important for contaminant detection and monitoring [58,63,64].Effective remediation requires coordinated physical, chemical, and biological approaches. Phytoremediation, mycoremediation, and bioremediation provide sustainable alternatives, while immobilization and stabilization can reduce contaminant mobility and bioavailability [57,64]. Long radionuclide half-lives and the non-biodegradable nature of heavy metals allow contamination to persist for generations, with implications for food and water security [58–60,62,63]. Climate change may further alter these risks through changing temperature, hydrology, and extreme events [65]. Management should

therefore combine prevention, monitoring, early-warning systems, sustainable remediation, cleaner production, hazardous-waste control, and GIS- and AI-based risk models [57,61,64,66,67]. Nature-based remediation can also support ecosystem-service restoration [57,67]. Ultimately, effective management requires integration of chemistry, ecology, toxicology, radioecology, data science, and environmental engineering. One Health and Planetary Health frameworks provide a broader basis for protecting human health, ecosystem resilience, and socioeconomic security [66,68]. Interdisciplinary strategies are essential for reducing contamination, protecting biodiversity, maintaining ecosystem integrity, and promoting a safer and more sustainable environment for future generations [57–68].

REFERENCES

1. World Health Organization. (2017). Guidelines for drinking-water quality: Fourth edition incorporating the first addendum. World Health Organization.
2. United Nations Scientific Committee on the Effects of Atomic Radiation. (2020). Sources and effects of ionizing radiation. United Nations.
3. U.S. Environmental Protection Agency. (1989). Risk assessment guidance for Superfund: Volume I—Human health evaluation manual (Part A) (EPA/540/1-89/002). U.S. Environmental Protection Agency.
4. International Commission on Radiological Protection. (2007). The 2007 recommendations of the International Commission on Radiological Protection (ICRP Publication 103). Elsevier.
5. Alloway, B. J. (2013). Heavy metals in soils: Trace metals and metalloids in soils and their bioavailability (3rd ed.). Springer.
6. Kabata-Pendias, A. (2011). Trace elements in soils and plants (4th ed.). CRC Press.
7. Agency for Toxic Substances and Disease Registry. (2019). Toxicological profile for arsenic. U.S. Department of Health and Human Services.
8. International Atomic Energy Agency. (2014). Radiation protection and safety of radiation sources: International basic safety standards (IAEA Safety Standards Series No. GSR Part 3). IAEA.
9. Alloway, B. J., & Ayres, D. C. (1997). Chemical principles of environmental pollution (2nd ed.). Blackie Academic & Professional.
10. Keith, L. H. (1996). Principles of environmental sampling (2nd ed.). American Chemical Society.
11. Förstner, U., & Wittmann, G. T. W. (2012). Metal pollution in the aquatic environment. Springer.
12. Chen, T. B., Zheng, Y. M., Lei, M., Huang, Z. C., Wu, H. T., Chen, H., Fan, K. K., Yu, K., Wu, X., & Tian, Q. Z. (2005). Assessment of heavy metal pollution in surface soils of Tianjin, China. Journal of Geographical Sciences, 15(1), 101–108.
13. Nagajyoti, P. C., Lee, K. D., & Sreekanth, T. V. M. (2010). Heavy metals, occurrence and toxicity for plants: A review. Environmental Chemistry Letters, 8(3), 199–216. https://doi.org/10.1007/s10311-010-0297-8
14. Adriano, D. C. (2001). Trace elements in terrestrial environments: Biogeochemistry, bioavailability, and risks of metals (2nd ed.). Springer.
15. Sparks, D. L. (2003). Environmental soil chemistry (2nd ed.). Academic Press.

16. Sposito, G. (2008). The chemistry of soils (2nd ed.). Oxford University Press.
17. Greenwood, N. N., & Earnshaw, A. (1997). Chemistry of the elements (2nd ed.). Butterworth-Heinemann.
18. Wedepohl, K. H. (1995). The composition of the continental crust. Geochimica et Cosmochimica Acta, 59(7), 1217–1232. https://doi.org/10.1016/0016-7037(95)00038-2
19. Baird, C., & Cann, M. (2012). Environmental chemistry (5th ed.). W. H. Freeman.
20. Manahan, S. E. (2017). Environmental chemistry (10th ed.). CRC Press.
21. Mason, B. (1966). Principles of geochemistry (3rd ed.). Wiley.
22. Fetter, C. W. (1999). Contaminant hydrogeology (2nd ed.). Prentice Hall.
23. Freeze, R. A., & Cherry, J. A. (1979). Groundwater. Prentice-Hall.
24. Christensen, J. B., Jensen, D. L., & Christensen, T. H. (2000). Effect of dissolved organic carbon on the mobility of metals in soil and groundwater. Environmental Science & Technology, 34(9), 1571–1577.
25. Stumm, W., & Morgan, J. J. (1996). Aquatic chemistry: Chemical equilibria and rates in natural waters (3rd ed.). Wiley.
26. Langmuir, D. (1997). Aqueous environmental geochemistry. Prentice Hall.
27. Smedley, P. L., & Kinniburgh, D. G. (2002). A review of the source, behaviour and distribution of arsenic in natural waters. Applied Geochemistry, 17(5), 517–568. https://doi.org/10.1016/S0883-2927(02)00018-5
28. United Nations Scientific Committee on the Effects of Atomic Radiation. (2008). Effects of ionizing radiation: UNSCEAR 2008 report to the General Assembly, with scientific annexes. United Nations.
29. International Commission on Radiological Protection. (2012). Compendium of dose coefficients based on ICRP Publication 60 (ICRP Publication 119). Elsevier.
30. International Atomic Energy Agency. (2018). Radiation protection of the public and the environment (IAEA Safety Standards Series No. GSG-8). IAEA.
31. U.S. Environmental Protection Agency. (2020). Integrated Risk Information System (IRIS). U.S. Environmental Protection Agency.
32. U.S. Geological Survey. (2019). Trace elements in the environment. U.S. Geological Survey.
33. Macklin, M. G. (1992). Historical problems of heavy metal mining and smelting in the English Lake District. Environmental Geochemistry and Health, 14, 15–19.

34. Adriano, D. C., & Wenzel, W. W. (2008). Phytoavailability of trace metals. Plant and Soil, 293, 1–29.
35. Gadd, G. M. (2010). Metals, minerals and microbes: Geomicrobiology and bioremediation. Microbiology, 156(3), 609–643.
36. Raskin, I., & Ensley, B. D. (Eds.). (2000). Phytoremediation of toxic metals: Using plants to clean up the environment. Wiley.
37. Baker, A. J. M., Reeves, R. D., & Hajar, A. S. M. (1994). Heavy metal accumulation and tolerance in British populations of the metallophyte Thlaspi caerulescens J. & C. Presl (Brassicaceae). New Phytologist, 127(1), 61–68.
38. Salt, D. E., Blaylock, M., Kumar, N. P. B. A., Dushenkov, V., Ensley, B. D., Chet, I., & Raskin, I. (1995). Phytoremediation: A novel strategy for the removal of toxic metals from the environment using plants. Bio/Technology, 13, 468–474.
39. Cunningham, S. D., Berti, W. R., & Huang, J. W. (1995). Phytoremediation of contaminated soils. Trends in Biotechnology, 13(9), 393–397.
40. Burrough, P. A., & McDonnell, R. A. (1998). Principles of geographical information systems. Oxford University Press.
41. Hsu, M. J., Selvaraj, K., & Agoramoorthy, G. (2006). Taiwan's industrial heavy metal pollution threatens terrestrial biota. Environmental Pollution, 143(2), 327–334.
42. Paustenbach, D. J. (Ed.). (2002). Human and ecological risk assessment: Theory and practice. Wiley.
43. International Commission on Radiological Protection. (2009). Nuclear decay data for dosimetric calculations (ICRP Publication 107). Elsevier.
44. International Atomic Energy Agency. (2011). Handbook of parameter values for the prediction of radionuclide transfer in terrestrial and freshwater environments (Technical Reports Series No. 472). IAEA.
45. Longley, P. A., Goodchild, M. F., Maguire, D. J., & Rhind, D. W. (2015). Geographic information science and systems (4th ed.). Wiley.
46. Goodchild, M. F. (2007). Citizens as sensors: The world of volunteered geography. GeoJournal, 69, 211–221.
47. Hastie, T., Tibshirani, R., & Friedman, J. (2009). The elements of statistical learning: Data mining, inference, and prediction (2nd ed.). Springer.
48. Bishop, C. M. (2006). Pattern recognition and machine learning. Springer.
49. American Public Health Association, American Water Works Association, & Water Environment Federation. (2017). Standard methods for the

examination of water and wastewater (23rd ed.). American Public Health Association.
50. International Organization for Standardization. (2016). Environmental sampling standards. ISO.
51. Knoll, G. F. (2010). Radiation detection and measurement (4th ed.). Wiley.
52. Skoog, D. A., Holler, F. J., & Crouch, S. R. (2017). Principles of instrumental analysis (7th ed.). Cengage Learning.
53. Hou, X., & Roos, P. (2008). Critical comparison of radiometric and mass spectrometric methods for the determination of radionuclides in environmental samples. Analytical Chemistry, 80(12), 449–462.
54. Intergovernmental Panel on Climate Change. (2021). Climate change 2021: The physical science basis. Cambridge University Press.
55. Schlesinger, W. H. (1997). Biogeochemistry: An analysis of global change (2nd ed.). Academic Press.
56. Zhang, C., & others. (2019). Remote sensing of soil contamination. Remote Sensing of Environment, 231, 111–123.
57. Sharma, S. K., & Sanghi, R. (Eds.). (2012). Wastewater reuse and management. Springer.
58. Gupta, V. K., Nayak, A., & Agarwal, S. (2015). Bioadsorbents for remediation of heavy metals: Current status and their future perspectives. Environmental Science and Pollution Research, 22, 17987–18008.
59. Wang, J., & Chen, C. (2009). Biosorbents for heavy metals removal and their future. Biotechnology Advances, 27(2), 195–226. https://doi.org/10.1016/j.biotechadv.2008.11.002
60. U.S. Environmental Protection Agency. (2022). Nanomaterial environmental risk assessment. U.S. Environmental Protection Agency.
61. Brusseau, M. L. (2018). Assessing the importance of transport processes in environmental contaminant transport. Water Research, 133, 1–14.
62. Reddy, K. R., & Cameselle, C. (2009). Electrochemical remediation technologies for contaminated soils, sediments and groundwater. Wiley.
63. Chen, G. (2004). Electrochemical technologies in wastewater treatment. Separation and Purification Technology, 38(1), 11–41.
64. Holling, C. S. (Ed.). (1978). Adaptive environmental assessment and management. Wiley.
65. Walters, C. J. (1986). Adaptive management of renewable resources. Macmillan.
66. Vitousek, P. M., Mooney, H. A., Lubchenco, J., & Melillo, J. M. (1997). Human domination of Earth's ecosystems. Science, 277(5325), 494–499. https://doi.org/10.1126/science.277.5325.494

67. United Nations. (2015). Transforming our world: The 2030 Agenda for Sustainable Development. United Nations.
68. Rockström, J., Steffen, W., Noone, K., Persson, Å., Chapin, F. S., III, Lambin, E., Lenton, T. M., Scheffer, M., Folke, C., Schellnhuber, H. J., Nykvist, B., de Wit, C. A., Hughes, T., van der Leeuw, S., Rodhe, H., Sörlin, S., Snyder, P. K., Costanza, R., Svedin, U., ... Foley, J. A. (2009). A safe operating space for humanity. Ecology and Society, 14(2), Article 32. https://doi.org/10.5751/ES-03180-140232

Chapter 14

Single-Atom Catalysts for Pem Fuel Cells: From Catalyst Design to Reaction Mechanisms

Alpaslan GÜRBÜZ[1], Bülent KUTLU[2]

1. INTRODUCTION

One of the greatest technological challenges of the early 21st century is meeting the continuously growing demand for energy while reducing greenhouse gas emissions. Renewable energy sources such as solar and wind power have expanded over the past decades, but their intermittent nature necessitates efficient methods for storing and converting energy. Hydrogen emerged as one of the most promising energy sources, providing electricity with water being the reaction product. Among hydrogen-based technologies, Proton Exchange Membrane Fuel Cells (PEMFC's) present themselves as viable alternative energy sources because of their high efficiency, rapid start-up and suitability for portable applications. Despite decades of research and technological progress, the widespread commercialization of PEM fuel cells is held back by the need for highly active, durable, and economically viable electrocatalysts.Catalysis, an atomic scale phenomenon, plays a central role for energy conversion in fuel cells. Electrochemical reactions begin with the adsorption of reactants onto the catalyst surface, proceed through a sequence of elementary reactions steps, and conclude with the desorption of products. Platinum is considered as the benchmark electrocatalyst because of its exceptional activity toward both the hydrogen oxidation reaction (HOR) and oxygen reduction reaction (ORR), which take place at the anode and cathode of a PEM fuel cell. Its scarcity, high cost and degradation in the long-term motivated the search for alternative catalyst materials.Among the various strategies explored, metal single-atom catalysts (SAC), where isolated metal atoms are dispersed onto engineered support materials, have emerged as one of the most promising developments in heterogenous catalysis. They maximize atomic utilization while enabling the electronic structure of the active site to be tuned through strong metal-support interactions.

[1] Department of Physics, Institute of Science, Gazi University, Ankara, Türkiye.
E-mail: alpaslan.gurbuz@gazi.edu.tr. ORCID: 0000-0003-1740-5875
[2] Department of Physics, Faculty of Science, Gazi University, Ankara, Türkiye.
E-mail: bkutlu@gazi.edu.tr. ORCID: 0000-0003-4315-9778

Parallel to catalyst and materials design, advances in experimental characterization techniques and first-principles electronic structure calculations have transformed our ability to investigate catalytic mechanisms at the atomic scale. Modern microscopy and spectroscopy can identify catalytic sites of engineered materials experimentally with high precision, while theoretical methods like density functional theory (DFT) allows the determination of adsorption energies, activation barriers, and reaction pathways before a catalyst is synthesized. The following sections present the operating principles of PEM fuel cells, the elementary reaction mechanisms governing the hydrogen oxidation and oxygen reduction reactions, and the principal degradation processes affecting long-term performance. Particular emphasis is then placed on the development of metal single-atom catalysts supported on two-dimensional carbon-based materials, recent catalyst design strategies and trends. Finally, the application of density functional theory to investigate adsorption phenomena, reaction pathways, and activation barriers are discussed.

2. PEM FUEL CELLS: OPERATION AND DEGRADATION

A simplified structure of a PEM fuel cell is shown in Figure 1. The proton conducting membrane is placed between the two electrodes, the anode and cathode, together referred to as the Membrane-Electrode Assembly (MEA). The catalyst layer, where the reactions take place, is located between the electrodes and the membrane.

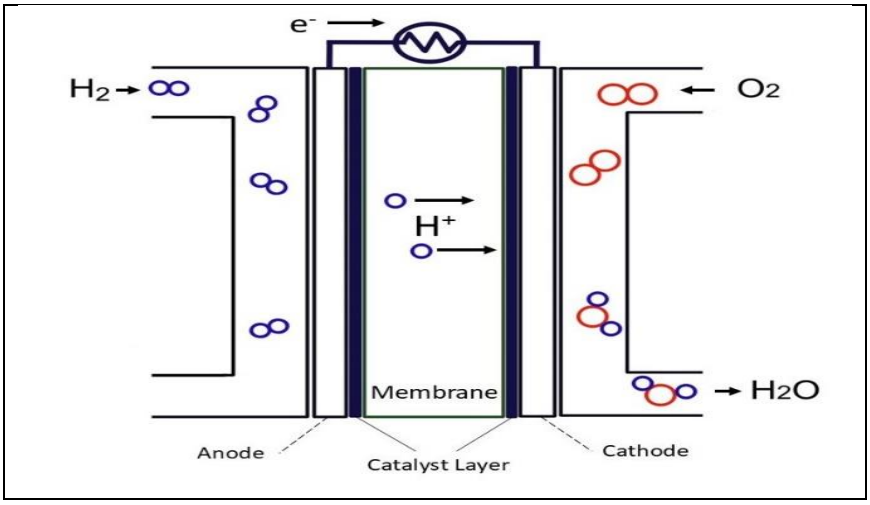


Figure 1. Structure of a PEM fuel cell.

The reactants are delivered through flow channels in the collector plates. The electrodes have a porous structure, which allows the diffusion of the reactants to the catalyst layer. On reaching the catalyst layer, the H_2 molecule dissociates into two hydrogen atoms. The H atom is stripped from its electron, which reaches the cathode through the external circuit. The proton is transferred to the cathode through the membrane, which is highly selective for H^+. At the cathode catalyst layer the H^+ recombine with e^- and interact with oxygen to form water, which is the end product of this energy generating process.The overall reaction is divided into two half-reactions at the anode and cathode:

Anode reaction $: 2\,H_2 \rightarrow 4\,H^+ + 4\,e^-$

Cathode reaction $: 4\,H^+ + 4\,e^- + O_2 \rightarrow 2\,H_2O$

Under ambient conditions (25ºC) the theoretical cell voltage is calculated to be 1.23 V [1]. For applications with high energy requirements, the desired energy output can be achieved through stacking multiple cells.Although the reaction of H_2 with O_2 to produce H_2O being essentially an exothermic one, doesn't take place spontaneously under ambient conditions, because it is associated with a high energy barrier [2]. This high activation barrier for the reaction to start makes it a necessity to use catalysts. Because of the slower reaction kinetics, the cathode requires a higher catalyst load than the anode [3].The catalyst of choice for both half-reactions is platinum on carbon-based support (Pt/C) because of its efficiency towards those reactions [4]. Support materials are necessary for the catalyst to stay dispersed and achieve high currents, at the same time shaping the architecture of the catalyst layer by controlling the porous structure and three-phase boundaries, affecting reactant and product transfer from and to the active sites. Carbon based materials like carbon black and graphene are chosen for their conductive properties, low cost and ease of synthesis.Due to operating conditions, the fuel cell components are subject to various degradation processes. Typical operating temperature is about 80ºC and the acid-based electrolyte, makes the environment highly acidic [5]. Because of the insufficient interaction strength with the support material, catalyst degradation is dominated by Pt dissolution, migration and agglomeration, thus reducing electrochemical surface area. This type of degradation is associated with the loss of catalytic activity. Carbon support suffers from degradation as well. High operating potentials and temperatures can cause corrosion, leading to the loss of the support material and contribute to Pt detachment [6].The membrane can degrade through chemical, mechanical and thermal pathways. For the membrane to achieve full conductivity, it needs to be saturated with water. High temperatures can cause loss of humidity and drying,

causing mechanical stress and cracks of the membrane which can result in loss of conductivity. The introduction of metals through catalyst degradation and impurities can cause chemical degradation through the formation of radicals, thereby changing the structure and properties of the membrane [7]. The limitations of the catalyst–support material systems discussed above have motivated the search for alternative electrocatalysts that combine Pt-like catalytic activity with improved durability, strong catalyst–support interactions, efficient electrical conductivity, resistance to corrosion and metal aggregation, and reduced cost through the use of earth-abundant transition metals and advanced carbon-based support materials.

3. CATALYSTS: FROM BULK METAL TO SAC'S

The development of heterogenous electrocatalysts has been a continuous effort to maximize catalytic activity while minimizing the consumption of expensive materials. At the early stages of fuel cell research, bulk metallic electrodes were used, in particular platinum, because of its excellent catalytic activity towards HOR and ORR. The electronic structure of Pt provides a balance between adsorption and desorption of reaction intermediates. However, the use of a bulk catalyst has its limitation. As catalysis is a surface phenomenon, only the atoms at or near the surface contribute to catalytic activity. Thus, a substantial fraction of the catalyst material remains inactive and as in the case of Pt, significantly increasing the cost of fuel cell systems.To improve catalyst utilization, research shifted towards nanostructured catalysts like Pt nanoparticles on electrically conductive support materials. The reduction of particle size increases the surface-to-volume ratio and a larger fraction of metal atoms is exposed to the reactant molecules. In addition to improved utilization, nanoparticles exhibit size dependent electronic and geometric properties that can influence adsorption energies and catalytic activity. The amount of platinum was reduced even further by alloying Pt with other metals and the development of core-shell structures where Pt forms the shell of a core made up of a different metal. Nanoparticles have their own limitations. As discussed earlier, they are prone to degradation mechanisms such as migration, agglomeration, Ostwald ripening, and dissolution. Over time, these degradation processes cause a gradual decline in catalytic performance by reducing the electrochemically active surface area [8,9].The emergence of single-atom catalysts is the next step in reduction of catalyst size. Isolated metal atoms are anchored onto support materials, each of them functioning as active sites. Electronic properties and catalytic activity of these active sites can be influenced by the local coordination environment, i.e. the surrounding atoms they interact with.

While presenting themselves as a solution to most of the known issues regarding size and cost, SAC's come with their own issues: their stability as isolated atoms. In contrast to bulk metals, isolated atoms possess high surface free energies because of their unsaturated coordination environments [10]. They tend to migrate across the surface and form clusters or nanoparticles, thereby eliminating active sites. Thus, properties of supporting materials to stabilize SAC's become as important as the choice of metals atoms themselves.

4. SUPPORT MATERIALS FOR SAC'S

Conventional support materials were substrates that were electrically conducting and provided mechanical stability for catalyst particles. With SAC's the support itself is no more standing passively in the background but becomes an active component of the catalyst system [11]. Strong interaction of the metal atom with the support material plays an important role in the electronic structure of the active site and influence charge redistribution. This can lead to a modification in adsorption characteristics and thereby affect the catalytic activity.

Strong catalyst-support interaction is unfortunately not the whole story. There are other requirements which a support material needs to satisfy. Providing anchoring sites which are strong enough to suppress migration of catalyst atoms, while preserving accessibility of actives sites for reactant molecules, as well as electrical conductivity to facilitate electron transport. In addition to mechanical stability, it should possess chemical stability to withstand the acidic and oxidative environment present in a PEM fuel cell. Carbon-based support materials like carbon black, being the support of choice, suffer from oxidation related degradation [12]. Graphene, a two dimensional hexagonally arranged carbon structure with a single atom thickness, was the starting point for 2-D support materials (Fig. 2.a). A lattice composed of sp-2 hybridized bonds with high chemical stability [13].Despite its favorable properties, pristine graphene doesn't bind metal atoms strong enough. A DFT study on adsorption of different metal atoms on graphene reveals why metals atoms are prone to migration and agglomeration. Adsorption energies of the metals subject to the study were lower than their corresponding bulk cohesive energies [14]. Energetically, the metal atoms prefer to stay together when brought close to each other. A strategy to overcome this anchoring problem is to embed the metal atom into the lattice instead of just adsorbing it. This can be achieved through replacing a carbon atom with a metal atom by creating a defect in the graphene layer. Alternatively, multiple neighboring carbon atoms are removed and nitrogen atoms are used to stabilize the metal atom (Fig. 2.b) [15].

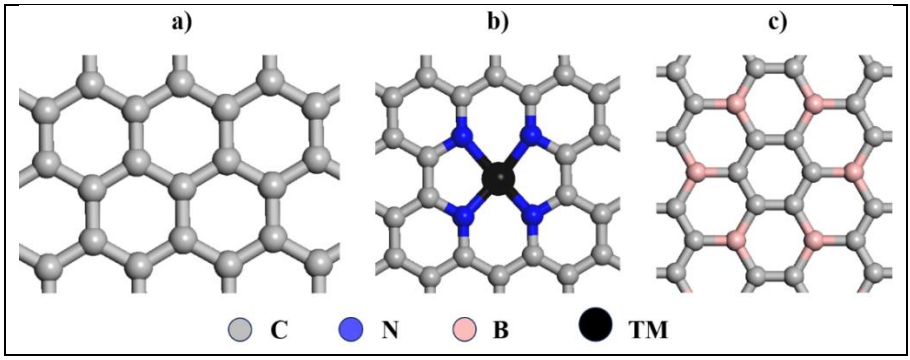


Figure 2. a) Pristine graphene, b) N-coordinated TM anchored graphene (TM-N4-C), and c) BC_3.

A DFT comparison of the binding energies of various metal atoms with their cohesive energies reveals that the binding energies of almost all of the included metal atoms in the study are higher than their cohesive energies [16]. Although a strong metal-support can be achieved through embedding metal atoms into the graphene layer using nitrogen, the majority of the support material still consists of graphene and is subject to carbon degradation mechanisms as mentioned before, as well as demetallation of active sites through radical attacks and loss of support material [15].Functionalizing graphene through dopants made it possible to explore numerous alternative graphene-based materials. One of these materials is graphyne, a pure carbon-based two-dimensional structure, can be achieved by connecting hexagonal carbon rings via two linearly arranged carbon atoms. Other variants include the substitution of carbon atoms with boron and/or nitrogen, forming a periodic arrangement over the entire surface. One such arrangement is BC_3 (Fig. 2.c). Such a surface provides numerous identical adsorption sites for metal SAC's, which doesn't require the post-synthesis engineering of defects to embed metal and coordination atoms. A DFT study of transition metal adsorption on BC_3 shows strong metal-support interaction, with adsorption energies of alkali and early transition metals higher than their cohesive energies [17]. In addition to being a support material, the BC_3 surface itself is able to display catalytic activity towards ORR [18]. Carbon based materials are by no means the only structures that are being considered for use as support. Transition metal dichalcogenides like MoS_2, $MoSe_2$ and WS_2 have been used as support material for anode side reactions with higher activity compared to Pt/C [19]. Another family of materials which have been investigated as catalyst supports are MXenes, transition metal carbides, nitrides and carbonitrides with -O, -OH and -F surface terminations. Cu atoms on Ti_2CO_2 have been reported as highly efficient cathode catalyst for PEM fuel cells [20].

With the rapidly expanding number of possible metals, support materials, dopants, defects and other design strategies, experimental investigation of catalysts becomes a challenging task. Computational approaches provide the means to investigate promising catalyst-support combinations before their experimental synthesis. First principles calculations make it possible to investigate the strength of metal-support interactions, adsorption characteristics of reaction intermediates and structural stability at the atomic level. It should be noted that computational calculations are no replacement for experimental methods, but can play a complementary role.

5. DENSITY FUNCTIONAL THEORY AS A TOOL FOR CATALYST DESIGN

With quantum mechanics at its core, density functional theory tries to solve the many-body Schrödinger equation, which is not possible analytically, by reformulating it to an equivalent system of non-interacting electrons subject to an effective potential. Through consecutive iterations arriving at the lowest possible energy, the ground state energy and electron configuration of the system. When proposing a new catalyst that has not been experimentally synthesized, the starting point should be its structural stability. Geometry optimization is performed to identify the atomic arrangement with the lowest energy. For single or multi-layered support materials the calculation of formation energies can be used to make an initial evaluation on the stability of the proposed system. Additional criteria include the calculation of elastic constants and phonon dispersion calculations, the latter providing information on the structures dynamic properties by determining lattice vibrational frequencies. The presence of imaginary (negative) frequencies across the Brillouin zone would indicate that the system is unstable.Beyond structural stability, DFT also provides information on the electronic structure. Through band structure calculations information on the density of states can be gained (DOS). The presence (or absence) of a band-gap indicates whether the system is a conductor, semiconductor, or an insulator. The introduction of dopants for the modification of the support material, and even the catalyst itself can alter the electronic structure of the whole system. DOS and band structure analysis can help to identify if the change in electronic properties is a wanted one.As an example, the phonon dispersion together with the band structure and density of states plot for the unit cell of the BC_3 monolayer - obtained through band structure and phonon calculations in CASTEP - is given in Fig. 3. This monolayer exhibits no negative frequencies and is considered a stable structure. It, has been experimentally synthesized, by replacing boron

atoms on the hexagonally arranged boron containing layer of NbB_2 [21]. The band gap reflects the semiconducting character.

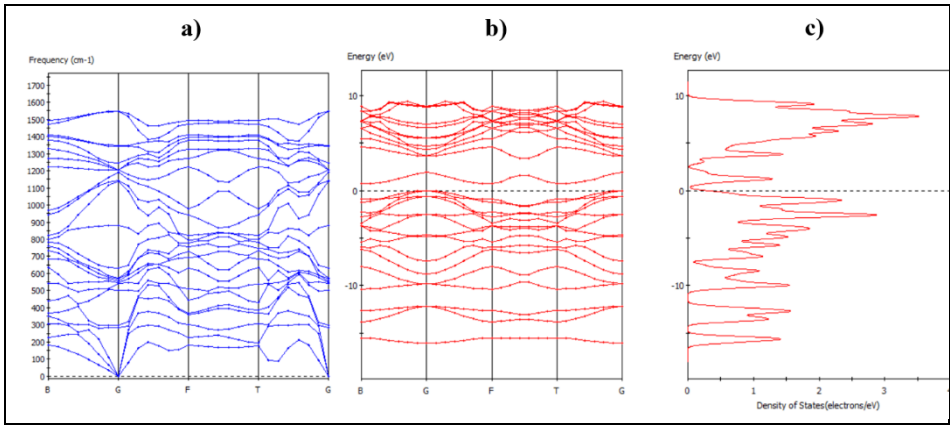


Figure 3. a) Phonon dispersion, b) band structure and c) density of states (DOS) for BC_3.

As stated earlier, the strength of interaction between catalyst and support material is of utmost importance. The adsorption energy (E_{ads}), also referred to as the binding energy, provides a way of quantifying this interaction. With the help of the total energies of the species the adsorption energy is calculated as follows:

$$E_{ads} = E_{supp+cat} - (E_{supp} + E_{cat})$$

Here the quantities E_{supp} and E_{cat} refer to the total energies of the support material and single atom catalyst, respectively, whereas $E_{supp+cat}$ refers to the total energy of the system consisting of the catalyst adsorbed onto the support. This relation for the adsorption energy can be applied to any adsorbent-adsorbate pair. A more negative value means stronger adsorption. To give an idea on how dopants can change adsorption characteristics, we will mention the adsorption energies of Ti on graphene and boron-carbide (BC_3), which are 1.45 eV and ~5.5 eV, respectively [14,17].Additional information can be gained from charge distribution, electron density and density difference analysis. Dopants like nitrogen and boron can act as electron acceptors and/or donors. With the addition of metal atoms, the charge distribution can further be altered, creating suitable environments for catalytic activity [22]. Charge density maps on the other hand can help identify localization (accumulation/depletion) of electrons and provide insight as to the nature of bonds between atoms.

At this point it should be noted that, being a powerful tool for the theoretical investigation of systems at the atomic scale, density functional theory comes with its own limitations. The accuracy of the calculated properties depends on the chosen exchange-correlation functional. Metallic, semiconductor, organic etc. are just a few of the numerous types of systems that can be subject to investigation.

The chosen functional may deliver accurate results for a calculated property while over- or underestimating another property of interest. In DFT calculations, precision is closely related to computing power. While an increase in precision after a certain point may not cause a change in the calculated quantities, the time or computing power needed to complete the task can increase dramatically. A balance between the two is needed to obtain acceptable results.

6. REACTION PATHWAYS AND EVALUATION METHODS

Although chemical reactions, including the overall reaction in a fuel cell, can be expressed with a single equation, they don't proceed through a single elementary process, but involve a sequence of adsorption, dissociation, hydrogenation and desorption steps at the catalytically active site. Each step having their own energy requirements, the overall catalytic activity is governed by the slowest step within the reaction sequence. Therefore, an understanding of the complete reaction pathway, rather than the overall reaction, is essential in the evaluation of catalytic performance.

The anode reaction (HOR) is straightforward and includes the adsorption of the H_2 molecule onto the active site followed by its dissociation. By computing the total energies of the surface (including the catalyst and support material) and H_2 in the gaseous state, and also the total energies of H_2 adsorbed on the surface, as well as the total energy of the surface with two hydrogen atoms adsorbed, we can determine which of these steps is energetically favorable.

$$H_2\,(g) \rightarrow {}^*H_2 \rightarrow {}^*H + {}^*H$$

The asterisk (*) indicates adsorbed species. The variation of the total energies may point out whether a reaction step is exothermic or endothermic, but this quantity alone does not provide information on how much energy is required for the reaction to proceed. The quantity of interest is the activation energy and the performance of a catalyst is directly related to on how much it can lower energy barrier. As an example for the catalytic performance of Pt, activation energies for the dissociation of H_2 and O_2 molecules on the Pt(111) surface are given as 0.20 eV and 0.63 eV, respectively [23,24]. The bond dissociation energies for the same molecules without a catalyst are reported as 4.52 eV for H_2 and 5.15 eV for O_2

(at 298K) [25].The cathode reaction (ORR) on the other hand is a rather complex multi-step reaction. The possible reaction pathways are summarized in Fig. 4. After the adsorption of the O_2 molecule, the reaction can proceed either through the dissociative pathway, where the oxygen molecule dissociates into two adsorbed oxygen atoms. From there, the oxygen atom captures a hydrogen atom to form the OH intermediate and then a second atom to form H_2O which is then desorbed from the surface.

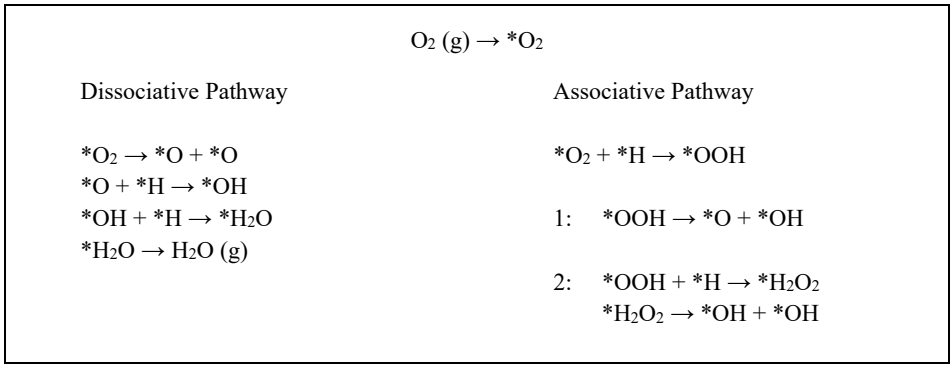


Figure 4. Possible pathways for the oxygen reduction reaction

Alternatively, the adsorbed O_2 molecule can capture a hydrogen atom to form an OOH intermediate, following the associative pathway. From there the intermediate can either dissociate into an O and OH (associative path: 1), or capture yet another hydrogen atom to form the H_2O_2 intermediate, and then dissociate into two OH (associative path: 2). For each of the paths, the next step is the capture of a hydrogen atom to produce water, with the final step being the desorption of the H_2O molecule from the surface.Which path is preferred depends on the catalyst and the energetics of the intermediate steps. Adsorption energies provide a measure for the interaction strength of the intermediates with the catalyst surface. For the HOR and ORR, the adsorption energies of H, O, H_2, O_2, OH, OOH, H_2O_2 and H_2O would need to be calculated. According to Sabatier's principle, the interaction between reaction intermediates and catalyst should not be too strong as to prevent them from leaving the surface, blocking the active site and making the catalyst unavailable for other molecules. The interaction should not be too weak either, which would prevent the activation of molecules and molecules might even desorb from the surface without entering a reaction [26].

With this principle in mind, various descriptors have been constructed to correlate adsorption energies with catalytic activity. One of these descriptors are the well-known volcano plots, where catalytic activities are plotted against adsorption energies. Catalysts near the summit of the volcano plot have optimal

binding strengths. Catalysts positioned on the sides of the plot either bind intermediates too strongly or too weakly. The inclusion of zero-point energy (ZPE), entropy and applied voltage terms for a reaction taking place under operating conditions contribute to the calculation of free energies, which allow for the construction of free energy diagrams [27]. Plotting the adsorption energies of two intermediates against each other reveals a highly linear relationship between them, indicating that if an intermediate binds strongly to the surface, then the other is likely to bind strongly as well. This relationship forms the basis for the so-called scaling relations [28]. These descriptors make it possible to rapidly screen a large number of catalysts. For two catalysts to exhibit similar adsorption characteristics doesn't necessarily mean they also show the same activity, as they might have very different activation energies towards various reaction steps or the formation of intermediates. Quantities that depend on the initial and final states of the system can therefore provide only indirect information. The behavior of electrocatalytic reactions is closely related to the potential energy surface connecting the reactants and products. Reaction steps proceed through a transition state, which corresponds to an energy maximum along the minimum energy path, connecting the reactants with the products (Fig. 5). The energy difference between the initial state (reactants) and the transition state defines the activation energy. The determination of activation energies requires calculation of transition states. Methods like Nudged Elastic Band (NEB) and Linear/Quadratic Synchronous Transit (LST/QST) are used to find the minimum-energy pathway connecting the two stable structures and locate the saddle point which corresponds to the transition state [29,30].

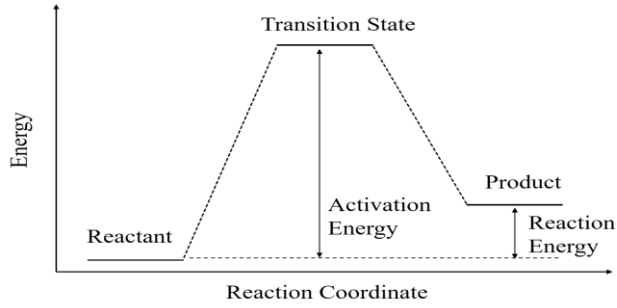


Figure 5. Transition state along reaction coordinate with highest energy configuration

Together with reaction free energies, transition state search and activation energy calculations provide a more complete evaluation of electrocatalytic reactions.

7. CONCLUSION

The previous sections presented a brief overview of PEM fuel cell operation principles and several of the degradation mechanisms associated with its operation, as well as the emergence of single atom catalysts and major families of support materials, their limitations giving rise to a new material or even a whole family of new materials. Density functional theory was introduced as a theoretical approach to calculate the ground state electronic structure and related properties of materials, enabling the investigation of catalytic systems at the atomic scale.The discussion was rounded off with presenting possible reaction pathways and elementary reaction steps for both HOR and ORR, introducing some of the relevant quantities and descriptors essential for the evaluation of catalytic activity. Structural descriptors evaluate catalyst stability, electronic descriptors explain catalyst-support interactions, adsorption energies characterize binding, free energy diagrams allow evaluation of thermodynamic feasibility, and transition-state calculations determine activation energies. Together they complement each other, providing a comprehensive description of catalytic performance. Computational electrocatalysis is no longer a screening of individual catalysts, evolving into a mechanism-driven catalyst design.Over the past decades, an enormous body of research has accumulated on electrocatalysts and support materials for proton exchange membrane fuel cells, resulting in significant advances in catalyst architecture, materials engineering, and a better understanding of reaction mechanisms.Degradation and stability issues continue to be a major concern. Achieving an optimal combination of catalytic activity, durability and economic viability remains a major challenge, motivating the research of new catalyst materials, support structures, and computational design strategies.

REFERENCES

1. Barbir, F. (2013). *PEM fuel cells: theory and practice* (2nd Ed.). Elsevier.
2. Zaccaria F, Menendez Rodriguez G, Rocchigiani L and Macchioni A (2022) Molecular Catalysis in "Green" Hydrogen Production. Front. Catal. 2:892183. doi:10.3389/fctls.2022.892183
3. Alabi, A. S., Popoola, I., Popoola, O. M., Mathe, N., & M. Abdulwahab. (2023). Materials for electrocatalysts in proton exchange membrane fuel cell: A brief review. *Frontiers in Energy Research*, *11*. doi:10.3389/fenrg.2023.1091105
4. Hu, X., Yang, B., Ke, S., Liu, Y., Fang, M., He, C., & Min, X. (2023). Review and Perspectives of Carbon-Supported Platinum-Based Catalysts for Proton Exchange Membrane Fuel Cells. *Energy & Fuels*. doi:10.1021/acs.energyfuels.3c01265
5. Kaur, G. (2021). *PEM Fuel Cells*. Elsevier.
6. Ren, P., Pei, P., Li, Y., Wu, Z., Chen, D., & Huang, S. (2020). Degradation mechanisms of proton exchange membrane fuel cell under typical automotive operating conditions. *Progress in Energy and Combustion Science*, *80*, 100859. doi:10.1016/j.pecs.2020.100859
7. Dharmjeet Madhav, Wang, J., Rajesh Keloth, Mus, J., Buysschaert, F., & Veerle Vandeginste. (2024). A Review of Proton Exchange Membrane Degradation Pathways, Mechanisms, and Mitigation Strategies in a Fuel Cell. *Energies*, *17*(5), 998–998. doi:10.3390/en17050998
8. Yuan, C., Zhang, S., & Zhang, J. (2023). Oxygen reduction electrocatalysis: From conventional to single-atomic platinum-based catalysts for proton exchange membrane fuel cells. *Frontiers in Energy*, *18*(2), 206–222. doi:10.1007/s11708-023-0907-3
9. Wang, X., Li, Z., Qu, Y., Yuan, T., Wang, W., Wu, Y., & Li, Y. (2019). Review of Metal Catalysts for Oxygen Reduction Reaction: From Nanoscale Engineering to Atomic Design. *Chem*, *5*(6), 1486–1511. doi:10.1016/j.chempr.2019.03.00
10. Rigby, K., & Kim, J.-H. (2023). Deciphering the issue of single-atom catalyst stability. *Current Opinion in Chemical Engineering*, *40*, 100921. doi:10.1016/j.coche.2023.100921
11. Gloag, L., Somerville, S.V., Gooding, J.J. *et al.* (2024). Co-catalytic metal–support interactions in single-atom electrocatalysts. *Nat Rev Mater* **9**, 173–189. doi:10.1038/s41578-023-00633-2
12. Dubau, L., Castanheira, L., Maillard, F., Chatenet, M., Lottin, O., Maranzana, G., Dillet, J., Lamibrac, A., Perrin, J. C., Moukheiber, E., ElKaddouri, A., De Moor, G., Bas, C., Flandin, L., & Caqué, N. (2014). A

review of PEM fuel cell durability: materials degradation, local heterogeneities of aging and possible mitigation strategies. *WIREs Energy and Environment*, *3*(6), 540–560. doi:10.1002/wene.113

13. Fei, H., Dong, J., Chen, D., Hu, T., Duan, X., Shakir, I., Huang, Y., & Duan, X. (2019). Single atom electrocatalysts supported on graphene or graphene-like carbons. *Chemical Society Reviews*, *48*(20), 5207–5241. doi:org/10.1039/c9cs00422j
14. Hu, L., Hu, X., Wu, X., Du, C., Dai, Y., & Deng, J. (2010). Density functional calculation of transition metal adatom adsorption on graphene. *Physica B: Condensed Matter*, *405*(16), 3337–3341. doi:10.1016/j.physb.2010.05.001
15. He, Y., Liu, S., Priest, C., Shi, Q., & Wu, G. (2020). Atomically dispersed metal–nitrogen–carbon catalysts for fuel cells: advances in catalyst design, electrode performance, and durability improvement. *Chemical Society Reviews*, *49*(11), 3484–3524. doi:10.1039/c9cs00903e
16. Wei, S., Tian, X., Rao, Z., Wang, C., Tang, R., He, Y., Luo, Y., Fan, Q., Fan, W., & Hu, Y. (2025). The Potential of MN4-GPs (M = Mn, Fe, Co, Ni, Cu, Mo) as Adsorbents for the Efficient Separation of CH4 from CO2 and H2S. *Materials*, *18*(12), 2907. doi:10.3390/ma18122907
17. Wang, J., Yang, Y., Liu, H., Dong, H., Ding, L., & Li, Y. (2022). Adsorption of metal atoms on two-dimensional BC3 and AlC3 nanosheets: Computational studies. *Chemical Physics Letters*, *792*, 139403. doi:10.1016/j.cplett.2022.139403
18. Fazio, G., Ferrighi, L., & Di Valentin, C. (2014). Boron-doped graphene as active electrocatalyst for oxygen reduction reaction at a fuel-cell cathode. *Journal of Catalysis*, *318*, 203–210. doi:10.1016/j.jcat.2014.07.024
19. Shi, Y., Ma, Z.-R., Xiao, Y.-Y., Yin, Y.-C., Huang, W.-M., Huang, Z.-C., Zheng, Y.-Z., Mu, F.-Y., Huang, R., Shi, G.-Y., Sun, Y.-Y., Xia, X.-H., & Chen, W. (2021). Electronic metal–support interaction modulates single-atom platinum catalysis for hydrogen evolution reaction. *Nature Communications*, *12*(1). doi:10.1038/s41467-021-23306-6
20. Peng, Q., Zhou, J., Chen, J., Zhang, T., & Sun, Z. (2019). Cu single atoms on Ti_2CO_2 as a highly efficient oxygen reduction catalyst in a proton exchange membrane fuel cell. *Journal of Materials Chemistry A*, *7*(45), 26062–26070. doi:10.1039/c9ta08297b
21. Ueno, A., Fujita, T., M. Matsue, Yanagisawa, H., Oshima, C., F. Patthey, H.-C. Ploigt, Schneider, W.-D., & Otani, S. (2006). Scanning tunneling

microscopy study on a BC3 covered NbB2(0001) surface. *Surface Science*, *600*(17), 3518–3521. doi:10.1016/j.susc.2006.07.007

22. He, K., Huang, Z., Chen, C., Qiu, C., Zhong, Y. L., & Zhang, Q. (2023). Exploring the Roles of Single Atom in Hydrogen Peroxide Photosynthesis. *Nano-Micro Letters*, *16*(1).doi:10.1007/s40820-023-01231-1
23. Wang, J. X., Springer, T. E., Liu, P., Shao, M., & Adzic, R. R. (2007). Hydrogen Oxidation Reaction on Pt in Acidic Media: Adsorption Isotherm and Activation Free Energies. *The Journal of Physical Chemistry C*, *111*(33), 12425–12433. doi:10.1021/jp073400i
24. Duan, Z., & Wang, G. (2011). A first principles study of oxygen reduction reaction on a Pt(111) surface modified by a subsurface transition metal M (M = Ni, Co, or Fe). *Physical Chemistry Chemical Physics*, *13*(45), 20178. doi:10.1039/c1cp21687b
25. Luo, Y.-R. (2007). *Comprehensive Handbook of Chemical Bond Energies*. CRC Press.
26. Chorkendorff, & Niemantsverdriet, J. W. (2003). *Concepts of Modern Catalysis and Kinetics*. Wiley-VCH.
27. Nørskov, J. K., Rossmeisl, J., Logadottir, A., Lindqvist, L., Kitchin, J. R., Bligaard, T., & Jónsson, H. (2004). Origin of the Overpotential for Oxygen Reduction at a Fuel-Cell Cathode. *The Journal of Physical Chemistry B*, *108*(46), 17886–17892. doi:10.1021/jp047349j
28. Man, I. C., Su, H. Y., Calle-Vallejo, F., Hansen, H. A., Martínez, J. I., Inoglu, N. G., Kitchin, J., Jaramillo, T. F., Nørskov, J. K., & Rossmeisl, J. (2011). Universality in Oxygen Evolution Electrocatalysis on Oxide Surfaces. *ChemCatChem*, *3*(7), 1159–1165. doi:10.1002/cctc.201000397
29. Jonsson, H., Mills, G., & Jacobsen, K. W. (1998). Nudged elastic band method for finding minimum energy paths of transitions. *Classical and Quantum Dynamics in Condensed Phase Simulations*. doi:10.1142/9789812839664_0016
30. Halgren, T. A., & Lipscomb, W. N. (1977). The synchronous-transit method for determining reaction pathways and locating molecular transition states. *Chemical Physics Letters*, *49*(2), 225–232. doi:10.1016/0009-2614(77)80574-5

Chapter 15

Artificial Intelligence for Education for Sustainable Development: An Integrative Review of Environmental Sustainability, Resource Management, And Future Green Competencies

Meltem KAYGUSUZ[1]

1. INTRODUCTION

Environmental issues such as climate change, biodiversity loss, pollution, and the growing demands on energy, water, food, and material resources are deeply interconnected socioecological challenges. These challenges are shaped by a complex interplay of technological systems, economic priorities, governance structures, societal values, and uneven patterns of exposure and vulnerability (IPCC, 2023; IPBES, 2024). ESD seeks to address this complexity by fostering the knowledge, skills, values, attitudes, and capacity for action necessary to achieve environmentally sustainable and socially just futures. UNESCO's "Education for Sustainable Development: A Roadmap" emphasises education as a transformative process and outlines five key action areas: advancing policy, transforming learning environments, building educators' capacities, empowering and mobilising youth, and accelerating local-level action [29].

Competence-oriented methodologies have shifted sustainability education from teaching sustainability to learning for sustainability transformations. Wiek et al. [35] introduced five competencies: systems, anticipatory, normative, strategic, and interpersonal thinking for research and problem-solving. Brundiers et al. [7] added intrapersonal and implementation competencies, made values-thinking foundational, expanded learning objectives, and noted debate over intrapersonal competency and the need to theorise implementation competency. GreenComp groups 12 sustainability competencies into four domains [6], collectively requiring analysis, collaboration, and action.Artificial intelligence is significant in educational contexts. Technologies such as machine learning, natural language processing, predictive analytics, and generative AI identify patterns, model scenarios, aid decision-making, and provide feedback. AI applications are utilised in climate-risk assessment, renewable-energy

[1] Dr., Tarsus University, School of Foreign Languages, Mersin, Türkiye, meltemkaygusuz@tarsus.edu.tr (ORCID: 0000-0003-1892-8934)

forecasting, environmental monitoring, precision agriculture, water-resource management, biodiversity conservation, and waste classification [1-5-24-25-26-37]. According to Vinuesa et al. [32], AI can advance 134 Sustainable Development Goal targets but may hinder 59. Risks include inequalities, high computational and energy demands, insufficient transparency and accountability, and poor regulatory oversight. Few studies have integrated AI with sustainability expertise and contextualisation [12].Educational implications extend beyond AI technology. AI supports ESD through environmental-data visualisation, analysis, simulation, scaffolding, feedback, and stakeholder perspectives. It is a learning object when students examine algorithmic systems classifying habitats, forecasting energy demand, and informing resource-allocation decisions. Educators identified project-based and virtual learning for AI support but raised concerns about plagiarism, hallucination, data privacy, bias, digital divide, and training costs [3]. Review stressed conditions [20]. While AI can aid the environment, it can introduce challenges. Sustainable AI includes using AI to promote sustainability and ensuring AI sustainability [31]. Data-centre electricity demand, cooling water, hardware manufacturing, mineral extraction, and electronic waste complicate claims that AI is eco-friendly [30]. According to the International Energy Agency [13], data-centre electricity consumption might reach 945 TWh by 2030, more than double 2024 levels. Therefore, ESD must enable learners to distinguish efficiency from sustainability and capability from socioecological desirability.

The literature on AI and ESD remains fragmented. Research on AI in education covers adaptive and personalised learning, intelligent tutoring systems, assessment, management, profiling, prediction, and AI-based educational products [33]. Research on AI for sustainability emphasises performance and optimisation, while sustainable AI scholarship explores environmental footprints, governance, or ethics without integrating them into curriculum and pedagogy [31]. Sustainability competence frameworks do not delineate environmental data literacy, algorithmic judgment, and life-cycle reasoning necessary for AI-mediated environmental decision-making. This gap is technological, curricular, and epistemic. Learners comprehend what AI discloses, what models may overlook, how outputs should be validated, whose interests and knowledge are represented, and whether optimisation shifts costs to communities, systems, or generations.This review seeks to fill the existing gap by examining three interconnected perspectives: (1) the role of AI in facilitating learning about sustainability, where AI aids in enquiry, simulation, visualisation, and feedback; (2) the integration of AI applications into sustainability education, where environmental and resource management applications serve as genuine curricular

examples; and (3) the critical evaluation and responsible use of AI from a sustainability standpoint, focusing on environmental impact, justice, uncertainty, and governance as explicit subjects of study,

The review addresses four key questions;

1. How can AI applications in environmental sustainability and resource management be adapted for ESD contexts?
2. What are the pedagogical advantages and limitations of AI-supported ESD?
3. What future green competencies arise at the intersection of sustainability competence and AI literacy?
4. What environmental, ethical, social, and epistemic challenges need to be addressed for responsible integration?

2. REVIEW APPROACH

This study employed a structured, integrative review approach. This type of review is suitable when a research issue encompasses various theoretical and methodological frameworks, aiming to create a conceptually unified synthesis rather than determining a common effect size [27-34]. Consequently, the evidence base comprises empirical educational research, review articles, conceptual studies, environmental AI research, and recognised competence and policy frameworks related to AI. This review does not aim to cover every technical AI application comprehensively; rather, it focuses on providing a broad conceptual overview of the educationally pertinent connections between AI applications, teaching methods, competencies, and sustainability challenges.

Concept-driven searches, March–July 2026, identified literature on artificial intelligence, machine learning, generative AI, ESD, sustainability education, environmental education, environmental sustainability, resource management, green skills, sustainability competencies, AI literacy, responsible/sustainable AI, climate modelling, environmental monitoring, renewable energy, water management, agriculture, biodiversity, waste management, and circular economy. Databases: Scopus, Web of Science Core Collection, ERIC, IEEE Xplore, ScienceDirect, plus backward/forward tracking. UNESCO, European Commission's Joint Research Centre, UNEP, and IEA documents were gathered. Emphasis: 2019–July 2026; foundational studies included for ESD, sustainability competencies, or integrative-review methodology.

Sources were included if they contributed to four domains: AI-supported sustainability teaching-learning; pedagogically relevant AI applications for environmental sustainability or resource management; sustainability competence or AI literacy; and environmental, ethical, or justice implications of AI. Technical

comparisons lacking connections to environmental decision-making, public learning, curricula, or competence development were excluded. Publications referring to sustainable education solely as institutional-operational continuity were excluded. Evidence prioritised peer-reviewed syntheses, empirical studies with transparent methodologies, established competence frameworks, and authoritative international agency reports.The analysis employed deductive and inductive thematic synthesis. Initial coding was informed by three perspectives: AI as a pedagogical tool, AI as an environmental application domain, and AI as a subject of critical sustainability enquiry. Sensitising categories included sustainability values, systems thinking, futures reasoning, action, a human-centred mindset, AI ethics, AI techniques and applications, and AI system design derived from GreenComp, the sustainability competence literature, and UNESCO's AI competency framework [6-21]. Inductive comparison identified recurring concepts not fully integrated across sustainability competence and AI literacy frameworks, such as environmental data judgment, model uncertainty, life-cycle reasoning, human–AI collaboration, and distributive justice. Implementation competence was examined against Brundiers et al.'s framework [7]. Given the heterogeneity in the included evidence purpose and design, the findings are presented as narrative and conceptual synthesis rather than causal estimates.

3. AI APPLICATIONS FOR ENVIRONMENTAL SUSTAINABILITY AND RESOURCE MANAGEMENT

The educational significance of environmental AI is not merely introducing learners to a growing array of technologies. Instead, it converts real-world applications into structured opportunities for system investigation, data interrogation, alternative comparison, and trade-off evaluation. In various domains, the most valuable ESD tasks highlight model assumptions, uncertainties, stakeholders, and environmental consequences, rather than presenting AI-generated outputs as definitive answers.

3.1 Climate Modelling and Environmental Monitoring

Machine learning is used to estimate emissions, integrate renewable energy, forecast extreme weather, assess climate risks, remote sensing, and detect land-use changes. Rolnick et al. [24] highlighted the opportunities to mitigate and adapt to climate change, stressing machine-learning researcher collaboration with experts. Similarly, Kaack et al. [14] suggested assessing AI's climate impacts in three categories: computing-related impacts, direct effects of machine learning applications, and system-level consequences. Educationally, models might yield

unsustainable outcomes if poorly defined goals or rebound effects are addressed.In ESD, climate modelling and environmental monitoring support exploration. Students compare data with modelled trends, investigate satellite deforestation images, or assess flood-risk scenarios. They require tracing origins, distinguishing predictions from explanations, interpreting uncertainty, and considering included and excluded communities and conditions. Students evaluated two AI-generated climate adaptation plans using demographic, ecological and environmental justice criteria. AI reveals complexity, but its value depends on the examination of assumptions and results.

3.2 Renewable Energy And Resource Optimisation

AI enhances energy systems through demand forecasting, predictive maintenance, building energy management, grid balancing, and solar and wind generation forecasting. AI-driven forecasting supports integration of variable renewable sources, while fault detection, predictive maintenance, and real-time management improve the reliability and efficiency of electricity systems [13]. However, these applications depend on high-quality data, secure digital infrastructure, interoperability, and technical and institutional capabilities. Similar optimisation strategies can be used in campus buildings, transportation systems, and industrial energy and resource utilisation. From an educational standpoint, energy optimisation offers a practical framework for systems thinking and normative reasoning. Students are able to examine a campus energy profile, employ an AI-supported tool to develop reduction scenarios, and evaluate the alternatives based on emissions, cost, reliability, accessibility, and their impacts on various user groups. The aim is not to determine a singular mathematically optimal solution, but to understand that optimisation criteria reflect specific priorities and values. A model primarily focused on minimising financial costs may neglect aspects such as thermal comfort, accessibility, distributional impacts, and the environmental burdens associated with infrastructure and material usage. Therefore, ESD must integrate optimisation literacy with a clear consideration of values, trade-offs, and the stakeholders affected.

3.3 Water, Agriculture, And Food Systems

Water and agricultural systems exemplify the capabilities and constraints of data-intensive decision support. AI supports water-demand forecasting, leak detection, water-quality monitoring, irrigation management, crop disease recognition, and soil monitoring. Recent literature reviews suggest that AI and data analytics can enhance monitoring, forecasting, resource allocation, and operational responsiveness, provided representative data, appropriate

infrastructure, and domain expertise [15-36]. Nonetheless, disparities in access to sensors, connectivity, data, and capacity persist, particularly among smallholders and resource-limited communities. Farm- or utility-level optimisation does not inherently guarantee watershed resilience, equitable access, or long-term ecological sustainability.

Water and food systems are well-suited for problem-based ESD because of the tensions they create. Students might navigate a drought where households, agriculture, industry, and ecosystems compete for scarce water resources. Although AI can predict and suggest allocation models, students must assess them against environmental flow needs, food security, cost, and the rights of marginalised communities. Learners might explore precision agriculture by weighing yield increases against soil health, pesticide usage, biodiversity, farmer independence, and data management. These exercises challenge the belief that productivity leads to sustainability and emphasise how benefits, risks, and decision-making power are distributed.

3.4 Biodiversity, Waste, And Circular Systems

Computer vision, acoustic recognition, remote sensing, and predictive modelling are used for species identification, wildlife monitoring, habitat assessment, and conservation planning. According to Tuia et al. [28], machine learning can convert images, audio, movement, and other sensor data in animal ecology into ecologically significant insights, especially when computational methods integrate domain expertise and consider data quality and bias. AI-supported conservation planning can incorporate biodiversity data with anthropogenic pressures, climate-related changes, protection costs, and alternative conservation objectives [26]. Nonetheless, AI should not supplant human judgment, and conservation decisions must account for social priorities and the ways in which individuals interact with nature.

Waste management and circular systems support sorting, waste-generation forecasting, collection-route optimisation, recycling-assistance, and material tracking through waste processes [23-25]. Digitalisation and AI enhance transparency, adaptability, and effectiveness, supporting circular economy strategies. In ESD, students conduct waste audits, use AI-assisted classification, map life cycles, and redesign systems for waste reduction, repair, reuse, recycling, and recovery. Pedagogy must ensure that collection/sorting efficiency does not replace questioning production-consumption patterns. Circularity education should examine product design, material demand, rebound effects, working conditions, and whether technological solutions prevent waste or shift environmental-social impacts.

Table 1. AI applications and their pedagogical translation into ESD

Domain	Representative AI application	ESD learning task	Primary competence	Critical question
Climate and monitoring	Risk prediction, remote sensing, emissions and air-quality analysis	Compare modelled and observed local data; revise an adaptation scenario	Anticipatory reasoning; data literacy	What assumptions and uncertainties shape the prediction?
Energy	Demand forecasting, smart grids, building optimisation	Design and justify a campus energy transition plan	Systems thinking; normative judgement	Efficient for whom, and according to which criteria?
Water and agriculture	Leak detection, smart irrigation, crop and soil monitoring	Allocate scarce water among competing users and ecosystems	Resource reasoning; justice	How are rights, access, and ecological thresholds represented?
Biodiversity	Species recognition, acoustic monitoring, habitat mapping	Conduct a local biodiversity inquiry and audit dataset coverage	Environmental data literacy	Which species, places, and knowledge systems are missing?
Waste and circularity	Sorting, material tracking, demand and route prediction	Redesign a product or campus waste system using life-cycle evidence	Life-cycle reasoning; action competence	Does optimisation prevent waste or merely manage more of it?

4. PEDAGOGICAL PATHWAYS FOR AI-SUPPORTED ESD

4.1 Inquiry, Problem, And Project-Based Learning

AI-supported ESD is justified when technology aligns with a pedagogical framework. Analyses of AI in education highlight key application areas: adaptive learning and personalised tutoring, intelligent assessment and management, profiling and prediction, and new AI-based products [33]. In ESD, the challenge is not just personalisation but empowering learners to explore complex sustainability issues without singular, technically correct solutions. Consequently, enquiry-, problem-, project-, and challenge-based methodologies suit environmental AI applications, enabling learners to formulate questions, assess evidence, consider stakeholder perspectives and substantiate decisions [18]. In an urban heat project, students can integrate open environmental data, AI-enhanced mapping tools, field observations, and resident interviews to identify heat-vulnerable zones, evaluate model resolution and limitations, and

suggest interventions that balance cooling, biodiversity, public access, and cost. Here, AI acts as a cognitive and representational aid, complementing enquiry and judgment. Documenting prompts, datasets, assumptions, sources, and revisions improves the transparency of reasoning.

4.2 Simulation, Scenario Building, And Futures Thinking

Simulation- and scenario-based learning can make uncertain, nonlinear consequences tangible. AI-supported tools facilitate the exploration of pathways, stakeholder perspectives, and outcomes as assumptions change, aligning with sustainability education, which prioritises the future, uncertainty, learner agency, and envisioning sustainability transformation [17]. Climate change education research suggests that such activities enhance students' future literacy and environmental agency [8]. However, learners must recognise modelled futures as shaped by data, assumptions, and variables, not predictions.

Generative AI can aid sustainability narratives, but its application must be delimited. In education, it can enhance explanations, foster ideas, personalise interactions, and support problem-solving. Nonetheless, it may generate inaccurate, unverifiable information, perpetuate training-data biases, oversimplify issues, and promote overreliance [20]. Consequently, tasks require evaluating and amending AI-generated proposals using literature, local knowledge, and stakeholder evidence, enabling human–AI collaboration.

4.3 Human–AI Collaboration And The Role Of The Educator

Educators implement responsible AI-supported ESD. Teachers frame sustainability issues, guide assessing evidence relevance and credibility, facilitate dialogue, and ensure that students confront value conflicts rather than depoliticized solutions. UNESCO's AI competency frameworks highlight human-centred mindset, agency, ethical judgment, responsible AI use, and developing learners and teachers as users and co-creators of AI [21-22]. In AI-supported ESD, educators address data, systems reasoning, uncertainty, justice, and lifecycle awareness, linking AI to sustainability education's epistemic and ethical challenges. Assessment should prioritise learners' reasoning over AI-assisted outputs. Evidence may include decisions, triangulation, and oral defence. Human–AI collaboration matters when learners remain accountable for claims. AI should augment access and feedback, not replace verification, ethical deliberation, creativity, or collective judgment.

5. FUTURE GREEN COMPETENCIES IN AN AI-MEDIATED WORLD

GreenComp and established sustainability competence frameworks offer a robust basis for comprehending the values, complexity, potential futures, and actions pertinent to sustainability. AI literacy augments this foundation by focusing on the capacity to comprehend and utilise AI, critically assess AI technologies, collaborate effectively with AI systems, and acknowledge ethical implications [19]. Nevertheless, their intersection necessitates a more explicit set of competencies for making environmentally responsible decisions in AI-mediated contexts. Consequently, the following seven competencies are proposed as a conceptual synthesis derived from this review, rather than as an empirically validated framework or a measurement scale.

5.1 AI-Enhanced Systems Thinking

The ability to evaluate the connections between ecological, technological, economic, and social systems while scrutinising the assumptions and limitations of AI models is crucial in this regard. Learners need to pinpoint feedback loops, indirect impacts, time lags, and outcomes across different spatial and temporal dimensions. They must also understand that AI models simplify intricate systems and may exclude cultural, institutional, or political factors that are crucial for implementation. Predictive associations should not be mistaken for causal explanations without corroborating evidence [6-35]. This skill thus broadens traditional systems thinking by urging learners to investigate not only the sustainability system depicted, but also the epistemic framework of the model that reveals that system. It is necessary to question how data selection, indicators, system boundaries, and optimisation goals influence the conclusions drawn by an AI system. In educational settings, this competence is demonstrated when learners contrast model outputs with contextual evidence, detect absent relationships, and adjust a proposed intervention considering potential cross-system and long-term impacts.

5.2 Environmental Data And AI Literacy

The ability to identify, interpret, verify, and communicate environmental data and outputs generated by artificial intelligence encompasses several critical components. These include understanding data provenance, sampling methods, representation, measurement errors, bias, validation, correlation, and the differentiation between prediction and explanation. It is essential for learners to discern when AI outputs are incomplete or unreliable and to recognize when the expertise of scientific, professional, local, or community sources is necessary.

5.3 Anticipatory Modelling and Uncertainty Reasoning

The ability to employ scenarios and predictions without considering them as definitive futures is crucial. Learners are expected to compare alternative models, identify underlying assumptions, interpret levels of confidence and uncertainty, and consider plausible but potentially high-impact outcomes. This competence links future thinking with epistemic humility, cautious judgment, and informed decision-making.

5.4 Life-Cycle and Resource Reasoning

The evaluation of AI-enabled solutions should encompass all significant phases of the material and energy life cycle. Learners must analyse various components, including the processes of model training and inference, the consumption of electricity and water by data centres, the production of hardware, the extraction of essential minerals, and infrastructure maintenance. In addition, the examination of electronic waste is crucial. It is also important to consider rebound and displacement effects and question whether improvements in efficiency genuinely reduce environmental impacts or inadvertently lead to increased consumption in other areas.

5.5 Human–AI Collaborative Problem-Solving

The integration of AI-assisted analysis with disciplinary knowledge, stakeholder insights, and collaborative discussions is a crucial skill. Learners are expected to develop the ability to pose relevant questions, choose and modify suitable tools, validate results, articulate limitations, and uphold human accountability in decision making. Additionally, this competence involves the ability to discern when AI is not required or when a more resource-efficient, locally focused, or participatory method is suitable.

5.6 Justice-Oriented Ethical Judgement

The evaluation of who benefits from AI-supported decisions, who incurs environmental and social costs, whose data and knowledge are represented, and who has the ability to challenge these decisions is essential. This assessment involves considerations of environmental and data justice, intergenerational responsibility, privacy, accessibility, and disparities in digital infrastructure and technological capacity of the community. Thus, ethical judgment must move beyond theoretical principles to address the specific distributional impacts of AI applications.

5.7 Sustainability Action Competence

The ability to convert insights derived from artificial intelligence into actions that are contextually appropriate, feasible, and widely accepted involves several stages. These stages encompass planning, stakeholder engagement, strategy execution, development monitoring, adaptation to new circumstances, and result assessment. It is crucial for learners to understand that even the most technically advanced proposals may not succeed if they do not consider institutional feasibility, community trust, behavioural relevance, political endorsement, or sensitivity to local conditions.

Table 2. Proposed future green competencies at the intersection of sustainability competence and AI literacy

Proposed competence	Related sustainability competence	Related AI competence	Indicative evidence of learning
AI-enhanced systems thinking	Systems and integration competence	Understanding AI applications and model boundaries	System map that identifies feedback, omitted variables, and indirect effects
Environmental data and AI literacy	Critical thinking and embracing complexity	Data, algorithm, and output evaluation	Audit of data provenance, bias, validity, and uncertainty
Anticipatory modelling and uncertainty reasoning	Anticipatory competence; envisioning futures	Critical interpretation of predictive systems	Comparison of alternative scenarios and assumptions
Life-cycle and resource reasoning	Sustainability values; systems competence	Ethics and sustainable design	Life-cycle comparison including energy, water, materials, and rebound effects
Human–AI collaborative problem-solving	Strategic and interpersonal competence	Human-centred use and co-creation	Documented workflow showing verification and human decision responsibility
Justice-oriented ethical judgement	Normative and intrapersonal competence	AI ethics and citizenship	Stakeholder and distributional impact analysis
Sustainability action competence	Implementation and action competence	Responsible design and application	Feasible intervention plan with monitoring and adaptation criteria

6. RISKS, PARADOXES, AND PRINCIPLES FOR RESPONSIBLE INTEGRATION

6.1 The Environmental Footprint of AI

AI-supported environmental learning presents a paradox: technologies analysing sustainability issues may exacerbate pressures on electricity and water consumption, mineral extraction, hardware production, and electronic waste. Estimating AI's environmental footprint is challenging given the variation in model architecture, hardware, utilisation, electricity sources, geographic conditions, and reporting practices. Data-centre electricity demand is increasing. The IEA [13] forecasts that data-centre electricity consumption will more than double by 2030; accelerated servers driven by AI adoption account for nearly half the net increase. Dokic et al. stress that assessments should cover the AI lifecycle, not solely operational electricity consumption [11].

In ESD, the response is neither uncritical adoption nor rejection of AI. Instead, this review advocates environmental proportionality: an AI-supported task's educational or sustainability value should be evaluated against computational and material demands. Consider less resource-intensive models, shared tools, limited generation, reusing outputs, and non-AI alternatives. Learners assess an AI model's value against simpler statistical, observational, or participatory methods. Thus, sustainable AI literacy encompasses questioning whether AI is necessary and proportionate, rather than its deployment.

6.2 Bias, Misinformation, and Environmental Data Justice

The distribution of environmental datasets and monitoring capabilities is not uniform, leading to the underrepresentation of communities and regions that lack research funding, digital infrastructure, or involvement in formal monitoring systems. This imbalance can perpetuate existing disparities in environmental knowledge and decision-making. The issue extends beyond statistical bias to include environmental data justice, which encompasses participation in data collection, control over data, recognition of indigenous and local knowledge, and the ability to challenge data-driven decisions.

Generative AI introduces epistemic risks. Large language models may produce fluent but inaccurate or unverifiable explanations and authoritative responses to disputed questions. Bender et al. [4] warned that language models generate outputs from statistical patterns in training data without grounded understanding. In education, Kasneci et al. [16] emphasise critical evaluation, human oversight, and systematic fact-checking. In ESD, verification should be integrated into AI-supported tasks through source triangulation, primary

evidence, acknowledgement of uncertainty, and comparison with local or disciplinary expertise.

6.3 Technological Solutionism and Rebound Effects

Another issue is technological solutionism, which interprets political, behavioural, cultural, or distributional challenges as information, prediction, or optimisation issues. While AI can enhance forecasting and decision-making, it cannot replace democratic governance, institutional reforms, public involvement, or shifts in production and consumption. Traffic models cannot decide whether cities should focus on private cars or public transportation; likewise, precision agriculture cannot address land ownership, farmer reliance, or food justice issues.

Rebound effects add to these concerns. Although advances in hardware and model efficiency may reduce the resources and costs of AI tasks, they can increase electricity consumption [10]. Thus, AI-driven optimisation may improve relative efficiency without achieving absolute environmental reduction. Learners should consider immediate, indirect, and system-wide effects, distinguishing enhancements from impacts that shift across sectors, regions, or time. This review suggests six principles for integration: human agency, transparency, verification, justice and inclusion, life-cycle awareness, and action orientation to evaluate AI-supported learning against ESD goals [1].

7. DISCUSSION: AN INTEGRATIVE AI–ESD FRAMEWORK

The analysis reveals AI-ESD interaction from three perspectives. First, AI for understanding sustainability highlights visualisation, simulation, feedback, explanations, and enquiry facilitation. Second, AI in sustainability uses environmental and resource management systems as curriculum models. Third, assessing AI for sustainability addresses environmental, ethical, epistemic, and justice-related implications as learning objectives. Integrating these perspectives provides a foundation. The framework adapts seven competencies for AI-mediated environmental judgment: systems thinking, data literacy, anticipatory, normative, action, life-cycle, and resource reasoning.

This framework significantly influences curriculum development. Instead of treating AI and sustainability as separate subjects connected only by occasional examples, they should be integrated through problem-based learning that requires environmental evidence, modelling, stakeholder analysis, ethical assessment and practical outcomes. A module might be designed to start with gathering local data, followed by AI-supported analysis, scenario evaluation, stakeholder feedback, life cycle assessment, and planning for implementation. This method

ensures that technology does not overshadow the learning process, thus preserving the focus of ESD on empowerment and change.

Teacher education is crucial for the implementation of such strategies. Educators require tools and examples, but professional learning must transcend techniques for long-term effectiveness. UNESCO's frameworks offer a foundation, emphasising agency, AI ethics, technical understanding, pedagogy, and responsible AI use in education. In ESD, learning should encompass environmental data quality, model limitations, sustainability competence, assessment design, and contested values. Institutions must establish policies for data protection, accessibility, academic integrity, procurement, resource implications, and meaningful human support.

This synthesis suggests several research priorities. Investigations should extend beyond attitudes and perceived usefulness to sustainability-learning outcomes. The proposed competencies require operational definitions, developmental progressions, and valid assessment instruments. Longitudinal comparative studies are essential in schools, universities, vocational, and community settings. Research should prioritise the Global South, rural low-connectivity contexts, and Indigenous and local knowledge. The educational benefits must be evaluated alongside computational and material costs. The question is whether AI enhances tasks in isolation or generates educational and sustainability values that are not more responsibly achieved through alternatives.

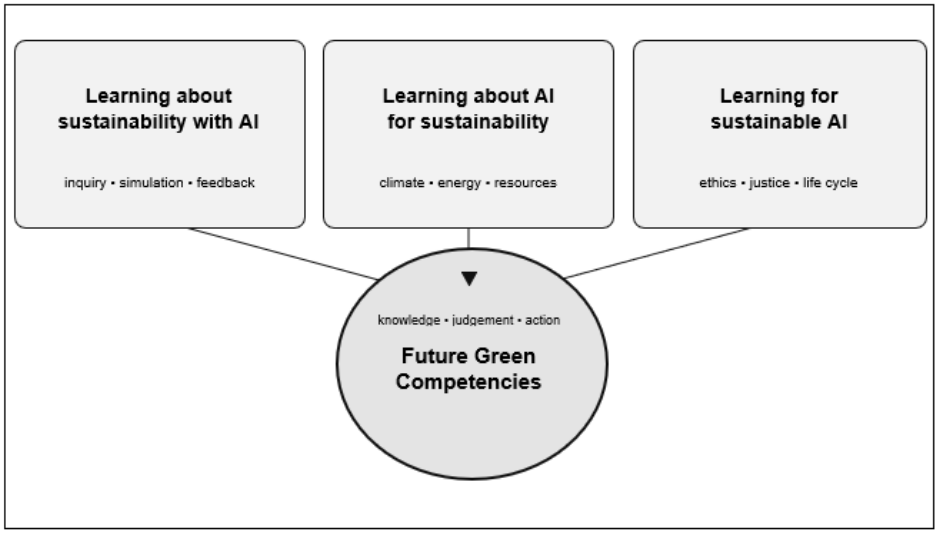


Figure 1. The integrative AI–ESD triple-lens framework

8. CONCLUSION

Artificial intelligence has the potential to enhance Education for Sustainable Development by facilitating learners' interaction with environmental data, modelling of alternatives, exploration of complex systems, and examination of technologies that are increasingly employed in decision-making related to energy, water, food, biodiversity, and material resources. However, its educational impact is not solely derived from its technical capabilities. It is contingent upon pedagogical frameworks that preserve human judgment, highlight assumptions and uncertainties, integrate optimisation with values and justice, and necessitate that learners convert analysis into responsible actions.

This review delineates three concurrent roles for AI: as a pedagogical tool for sustainability education, an application domain for examining environmental problem-solving, and a subject of critical sustainability enquiry. The proposed future green competencies link sustainability competence with AI literacy by focusing on systems thinking, environmental data literacy, uncertainty reasoning, life cycle impacts, human–AI collaboration, justice-oriented judgment, and implementation. This integration is crucial because AI has the potential to support sustainability while simultaneously perpetuating inequality, misinformation, resource pressure, and technological solutionism. Education should not condition learners to passively accept automated environmental decisions. Instead, it should equip them with the ability to comprehend, critically evaluate, enhance, challenge, and, when warranted, reject these decisions. This approach ensures their competent and ethical participation in the development of sustainable futures.

REFERENCES

1. Ahmad, T., Zhang, D., Huang, C., Zhang, H., Dai, N., Song, Y., & Chen, H. (2021). Artificial intelligence in sustainable energy industry: Status quo, challenges and opportunities. *Journal of Cleaner Production, 289*, Article 125834. https://doi.org/10.1016/j.jclepro.2021.125834

2. Al-Hamdani, D. (2026). Applied Artificial Intelligence in Sustainable Education: Toward an Integrative Model Bridging Technology, Human Values, and Sustainable Development. *Applied Computing Journal*, *6*(2), 461–470. https://doi.org/10.52098/acj.20266272

3. Asrifan, A., Khristianto, K., Aini, N., & Wahira, W. (2025). Integrating AI and Sustainability In Education: A New Paradigm for Modern Literacy. In A. Diogo, A. Joaquim, & C. de Almeida (Eds.), *Rethinking Literacy in the Era of Sustainability and Artificial Intelligence* (pp. 43-72). IGI Global Scientific Publishing. https://doi.org/10.4018/979-8-3373-0725-1.ch002

4. Bender, E. M., Gebru, T., McMillan-Major, A., & Shmitchell, S. (2021). On the dangers of stochastic parrots: Can language models be too big? In *Proceedings of the 2021 ACM Conference on Fairness, Accountability, and Transparency* (pp. 610–623). Association for Computing Machinery. https://doi.org/10.1145/3442188.3445922

5. Benos, L., Tagarakis, A. C., Dolias, G., Berruto, R., Kateris, D., & Bochtis, D. (2021). Machine learning in agriculture: A comprehensive updated review. *Sensors, 21*(11), Article 3758. https://doi.org/10.3390/s21113758

6. Bianchi, G., Pisiotis, U., & Cabrera Giraldez, M. (2022). *GreenComp: The European sustainability competence framework*. Publications Office of the European Union. https://doi.org/10.2760/13286

7. Brundiers, K., Barth, M., Cebrián, G., Cohen, M., Diaz, L., Doucette-Remington, S., Dripps, W., Habron, G., Harré, N., Jarchow, M., Losch, K., Michel, J., Mochizuki, Y., Rieckmann, M., Parnell, R., Walker, P., & Zint, M. (2021). Key competencies in sustainability in higher education—Toward an agreed-upon reference framework. *Sustainability Science, 16*, 13–29. https://doi.org/10.1007/s11625-020-00838-2

8. Chan, J., & Erduran, S. (2025). Future-oriented science learning and its effects on students' emotions, futures literacy and agency in the Anthropocene. *Research in Science Education, 55*, 899–919. https://doi.org/10.1007/s11165-024-10213-1

9. Crawford, K. (2021). *Atlas of AI: Power, politics, and the planetary costs of artificial intelligence*. Yale University Press.

10. de Vries, A. (2023). The growing energy footprint of artificial intelligence. *Joule, 7*(10), 2191–2194. https://doi.org/10.1016/j.joule.2023.09.004

11. Dokic, D., Groen In'T Woud, F., & Maass, W. (2024, January 1). Towards Sustainability of AI: A Systematic Review of Exisiting Life Cycle Assessment Approaches and Key Environmental Impact Parameters of Artificial Intelligence. https://doi.org/10.24251/hicss.2024.518

12. Gohr, C., Rodríguez, G., Belomestnykh, S., Berg-Moelleken, D., Chauhan, N., Engler, J.-O., Heydebreck, L. V., Hintz, M. J., Kretschmer, M., Krügermeier, C., Meinberg, J., Rau, A.-L., Schwenck, C., Aoulkadi, I., Poll, S., Lemke, O., Frank, E., Creutzig, F., Maushart, M., … von Wehrden, H. (2025). Artificial intelligence in sustainable development research. *Nature Sustainability, 8*, 970–978. https://doi.org/10.1038/s41893-025-01598-6

13. International Energy Agency. (2025). *Energy and AI*, IEA, Paris https://www.iea.org/reports/energy-and-ai

14. Kaack, L. H., Donti, P. L., Strubell, E., Kamiya, G., Creutzig, F., & Rolnick, D. (2022). Aligning artificial intelligence with climate change mitigation. *Nature Climate Change, 12*, 518–527. https://doi.org/10.1038/s41558-022-01377-7

15. Kamyab, H., Khademi, T., Chelliapan, S., SaberiKamarposhti, M., Rezania, S., Yusuf, M., Farajnezhad, M., Abbas, M., Jeon, B. H., & Ahn, Y. (2023). The latest innovative avenues for the utilization of artificial intelligence and big data analytics in water resource management. *Results in Engineering, 20*, Article 101566. https://doi.org/10.1016/j.rineng.2023.101566

16. Kasneci, E., Sessler, K., Küchemann, S., Bannert, M., Dementieva, D., Fischer, F., Gasser, U., Groh, G., Günnemann, S., Hüllermeier, E., Krusche, S., Kutyniok, G., Michaeli, T., Nerdel, C., Pfeffer, J., Poquet, O., Sailer, M., Schmidt, A., Seidel, T., … Kasneci, G. (2023). ChatGPT for good? On opportunities and challenges of large language models for education. *Learning and Individual Differences, 103*, Article 102274. https://doi.org/10.1016/j.lindif.2023.102274

17. Laherto, A., Rasa, T., Miani, L., Levrini, O., & Erduran, S. (2023). Future-oriented science education building sustainability competences: An approach to the European GreenComp framework. In X. Fazio (Ed.), *Science curriculum for the Anthropocene, volume 2: Curriculum models for our collective future* (pp. 83–105). Palgrave Macmillan. https://doi.org/10.1007/978-3-031-37391-6_5

18. Leal Filho, W., Kim, E., Borsatto, J. M. L. S., & Marcolin, C. B. (2025). Using artificial intelligence in sustainability teaching and learning.

Environmental Sciences Europe, 37, Article 124. https://doi.org/10.1186/s12302-025-01159-w

19. Long, D., & Magerko, B. (2020). What is AI literacy? Competencies and design considerations. In *Proceedings of the 2020 CHI Conference on Human Factors in Computing Systems* (pp. 1–16). Association for Computing Machinery. https://doi.org/10.1145/3313831.3376727

20. Mbah, M. F., Nugraha, T. R., & Kushnir, I. (2025). Challenges And Opportunities for Leveraging Generative AI for Sustainability Education: A critical review. *Sustainability, 17*(23), Article 10623. https://doi.org/10.3390/su172310623

21. Miao, F., & Cukurova, M. (2024). *AI competency framework for teachers*. UNESCO. https://doi.org/10.54675/ZJTE2084

22. Miao, F., Shiohira, K., & Lao, N. (2024). *AI competency framework for students*. UNESCO. https://doi.org/10.54675/JKJB9835

23. Olawade, D. B., Fapohunda, O., Wada, O. Z., Usman, S. O., Ige, A. O., Ajisafe, O., & Oladapo, B. I. (2024). Smart waste management: A paradigm shift enabled by artificial intelligence. *Waste Management Bulletin, 2*(2), 244–263. https://doi.org/10.1016/j.wmb.2024.05.001

24. Rolnick, D., Donti, P. L., Kaack, L. H., Kochanski, K., Lacoste, A., Sankaran, K., Ross, A. S., Milojevic-Dupont, N., Jaques, N., Waldman-Brown, A., Luccioni, A. S., Maharaj, T., Sherwin, E. D., Mukkavilli, S. K., Kording, K. P., Gomes, C. P., Ng, A. Y., Hassabis, D., Platt, J. C., … Bengio, Y. (2022). Tackling climate change with machine learning. *ACM Computing Surveys, 55*(2), Article 42. https://doi.org/10.1145/3485128

25. Seyyedi, S. R., Kowsari, E., Gheibi, M., Chinnappan, A., & Ramakrishna, S. (2024). A comprehensive review integration of digitalization and circular economy in waste management by adopting artificial intelligence approaches: Towards a simulation model. *Journal of Cleaner Production, 460*, Article 142584. https://doi.org/10.1016/j.jclepro.2024.142584

26. Silvestro, D., Goria, S., Sterner, T., & Antonelli, A. (2022). Improving biodiversity protection through artificial intelligence. *Nature Sustainability, 5*, 415–424. https://doi.org/10.1038/s41893-022-00851-6

27. Torraco, R. J. (2016). Writing İntegrative Literature Reviews: Using The Past And Present to Explore the Future. *Human Resource Development Review, 15*(4), 404–428. https://doi.org/10.1177/1534484316671606

28. Tuia, D., Kellenberger, B., Beery, S., Costelloe, B. R., Zuffi, S., Risse, B., Mathis, A., Mathis, M. W., van Langevelde, F., Burghardt, T., Kays, R., Klinck, H., Wikelski, M., Couzin, I. D., van Horn, G., Crofoot, M. C., Stewart, C. V., & Berger-Wolf, T. (2022). Perspectives in machine

learning for wildlife conservation. *Nature Communications, 13*, Article 792. https://doi.org/10.1038/s41467-022-27980-y

29. UNESCO. (2020). *Education for sustainable development: A roadmap*. https://doi.org/10.54675/YFRE1448

30. United Nations Environment Programme. (2024). *Artificial intelligence (AI) end-to-end: The environmental impact of the full AI lifecycle needs to be comprehensively assessed*.

31. van Wynsberghe, A. (2021). Sustainable AI: AI for sustainability and the sustainability of AI. *AI and Ethics, 1*, 213–218. https://doi.org/10.1007/s43681-021-00043-6

1**32.** Vinuesa, R., Azizpour, H., Leite, I., Balaam, M., Dignum, V., Domisch, S., Felländer, A., Langhans, S. D., Tegmark, M., & Fuso Nerini, F. (2020). The role of artificial intelligence in achieving the Sustainable Development Goals. *Nature Communications, 11*, Article 233. https://doi.org/10.1038/s41467-019-14108-y

33. Wang, S., Wang, F., Zhu, Z., Wang, J., Tran, T., & Du, Z. (2024). Artificial intelligence in education: A systematic literature review. *Expert Systems with Applications, 252*, Article 124167. https://doi.org/10.1016/j.eswa.2024.124167

34. Whittemore, R., & Knafl, K. (2005). The integrative review: Updated methodology. *Journal of Advanced Nursing, 52*(5), 546–553. https://doi.org/10.1111/j.1365-2648.2005.03621.x

35. Wiek, A., Withycombe, L., & Redman, C. L. (2011). Key competencies in sustainability: A reference framework for academic program development. *Sustainability Science, 6*, 203–218. https://doi.org/10.1007/s11625-011-0132-6

36. Wu, P., & Zhong, Y. (2025). Artificial intelligence in sustainable agriculture: Towards a socio-technical roadmap. Smart Agricultural Technology, 12, Article 101578. https://doi.org/10.1016/j.atech.2025.101578

37. Xiang, X., Li, Q., Khan, S., & Khalaf, O. I. (2021). Urban water resource management for sustainable environment planning using artificial intelligence techniques. *Environmental Impact Assessment Review, 86*, Article 106515. https://doi.org/10.1016/j.eiar.2020.106515

Chapter 16

Assessment of Radinucluide (Radon, Radium, Thorium and Potassium) Activity Concentration and Exhalation Rates in Building Materials Utilized in Türkiye

Aslı KURNAZ[1], Şeref TURHAN[2], Aybaba HANÇERLİOĞULLARI[3]

1. INTRODUCTION

This study presents a comprehensive systematic review of the radiological risks associated with building materials utilized across various regions in Türkiye, focusing on radon (^{222}Rn) activity concentrations, mass/surface exhalation rates, and natural radioactivity levels (^{226}Ra, ^{232}Th, and ^{40}K). Data collected from localized studies spanning major urban and industrial hubs including İstanbul, İzmir, Manisa, and the Eastern Mediterranean region synthesized and cross-examined. The primary experimental methodologies evaluated include passive Solid-State Nuclear Track Detection (SSNTD via CR-39) utilizing the sealed-can technique, alongside active Gamma-Ray Spectroscopy (NaI(Tl)/HPGe detectors). The calculated surface radon exhalation rates, mass exhalation rates, radium equivalent activities (Ra_{eq}), and annual effective dose equivalents (AEDE) reported across the literature were evaluated against safety criteria established by international bodies, including the United Nations Scientific Committee on the Effects of Atomic Radiation (UNSCEAR) and the International Commission on Radiological Protection (ICRP). The synthesized data demonstrate that while specific commercial composite matrices such as fly-ash blended mortars and highly crystalline granitesexhibit elevated localized exhalation kinetics, the overarching radiological profile of commercial building materials in Türkiye remains well within internationally accepted safety thresholds.

[1] Prof. Dr., Department of Physisc/Faculty of Science, Kastamonu University, Türkiye, akurnaz@kastamonu.edu.tr, (ORCID: 0000-0002-7910-3461)
[2] Prof. Dr., Department of Physics/Faculty of Science, Kastamonu University, Türkiye serefturhan63@gmail.com, (ORCID: 0000-0000-1700-8480)
[3] Prof. Dr., Department of Physics/Faculty of Science, Kastamonu University, Türkiye aybaba@kastamonu.edu.tr, (ORCID:0000-0005-5303-3680)

1.1. Background and Radiological Significance

Human populations in modern urban environments spend upwards of 80–90% of their lifespans inside enclosed residential or occupational structures [1-8,9]. Consequently, the radiological quality of the indoor atmospheric environment has emerged as a primary determinant of long-term public health. Natural background radiation originates predominantly from primordial radionuclides persisting within the Earth's crust [5-7] Among these, Uranium (^{238}U) and Thorium (^{232}Th) decay series, along with the singular primordial isotope Potassium-40 (^{40}K), represent the primary contributors to terrestrial gamma exposure. Radon-222 (^{222}Rn), an alpha-emitting inert gas with a physical half-life of 3.82 days, arises directly from the alpha decay of Radium-226 (^{226}Ra) within the ^{238}U chain. Because it is a gas, radon possesses the kinetic capacity to diffuse through the interstitial pore networks of geological matrices, escaping into ambient air. When inhaled, radon gas decays rapidly into short-lived particulate progeny (^{218}Po, ^{214}Pb, ^{214}Bi, and ^{214}Po). These heavy-metal radioisotopes lodge within the epithelial lining of the human respiratory tract. Subsequent localized alpha-particle emissions induce dense ionization tracks within the DNA architecture of bronchial cells, significantly accelerating the risk of bronchogenic carcinoma. Globally, radon exposure stands as the second leading cause of lung cancer after tobacco smoking [8,9].

1.2. Role of Building Materials as Radon Sources

While geogenic radon entry via sub-structure soil gas migration constitutes the dominant indoor radon source in ground-level dwellings, the structural and decorative building materials utilized in construction serve as the primary source of indoor radon in multi-story buildings and high-rise apartments [7-9]. Materials such as concrete, clay bricks, cement, gypsum, and natural ornamental stones (e.g., granites and marbles) naturally contain varying trace quantities of ^{226}Ra, ^{232}Th, and ^{40}K [3,9]. The continuous emission of radon from a structural element into an indoor room is governed by two sequential physical processes;

1. *Emanation: The dislodgement of newly created radon atoms from the solid mineral grains into the pore spaces due to alpha-recoil energy.*
2. *Exhalation: The subsequent transport of emanated radon through the material's interconnected pore system via molecular diffusion and advection, culminating in its release from the material's surface into the surrounding air layer.*

1.3. Scope and Objectives within the Turkish Context

In Türkiye, the rapid expansion of the construction sector over the past few decades has led to a diversification of raw materials, including increased incorporation of industrial by-products such as fly ash and blast-furnace slag into commercial cements and concrete aggregates. Furthermore, the extensive domestic quarrying and importation of highly crystalline granites for interior cladding and flooring have altered the indoor radiological landscapes of modern Turkish dwellings. Recognizing these shifts, independent research groups across Türkiye have conducted localized radiological assessments. However, these investigations are often fragmented by region or material type. This paper provides a rigorous, unified systematic review of the peer-reviewed scientific literature tracking radon activity concentrations and exhalation kinetics within building elements utilized across Türkiye. By synthesizing data from key regional studies ranging from the high-density urban expanses of İstanbul and the industrial sectors of the Ege Region (İzmir and Manisa) to the geological variations of the Eastern Mediterranean zone this paper establishes a comprehensive baseline of domestic structural radiation profiles and directly assesses their public health implications against global safety mandates.

2. THEORETICAL AND MATHEMATICAL CALCULATIONS

To compare data across different scientific investigations, it is necessary to establish the standard mathematical equations used to determine radon exhalation rates and index hazards.

2.1. Radon Exhalation Kinetics

The transport of radon through structural materials is mathematically modeled using steady-state one-dimensional diffusion theories [1,7]. When using the standard "sealed-can technique" with Solid-State Nuclear Track Detectors (SSNTDs), the time-dependent growth of radon activity concentration (C) within the enclosed chamber air volume is expressed via the following differential relationship;

$$C(t)=Ex.A(1-Ex(-\lambda_{eff.}.t\ ).(1/V.\ \lambda_{eff.})\ +C_0.\ Ex(-\lambda_{eff.}.t)$$

Where;C(t) is the radon activity concentration at exposure time t ($Bq\cdot m^{-3}$),C_0 is the initial indoor background radon concentration ($Bq\cdot m^{-3}$),Ex is the surface radon exhalation rate ($Bq\cdot m^{-2}\cdot h^{-1}$)., A is the exposed surface area of the structural

sample (m^2),V is the net free air volume inside the sealed measurement chamber (m^3),λ_{eff} is the effective decay constant (h^{-1}), defined as

$$\lambda_{eff} = \lambda_{Rn} + \lambda_{leak}$$

Where,λ_{Rn} is the physical decay constant of ^{222}Rn (0.00756 h^{-1}) and λleak is accounts for any microscopic leakage rate of the experimental chamberWhen evaluating granular, crushed, or powder-form building constituents (such as raw cement powders or fly ash aggregates), the mass radon exhalation rate (Em, expressed in $Bq \cdot kg^{-1} \cdot h^{-1}$) is preferred over the surface-derived parameter, calculated as M, the total dry mass of the sample under investigation (kg).

$$E_m = E_x . A(1/M)$$

2.2. Evaluation of Radiological Risk Indices

To evaluate the cumulative gamma and alpha hazards induced by the structural samples, researchers calculate several standard regulatory indexes.

2.2.1. Radium Equivalent Activity (Raeq)

Because the distribution of primordial radionuclides within geological building blocks is fundamentally non-uniform, a mathematically weighted index known as the Radium Equivalent Activity is universally adopted to compare the specific activities of ^{226}Ra, ^{232}Th, and ^{40}K on a uniform radiological basis [7]. It is formulated on the assumption that 370 $Bq \cdot kg^{-1}$ of ^{226}Ra, 259 $Bq \cdot kg^{-1}$ of ^{232}Th, and 4810 $Bq \cdot kg^{-1}$ of ^{40}K generate an identical gamma radiation dose rate:

$$Ra_{eq} = A_{Ra} + 1.43A_{Th} + 0.0077A_K$$

Where A_{Ra}, A_{Th}, and $A_K$are the specific activity concentrations of ^{226}Ra, ^{232}Th, and ^{40}K in $Bq \cdot kg^{-1}$, respectively. To comply with the safety limits recommended by UNSCEAR, the maximum value of Raeq for materials used in residential buildings must not exceed 370 $Bq \cdot kg^{-1}$.

2.2.2. Internal Hazard Index (Hin)

To specifically regulate the internal hazard posed by the inhalation of radon gas and its short-lived alpha-emitting daughters, the internal hazard index is employed. For structural materials to be deemed radiologically safe for indoor use, must strictly remain below unity (Hin<1) (UNSCEAR, 2008; ICRP, 2010).

$$H_{in} = A_{Ra}.0.006 + A_{Th}.0.004 + A_K.0.0002$$

3. Methodological Approaches in the Reviewed Studies

The data gathered in this review reflect two primary analytical methods used across academic institutions in Türkiye.

3.1. Passive Radon Tracking: Sealed-Can Technique with CR-39

The dominant technique for isolating radon gas exhalation kinetics across the reviewed Turkish literature involves the use of Allyl Diglycol Carbonate sheets, commercially classified as **CR-39** Solid-State Nuclear Track Detectors (SSNTDs) [1,2]. This passive approach is preferred due to its long-term integration capabilities and resistance to environmental moisture distortions.In a typical experimental setup, the building material sample is dried in a temperature-controlled oven at 105°C until it reaches a constant mass, eliminating volatile moisture that could artificially impede radon pore diffusion. The sample is then placed at the bottom of a cylindrical chamber of known dimensions. A CR-39 chip is fixed to the inside top of the container, at a distance sufficient to prevent alpha particles emitted directly from the sample's surface from reaching the plastic track detector. This ensures that only alpha particles originating from the decayed radon gas within the upper air volume are recorded.The container is hermetically sealed for an integration period typically ranging from 30 to 90 days. During this time, alpha particles striking the CR-39 sheet create microscopic, latent damaged zones known as latent tracks. After the exposure period, the CR-39 detectors are removed and subjected to chemical etching typically using a 6.25 M Sodium Hydroxide (NaOH) solution at 70°C for a precise period of 6 to 7 hours. This process enlarges the latent tracks into visible pits. These pits are then counted using automated optical track-analysis microscopes to calculate the net track density (tracks·cm^{-2}·h^{-1}), which is directly proportional to the integrated radon concentration.

3.2. Gamma-Ray Spectroscopy

To establish the elemental origin of the exhaled radon, researchers across Türkiye rely on active high-resolution gamma-ray spectroscopy. This method uses either Thallium-activated Sodium Iodide(NaI(Tl)) scintillation detectors or High-Purity Germanium (HPGe) semiconductor detectors enclosed in thick lead shields to suppress ambient cosmic background interference.Samples are crushed, sieved through standard mesh matrices, weighed, and sealed inside standardized geometry containers (such as Marinelli beakers) for a minimum of 4 weeks [3,7]. This sealing period is critical to establish a state of secular radioactive equilibrium between ^{226}Ra and its short-lived daughters (^{214}Pb and

^{214}Bi), as well as between ^{228}Ac and ^{208}Tl in the Thorium series. The gamma photopeaks typically analyzed include;

- ^{226}Ra, Evaluated indirectly via the 351.9 keV photopeak of ^{214}Pb and the 609.3 keV photopeak of ^{214}Bi
- ^{232}Th, Measured through the 911.2 keV line of ^{228}Ac or the 583.1 keV line of ^{208}Tl.
- ^{40}K, Determined directly via its single distinct rest-energy gamma emission at 1460.8 keV.

4. Synthesis of Regional and Material-Specific Findings

The compiled findings from across Türkiye show significant variations that depend directly on the geological origin of the raw materials and the manufacturing formulations used. To provide a clear overview of the findings, the typical in Table-1 ranges of radioactivity concentrations and radon kinetics extracted from the core literature are summarized below;

Table-1 ranges of radioactivity concentrations and radon kinetics extracted

Material Type	Primary Region	Investigated ^{26}Ra Concentration (Bq·kg^{-1})	^{232}Th Concentration (Bq·kg^{-1})	^{40}K Concentration (Bq·kg^{-1})	Surface Exhalation Rate (Ex) (Bq·m^{-2}·h^{-1})	Primary Experimental Methodology
Commercial Granites	National Market / Imports	20 – 140	30 – 160	600 – 1500	0.25 – 2.10	CR-39 / HPGe Spectroscopy
Standard Bricks / Clays	İstanbul / Marmara	15 – 65	20 – 70	300 – 800	0.05 – 0.45	CR-39 / NaI(Tl) Detection
Fly-Ash Blended Mortars	İzmir / Ege	45 – 110	35 – 90	400 – 950	0.18 – 0.85	CR-39 Closed-Can System
Aggregates & Tuffs	Mediterranean / Osmaniye	10 – 55	12 – 60	150 – 700	0.08 – 0.50	NaI(Tl) / Mathematical Modeling
Natural Marbles	Aegean / West Anatolia	2 – 15	1 – 12	20 – 120	0.01 – 0.12	CR-39 Passive Tracking

Granite samples utilized within the Turkish building sector show the highest variance and upper-bound extremes for both specific activity and radon exhalation [1,6]. As analyzed by Aykamış et al. and further corroborated by the text of Akkaş, 2025., granites exhibit elevated ^{226}Ra and ^{232}Th concentrations due to the geochemical partitioning of incompatible lithophile elements during magma solidification.The surface radon exhalation rates (Ex) of certain highly crystalline granite variants reached up to 2.10 $Bq \cdot m^{-2} \cdot h^{-1}$. This is significantly higher than the baseline values found in sedimentary rocks like limestone or marble. This elevation is directly linked to the micro-fissuring characteristic of granitic crystal sheets, which provides high internal surface areas that facilitate the migration of emanated radon into interstitial channels.In industrial sectors like İzmir and Manisa, economic and environmental considerations have led to the widespread use of coal combustion products specifically fly ash as pozzolanic additives in cement formulations. Investigations targeting these specific composite matrices indicate that fly-ash blended mortars consistently exhibit higher ^{226}Ra concentrations compared to conventional Portland cement blocks [4,5]. The combustion of coal concentrates non-volatile trace radyonuklides within the residual ash phase. Consequently, the incorporation of fly ash slightly elevates the internal hazard index (Hin) and shifts the mass radon exhalation rate upward. However, this effect is partially mitigated by the physical characteristics of the fly ash itself; its fine particulate nature alters the pore-size distribution of the cured concrete matrix, increasing tortuosity and reducing the effective diffusion coefficient of radon gas.

In contrast to granites and industrial composite mixes, natural marbles and limestones quarried across Western Anatolia and the Mediterranean shelf exhibit minimal radiological activity [3,7]. Because these rocks are formed through sedimentary deposition and subsequent low-temperature metamorphism, they naturally exclude heavy radioelements. The radon exhalation rates from marble blocks rarely exceed 0.12 $Bq \cdot m^{-2} \cdot h^{-1}$, making them the safest structural choice for minimizing internal alpha exposure. Studies conducted on structural components sold in the İstanbul area focused on mapping the baseline emissions of materials used in high-density residential developments. The results indicate that standard clay bricks, lightweight autoclaved aerated concrete (AAC), and blocks produced by local manufacturers align closely with worldwide averages [2,7]. The radon exhalation rates from these materials do not pose an elevated risk when evaluated against the global background standards compiled by UNSCEAR.The İzmir and Manisa corridor represents a unique industrial landscape where extensive geothermal and tectonic activity intersects with heavy manufacturing. Studies mapping this region indicate that building blocks utilizing local volcanic tuffs or industrial slag show slightly elevated radiological baselines (Topcu et al., 2013; Hatungimana et al., 2020.

However, tracking programs using CR-39 arrays over extended integration windows confirm that even the maximum recorded radon exhalation fluxes remain within safe limits, preventing indoor radon concentrations from exceeding the national regulatory action level of 300 $Bq \cdot m^{-3}$.In the Eastern Mediterranean zone, centered around Osmaniye and its surrounding plains, research focused on evaluating radiological hazard indices via gamma-ray spectroscopy. These studies assessed the Radium Equivalent Activity (Raeq) and external hazard indices of raw soil blocks, regional aggregates, and concrete products. The data confirm that the geological materials of the Mediterranean shelf present low risk profiles, with Raeq values falling well below the mandatory international cap of 370 $Bq \cdot kg^{-1}$ [4,5].

5. RADıOLOGICAL RISK EVALUATION AND PUBLIC HEALTH IMPLICATIONS

To contextualize these experimental values within a public health framework, the compiled data must be evaluated against the dose limitation systems established by the ICRP and UNSCEAR.

5.1. Annual Effective Dose Equivalent (AEDE) Assessment

The ultimate parameter used to assess public health risk is the Annual Effective Dose Equivalent (AEDE), measured in milliSieverts per year ($mSv \cdot y^{-1}$). This metric accounts for both external gamma radiation emitted by the walls and floor, and internal alpha exposure delivered to the lungs by inhaled radon progeny.The studies reviewed indicate that the typical annual effective dose derived from indoor exposure to standard Turkish building components clusters between 0.25 $mSv \cdot y^{-1}$ and 0.75 $mSv \cdot y^{-1}$. This range is well below the conservative public dose limit of 1.0 $mSv \cdot y^{-1}$ recommended by the ICRP for civilian dwellings [7-9].

5.2. Mitigation Strategies for Borderline Materials

While the average structural sample poses no hazard, specific premium granite claddings and fly-ash rich composites present borderline values that approach regulatory thresholds under poor ventilation conditions. To manage these specific instances, two practical mitigation strategies are recommended;

1. Enhanced Indoor Ventilation Rates: Increasing the air exchange rate (ACH) of a room from a poor baseline of 0.2 h^{-1} to a standard mechanical or natural ventilation rate of 0.5 h^{-1} rapidly dilutes accumulated radon gas, preventing the build-up of short-lived alpha-emitting daughters regardless of the material's surface exhalation rate.
2. Surface Sealants and Epoxies: Applying non-porous chemical sealants, polyurethane coats, or specialized anti-radon paints to the exposed surfaces

of high-exhalation ornamental stones forms a physical barrier. This barrier impedes the diffusion of radon gas, forcing it to undergo radioactive decay within the solid matrix before it can escape into the indoor atmosphere.

6. CONCLUSION

This review synthesized peer-reviewed data tracking radon activity concentrations and exhalation kinetics within structural and decorative building components utilized across Türkiye. The primary conclusions are summarized as follows;Experimental Consistency: The integration of passive CR-39 sealed-can testing and active gamma spectroscopy provides a reliable framework for assessing the radiological profiles of structural materials,Safety Threshold Compliance: The overarching baseline of commercial bricks, conventional cements, and structural concretes produced in Türkiye complies with the safety guidelines set by UNSCEAR and the ICRP [2,7-9]. The calculated Radium Equivalent Activities (Raeq) and Internal Hazard Indices (Hin) consistently remain below 370 $Bq \cdot kg^{-1}$ and unity, respectively,Material Matrix Variations: Natural granites and industrial fly-ash composite mortars exhibit the highest radon exhalation rates (Ex up to 2.10 $Bq \cdot m^{-2} \cdot h^{-1}$). Conversely, metamorphic marbles present negligible radiological risks ([1,4,6] Public Health Outlook: The average indoor annual effective dose derived from domestic structural components is well within safe limits, indicating no immediate radiological risk to the Turkish population under standard living conditions[7-9].

REFERENCES

[1] Aykamış, A.Ş., Turhan, Ş., Ugur F.A, Baykan U. N.,. Kılıç A. M. (2013). Natural radioactivity, radon exhalation rates and indoor radon concentration of some granite samples used as construction material in Turkey. 157, 1, 105-111.

[2] Kaynar, S.Ç., Özbey, E., & Ereeş F.S. (2015). Determination of radon exhalation rate and natural radioactivity levels of building materials used in İstanbul, Turkey. *Journal of Radioanalytical and Nuclear Chemistry*, 305, 337-343.

[3] Turhan, Ş., Kurnaz A., & Karataşlı M. (2021). Evaluation of Natural Radioactivity Levels and Potential Radiological Hazards of Common Building Materials Utilized in Mediterranean Region, Turkey. *Environmental Science and Pollution Research*, 29, 10575-10584.

[4] Topcu N., Bicak D., ÇAM KAYNAR S., Erees F. (2013). Radon exhalation rate from building materials using cr-39 nuclear track detector. *Indoor and Built Environment,* 22(2), 384-387,

[5] Hatungimana, D., Taşköprü, C., İçhedef, M., Saç, M.M. Yazıcı, Ş., & Mardani-Aghabaglou, A. (2020). Determination of Radon and Natural Radioactivity Concentration in Some Building Materials Used in İzmir, Turkey. *Journal of Green Building*, 15(1), 107-118.

[6] Akkaş. A., (2025). Radioactivity and radon exhalation rate of some granite building materials in Türkiye. *Applied Radiation and Isotopes*, 225, 112024.

[7] United Nations Scientific Committee on the Effects of Atomic Radiation (UNSCEAR). (2008). *Sources and Effects of Ionizing Radiation*. Report to the General Assembly, New York.

[8] International Commission on Radiological Protection (ICRP). (2010). *Radiological Protection in Biomedical Research*. ICRP Publication 115, Annals of the ICRP.

[9] World Health Organization. (2009). WHO handbook on indoor radon: A public health perspective. World Health Organization. ISBN: 978-92-4-154767-3.

Chapter 17

Analysing Naturally Occurring Radioactive Materials (NORM) in Structural Building Materials Used in Türkiye and Radiological Health Risk Evaluation

Şeref TURHAN[1], Aybaba HANÇERLİOĞULLARI[2], Aslı KURNAZ[3]

1. INTRODUCTION

Naturally occurring radioactive materials (NORM) are ubiquitous components of the Earth's crust and are present in varying concentrations in geological formations used as raw materials for construction. Structural building materials such as cement, concrete, clay bricks, pumice, natural stone, marble, granite, and volcanic tuff may contain measurable amounts of radionuclides belonging to the uranium (^{238}U) and thorium (^{232}Th) decay series as well as potassium (^{40}K). Since these materials are extensively used in residential, commercial, and industrial buildings, they may contribute to external gamma radiation exposure and indoor radon accumulation, potentially affecting public health.Türkiye possesses diverse geological formations that provide abundant natural resources for the construction industry. Consequently, numerous investigations have evaluated the activity concentrations of natural radionuclides in Turkish building materials using high-resolution gamma-ray spectrometry and have assessed their radiological hazards according to international recommendations issued by UNSCEAR, the International Atomic Energy Agency (IAEA), and the European Commission.This review summarizes the current knowledge regarding NORM levels in structural building materials used in Türkiye and discusses radiological hazard indices including radium equivalent activity (Raeq), absorbed gamma dose rate, annual effective dose (AED), external hazard index (Hex), internal hazard index (Hin), and activity concentration index (Iγ). Previous studies indicate that although radionuclide concentrations vary considerably depending on geological origin and manufacturing processes, most commonly used Turkish construction materials remain within internationally accepted radiological safety limits. Nevertheless, certain volcanic and granitic

[1] Prof. Dr., Department of Physics/Faculty of Science, Kastamonu University, Türkiye serefturhan63@gmail.com, (ORCID: 0000-0000-1700-8480)
[2] Prof. Dr., Department of Physics/Faculty of Science, Kastamonu University, Türkiye aybaba@kastamonu.edu.tr, (ORCID:0000-0005-5303-3680)
[3] Prof. Dr., Department of Physisc/Faculty of Science, Kastamonu University, Türkiye, akurnaz@kastamonu.edu.tr, (ORCID: 0000-0002-7910-3461)

materials exhibit elevated radionuclide concentrations that justify continuous monitoring. The review also identifies current research gaps and provides recommendations for future investigations aimed at improving radiation protection in the Turkish construction sector.Natural radioactivity has existed since the formation of the Earth and represents the largest contributor to the radiation dose received by the general population (UNSCEAR, 2000; UNSCEAR, 2008). Naturally occurring radioactive materials (NORM) originate primarily from primordial radionuclides, particularly members of the uranium (^{238}U) and thorium (^{232}Th) decay series together with the naturally occurring isotope of potassium (^{40}K) (IAEA, 2004; IAEA, 2007). These radionuclides are widely distributed in rocks, soils, sediments, and minerals, which subsequently become raw materials for the production of structural building materials. The rapid growth of urbanization and infrastructure development has substantially increased the global consumption of construction materials. Concrete, cement, clay bricks, aggregates, pumice, limestone, marble, granite, volcanic tuff, gypsum, and ceramic products are routinely incorporated into residential and commercial buildings.

Because these materials retain varying concentrations of naturally occurring radionuclides inherited from their geological sources, they may contribute to indoor gamma radiation exposure and radon generation throughout the service life of buildings (European Commission, 1999; UNSCEAR, 2008).Assessment of natural radioactivity in building materials has therefore become an important component of environmental radiation protection. International organizations including UNSCEAR, the IAEA, and the European Commission have developed methodologies for evaluating radiological hazards associated with construction materials. Widely accepted parameters include activity concentration, absorbed dose rate, radium equivalent activity (Raeq), external and internal hazard indices (Hex and Hin), annual effective dose (AED), and the activity concentration index (Iγ). These indices provide standardized approaches for determining whether construction materials satisfy recommended radiological safety criteria (European Commission, 1999; IAEA, 2007; UNSCEAR, 2000).Türkiye is characterized by remarkable geological diversity, including extensive volcanic provinces, sedimentary basins, metamorphic terrains, and granitic formations. This geological variability influences the natural radionuclide content of raw materials used by the Turkish construction industry. During the last two decades, numerous investigations have measured radionuclide concentrations in Turkish cement, concrete, pumice blocks, clay bricks, natural stones, granites, marbles, volcanic tuffs, and ceramic products (Erkan, 2007; Ereeş and Kaynar, 2006). Most studies employed high-purity germanium (HPGe) gamma-ray spectrometry

and evaluated radiological hazards according to internationally accepted standards (Turhan et al., 2015; Turhan et al., 2018; Özdiş et al., 2017).Although the majority of published studies conclude that Turkish construction materials generally comply with international radiological safety criteria, significant regional variations have been reported due to differences in geological origin, mineralogical composition, and industrial processing. Materials derived from volcanic formations may exhibit relatively higher concentrations of uranium and thorium series radionuclides compared with sedimentary materials (Baltas et al., 2014; Tufan and Dişci, 2013; Turhan et al., 2015; Çetin and Akkurt, 2010). Consequently, continuous monitoring remains essential to ensure radiation protection and public health.

The purpose of this review is to synthesize published findings regarding NORM concentrations in structural building materials used in Türkiye, summarize commonly employed measurement techniques and radiological indices, compare Turkish findings with international recommendations, and identify future research priorities for radiation safety assessment within the Turkish construction sector (IAEA, 2007; UNSCEAR, 2008).

2. FUNDAMENTALS OF NORM

Naturally Occurring Radioactive Materials (NORM) are radioactive substances that occur naturally in the Earth's crust without any human intervention. These radionuclides have existed since the formation of the Earth approximately 4.5 billion years ago and remain present because of their extremely long half-lives (UNSCEAR, 2000; IAEA, 2005). The most important naturally occurring radionuclides include members of the uranium (^{238}U) and thorium (^{232}Th) decay series together with potassium (^{40}K), which are widely distributed in rocks, soils, sediments, groundwater, and minerals. Consequently, they become incorporated into raw materials used for the manufacture of structural building materials such as cement, concrete, clay bricks, natural stones, ceramics, and aggregates (European Commission, 1999; IAEA, 2007).Unlike artificial radionuclides released from nuclear activities, NORM represents the natural background radioactivity of geological formations. However, mining, quarrying, mineral processing, and industrial manufacturing may increase the concentration or redistribution of these radionuclides in commercial products, leading to what is commonly referred to as technologically enhanced naturally occurring radioactive materials (TENORM) (IAEA, 2005). Therefore, evaluating NORM concentrations in construction materials is essential for environmental radiation protection and public health.

2.1 Origin of Natural Radioactivity

Natural radiation is the largest contributor to the annual effective dose received by the general population worldwide. According to the United Nations Scientific Committee on the Effects of Atomic Radiation (UNSCEAR,2020), approximately 80% of the annual radiation exposure originates from natural sources, whereas the remaining dose is mainly associated with medical and anthropogenic applications (UNSCEAR, 2000; UNSCEAR, 2008).Natural radiation consists of three principal components;Cosmic radiation originating from outer space,Terrestrial radiation emitted by naturally occurring radionuclides in rocks and soils, Internal radiation resulting from radionuclides incorporated into the human body through inhalation and ingestion (UNSCEAR, 2008).Among these components, terrestrial radiation is of particular significance in studies concerning building materials because radionuclides contained within construction materials continuously emit gamma radiation throughout the lifetime of buildings (European Commission, 1999).

2.2 Major Primordial Radionuclides

The radionuclides most commonly investigated in environmental radioactivity studies are uranium-238 (^{238}U), thorium-232 (^{232}Th), and potassium-40 (^{40}K). These radionuclides differ in terms of abundance, decay mechanisms, radiological significance, and contribution to external and internal radiation exposure (UNSCEAR, 2000).Uranium-238 Series: The uranium-238 decay series contains fourteen daughter radionuclides and ultimately decays into stable lead-206 (^{206}Pb). Among its decay products, radium-226 (^{226}Ra) and radon-222 (^{222}Rn) are considered the most radiologically important. Radon is a radioactive noble gas capable of migrating through porous construction materials into indoor environments, where prolonged exposure has been associated with an increased risk of lung cancer (IAEA, 2003; UNSCEAR, 2008).Uranium concentrations vary considerably depending on geological conditions. Granitic rocks, volcanic tuffs, phosphate deposits, and some metamorphic formations generally exhibit higher uranium concentrations than sedimentary carbonate rocks (UNSCEAR, 2000).

Thorium-232 Series: Thorium-232 possesses a half-life of approximately 1.4×10^{10} years and represents another major contributor to terrestrial radioactivity. Because thorium has low chemical mobility, its concentration largely depends on the mineralogical composition of the parent rock (UNSCEAR, 2000). Minerals such as monazite and zircon frequently contain elevated thorium concentrations, resulting in increased gamma radiation emitted by their daughter radionuclides, particularly ^{228}Ac and ^{208}Tl (IAEA, 2004).Potassium-40: Potassium is one of the

most abundant elements in the Earth's crust, and approximately 0.0117% of natural potassium consists of the radioactive isotope ^{40}K (UNSCEAR, 2000). Unlike uranium and thorium, ^{40}K does not belong to a radioactive decay series but decays directly through beta emission and electron capture, producing a characteristic gamma photon of 1460.8 keV (IAEA, 2004).Clay minerals, feldspars, micas, and volcanic rocks generally contain elevated potassium concentrations; consequently, clay bricks, ceramics, and granitic building stones often exhibit relatively high ^{40}K activity concentrations (Eissa et al., 2008; Turhan et al., 2018; Özdiş et al., 2017).

2.3 Geological Controls on NORM Distribution

The distribution of natural radionuclides is primarily governed by geological processes, including magmatic differentiation, sedimentation, metamorphism, and weathering. Acidic igneous rocks such as granite and rhyolite generally exhibit higher uranium and thorium concentrations than sedimentary limestones because incompatible elements become enriched during magma evolution (UNSCEAR, 2000; IAEA, 2007). Türkiye possesses highly diverse geological formations, including extensive volcanic provinces, granitic intrusions, sedimentary basins, and metamorphic belts. This geological diversity leads to considerable regional variations in radionuclide concentrations observed in Turkish construction materials (Turhan et al., 2015; Turhan et al., 2018).

3. NORM AND BUILDING MATERIALS USED IN TÜRKİYE

3.1 Geological Origin of NORM in Construction Materials

NORM in structural building materials are fundamentally controlled by geological processes that govern the formation, differentiation, and alteration of rocks. Natural radionuclides such as uranium (^{238}U), thorium (^{232}Th), and potassium (^{40}K) are incorporated into minerals during the crystallization of igneous rocks and subsequent sedimentary and metamorphic processes. Their abundance in construction materials therefore reflects the geochemical composition of the parent geological formations (UNSCEAR, 2000; IAEA, 2005).Igneous processes play a particularly important role in controlling radionuclide concentrations. During magma cooling and differentiation, incompatible elements such as uranium and thorium tend to concentrate in the residual melt, leading to elevated activity concentrations in acidic igneous rocks such as granite, rhyolite, and volcanic tuff. These rock types are widely used as decorative stones and sometimes as aggregates in construction, resulting in enhanced gamma radiation levels in buildings (UNSCEAR, 2000; IAEA, 2007).Sedimentary rocks generally exhibit lower radionuclide concentrations due

to dilution processes during weathering and transport. Carbonate rocks such as limestone and dolomite typically contain relatively low levels of uranium, thorium, and potassium. However, clay-rich sediments may retain higher potassium-40 (^{40}K) concentrations due to the presence of feldspar and mica minerals (European Commission, 1999).Metamorphic processes can modify the distribution of radionuclides by recrystallization and mineral phase changes, although they do not introduce new radioactivity. Instead, they may concentrate or redistribute existing radionuclides depending on temperature, pressure, and fluid interactions during metamorphism (IAEA, 2005).In addition to natural geological processes, human industrial activities such as quarrying, crushing, and cement production may alter the distribution of radionuclides in final construction products. This does not create radioactivity but can lead to relative enrichment of radionuclides in processed materials compared with bulk rock (IAEA, 2007).

3.2 Building Materials Used in Türkiye

Türkiye is characterized by highly diverse geological formations, including extensive volcanic provinces (Central Anatolia and Eastern Anatolia), granitic intrusions (Western Anatolia), carbonate platforms, and metamorphic belts. This geological diversity results in a wide range of radionuclide concentrations in construction materials used across the country (UNSCEAR, 2008; Turhan et al., 2015).

The most commonly used structural building materials in Türkiye include cement, concrete, clay bricks, pumice blocks, volcanic tuffs, natural stones (granite, marble, basalt, travertine), aggregates, and ceramic products. Each of these materials exhibits distinct radiological characteristics depending on its mineralogical and geological origin.Cement and concrete are among the most widely used construction materials and generally show moderate levels of natural radioactivity. Cement raw materials such as limestone and clay contribute uranium, thorium, and potassium in varying proportions (Özdiş et al., 2017). Concrete, being a composite material, reflects the combined radiological properties of cement and aggregates (Özdiş et al., 2017). Clay bricks and ceramic products often contain relatively higher ^{40}K activity concentrations due to the potassium-rich nature of clay minerals. Studies conducted in Türkiye have shown that brick samples may exhibit significant variability in radionuclide content depending on the clay source and firing conditions (Turhan et al., 2018). Volcanic materials such as pumice and tuff are widely used, particularly in central and eastern regions of Türkiye. These materials may exhibit elevated uranium and thorium concentrations due to their volcanic origin. As a result, they can contribute more significantly to external gamma radiation compared with

sedimentary materials (Turhan et al., 2015). Natural stones such as granite, basalt, marble, and travertine are also important construction materials. Among these, granite typically shows higher radionuclide concentrations due to its felsic composition, while carbonate-based stones such as marble and travertine generally exhibit lower activity levels. Basalt, being of mafic volcanic origin, usually contains intermediate radionuclide concentrations.

Aggregates used in concrete production may originate from various geological sources, and their radionuclide content significantly influences the overall radioactivity of concrete structures. Therefore, aggregate selection is an important factor in controlling radiological exposure in buildings.

3.3 Radiological Characteristics of Building Materials in Türkiye

Numerous studies conducted in Türkiye have demonstrated that natural radionuclide concentrations in building materials vary widely depending on geological origin, mineral composition, and industrial processing. Measurements performed using high-resolution gamma-ray spectrometry indicate that ^{226}Ra, ^{232}Th, and ^{40}K activity concentrations differ significantly among material types (Turhan et al., 2015; Turhan et al., 2018; Özdiş et al., 2017).In general, volcanic materials and clay-based products tend to exhibit higher activity concentrations compared with carbonate-based materials. However, most studied samples remain within internationally recommended safety limits established by the European Commission and IAEA guidelines (European Commission, 1999; IAEA, 2007).Radiological hazard indices calculated in Turkish studies, including radium equivalent activity (Raeq), external hazard index (Hex), internal hazard index (Hin), and absorbed gamma dose rate, typically indicate that construction materials used in Türkiye do not pose significant radiological risk to the public. Nevertheless, localized variations highlight the importance of continuous monitoring, particularly in regions with volcanic geology (UNSCEAR, 2008).

4. ANALYTICAL TECHNIQUES FOR NORM DETERMINATION

NORM in structural building materials relies primarily on the accurate determination of radionuclide activity concentrations. Since naturally occurring radionuclides such as ^{238}U, ^{232}Th, and ^{40}K emit gamma radiation of characteristic energies, high-resolution gamma-ray spectrometry is widely recognized as the standard analytical technique for their quantification (IAEA, 2004; IAEA, 2007). This method allows non-destructive, simultaneous, and reliable measurement of multiple radionuclides in complex matrices such as cement, concrete, bricks, and natural stones.

4.1 Sample Collection and Preparation

Proper sample collection and preparation are essential to ensure representativeness and measurement accuracy. Building material samples are typically collected from production sites, construction areas, or quarries. In many studies conducted in Türkiye, samples are first crushed and homogenized to obtain a uniform particle size distribution, usually below 1–2 mm, to minimize heterogeneity effects (Turhan et al., 2015; Özdiş et al., 2017).After homogenization, samples are dried at approximately 105°C to remove moisture content, which may otherwise affect density and gamma attenuation characteristics. The dried samples are then weighed and sealed in airtight containers, typically Marinelli beakers or cylindrical plastic containers, to prevent the escape of radon (^{222}Rn) and its progeny. Sealing is a critical step, as radon equilibrium between ^{226}Ra and its decay products must be achieved before measurement, usually requiring a storage period of 3–4 weeks (IAEA, 2004).

4.2 High-Purity Germanium (HPGe) Gamma Spectrometry

High-Purity Germanium (HPGe) detectors are the most widely used instruments for NORM analysis due to their superior energy resolution compared to scintillation detectors. HPGe detectors allow precise identification of gamma-emitting radionuclides based on their characteristic energy peaks.Typical gamma emissions used for activity determination include.^{40}K; 1460.8 keV gamma line, ^{214}Bi and ^{214}Pb (from ^{238}U series): multiple gamma lines (e.g., 609 keV, 352 keV), ^{228}Ac, ^{212}Pb, ^{208}Tl (from ^{232}Th series): multiple gamma emissions (e.g., 911 keV, 583 keV, 2614 keV)Because ^{238}U and ^{232}Th themselves do not emit strong gamma rays, their activity concentrations are usually determined indirectly through their decay products, assuming secular equilibrium (UNSCEAR, 2000; IAEA, 2007).

4.3 Calibration and Efficiency Determination

Accurate gamma spectrometric analysis requires energy and efficiency calibration of the detector system. Energy calibration is performed using standard radioactive sources with known gamma energies, while efficiency calibration is conducted using reference materials that match the geometry and density of the measured samples.Efficiency calibration is one of the most critical steps, as it directly influences the accuracy of calculated activity concentrations. Monte Carlo simulations or certified reference materials (CRMs) are often used to improve calibration accuracy, especially for complex geometries such as Marinelli beakers (IAEA, 2004).

4.4 Activity Concentration Calculation

The activity concentration (A) of a radionuclide is calculated using the following general equation:

$$A = C / (\varepsilon \times P\gamma \times m \times t)$$

where:C ; net peak count rate, ε ; detector efficiency at specific gamma energy, Pγ ; gamma emission probability, m ; mass of the sample (kg) and t = counting time (s).This formulation ensures that detector response, measurement time, and radionuclide decay probabilities are properly accounted for.

4.5 Minimum Detectable Activity (MDA)

The sensitivity of gamma spectrometric measurements is expressed through the Minimum Detectable Activity (MDA), which represents the lowest activity level that can be statistically distinguished from background radiation. MDA depends on background count rate, counting time, detector efficiency, and sample mass. Lower MDA values are achieved by using longer counting times, low-background shielding (commonly lead shielding), and high-efficiency detectors. In environmental radioactivity studies, particularly those involving building materials, achieving low MDA is essential for accurate quantification of low-level radionuclides (IAEA, 2004).

4.6 Quality Assurance and Uncertainty Analysis

Quality assurance is a critical component of radiometric analysis. It includes regular calibration checks, background measurements, use of certified reference materials, and interlaboratory comparisons. Measurement uncertainty arises from counting statistics, efficiency calibration, sample heterogeneity, and decay corrections. Most studies report combined uncertainties ranging from 5% to 15%, depending on radionuclide concentration and measurement conditions (Turhan et al., 2018).

4.7 Alternative and Complementary Techniques

Although HPGe gamma spectrometry is the primary method for NORM analysis, several complementary techniques may also be used;Alpha spectrometry: Used for direct measurement of alpha-emitting radionuclides such as ^{238}U and ^{232}Th after chemical separation.Liquid scintillation counting (LSC): Commonly used for radon and low-energy beta emitters.Inductively Coupled Plasma Mass Spectrometry (ICP-MS): Provides ultra-trace elemental concentrations of uranium and thorium.Radon exhalation measurements: Used to

assess radon release rates from building materials under controlled conditions.However, these techniques often require complex sample preparation and are not as widely applied in routine building material studies as gamma spectrometry.

4.8 Application in Turkish Studies

In Türkiye, most studies on building materials have employed HPGe gamma spectrometry due to its reliability and non-destructive nature. Research conducted on cement, clay bricks, pumice, volcanic tuff, and natural stones has consistently followed similar methodologies, enabling comparison across different regions (Turhan et al., 2015; Turhan et al., 2018; Özdiş et al., 2017).These standardized approaches have allowed researchers to establish a comprehensive database of natural radioactivity levels in Turkish construction materials, forming the basis for radiological risk assessments and regulatory evaluations.

5. RADIOLOGICAL HEALTH RISK ASSESSMENT

The evaluation of radiological health risks associated with Naturally Occurring Radioactive Materials (NORM) in building materials is a critical component of environmental radiation protection. Since structural materials such as cement, concrete, bricks, and natural stones contain varying concentrations of ^{226}Ra, ^{232}Th, and ^{40}K, their long-term use in buildings may contribute to external gamma exposure and internal exposure through radon inhalation. To standardize risk evaluation, several radiological hazard indices have been developed by international organizations such as UNSCEAR, the International Atomic Energy Agency (IAEA), and the European Commission (UNSCEAR, 2000; IAEA, 2007; European Commission, 1999).

5.1 Radium Equivalent Activity (Ra_{eq})

Radium equivalent activity (Raeq) is a widely used index that provides a single parameter to describe the gamma output from ^{226}Ra, ^{232}Th, and ^{40}K in building materials. It is based on the assumption that 370 Bq/kg of ^{226}Ra, 259 Bq/kg of ^{232}Th, and 4810 Bq/kg of ^{40}K produce the same gamma dose rate.

The Raeq is defined as:

$$Ra_{eq}\ (Bq/kg) = A_{Ra} + 1.43\ A_{Th} + 0.077\ A_K$$

Where; A_{Ra}, A_{Th}, and A_K are the activity concentrations of ^{226}Ra, ^{232}Th, and ^{40}K, respectively.According to the European Commission (1999), Raeq should not exceed 370 Bq/kg for safe use of materials in dwellings. Most building

materials studied in Türkiye generally remain below this limit, although volcanic-origin materials may approach higher values (Turhan et al., 2015; Turhan et al., 2018).

5.2 Absorbed Gamma Dose Rate (D)

The absorbed gamma dose rate in indoor air at 1 m above ground is calculated using activity concentrations of radionuclides:

$$D\ (nGy/h) = 0.92\ A_{Ra} + 1.10\ A_{Th} + 0.08\ A_K$$

This parameter represents the external exposure due to gamma radiation emitted from building materials.

(UNSCEAR ,2000) reports a global average outdoor terrestrial gamma dose rate of approximately 60 nGy/h, while indoor values are typically higher due to building material contribution. In Turkish studies, dose rates vary depending on material type and geological origin, with higher values generally observed in volcanic tuffs and granitic materials (Turhan et al., 2015).

5.3 Annual Effective Dose (AED)

The annual effective dose (AED) estimates the effective radiation dose received by individuals spending time indoors. It is calculated from absorbed dose rate using occupancy factors and dose conversion coefficients:

$$AED\ (mSv/y) = D \times 8760 \times 0.8 \times 0.7 \times 10^{-6}\ (indoor)$$

Where, 8760 = hours per year, 0.8 = indoor occupancy factor, 0.7 Sv/Gy = dose conversion coefficient

The worldwide average annual effective dose from natural sources is approximately 2.4 mSv/year, of which indoor terrestrial gamma radiation contributes a significant portion (UNSCEAR, 2008). Studies in Türkiye indicate that AED values from building materials generally remain within recommended limits.

5.4 External and Internal Hazard Indices

To assess potential radiological hazards, two important indices are used:

External Hazard Index (Hex): Hex evaluates external gamma radiation hazard and is defined as:

$$H_{ex} = A_{Ra}/370 + A_{Th}/259 + A_K/4810$$

For safe use, Hex must be less than 1.Internal Hazard Index (Hin): Hin accounts for internal exposure due to radon inhalation and is defined as:

$$H_{in} = A_{Ra}/185 + A_{Th}/259 + A_K/4810$$

Hin should also be less than 1 to ensure radiological safety.Radon contribution is particularly important because ^{226}Ra decay produces ^{222}Rn gas, which can accumulate indoors and significantly increase lung cancer risk (IAEA, 2003; UNSCEAR, 2008).

5.5 Gamma Activity Concentration Index (Iγ)

The gamma index (Iγ) is recommended by the European Commission for assessing compliance of building materials:

$$I\gamma = ARa/300 + ATh/200 + AK/3000$$

Interpretation, $I\gamma \leq 1$ → material is safe for use in bulk quantities, $1 < I\gamma \leq 6$ → restricted use may be required.This index is particularly useful for regulatory screening of construction materials (European Commission, 1999).

5.6 Radon Exhalation and Internal Exposure

Radon exhalation from building materials is a major contributor to internal radiation dose. The rate of radon release depends on ^{226}Ra content, porosity, moisture, and diffusion properties of materials.

Materials such as pumice, tuff, and certain granites may exhibit higher radon exhalation rates compared with dense carbonate rocks. Once released, radon and its short-lived progeny (^{218}Po, ^{214}Pb, ^{214}Bi) contribute to alpha radiation dose in the respiratory system (IAEA, 2003; UNSCEAR, 2008).

Although most Turkish studies report radon levels within acceptable limits, localized variations emphasize the importance of ventilation and material selection in building design (Turhan et al., 2015).

5.7 Interpretation of Radiological Risk in Turkish Building Materials

Studies conducted in Türkiye consistently show that cement, concrete, clay bricks, and most natural stones exhibit Raeq, Hex, Hin, and Iγ values below internationally recommended limits (Baş et al., 2025; Turhan et al., 2018; Özdiş

et al., 2017). However, volcanic-origin materials such as pumice and tuff may present relatively higher values due to elevated uranium and thorium content.

Despite these variations, overall radiological risk from commonly used construction materials in Türkiye is generally considered low. Nevertheless, continuous monitoring is recommended, particularly in regions with volcanic geology, to ensure long-term radiation protection compliance.

6. CRITICAL REVIEW OF STUDIES CONDUCTED IN TÜRKİYE

Research on Naturally Occurring Radioactive Materials (NORM) in building materials in Türkiye has expanded significantly over the last two decades, largely driven by increased awareness of indoor radiation exposure and the availability of high-resolution gamma spectrometry systems. The majority of studies focus on the determination of ^{226}Ra, ^{232}Th, and ^{40}K activity concentrations in commonly used construction materials such as cement, concrete, bricks, natural stones, pumice, and volcanic tuff, followed by radiological hazard assessment using internationally standardized indices (Baş et al., 2025; Baykara et al., 2011; Solak et al., 2014; Turhan et al., 2008, 2015, 2018; Özdiş et al., 2017; UNSCEAR, 2008).Most investigations conducted in Türkiye employ a similar methodological framework based on HPGe gamma-ray spectrometry, long counting times, and secular equilibrium assumptions for uranium and thorium decay series. This methodological consistency enables meaningful comparison between different regions and material types (IAEA, 2007).

Studies are geographically distributed across various geological provinces, including Central Anatolia, Western Anatolia, Eastern Anatolia, and the Mediterranean region. This spatial diversity is particularly important because Türkiye's complex geology comprising volcanic fields, granitic intrusions, sedimentary basins, and metamorphic zones directly influences radionuclide distribution in construction materials (UNSCEAR, 2000).

6.1 Cement and Concrete Studies

Cement and concrete have been extensively studied due to their widespread use in residential and industrial construction. Research indicates that activity concentrations in cement generally reflect the composition of raw materials such as limestone and clay, with moderate contributions from uranium, thorium, and potassium-bearing minerals. Özdiş et al. (2017) reported that cement samples used in Türkiye typically exhibit radionuclide concentrations within global average ranges. Similarly, concrete samples show slightly higher variability due to the influence of aggregates, which may originate from different geological sources. Overall, cement-based materials in Türkiye are consistently reported to

comply with international radiological safety limits defined by the European Commission and IAEA guidelines (European Commission, 1999; IAEA, 2007).

6.2 Clay Bricks and Ceramic Materials

Clay bricks and ceramic materials are significant contributors to indoor radiation exposure due to their high surface area and widespread use in building interiors. Studies indicate that these materials often contain relatively higher ^{40}K activity concentrations compared with cement and concrete, due to potassium-rich clay minerals. Turhan et al. (2018) demonstrated that brick samples and pumice-based construction materials exhibit noticeable variability in radionuclide content depending on raw material origin and manufacturing conditions. However, even in cases where activity concentrations are elevated, calculated hazard indices generally remain within permissible limits.

6.3 Volcanic Tuff and Pumice Materials

Volcanic-origin materials such as tuff and pumice are widely used in Türkiye, particularly in Central Anatolia and Eastern Anatolia regions. These materials are of special interest because they may contain higher concentrations of uranium and thorium due to magmatic differentiation processes. Turhan et al. (2015) reported that volcanic tuff stones used as ornamental and structural materials exhibit relatively higher gamma dose rates compared with sedimentary rocks. Nevertheless, calculated radiological hazard indices such as Raeq, Hex, and Iγ were generally below recommended safety thresholds.

This indicates that although volcanic materials may show elevated natural radioactivity relative to other construction materials, their use in building applications does not typically pose significant radiological risk under normal conditions.

6.4 Natural Stones (Granite, Marble, Basalt, Travertine)

Natural stones used in Türkiye show strong lithological dependence in terms of radionuclide content. Granitic rocks generally contain higher concentrations of ^{238}U and ^{232}Th due to their felsic composition, whereas carbonate rocks such as marble and travertine exhibit lower activity levels. Basaltic rocks typically present intermediate radionuclide concentrations, reflecting their mafic composition. These variations highlight the importance of geological origin in determining radiological characteristics of construction materials.Across studies, most natural stones used in Türkiye remain within internationally accepted radiological safety limits, although granite occasionally shows higher values compared to other stone types.

6.5 Radiological Hazard Indices in Turkish Studies

A common feature across Turkish studies is the application of standardized radiological hazard indices, including radium equivalent activity (Raeq), absorbed dose rate (D), annual effective dose (AED), external hazard index (Hex), internal hazard index (Hin), and gamma index (Iγ).

In general, reported values for these indices remain below internationally recommended limits:

$$Raeq < 370\ Bq/kg;\ \ Hex < 1;\ \ Hin < 1;\ I\gamma \leq 1$$

These results suggest that most building materials used in Türkiye do not pose significant radiological health risks to occupants (UNSCEAR, 2008; IAEA, 2007). However, variability among material types and regions indicates that localized assessments are necessary rather than relying solely on national averages.

6.6 Comparative Evaluation of Regional Differences

Regional differences in radionuclide concentrations are strongly influenced by geological variability. Volcanic regions tend to exhibit higher activity concentrations compared with sedimentary basins. For example, Central Anatolia and parts of Eastern Anatolia, which are rich in volcanic deposits, show relatively higher values in pumice and tuff-based materials. In contrast, Western Anatolia and coastal sedimentary regions generally produce construction materials with lower radionuclide content. These differences underline the importance of source material selection in construction practices.

6.7 Research Limitations and Methodological Considerations

Despite the increasing number of studies, several limitations exist in the Turkish NORM literatüre;

1. Limited radon exhalation data: Most studies focus on gamma-emitting radionuclides, while radon exhalation measurements remain relatively scarce.2. Small sample sizes: Many studies analyze limited numbers of samples, reducing statistical representativeness.3. Lack of long-term monitoring: Temporal variations in radionuclide concentrations are rarely considered.4. Inconsistent material classification: Different studies sometimes use varying definitions for material categories, making comparisons difficult.Addressing these limitations would significantly improve the robustness of radiological assessments in future research.The collective evidence from Turkish studies indicates that natural radioactivity levels in structural building materials are generally within safe limits defined by international organizations. While volcanic-origin materials may exhibit

elevated radionuclide concentrations compared to sedimentary materials, their contribution to overall radiation exposure remains within acceptable bounds under normal usage conditions. Nevertheless, continued monitoring and more comprehensive datasets are necessary to ensure long-term radiological safety, particularly in regions with active volcanic geology or extensive use of natural stone materials.

10. CONCLUSIONS

This review comprehensively evaluated the presence of Naturally Occurring Radioactive Materials (NORM) in structural building materials used in Türkiye and assessed the associated radiological health risks. The analyzed literature demonstrates that the primary radionuclides of concern in construction materials are ^{226}Ra, ^{232}Th, and ^{40}K, which originate from primordial decay series and are naturally embedded in geological formations.The findings from Turkish studies indicate that the activity concentrations of these radionuclides vary significantly depending on geological origin, mineral composition, and industrial processing of materials. Volcanic-derived materials such as pumice and tuff generally exhibit relatively higher radionuclide concentrations compared with sedimentary carbonate-based materials such as limestone, marble, and travertine. Clay-based materials and ceramics tend to show elevated ^{40}K activity due to potassium-rich mineral phases.Despite these variations, radiological hazard indices including radium equivalent activity (Raeq), external hazard index (Hex), internal hazard index (Hin), gamma index (Iγ), absorbed gamma dose rate, and annual effective dose (AED) are generally reported to be within internationally accepted safety limits established by the European Commission, IAEA, and UNSCEAR. This indicates that commonly used structural building materials in Türkiye do not pose significant radiological health risks under normal conditions of use. However, the review also highlights important research gaps, particularly the limited number of radon exhalation studies, insufficient large-scale regional datasets, and lack of long-term monitoring of building material radioactivity. Given Türkiye's complex geological structure, localized assessments remain essential to ensure accurate radiological risk evaluation.Future research should focus on expanding datasets across different geological provinces, integrating radon exhalation measurements with gamma spectrometry data, and developing standardized national databases for building material radioactivity. Such efforts would strengthen radiation protection policies and contribute to safer construction practices. Overall, while natural radioactivity in Turkish building materials is generally within safe limits, continuous monitoring and improved methodological consistency are recommended to maintain radiological safety in the built environment.

REFERENCES

[1] Çetin, B. & Akkurt, I. (2010). Natural radioactivity and radiation hazards in some building materials used in Isparta, Turkey. *Radiation Physics and Chemistry*, 79 (9): 933-937.

[2] Eissa, M.F., Mostafa, R.M., Shahin, F., Hassan, K.F., & Saleh, Z.A. (2008). Natural radioactivity of some Egyptian building materials. International Journal of Low Radiation 5(1), 1.

[3] Turhan, Ş., Baykan, U.N. & Sen, K. (2008). Measurement of the natural radioactivity in building materials used in Ankara and assessment of external doses. *Journal of Radiological Protection*, 28(1):83-91

[4] Erkan, A., (2007). An Investigation on the Natural Radioactivity of Building Materials, Raw Materials and Interior Coatings in Central Turkey. *Turkish Journal of Medical Sciences* 37(4), 199-203.

[5] Erees, F.S., & Kaynar S.Ç. (2006). Natural radionuclides in building materials used in Manisa City, Turkey. Indoor and Built Environment 15(5), 495-498.

[6] European Commission, 1999. Radiological Protection Principles Concerning the Natural Radioactivity of Building Materials. Radiation Protection Report 112. Luxembourg.

[7] Özdiş, B.E., Çam, N.F., & Canbaz Öztürk, B. 2017. Assessment of natural radioactivity in cements used as building materials in Turkey. *Journal of Radioanalytical and Nuclear Chemistry,* 311, 307-316.

[8] IAEA, 2003. Radiation Protection against Radon in Workplaces Other than Mines. Safety Reports Series No. 33. Vienna.

[9] IAEA, 2004. Measurement of Radionuclides in Food and the Environment. Technical Reports Series No. 295. Vienna.

[10] IAEA, 2005. Naturally Occurring Radioactive Materials (NORM IV). TECDOC-1472. Vienna.

[11] IAEA, 2007. Assessing the Need for Radiation Protection Measures in Work Involving Minerals and Raw Materials. Safety Reports Series No. 49. Vienna.

[12] Baş, M., Mavi, A., & Yıldız Yorgun, N. (2025). Natural Radionuclide Analysis in Building Materials Used in Bursa. *Yuzuncu Yil University Journal of the Institute of Natural & Applied Sciences*. 30(2), 524-536.

[13] Tufan, M.Ç., & Dişci, T. (2013). Natural radioactivity measurements in building materials used in Samsun, Turkey. *Radiation Protection Dosimetry*, 156 (1), 87–92.

[14] Baltas, H., Kırıs, E., Ustabas, I., Yılmaz, E., Sırın, M., Kuloglu, E., & Erdogan Gunes, B. (2014). Determination of Natural Radioactivity Levels

of Some Concretes and Mineral Admixtures in Turkey. *Asian Journal of Chemistry*, 26 (13), 3946-3952.

[15] Baykara, O., Karatepe, Ş. & Doğru, M. (2011). Assessments of natural radioactivity and radiological hazards in construction materials used in Elazig, Turkey. *Radiation Measurements*, 46, 153-158.

[16] Solak, S., Turhan, Ş., Uğur, F. A., Gören, E., Gezer, F., Yeğingil, Z., & Yeğingil, İ. (2014). Evaluation of potential exposure risks of natural radioactivity levels emitted from building materials used in Adana, Turkey. *Indoor and Built Environment*, 23 (4), 594-602.

[17] Turhan, Ş., Atıcı, E., & Varinlioğlu, A. (2015). Radiometric analysis of volcanic tuff stones used as ornamental and structural building materials in Turkey and evaluation of radiological risk. *Radioprotection*, 50 (4), 273–280.

[18] Turhan, Ş., Demir, K., & Karataşlı, M. (2018). Radiological evaluation of the use of clay brick and pumice brick as a structural building material. *Applied Radiation and Isotopes*, 141, 95–100.

[19] UNSCEAR, 2000. Sources and Effects of Ionizing Radiation. United Nations, New York.

[20] UNSCEAR, 2008. Sources and Effects of Ionizing Radiation. United Nations, New York.

Chapter 18

Applications of Radon In Earthquake Forecasting and Geohazard Assessment

Mehmet ERDOĞAN[1]

1. INTRODUCTION

Radon is a naturally occurring radioactive noble gas generated in the Earth's crust through the radioactive decay of radium isotopes. The three naturally occurring isotopes of radon are ^{222}Rn (radon), ^{220}Rn (thoron), and ^{219}Rn (actinon), which are produced by the decay of ^{226}Ra, ^{224}Ra, and ^{223}Ra, respectively, in the ^{238}U, ^{232}Th, and ^{235}U decay series as shown in Fig. 1 [1]. During the α-decay of radium, the newly formed radon atom receives recoil energy, which may displace it from its original position within the mineral lattice. If the decay occurs sufficiently close to a mineral grain surface, the recoiling radon atom may escape into an adjacent pore space. This process, known as radon emanation, determines the fraction of radon that becomes available for subsequent transport. Once released into pore spaces, radon can migrate through the pore network by diffusion and advection, depending on the physical properties of the porous medium and the prevailing pressure and fluid-flow conditions. Because radon is soluble in water, a fraction of the radon released from mineral grains can dissolve in pore water and groundwater. Its solubility generally decreases with increasing temperature, which can influence the partitioning and transport of radon between the aqueous and gas phases. In interconnected aquifers, dissolved radon may subsequently be transported by groundwater flow, whereas radon in the gas phase can migrate through soil pores and fractures and may eventually be released into the atmosphere through soil exhalation [2].

The amount of radon available for migration is strongly influenced by the concentration and distribution of radium in rocks and soils, as well as by the physical properties of the geological medium. Although some general trends can be identified among different rock types, radium concentrations may vary considerably within the same lithological group. Granitic rocks commonly contain relatively high concentrations of radium, whereas many sedimentary and metamorphic rocks generally show intermediate concentrations, while basalts and many limestones tend to have lower concentrations. However, substantial exceptions occur because radium

[1]Prof. Dr., Department of Physics, Faculty of Science, Selçuk University, Türkiye, merdogan@selcuk.edu.tr, meerdogan291@gmail.com, (ORCID: 0000-0003-1879-8500)

distribution is controlled by mineral composition, weathering, depositional history, and other geological processes. Soil radium concentrations are likewise highly variable and may reflect both the characteristics of the underlying bedrock and the composition of the overlying materials. In addition to radium content, the emanation and subsequent migration of radon are strongly affected by porosity, permeability, moisture content, and the presence of fractures and fissures. These properties control the availability of connected pathways through which radon can migrate from mineral grains into pore spaces and subsequently toward the surface. Consequently, variations in lithology, soil properties, and subsurface structure can produce substantial spatial differences in radon concentrations even within relatively small geographic areas [2].

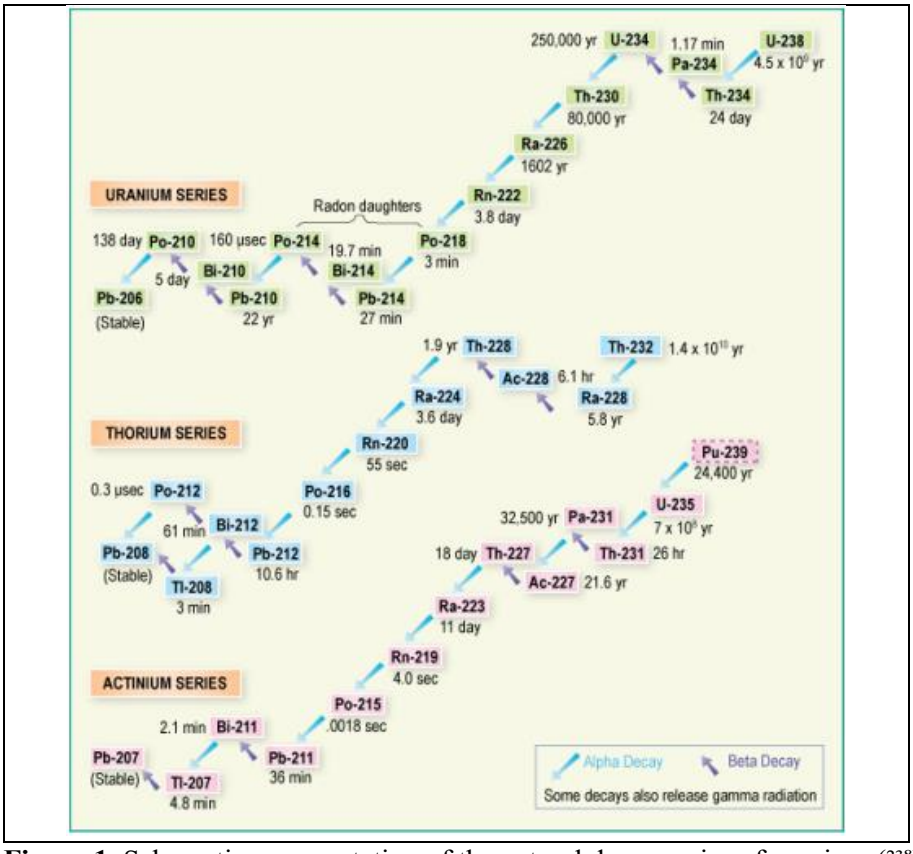


Figure 1. Schematic representation of the natural decay series of uranium (^{238}U and ^{235}U) and thorium (^{232}Th), illustrating the decay mode (α or β^-) and the half-life of each radionuclide [1].

Radon generated at greater depths may migrate toward the surface through advective transport in the gas phase and through groundwater flow. Carrier gases such as carbon dioxide (CO_2), methane (CH_4), hydrogen (H_2), helium (He), and nitrogen (N_2) may facilitate the upward transport of radon from deeper geological formations under favorable subsurface conditions [3]. Groundwater can also transport dissolved radon through interconnected pore spaces and fractures. Faults, fractures, fissures, and other highly permeable structures can provide preferential pathways for the upward migration of radon-bearing gases and groundwater [3]. The transport and accumulation of radon in soil gas, groundwater, and the atmosphere are therefore governed by the combined effects of geological, hydrogeological, and atmospheric conditions [4,5,6]. These characteristics have made radon a useful natural geochemical tracer in a variety of geological and environmental applications. In particular, radon measurements have been used in uranium exploration to identify areas with elevated uranium mineralization [7,8]. The application of radon measurements to the investigation of seismic activity emerged later, with Okabe (1956) reporting one of the earliest observations of a possible relationship between atmospheric radon variations and local seismic activity [9]. This observation stimulated subsequent research into the potential use of radon as a geochemical indicator in earthquake studies.

These properties have made radon a useful natural geochemical tracer in a variety of geological and environmental applications. In particular, radon measurements have been applied in uranium exploration as a means of identifying areas potentially associated with uranium-bearing formations [7,8]. Radon has also been investigated in relation to geological and environmental processes, including subsurface fluid circulation and structural discontinuities. One of the early observations linking radon variations to seismic activity was reported by Okabe (1956), who investigated variations in atmospheric radon concentration in relation to local seismic activity in Japan [9]. This observation contributed to subsequent research on the potential use of radon measurements as a geochemical indicator of seismic activity and, later, in the context of earthquake forecasting. Beyond their application to seismic activity, variations in radon concentrations have also been investigated as potential indicators of various geological and environmental processes and hazards, including active faulting, volcanic activity, sinkhole formation, geothermal activity, and groundwater circulation [1,4,10-13]. However, the interpretation of radon variations in relation to seismic activity remains challenging because radon concentrations are influenced by multiple geological, hydrogeological, and meteorological factors [4,5,6]. Therefore, evaluating the potential application of radon monitoring to

earthquake forecasting requires long-term observations and, preferably, simultaneous monitoring of other environmental and geophysical parameters.

2. HISTORICAL DEVELOPMENT AND CURRENT STATUS OF RADON RESEARCH IN EARTHQUAKE FORECASTING

Radon gas emissions are used as a tracker of moving air and groundwater masses to monitor groundwater movements and determine uranium deposits on Earth [1,7,8]. In addition, Okabe investigated temporal variations in atmospheric radon concentration in relation to local seismicity in Japan, providing one of the early observations that stimulated subsequent research into the possible relationship between radon anomalies and seismic activity [9]. Many studies have reported anomalous variations in radon concentrations in groundwater and soil gas in association with seismic activity, suggesting that radon anomalies may serve as potential geochemical indicators of subsurface processes related to earthquakes. Changes in crustal stress and strain may modify rock permeability and fluid pathways, potentially affecting the transfer of radon from rocks into groundwater and soil gas [4,11,14,15]. Research on radon anomalies associated with seismic activity, measurements of soil gas along fault lines, which can act as preferential pathways for the emission of crustal gases, and radon concentrations in spring waters, together with other gas measurements, can be influenced by meteorological factors such as atmospheric pressure, temperature, and precipitation, as well as by geological and structural conditions [4,5,6,11,15,16]. During periods of increased tectonic stress, enhanced gas flow through permeable fault zones may therefore produce detectable radon anomalies in soil gas, groundwater, and, in some cases, near-surface air [4].Many studies have indicated that abnormal changes in radon gas, which originates from the Earth and is soluble in water, in groundwater and soil gas can be a possible geochemical signal associated with seismic activity for many earthquakes, and that these radon anomalies can be a useful geochemical tracer in seismic events. Long-term measurements of radon activity are crucial for identifying these anomalies. Some of these studies are as follows:Press (1975) reported radon anomalies in well water in association with the magnitude 5.3 earthquake in Tashkent, Uzbekistan in 1966 and the subsequent magnitude 4.0 aftershock in 1967. As shown in figure -2, radon activity in well water increased before the seismic events and decreased after the earthquakes [17].

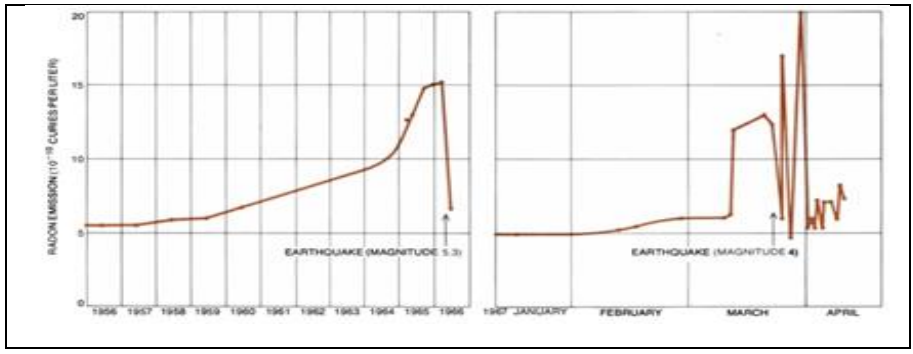


Figure 2. Variation of radon emission in water from deep wells before and after the 1966 magnitude 5.3 Tashkent earthquake (left) and the 1967 magnitude 4.0 earthquake (right) [17].

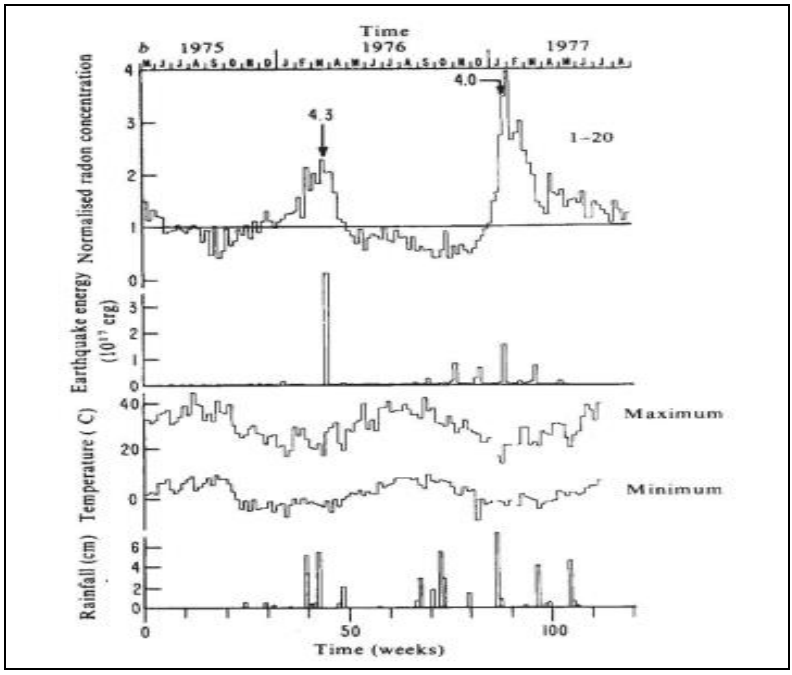


Figure 3. Temporal variation of normalized radon concentration, earthquake energy, maximum and minimum air temperatures, and rainfall at a monitoring site along the San Andreas Fault from 1975 to 1977 [18].

King (1978) monitored radon emissions weekly along an active section of the San Andreas Fault in central California from early May 1975 to late August 1977. The study revealed temporal variations in radon concentration that appeared to be associated with local seismic activity. As shown in Figure-3, distinct radon peaks occurred at the times of two relatively large earthquakes of magnitudes 4.3

and 4.0. In both cases, radon concentrations appeared to increase before and decrease after the seismic events. The study also considered meteorological parameters, including maximum and minimum temperature and precipitation, which could contribute to variations in radon concentration [18]. reported a precursory change in groundwater radon concentration before the magnitude 7.0 Izu-Oshima-kinkai earthquake in Japan on January 14, 1978. Continuous radon monitoring was conducted at a station approximately 25 km from the earthquake epicenter. On January 9, about five days before the earthquake, the radon concentration exhibited a sudden decrease followed by a subsequent increase. A remarkable increase in radon concentration was also observed after the earthquake. These observations were interpreted as a possible relationship between changes in groundwater radon concentration and the earthquake [19].Investigated the relationship between the Wenchuan (Ms = 8.0; 12 May 2008) and Lushan (Ms = 7.0; 20 April 2013) earthquakes along the Longmenshan Fault in China and variations in water and gas radon concentrations. Data on water radon, gas radon, groundwater level, and water temperature collected from monitoring stations between 2002 and 2014 were analyzed. The results revealed pronounced variations in radon concentrations around the periods of both earthquakes. The temporal variations in water radon concentrations recorded at the Guza and Ya'an stations are presented in Fig. 4. At Guza, water radon concentration decreased approximately 10 days before the Lushan earthquake, followed by a pronounced increase, while a sharp decrease was observed approximately 15 days before the Wenchuan earthquake (as shown Fig. 4a). At Ya'an, increases in water radon concentration were observed approximately two weeks before both earthquakes (as shown Fig. 4b). An inverse relationship between water radon concentration and groundwater level was also observed at Guza station prior to the Wenchuan earthquake. The temporal variation in gas radon concentration and groundwater level at Huize station is shown in Figure 4c,d. A pronounced peak in gas radon concentration was observed several days before the Wenchuan earthquake, whereas a sharp decrease occurred approximately five days before the Lushan earthquake. The study also showed that water radon concentrations were strongly influenced by seasonal and hydrological factors, particularly rainfall and groundwater-level variations. The authors suggested that some radon anomalies may be associated with changes in the stress regime, subsurface fracturing, and groundwater conditions. However, the magnitude and direction of the anomalies varied among the monitoring stations. Therefore, although radon variations may provide useful information on subsurface changes associated with seismic activity, radon alone cannot currently be regarded as a reliable tool for short-term earthquake forecasting [6].

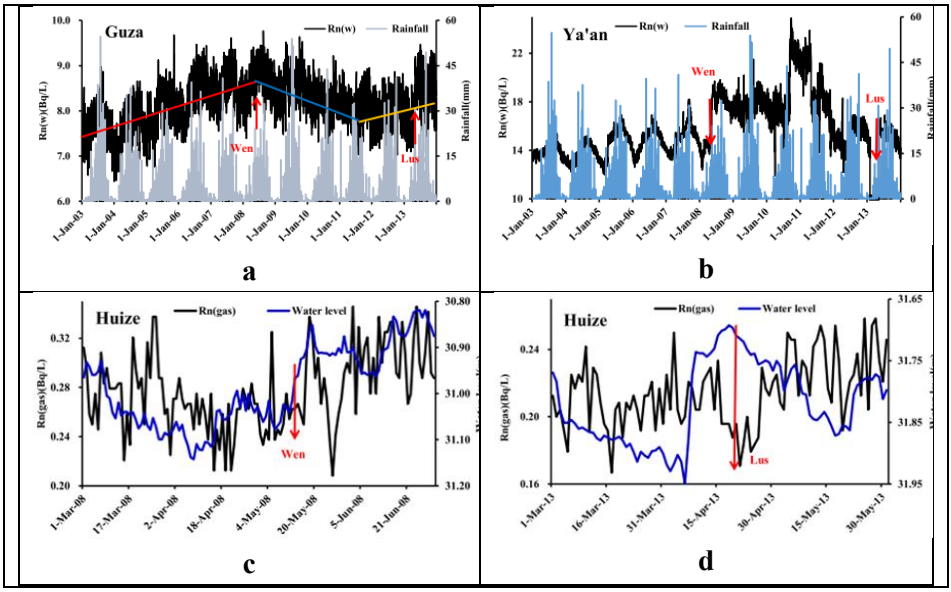


Figure 4. Temporal variations in radon concentration, rainfall, and groundwater level at selected monitoring stations along the Longmenshan Fault in relation to the Wenchuan and Lushan earthquakes: (a) water radon concentration and rainfall at the Guza station, (b) long-term variations in water radon concentration and rainfall at the Ya'an station, (c) gas radon concentration and groundwater level at the Huize station associated with the Wenchuan earthquake, and (d) gas radon concentration and groundwater level at the Huize station associated with the Lushan earthquake [6].

In a 26-year monitoring study covering 1994–2020, Zhou et al. (2020) reported significant radon anomalies in water at the Panjin observation station before earthquakes with magnitudes of $4.8 \leq M \leq 7.0$ occurring within a radius of 300 km. A significant increase in radon concentration in the water was observed in the 80 days before the 1999 Xiuyan earthquake, while a significant decrease was observed after the earthquake. Before the 4.8 magnitude Dengta and 5.0 magnitude Horqin earthquakes in 2013, a V-shaped change in radon concentration in the water was observed, followed by low values. However, it was observed that the radon concentration in the water fluctuated for 2 years after the earthquakes before gradually reaching a high threshold of 1.2 times the standard deviation. In this study, it was stated that not only anomalies were observed in radon concentration values in water before earthquakes, but also fluctuations in Ca^{2+}, Mg^{2+} and Cl^{-} concentrations were observed [20].In another study, Erdogan et al. (2025) investigated possible radon anomalies in groundwater associated with in 2023, Pazarcık (MW 7.7) and Elbistan (MW 7.6)

earthquakes and subsequent aftershocks in the Hatay region of Türkiye. Radon activity, pH, and temperature were measured in water samples collected from nine groundwater sources during four measurement periods between March 17 and June 25, 2023. According to the results, significant radon anomalies were observed at two sites, Hamamat (site 6) and Tahtaköprü-1 (site 8), where radon activity changed by approximately a factor of five between measurements. In addition to changes in the pH and radon concentrations of water samples collected from these sites, strain effects associated with aftershocks of magnitude 3.5 and above were calculated. The results of this study are presented in Fig. 5. These radon variations were accompanied by significant changes in pH and coincided with periods of strong seismic activity and calculated strain effects, suggesting a possible relationship between the observed anomalies and earthquake-related crustal deformation. Although the authors suggested that the observed changes may be related to seismic activity and changes in groundwater conditions, they emphasized that the short monitoring period limits the ability to draw definitive conclusions. Therefore, they recommended long-term radon monitoring at these two sites to better determine the relationship between groundwater radon anomalies and seismic activity [11].

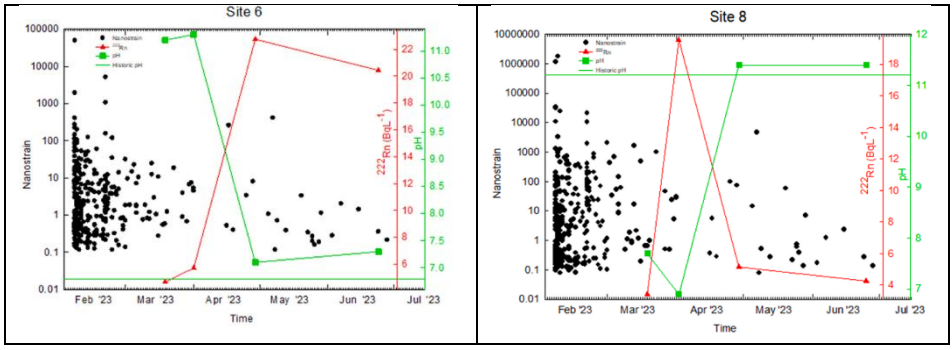


Figure 5. Temporal variations in radon activity, pH, temperature, aftershock activity, and calculated strain effects at the Hamamat (site 6, left) and Tahtaköprü-1 (site 8, right) groundwater sources following the February 6, 2023 earthquakes in the Hatay region, Türkiye [10].

3. CONCLUSIONS

Radon monitoring has emerged as a valuable geochemical approach for investigating subsurface processes associated with earthquakes and other geohazards. Its generation from radium-bearing rocks, mobility through pore spaces, groundwater, soil gas, and fault-related fractures, and sensitivity to changes in subsurface conditions make radon a potentially useful indicator of

crustal deformation and fluid–rock interactions. The studies reviewed in this chapter demonstrate that temporal and spatial variations in radon concentrations have been observed before, during, and after several earthquakes, particularly in groundwater and soil gas. However, the magnitude, direction, and timing of these anomalies are not consistent among different monitoring sites and seismic events. Moreover, radon concentrations can be strongly affected by meteorological, seasonal, hydrological, geological, and hydrogeological factors, which may complicate the identification of earthquake-related signals. Therefore, radon anomalies should not be interpreted as definitive evidence of an impending earthquake or as a stand-alone parameter for short-term earthquake prediction. Instead, long-term and continuous radon monitoring, combined with measurements of groundwater level, temperature, pH, major ion chemistry, other soil and carrier gases, meteorological parameters, and seismic activity, may provide a more reliable framework for distinguishing tectonic signals from environmental variations. In this context, radon should be regarded not as a deterministic earthquake prediction tool, but as a complementary geochemical indicator that can contribute to the assessment of subsurface processes, earthquake-related crustal deformation, and broader geohazards. Further long-term, multiparameter, and site-specific studies are required to clarify the physical mechanisms responsible for radon anomalies and to identify the environmental and tectonic conditions under which radon monitoring can provide meaningful information for earthquake forecasting and broader geohazard assessment.

REFERENCES

[1] Vinícius V. M. Ferreira, Raquel L. M. Fonseca, Zildete Rocha, Amanda L. Oliveira, Rubens M.Moreira, Nayron C. Lemos, Cláudio J. Chagas, Maria Angela B. C. Menezes & Talita O. Santos, 2015. Use of Radon as Water Tracer at Juatuba Basin. Journal of Geography and Geology, 7(3), 49-60.

[2] UNSCEAR (United Nations Scientific Committee on the Effects of Atomic Radiation), 2000. Sources and Effects of Ionizing Radiation, Annex B.

[3] Ciotoli, G., Bilgi, S., Tartarello, C., Sacco, P., Lombardi, S., Ascione, A., Mazzoli, S., 2013. Soil gas distribution in the main coseismic surface rupture zone of the 1980, Ms = 6.9, Irpinia earthquake (southern Italy). Journal of Geophysical Research: Solid Earth, 119, 2440–2461.

[4] Woith, H., 2015. Radon earthquake precursor: A short review. Eur. Phys. J. Special Topics, 224(4), 611–627.

[5] Ülküm, Ö., Taşköprü, C., İçhedef, M., Saç, M.M., Kumru, M.N., 2018. Ground water radon anomalies in Bodrum Peninsula. Terra Nova, 30(2), 152–161.

[6] Ye, Q., Singh, R. P., He, A., Ji, S., and Liu, C., 2015. Characteristic behavior of water radon associated with Wenchuan and Lushan earthquakes along Longmengshan fault. Radiation Measurements, 76, 44–53.

[7] George, A.C., 2008. World history of radon research and measurement from the early 1900's to today. 8th International Symposium on Natural Radiation Environment, AIP Conf. Proc., 1034, 20–33.

[8] Wattananikorn, K., Techakosit, S., & Jitaree, N., 1995. A combination of soil gas radon measurements in uranium exploration. Nuclear Geophysics, 9(6), 643–652.

[9] Okabe, S., 1956. Time variation of the atmospheric radon content near the ground surface with relation to some geophysical phenomena. Memoirs of the College of Science, University of Kyoto, Series A, 28, 99-115.

[10] Schubert, M., Knoeller, K., Mueller, C., Gilfedder, B., 2020. Investigating River Water/Groundwater Interaction along a Rivulet Section by 222Rn Mass Balancing. Water, 12, 3027, DOI:10.3390/w12113027.

[11] Erdogan, M., Atav, U., Manisa K., Acar, M., Satılmış, H., Bozdag, A., 2025. Radon anomalies in water sources in Hatay region after the 2023 Kahramanmaras earthquake. Journal of Environmental Radioactivity 290,107792.

[12] Giammanco, S., Maiolino, V., Ursino, A., Neri, M., Frasca, L., Maugeri, SR., Murè, F., Principato, P., 2026. Integrated Monitoring of Soil Radon Gas and Seismic Activity to Detect Volcanic Unrest at Mount Etna (Italy), 2023–2025. Quaternary, 9(1), 16, doi:10.3390/quat9010016.

[13] Tuccimei, P., Salvati, R., Capelli, G., Delitala, M.C., Primavera, P., 2005. Groundwater fluxes into a submerged sinkhole area, Central Italy, using radon and water chemistry. Applied Geochemistry, 20, 1831–1847.

[14] Ghosh, D., Deb A., Sengupta, R., 2009. Anomalous radon emission as precursor of earthquake. Journal of Applied Geophysics, 69(2), 67-81.

[15] Manisa, K., Erdogan, M., Zedef, V., Bircan, H., Bicer, A., 2022. Variations of 222Rn concentrations over active fault system in Simav, Kütahya, Western Turkey: Possible causes for soil-gas ^{222}Rn anomalies. Applied Radiation and Isotopes, 190, 110484.

[16] Friedmann, H., Aric, K., Gutdeutsch, R., King, C.Y., Altay, C., & Sav, H. (1988). Radon measurements for earthquake prediction along the North Anatolian Fault Zone: a progress report. Tectonophysics, 152(3–4), 209–214. DOI: 10.1016/0040-1951(88)90047-9.

[17] Press, F., 1975. Earthquake Prediction. Scientific American, 232(5), 14–23.

[18] King, C.Y., 1978. Radon emanation on San Andreas Fault. Nature, 271(5645), 516–519.

[19] Wakita, H., Nakamura, Y., Notsu, K., Noguchi, M., & Asada, T., 1980. Radon anomaly: A possible precursor of the 1978 Izu-Oshima-kinkai earthquake. Science, 207(4433), 882–883.

[20] Zhou, Z., Tian, L., Zhao, J., Wang, H., Liu, J., 2020. Stress-Related Pre-Seismic Water Radon Concentration Variations in the Panjin Observation Well, China (1994–2020). Frontiers in Earth Science, 8, 596283.

Chapter 19

Natural Radiation: Sources and Human Exposure

Fatih ÖZDEMİR[1], Mehmet ERDOĞAN[2]

1. INTRODUCTION

All living things, including humans, are exposed to natural radiation originating from naturally occurring radioactive nuclei. Radioactive nuclei are unstable systems that undergo radioactive decay by emitting particles, such as alpha and beta particles, or electromagnetic radiation, such as gamma rays. As a result, materials containing these radionuclides exhibit radioactive properties. The particles and electromagnetic radiation emitted during radioactive decay are forms of ionizing radiation when they possess sufficient energy to ionize atoms or molecules. Natural radiation comes from two main sources: cosmic radiation and radiation emitted during the radioactive decay of naturally occurring radionuclides. These naturally occurring radionuclides consist of primordial radioactive isotopes found in the Earth's crust, their decay products, and radionuclides formed as a result of interactions between cosmic radiation and stable atomic nuclei. Primordial radionuclides are characterized by half-lives on the same order of magnitude as the age of the Earth. In contrast, cosmogenic radionuclides are continuously generated through interactions between cosmic rays and nuclei in the Earth's atmosphere and at its surface.Human exposure to natural radiation occurs through external sources such as radiation emitted by radionuclides in the Earth's environment and cosmic rays, as well as internal sources from ingested radioactive substances. The main ways of ingesting radionuclides are through the consumption of food and water containing radioactive elements and the inhalation of radioactive substances. Among internal exposures, the irradiation of the bronchial epithelium with alpha particles emitted from the short-lived decay products of radon (^{222}Rn) makes a significant contribution and constitutes a substantial portion of the radiation dose received from natural sources. In addition to natural radiation, humans are also exposed to radiation from artificial (man-made) sources, with the majority of this exposure resulting from medical applications Natural sources are the largest contributor to

[1]PhD Student, Department of Physics, Institute of Science, Selçuk University, Türkiye, mr.fatihozdemir@yahoo.com, (ORCID: 0009-0006-9513-7414)
[2]Prof. Dr., Department of Physics, Faculty of Science, Selçuk University, Türkiye, merdogan@selcuk.edu.tr, meerdogan291@gmail.com, (ORCID: 0000-0003-1879-8500)

population exposure to ionizing radiation, with a worldwide average annual effective dose of approximately 2.4 mSv [1].

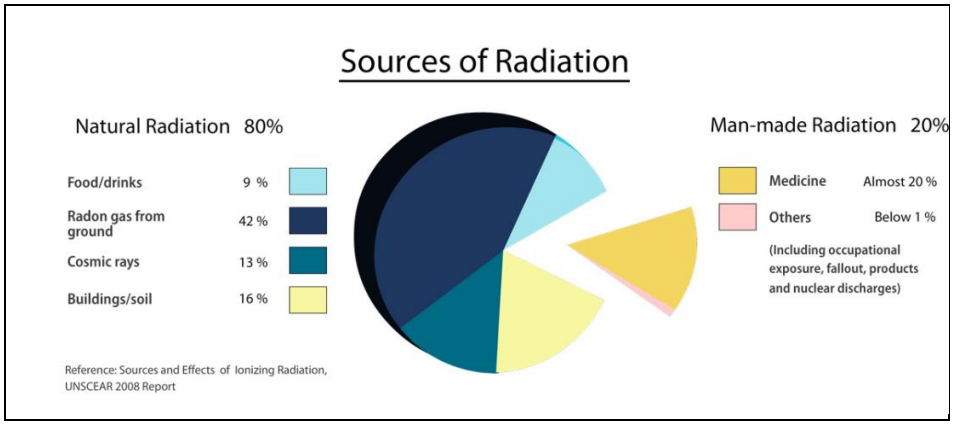


Figure 1. Natural and artificial sources of background radiation for humans [1]

Extensive research into the biological processes by which radiation exposure, unavoidable for living organisms, can affect them has been conducted since the discovery of radiation. Accordingly, it is well known that radiation can cause cellular damage primarily by directly damaging deoxyribonucleic acid (DNA) in chromosomes, leading to cell death or structural changes. It is well established that radiation can induce cellular damage by causing cell death or structural alterations, primarily through direct damage to the deoxyribonucleic acid (DNA) within chromosomes. When a sufficiently large number of cells are destroyed or impaired, normal organ function may be compromised, potentially leading to severe health consequences or even death. Radiation may also produce DNA damage that does not immediately result in cell death. In most cases, such damage is accurately repaired; however, if repair is incomplete or incorrect, permanent changes known as mutations may occur. These mutations can be propagated during subsequent cell divisions and, over time, may contribute to the development of cancer. Furthermore, if the affected cells are germ cells responsible for transmitting genetic information to future generations, hereditary abnormalities may occur. Much of the current understanding of these biological mechanisms and inherited effects has been obtained through experimental studies conducted under laboratory conditions [2].Various international organizations work together to minimize the health and environmental impacts of ionizing radiation. These organizations play complementary roles in scientific research, radiation protection, standardization, and practical application. UNSCEAR (United Nations Scientific Committee on the Effects of Atomic Radiation)

collects, evaluates, and reports global scientific data to assess the biological and environmental impacts of radiation exposure [3]. Based on these scientific assessments, ICRP (International Commission on Radiological Protection) develops independent recommendations and fundamental principles for radiation protection [4]. Building on these recommendations, the IAEA (International Atomic Energy Agency) establishes internationally accepted safety standards and promotes the safe, secure, and peaceful use of nuclear technology [5]. The WHO (World Health Organization) integrates this scientific knowledge into public health policies and medical radiation safety guidelines to protect human health [6]. Furthermore, IRPA (International Radiation Protection Association) brings together radiation protection experts worldwide to foster a strong radiation protection culture and facilitate the practical application of internationally accepted radiation protection principles [7].The fundamental principles of radiation protection are based on the recommendations of the ICRP and are designed to minimize the harmful effects of ionizing radiation on individuals and the environment. Radiation protection is founded on three core principles: justification, optimization, and dose limitation. The principle of justification states that any practice involving exposure to ionizing radiation should produce a net benefit that outweighs the associated radiation risks. The optimization principle, commonly known as the ALARA (As Low As Reasonably Achievable) principle, requires that radiation exposures be kept as low as reasonably achievable, taking into account economic and societal factors. The principle of dose limitation ensures that individual radiation doses from planned exposure situations do not exceed the regulatory limits established for occupationally exposed workers and members of the public. In practical radiation protection, these principles are implemented through measures designed to reduce the duration of exposure, increase the distance from radiation sources, and provide adequate shielding. Together, these principles provide the foundation of modern radiation protection and are universally applied in medical, industrial, research, and nuclear energy applications [8]. Table 1 shows the recommended dose limits for the general public and occupationally exposed workers, in accordance with IAEA GSR Part 3 [9].

Table 1. Recommended dose limits for the general public and occupationally exposed workers [9]

Exposure Category	Occupationally exposed workers	Members of the Public
Effective dose	20 mSv per year averaged over five consecutive years (100 mSv in total), with a maximum of 50 mSv in any single year.	1 mSv per year
Equivalent dose to the lens of the eye	An average annual effective dose of 20 mSv over a five-year period, with the dose not exceeding 50 mSv in any single year.	15 mSv per year
Equivalent dose to the skin (averaged over any 1 cm^2 of skin)	500 mSv per year	50 mSv per year
Equivalent dose to the hands and feet	500 mSv per year	Not specifically prescribed (covered by skin dose limit)
Declared pregnancy of an occupationally exposed worker	The equivalent dose to the embryo/fetus should not exceed approximately 1 mSv for the remainder of the pregnancy after declaration.	Not applicable

2. NATURAL SOURCES OF EXTERNAL IONIZING RADIATION

2.1. Cosmic Radiation

Earth's atmosphere and geomagnetic field protect us from cosmic radiation originating from outer space. The geomagnetic shielding effect is strongest near the equator and weakest near the poles. While Earth's magnetic field deflects many charged particles associated with cosmic radiation away from the Earth, the atmosphere absorbs most of the remaining radiation that penetrates the magnetic field. The level of cosmic radiation exposure depends partly on the altitude at which we live. Another factor that affects our exposure to cosmic radiation is the number and duration of air travels we undertake. During air travel, we fly at high altitudes where the atmosphere provides less shielding against cosmic radiation. As a result, we are exposed to higher levels of cosmic radiation compared with being at ground level. Also, flights over polar regions are generally associated with higher cosmic-radiation exposure than flights over equatorial regions. The amount of cosmic radiation received during flights depends on several factors, with altitude and flight duration being the most important [10]. The flights associated with the highest cosmic radiation exposure are primarily ultra-long-haul routes over polar regions or at high latitudes (above approximately 45°N). For example, a passenger on a Bangkok–New York (JFK) flight receives an average one-way radiation dose of approximately 101 μSv, which may increase

to about 107 μSv during periods of solar minimum. Consequently, five round-trip flights on this route could result in a cumulative dose of approximately 1 mSv, illustrating that frequent long-haul air travel can contribute measurably to annual radiation exposure [11]. In addition, approximate doses for some different flights are given in Table -2.

Table 2. Average Radiation Doses for Passengers and Flight Crew on Selected Flight Routes

Number	Route	Dose/Flight (μSv)	References
1	Frankfurt-Rome	3-6	[12]
2	Frankfurt-New York	32-75	[12]
3	Detroit Wayne County - Hong Kong	94.9	[13]
4	Cairo - Los Angeles	92.6	[13]
5	Bangkok Suvarnabhumi - John F Kennedy	101	[13]

Space stations and spacecraft do not benefit from Earth's natural protection against cosmic radiation provided by the atmosphere and geomagnetic field. Therefore, radiation shielding materials are incorporated into spacecraft and space habitats to reduce astronauts' exposure to potentially significant levels of cosmic radiation [10].Numerous national and international scientific and regulatory organizations have developed policies and guidance concerning radiation exposure in aviation and spaceflight. Among these organizations are the European Union Aviation Safety Agency (EASA), the International Commission on Radiological Protection (ICRP), and the Federal Aviation Administration (FAA) [14–16].In accordance with the recommendations of the ICRP and the National Council on Radiation Protection and Measurements (NCRP), the FAA recommends the following occupational radiation dose limits for flight crew [16]:

- An annual effective dose limit of 20 mSv, averaged over five years, with a maximum of 50 mSv permitted in any single year.
- For pregnant flight crew members, the recommended equivalent dose to the embryo/fetus should not exceed 1 mSv for the remainder of the pregnancy after declaration, with efforts to limit exposure to approximately 0.5 mSv per month.

2.2. Terrestrial Sources of External Radiation

Naturally occurring radionuclides of terrestrial origin, commonly referred to as primordial radionuclides, are found in varying concentrations throughout the environment, including within the human body. Only radionuclides with half-lives comparable to the age of the Earth, together with their radioactive decay products, remain present in appreciable amounts. External exposure to natural terrestrial radiation arises primarily from gamma rays emitted by radionuclides belonging to the uranium-238 (^{238}U) and thorium-232 (^{232}Th) decay series, as well as from potassium-40 (^{40}K). These radionuclides can also enter the human body through ingestion and inhalation, thereby contributing to internal radiation exposure. Although other naturally occurring terrestrial radionuclides, including those belonging to the ^{235}U decay series and primordial radionuclides such as rubidium (^{87}Rb), samarium (^{147}Sm), lanthanum (^{138}La), and lutetium (^{176}Lu), are also present in nature, their contributions to the total population dose are generally much smaller than those from the ^{238}U and ^{232}Th decay series and ^{40}K [17]. Three naturally occurring radioactive decay chains and the nuclei involved in these decays are shown in Figure 2 [18].

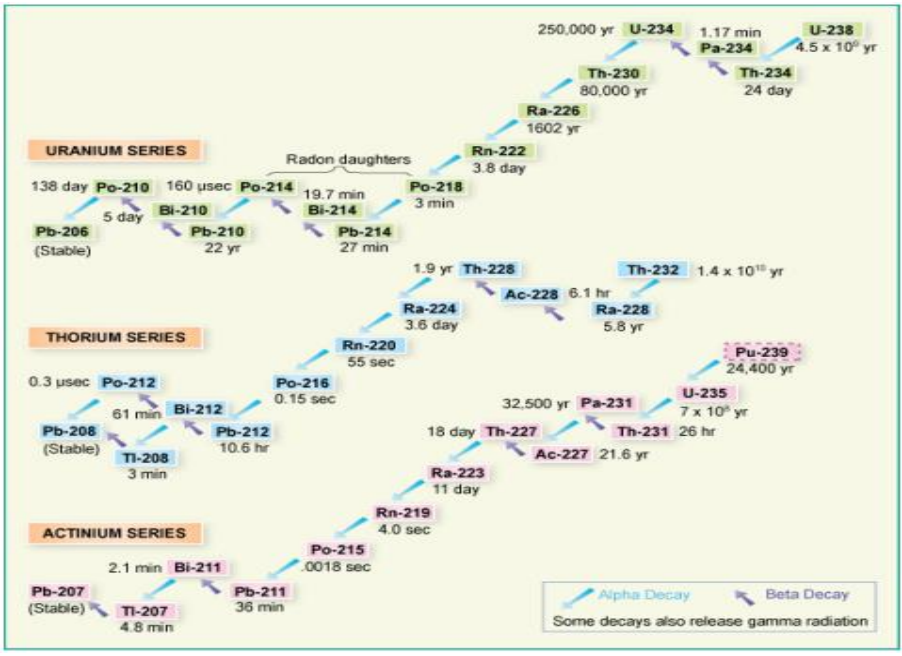


Figure 2. Schematic representation of the natural decay series of uranium (^{238}U and ^{235}U) and thorium (^{232}Th), illustrating the decay mode (α or β^-) and the half-life of each radionuclide [18].

External exposure in outdoor environments is primarily caused by terrestrial radionuclides that occur naturally at trace concentrations in soils. The activity concentrations of these radionuclides depend largely on the geological characteristics of the parent rocks from which the soils are derived. In general, soils originating from igneous rocks, particularly granite, contain higher concentrations of naturally occurring radionuclides and therefore produce higher external radiation levels than soils formed from sedimentary rocks. However, this trend is not universal, as certain sedimentary rocks, including shale and phosphate-bearing formations, may also contain elevated concentrations of natural radionuclides [17].Numerous investigations have been carried out worldwide to characterize the distribution of naturally occurring radionuclides in soils and to evaluate the resulting external radiation environment. Measurements of radionuclide activity concentrations can be used to estimate the absorbed gamma dose rate in air, while direct measurements of air dose rates provide a practical and reliable means of assessing natural background radiation levels over large geographical areas. These surveys have generated extensive datasets that allow comparisons of external exposure levels among different regions and countries [19-22].

Gamma spectrometric studies have consistently demonstrated that the terrestrial external gamma radiation field is dominated by three naturally occurring radionuclide groups: the ^{238}U decay series, the ^{232}Th decay series, and ^{40}K. Under typical environmental conditions, these three sources contribute approximately equally to the external gamma radiation dose received by the population, both in outdoor and indoor environments. Radionuclides belonging to the uranium and thorium decay series do not necessarily exist in complete secular equilibrium under natural environmental conditions. Within the uranium decay chain, ^{238}U and ^{234}U are often close to radioactive equilibrium in undisturbed minerals because they are separated only by the relatively short-lived radionuclides ^{234}Th and protactinium (^{234}Pa). Nevertheless, radioactive decay processes and subsequent geochemical interactions may disrupt this equilibrium by allowing daughter radionuclides to become separated from their parent materials and transported through the environment. As a result, ^{234}U is often slightly depleted relative to ^{238}U in soils, while its concentration may become enriched in surface waters and marine environments. The activity concentration of radium (^{226}Ra) may also differ from that of ^{238}U owing to its greater environmental mobility and the possible separation from its parent radionuclide, ^{230}Th. Furthermore, the decay of ^{226}Ra produces the noble gas radon (^{222}Rn), which can readily escape from soil pores into the atmosphere. This radon emanation reduces the contribution of the uranium series to external terrestrial

gamma radiation while simultaneously increasing the potential for internal exposure through inhalation. Although ^{222}Rn has a half-life of only 3.82 days, its longer-lived progeny, particularly lead (^{210}Pb) and polonium (^{210}Po), persist in the environment and play a significant role in radiation dose assessments because of their radiological importance. Comparable processes occur within the thorium decay series. The radionuclide ^{228}Ra has a sufficiently long half-life to permit partial separation from its parent, ^{232}Th, under suitable environmental conditions. In contrast, the gaseous radionuclide ^{220}Rn (thoron) has a very short half-life of approximately 56 seconds, which greatly limits its migration from its source material. Because of its very short half-life, ^{220}Rn has limited migration potential compared with radon, although its progeny can contribute to radiation exposure near its source [17].A substantial fraction of natural background radiation originates from terrestrial sources, with radon and its short-lived progeny (as seen Fig. 3) representing the largest single contributor to the radiation dose received by the general population. As shown in Figure 3, radon, a member of the natural uranium-238 decay series, decays into a series of short-lived radioactive progeny that exist in solid form. These radioactive decay products readily attach to airborne aerosol particles and can be inhaled into the respiratory tract, particularly in enclosed indoor environments. Once deposited in the lungs, the short-lived radon progeny emit predominantly alpha particles, which deliver a high radiation dose to bronchial epithelial cells and can damage DNA, thereby increasing the risk of lung cancer. Consequently, prolonged exposure to elevated indoor radon concentrations is recognized as the second leading cause of lung cancer after tobacco smoking [23]. Terrestrial radiation arises primarily from naturally occurring radionuclides in rocks and soils, particularly the ^{238}U and ^{232}Th decay series and ^{40}K, which contribute to external gamma radiation. According to the latest assessments by UNSCEAR, the worldwide average annual effective dose from external terrestrial gamma radiation is approximately 0.48 mSv, although this value varies considerably depending on local geology, soil composition, and altitude. In contrast, inhalation of ^{222}Rn and its short-lived progeny accounts for a much larger average annual effective dose of approximately 1.26 mSv, making radon the dominant source of natural radiation exposure for most individuals.

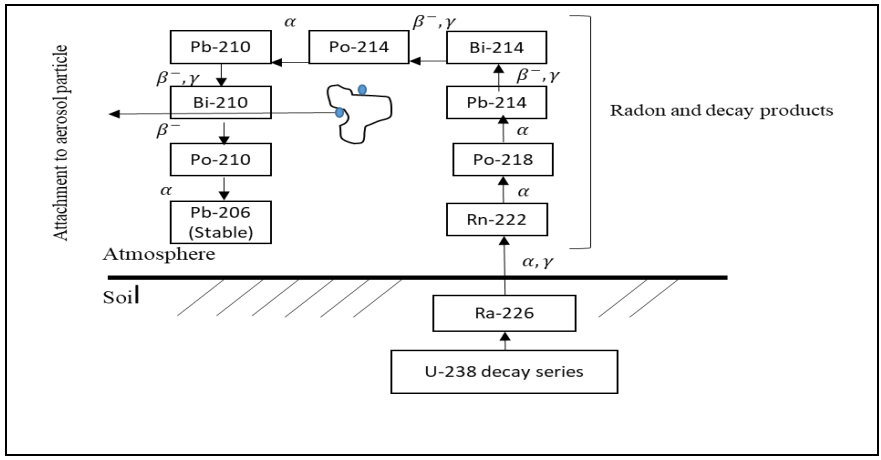


Figure 3. Schematic representation of the migration of radon (^{222}Rn) from soil to the atmosphere and the formation of airborne radioactive decay products attached to aerosol particles.

Because radon is continuously generated from the decay of ^{226}Ra in uranium-bearing rocks and soils, its concentration is strongly influenced by geological conditions, soil permeability, building characteristics, and ventilation rates. Consequently, regions with uranium-rich geological formations or elevated indoor radon concentrations may experience radiation doses that significantly exceed the global average [1,17].

2.3. Radyoactivity in Food

Natural radionuclides are widely distributed in the environment and are therefore present in virtually all foods at varying concentrations. These radionuclides enter the food chain through the uptake of minerals from soil and water by plants, followed by their transfer to animals and humans. Among naturally occurring radionuclides, ^{40}K is generally the most important contributor to internal radiation exposure from food. Other naturally occurring radionuclides, including members of the ^{238}U and ^{232}Th decay series, such as radium-226 (^{226}Ra), lead-210 (^{210}Pb), and polonium-210 (^{210}Po), may also be present in food depending on local geological conditions, agricultural practices, and environmental factors. Marine foods, nuts, cereals, leafy vegetables, mushrooms, and mineral-rich drinking water may contain relatively higher concentrations of certain natural radionuclides. The ingestion of these radionuclides contributes to the internal radiation dose received by humans throughout life. According to UNSCEAR, the annual effective dose received through the inhalation and ingestion of terrestrial radionuclides is estimated to average 0.29 mSv worldwide.

Potassium-40 (^{40}K), an essential naturally occurring radionuclide in the human body, contributes approximately 0.17 mSv, whereas long-lived radionuclides from the ^{238}U and ^{232}Th decay series contribute the remaining 0.12 mSv. Although the concentrations of natural radionuclides vary among different foods and geographical regions, the resulting doses are generally low and represent a normal component of natural background radiation [1]. Annual effective dose values based on consumption of certain commonly consumed foods from different geographical regions are given in Table 3.

Table 3. Estimated annual effective doses due to ^{40}K, ^{226}Ra, and ^{232}Th in selected food samples

Sample	Annual Effective Dose (μSvy^{-1})			References
	^{40}K	^{226}Ra	^{232}Th	
Pumpkin seed	1.34±0.18	0.35±0.02	0.35±0.02	[24]
Beans	7.5±0.96	1.35±0.19	0.74±0.07	[24]
Bulgur	12.5±1.69	7.56±1.08	4.41±0.63	[24]
Rice	1.13±0.14	4.20±0.60	4.12±0.57	[24]
Corn	3.42±0.45	4.83±0.65	6.60±0.88	[24]
Wheat	37.08±5.29	49.88±7.01	49.68±6.59	[24]
Fragrant rice	5.80±1.56	52.38±11.99	-	[25]
Rice	18.64	-	18.96	[26]

3. CONCLUSION

Natural radiation is an unavoidable component of the environment and represents the principal source of ionizing radiation exposure for the general population. Human exposure arises from both external sources, including cosmic and terrestrial radiation, and internal sources through the inhalation and ingestion of naturally occurring radionuclides. Although the levels of natural radiation vary according to geographical location, geological characteristics, altitude, lifestyle, and dietary habits, the associated doses are generally within the range of normal background exposure. Among the major natural radiation exposure pathways, inhalation of radon and its short-lived decay products constitutes the largest contribution to the annual effective dose received by humans and therefore remains one of the most important topics in environmental radiation protection.

A sound understanding of the origin, distribution, and behavior of natural radionuclides is essential for evaluating radiation exposure, assessing potential health risks, and establishing appropriate radiation protection strategies. Continuous monitoring of natural radiation levels in air, soil, water, and food, together with the application of internationally accepted radiation protection

principles and safety standards, plays a vital role in protecting public health. As scientific knowledge and measurement technologies continue to advance, more comprehensive assessments of natural radiation exposure will further improve environmental monitoring programs, epidemiological studies, and evidence-based radiation protection policies.

REFERENCES

[1] UNSCEAR (United Nations Scientific Committee on the Effects of Atomic Radiation), 2008. Sources and Effects of Ionizing Radiation, Annex B.

[2] UNEP (United Nations Environment Programme), 2016. Radiation Effects and Sources.

[3] https://www.unscear.org/unscear/en/about-us/index.html, access date:28.07.2026.

[4] https://www.icrp.org/, access date: 28.07.2026.

[5] https://www.iaea.org/about/overview/sustainable-development-goals, access date: 28.07.2026.

[6] https://www.who.int/about, access date: 28.07.2026.

[7] https://www.irpa.net/, access date: 28.07.2026.

[8] ICRP (International Commission on Radiological Protection), 2007. The 2007 Recommendations of the International Commission on Radiological Protection. ICRP Publication 103. *Annals of the ICRP*, 37(2–4):1–332.

[9] IAEA (International Atomic Energy Agency). Radiation Protection and Safety of Radiation Sources: International Basic Safety Standards. IAEA Safety Standards Series No. GSR Part 3. Vienna: IAEA; 2014.

[10] https://www.epa.gov/radtown/cosmic-radiation, access date: 29.07.2026.

[11] Cican, G. and Silivestru, V., 2025. Cosmic radiation and airline passengers: Sources, exposure levels, health risks, and protective measures - A review. Journal of Space Safety Engineering 12, 615–630.

[12] https://www.bfs.de/EN/topics/ion/environment/air/flight/flight_node.html, access date: 04.08.2026.

[13] Alvarez, L.E., Eastham, S.D., Barrett, S.R.H., 2016. Radiation dose to the global flying population, J. Radiol. Protect. 36 (93).

[14] Rees, C., Catachpole, J., Ryden, K., 2024. A discussion on policies and regulations governing the risks associated with radiation exposure for space tourism flight participants, Space Policy. 68.

[15] ICRP (International Commission on Radiological Protection), 2016. Radiological Protection from Cosmic Radiation in Aviation. ICRP Publication 132. Ann. ICRP 45(1), 1–48.

[16] FAA (Federal Aviation Administration), 2014. AC 120-61B: In-flight Radiation Exposure. U.S. Department of Transportation, Washington, DC.

[17] UNSCEAR (United Nations Scientific Committee on the Effects of Atomic Radiation), 2000. Sources and Effects of Ionizing Radiation, Annex B.

[18] Vinícius V. M. Ferreira, Raquel L. M. Fonseca, Zildete Rocha, Amanda L. Oliveira, Rubens M.Moreira, Nayron C. Lemos, Cláudio J. Chagas, Maria

Angela B. C. Menezes & Talita O. Santos, 2015. Use of Radon as Water Tracer at Juatuba Basin. Journal of Geography and Geology, 7(3), 49-60.

[19] Sahin, L., Hafizoglu, N., Çetinkaya, H., Manisa, K., Bozkurt, E., Biçer, A., 2017. Assessment of radiological hazard parameters due to natural radioactivity in soils from granite-rich regions in Kütahya Province, Turkey. Isotopes In Environmental and Health Studies, 53(2), 212-221.

[20] Manisa, K., Erdogan, M., Usluer, A., Cetinkaya, H., Isik, U., Sahin, L., Zedef, V., 2021. Assessment of natural radioactivity level of soil and water in the region of Çorlu (Turkey). Journal of Radioanalytical and Nuclear Chemistry, 329(3), 1213-1221.

[21] Siraz, MMM., et al., 2026. Pioneering Radiometric Analysis of Quarry Pit Soils in Bangladesh and Estimation of Associated Risks using Multivariate Statistical Analysis. Soil & Sediment Contamination, Doi:10.1080/15320383.2026.2673898.

[22] Siraz, MMM., et al., 2025. Assessment of radioactivity in soil from the vicinity of Srikail gas field, Bangladesh: implications for public health and environment. Isotopes in Environmental and Health Studies, Doi:10.1080/10256016.2025.2596044.

[23] ICRP (International Commission on Radiological Protection), 2014. Radiological Protection against Radon Exposure. ICRP Publication 126.

[24] Altikulac, A., 2021. Analysis of Natural Radioactivity and Determination of Potassium Content in Foods. Fresenius, Environmental Bulletin, 30,06B, 7859-7865.

[25] Nahar, A. et al., 2018. Assessment of Natural Radioactivity in Rice and Their Associated Population Dose Estimation. Radiation Effects and Defects in Solids, 173, 11-12, 1105-1114.

[26] Ibikunle, S.B., 2022. Assessment of Natural Radioactivity of Some Food Samples Commonly Consumed in Nigeria and Its Radiological Impact. International Journal of Environmental Science and Technology, 20,3085–3090.

Chapter 20

Examining The Integration of Environmental Physics and Radiation Health into the Physics Curriculum

Mehmet Altan KURNAZ[1]

1. INTRODUCTION

This study critically examines the "Turkish Century Education Model Secondary School Physics Curriculum (2026)," which is being gradually implemented in Turkey, with respect to the integration of environmental physics and radiation health concepts and the development of "radiation literacy." Using qualitative research methods, specifically document review and content analysis, the high school physics curriculum (grades 9-12) was examined in a spiral manner. The findings confirm that the new curriculum has a strong theoretical foundation in fluid mechanics, thermodynamics, optics, and quantum physics, all of which are necessary for modeling macroscale environmental problems. However, it was determined that the current structure completely confines this potential to classical engineering contexts and abstract mathematical equations. According to the research results, although quantum-mechanical infrastructure, such as atomic absorption spectra, is presented in the context of heavy metals, their functional counterparts in environmental analytics remain in a gray area. In the realm of radionuclides, the thermal pollution created by nuclear power plants in aquatic ecosystems and the atmospheric transport/deposition dynamics of radioactive clouds have not been correlated with existing physics outputs such as relative motion and terminal velocity. In the context of human health, the failure to clearly distinguish between ionizing and non-ionizing radiation at an early age is likely to fuel societal radiophobia; furthermore, current chronic exposure risks, such as 5G and electromagnetic pollution have not been addressed in depth at the pedagogical level. Ultimately, the study demonstrates the need for physics education to be adapted to socio-scientific issues by moving away from formulaic frameworks and suggests concrete learning outcome statements, interdisciplinary STEM activity designs, and teacher in-service training for future curriculum revisions.

[1] Prof. Dr., Department of Mathematics and Science Education/Faculty of Education, Kastamonu University, Türkiye, makurnaz@kastamonu.edu.tr, (ORCID: 0000-0003-2824-4077)

1.1. The Concept and Scope of Environmental Physics

The twenty-first century represents a period in which humanity's technological dominance over nature has reached its peak and is now facing devastating environmental repercussions. Macro-scale problems such as global climate change, industrial waste, ecosystem degradation, heavy metal accumulation, and radioactive pollution have a complex physical background that cannot be explained solely by biological or chemical processes. At this point, 'Environmental Physics' stands out as an interdisciplinary and vital field that aims to understand the functioning of complex environmental systems, energy flows, and the behavior of pollutants in nature using fundamental principles of physics (Boeker & van Grondelle, 2011; Monteith & Unsworth, 1990).One of the most fundamental elements forming the theoretical backbone of environmental physics is the laws of thermodynamics. The thermodynamic principles that govern all energy transformations, heat transfers, and entropy increases in the universe also define the boundaries of environmental problems. The first law of thermodynamics (conservation of energy) allows us to account for the energy entering and leaving ecosystems, while the second law (law of entropy) states that any energy converted will inevitably be released into the environment as low-quality waste heat (thermal pollution). For example, high-temperature cooling water released from fossil-fuel power plants or nuclear reactors into environmental water sources can disrupt the oxygen balance of aquatic ecosystems, creating a serious environmental problem. Similarly, the accumulation of greenhouse gases in the atmosphere, which disrupts the planet's thermal balance and traps long-wave infrared radiation that the Earth should radiate back into space, is a global energy budget crisis directly explained by the laws of thermodynamics and optics. However, the transport processes of pollutants among the atmosphere, hydrosphere, and lithosphere are governed entirely by the principles of atmospheric physics and fluid mechanics. The transport of particulate matter or radioactive fallout released into the air by wind currents is modeled by turbulent diffusion mechanisms and the laws of gravitational deposition (Karimi et al., 2025). Similarly, the hydrodynamic transport of heavy metals in streams or the infiltration processes of radionuclides between soil layers are areas of study within the sub-disciplines of soil and fluid mechanics physics. Therefore, modeling environmental problems by moving beyond a superficial perception of pollution and delving into their root causes is only possible with these fundamental conceptual tools of physics.

1.2. Radiation Health and Social Awareness: ‘Radiation Literacy’

Modern industrial societies, while facing enormous energy needs, are becoming increasingly dependent on radiation sources in medical, military, and technological fields. While nuclear power plants are presented as a zero-carbon emission energy

alternative to combat the global climate crisis, the socio-environmental and biological effects of historical nuclear accidents such as Chernobyl and Fukushima have left deep marks and a profound 'radiophobia' in the collective memory of societies (Bromet, 2014). On the other hand, applications such as computed tomography (CT), positron emission tomography (PET), X-rays, and mammography, which are indispensable elements of modern medicine, have dramatically increased individuals' exposure to ionizing radiation. In addition to the medical dimension, non-ionizing electromagnetic radiation pollution is also a subject of continuous debate in our living spaces surrounded by smartphones, base stations, high-voltage power lines, microwaves, and 5G technologies.

The effects of this complex micro-world on human health manifest through deterministic and stochastic mechanisms of biological damage. Damage caused by ionizing radiation (alpha, beta, gamma particles, and X-rays) directly to the DNA helix or indirectly through free radicals by radiolyzing water molecules encompasses a wide spectrum, from cancer development to genetic mutations (ICRP, 2007). For the modern individual living in such a high-risk and uncertain technological age, 'radiation literacy' has ceased to be an academic luxury or a marginal piece of knowledge that only nuclear engineers should possess; it has become a contemporary civic necessity and a survival skill.Radiation literacy refers to an individual's ability to scientifically distinguish between ionizing and non-ionizing radiation sources, rationally evaluate the radiation dose received, and apply protection principles to daily-life decisions to mitigate exposure risks. A radiation-literate individual can perform a benefit-risk analysis of the diagnostic dose they will be exposed to in medical imaging procedures; take ventilation measures against the risk of natural radon gas accumulation in their home (Sarıhan, 2022); and make rational decisions about base stations based on wavelength, frequency, and energy levels instead of relying on hearsay speculation. In this context, building public awareness based on scientific facts, free from manipulation, is only possible through a mass radiation literacy campaign.

1.3. The Role of Physics Education and the Necessity of Curriculum Integration

Formal education systems are the primary and most strategic platforms for building environmental physics awareness and radiation literacy at the societal level. At this point, physics education must go beyond merely transmitting abstract laws of the universe or mechanical problem-solving skills based on formulas to the young generations. The 'Socio-Scientific Issues' approach, which has long been emphasized in the educational sciences literature, argues that science should be addressed together with its social, ethical, environmental, and political dimensions.

Environmental pollution, radionuclides, the safety of nuclear power plants, and the biological effects of electromagnetic fields are truly open-ended, controversial socio-scientific issues that directly concern society.The fundamental role of physics education is not to present these interdisciplinary and current topics as purely theoretical subtopics, formula patterns, or rote memorization, but to transform them into functional, life-integrated achievements in the minds of high school and university students—the future decision-makers. If a physics curriculum limits the topic of radioactivity to only mathematical equations for nuclear reactions or half-life equations for unstable atoms, then that education has failed to develop radiation literacy in students. It is essential that educational processes be deepened to the point where students can connect these abstract concepts to environmental health, ecological balance, and societal risk management.Accordingly, physics curricula need to be structurally revised in the context of environmental physics principles and radiation health standards, and an interdisciplinary integration model should be adopted. While students learn mechanics, thermodynamics, optics, and modern physics units in high school, they should simultaneously explore how these physical tools can be used to detect environmental pollution, monitor radioactive risks, and protect human health. This integration will break the perception of physics courses as detached from daily life and overly abstract, increase the course's meaningfulness, and raise students' scientific literacy to global standards.

2. METHODOLOGICAL FRAMEWORK

The main objective of this book chapter is to critically examine the 'Turkish Century Education Model Secondary School Physics Curriculum (2026)', which constitutes the most current link in the chain of education reforms in Turkey and is being implemented gradually, in terms of the level, depth, and potential of integration of environmental physics and radiation health concepts. The study examines the extent to which the philosophical transformation, skill-oriented approach, and claims of interdisciplinary horizontal/vertical integration brought about by the new curriculum can address issues at the intersection of environmental pollutants, radionuclides, radiation exposure, and human health, which also form the main vision of the book.To achieve this objective, qualitative research methodologies, specifically document review and content analysis, were employed in this study. The primary data source for the research is the text of the 2026 Physics Curriculum published by the Ministry of National Education, Board of Education (MoNE, 2026). During the review process, the curriculum was coded and scanned within the framework of fundamental analytical topics: (i) Thermal pollution, energy transformations, and atmospheric phenomena within the framework of Environmental Pollutants and Physical Processes; (ii) Ionizing and non-ionizing

radiation within the framework of Radiation Physics and the Electromagnetic Spectrum; and (iii) Effects on human health, biological risks, and reasonable levels within the framework of Radiation Health, Dosimetry, and Protection Principles.By classifying the 9th-, 10th-, 11th-, and 12th-grade physics achievements, learning outcomes, and process components in the current program in the context of these themes, the strengths of the program were revealed, and the gray areas open to structural improvement were evaluated. In light of the findings, the aim is to make an original and practical contribution to the literature by offering concrete suggestions for future curriculum revisions, textbook authors, and physics educators working in the field.

3. FINDINGS AND DISCUSSION

As a result of the examinations carried out on the program text, the current levels of representation, pedagogical approaches, and future integration potentials of the concepts of 'Thermal Pollution, Electromagnetic Pollution, Spectroscopic Analysis of Heavy Metals, and Atmospheric Transport and Pollutant Dynamics' in the 2026 curriculum were subjected to a structural critique.

3.1. Thermal Pollution

The findings obtained for 'Thermal Pollution' as a result of the examination of the program text are presented in Table 1. The sub-theme of Thermal Pollution at the 9th-grade level appears to focus on micro- or individual-scale contexts, such as domestic insulation techniques, energy savings in buildings, and theoretical heat transfer mechanisms (conduction, convection, radiation). However, the study points out that this emphasis should evolve to address macro-scale environmental problems. It can be said that the ecological damage (thermal pollution) caused by the high-temperature waters discharged by industrial facilities and thermal and nuclear power plants into receiving environments (seas, lakes, and rivers), and the disruptions in the Earth's global radiation balance, remain as gray areas in the curriculum.

Table 1. Spiral Representation Matrix of Thermal Pollution Concepts in the 2026 Curriculum (9-12)

Grade	Unit	Relevant Learning Outcome / Content Context	Curriculum Approach / Representation	Deficiency / Potential
9	Energy	PHYS.9.4.5, PHYS.9.4.6 Heat transfer mechanisms, heat conduction rate, domestic insulation, greenhouse effect.	Theoretical approach focusing on micro-scale domestic insulation and energy conservation in buildings.	The impact of waste heat (thermal pollution) released by macro-industrial plants into the ecosystem remains a gray area.
10	Energy	PHYS.10.2.5 Comparison of renewable and non-renewable energy sources, and global warming.	Socio-scientific context of "global warming" and awareness of "conservation/efficiency".	While the disadvantages of non-renewable power plants are addressed, pollution is limited to gas emissions; thermal pollution of water is not mentioned.
11	Electricity and Magnetism	PHYS.11.2.9 Generators, electric motors, and electric vehicle technologies.	Green technology-oriented approach.	The environmental physics dimension regarding the thermal waste generated by energy conversion inefficiency and the local thermal loads of battery systems is missing.
12	Matter and Its Nature	PHYS.12.4.8 Nuclear energy (fission-fusion): advantages and disadvantages of nuclear power plants.	Environmental and economic impacts of nuclear energy.	Thermal pollution and thermal shock effects caused by the cooling water of nuclear reactors in marine/river ecosystems remain a potential area for discussion.

The explicit reference to atmospheric pollution components such as 'global warming' and 'carbon footprint' when discussing non-renewable energy sources (thermal power plants, etc.) in the 10th-grade program is a significant empirical achievement. However, the danger of thermal pollution from discharging water used

in these plants' cooling cycles into river and marine ecosystems is not addressed at this level either. When listing the disadvantages of energy sources, limiting pollution solely to the atmospheric dimension (gas emissions) leads environmental physics to overlook the aquatic thermal ecosystem dimension.In the 11th-grade curriculum, the process of converting electrical energy into mechanical energy or mechanical energy into electrical energy via generators can be addressed as a physical pollution element, specifically focusing on ‘waste heat’ resulting from system inefficiencies and its release into the environment (increased entropy). The curriculum's direct contextualization of this topic through green technologies such as ‘clean energy and electric vehicles’ is positive. However, it should be noted that the high thermal loads (thermal management) generated by the battery management systems of these vehicles and the local microclimatic thermal effects created by large-scale generator centers have not been empirically examined.At the 12th-grade level, evaluating the advantages and disadvantages of nuclear energy using empirical data and source reliability represents the pinnacle of environmental physics analysis. The thermal energy released during the operational processes of nuclear power plants—not only the portion converted into electricity but also the enormous heat discharged into the environment (with the potential for thermal pollution)—is a fundamental thermodynamic problem. Expanding the curriculum beyond simply framing these disadvantages as ‘nuclear waste’ or ‘radiation risk’ to include ‘thermal shocks’ caused by reactor coolant in aquatic biomes could help elevate students' reasoning skills to the level of environmental engineering.

3.2. Electromagnetic Pollution (Non-ionizing Radiation)

Table -2 show that the verifiable status of the Physics Curriculum regarding electromagnetic pollution (non-ionizing radiation). Within the sub-theme of electromagnetic pollution, the first encounter with the word radiation occurs at the 9th-grade level in the context of thermal energy emission (radiation). The program's failure to address the distinction between ionizing and non-ionizing radiation at this stage is a deficiency, as it could lead to the development of 'radiophobia' (fear of radiation) among students in later years. When introducing the concept of radiation, mentioning not only thermal radiation but also other non-ionizing radiation encountered in daily life (e.g., microwaves or infrared) has strong potential for integration to awaken awareness of the electromagnetic environment at an early age

Table 2. Spiral Representation Matrix of Electromagnetic Pollution Concepts in the 2026 Curriculum (9-12)

Grade	Unit	Relevant Learning Outcome / Content Context	Curriculum Approach / Representation	Deficiency / Potential
9	Energy	PHYS.9.4.5 Theoretical analysis of the concept of 'Radiation' within the scope of energy transfer mechanisms.	The wave/ray mechanism explanation focused solely on thermal (heat) emission.	Preventing the fear of radiation (radiophobia) triggered by the word in students' minds, and introducing other non-ionizing everyday radiations (microwaves, infrared).
10	Waves	PHYS.10.4.3 Classifying waves based on their characteristics and the concept of electromagnetic waves.	Classification of electromagnetic waves along with water, sound, spring, and seismic waves.	By emphasizing the non-ionizing nature of the spectrum's low-energy bands (radio, microwave, Wi-Fi), the public health dimension of chronic exposure can be integrated into this classification.
11	Electricity and Magnetism	PHYS.11.2.9 Examination of electric vehicle technologies, electric motors, and the energy infrastructures of smart cities.	Innovative and industrial aspects of technological advancements, and alternating current mechanisms.	The 'Extremely Low Frequency Electromagnetic Field' (ELF-EMF) pollution created by high-voltage power lines and urban distribution transformers in residential areas, alongside ICNIRP safety standards, can be discussed.
12	Waves	PHYS.12.3.5 Classification of Electromagnetic Waves, general characteristics, and the electromagnetic wave spectrum.	Analyzing the spectrum (from radio waves to gamma rays) through ready-made datasets based on speed, frequency, wavelength, and energy variables.	Tissue-level differences between ionizing (X-rays, gamma rays) and non-ionizing (5G, IoT millimetric waves, microwaves) radiation, as well as the ALARA (As Low As Reasonably Achievable) principle, can be directly integrated into this learning outcome.
12	Matter and Its Nature	PHYS.12.4.4 Semiconductor materials (diodes, transistors, integrated circuits) and their roles in electronic devices such as mobile phones and computers.	Operating principles of microelectronic devices and quantum physics-based analysis of technological infrastructure.	"Electrosmog" (electromagnetic background load), created by the coexistence of billions of devices and now considered one of the largest next-generation pollutants of today's world, can be evaluated as a socio-scientific context.

The 10th-grade curriculum provides a complete theoretical foundation for electromagnetic pollution by introducing the spectrum mechanism. However, the biggest pedagogical gray area here is the insufficient emphasis, from an environmental health perspective, on the difference in biological effects between the low-energy portion of the spectrum (radio waves, microwaves, etc.) and the high-energy portion (X-rays, gamma rays). While students learn about the locations in the spectrum, it would be more appropriate for this unit to explore, within a socio-scientific context, that base stations or Wi-Fi devices (non-ionizing radiation) do not possess the energy to cause DNA breakage in tissues, but can create cellular stress through ‘thermal effects’ (electromagnetic pollution) in cases of chronic exposure.In the 11th-grade curriculum, transformers and high-voltage power lines are a primary source of 'Low Frequency Electromagnetic Field' (ELF-EMF) pollution in environmental physics. While the curriculum emphasizes the electrical efficiency and industrial importance of these devices, it does not discuss the magnetic field intensity they generate in surrounding settlements or the safe distance limits. While the innovative aspects of smart cities and electric vehicles are praised, the 'background electromagnetic pollution load' (electrosmog) generated by this dense technological ecosystem needs to be examined empirically, based on data, as a disadvantageous component in the unit's critical thinking and argumentation outcomes.The 12th-grade program, while teaching the operating principles of wireless communication technologies and modern medical devices, clearly defines the boundary between 'ionizing and non-ionizing' radiation. However, despite this clear distinction, the millimeter-wave pollution created by 5G technologies and the Internet of Things (IoT), considered an ‘Emerging Contaminant’ in modern urban life, and its potential bio-effects on human sleep quality, melatonin hormone secretion, or overall environmental health, are not discussed in depth in the curriculum. Consequently, 12th-grade topics offer enormous potential for integration to critically examine the reflections of modern environmental exposure risks, such as wireless networks, 5G, and electrosmog, in the curriculum.

3.3. Spectroscopic Analysis of Heavy Metals

Table 3 shows the status of the spectroscopic analysis of heavy metals in the Physics Curriculum. While the concepts of optics and atomic physics are introduced at the 9th-grade level in the context of spectroscopic analysis of heavy metals, the role of these fields in detecting environmental pollution is not addressed. It should be noted that heavy metals, in addition to being chemical elements, possess unique ‘physical spectrum fingerprints,’ and that environmental pollution analyses are performed using physical spectroscopy devices. This could be presented as an interdisciplinary bridge (Physics-Chemistry-Environment) at this initial stage of

career exploration. Due to the relocation of the 'Optics' unit to the 11th grade in the new unit structure of the 2026 curriculum, the 10th-grade level is left completely empty in the context of the optical or spectroscopic analysis of heavy metals.

Table 3. Spiral Representation Matrix of the Concepts of Spectroscopic Analysis of Heavy Metals in the 2026 Curriculum (9-12)

Grade	Unit	Relevant Learning Outcome / Content Context	Curriculum Approach / Representation	Deficiency / Potential
9	Physics as a Science and Career Exploration	**PHYS.9.1.1** Sub-branches of physics (Optics, Atomic Physics) and the definition of interdisciplinary relations.	A conceptual, surface-level classification and an introduction to career fields.	The first interdisciplinary approach to detecting the chemical presence of heavy metals through physical methods (spectroscopy) is presented here.
11	Optics	**PHYS.11.3.1, …** Interaction of light with matter, absorption of light by media, and the color spectrum.	A theoretical/ geometric approach focused on light filters and the phenomenon of visible color.	A bridge can be established using UV-Vis spectrophotometry, which measures heavy metal concentrations in water based on the light absorbed as light passes through the sample.
12	Matter and Its Nature	**PHYS.12.4.1** **PHYS.12.4.2** Bohr atomic model, methods of atomic excitation, discrete energy levels, 'Emission and Absorption Spectra'.	Theoretical and mathematical analysis of line spectra at an introductory level to quantum physics.	This is the strongest point of intersection with the textbook vision. The role of Atomic Absorption Spectroscopy (AAS) in environmental analytics (mercury and lead determination) can be directly integrated into this learning outcome.
12	Matter and Its Nature	**PHYS.12.4.8** Applications in modern technology: the 'Photoelectric Effect' and the production/properties of 'X-Rays'.	Quantum-scale analysis of the operating principles of medical imaging and industrial sensors.	The physical background of XRF (X-ray fluorescence) devices, which measure heavy metals in soil and sediments in situ and rapidly, can be transformed into a socio-scientific performance indicator for this learning outcome.

The 11th-grade optics unit is where the concept of 'spectrum,' the foundation of spectroscopy, is concretized in the minds of students. When discussing the absorption of light by matter and color spectra, the context should not be limited solely to rainbow formation or simple lighting technologies. An empirical socio-scientific context, where each heavy metal has different light absorption/reflection characteristics and the amount of mercury or lead in water samples is determined by spectroscopic analysis (color intensity and wavelength) in environmental laboratories, can be directly integrated into this unit.The 12th-grade curriculum is the most perfect and highest-level empirical data source for the theme of 'Spectroscopic Analysis of Heavy Metals'. The 'Emission and Absorption Spectra' section in the curriculum is the working principle of the Atomic Absorption Spectroscopy (AAS) instrument used in environmental engineering. Similarly, the 'X-rays' topic in the curriculum forms the basis of the X-ray Fluorescence (XRF) technique, which performs non-destructive analysis of heavy metals in solid waste and soil. This demonstrates the functional and concrete application of quantum mechanics principles in environmental analytics.

3.4. Atmospheric Transport and Pollutant Dynamics

The intercontinental transport of industrial emissions, radioactive fallout, and new generation pollutants such as microplastics through the atmosphere is one of the most dynamic components of global environmental health. Physically, these processes depend on parameters such as fluid velocity, pressure gradient forces, thermal convection currents, and gravitational deposition velocity. An examination of the 2026 Physics Curriculum reveals that the mechanical infrastructure required for this macro-environmental modeling is incorporated into the curriculum in a spiral pattern. The 9th-grade 'Fluids' unit provides the most important theoretical foundation for explaining the principles of vertical and horizontal atmospheric transport of pollutants. The suspension or dispersal of particulate matter or heavy metal gases over cities by wind can be entirely attributed to Bernoulli's Principle and pressure gradients. Similarly, the phenomenon of thermal inversion (temperature reversal) observed in urban areas during winter months, causing polluted air to settle to the ground, is a direct application of the principles of buoyancy and density difference in fluids within environmental physics.

At the 10th-grade level, the topic is presented directly within the context of 'environmental pollution.' While the disadvantages of thermal power plants are discussed, it is acknowledged that heavy metals and gases emitted from chimneys are released into the environment. However, the relationship between the atmospheric transport of this emission and wind direction is not addressed. The focus is solely on the presence of pollutants at the source; the physical processes by which

these substances are ‘transported’ and deposited in distant ecosystems through atmospheric dynamics (precipitation or dry deposition) are neglected.

Table 4. Spiral Representation Matrix of Atmospheric Transport and Pollutant Dynamics Concepts in the 2026 Curriculum (9-12)

Grade	Unit	Relevant Learning Outcome / Content Context	Curriculum Approach / Representation	Deficiency / Potential
9	Fluids	PHYS.9.3.3, PHYS.9.3.4 Atmospheric pressure, buoyant force, fluid speed, and the Bernoulli Principle.	Focus on classical mechanical contexts such as airplane wings and roofs.	It serves as a fundamental framework for explaining the distribution of pollutants in cities, based on wind speed and the physics of thermal inversion (the trapping of air pollution).
10	Energy	PHYS.10.2.5 Advantages/disadvantages of energy sources, global warming, and carbon emissions.	Socio-scientific awareness of pollution.	The focus is solely on the presence of pollutants at the source; the dynamics of their transport and accumulation in the ecosystem via atmospheric winds remain a gray area.
11	Force and Motion	PHYS.11.1.1, PHYS.11.1.3 Addition of vectors in two dimensions, relative motion, and river problems.	A theoretical-mathematical approach in the context of riverboats/swimmers navigating a river with a current.	This can be transformed into horizontal transport (advection) models of radionuclide clouds released into the air, driven by atmospheric wind vectors.
12	Force and Motion	PHYS.12.1.3 Falling motion under fluid (air) resistance and the concept of 'Terminal Velocity'.	A mechanical approach limited to raindrops and parachutist analogies.	This is an excellent integration site for calculating the settling/deposition velocities (Physics of Dry Deposition) and suspension times of heavy metals and radioactive dust in the atmosphere.

The relative motion and river problems in 11th grade are mathematical twins of the vectorial transport (advection) mechanism for pollutants driven by wind currents in environmental physics. The direction and speed of a radionuclide cloud released into the air (for example, the cesium cloud after the Chornobyl accident) is the resultant sum (vector sum) of the cloud's own diffusion velocity vector and the current atmospheric wind speed vector. Making such interdisciplinary connections can contribute to students' learning in terms of environmental physics.In the 12th-grade curriculum, the topic of terminal velocity is usually covered only with classic examples such as 'a raindrop falling to the ground at a safe speed' or 'parachutists jumping'. However, the process by which heavy metal particles, radioactive dust, or microplastics fall to the ground and settle within the ecosystem is called 'Dry Deposition' in environmental physics and is governed entirely by the laws of terminal velocity. The particle's mass, radius, and air friction coefficient determine how long the pollutant will remain suspended in the atmosphere and how quickly it will settle to the ground. Therefore, this output is highly suitable for integration into advanced environmental physics problems, such as mapping environmental risk zones and establishing public health protection corridors, based on analyses of limiting velocity for micron-scale lead or cadmium dust emitted from industrial chimneys.

4. CONCLUSION

In this study, the renewed high school physics curriculum, within the scope of the ‘Turkish Century Education Model Secondary School Physics Curriculum (2026)’, was systematically examined through document review and content analysis to assess its alignment with the goals of building mass ‘radiation literacy’, environmental physics principles, and radiation health standards. The empirical findings confirm that the program has the theoretical mechanics and quantum infrastructure (Bernoulli principle, relative motion, terminal velocity, emission/absorption spectra) needed to model macroscale environmental problems. However, the current curriculum structure has confined these powerful physical tools entirely to classical engineering contexts and abstract mathematical equations. When the curriculum is analyzed in terms of the macro and micro dynamics within the triangle of Heavy Metals, Radionuclides, and Human Health, which forms the main vision of the book, the following fundamental conclusions have been reached:;

- Heavy Metals Context: Although the curriculum flawlessly presents the absorption of light at the 11th-grade level and the quantum mechanical infrastructure with atomic emission/absorption spectra at the 12th-grade level, it leaves the application of these physical principles in environmental analytics, in the determination of heavy metals such as mercury, lead, and cadmium in soils and aquatic ecosystems (via AAS and XRF technologies)

entirely in a gray area. The presence of heavy metals is only a superficial indicator of pollution at the 10th-grade level and cannot be translated into spectroscopic fingerprint analyses.

- Radionuclides Context: Nuclear energy (fission-fusion) and nuclear power plants are discussed at the 12th-grade level on a socio-scientific level. However, the macro-level 'thermal pollution' and thermal shock waves generated by cooling water during the operational processes of nuclear power plants in aquatic ecosystems have been overlooked. The most critical weakness is that the horizontal transport (advection) mechanisms of released radionuclide clouds under atmospheric wind currents have not been integrated into the 11th-grade relative motion (river problems) curriculum, and the dynamics of ground deposition (dry deposition) have not been integrated into the 12th-grade limiting velocity outputs.
- Human Health Context: The failure to clearly distinguish between ionizing and non-ionizing radiation in the first encounter with the concept of radiation in the 9th grade is likely to fuel societal 'radiophobia' tendencies. In the 12th grade, the biological risks at the tissue level of non-ionizing electromagnetic pollution, such as wireless networks (5G, IoT) and 'Electrosmog', to which modern humans are constantly exposed, and their chronic effects on melatonin hormone secretion and human health have not been subjected to a pedagogical filter.Ultimately, the study found that the emphasis on human health and the environment in the 2026 physics curriculum is theoretically strong but weak in terms of functional application. These results empirically demonstrate that physics education needs to be freed from formulaic frameworks and instead delve deeply into socio-scientific environmental and radiation literacy, a necessity for contemporary citizenship.

5. RECOMMENDATIONS

Based on the findings of the review and the structural gray areas in the program, the following concrete and functional strategies are suggested for future curriculum revisions, textbook authors, and field educators:

- Learning outcome suggestions for curriculum revision: Abstract mechanical and modern physics outcomes in the curriculum should be expanded with concrete learning outcome statements that can be directly added at the intersection of environmental physics and human health. For example:
  - 'Students analyze the chronic and acute effects of environmentally released radionuclides on human health by relating them to the concepts of physical half-life and biological half-life.'

- ‘Students understand the principles of friction and terminal velocity in fluids; • ‘Students model and present the rates at which microplastics and heavy metal particles in the atmosphere fall into the ecosystem (dry deposition physics).’

❖ ‘Students correlate the working principles of spectroscopic methods used to detect heavy metals in industrial waste with absorption spectra in quantum mechanics.’

❖ Suggestions for interdisciplinary STEM activity designs: Instead of memorizing formulas in physics lessons, micro-activities that will increase students' scientific literacy should be designed. In the 11th-grade Optics unit, while covering the visible color spectrum and filters, a simple ‘UV-Vis Spectrophotometer’ simulation or analogy that measures the number of heavy metals (pollution intensity) in water through color spectrum and light absorption should be developed and transformed into STEM-based projects. In the 12th-grade Electromagnetic Waves unit, while discussing ionizing and non-ionizing radiation bands, students should be given argumentation tasks that require them to calculate safe exposure limits for Wi-Fi or base station signals in their homes using the ICNIRP (International Commission on Non-Ionizing Radiation Protection) and ALARA principles.

❖ Recommendations for teacher training and pedagogical content knowledge: In-service training and pedagogical content knowledge development seminars should be urgently planned for physics teachers to enable them to keep up with current developments in environmental physics, ecotoxicology, and radiation health. Supporting teachers with an interdisciplinary vision that can transform abstract river problems into atmospheric pollutant transport vectors and classic limit-velocity parachutist examples into dry deposition dynamics of heavy-metal dust will directly determine the success of education reform in classrooms.

REFERENCES

Boeker, E., & van Grondelle, R. (2011). *Environmental physics: Sustainable energy and climate change* (3rd ed.). Wiley.

Bromet, E. J. (2014). Emotional consequences of nuclear power plant disasters. *Health Physics, 106*(2), 206–210. https://doi.org/10.1097/HP.0000000000000012

ICRP. (2007). *The 2007 recommendations of the International Commission on Radiological Protection (ICRP Publication 103).* Elsevier.

Karimi, M. S., Arif, S., & Noori, B. (2025). Greenhouse gases and their role in air pollution and global warming. *International Journal of Biological, Physical and Chemical Studies, 7*(1), 6–12. https://doi.org/10.32996/ijbpcs

Ministry of National Education of the Republic of Türkiye. (2026). *Türkiye century education model secondary school physics curriculum*. Board of Education. https://mufredat.meb.gov.tr/

Monteith, J. L., & Unsworth, M. H. (1990). *Principles of environmental physics* (2nd ed.). Elsevier.

Sarıhan, M. (2022). Nükleer tıp öğrencilerinin radyasyon okur-yazarlığının değerlendirilmesi [Evaluation of radiation literacy of nuclear medicine students]. *European Journal of Science and Technology, 41*, 85–91. https://doi.org/10.31590/ejosat.1114547

Chapter 21

Mapping The Thematic Evolution of Radionuclides, Toxic Metals, and Emerging Contaminants: A Bibliometric Study of the Last Decade

Mehmet Altan KURNAZ[1]

1. INTRODUCTION

Environmental pollution has evolved from a problem that can be explained by the effects of a single pollutant to a complex structure involving the simultaneous interactions of numerous pollutants released into the environment from different sources. Particularly as a result of industrial activities, mining operations, and intensive agricultural production processes, significant amounts of heavy metals and radionuclides such as aluminum (Al), iron (Fe), manganese (Mn), zinc (Zn), copper (Cu), lead (Pb), chromium (Cr), nickel (Ni), cobalt (Co), arsenic (As), cadmium (Cd), cesium (Cs), and uranium (U) are transported into the environment (Ustaoğlu and Islam, 2020; Vetrimurugan et al., 2017). These pollutants often do not exist alone in the environment; they combine in different compositions, creating synergistic effects on living organisms and ecosystems. This situation necessitates a more comprehensive investigation of the environmental behavior of pollutants and their combined effects on human health (Martinez-Morata et al., 2023). The mobility of heavy metals and radionuclides in the environment is determined by complex physical, chemical, and biological processes between water, soil, and sediment systems. While sediments function as long-term storage environments for these pollutants, pH, organic matter content, and the geochemical properties of the environment can affect the re-dissolution of pollutants and their transport to biological systems (Ustaoğlu and Islam, 2020). Similarly, agricultural activities, groundwater intrusions, and surface runoff play a significant role in the transport of pollutants to different environmental settings (Ustaoğlu and Islam, 2020; Vetrimurugan et al., 2017). In soil-plant systems, the uptake of toxic elements such as uranium by roots, their transport within the plant, and their impact on various metabolic processes further increase environmental risks (Chen et al., 2021).

The long-term persistence of pollutants in the environment affects not only physical and chemical systems but also the biological components of ecosystems. In

[1] Prof. Dr., Department of Mathematics and Science Education/Faculty of Education, Kastamonu University, Türkiye, makurnaz@kastamonu.edu.tr, (ORCID: 0000-0003-2824-4077)

particular, heavy metals are reported to alter the structure of soil microbial communities and reduce biodiversity in mining areas, waste disposal sites, and contaminated agricultural lands (Zhao et al., 2019). However, some microorganism species have been shown to develop resistance to heavy metals over time, and these properties can be utilized in bioremediation applications (Zhao et al., 2019; Kumari et al., 2016). The risks posed by heavy metals and radionuclides in environmental settings have also accelerated the development of new technologies for the removal of these pollutants. Due to the limitations of traditional treatment methods, especially in multi-pollutant systems, various approaches such as membrane technologies, electrodialysis applications, and chemical precipitation methods have been developed (Zhang et al., 2019; Wang and Zhuang, 2019). In recent years, advanced materials such as zeolitic imidazolate framework (ZIF) based nanomaterials, functionalized biopolymers, and metal hexacyanoferrate compounds have shown remarkable results in heavy metal and radionuclide removal (Liu et al., 2021). Furthermore, biological approaches such as microbial-derived carbonate precipitation and mycorrhizal fungus-assisted phytoremediation applications are also prominent among sustainable environmental technologies (Kumari et al., 2016; Chen et al., 2021). The mobility and accumulation of these pollutants in environmental settings lead to significant consequences that directly affect human health. In particular, the contamination of drinking water sources is considered one of the primary routes of exposure for the entry of heavy metals and radionuclides into the human body (Zhang et al., 2019). It has been reported that lead, nickel, cadmium, and similar elements detected in drinking water sources in areas with intensive agricultural activities and settlements near mining areas pose significant health risks (Vetrimurugan et al., 2017; Ustaoğlu and Islam, 2020). Therefore, determining exposure levels through biological indicators such as human blood, urine, hair, and nail samples has become an important research area in terms of protecting public health (Martinez-Morata et al., 2023). Research on heavy metals and radionuclides has increased significantly in recent years; a vast body of knowledge has accumulated around different research themes such as environmental transport mechanisms, biological effects, exposure assessments, and remediation technologies. However, studies that comprehensively present the development process of the field, research trends, prominent research topics, collaborations among researchers, and future research directions are limited. Therefore, in this study, scientific publications in the field of heavy metals and radionuclides were examined using bibliometric analysis methods; the aim was to reveal the intellectual structure, research trends, and development dynamics of the field.

2. DATA SOURCE AND LITERATURE REVIEW PROCESS

The Web of Science (WoS) database was chosen as the data source to access the scientific publications examined within the scope of the research. WoS's broad interdisciplinary scope, its indexing of high-impact academic journals and conference proceedings, and its provision of detailed bibliographic records such as author information, abstracts, keywords, and citation data necessary for bibliometric studies were decisive factors in this choice.During the literature review, fundamental concepts related to the research topic were first identified, and then a comprehensive search strategy was developed using field expertise and relevant literature reviews. Accordingly, the following query was developed using Boolean operators:

(("radiation exposure" OR "radionuclide" OR "uranium" OR "thorium" OR "radon") AND ("toxic metal*" OR "heavy metal*" OR "lead" OR "cadmium" OR "mercury") AND ("human health" OR "risk assessment" OR "carcinogenicity"))*

The search process was limited to the years 2016–2025. This period was chosen because it allows for the evaluation of current scientific trends in the research area and provides more holistic and standardized data for bibliometric analyses. Records obtained according to the defined criteria were exported from the Web of Science platform in BibTeX format and organized to make them suitable for the analysis process.

3. DATA ANALYSIS

The obtained bibliographic data were evaluated through bibliometric analyses performed in the R programming environment. Various statistical and bibliometric tools were used in the analysis process, primarily the Bibliometrix package (Aria & Cuccurullo, 2017). The analyses aimed to reveal publication production trends, research themes, keyword structures, prolific researchers and their countries, and the development dynamics of the field over time. These analyses allowed for a systematic evaluation of the intellectual structure and knowledge production processes of the research area. The study was conducted using only publicly available bibliographic data. No data was collected from human participants, no personal information was used, and no experimental procedures were performed. Therefore, the study was prepared in accordance with research and publication ethics principles.

4. RESULTS

4.1. Data Overview and Descriptive Statistics

The comprehensive bibliometric analysis of the retrieved dataset spans an 10-year period from 2016 to 2025 (Table, 1).

Table 1. The main information

Description	Results
Timespan	2016:2025
Sources	270
Documents	605
Annual Growth Rate %	-11.45
Document Average Age	4.45
Average citations per doc	21.85
Author's Keywords	1989
Authors	3276
Authors of single-authored docs	16
Single-authored docs	17
Co-Authors per Doc	6.64
International co-authorships %	29.26
Document Types	
Article	496
Article; book chapter	4
Article; early access	2
Article; proceedings paper	9
Editorial material	3
Letter	1
Proceedings paper	12
Review	76
Review; book chapter	2

A total of 605 documents were recovered from 270 distinct sources (journals, books, etc.), reflecting a diverse publishing landscape. The dataset exhibits a negative annual growth rate of -11.45%, suggesting a consolidation or shifts in research intensity over the final years of the analyzed decade. The average age of the published documents is 4.45 years, and they have garnered an average of 21.85 citations per document, indicating strong scientific impact and relevance within the community.Regarding authorship and collaboration patterns, 3,276 authors contributed to the dataset. Single-authored publications are rare, with only 16 authors publishing 17 single-authored documents. This highlights that the vast majority of the research is the product of collaborative efforts, as further evidenced by a high co-authorship average of 6.64 authors per document. Furthermore, international collaboration is quite prominent, with an international co-authorship rate of 29.26%, demonstrating strong global networks and cross-border academic exchange. A total of 1,989 unique author keywords were identified, reflecting a wide conceptual structure within the field.Regarding document types, traditional peer-reviewed articles constitute the largest share of the literature with 496 documents, supplemented by 76 review papers. The

remaining dataset comprises various formats, including proceedings papers, book chapters, editorial materials, and letters.

4.2. Scientific Production: Analyzing the Modern Decade of Research (2016–2025)

Although the roots and foundational frameworks of this research field date back several decades, this study deliberately focuses on the modern era through 2025. This specific timespan was chosen because the field has experienced an unprecedented paradigm shift, technological integration, and rapid expansion over the last decade, making contemporary literature more representative of current trends than historical data. Figure 1 displays the annual scientific production within this modern analytical window.

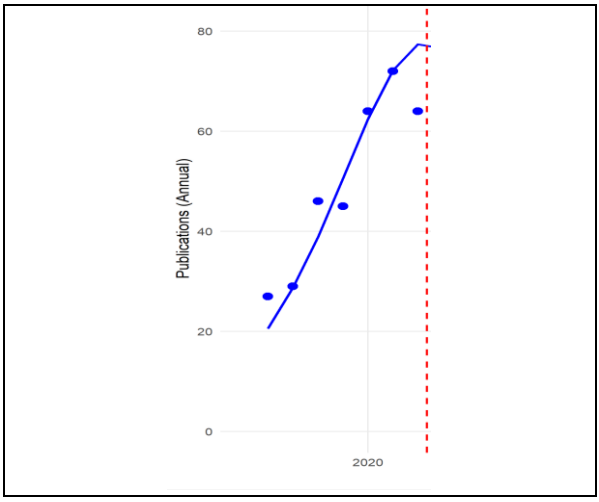


Figure 1. Life cycle of annual publications.

As observed in the temporal trajectory, the decade opens in 2016 with 27 documents. Rather than showing a stagnant or slowly evolving field, the empirical data demonstrate a strong, continuous escalation in scientific production. The annual output nearly doubles by 2019 (45 documents) and crosses the half-century mark in 2020 with 64 publications. This sharp and steady increase indicates that while the field has a long historical background, it has entered its "hyper-growth" or institutionalized phase in recent years, capturing massive academic attention and funding worldwide. The publication volume reached its contemporary zenith in 2025 with an impressive 93 documents, showcasing a highly active, dense, and rapidly expanding research ecosystem at the close of the observed period.

A critical methodological limitation and critique arise when evaluating the automated cumulative growth modeling plotted alongside this empirical data. In the predictive model, 2026 had no empirical observations and was excluded from the actual data collection. However, the software's logistic growth algorithm attempts to project a theoretical distribution across the timeline. Because the algorithm forces the data into a strict S-shaped curve, it mathematically assumes that the field must reach a natural saturation point. Consequently, the model back-propagates this theoretical ceiling, artificially forecasting a downward trend in annual velocity starting prematurely in 2024 (declining from 77.36 to 69.96 in 2024, and 59.45 in 2025) to allocate a fitted value of 47.48 for the unobserved year 2025.Therefore, this study emphasizes that the software's automated post-2024 stabilization and decline forecast is a purely mathematical artifact of the logistic model's boundary constraints rather than a reflection of actual scientific exhaustion. In reality, the empirical momentum -culminating in the historical peak of 93 documents in 2025- strongly indicates that the paradigm is still in a powerful hyper-growth phase and has not yet reached its real-world carrying capacity.To better understand the long-term trajectory and maturity stage of the analyzed decade, a logistic cumulative growth curve was modeled using the historical dataset from 2016 to 2025, with a future projection (Figure -2).

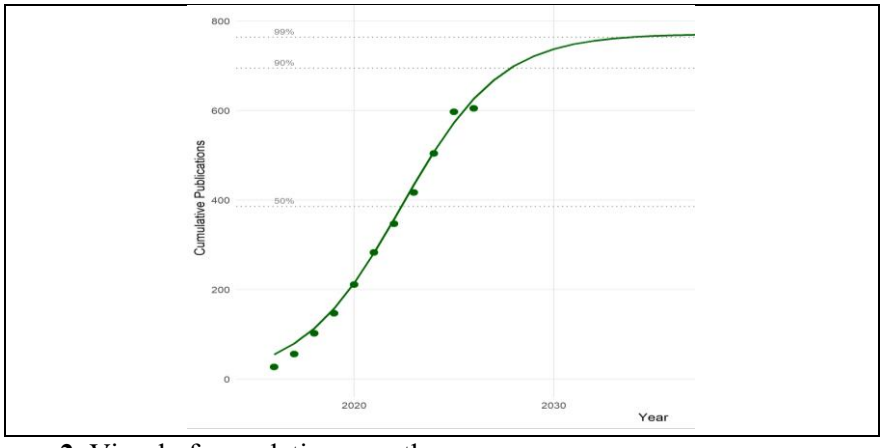


Figure 2. Visual of cumulative growth curve

Although the core concepts of this field have developed over a much longer historical timeline, restricting the empirical window to the modern decade reveals a classic S-shaped growth pattern (logistic growth), typical of rapidly evolving, institutionally consolidating scientific disciplines. The cumulative distribution highlights three distinct phases within this contemporary window;

- ❖ The Initial Acceleration Phase (2016–2020): In the early years of the analyzed decade, the cumulative volume rose steadily, transitioning from a baseline of under 100 publications to over 200 documents by 2020. This indicates the period when long-standing theoretical ideas began to expand into active, structured research lines.
- ❖ The Hyper-Growth Phase (2021–2025): Between 2021 and 2025, the curve exhibits a steep, nearly linear vertical climb, cutting through the 50% cumulative threshold around 2023. This dramatic surge indicates a period of intense paradigm convergence, massive literature production, and widespread academic adoption. The empirical data points (green dots) tightly align with the estimated growth model, demonstrating a highly predictable and robust expansion over the last few years.
- ❖ The Maturation and Saturation Projection (Post-2025): The logistic model projects that the current intensive growth wave will gradually transition into a stabilization phase as the conceptual boundaries of this specific decade's paradigm become saturated. According to mathematical estimates, the literature is expected to reach its 90% maturity capacity around 2030, eventually plateauing near its 99% theoretical carrying capacity (approximately 770 cumulative documents) post-2035.

This modeled saturation does not suggest that research in the broader field will cease; rather, it indicates that the specific research questions, technological tools, and thematic frameworks that characterized the 2016–2025 era will reach their natural scientific maturity. This statistical behavior fully justifies the methodological decision to isolate this specific ten-year window, as it successfully captures the entire lifespan -from acceleration to peak expansion- of the modern research wave.

4.3. Source Dispersion and Bradford’s Law of Citation

To evaluate the structural dispersion of literature across scientific journals and identify the core venues driving the contemporary era (2016–2025), Bradford’s Law of Scattering was applied. Bradford's formulation divides the total 270 sources into three distinct zones (Core, Zone 2, and Zone 3), each containing approximately one-third of the total 605 documents (Figure 3).

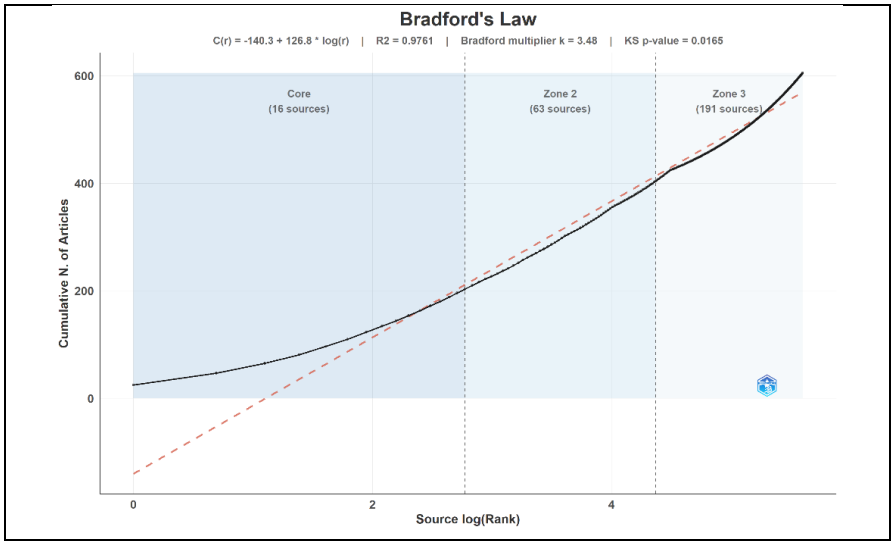


Figure 3. Visual of structural dispersion of literature.

The mathematical modeling reveals a highly institutionalized and concentrated publishing ecosystem within this modern decade:

- Zone 1 (The Core Zone): Comprising merely 16 core sources, this elite zone accounts for approximately one-third of the entire decade's scientific output. This high concentration indicates that, although the subject matter has a long historical background across various disciplines, its modern consolidation and high-impact breakthroughs over the last ten years are driven primarily by a specialized group of journals. These 16 journals represent the primary intellectual arenas for contemporary discussions.
- Zone 2 (Secondary Zone): Contains 63 sources. This area represents a broader boundary of journals that frequently accommodate the field's expanding scope as it integrates with adjacent disciplines.
- Zone 3 (Peripheral Zone): Encompasses 191 sources. This vast periphery consists mostly of journals that publish only one or two isolated papers related to the topic, highlighting the field's interdisciplinary reach and sporadic application across diverse fields.

The mathematical verification of the model is exceptionally robust, with a logarithmic regression formula of $C(r) = -140.3 + 126.8 \times log\ (r)$ and an explanatory power (R^2) of 0.9761. This indicates that 97.6% of the variance in document distribution is accounted for by Bradford's theoretical framework. The Bradford multiplier (k) is calculated as 3.48, meaning that as one moves from the core to the peripheral zones, the number of required journals increases by a factor

of roughly 3.5 ($16 \rightarrow 16 \times 3.5 \approx 56 \rightarrow 56 \times 3.5 \approx 196$), maintaining mathematical consistency across the three zones.Limiting the analysis to the 2016–2025 window demonstrates that the modern rapid growth of the discipline did not lead to an uncontrolled fragmentation across the scientific literature. Instead, the knowledge production remains anchored in a well-defined, elite core of 16 journals, providing clear direction for future researchers seeking high-impact publishing venues or literature reviews. The list of journals included in Zone -1 is given in Table- 2.

Table 1. The list of journals included in Zone 1

Source	Rank	Freq	Cumfreq	Zone
Environmental Science and Pollution Research	1	25	25	Zone 1
Science of the Total Environment	2	22	47	Zone 1
Journal of Radioanalytical and Nuclear Chemistry	3	18	65	Zone 1
Chemosphere	4	16	81	Zone 1
Environmental Monitoring and Assessment	5	16	97	Zone 1
Journal of Environmental Radioactivity	6	13	110	Zone 1
Journal of Hazardous Materials	7	13	123	Zone 1
Marine Pollution Bulletin	8	11	134	Zone 1
Environmental Geochemistry and Health	9	10	144	Zone 1
Heliyon	10	10	154	Zone 1
International Journal of Environmental Analytical Chemistry	11	9	163	Zone 1
Scientific Reports	12	9	172	Zone 1
Environmental Earth Sciences	13	8	180	Zone 1
Environmental Pollution	14	8	188	Zone 1
Water, Air, and Soil Pollution	15	8	196	Zone 1
Ecotoxicology and environmental safety	16	7	203	Zone 1

4.4. Conceptual Structure and Word Frequency Growth Analysis

To map the contemporary conceptual evolution and shifting research fronts within the analyzed domain, the cumulative growth velocity of the top author keywords was investigated across the designated ten-year window from 2016 to 2025 (Figure 4).

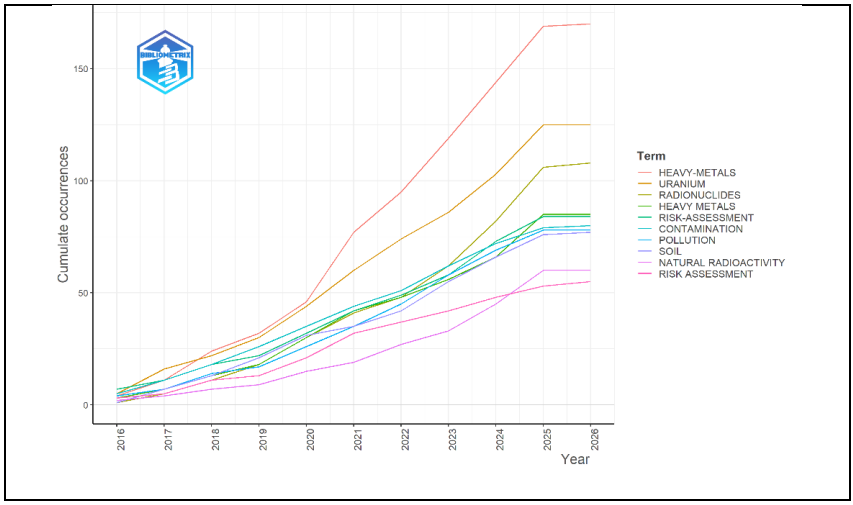


Figure 4. Words' frequency over time

It is methodologically vital to emphasize that the concepts tracked in this analysis -such as radionuclides, toxic elements, and risk models- possess extensive, decades-long historical foundations in environmental science prior to 2016. Therefore, the baseline values observed at the starting point of the graph do not signify the birth or historical emergence of these terms; rather, they represent the absolute zero-point calibration of our specific, isolated analytical window. Tracking their cumulative occurrences from this 2016 baseline allows the study to measure the immediate acceleration, modern intensity, and thematic densification of these established terms in the current era. The dynamic trajectory of word growth highlights a highly interconnected and specialized contemporary research focus:Primary Conceptual Anchors: The term "Heavy-Metals" operates as the dominant conceptual axis of the decade. While historically well documented, the term exhibited a massive, nearly linear acceleration after 2020 in this dataset, culminating in the highest cumulative volume by 2025 (over 160 occurrences). This sharp rise underscores that heavy metal contamination experienced a powerful resurgence and remained the central operational focus of modern literature.Radiological and Nuclear Intersections: This contemporary environmental focus is heavily intertwined with radiological hazards, as evidenced by the high-velocity growth of "Uranium" (reaching ~125 cumulative occurrences) and "Radionuclides" (crossing 100 cumulative occurrences) by 2025. The parallel, steeply upward trajectories of these keywords from 2018 onward indicate a structured, modern paradigm shift in which toxic heavy metals and nuclear contaminants are studied simultaneously within integrated environmental safety frameworks.Methodological and Media Vectors: The modern conceptual network is structurally sustained by terms reflecting target media and administrative goals, such

as "Risk-Assessment", "Contamination", "Pollution", and "Soil". These terms serve as operational linkages, demonstrating that the modern literature is not merely descriptive of historical contamination but is also heavily oriented toward contemporary risk mitigation, environmental remediation, and multi-media safety modeling.Emerging Natural Benchmarks: Notably, "Natural Radioactivity" exhibited a later but distinct acceleration phase after 2022, signaling a shifting modern research front toward distinguishing anthropogenic nuclear pollution from background naturally occurring radioactive materials.A prominent visual feature in the word frequency graph is the complete flattening of all cumulative trajectories between 2025 and 2026. In line with the previous chronological production analysis, this stagnation is a strict technical artifact of data limitations, as the year 2026 contained zero empirical observations and was excluded from active data indexing. The absolute horizontal lines do not reflect a sudden loss of thematic relevance or a conceptual freeze in the scientific community. Instead, they mathematically confirm that the cumulative frequency reached its empirical cap at the close of 2025. Consequently, the true conceptual momentum of the discipline remains anchored in the intensive vertical acceleration observed up to 2025, proving that the modern paradigm was still actively radiating and diversifying at the end of the observed decade.

4.5. Conceptual Network Mapping and Co-word Cluster Analysis

To decipher the intellectual topology and thematic intersections of the literature within the designated contemporary window (2016–2025), a keyword co-occurrence network analysis was executed. This network map visualizes how established scientific terms co-occur across individual documents, delineating the cognitive subfields and integrated paradigms that define the modern era. The analysis structurally subdivides the core literature into three primary thematic clusters, distinguished by color coding (Figure 5).

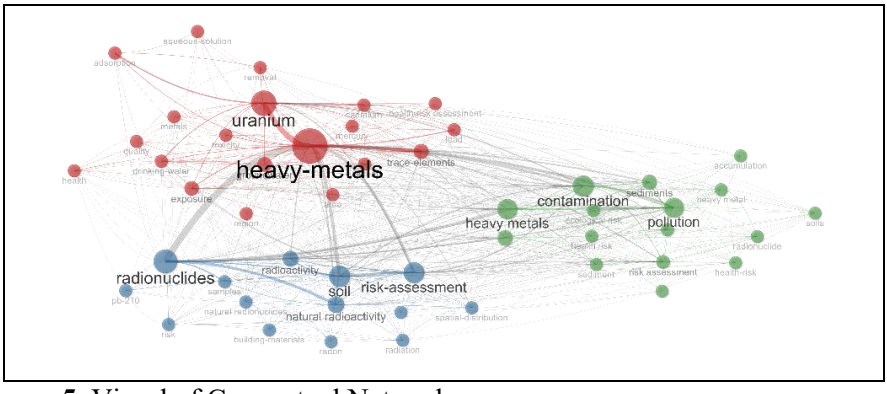


Figure 5. Visual of Conceptual Network

It is essential to reinforce that while individual core components like heavy metals, soil contamination, and uranium radioactivity possess well-documented independent histories stretching back several decades, their close spatial clustering in this contemporary network maps a unique, multidisciplinary paradigm merger characteristic of the 2016–2025 literature.The Source and Nuclear Contaminant Cluster (Red): Centered primarily around "uranium" and "heavy metals," this prominent cluster maps the foundational chemical and radiological agents under investigation. The strong, thick line linking uranium directly to heavy metals highlights a dense cross-disciplinary focus on nuclear mining legacies, industrial processing, and waste streams. Sub-themes filtering through this cluster -such as "removal," "adsorption," and "aqueous-solution" - indicate a strong experimental and technological push within the modern decade toward environmental engineering, focusing on extracting these specific pollutants from aquatic and ecological systems.

The Environmental Media and General Pollution Cluster (Green): This cluster acts as the geographic and ecological focus of the literature, anchored by terms such as "contamination", "pollution", and "heavy metals" (variant). This thematic group primarily captures how these hazardous substances migrate into different environmental sinks, particularly "sediments" and agricultural matrices. The network architecture positions this cluster as a vital conceptual bridge, linking raw chemical components to broader ecological risk frameworks.The Radiological Risk and Media Mapping Cluster (Blue): Dominating the lower-left sector of the network, this cluster is defined by "radionuclides", "soil", "risk-assessment", and "natural radioactivity". This grouping demonstrates the operational focus of the contemporary decade. It indicates that modern research is heavily invested in quantifying the precise biological and environmental exposure risks of both naturally occurring radioactive materials (NORM) and anthropogenic radio-isotopes in terrestrial media. Key nodes like "spatial-distribution," "building-materials," and "radon" suggest that spatial modeling and public health risk assessments within human habitats represent a major contemporary research front.The structural maturity of the 2016–2025 dataset is further verified by the dense, cross-cluster lines connecting the blue (risk/radionuclides), red (uranium/source), and green (pollution/media) zones. For instance, the prominent link spanning from "radionuclides" to "soil" and then to "heavy metals" mathematically proves that the modern literature has successfully broken out of isolated disciplinary silos. Rather than treating toxicological metal research and nuclear physics as separate domains, the contemporary era has fused them into a coherent, tripartite research nexus in which sources, media, and risk assessment are evaluated simultaneously.

4.6. Strategic Thematic Mapping and Evolutionary Maturity

To evaluate the structural maturity, operational relevance, and evolutionary trajectory of the conceptual building blocks within the modern decade (2016–2025), a strategic thematic map was constructed. By plotting keyword clusters based on Callon's centrality (relevance degree to the entire network) and density (internal development degree), the core research themes are categorized into four distinct strategic quadrants (Figure 6).

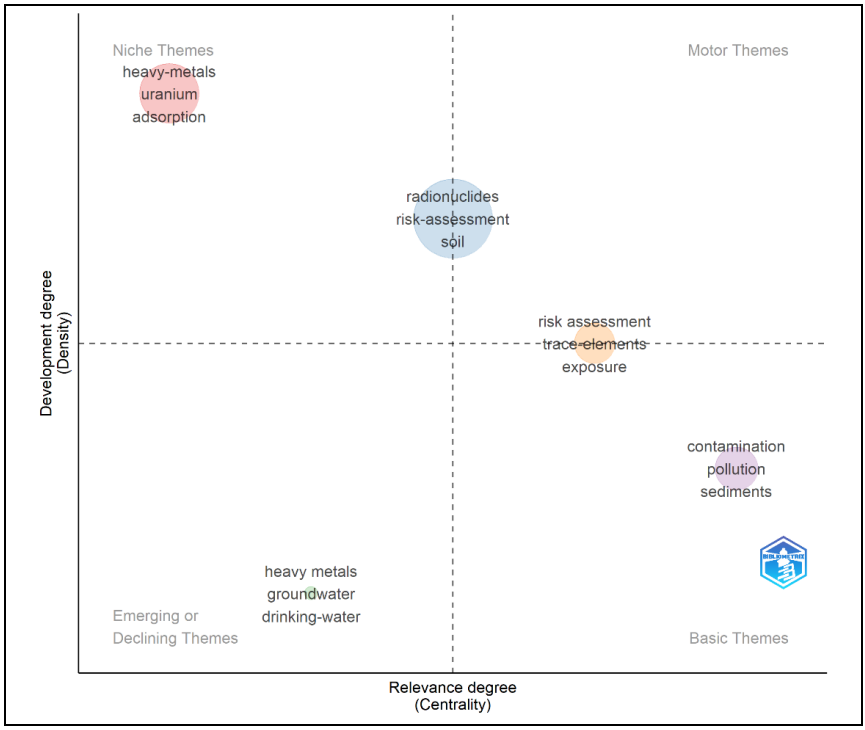


Figure 6. Strategic diagram of conceptual keyword clusters driving the modern research era.

Consistent with the chronological boundary limitations established earlier, this mapping does not imply that these environmental or radiological concepts were newly invented in the post-2016 window. Rather, it reveals how decades-long established topics have been strategically prioritized and conceptually restructured by the scientific community during this highly intensive recent decade.Motor Themes (Upper-Right Quadrant): Characterized by high density and high centrality, this quadrant traditionally hosts the driving forces of a discipline. Interestingly, the cluster containing "radionuclides", "risk-assessment", and "soil" sits directly on the border of this quadrant, tilting toward

the center. This strategic positioning proves that in the 2016–2025 era, the terrestrial modeling of radioactive hazards and integrated public health risk mapping achieved the status of a mature, well-developed, and mathematically structured cornerstone that actively bridges technical radio-physics with practical environmental monitoring.Basic and Transversal Themes (Lower-Right Quadrant): Exhibited by high centrality but low density, these themes represent the foundational underpinnings of the field. The cluster containing "contamination", "pollution", and "sediments" occupies a deep position here. This indicates that general pollution monitoring across geological media serves as the essential vocabulary and cross-cutting foundation of the entire discipline. While these topics lack highly specialized or novel internal methodologies (low density), no study in the modern era can operate without referencing them.Niche Themes (Upper-Left Quadrant): Defined by high density but low centrality, this quadrant contains highly specialized, technically advanced, yet isolated lines of research. The cluster comprising "heavy-metals", "uranium", and "adsorption" is deeply embedded in this sector. This structural placement reveals an important modern trend: while uranium and heavy metals are major chemical entities, contemporary research investigates them through highly specialized chemical engineering lenses (such as advanced adsorption materials and specific removal kinetics in aqueous solutions). These topics are technically sophisticated and internally well-developed, yet they remain somewhat marginalized from the broader environmental health policy discussions.Emerging or Declining Themes (Lower-Left Quadrant): Marked by low centrality and low density, this quadrant highlights peripheral or transitioning topics. The cluster involving "heavy metals" (variant), "groundwater", and "drinking-water" resides in this area. Within the specific context of this modern decade, this position indicates that hydro-toxicological tracking and water resource vectors are either in an early, nascent stage of methodological integration or are being overshadowed by the more dominant terrestrial (soil and sediment) frameworks.

4.7. Analysis of Scientific Stakeholders: Productive Authors, High-Impact Documents, and Global Collaboration (2016–2025)

To fully map the social architecture and intellectual leadership driving the modern decade of research (2016–2025), a comprehensive analysis of the most productive authors, globally cited documents, and corresponding author countries was conducted. While research on environmental radionuclides and toxic elements has a rich global history prior to 2016, evaluating these parameters within the isolated modern window reveals which specific academic actors, foundational papers, and geographical clusters have actively restructured and

spearheaded the contemporary paradigm.Author Productivity and Intellectual Leadership: The distribution of the most relevant authors highlights a highly active core of researchers driving the contemporary literature (Figure 7). Wang emerges as the most prolific author of the decade, leading the field with 15 distinct documents, followed closely by Liu (11) and Liu (10). A tightly packed cluster of investigators -including Chen, Khan, and Wang- each contributed 9 publications within this timespan. This concentration of productivity indicates that while the broader literature is expanding globally, a specialized cohort of key scientists provides the sustained empirical output and structural continuity that characterizes the 2016–2025 research wave.

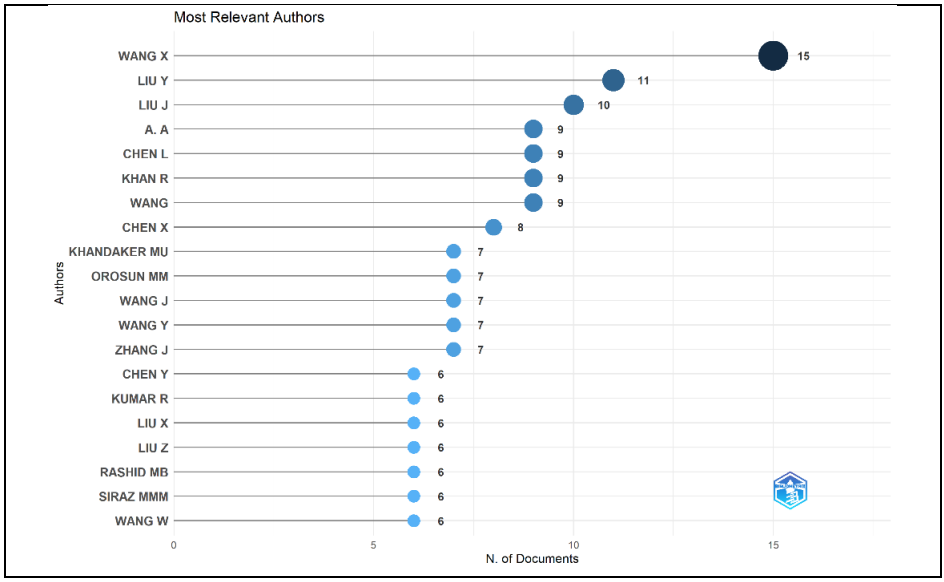


Figure.7 The social and intellectual structure of the domain during the modern era (Top 20 most relevant authors based on total document frequency).

Analysis of High-Impact Documents: Evaluating global citation footprints identifies the primary intellectual pillars that defined the decade's theoretical boundaries (Figure 8). The most globally cited document is authored by Zhao (2019) in *Ecotoxicology and Environmental Safety*, with 307 citations within a relatively short exposure window. This is closely followed by Wang (2019) in *Reviews in Environmental Science and Bio-Technology* (275 citations) and Ustaoglu (2020) in *Ecological Indicators* (261 citations). The fact that the most defining, high-impact papers are heavily concentrated between 2019 and 2021 mathematically aligns with the hyper-growth phase observed in the general temporal trajectory. These documents provided the updated risk-assessment

methodologies and heavy-metal tracking frameworks that the rest of the decade subsequently built upon.

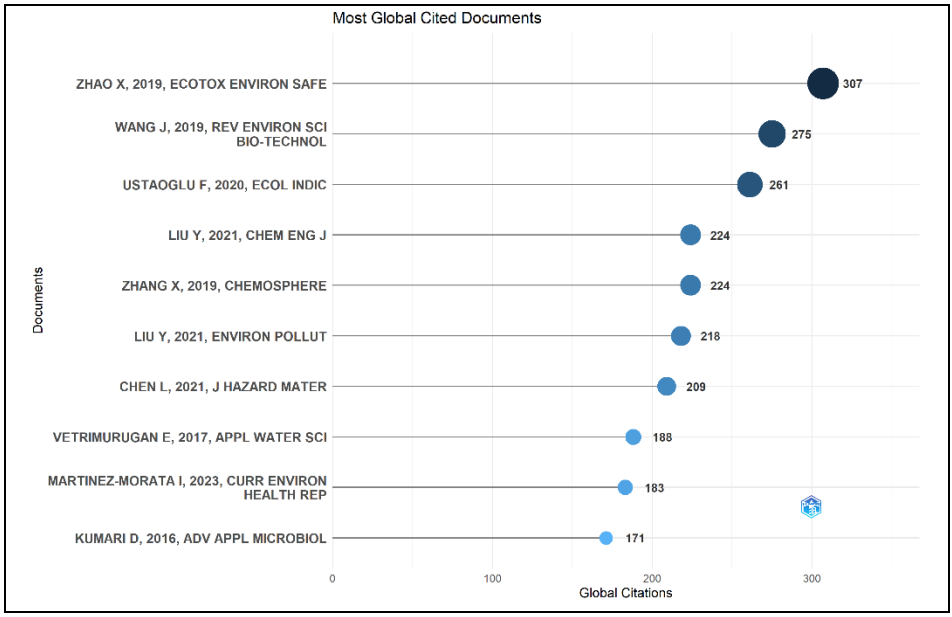


Figure.8 The social and intellectual structure of the domain during the modern era (Top 10 most globally cited documents, highlighting the foundational pillars established during the 2019–2021 hyper-growth turn).

Geographical Distribution and Collaboration Dynamics: The spatial distribution of scientific production is dominated by a clear geopolitical hierarchy led by Asian and Western research hubs (Figure 9). China stands as the undisputed global leader in this domain, producing well over 125 total documents. Notably, China also demonstrates a substantial volume of Multiple Country Publications (MCP, red bars), signaling strong international integration, alongside its high volume of Single Country Publications (SCP, blue bars). India ranks second, with approximately 60 documents, followed closely by the USA (around 55).

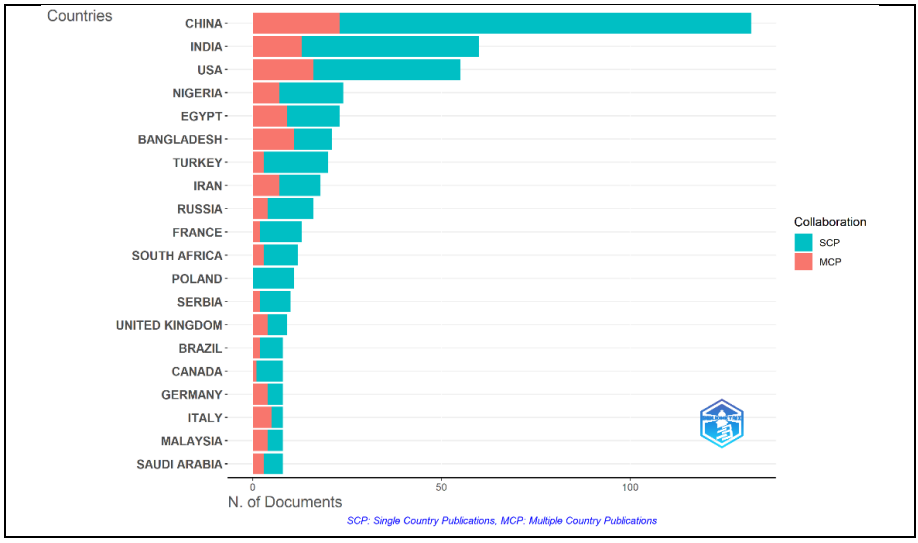


Figure.9 The social and intellectual structure of the domain during the modern era (Countries, partitioned by Single Country Publications (SCP) and Multiple Country Publications (MCP), showcasing the geopolitical distribution ratios.).

Middle Eastern and regional contributors also have a highly specialized presence in the top ten, with countries like Türkiye, Egypt, and Iran generating significant localized literature. Interestingly, countries like Turkey and Poland exhibit an overwhelmingly high ratio of Single Country Publications (SCP) relative to their total output. This operational behavior suggests that while these nations are actively generating vital, high-density empirical data targeting their local terrestrial or aquatic ecosystems, their research frameworks remain structurally localized. This highlights a clear strategic opportunity for future researchers in these regions to actively seek multinational partnerships (MCPs) to enhance the global scalability of their findings.

In conclusion, the social structure of the 2016–2025 era is characterized by a powerful publishing core in China and India, anchored conceptually by a select group of high-impact papers published at the turn of the decade, and driven forward by a dedicated elite of prolific scientists.

5. DISCUSSION

The empirical and structural mapping of the literature from 2016 to 2025 outlines a highly dynamic, institutionalized, and rapidly consolidating research paradigm. While individual conceptual pillars of this domain, such as heavy-metal toxicological monitoring, uranium mining environmental impacts, and radionuclide decay dynamics, have an extensive history in environmental science

stretching back several decades, their strategic integration over the last ten years marks an unprecedented modern paradigm shift. This context outlines the mathematical models, conceptual evolutions, and socio-geopolitical structures that have characterized the discipline during this hyper-growth decade. The chronological distribution of scientific production establishes that the 2016–2025 window represents a distinct "golden era" of literature expansion. The steady rise from 27 documents in 2016 to a historical peak of 93 documents in 2025 visually and mathematically aligns with the concept of a disciplined hyper-growth phase. This surge indicates that the field has successfully moved beyond isolated, esoteric investigations and has crystallized into a major, well-funded global academic priority. However, a critical epistemological contribution of this study lies in the deliberate methodological critique of automated bibliometric growth software. When plotted on a standard logistic S-curve, the mathematical model artificially forces the predictive annual velocity to plateau and to project a premature sharp decline starting in 2024 (from 77.36 to 59.45 by 2025). In traditional, uncritical bibliometric reporting, an author might blindly accept this output and conclude that the discipline is experiencing "thematic exhaustion" or a decline in academic interest. In reality, the empirical data completely refute the software's boundary constraints, showing an active vertical trajectory with 87 papers in 2024 and 93 in 2025. The mathematical model back-propagates an artificial saturation because it forces the dataset into a strict logistic carrying capacity ceiling to accommodate the zero-observation boundary of 2026. This technical artifact emphasizes an important caveat for contemporary bibliometricians: automated mathematical growth projections must always be balanced against real-world empirical momentum. The field has clearly not yet reached its conceptual carrying capacity, and its intense momentum is highly likely to continue to accelerate throughout the late 2020s.The verification of Bradford's Law provides robust evidence regarding how the scientific community publishes within this domain. A common critique of fields experiencing a sudden explosion in literature volume is that the knowledge production becomes highly fragmented, scattered across hundreds of predatory or non-specialized peripheral journals. However, the exceptionally high explanatory power (R^2 = 0.9761) and a Bradford multiplier (k) of 3.48 mathematically confirm that the contemporary expansion did not lead to uncontrolled fragmentation. Instead, the literature remains deeply anchored in a highly concentrated, elite core of just 16 journals, which account for one-third of the entire decade's scientific output. This structural concentration indicates that the modern era has established recognized, highly authoritative institutional arenas. These 16 core journals act as the primary intellectual gatekeepers,

ensuring that, even as empirical investigations accelerate, they are filtered through rigorous peer-review processes. For future researchers and academic stakeholders, this provides an actionable roadmap: these core venues represent the most strategic targets for both high-impact publishing and targeted literature reviews, maximizing the visibility and cross-cohesion of future studies. Analyzing the cumulative growth of author keywords and their co-occurrence networks over the 2016–2025 period reveals a major multidisciplinary paradigm shift. It is vital to reiterate that terms like "heavy metals," "uranium," and "radionuclides" did not originate in 2016; the zero-point baseline at the beginning of the temporal frequency charts is simply a technical calibration of this study's analytical window. However, the explosive vertical velocity of these terms after 2020 tells a story of modern urgency. The spatial configuration of the co-word network demonstrates that contemporary research has successfully shattered historical disciplinary silos. Rather than treating toxic heavy metal chemistry and nuclear radio-physics as isolated fields, the modern decade has forged a coherent, tri-partite research nexus linking sources, media, and risk assessment. The close proximity of "uranium" and "heavy metals" (the hyphenated variant in the network) alongside terms such as "adsorption" and "removal" reveals a highly specialized chemical engineering domain. This sub-field focuses intensely on remediation kinetics, seeking innovative, high-capacity materials to extract contaminants from aqueous solutions, driven by mining legacies and industrial effluents. Concepts like "contamination," "pollution," and "sediments" act as the vital conceptual bridge. They illustrate how these raw radioactive and heavy metal sources migrate across ecosystems, tracking their accumulation patterns in geological sinks. The network sector driven by "radionuclides," "soil," and "risk-assessment" represents the operational endpoint of the modern era. Research is no longer purely descriptive; it is heavily oriented toward human safety. The strong inclusion of "natural radioactivity," "building materials," and "radon" proves that quantifying radiological exposure risks within human habitats has become a dominant contemporary priority. The dense cross-cluster linkages weaving these zones together prove that a standard contemporary paper in this field now simultaneously evaluates the raw pollutant source, tracks its environmental media pathway, and models its biological risk assessment to human populations. The strategic thematic map further refines this structural understanding by analyzing the internal development (density) and external interaction (centrality) of these keyword clusters. The spatial distribution of the clusters reveals a compelling operational division in the modern era. The cluster containing "radionuclides," "risk-assessment," and "soil" sits directly on the border of the motor themes quadrant, acting as the driving engine of the

discipline. This high centrality and balanced density signify that terrestrial modeling of radioactive hazards has achieved full structural maturity. It is highly integrated into the broader environmental science discourse and serves as a core shared vocabulary. Conversely, the cluster containing "contamination," "pollution," and "sediments" occupies the basic themes quadrant, confirming its role as the essential, cross-cutting background knowledge that sustains the field without requiring novel internal methodological shifts. The most critical strategic insight emerged from the distinct separation of the heavy metal variants across the diagram. The hyphenated cluster ("heavy-metals," "uranium," "adsorption") resides deeply within the niche themes quadrant. This shows that laboratory-based chemical engineering approaches to pollutant removal are technically sophisticated, hyper-specialized, and internally well-developed (high density), yet structurally isolated from broader environmental health policy frameworks (low centrality). In sharp contrast, the unhyphenated cluster ("heavy metals," "groundwater," "drinking-water") is positioned in the emerging themes quadrant. This structural separation provides a vital diagnostic insight for the late 2020s: while advanced adsorption engineering has achieved high maturity as a specialized niche, the hydro-toxicological modeling of these contaminants in freshwater and drinking-water vectors represents the true emerging frontier that the scientific community must actively expand. The social architecture of the 2016–2025 era reveals a powerful geopolitical concentration dominated by Asian and Western research hubs. China is the undisputed global superpower in this domain, leading with an elite volume of publications, followed by India and the USA. The intellectual backbone of this decade was solidified between 2019 and 2021, with foundational papers such as Zhao (2019), Wang (2019), and Ustaoglu (2020) accruing hundreds of global citations. These milestone documents provided the refined heavy-metal risk indices and ecotoxicological frameworks that the prolific author networks (led by pioneers like Wang and Liu) subsequently deployed at a global scale. A particularly critical finding emerges when evaluating the collaboration dynamics of regional contributors like Türkiye and Poland. While Türkiye ranks highly among the top nations for absolute publication volume - demonstrating a highly active, dedicated local research community - its output is characterized by an overwhelmingly high ratio of Single Country Publications (SCP) relative to Multiple Country Publications (MCP). This structural behavior exposes a phenomenon known as the localization trap. Researchers in these regions are exceptionally productive in collecting vital, high-density empirical data targeting their specific local terrestrial, agricultural, or aquatic ecosystems. However, because these studies are conducted predominantly within isolated national boundaries and lack multinational co-

authorships, their findings remain localized in scope. To break out of this peripheral positioning and elevate local data into globally scalable frameworks, academic stakeholders in these regions must strategically pivot toward international collaborative networks and actively engage in cross-border partnerships (MCP) to amplify the global citation footprint and policy impact of their research. In conclusion, the social structure of the 2016–2025 era is characterized by a powerful publishing core in China and India, anchored conceptually by a select group of high-impact papers published at the turn of the decade, and driven forward by a dedicated elite of prolific scientists.

6. CONCLUSIONS AND RECOMMENDATIONS

The bibliometric mapping of the literature from 2016 to 2025 provides a conclusive evaluation of a rapidly consolidating, high-velocity research paradigm. While the individual environmental and radiological components of this domain possess extensive, decades-long historical roots, their structural integration over the modern decade has crystallized into a mature, well-funded global academic priority. Chronological analysis refutes automated software assumptions regarding paradigm saturation, mathematically demonstrating that the discipline remains in a powerful hyper-growth phase peaking at 93 documents annually by the close of 2025. Furthermore, the verification of Bradford's Law confirms that this rapid expansion has not led to knowledge fragmentation; instead, production remains rigorously institutionalized within an elite core of 16 specialized journals.

Conceptually, the modern era is defined by a successful transition from isolated disciplinary silos into a tri-partite research nexus that simultaneously links pollutant sources, ecological media pathways, and human risk mitigation. Strategic thematic mapping confirms that while laboratory-based chemical engineering approaches to heavy metal and uranium removal have achieved high internal technical maturity as specialized niches, they remain structurally isolated from broader public health policy. Conversely, the hydro-toxicological modeling of these contaminants within groundwater and drinking-water vectors represents the primary emerging frontier for the scientific community. Geopolitically, the field is dominated by a powerful publishing core led by China, India, and the USA, supported by foundational intellectual pillars established at the turn of the decade. However, a critical socio-structural limitation characterizes regional contributors like Turkey, where highly productive empirical data collection remains trapped within isolated national boundaries due to an exceptionally low international collaboration ratio.

Based on these structural insights, the following strategic recommendations are proposed for future researchers, funding agencies, and academic stakeholders;

i. *Pivoting to Freshwater Vectors: Researchers should actively transition from heavily saturated terrestrial and sediment frameworks toward modeling the migration kinetics and bioaccumulation profiles of radionuclides and heavy metals in freshwater and drinking-water systems.*
ii. *Breaking the Localization Trap: Prolific research communities in regional hubs, particularly in Turkey and Poland, must strategically restructure their publishing behavior by establishing multi-national co-authorships and cross-border environmental tracking projects to enhance global citation footprints and policy scalability.*
iii. *Bridging Engineering and Policy: Future studies in chemical engineering must explicitly connect laboratory adsorption and removal mechanisms to practical, macro-level public health risk assessment models, ensuring that technical remediation protocols directly influence environmental safety standards and human habitat protection.*
iv. *Critical Algorithmic Evaluation: Future bibliometric investigators must exercise rigorous methodological caution when utilizing automated growth projections near boundary data limits, ensuring that theoretical mathematical models are critically balanced against actual, real-world empirical production trends.*

REFERENCES

1. Aria, M., & Cuccurullo, C. (2017). Bibliometrix: An R tool for comprehensive science mapping analysis. Journal of Informetrics, 11(4), 959–975. https://doi.org/10.1016/j.joi.2017.08.007
2. Chen, L., Liu, J., Zhang, W., Zhou, J., Luo, D., & Li, Z. (2021). Uranium (U) source, speciation, uptake, toxicity, and bioremediation strategies in soil-plant system: A review. Journal of Hazardous Materials, 413, 125319.
3. Kumari, D., Qian, X. Y., Pan, X., Achal, V., Li, Q., & Gadd, G. M. (2016). Microbially-induced Carbonate Precipitation for Immobilization of Toxic Metals. Advances in Applied Microbiology, 94, 79-108.
4. Liu, Y., Pang, H., Wang, X., Yu, S., Chen, Z., Zhang, P., Chen, L., Song, G., Alharbi, N. S., Rabah, S. O., & Wang, X. (2021). Zeolitic imidazolate framework-based nanomaterials for the capture of heavy metal ions and radionuclides: A review. Chemical Engineering Journal, 406, 127139.
5. Liu, Y., Wang, P., Gojenko, B., Yu, J., Wei, L., Luo, D., & Xiao, T. (2021). A review of water pollution arising from agriculture and mining activities in Central Asia: Facts, causes and effects. Environmental Pollution, 291, 118209.
6. Martinez-Morata, I., Sobel, M., Tellez-Plaza, M., Navas-Acien, A., Howe, C. G., & Sanchez, T. R. (2023). A State-of-the-Science Review on Metal Biomarkers. Current Environmental Health Reports, 10(3), 215-249.
7. Ustaoğlu, F., & Islam, M. S. (2020). Potential toxic elements in sediment of some rivers at Giresun, Northeast Turkey: A preliminary assessment for ecotoxicological status and health risk. Ecological Indicators, 113, 106237.
8. Vetrimurugan, E., Brindha, K., Elango, L., & Ndwandwe, O. M. (2017). Human exposure risk to heavy metals through groundwater used for drinking in an intensively irrigated river delta. Applied Water Science, 7, 3267-3280.
9. Wang, J., & Zhuang, S. (2019). Removal of cesium ions from aqueous solutions using various separation technologies. Reviews in Environmental Science and Bio/Technology, 18, 231-269.
10. Zhang, X., Gu, P., & Liu, Y. (2019). Decontamination of radioactive wastewater: State of the art and challenges forward. Chemosphere, 215, 543-553.
11. Zhao, X., Huang, J., Lu, J., & Sun, Y. (2019). Study on the influence of soil microbial community on the long-term heavy metal pollution of different land use types and depth layers in mine. Ecotoxicology and Environmental Safety, 170, 218-226

Chapter 22

Radioactivity Levels in Mushroom Samples

Aydan ALTIKULAÇ [1]

1. INTRODUCTION

Radioactivity in foods can be defined as foods containing natural radionuclides (^{238}U, ^{232}Th, and ^{40}K) or artificial radionuclides (^{137}Cs, ^{90}Sr, and ^{131}I) at certain levels as a result of human activities. Natural radioactivity occurs when radionuclides naturally found in the earth's crust pass to plants and animals through soil, water, and air. Artificial radioactivity involves radionuclides released into the environment as a result of nuclear activities or accidents. Radionuclides taken through foods cause internal exposure. The radiation dose received varies depending on the type of radionuclide, activity concentration, consumption amount, and biological behavior. Under normal conditions, exposure to natural radionuclides is at low levels and is accepted within the limits determined by international organizations. However, in cases of high-level radioactive contamination, long-term exposure may lead to various health effects, particularly an increase in cancer risk. Therefore, the regular monitoring of foods is of great importance. Mushrooms are among the important food sources widely consumed around the world due to their high nutritional value and low energy content. They are considered an important part of a healthy diet because they are rich in protein, dietary fiber, B-group vitamins, vitamin D, potassium, phosphorus, selenium, and various antioxidant components. Furthermore, their low fat and sodium contents and the fact that they do not contain cholesterol make mushrooms a valuable food in terms of balanced nutrition[1-3].Mushrooms are considered important bioindicators of environmental radioactivity because they can absorb nutrient elements and radionuclides from a large soil volume through their mycelia. In studies conducted in the Eastern Black Sea Region of Türkiye after the Chernobyl accident, it determined that ^{137}Cs activity concentrations in wild mushrooms were higher than those in cultivated plants. The reason for this is that cesium is chemically similar to potassium and is easily taken up by mushrooms [4-7]. Several studies have been conducted to determine ^{137}Cs activity concentrations in mushrooms grown in different regions of the world [8-15].

[1] Assoc.Prof. Dr., Ula Ali Koçman Vocational School, Muğla Sıtkı Koçman University, Turkey; aydanaltikulac@mu.edu.tr , (ORCID:0000-0002-2041-4193)

In this study, wild mushroom samples naturally growing in 14 different locations within the borders of the province of Samsun in the Black Sea Region of Türkiye were collected, and gamma spectrometric radioactivity analyses were performed on these samples to determine the activity concentrations of natural and artificial radionuclides. The main reason for investigating radiation in mushrooms in the Black Sea Region is the radioactive fallout transported to the region after the 1986 Chernobyl Nuclear Power Plant accident. Especially in the Eastern Black Sea Region, where precipitation is high, Cesium-137 (^{137}Cs) remained in the soil for many years and was taken up by mushrooms more effectively than many other plants. Today, while nearly 40 years have passed since Chernobyl, the amount of ^{137}Cs in the environment has significantly decreased due to the physical half-life of Cs being approximately 30 years. However, because the organic layer in forest ecosystems renews slowly, measurable levels of ^{137}Cs can still be found in some wild mushroom species. The levels show great variability depending on the mushroom species, the characteristics of the soil in which it grows, altitude, and the microregion where it is found [16-17].

2. MATERIALS AND METHODS

Figure-1 show that the locations where the mushroom samples analyzed in the study were collected. Within the scope of the study, plant samples were collected from garden and agricultural areas located at 14 different sampling points shown in Figure -1. The fresh masses of the samples delivered to the laboratory were determined using an analytical scale and recorded. The samples were then cut into small pieces using stainless steel knife to ensure homogeneous drying. The prepared samples were dried at 105°C for 12 hours in preheated drying oven to remove their moisture content. After the drying process, the samples transferred into high-temperature-resistant porcelain crucibles, and the incineration process was carried out in a controlled manner. The temperature gradually increased to the 300-350°C range to ensure the complete removal of organic components and obtain homogeneous ash. After the obtained ash samples were cooled to room temperature, they were transferred into standard measurement containers whose tare weights had been previously recorded, and their net masses were determined using an analytical scale and recorded. During measurement, to prevent radon gas loss and to ensure secular equilibrium between the ^{226}Ra decay series and short half-life decay products, the sample containers tightly sealed, and the joints of the containers were sealed with parafilm to make them leakproof. The prepared samples were kept for one month before gamma spectrometric analysis to allow secular equilibrium to be established. The gamma spectrometric analyses of the mushroom samples were performed using a gamma-ray spectrometer (ORTEC-

905-4) equipped with a 7.62 × 7.62 cm NaI(Tl) detector placed inside a tabletop lead shield. The efficiency calibration of the system was performed using RGU-1, RGTh-1, and RGK-1 reference materials certified by the International Atomic Energy Agency (IAEA). Each soil sample was measured for 80,000 seconds while preserving the source-detector geometry used in the efficiency calibration process. The gamma spectrum of each sample was analyzed using the ORTEC ScintiVision software. The ^{238}U activity concentration was determined using the 1764.5 keV gamma photopeak of ^{214}Bi. The ^{232}Th activity concentration was determined using the 2614.4 keV gamma photopeak of ^{208}Tl. The ^{40}K and ^{137}Cs activity concentrations were calculated based on their characteristic gamma energy lines at 1460.8 keV and 661.7 keV, respectively [18].

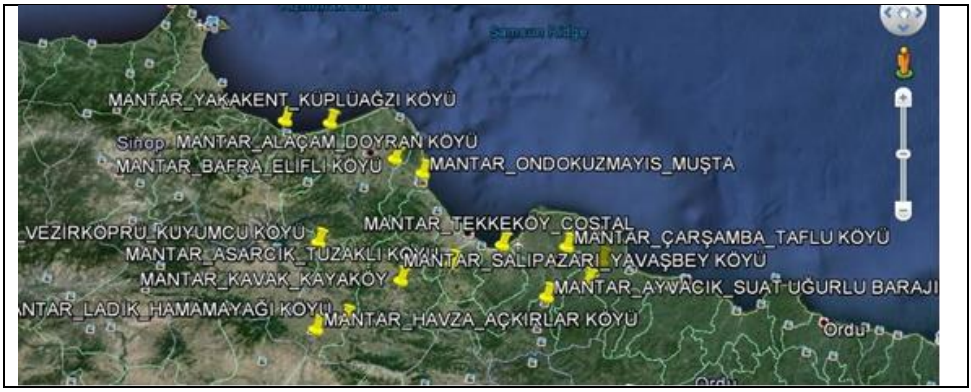


Figure 1.14 different locations within the borders of the province of Samsun in the BlackSea Region of Türkiye

2.1 Calculated radiological parameters

2.1.1 Method detection limit

The method detection limit (MDL) is a term that refers to the detection capacity of a measurement system under certain conditions. MDL is calculated as follows:

$$MDL = 4,66\sqrt{Background} \,/\, (t.Y.m.\eta) \tag{1}$$

Here, Background is the background radiation value, t is the counting time, Y is abundance, m is mass, and η is efficiency at photopeak [19].

2.1.2 Activity measurement

After the detector's energy and efficiency calibrations are completed, the energy and detection efficiency values of the gamma energy peaks to be used in activity calculations are determined. In the gamma spectrum obtained as a result of the counting process, the net areas of the photopeaks of interest are calculated by applying background radiation correction. Using the obtained net peak areas, the activity concentrations of the relevant radionuclides were calculated utilizing Formula 1.

$$A(Bq/kg) = \frac{N_{net}}{\varepsilon_\gamma t I_\gamma m} \quad (2)$$

Here, A is the calculated activity, N_{net} is the net peak area, ε_γ is the detector efficiency for the peak of interest, t is the counting time, m is the mass of the sample (kg), and I_γ is the emission probability of the gamma energy [20].

Table 1: Radioactivity concentrations measured in mushroom samples

Mushroom samples	Activity concentrations ($Bqkg^{-1}$)			
	^{238}U	^{232}Th	^{40}K	^{137}Cs
1-Ondokuzmayıs	0.309±0.051	0.249±0.028	54.97±1.78	0.602±0.039
2-Terme	< 0.021	0.32±0.12	72.03±2.15	0.523±0.013
3-Salıpazarı	0.076±0.038	0.077±0.020	85.88±2.57	3.64±0.114
4-Ayvacık	<0.033	0.086±0.018	81.32±2.46	0.265±0.026
5-Alaçam	<0.052	0.186±0.024	131.67±3.99	0.075±0.024
6-Yakakent	0.344±0.122	0.207±0.053	166.19±5.16	<0.027
7-Bafra	0.184±0.037	0.093±0.014	75.36±2.26	0.041±0.016
8-Asarcık	<0.035	0.060±0.015	44.28±1.39	0.663±0.041
9-Ladik	0.516±0.139	0.192±0.030	160.81±5.13	0.415±0.031
10-Çarşamba	0.182±0.051	0.109±0.031	121.12±3.67	0.072±0.023
11-Tekkeköy	<0.045	0.109±0.022	147.57±4.42	0.311±0.037
12-Kavak	0.112±0.082	0.152±0.026	102.89±3.19	0.390±0.033
13-Havza	0.18±0.037	0.140±0.023	102.25±3.07	0.052±0.015
14-Vezirköprü	0.211±0.041	0.172±0.022	80.20±2.44	0.480±0.029
Mean	0.16	0.15	101.89	0.53

2.1.3 Annual Effective Dose

The calculation of the annual effective dose (AED) resulting from internal exposure caused by radionuclides present in foods is important for evaluating the potential radiological risk to human health. The contribution from food consumption within the AED naturally received by an adult individual was

calculated by considering the activity concentrations of radionuclides measured in foods, effective dose conversion factors, and the average amount of food consumed by an adult individual in one year. The radiation dose taken by humans through nutrition and varying depending on mushroom consumption amounts was calculated using formula -2 [21-22].

Table2:

Mushroom samples	Annual effective dose (μSv/y)			
	^{238}U	^{232}Th	^{40}K	^{137}Cs
1-Ondokuzmayıs	0.0030±0.0005	0.0123±0.0014	0.0748±0.0024	0.00175±0.00011
2-Terme	MDL	0.0161±0.0060	0.0982±0.0029	0.00140±0.00003
3-Salıpazarı	0.0007±0.0003	0.0038±0.0010	0.1171±0.0035	0.01041±0.0003
4-Ayvacık	MDl	0.0043±0.0009	0.1109±0.0033	0.00073±0.00007
5-Alaçam	MDL	0.0094±0.0012	0.1795±0.0054	0.00027±0.00006
6-Yakakent	0.0034±0.0012	0.0104±0.0026	0.2266±0.0070	MDL
7-Bafra	0.0018±0.0003	0.0047±0.0007	0.1027±0.0030	0.00011±0.00004
8-Asarcık	MDL	0.0030±0.0007	0.0603±0.0018	0.0018±0.0001
9-Ladik	0.0051±0.0013	0.0098±0.0015	0.2193±0.0069	0.00118±0.00008
10-Çarşamba	0.0018±0.0005	0.0055±0.0015	0.1652±0.0050	0.00020±0.00006
11-Tekkeköy	MDL	0.0055±0.0011	0.2012±0.0060	0.00088±0.00010
12-Kavak	0.0011±0.0008	0.0076±0.0013	0.1403±0.0043	0.00111±0.00009
13-Havza	0.0017±0.0003	0.0070±0.0011	0.1403±0.0041	0.00014±0.00004
14-Vezirköprü	0.0020±0.0004	0.0087±0.0011	0.1093±0.0033	0.00137±0.00008

$$H_{T,r}=\Sigma\ (\ U_i\ C_i\ )g_{T,r} \quad (3)$$

In this formula,H expresses the effective dose value (μSv/year),Ui and Ci respectively represent the annual consumption amount (kg) and activity concentration ($Bqkg^{-1}$),gT,r expresses the dose conversion coefficient of the relevant radionuclide ($SvBq^{-1}$),The gT,r value for ^{40}K, ^{238}U, ^{232}Th, and ^{137}Cs is respectively 6.2×10^{-3} , 0.045, 0.23, and 1.3×10^{-2} [23].

3. RESULT AND DISCUSSION

In the analyzed mushroom samples, the activity concentrations of ^{238}U, ^{232}Th, ^{40}K, and ^{137}Cs radionuclides were determined, and the AED values resulting from these radionuclides were calculated. The obtained activity concentrations are

presented in Table 1, and the AED values are presented in Table 2. As a result of the gamma spectrometric analyses performed on the mushroom samples, the mean activity concentrations of ^{238}U, ^{232}Th, ^{40}K, and ^{137}Cs radionuclides were determined as 0.16, 0.15, 101.89, and 0.53 Bq kg^{-1}, respectively. Among the analyzed samples, the highest ^{238}U activity concentration was measured in the mushroom sample taken from the Ladik district as 0.516±0.139 Bq kg^{-1}. In contrast, in the samples taken from the Terme, Ayvacık, Alaçam, Asarcık, and Tekkeköy districts, ^{238}U activity concentrations could not be determined because they remained below the minimum detectable activity (MDL) value. In the examined mushroom samples, ^{232}Th activity concentrations ranged between 0.060±0.015 and 0.320±0.120 Bq kg^{-1}. As shown in Table 1, the lowest ^{40}K activity concentration was determined in the mushroom samples taken from the Asarcık district as 44.28±1.39 Bq kg^{-1}, while the highest value was determined in the samples taken from the Yakakent district as 166.19±5.16 Bq kg^{-1}. The ^{137}Cs activity concentration in the mushroom samples taken from the Yakakent district remained below the MDL value. Among the measurable samples, the highest ^{137}Cs activity concentration was detected in the samples taken from the Salıpazarı district as 3.64±0.114 Bq kg^{-1}, while the lowest value was detected in the samples taken from the Bafra district as 0.041±0.016 Bq kg^{-1}. The AED values to which individuals are exposed through mushroom consumption and the contributions of ^{238}U, ^{232}Th, ^{40}K, and ^{137}Cs radionuclides to the total dose were calculated using Formula 2, and the results are presented in Table - 2. In the calculations, the annual per capita mushroom consumption amount was accepted as 0.22 kg, and this value was based on annual mushroom consumption data reported by Demir [24].

Table 3. radionuclide activity concentrations in mushroom samples regions

	^{238}U	^{232}Th	^{40}K	^{137}Cs	Reference
Czechia- Opava region				11,8-8.77	Harkut et al. (2021)
Türkiye	2.33-8.54	0.35-543	4.3-90.0		Akça et al. (2014)
Poland			1316±40-1895±79	118±2 - 1647±12	Strumińska-Parulska, et al. (2025)
Türkiye			715-1779	2.4- 109	Turhan et al.(2207)
China	1-34.3	2.26-32.3	208-2.38	0.6-130.3	Wang et al. (2021)
Northern Norway			733 ± 1.2 Bq/kg	218 ± 3.0 Bq/kg	Gwynn et al. (2013)
Italy				300- 1800	Cocchi et al. (2017)
Rogozno area of Poland			450-3519	437-8855	Bem et al. (1990)

According to the calculated AED values, the dose originating from ^{40}K in mushroom samples was determined to range between 0.07 and 0.22 μSv year^{-1}, while the dose originating from ^{137}Cs was determined to range between 0.0001 and 0.001 μSv year^{-1}. These values were lower than the 0.99-3.56 μSv year^{-1} dose range reported for 40K in mushroom samples in the TAEK report, and they were consistent with the results indicating that ^{137}Cs-related doses were below measurable levels in the vast majority of analyzed samples [25]. These results show that the radiological effective dose resulting from the consumption of the examined mushroom samples was at quite low levels. Furthermore, Table 3 presents the results of studies conducted to determine radionuclide activity concentrations in mushroom samples in different regions of the world. These studies allow the comparison of natural radionuclide activity concentrations, especially for ^{137}Cs, measured in mushrooms grown in different geographical regions.

4. CONCLUSION

The presence of the fission product ^{137}Cs detected in the analyzed mushroom samples is largely considered to originate from the radioactive fallout released into the environment after the Chernobyl Nuclear Power Plant accident in 1986. Because the organic layer in forest ecosystems renews slowly, and Cs can maintain long-term persistence in soil, wild mushrooms, in particular, can still contain measurable levels of ^{137}Cs today. Due to the limited nature of fossil fuel reserves, nuclear energy is considered one of the important options for ensuring energy supply security in Türkiye, as in many other countries. Studies aimed at determining the reserves of uranium and thorium, which are natural radioactive elements, monitoring their environmental distributions, and revealing their radiological characteristics are important for the development and safe use of nuclear energy technologies. Furthermore, the regular monitoring of the levels of natural and artificial radionuclides in environmental media provides scientific data for evaluating the radiation doses to which the public is exposed and determining possible environmental effects.

REFERENCES

1-Kalač, P. (2013). A review of chemical composition and nutritional value of wild-growing and cultivated mushrooms. Journal of the Science of Food and Agriculture, 93(2), 209–218. https://doi.org/10.1002/jsfa.5960

2- Valverde, M. E., Hernández-Pérez, T., & Paredes-López, O. (2015). Edible mushrooms: Improving human health and promoting quality life. International Journal of Microbiology, 2015, 376387. https://doi.org/10.1155/2015/376387

3- U.S. Department of Agriculture. (2024). FoodData Central. https://fdc.nal.usda.gov/

4- International Atomic Energy Agency. (2006). Environmental consequences of the Chernobyl accident and their remediation: Twenty years of experience (Report of the Chernobyl Forum Expert Group "Environment"). IAEA. https://www.iaea.org/publications/7382/environmental-consequences-of-the-chernobyl-accident-and-their-remediation-twenty-years-of-experience

5- United Nations Scientific Committee on the Effects of Atomic Radiation. (2008). Sources and effects of ionizing radiation. UNSCEAR 2008 Report to the General Assembly with Scientific Annexes. Volume I. United Nations.

6- Rühm, W., Kammerer, L., Hiersche, L., & Wirth, E. (2013). Long-term changes of ^{137}Cs concentrations in wild mushrooms after the Chernobyl accident. Journal of Environmental Radioactivity, 126, 231–238.

7- Karadeniz, Ö., & Yaprak, G. (2007). Transfer of radiocaesium from soil to wild mushrooms collected in the eastern Black Sea region of Turkey. Journal of Environmental Radioactivity. (Doğu Karadeniz'de yabani mantarlarda ^{137}Cs düzeylerini inceleyen Türkiye kaynaklı çalışma.)

8- Harkut, O., Alexa, P., & Uhlář, R. (2021). Radiocaesium Contamination of Mushrooms at High- and Low-Level Chernobyl Exposure Sites and Its Consequences for Public Health. Life (Basel, Switzerland), 11(12), 1370. https://doi.org/10.3390/life11121370

9-Akca, S., Söğüt, Ö., Küçükönder, E., Doğru, M., et al. (2014). Radioactivity levels in some mushroom species and consequent doses. Asian Journal of Chemistry, 26(3), 879–882. https://doi.org/10.14233/ajchem.2014.15671

10- Strumińska-Parulska, D., Moniakowska, A., Szymańska, K., et al. (2025). Evaluation of radioactivity in chanterelle (Cantharellus cibarius) and health implications. Environmental Geochemistry and Health, 47, 258. https://doi.org/10.1007/s10653-025-02576-9

11- Turhan, Ş., Köse, A., & Varinlioğlu, A. (2007). Radioactivity levels in some wild edible mushroom species in Turkey. Isotopes in Environmental and Health Studies, 43(3), 249–256. https://doi.org/10.1080/10256010701562794

12- Wang, S., Yang, B., Zhou, Q., Li, Z., Li, W., Zhang, J., & Tuo, F. (2021). Radionuclide content and risk analysis of edible mushrooms in northeast China. Radiation Medicine and Protection, 2(4), 165–170.

13 - Gwynn, J. P., Nalbandyan, A., & Rudolfsen, G. (2013). ^{210}Po, ^{210}Pb, ^{40}K and ^{137}Cs in edible wild berries and mushrooms and ingestion doses to man from high consumption rates of these wild foods.Journal of Environmental Radioactivity, 116, 34–41. https://doi.org/10.1016/j.jenvrad.2012.08.016

14- Cocchi, L., Kluza, K., Zalewska, T., Apanel, A., & Falandysz, J. (2017). Radioactive caesium (134Cs and 137Cs) in mushrooms of the genus Boletus from the Reggio Emilia in Italy and Pomerania in Poland. Isotopes in Environmental and Health Studies, 53(6), 620–627. https://doi.org/10.1080/10256016.2017.1337761

15 - Bem, H., Lasota, W., Kuśmierek, E., & Witusik, M. (1990). Accumulation of 137 Cs by mushrooms from Rogozno area of Poland over the period 1984–1988. Journal of radioanalytical and nuclear chemistry, 145(1), 39-46.

16- Falandysz, J., & Borovička, J. (2013). Macro and trace mineral constituents and radionuclides in mushrooms: Health benefits and risks. Applied Microbiology and Biotechnology, 97(2), 477–501. https://doi.org/10.1007/s00253-012-4552-8.

17- Yoshida, S., & Muramatsu, Y. (1998). Concentrations of alkali and alkaline earth elements, rare earth elements, and radionuclides in mushrooms. Science of the Total Environment, 205(2–3), 195–206.

18- Altıkulaç, A., Turhan, Ş., & Gümüş, H. (2016). Activity concentration of terrestrial and anthropogenic radionuclides (226Ra, 222Rn, 232Th, 40K, and 137Cs) in soil samples. Environmental Earth Sciences, 75, 41. https://doi.org/10.1007/s12665-015-4841-5.

19- International Atomic Energy Agency. (1989). Measurement of radionuclides in food and the environment: A guidebook (Technical Reports Series No. 295). International Atomic Energy Agency.

20-Debertin, K., & Helmer, R. G. (1988). Gamma- and X-ray spectrometry with semiconductor detectors. North-Holland.

21- United Nations Scientific Committee on the Effects of Atomic Radiation. (2000). Sources and effects of ionizing radiation: UNSCEAR 2000 report

to the General Assembly, with scientific annexes (Vol. I). United Nations.
22- International Commission on Radiological Protection. (1996). Age-dependent doses to members of the public from intake of radionuclides: Part 5. Compilation of ingestion and inhalation dose coefficients (ICRP Publication 72). Annals of the ICRP, 26(1). Elsevier.
23- ICRP. (1996). Age-dependent doses to members of the public from intake of radionuclides: Part 5. Compilation of ingestion and inhalation dose coefficients. ICRP Publication 72. Annals of the ICRP, 26(1). https://doi.org/10.1016/S0146-6453(96)90010-9
24- Demir, A. (2003). Mantar. T.E.A.E.–BAKIL, 3–14.
25- Taek, 2009. Taek ile Üniversiteler Arasında Çevresel Radyoaktivitenin Belirlenmesi ve İzlenmesine Yönelik İş birliği Projesi, Birinci Çalıştayı, Taek-Sanaem, Ankara.

Chapter 23

Radiological Assessment of Coal-Fired Thermal Power Plants

Aydan ALTIKULAÇ [1]

1. INTRODUCTION

Global energy demand is continuously increasing, and a significant part of this demand is currently met by using coal, which is a fossil fuel. For this reason, coal has been at the center of energy policies worldwide for many years. Approximately 34% of the electrical energy needed in Türkiye is supplied from coal, and 39% of the coal used in these processes is met by domestic lignite and hard coal resources [1]. The Muğla basin, which has significant lignite reserves in Türkiye, and the Yatağan Thermal Power Plant operating in this basin have played a critical role in regional and national energy supply. However, the ecological cost of this production manifests as a progressively worsening picture of environmental pollution over the years. While the form of environmental degradation caused by coal-fired thermal power plants is mostly known as carbon emissions, sülfür dioxide (SO 2) gases that cause acid rain, and heavy metal pollution, another serious and lesser known danger arising from the structure of coal is radioactive pollution due to its crustal origin. Since coal originates from the Earth's crust, its composition contains, albeit in small amounts, natural radioactive elements such as ^{238}U, ^{232}Th and ^{40}K. These elements do not completely disappear as a result of the combustion of coal. On the contrary, they become concentrated in combustion residues, such as fly ash and bottom ash, and gain the potential to spread into the environment. This situation can create long-term effects on soil, water, and air quality in regions where thermal power plants are located. This study aims to address the formation mechanisms of radioactive pollution originating from the Yatağan Thermal Power Plant, its environmental dispersion, and its potential effects on human health in light of scientific data. Thus, it is aimed to raise awareness regarding the preservation of the balance between energy production and environmental and public health. In the literature, studies on the environmental distribution of natural radionuclides around the Yatağan Thermal Power Plant and the evaluation of the associated radiological risk are limited in number [2-7]. In this context, we previously determined natural radionuclide activity concentrations in coal used as fuel and in fly ash samples formed as a result of combustion in the same power plant and evaluated radiological risk [8]. This study

[1] Assoc.Prof. Dr., Ula Ali Koçman Vocational School, Muğla Sıtkı Koçman University, Turkey; aydanaltikulac@mu.edu.tr , (ORCID:0000-0002-2041-4193)

is a continuation of the previous study, and this time, natural radionuclide levels in samples taken from the ash storage area where ashes formed as a result of coal combustion are stored were examined, and environmental radiological risk was evaluated.

2. MATERIAL AND METHOD

The Thermal Power Plant, whose location is given in Figure 1, is a lignite-fired thermal power plant located in the province of Muğla, which contains a significant proportion of the lignite reserves of Türkiye, and has an installed capacity of 3×2^{10} MW [9]. In this study, activity concentrations of ^{238}Ra, ^{232}Th, and ^{40}K were determined in 19 ash samples taken from the area where ashes formed as a result of coal combustion in the Thermal Power Plant are stored. Samples on which measurements would be carried out were dried for one day in a stove preheated up to 100 C. The dried samples were placed in standard containers of 6×5 cm with the same geometry as the RGU, RGTh, and RGK standards, and to prevent leakage, the opening of each container was tightly wrapped with parafilm. Before measurements, the prepared samples were kept for 4 weeks to ensure secular equilibrium between ^{226}Ra and its decay product ^{222}Rn. At the end of this period, the gamma spectrum of each sample was obtained with a high-resolution HPGe gamma spectrometer system. The obtained spectra were analyzed with the GammaVision software, and ^{226}Ra, ^{232}Th, and ^{40}K activity concentrations in each sample were calculated. In the measurements, a high-resolution gamma spectrometer from ORTEC with 30% relative efficiency and an HPGe detector was used. The energy resolution of the device is 0.85% at 122 keV and 1.85% at 1.33 MeV. The detector is cooled using a liquid nitrogen container with a capacity of 30L. The detector can be used in the energy range between 40 keV and 10 MeV. To prevent cosmic rays and natural background gamma rays originating from the environment from reaching the detector, a protective shield consisting of 9.5 mm thick steel and 101 mm thick lead shielding was used. The inner surface of the lead shielding was covered with a 0.5 mm thick tin and a 1.5 mm thick copper plate to prevent characteristic X-rays formed as a result of the interaction of gamma rays with lead from reaching the detector [10].

2.1 Gamma-Spectrometric Measurements

2.1.1 Activity Measurement

In the analyses of the samples, for ^{226}Ra activity, the 295.2 keV photopeak of ^{214}Pb, the 351.9 keV photopeak of ^{214}Pb, the 609.3 keV photopeak of ^{214}Bi, and the 1764.5 keV photopeak of ^{214}Bi were used. For ^{232}Th activity, the 583.2 keV photopeak of ^{208}Tl and the 911.2 keV photopeak of ^{228}Ac were used. For ^{40}K activity,

the 1460.8 keV photopeak was used. Using Formula 1, the activity values of the relevant radionuclides were calculated [11].

$$A(\text{Bqkg}^{-1}) = (\text{N net})/(\epsilon\gamma \text{ t } I\gamma \text{ m}) \quad (1)$$

Here, A denotes the calculated activity concentration (Bq kg $^{-1}$), Nnet denotes the net peak area, εγ denotes the detector efficiency for the relevant gamma energy, t denotes the counting time, m denotes the sample mass (kg), and Iγ denotes the emission probability of the relevant gamma ray.

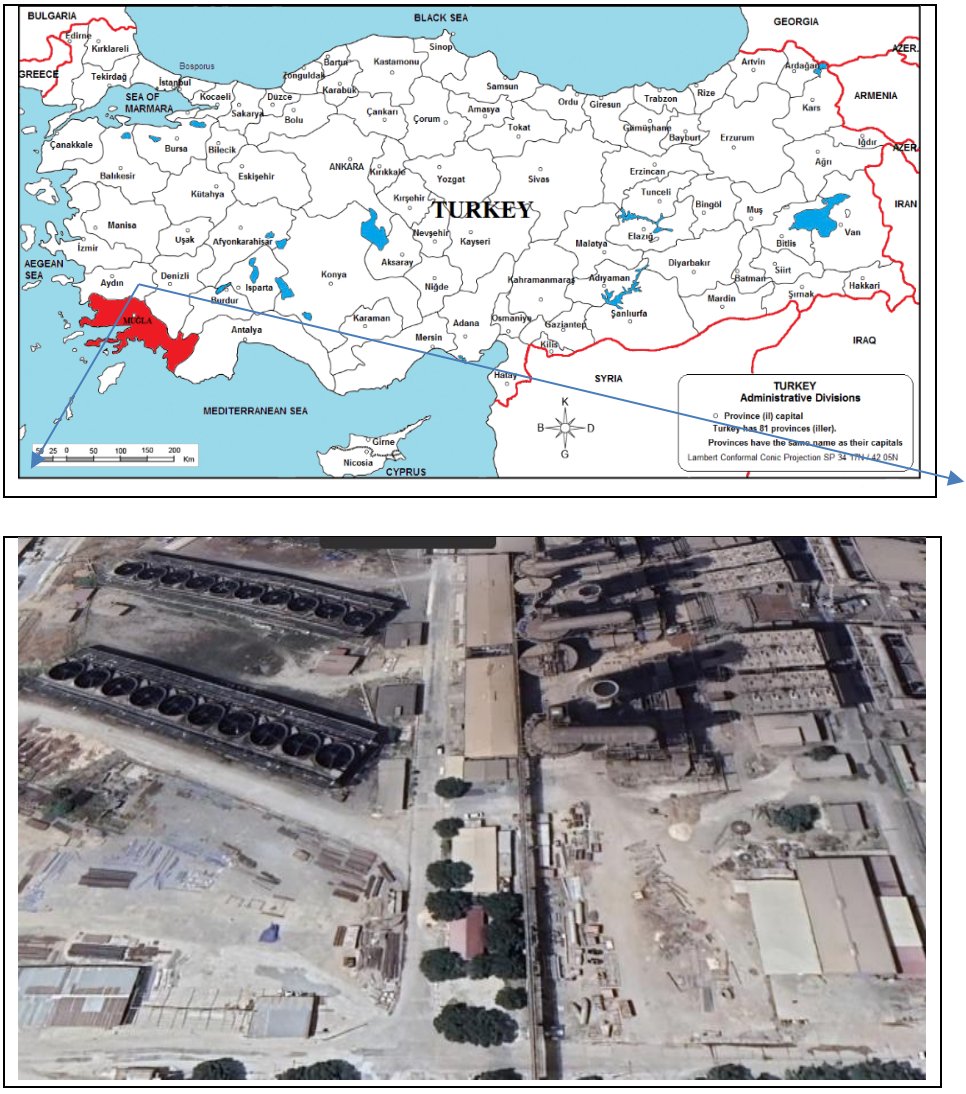


Figure 1. Sampling area

2.2 Radiological parameters

2.2.1 Radium equivalen

One of the parameters used to compare radioactivity originating from radium, thorium, and potassium in the uranium decay series is radium equivalent activity (Raeq). Radium equivalent activity was calculated using Formula 2 [12].

$$Raeq = C_{Ra} + 1.423\ C_{Th} + 0.077\ C_K \quad (2)$$

C_{Ra}, C_{Th}, and C_K values are the activity concentrations of ^{226}Ra, ^{232}Th, and ^{40}K radioisotopes in units of Bqkg $^{-1}$, respectively. In the definition of radium equivalent activity, it is assumed that activity concentrations of 10 Bq kg $^{-1}$ for ^{226}Ra, 7 Bq kg $^{-1}$ for ^{232}Th, and 130 Bq kg $^{-1}$ for ^{40}K produce equal gamma dose rates [13]. In the report published by OECD-NEA in 1979, the upper limit of radium equivalent activity for materials produced for permanent use in residential and workplace buildings was set as 370 Bqkg $^{-1}$ [14].

2.2.2 Absorbed gamma dose rate (D)

The absorbed gamma dose rate in air at 1 m above the ground surface due to 226Ra, 232Th, and 40K radioisotopes present in soil was calculated using Formula 3.

$$D\ (\ nGyh^{-1}) = 0.92\ C_{Ra} + 1.1\ C_{Th} + 0.08\ C_K \quad (3)$$

Here, 0.92 nGyh $^{-1}$ /Bqkg $^{-1}$, 1.1 nGyh $^{-1}$ /Bqkg $^{-1}$, and 0.08 nGyh $^{-1}$ /Bqkg $^{-1}$ are the dose rate conversion factors for ^{226}Ra, ^{232}Th, and ^{40}K, respectively. The population-weighted world average of the absorbed gamma dose rate in air due to external exposure from crustal radionuclides has been calculated as 59 nGyh $^{-1}$ (40–200 nGyh $^{-1}$) [15-16].

2.2.3 Annual effective dose value

Using the calculated gamma dose values, the annual effective dose value (AED), that is, the döşe amount that a person will receive from radiation emitted by natural radiation sources, is obtained. Taking into account the conversion factor for absorbed dose (0.7 Sv/Gy) and the outdoor occupancy factor (0.2), the effective dose was calculated using Formula 4.

$$AED\ (mSvy^{-1}) = D\ (\ nGyh\text{-}^{1}) \times 8760 \times 0.8 \times 0.7\ (\ SvGy\text{-}^{1}) \times 10^{-6} \quad (4)$$

According to the UNSCEAR (2008) report, the average activity concentrations of natural radionuclides in soil worldwide are reported as 32, 45, and 412 Bq kg $^{-1}$

for ^{226}Ra, ^{232}Th, and ^{40}K, respectively. In the same report, the annual average effective dose that individuals receive from natural and artificial radiation sources is stated as 2.8 mSv, and approximately 85% of this dose isreported to originate from natural radiation sources [17].

Table 1. Activity concentrations measured in the samples

Sample ID	^{226}Ra ($Bqkg^{-1}$)	^{232}Th $Bqkg^{-1}$)	^{40}K ($Bqkg^{-1}$)
W1	83.8	55.3	731.6
W2	86.8	56.7	938.8
W3	88.52	76.66	764.3
W4	96.74	90.48	598.0
W5	147.96	67.9	612.1
W6	126.56	85.1	982.0
W7	92.34	71.48	709.0
W8	146.93	113.87	728.0
W9	120.2	98.16	615.8
W10	136.38	59.45	1023.3
W11	125.62	77.23	598,5
W12	131.77	64.49	642.4
W13	73.85	81.15	829.6
W14	78.67	45.18	679.7
W15	93.77	62.26	1195.8
W16	79.57	72.01	657.1
W17	82.92	69.9	751.0
W18	79.81	67.71	692.6
W19	90.19	48.72	698.4
Average	103.28	71.76211	760±11.1

2.2.4 Lifetime cancer risk

Lifetime cancer risk (LCR) is a parameter that indicates the maximum number of cancer cases observed for a limited number of individuals exposed to a certain level of ionizing radiation. In the assessment of the potential effects of radioactive pollution on human health, LCR is an important radiological risk indicator. Therefore, determining the LCR value, which expresses the probabilitythat individuals will develop cancer during their lifetime as a result of exposure to ionizing radiation, is of great importance. For the radiation dose values obtained in this study, the LCR value was calculated using Formula 5.

$$LCR= AED . O\ddot{O} . RF \quad (5)$$

Here, AED is the annual effective radiation dose rate, OÖ is the average lifetime for a Turkish individual, and RF is the risk factor, which is 0.05. The world average for LCR is 2.5×10^{-4} [18].

3. RESULT AND DISCUSSION

In the Yatağan Thermal Power Plant, coal combustion results in ash that is subsequently stored in the ash storage area for later utilization. In this study, natural radioactivity levels of 19 ash samples taken from the storage area were determined using a high-resolution gamma spectrometer system equipped with an HPGe detector. Using the obtained data, radiological hazard indices such as radium equivalent activity (Ra_eq), absorbed gamma dose rate, AED, and LCR were determined. The results were evaluated by comparing them to limit values recommended by international organizations. The measured ^{226}Ra activity concentrations varied between 73.86 and 146.93 Bq kg $^{-1}$ as shown in the second column of Table 1. The mean ^{226}Ra activity concentration of the samples was calculated as 103.28 Bq kg $^{-1}$. This value corresponds to approximately 3.2 times the world average value of 32 Bq kg $^{-1}$ reported for soil by UNSCEAR (2008). The measured ^{232}Th activity concentrations varied between 48.72 and 113.87 Bq kg $^{-1}$ as shown in the third column of Table 1. The mean ^{232}Th activity concentration of the samples was calculated as 71.76 Bq kg $^{-1}$. This value corresponds to approximately 1.6 times the world average value of 45 Bq kg $^{-1}$ reported for soil by UNSCEAR (2008). The measured mean ^{40}K activity value was 760 Bq kg $^{-1}$, and it is approximately twice the World average. According to the UNSCEAR (2008) report, the world average activity concentrations of ^{226}Ra, ^{232}Th, and ^{40}K radionuclides in soil are 32, 45, and 412 Bq kg $^{-1}$, respectively. Based on these average activity concentrations, the radium equivalent activity (Raeq) is approximately 128 Bq kg $^{-1}$, and in the same report, the average absorbed gamma dose rate (D) for outdoor environments is given as 59 nGy h $^{-1}$, while the corresponding AED is 0.07 mSv year $^{-1}$ (70 μSv year $^{-1}$). These reference values were used as comparison criteria in the evaluation of the radiological parameter values obtained in the study. LCR is not directly provided in the UNSCEAR (2008) report and is calculated using AED, life expectancy, and the nominal cancer risk coefficient recommended by ICRP. According to this approach, the world average LCR is approximately 2.5×10^{-4} . The radium equivalent activity (Ra_eq) values calculated using the measured activity concentrations varied between 195.56 and 365.82 Bq kg $^{-1}$ as shown in the second column of Table 2, with a mean value of 229.91 Bq kg $^{-1}$. This value corresponds to approximately 1.8 times the world avaraya Raeqvalue of about 128 Bq kg $^{-1}$.

Table 2. Calculated radiological parameters

Sample ID	Raeq (Bqkg $^{-1}$)	D (nGy $h^{-1)}$	AED (m Svy^{-1})	LCR
W1	218.77	102.43	0.5	1.8 x 10^{-3}
W2	240.10	113.46	0.5	1.8 x 10-^{3}
W3	256.97	119.05	0.5	1.8 x 10^{-3}
W4	272.17	124.28	0.6	2.2 x 10^{-3}
W5	292.18	134.88	0.6	2.2 x 10^{-3}
W6	323.86	150.82	0.7	2.6 x 10^{-3}
W7	249.14	115.40	0.5	1.8 x 10^{-3}
W8	365.82	167.01	0.8	3.0 x 10^{-3}
W9	307.92	140.46	0.6	2.2 x 10^{-3}
W10	300.16	141.57	0,6	2.2 x 10^{-3}
W11	282.10	129.61	0.6	2.2 x 10^{-3}
W12	273.42	126.60	0.6	2.2 x 10^{-3}
W13	253.72	117.70	0.5	1.8 x 10^{-3}
W14	195.56	91.948	0.4	1.5 x 10^{-3}
W15	274.81	130.75	0.6	2.2 x 10^{-3}
W16	233.13	107.65	0.5	1.8 x 10^{-3}
W17	240.70	111.84	0.5	1.8 x 10^{-3}
W18	229.91	106.62	0.5	1.8 x 10^{-3}
W19	213.60	100.20	0.4	1.5 x 10^{-3}
Average	216.19	10.31	0.5	1.6x10^{-3}

The mean absorbed gamma dose rate (D) in this study was calculated as 106.62 nGy h^{-1} , and it isapproximately 1.8 times the world average value of 59 nGy h^{-1} reported by UNSCEAR (2008). Themean AED value corresponding to this dose was determined as 0.50 mSv $year^{-1}$ and was found to be approximately seven times the world average of 0.07 mSv $year^{-1}$. Accordingly, the calculated LCR also reached approximately seven times the world average value of 2.5×10^{-4}. These results show that the radiological risk level arising from natural radionuclides in the examined samples was significantly above the world average values. Furthermore, Table 3 presents results from some radioactivity studies conducted on coal ash samples in different regions of the world. These studies allow for the comparison of the obtained results to values reported in the literature.

Table 3. Studies conducted in various parts of the world

Country	^{226}Ra	^{232}Th	^{40}K	Reference
China	40.3	59.6	751.2	Lu et al. (2012)
Türkiye	150	96	621	Turhan et al. (2025)
Vietnam	77	92	938	Loan et al. (2022)
Bangladesh	19-32	31-90	420-870	Siraz et al. (2025)
Malaysia	22-150	20-153	68-1594	Mohamed et al. (2023)
Dhaka	19-57	23-97	78-170	Yeasmin et al. (2025)
Brazil	17-60	11-64	140-850	Flues et al. (2002)
Pakistan	86	36	85	Saleem et al. (2026)
India	81-177	116-178	365- 495	Gupta et al. (2013)

4. CONCLUSION

Lignite obtained from lignite fields in the region is used as fuel in the examined power plant. Ash formed as a result of lignite combustion can be recycled in many areas such as cement and concrete production, brick and other construction material manufacturing, road construction, soil improvement, and the rehabilitation of mining sites. However, due to the natural radionuclides contained in these materials, before recycling, there is a need for radiological evaluations and the determination of compliance with international radiation safety criteria. Within the scope of this study, analyses performed on ash samples formed as a result of combustion in the thermal power plant and accumulated in the ash storage area revealed that natural radioactivity concentrations were above world average values, and the radiological hazard indices calculated accordingly also showed an increase. The obtained results demonstrated the importance of radiological evaluations of these ashes before their use in recycling applications and the necessity of taking the required measures in terms of environmental radiation safety.

REFERENCES

1-T.C. Enerji ve Tabi, Kaynaklar Bakanlığı.29.06.2026. https://enerji.gov.tr/bilgi-merkezi-enerji-elektrik.

2-Tanıl, A., Sevim, A., Ahmet, V., & Abdullah, K. (2004). Natural radioactivity and EDXRF analysis of ashes from coal power plants of Turkey. İstanbul Kültür Üniversitesi Yayınları, 2(1), 39–43.

3-Baba, A. (2002). Assessment of radioactive contaminants in by-products from Yatagan (Mugla, Turkey) coal-fired power plant. Environmental Geology, 41, 916–921.

4-Ayçık, G. A., & Ercan, A. (1997). Radioactivity measurements of coals and ashes from coal-fired power plants in the southwestern part of Turkey. Journal of Environmental Radioactivity, 35(1), 23–35.

5-Büke, T., & Köne, A. Ç. (2011). Estimation of the health benefits of controlling air pollution from the Yatağan coal-fired power plant. Environmental Science & Policy, 14(8), 1113–1120.

6- Uğur, A., Özden, B., Saç, M. M., Yener, G., Altınbaş, Ü., Kurucu, Y., & Olcay, M. (2004). Lichens and mosses for correlation between trace elements and ^{210}Po in the areas near the coal-fired power plant at Yatağan, Turkey. Journal of Radioanalytical and Nuclear Chemistry, 259(1), 87–92. https://doi.org/10.1023/B:JRNC.0000015814.03156.80

7- Özden, B., Güler, E., Vaasma, T., Horváth, M., Kiisk, M., & Kovács, T. (2018). Enrichment of naturally occurring radionuclides and trace elements in Yatağan and Yeniköy coal-fired thermal power plants, Turkey. Journal of Environmental Radioactivity, 188, 100–107. https://doi.org/10.1016/j.jenvrad.2018.02.013

8- Altıkulaç, A., Turhan, Ş., & Gümüş, H. (2017). Analysis of natural radioactivity in Yatağan coal-fired power plant in Turkey. EPJ Web of Conferences, 154, Article 01009. https://doi.org/10.1051/epjconf/201715401009

9- Elektrik Üretim A.Ş. (EÜAŞ). (2024). Yatağan Termik Santrali. https://www.euas.gov.tr

10-Altıkulaç, A. (2022). Investigation of radiological and chemical contents of bauxite ore extracted in Turkey. ACS Omega .7(44), 39917–39923.

11-Debertin, K., & Helmer, R. G. (1988). Gamma- and X-ray spectrometry with semiconductor detectors. North-Holland.

12-Beretka, J., & Mathew, P. J. (1985). Natural radioactivity of Australian building materials, industrial wastes and by-products. Health Physics, 48(1), 87–95. https://doi.org/10.1097/00004032-198501000-00007

13-Stranden, E. (1976). Some aspects on radioactivity of building materials. Physics and Chemistry of the Earth (Physica Norvegica), 8, 167–177.

14- OECD Nuclear Energy Agency. (1979). Exposure to radiation from the natural radioactivity in building materials. Organisation for Economic Co-operation and Development.

15-European Commission. (1999). Radiation protection 112: Radiological protection principles concerning the natural radioactivity of building materials. Directorate-General Environment, Nuclear Safety and Civil Protection..

16 - Markkanen, M. (1995). Radiation dose assessments for materials with elevated natural radioactivity (STUK-B-STO 32). Radiation and Nuclear Safety Authority (STUK).

17-United Nations Scientific Committee on the Effects of Atomic Radiation. (2008). Sources and effects of ionizing radiation: UNSCEAR 2008 report to the General Assembly with scientific annexes. Volume I: Scientific annexes A and B. United Nations.

18- International Commission on Radiological Protection. (2007). The 2007 recommendations of the International Commission on Radiological Protection (ICRP Publication 103). Annals of the ICRP, 37(2–4).

19- Lu, X., Li, X., Yun, P., Luo, D., Wang, L., Ren, C., & Chen, C. (2012). Measurement of natural radioactivity and assessment of associated radiation hazards in soil around Baoji second coal-fired thermal power plant, China. *Radiation Protection Dosimetry, 148*(2), 219–226. https://doi.org/10.1093/rpd/ncr016

20- Turhan, Ş., & Jamasali, Y. D. (2025). Technologically enhanced natural radioactivity level in fly ash produced in lignite-fired thermal power plant and assessment of radiological hazards. Environmental geochemistry and health, 47(9), 374. https://doi.org/10.1007/s10653-025-02668-

21- Loan, T. T. H., Ba, V. N., & Thien, B. N. (2022). Natural radioactivity level in fly ash samples and radiological hazard at the landfill area of the coal-fired power plant complex, Vietnam. Nuclear Engineering and Technology, 54(4), 1431–1438.

22- Siraz, M. M. M., Reza, A., Khan, M., Alam, M. S., Al Mahmud, J., Rashid, Md. B., … Yeasmin, S. (2025). Pioneering study of radioactivity in soil near the Payra 1320 MW Thermal Power Plant, the largest coal-fired thermal power plant in Bangladesh. International Journal of Environmental Analytical Chemistry, 105(17), 5757–5775. https://doi.org/10.1080/03067319.2024.2404526

23- Mohamed, H., Pauzi, A. M., Ahmad, N., Karim, N. A., Wazir, M. N. U. I., Bahri, C. Z., & Idris, M. I. (2023). Natural radioactivity analysis and radiological

impact assessment from a coal power plant. International Journal of Radiation Research, 21(4), 797–804.

24- Yeasmin, S., Das, S. K., Siraz, M. M., & Rahman, M. S. (2025). Assessing radioactivity and hazards: analysis of soil, water, and coal samples near a coal-fired thermal power plant and their implications for human health and the environment. International Journal of Environmental Analytical Chemistry, 105(3), 618-635.

25- Flues, M., Moraes, V., & Mazzilli, B. P. (2002). The influence of a coal-fired power plant operation on radionuclide concentrations in soil. Journal of Environmental Radioactivity, 63(3), 285–294.

26- Saleem, N., Naheed, R., & Ali, A. (2026). Evaluation of naturally occurring radioactive material and associated radiological risks at coal-fired power plants of Pakistan. Journal of Radioanalytical and Nuclear Chemistry, 335(4), 3233–3242.

27- Gupta, M., Mahur, A. K., Varshney, R., Sonkawade, R. G., Verma, K. D., & Prasad, R. (2013). Measurement of natural radioactivity and radon exhalation rate in fly ash samples from a thermal power plant and estimation of radiation doses. Radiation Measurements, 50, 160-165.

Chapter 24

Radiation Dosimetry and Environmental Monitoring: Modern Approaches for Assesing Population Exposure

Celal Tuğrul ZEYREK[1]

1. INTRODUCTION

Ionizing radiation has become an integral part of modern society, with applications spanning medicine, industry, energy production, and scientific research. While these uses provide significant benefits—from advanced diagnostic imaging and cancer therapy to industrial quality control and nuclear power generation—they also introduce potential risks to human health and the environment. Understanding and quantifying radiation exposure is therefore essential for establishing protective measures that safeguard workers, the public, and ecosystems.Radiation dosimetry serves as the foundation of this protective framework. As a multidisciplinary science, it unites physics, chemistry, and biology to measure and interpret the energy deposited by ionizing radiation in matter, particularly in living tissues. The discipline provides the standardized quantities and concepts necessary to translate absorbed energy into meaningful indicators of biological effect and risk. These metrics underpin international radiation protection guidelines, enabling regulators, clinicians, and researchers to set dose limits, define reference levels, and implement safety protocols across diverse exposure scenarios [1-3].The evolution of dosimetric methodologies reflects both technological progress and the growing complexity of radiation applications. Classical approaches—ranging from thermoluminescent and chemical dosimeters to cytogenetic and molecular assays—have been complemented by modern innovations such as retrospective dosimetry using everyday materials, environmental monitoring networks, and wearable sensors. Together, these strategies illustrate a paradigm shift toward integrated, scalable, and individualized assessment of radiation exposure [4,5]. The environmental monitoring has emerged as a critical dimension in assessing population-level exposure. Modern approaches integrate sensor networks, geostatistical sampling, and portable instruments to provide real-time surveillance and retrospective analysis. Studies emphasize the role of environmental dosimetry in large-scale radiological emergencies, where rapid triage and reliable dose estimation are essential for public health protection [6,7]. Moreover, the incorporation of wearable sensors, smartphone-based monitoring, and

[1] Prof. Dr., Institute of Nuclear Sciences, Ankara University, Türkiye, celaltugrulzeyrek@ankara.edu.tr, (ORCID: 0000-0001-6744-7841)

omics technologies has expanded the scope of exposure assessment, bridging individual-level biodosimetry with community-wide surveillance [8].

This chapter introduces the fundamental principles of radiation dosimetry, outlines the established dose concepts that form the language of radiological sciences, and highlights contemporary advances that strengthen global radiation protection. By bridging physical measurement with biological interpretation, dosimetry continues to play a pivotal role in ensuring that the benefits of ionizing radiation are realized while minimizing its risks.

2. FUNDAMENTAL DOSE CONCEPTS AND QUANTITIES

Dose is the amount of any substance used or consumed within a certain period of time. Radiation dose, on the other hand, is the amount of radiation absorbed or received by the target medium within a specific timeframe. The effect that the radiation dose will produce in the target medium depends on the type of radiation, the dose rate, and the duration of exposure. In studies conducted with ionizing radiation, knowing the radiation dose is essential to achieve efficient results, determine harmful biological effects, and primarily ensure protection. Measuring the amount of radiation exposure is one of the most critical points to consider when working with radiation. For this purpose, it is first necessary to know the radiation measurement units and quantities.The specific fundamental units are utilized to characterize the attributes and impacts of radiation. As detailed in ICRU-85 [9], this framework encompasses electrical charge (Coulomb), energy (Joule), power (Watt), and activity (Becquerel). It also incorporates absorbed dose, kinetic energy released per unit mass (KERMA), converted energy per unit mass (CEMA), specific energy, and the gray (Gy) in the SI system applied to physical quantities. Among these metrics, the units of activity, exposure, absorbed dose, and dose equivalent—alternatively termed biological dose—are extensively utilized within the International System of Units (SI) for radiation protection monitoring. Different types of ionizing radiation interact distinctively with biological media, consequently producing varying biological effects. Equal amounts of absorbed doses—and thus equivalent amounts of deposited energy—do not necessarily result in the same biological outcome. For instance, identical dose values of alpha, beta, neutron particles, or photons within the same tissue will elicit disparate biological responses. Consequently, to evaluate the damage potentials of diverse ionizing radiation types in biological tissue based on uniform principles, a new quantity was required.

This novel quantity is the 'equivalent dose,' measured in 'sievert' (Sv) in honor of the Swedish physicist Rolf Sievert. Equivalent dose, a fundamental radiation protection quantity, is derived from the average absorbed dose ($D_{T,R}$) of radiation type (R) deposited in a specified organ or tissue volume (T). Here, radiation types

(R) are defined by the quality and energy of radiations, whether incident on the body or emitted from internal radionuclides.As the foundational physical quantity in radiological physics, the absorbed dose quantifies the mean ionizing radiation energy imparted to matter per unit mass. Mathematically, it is expressed as the quotient of the mean energy ($d\bar{\varepsilon}$) imparted by ionizing radiation within a specific volume element divided by the differential mass (dm) of the matter contained within that volume

$$D = \frac{d\bar{\varepsilon}}{dm} \quad (1)$$

Its SI unit is the joule per kilogram $J.kg^{-1}$, with the special name gray (Gy). Derived from the mean value of the stochastic energy imparted (ε) the absorbed dose averages out the random fluctuations inherent to individual interaction events within tissue. Although defined pointwise throughout matter, its practical value is determined by averaging over a differential mass element (dm), thereby encompassing a vast ensemble of constituent atoms or molecules. Consequently, absorbed dose represents a fundamentally measurable quantity, backed by established primary standards, while maintaining the rigorous scientific definition demanded of a baseline physical quantity. In the framework of radiological protection, the absorbed dose is systematically averaged over macro-scale tissue volumes. The underlying paradigm posits that under low-dose exposure scenarios, the mean absorbed dose within a specific organ or tissue correlates sufficiently with the radiation-induced detriment for stochastic effects. Consequently, this volumetric averaging is conventionally applied across defined anatomical structures, ranging from entire organs such as the liver, to complex tissue networks like the red bone marrow, or highly radiosensitive sub-regions including the endosteal surfaces of the skeleton. The organ or tissue equivalent dose (H_T) is thus expressed a

$$H_T = \sum_R W_R . D_{T,R} \quad (2)$$

In this expression, W_R represents the radiation weighting factor corresponding to radiation type R, where the total sum accounts for all types of radiation present. The equivalent dose carries the unit of $J.kg^{-1}$ which is specifically designated as the sievert (Sv). In early frameworks, radiation weighting within radiological protection quantities was determined by the radiation quality factor (Q) as a function of LET, designated as (L) in the Q(L) relationship of Publication 26 (ICRP, 1977) [10]. In its 1991 recommendations (ICRP Publication 60) [11], the International Commission on Radiological Protection revised the approach to radiation weighting in the

calculation of effective dose, introducing a defined set of radiation weighting factors (W_R). The assignment of radiation weighting factors W_R was guided primarily by experimental data on relative biological effectiveness (RBE). RBE is determined by comparing the doses of a test radiation with those of a reference low-LET radiation that yield the same biological outcome. Because the observed values depend on both the biological endpoint under study and the choice of reference radiation, a range of RBE values has been reported in the literature. The reported values of relative biological effectiveness (RBE) vary according to the biological endpoint investigated and the choice of reference radiation. Commonly employed references include high-energy x-rays (above approximately 200 kV), cobalt-60, and cesium-137 gamma rays. The radiation weighting factors (W_R) ultimately adopted by the International Commission on Radiological Protection are presented in Table 1 of ICRP Publication 103 (2007) [12]. As established by the International Commission on Radiological Protection, the effective dose (E)—conceptually defined in ICRP Publication 60 [13] and operationalized in ICRP Publication 103 [12]—is expressed by the following relationship:

$$E = \sum_T W_T \sum_R W_R D_{T,R} = \sum_T W_T H_T \quad (2)$$

where W_T denotes the tissue weighting factor for a specific tissue T, satisfying the normalization condition $\sum_T W_T = 1$. This summation encompasses all human organs and tissues for which distinct radiation detriment values can be quantified and corresponding tissue weighting factors are explicitly defined in Publication 103 [12].

Table 1. Radiation weighting factors (Publication 103).

Type of radiation	Radiation weighting factor, W_R
Photons	1
Electrons and muons	1
Protons and charged pions	2
Alpha particles, fission fragments, heavy ions	20
Neutrons	Depending of neutron energy

2.1. Operational quantities

For the assessment of external exposures, the ICRU has established operational dose equivalent quantities applicable to both area monitoring and individual monitoring [9]. Dose equivalent quantities are directly measurable, and radiation monitoring instruments are calibrated against these quantities. In routine monitoring, the recorded values are considered sufficiently accurate representations of the

effective dose, as well as of doses to the lens of the eye and the skin. For the monitoring of occupational exposure to external radiation, the operational quantity employed is the personal dose equivalent, Hp(d), defined as the dose equivalent in ICRU soft tissue at a specified depth d beneath a designated point on the human body. The reference point for personal dosimetry is generally the location at which the dosimeter is worn. To estimate effective dose, the personal dose equivalent at a depth of 10 mm, denoted as Hp(10), is used. When the dosimeter is positioned at a body site representative of whole-body exposure, Hp(10) is considered a sufficiently accurate approximation of effective dose for radiological protection purposes. For evaluating doses to the skin and extremities, the personal dose equivalent at a depth of 0.07 mm, Hp(0.07), is recommended as the operational quantity. In addition, a depth of 3 mm has been proposed for the monitoring of radiation exposure to the lens of the eye. While ICRP Publication 103 [12] indicated that routine monitoring based on Hp(3) was not considered essential, the reduction of the occupational dose limit for the lens of the eye to 20 mSv per year has increased the importance of eye lens dosimetry and prompted renewed consideration of the applicability of Hp(3) for radiation protection purposes [14].

3. MODERN RADIATION DOSIMETRY SYSTEMS

Radiation dosimetry is the science of measuring, calculating, and assessing the absorbed dose delivered by ionizing radiation to matter, biological tissues, workers, patients, and the environment. Advances in radiation protection, medical imaging, radiation therapy, nuclear power operations, industrial applications, and environmental monitoring have significantly increased the demand for accurate and reliable dosimetric techniques. Modern radiation dosimetry has evolved from simple exposure measurements to sophisticated systems capable of providing real-time, high-precision dose assessment under a wide range of radiation fields. The principal objectives of contemporary dosimetry are multifaceted. They encompass the quantification of absorbed dose and dose rate, the estimation of effective and equivalent doses, and the monitoring of occupational radiation exposure. In clinical contexts, dosimetry also plays a critical role in verifying the accuracy of radiation treatment delivery. Beyond the workplace and medical applications, it contributes to the assessment of environmental radiation levels and provides essential support for radiological emergency preparedness and response. Together, these functions define the scope of modern dosimetric practice and highlight its central role in radiation protection frameworks.Modern dosimetric approaches integrate advanced detector technologies, numerical modeling, digital signal processing, and computational algorithms to improve measurement accuracy and reduce uncertainties. These

developments have enhanced the capability of radiation protection programs and contributed significantly to compliance with international safety standards.

3.1. Radiation Dosimetry Types and Applications

Depending on the measurement detection mechanism and the field of application, radiation dosimetry is broadly classified into various types, including physical, chemical, and biological methods. Radiation dosimetry is broadly categorized into passive and active systems—such as Thermoluminescent Dosimeters (TLD) and Optically Stimulated Luminescence (OSL), Active Electronic Personal Dosimeters (EPDs) –each specifically engineered to meet the stringent demands of medical, industrial, and environmental applications.

Thermoluminescent dosimeters (TLD) remain among the most widely utilized passive radiation monitoring tools worldwide. TLD materials possess crystalline structures containing electron trapping centers created by impurities or defects within the lattice. When exposed to ionizing radiation, electrons are excited and become trapped within metastable energy states. Subsequent heating of the detector releases these electrons, producing visible light proportional to the absorbed radiation dose. Frequently employed thermoluminescent dosimeter (TLD) materials include lithium fluoride activated with magnesium and titanium (LiF:Mg,Ti), lithium fluoride activated with magnesium, copper, and phosphorus (LiF:Mg,Cu,P), calcium fluoride (CaF_2), and dysprosium-doped calcium sulfate ($CaSO_4$:Dy), all of which exhibit favorable luminescent properties for radiation dose measurement. Among these materials, LiF-based detectors are particularly favored because their effective atomic number closely approximates that of human tissue [15]. Thermoluminescent dosimeters (TLDs) remain among the most extensively utilized passive radiation detectors in occupational, medical, and environmental dosimetry because of their proven reliability and favorable dosimetric characteristics. One of the most important advantages of TLD systems is their high sensitivity, which enables the accurate measurement of low levels of ionizing radiation. In addition, TLDs possess a wide dynamic dose range, allowing their application in both routine personnel monitoring and higher-dose radiation environments. Materials such as lithium fluoride (LiF) exhibit near tissue-equivalent characteristics due to their effective atomic number being similar to that of soft tissue, thereby providing a dosimetric response that closely approximates human radiation absorption. Furthermore, TLD detectors are compact, lightweight, and available in different geometries, facilitating their use in personal monitoring badges, extremity dosimeters, and environmental monitoring networks. Another significant advantage is their reusability, as the stored radiation signal can be erased through an annealing process, permitting repeated use while maintaining acceptable measurement

performance. As passive devices, TLDs also do not require an external power source during radiation exposure, making them particularly suitable for long-term monitoring applications. These characteristics have established TLD technology as a standard method in radiation protection and dose assessment programs worldwide. Despite these strengths, TLD systems have several inherent limitations. Unlike active dosimetry technologies, TLDs cannot provide real-time information regarding radiation exposure because the absorbed dose information remains stored within the detector material until a subsequent laboratory readout is performed. As a result, dose evaluation is delayed until the dosimeter is processed.

Optically Stimulated Luminescence (OSL) dosimetry is considered one of the most significant developments in modern personal radiation monitoring. Similar to thermoluminescent dosimetry, OSL is based on the storage of energy in crystal lattice defects following exposure to ionizing radiation. However, unlike TLD systems, where trapped charge carriers are released through thermal heating, OSL dosimeters employ optical stimulation to liberate the stored electrons. When stimulated by a suitable light source, the trapped electrons recombine with luminescence centers and emit photons, producing a measurable light signal whose intensity is proportional to the absorbed radiation dose. This fundamental characteristic enables highly sensitive and accurate dose measurements over a broad range of radiation exposures [16]. Among the various materials investigated for OSL applications, carbon-doped aluminum oxide (Al_2O_3:C) has emerged as the most widely used detector material in personal and environmental radiation monitoring. The popularity of Al_2O_3:C is primarily attributed to its exceptional sensitivity to ionizing radiation, excellent signal-to-noise ratio, and remarkable long-term stability under normal storage conditions. In comparison with many traditional thermoluminescent materials, Al_2O_3:C exhibits a significantly stronger luminescence response, allowing reliable assessment of very low radiation doses. These characteristics have contributed substantially to its adoption in commercial personnel dosimetry systems used by radiation protection programs worldwide [16].

The OSL measurement process begins when ionizing radiation interacts with the detector material, generating electron-hole pairs within the crystal lattice. A fraction of these charge carriers becomes trapped at defect sites created by impurities or structural imperfections. The trapped charges remain stable until the detector is exposed to an external optical stimulation source, typically a laser or light-emitting diode (LED). Upon stimulation, the trapped electrons acquire sufficient energy to escape from their trapping sites and subsequently recombine with luminescence centers. This recombination process produces luminescent photons that are detected by highly sensitive photomultiplier tubes or photodiodes. The recorded luminescence intensity is then analyzed and converted into absorbed dose values

through calibration procedures established for the specific detector system. Because optical stimulation does not completely deplete the stored signal, a portion of the dosimetric information can often be preserved for repeated measurements and quality assurance purposes. OSL technology offers several advantages that have contributed to its widespread implementation in occupational radiation monitoring. One of its most important attributes is its exceptionally high sensitivity, enabling accurate measurement of doses in the microsievert range. OSL dosimeters also provide rapid readout procedures and require relatively simple instrumentation compared with some conventional dosimetric methods. A distinctive feature of OSL technology is its non-destructive readout capability, which allows the same dosimeter to be analyzed multiple times without significant loss of information. Furthermore, OSL systems exhibit reduced signal fading during storage and demonstrate excellent performance in low-dose monitoring applications. These characteristics enhance measurement reliability and facilitate retrospective dose verification when necessary. Consequently, OSL-based personnel monitoring systems have increasingly replaced conventional TLD systems in many countries and are now widely employed in occupational radiation protection programs, environmental monitoring networks, and medical radiation facilities.

Electronic Personal Dosimeters (EPDs) are among the most important active dosimetry systems used in contemporary radiation protection programs. Unlike passive dosimeters, which require subsequent laboratory processing to determine accumulated dose, EPDs provide continuous, real-time measurements of both radiation dose and dose rate during work activities. This capability enables radiation workers and radiation protection officers to assess exposure conditions instantaneously and to take corrective actions whenever necessary. As a result, EPDs have become an essential component of occupational radiation protection programs in nuclear power plants, research reactors, medical facilities, industrial radiography operations, and emergency response situations [17]. Modern EPDs typically incorporate semiconductor detectors, silicon diode sensors, or miniature Geiger-Müller counters that convert radiation interactions into electrical signals. These signals are processed electronically and displayed in terms of dose rate and cumulative dose. Advances in microelectronics have significantly improved detector sensitivity, energy compensation, battery life, and data storage capacity, allowing modern dosimeters to perform accurate measurements over a wide range of radiation fields. Many current-generation devices are capable of monitoring photon, beta, and, in some specialized configurations, neutron radiation exposure, thereby supporting comprehensive occupational dose assessment [18]. One of the most significant advantages of EPD technology is the availability of alarm functions that provide immediate notification when predefined dose or dose-rate thresholds are exceeded.

Audible, visual, and vibration alarms can alert workers to unexpected increases in radiation levels, enabling rapid evacuation or modification of work practices. Such real-time feedback supports the implementation of the ALARA (As Low As Reasonably Achievable) principle by helping workers minimize unnecessary radiation exposure during routine operations and maintenance activities. In environments where radiation fields may change rapidly, such as refueling outages, decommissioning projects, or industrial radiography operations, immediate warning capabilities contribute substantially to occupational safety [19]. Contemporary EPD systems also include advanced digital features that facilitate exposure management and regulatory compliance. Measurement records can be stored electronically and transferred to centralized databases through wireless communication technologies, including radiofrequency, Bluetooth, or network-based systems. This functionality enables radiation protection personnel to monitor worker exposures remotely, maintain accurate dose histories, and generate exposure reports efficiently. Integration with facility-wide radiation monitoring systems further enhances operational oversight and supports decision-making during radiological incidents or emergency situations [17]. Despite their numerous advantages, electronic dosimeters are not without limitations. Their performance may be influenced by environmental conditions such as temperature, humidity, mechanical shock, or electromagnetic interference. In addition, EPDs require periodic calibration, battery maintenance, and functional testing to ensure measurement reliability. For these reasons, many regulatory frameworks continue to recommend the complementary use of passive dosimeters, such as thermoluminescent dosimeters (TLDs) or optically stimulated luminescence (OSL) dosimeters, for official dose recording and long-term exposure verification. The combined use of active and passive monitoring systems provides a robust approach to occupational radiation protection and enhances confidence in dose assessments [20]. (ICRP, 2007). Ongoing developments in radiation monitoring technologies are expected to further expand the capabilities of EPDs. Emerging systems incorporate wireless sensor networks, cloud-based data management platforms, artificial intelligence-assisted exposure analysis, and integration with personal protective equipment. These innovations may improve real-time situational awareness, facilitate predictive exposure management, and strengthen radiation safety culture within facilities that utilize ionizing radiation. Consequently, Electronic Personal Dosimeters are expected to remain a central component of modern occupational dosimetry programs and radiation protection strategies for the foreseeable future.

Semiconductor-based dosimetry systems have become increasingly important in modern radiation measurements owing to their high sensitivity, excellent spatial resolution, rapid response characteristics, and compact detector architecture. In these

systems, ionizing radiation interacts with semiconductor materials and generates electron-hole pairs, producing electrical signals proportional to the deposited energy. Compared with conventional passive dosimeters, semiconductor detectors offer superior temporal resolution and can provide immediate measurement results, making them particularly suitable for applications requiring precise dose verification and quality assurance. Silicon-based detectors are among the most widely employed semiconductor dosimeters because of their reliability, well-characterized response, and compatibility with digital measurement systems. In addition, synthetic diamond detectors have attracted considerable attention due to their near-tissue equivalence, high radiation resistance, and stable dosimetric performance under high-dose conditions. These characteristics have led to their extensive use in radiation therapy beam characterization, diagnostic radiology, and medical physics quality control procedures [18,21]. A particularly important advancement in semiconductor dosimetry has been the development of Metal-Oxide-Semiconductor Field-Effect Transistor (MOSFET) dosimeters. MOSFET devices operate by measuring radiation-induced changes in transistor threshold voltage, which can be correlated directly with absorbed dose. Their small physical dimensions, lightweight design, and immediate readout capabilities make them highly suitable for in vivo dosimetry applications. Unlike larger conventional detectors, MOSFET dosimeters can be positioned directly on the patient surface or within anatomical cavities, enabling dose measurements at locations that are difficult to access using traditional dosimetric systems. This capability provides valuable information regarding the accuracy of dose delivery during radiotherapy procedures and supports comprehensive treatment verification [22,23]. In contemporary radiation oncology, MOSFET dosimeters are frequently employed for patient-specific quality assurance and treatment validation. Their ability to provide near real-time dose information is particularly valuable for advanced treatment modalities such as Intensity-Modulated Radiation Therapy (IMRT), Volumetric Modulated Arc Therapy (VMAT), Stereotactic Radiosurgery (SRS), and Image-Guided Radiation Therapy (IGRT). These highly conformal treatment techniques require accurate dose delivery to target volumes while minimizing radiation exposure to surrounding healthy tissues. MOSFET-based dose verification contributes to treatment accuracy by identifying potential deviations between planned and delivered doses, thereby enhancing patient safety and treatment effectiveness [18, 22]. Despite their many advantages, semiconductor and MOSFET dosimeters exhibit certain limitations that should be considered during clinical implementation. Factors such as energy dependence, angular dependence, accumulated radiation damage, and temperature sensitivity may influence detector response and necessitate appropriate calibration procedures. Furthermore, periodic quality control and performance verification are essential to ensure measurement

reliability and long-term stability. Nevertheless, continuous improvements in detector design, microelectronics, and signal-processing technologies have significantly enhanced the accuracy and robustness of semiconductor-based dosimetry systems, reinforcing their role as important tools in modern medical physics and radiation protection programs [18,22].

Computational dosimetry has become an indispensable component of modern radiation science, complementing experimental measurements and enabling detailed dose assessments in situations where direct measurements may be impractical or associated with significant uncertainty. The rapid growth in computational power and numerical modeling techniques has facilitated the widespread adoption of Monte Carlo simulation methods, which are currently regarded as the most accurate approach for modeling the transport of ionizing radiation through matter. Monte Carlo techniques employ probabilistic algorithms to simulate the interactions of radiation particles with materials by tracking large numbers of individual particles and their secondary products. Through repeated simulation of these stochastic processes, highly detailed information regarding energy deposition, particle fluence, and absorbed dose distributions can be obtained [24,25]. One of the principal strengths of Monte Carlo methods is their ability to accurately represent complex geometries, heterogeneous materials, and intricate radiation fields that are difficult to characterize using analytical techniques. This capability has made Monte Carlo simulations the reference standard for dose calculations in medical physics, radiation protection, nuclear engineering, and environmental radiological assessments. In medical applications, these techniques are extensively employed for treatment planning verification, patient-specific dose reconstruction, organ dose estimation, and optimization of advanced radiotherapy procedures. Their ability to model patient anatomy using voxel-based computational phantoms has significantly improved the accuracy of internal and external dose assessments [24]. Beyond clinical applications, computational dosimetry plays a critical role in occupational radiation protection. Monte Carlo calculations are used to estimate worker exposures in complex radiation environments, evaluate shielding effectiveness, and support the design of radiation protection measures in nuclear facilities, research reactors, and industrial installations. This methodology is extensively employed in the derivation of conversion coefficients linking operational quantities to protection quantities, thereby supporting the establishment and harmonization of international standards in radiation protection [19,20].

Environmental radiation monitoring and retrospective dose assessment further benefit from computational dosimetry techniques. Monte Carlo models can be applied to reconstruct historical exposure scenarios, estimate radiation doses resulting from radionuclide releases, and evaluate the transport of radiation through

environmental media. Such analyses support environmental impact assessments, emergency preparedness planning, and radiological risk evaluations. By integrating environmental monitoring data with computational models, researchers can achieve more realistic estimates of population exposure under a wide range of environmental conditions [26]. The combination of computational and experimental approaches has significantly enhanced the reliability of modern dose assessment methodologies. Experimental measurements obtained from dosimeters, survey instruments, and environmental monitoring systems are frequently used to validate simulation results, while computational models help interpret measurement data and reduce associated uncertainties. This synergy between measurement and modeling improves confidence in dose evaluations and supports evidence-based decision-making in radiation protection, medical physics, and environmental surveillance programs. As computational technologies continue to evolve, Monte Carlo-based dosimetry is expected to remain a cornerstone of advanced radiation assessment and optimization strategies [24,25].

4. ENVIRONMENTAL RADIATION MONITORING

The environment in which humans live constitutes an inherent source of ionizing radiation. Since the emergence of life on Earth, all living organisms have been continuously exposed to natural radiation originating from both terrestrial and extraterrestrial sources. Long-lived primordial radionuclides that have persisted since the formation of the Earth contribute to a permanent background radiation level in the environment. Natural background radiation remains the dominant source of radiation exposure for the global population [27]. Sources of ionizing radiation can generally be classified into two major categories: natural and anthropogenic (human-made) radiation sources. Natural radiation sources include cosmic radiation originating from outer space, terrestrial gamma radiation emitted from naturally occurring radionuclides in the Earth's crust, radon and its progeny present in the atmosphere, and naturally occurring radionuclides found in food and drinking water. In contrast, artificial radiation sources arise primarily from human activities and encompass medical diagnostic and therapeutic procedures, industrial applications utilizing radioactive materials, nuclear weapons testing, and radioactive fallout released into the environment following nuclear accidents. Together, these sources contribute to the overall radiation exposure received by individuals and populations [27]. Although radiation originating from natural sources generally does not produce significant biological effects at normal environmental levels, it is regarded as an unavoidable component of human exposure and is commonly referred to as natural background radiation. Because these sources are inherently present in the environment, their contribution to radiation exposure cannot be completely

eliminated. Among natural radiation sources, radon gas, a decay product of uranium naturally occurring in the Earth's crust, represents one of the most important contributors to population dose. The radiation dose associated with radon primarily arises from its short-lived progeny, which can be inhaled and deposited within the respiratory tract. Nevertheless, unlike many other natural radiation sources, indoor radon concentrations and the resulting radiation dose can be effectively reduced through relatively simple mitigation measures, such as improving ventilation and increasing air exchange rates within buildings [27]. In contrast to natural radiation sources, exposures arising from anthropogenic sources can generally be managed more effectively, provided that accidental releases do not occur. This is largely because the industrial, medical, or technological activities responsible for generating radiation can be modified, regulated, or discontinued when necessary. Therefore, the fundamental challenge in the beneficial use of ionizing radiation is to ensure an appropriate balance between the advantages obtained and the potential risks associated with exposure. Within the framework of radiological protection, this balance is achieved through the principle of optimization, which aims to maintain radiation doses at levels that are as low as reasonably achievable while taking social, economic, and practical considerations into account [20]. According to the UNSCEAR 2000 assessment, the worldwide average annual effective dose received by members of the public was estimated to be approximately 2.8 mSv. Of this total, about 2.4 mSv originated from natural radiation sources, while approximately 0.4 mSv was attributable to medical exposure, primarily from diagnostic X-ray procedures. Natural radiation sources account for more than 85% of the total annual dose received by the global population, with nearly half of this contribution arising from inhalation of radon and its short-lived decay products in indoor environments. Medical applications of ionizing radiation constitute the overwhelming majority of human-made radiation exposure, representing approximately 99% of the dose from anthropogenic sources. By comparison, exposures associated with industrial activities, nuclear power generation, and residual fallout from nuclear weapons testing contribute less than 1% of the overall population dose. These estimates highlight the dominant role of natural background radiation in determining global radiation exposure patterns and emphasize the significant contribution of indoor radon to the collective dose received by the public [27].

4.1. Environmental Monitoring Techniques

The assessment of environmental radioactivity relies on comprehensive monitoring systems that quantify both ambient radiation levels and radionuclide concentrations across various environmental matrices. Such programs serve multiple functions, ranging from the protection of public health to the evaluation of

environmental impacts associated with radiation exposure. Beyond routine surveillance, environmental monitoring provides a scientific basis for detecting deviations from normal background conditions, identifying contamination events, and verifying compliance with radiological protection regulations. Long-term datasets generated through these activities are invaluable for understanding trends in environmental radioactivity and for strengthening emergency response capabilities. Consequently, environmental radiation monitoring represents a fundamental element of modern radiological protection frameworks, supporting risk assessment, environmental stewardship, and evidence-based regulatory decision-making. Monitoring refers to the systematic measurement and evaluation of radiation levels or radioactive substances for the purpose of assessing, controlling, and managing radiation exposure. Within the framework of radiation protection, monitoring activities provide essential information for determining potential exposures and ensuring compliance with established safety requirements. Depending on the objective of the assessment, monitoring programs are commonly categorized into three principal areas: personal monitoring, which is used to determine the radiation dose received by individuals; environmental monitoring, which evaluates the presence and distribution of radionuclides and radiation levels in environmental media; and workplace or area monitoring, which focuses on the assessment of radiation conditions within occupational settings and controlled areas. Together, these monitoring approaches form the basis of comprehensive radiological protection programs and contribute to the protection of workers, the public, and the environment.

Gamma-ray spectrometry is among the most important analytical techniques employed in environmental radioactivity surveillance. This method enables the qualitative and quantitative determination of gamma-emitting radionuclides present in environmental samples such as soil, water, sediments, vegetation, and food products. Owing to their superior energy resolution and detection efficiency, high-purity germanium (HPGe) detectors are widely utilized for radionuclide identification and activity concentration measurements. The excellent spectroscopic performance of HPGe systems allows the discrimination of closely spaced gamma-ray peaks, thereby facilitating accurate characterization of natural and anthropogenic radionuclides in complex environmental matrices [18].Environmental gamma spectrometric analyses commonly focus on both naturally occurring and artificial radionuclides. Naturally occurring radionuclides include potassium-40 (40K) and members of the uranium-238 (238U) and thorium-232 (232Th) decay series, which contribute significantly to terrestrial background radiation. In addition, anthropogenic radionuclides such as cesium-137 (137Cs), cobalt-60 (60Co), and iodine-131 (131I) are frequently monitored because of their relevance to nuclear

activities, medical applications, and potential environmental contamination [27,28]. The measurement of these radionuclides provides valuable information for assessing background radiation levels, evaluating the impact of nuclear facilities, tracking contamination events, and supporting environmental radiation protection programs.

Monitoring of airborne radioactivity constitutes a critical component of environmental radiation surveillance programs, as it provides early information on the presence and dispersion of radioactive materials released into the atmosphere. The assessment of airborne radionuclides is particularly important for evaluating potential inhalation doses, which often represent a significant exposure pathway for members of the public and occupationally exposed individuals. To achieve this objective, air-sampling systems are routinely employed to collect suspended particulate matter from the atmosphere. These systems typically utilize high-efficiency filtration media capable of capturing radioactive aerosols over extended sampling periods. Following collection, the filters are subjected to radiometric analyses, such as gamma-ray spectrometry, alpha spectrometry, or beta counting, to identify radionuclides and quantify their activity concentrations. The resulting data provide valuable information for environmental impact assessments, regulatory compliance verification, emergency response planning, and long-term trend analysis of atmospheric radioactivity [27,28].The surveillance of radionuclides in *aquatic environments* plays a fundamental role in environmental radiation protection programs. Monitoring activities conducted in surface waters, groundwater resources, drinking water supplies, and marine ecosystems provide valuable information on the transport, dispersion, and accumulation of radioactive substances within the hydrological cycle. Such assessments are essential for understanding potential exposure pathways to human populations and for evaluating the long-term environmental consequences of radionuclide contamination. Routine *water monitoring* programs typically involve the collection and analysis of samples to determine overall radioactivity levels as well as the presence of specific radionuclides of interest. Measurements commonly include concentrations of gross alpha and beta activity, which serve as screening indicators of radioactive contamination. In addition, particular attention is given to radionuclides such as tritium and gamma-emitting isotopes because of their environmental mobility and significance in environmental impact assessments. The data generated through these monitoring efforts contribute to the evaluation of drinking water safety, the assessment of radionuclide migration processes, the verification of regulatory compliance, and the development of effective radiation protection strategies for both the public and the environment [28].Soil represents one of the most significant environmental compartments for the accumulation and retention of radioactive materials released into the atmosphere. Following deposition processes such as dry

fallout and precipitation-driven scavenging, radionuclides can persist in soil for extended periods, making it an important indicator of both historical and recent radiological contamination. As a result, *soil monitoring programs* are widely employed to characterize the distribution, persistence, and mobility of radionuclides within terrestrial ecosystems.Systematic soil sampling provides essential information for evaluating the long-term environmental consequences of radioactive releases and for understanding the mechanisms governing radionuclide transport in the environment. Measurements commonly focus on naturally occurring radionuclides, including members of the uranium and thorium decay series as well as potassium-40, together with anthropogenic radionuclides such as cesium-137 and cobalt-60. The data obtained from these investigations support environmental impact assessments, contamination mapping, radioecological studies, and the estimation of potential radiation doses to human populations. Furthermore, long-term soil monitoring contributes to the development of predictive models describing radionuclide migration through terrestrial pathways and assists regulatory authorities in making informed decisions regarding environmental protection and remediation strategies [27,28].Recent advances in radiation detection technologies, communication systems, and digital data processing have transformed environmental radiation surveillance from periodic measurement campaigns to continuously operating monitoring infrastructures. Modern environmental radiation monitoring networks consist of geographically distributed detector stations capable of recording radiological parameters automatically and transmitting measurement results to centralized data management systems in near real time. These integrated systems provide continuous information on the radiological status of the environment and enhance the effectiveness of routine surveillance programs.

A major advantage of real-time monitoring networks is their ability to perform uninterrupted measurements of ambient gamma dose rates over large geographical regions. The continuous collection of radiological data enables the establishment of reliable background radiation baselines and facilitates the identification of unusual variations that may indicate abnormal radiological conditions. Automated processing and communication technologies allow monitoring centers to receive and analyze measurement results immediately after acquisition, significantly reducing the time required to recognize potential radiological events.In addition to routine environmental surveillance, these networks play an important role in emergency preparedness and response. *Real-time monitoring* data can support rapid decision-making processes, improve situational awareness, and assist authorities in evaluating the magnitude and spatial distribution of radiological impacts. Advanced monitoring platforms frequently incorporate automated notification systems and geospatial analysis tools, enabling visualization of radiation levels and facilitating coordinated

emergency management activities. Such capabilities contribute to the timely implementation of protective actions when required [26].Consequently, many countries have established national environmental radiation monitoring networks as a key component of their radiological protection infrastructure. These systems strengthen the capacity to detect unexpected radiological releases, support regulatory oversight, and provide scientifically reliable information for protecting both public health and the environment. Their continued development remains an important element of modern environmental radiation monitoring and emergency preparedness strategies.

4.2. Artificial Intelligence and Digital Technologies in Radiation Monitoring

The rapid advancement of digital technologies has introduced new opportunities for improving the efficiency, accuracy, and responsiveness of radiation protection and environmental monitoring systems. Among these developments, artificial intelligence (AI) has emerged as a valuable tool for managing and interpreting the large volumes of data generated by modern radiation detection networks. By applying machine learning and advanced data analytics techniques, AI-based systems can identify complex patterns within radiological datasets that may not be readily apparent through conventional analytical approaches [29].In radiation monitoring applications, artificial intelligence can support a variety of tasks, including detector performance optimization, automated calibration procedures, anomaly recognition, radionuclide source characterization, and predictive dose assessment. Machine learning algorithms are particularly useful for detecting subtle deviations from normal background conditions and for distinguishing genuine radiological events from measurement uncertainties or environmental fluctuations. These capabilities contribute to improved reliability and efficiency in both routine monitoring activities and emergency response operations.Another important application of AI involves the analysis of long-term environmental monitoring records. By processing extensive historical datasets, intelligent algorithms can assist in identifying spatial and temporal trends in environmental radioactivity, evaluating the effectiveness of remediation measures, and supporting risk assessment studies. Such analytical capabilities provide valuable scientific evidence for decision-making processes related to environmental protection and radiological safety.Simultaneously, advances in cloud computing, wireless communication technologies, and the Internet of Things (IoT) have facilitated the development of interconnected radiation monitoring platforms. These systems integrate networks of distributed sensors capable of continuously collecting, transmitting, and processing radiological data from multiple locations. Cloud-based infrastructures enable secure

data storage, remote access, real-time visualization, and centralized management of monitoring information, thereby improving operational flexibility and scalability.

The integration of AI, IoT technologies, and advanced communication networks has given rise to intelligent radiation monitoring systems capable of providing continuous and geographically extensive surveillance. Such platforms enhance situational awareness, support rapid detection of abnormal radiological conditions, and strengthen emergency preparedness capabilities. As digital technologies continue to evolve, their incorporation into radiation protection programs is expected to further improve monitoring performance, data interpretation, and evidence-based decision-making, ultimately contributing to more effective protection of workers, the general public, and the environment.

4.3. Future Directions in Radiation Dosimetry and Environmental Monitoring

Radiation dosimetry and environmental monitoring technologies continue to evolve in response to increasing demands for improved measurement accuracy, rapid data acquisition, and comprehensive radiological risk assessment. Future progress in these fields is expected to be driven by innovations that enhance detector performance, facilitate automated monitoring procedures, and enable the integration of information obtained from multiple data sources. These developments will contribute to a more detailed understanding of radiation exposure conditions in both occupational and environmental settings. A major trend in dosimetry research involves the development of compact and highly sensitive monitoring devices capable of providing continuous exposure information. Advances in materials science, electronics, and sensor engineering are supporting the design of next-generation personal dosimeters that offer improved measurement precision while minimizing device size and power consumption. Such technologies may facilitate more effective exposure tracking in medical, industrial, research, and emergency response environments [30].Innovative detection systems are also emerging as important components of future radiation monitoring infrastructures. Novel detector materials, advanced semiconductor technologies, fiber-optic sensing systems, and nanoscale radiation-sensitive materials have demonstrated considerable potential for improving detection capabilities and expanding the range of monitoring applications. These technologies may provide enhanced sensitivity, improved spatial resolution, and increased adaptability to complex monitoring scenarios. In parallel with hardware developments, biological approaches to dose assessment are attracting growing scientific interest. Biological dosimetry methods, which evaluate radiation-induced changes in cells and tissues, may provide valuable complementary information in situations where conventional physical dosimetry data are unavailable

or incomplete. Such approaches have the potential to strengthen dose reconstruction efforts and support the assessment of exposure consequences following radiological incidents.Computational technologies are expected to assume an increasingly important role in future radiation protection programs. Advanced simulation techniques, coupled with environmental and operational monitoring data, can support the development of dynamic predictive models capable of representing radiological systems with greater realism. These computational frameworks may improve exposure forecasting, environmental impact assessment, and emergency preparedness planning. The expansion of digital infrastructures has also created opportunities for the application of artificial intelligence and data-driven analytical methods. As monitoring systems generate increasingly large and complex datasets, intelligent algorithms can assist in the interpretation of measurement results, identification of unusual radiological patterns, and evaluation of long-term environmental trends. The integration of automated analytics with modern monitoring networks may enhance decision-making processes by providing timely and reliable information to radiation protection specialists and regulatory authorities.

Looking ahead, radiation monitoring systems are likely to become more interconnected, combining advanced detectors, wireless communication technologies, cloud-based data management platforms, and sophisticated analytical tools within unified monitoring frameworks. The convergence of these technologies is expected to improve the efficiency of environmental surveillance, strengthen emergency response capabilities, and support evidence-based radiological protection practices. Ultimately, continued technological innovation will play a central role in ensuring the safe and sustainable application of ionizing radiation across a wide range of disciplines. Improvements in measurement accuracy, monitoring reliability, and predictive assessment methodologies are expected to enhance the protection of workers, the public, and the environment while enabling the continued advancement of beneficial radiation-related technologies [31].

5. CONCLUSION

Radiation dosimetry and environmental monitoring represent essential components of contemporary radiological protection systems and provide the scientific basis for evaluating human exposure to ionizing radiation. Through the quantification of radiation doses and the systematic assessment of environmental radioactivity, these disciplines support the protection of workers, the public, and the environment from the potential risks associated with radiation exposure [26,27]. Over recent decades, significant technological progress has transformed the capabilities of radiation monitoring and dose assessment. Advanced detection systems, comprehensive environmental surveillance networks, computational

modeling techniques, geographic information systems, and sophisticated data management platforms have improved the accuracy and reliability of radiological evaluations. Furthermore, the increasing incorporation of digital technologies, including artificial intelligence and automated monitoring infrastructures, has enhanced the capacity to analyze complex datasets and respond rapidly to changing radiological conditions [30].

Environmental monitoring remains a critical element of radiation protection because it enables the identification of exposure pathways, the evaluation of radionuclide behavior in environmental compartments, and the verification of compliance with regulatory requirements. When integrated with personal and area monitoring programs, environmental surveillance provides a comprehensive framework for assessing radiological conditions at local, regional, and global scales. These activities contribute not only to routine radiation protection practices but also to emergency preparedness and response efforts.

As the applications of ionizing radiation continue to expand in medicine, industry, agriculture, research, and energy production, the demand for accurate and efficient monitoring systems will continue to grow. Future developments are expected to focus on improving measurement sensitivity, increasing automation, strengthening data integration capabilities, and enhancing predictive assessment methodologies. The continued convergence of advanced detector technologies, computational tools, and intelligent analytical systems will further improve the effectiveness of radiological protection programs.In conclusion, radiation dosimetry and environmental monitoring will remain indispensable elements of sustainable radiation safety management. Ongoing scientific and technological innovations are expected to strengthen the ability of regulatory authorities, researchers, and radiation protection professionals to evaluate exposure scenarios, manage radiological risks, and ensure the safe use of ionizing radiation for the benefit of society.

REFERENCES

1- International Atomic Energy Agency. (2014). *Radiation protection and safety of radiation sources: International basic safety standards (IAEA Safety Standards Series No. GSR Part 3)*. International Atomic Energy Agency.

2- Das, I. J. (2026). Radiation detectors and methods in medicine therapy, diagnostic and radiation protection. Springer Nature Switzerland AG.

3- Ainsbury, E. A., Bakhanova, E., Barquinero, J. F., Brai, M., Chumak, V., Correcher, V., Darroudi, F., Fattibene, P., Grillón, C., Guclu, I., McKeever, S. W. S., O'Hagan, J. A., Roecklein, A. K., Trompier, F., & Wünsch, C. (2011). Review of retrospective dosimetry techniques for external ionising radiation exposures. *Radiation Protection Dosimetry*, 147(4), 573–592. https://doi.org/10.1093/rpd/ncq499

4- Giussani, A., Lopez, M. A., Romm, H., Ainsbury, E. A., Barnard, S., Barquinero, J. F., Burbidge, C., De Angelis, C., Eakins, J., Fattibene, P., Gilvin, P., Ginjaume, M., Gregoire, E., Horton, P., Hovhannisyan, G., Jaworska, A., Kulka, U., Malsch, D., Oestreicher, U., ... Sharpo, O. (2020). Eurados review of retrospective dosimetry techniques for internal exposures to ionising radiation and their applications. Radiation and Environmental Biophysics, 59(3), 357-387. https://doi.org/10.1007/s00411-020-00845-y

5- Bailiff, I. K., Sholom, S., & McKeever, S. W. S. (2016). Retrospective and emergency dosimetry in response to radiological incidents and nuclear mass-casualty events: A review. *Radiation Measurements*, 94, 83-139. https://doi.org/10.1016/j.radmeas.2016.09.004

6- World Health Organization. (2018). *Radiation emergency medical preparedness and response*. World Health Organization. https://www.who.int/groups/rempan

7- Kurihara, O., Kim, E., Tani, K., Ogawa, M., Yajima, K., Kowatari, M., & Tatsuzaki, H. (2022). Effective population monitoring for determination of the thyroidal radioiodine content of the public following a nuclear accident in Japan. *Environmental Advances*, 8, Article 100206. https://doi.org/10.1016/j.envadv.2022.100206

8- Dunster, H. J. (2001). The future of the ICRP recommendations. *Journal of Radiological Protection*, 21(3), 303-304. https://doi.org/10.1088/0952-4746/21/3/103

9- International Commission on Radiation Units and Measurements. (2011). *Fundamental quantities and units for ionizing radiation* (ICRU Report No. 85). International Commission on Radiation Units and Measurements.

10- International Commission on Radiological Protection. (1977). *Recommendations of the International Commission on Radiological Protection* (ICRP Publication 26). *Annals of the ICRP*, 1(3). Pergamon Press.
11- International Commission on Radiological Protection. (1991). *1990 recommendations of the International Commission on Radiological Protection* (ICRP Publication No. 60). *Annals of the ICRP*, 21(1-3). Pergamon Press.
12- ICRP, 2007. The 2007 *Recommendations of the International Commission on Radiological Protection*. ICRP Publication 103. Annals of the ICRP, 37 (2-4).
13- International Commission on Radiological Protection. (1991). *1990 recommendations of the International Commission on Radiological Protection (ICRP Publication 60)*. *Annals of the ICRP*, 21(1-3).
14- Bolch, W. E., Dietze, G., Petoussi-Henss, N., & Zankl, M. (2015). Dosimetric models of the eye and lens of the eye and their use in assessing dose coefficients for ocular exposures. *Annals of the ICRP*, 44(1 Suppl.), 91-111. https://doi.org/10.1177/0146645314562320
15- Bhatt, B. (2011). Thermoluminescence (TL), optically stimulated luminescence (OSL), and radiophotoluminescence (RPL). *Radiation Protection and Environment,* 34(1), 6-16.
16- Yukihara, E. G., & McKeever, S. W. S. (2011). *Optically stimulated luminescence: Fundamentals and applications*. John Wiley & Sons. https://doi.org/10.1002/9780470977064
17- Suliman, I. I., Yousif, E. H., Beineen, A. A., Yousif, B. E., & Hassan, M. (2010). Performance testing of selected types of electronic personal dosimeters used in Sudan. *Radiation Measurements*, 45(10), 1582-1584. https://doi.org/10.1016/j.radmeas.2010.05.032
18- Knoll, G. F. (2010). *Radiation detection and measurement* (4th ed.). John Wiley & Sons.
19- International Atomic Energy Agency. (2014). *Radiation protection and safety of radiation sources: International basic safety standards (General Safety Requirements No. GSR Part 3*). International Atomic Energy Agency.
20- International Commission on Radiological Protection. (2007). *The 2007 recommendations of the International Commission on Radiological Protection (ICRP Publication 103). Annals of the ICRP*, 37(2-4).
21- Andreo, P., Burns, D. T., Nahum, A. E., Seuntjens, J., Attix, F. H., Verdú, G., & Rogers, D. W. O. (2017). *Fundamentals of ionizing radiation dosimetry.* Wiley-VCH.
22- Beyer, G. P., Ebert, M., Fulham, M., Waterhouse, D., Binns, D., & Kutcher, G. J. (2008). An implantable MOSFET dosimeter for the measurement of

radiation dose in tissue during cancer therapy. *IEEE Sensors Journal*, 8(1), 38-51. https://doi.org/10.1109/JSEN.2007.912542

23- Kumar, A., Singh, I. R., Sharma, S., & Ravindran, B. (2015). Performance characteristics of mobile MOSFET dosimeter for kilovoltage X-rays used in image guided radiotherapy. *Journal of Medical Physics*, 40(3), 123–128. https://doi.org/10.4103/0971-6203.165074

24- Rogers, D. W. O. (2006). Fifty years of Monte Carlo simulations for medical physics. *Physics in Medicine & Biology*, 51(13), R287-R301. https://doi.org/10.1088/0031-9155/51/13/R17

25- Andreo, P., Burns, D. T., Nahum, A. E., Seuntjens, J., & Attix, F. H. (2017). *Fundamentals of ionizing radiation dosimetry*. Wiley-VCH.

26- United Nations Scientific Committee on the Effects of Atomic Radiation. (2020). *Sources, effects and risks of ionizing radiation*. United Nations Scientific Committee on the Effects of Atomic Radiation.

27- United Nations Scientific Committee on the Effects of Atomic Radiation (UNSCEAR). (2000). *Sources and Effects of Ionizing Radiation: UNSCEAR 2000 Report to the General Assembly*, Volume I: Sources. United Nations, New York.

28- International Atomic Energy Agency. (2005). *Environmental and source monitoring for purposes of radiation protection* (Safety Guide No. RS-G-1.8). International Atomic Energy Agency.

29- Arhouni, F. E., Abdo, M. A. S., Ouakkas, S., Bouhssa, M. L., & Boukhair, A. (2025). Artificial intelligence-driven advances in nuclear technology: Exploring innovations, applications, and future prospects. *Annals of Nuclear Energy*, 213, Article 111151. https://doi.org/10.1016/j.anucene.2024.111151

30- He, R., Niu, X. Y., Wang, Y., et al. (2023). Advances in nuclear detection and readout techniques. *Nuclear Science and Techniques*, 34, Article 205. https://doi.org/10.1007/s41365-023-01359-0

31- Iniewski, K., & Gadey, H. (2024). *Emerging radiation detection technology and applications*. Springer. https://doi.org/10.1007/978-3-031-63897-8

Chapter 25

Optoelectronic and Vibrational Properties of Half-Heusler Libaas Compounds

Yasemin O. CIFTCI [1]

1.INTRODUCTION

The structural, mechanical, electronic, vibrational, and optical properties of the α-, β-, and γ-phases of LiBaAs were systematically investigated using density functional theory (DFT). The structural optimization and energy–volume calculations reveal that the β phase possesses the lowest total energy among the three polymorphs, indicating that it is the thermodynamically most stable phase. The calculated elastic constants satisfy the Born stability criteria, confirming the mechanical stability of β-LiBaAs. The relatively low shear modulus (7.4 GPa), Young's modulus (20.8 GPa), and Debye temperature (144.6 K), together with a high Pugh's ratio (B/G = 4.72) and Poisson's ratio (0.40), suggest that the compound is mechanically soft and ductile. The electronic band structure and density of states demonstrate that β-LiBaAs is a semiconductor with a well-defined band gap. The phonon dispersion curves contain no imaginary frequencies, confirming the dynamical stability of the optimized structure. Optical calculations reveal a relatively high dielectric response, large refractive index, strong ultraviolet absorption, moderate reflectivity, and a pronounced plasma resonance at higher photon energies. The excellent agreement among the structural, elastic, electronic, vibrational, and optical results demonstrates the internal consistency of the calculations and establishes β-LiBaAs as a dynamically stable semiconductor with promising mechanical flexibility and attractive optoelectronic characteristics. These findings provide valuable theoretical guidance for future experimental synthesis and the development of Li-based semiconductor materials for optoelectronic and ultraviolet photonic applications.There is a pressing need for renewable energy alternatives to fossil fuels if the world energy economy is to be strengthened [1]. Materials scientists should pay close attention to the immense and growing reliance on fossil fuels. A considerable amount of waste heat is produced when fossil fuels are converted into energy. Most of the fuel is converted into waste heat which decreases the amount of energy obtained from the fuel and so waste heat from this fuel can

[1] Department of Physics, Faculty of Science, Gazi University, 06500 Ankara, Turkey,
ORCID: 0000-0003-1796-0270

destroy the valuable energy [2]. It is important to maximise the amount of energy from fossil fuel and this can be done by converting waste heat from fossil fuel combustion. Tackling these problems will reduce fossil fuel consumption and the negative environmental impacts of fossil fuels on life on Earth. Minimising the damaging effects of fossil fuels will mitigate the impact of global warming. Energy is turned into electricity by thermoelectric generators. The Seebeck effect [3, 4] is what makes this happen, converting waste heat directly into electricity. The thermoelectric materials currently being studied are compounds and alloys [5-11]. The study of half Heusler compounds is widespread because of their interesting properties such as a high bulk modulus, high thermal stability, simple crystal structure, high band degeneracy and a tunable electronic structure [12-13]. The ability of half-Heusler compounds to generate electricity through thermoelectric effects is very important. In fact, the 8 or 18 electron valence electron counts (VEC) of these compounds are very important. The 8 or 18 VEC half Heusler compounds are semiconductors and very high effective mass is possessed by the charge carriers of these compounds [14]. Half-Heusler compounds and alloys are very popular because of their extraordinary optoelectronic properties, and they are used in solar and photovoltaic applications [15-21]. Half-Heusler compounds with XYZ composition are a class of ternary materials in which researchers are currently working. Well, in these compounds, X, Y and Z are, respectively, transition or rare-earth metal, transition metal and main group element. Half-Heusler crystal structures crystallize in the C1b space group (F43m). As a result, they have a wide area of work on superconductivity, thermoelectricity, and spintronics [22-23]. As a result, in recent years, in materials science and nanotechnology, there has been a surge of interest in half-Heusler compounds, and it is currently a hot topic in research. Due to their semiconductor properties and high thermal and mechanical stability, these compounds can be applied in a wide variety of applications. Rising global energy demand and the depletion of fossil fuel reserves have also increased the need for energy storage solutions. LiBaAs has the potential to transform fields such as electric vehicles and renewable energy systems with a higher density and longer cycle life. Moreover, LiBaAs is eco-friendly, and this is a key factor in reducing the environmental impact of LiBaAs. In this paper, we will consider structural, electronic, vibrational and optical properties of LiBaAs compound. Investigation of the different phases of the compound, namely, beta (β), gamma (γ) and alpha (α) will allow us to better understand the material's physical properties. In particular, the stable structure of the beta phase suggests that this phase is the most suitable for use.

2. MATERIAL AND METHOD

We conducted first-principles (ab initio) calculations on LiBaAs to assess its structural, electronic, elastic, vibrational, and optical characteristics. The compound was represented in a cubic MgAgAs structure with space group 216 (see Figure 1). All computations were carried out using the VASP software package [24], applying the Generalized Gradient Approximation (GGA) with the Perdew–Burke–Ernzerhof (PBE) functional [25]. A plane-wave cutoff energy of 700 eV was employed to ensure total energy convergence within 10−8 eV. The valence configurations used for reliable electronic property calculations included Li($2s^1\ 2p^0$), Ba($5s^2\ 5p^6\ 6s^2$), and As($4s^2\ 4p^3$). Phonon calculations utilized a 2×2×2 supercell of LiBaAs; force constants were obtained through VASP, while phonon dispersions were calculated using the PHONOPY package [26]. The elastic constants were determined through the stress–strain method [27].

3. RESULTS AND DISCUSSION

3.1. Structural Properties

The optimized structures of LiBaAs are obtained by total energy minimization of the three phases of these compounds. The phases optimized are as follows: α with Li atom at 4c, Ba atom at 4b, and As atom at 4a, the β with Li atom at 4b, Ba atom at 4a, and As atom at 4c, and the γ with Li atom at 4a, Ba atom at 4c, and As atom at 4b.

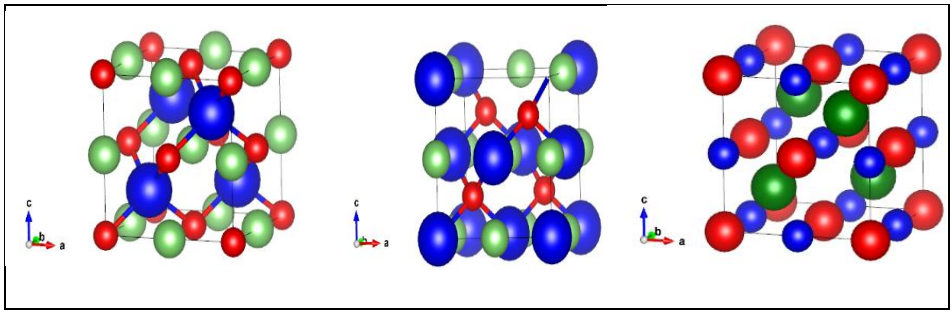


Figure 1. Unit cell of alpha, beta, and gamma phases of LiBaAs

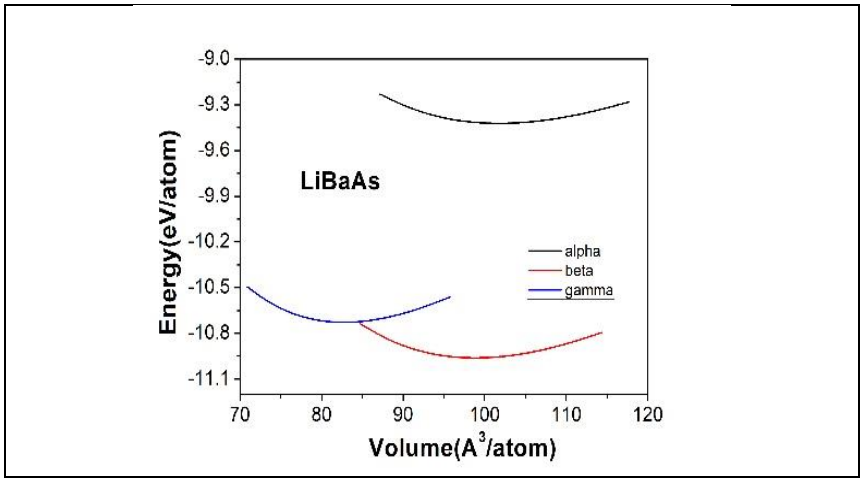


Figure 2. Energy-volume curves for LiBaAs

The energy–volume (E–V) curves for the α-, β-, and γ-phases of LiBaAs are illustrated in Fig. 2. These curves were derived by fitting the computed total energies to the Birch–Murnaghan equation of state, which facilitated the precise determination of each phase's equilibrium volume and minimum total energy. As depicted in Fig. 2, all phases demonstrate distinct parabolic E–V characteristics with a singular energy minimum, signifying that these three crystal structures represent mechanically stable equilibrium states. The gradual change in total energy relative to volume further validates the accuracy of the structural optimization.Among the studied polymorphs, the β phase exhibits the lowest minimum total energy, indicating it is thermodynamically the most stable configuration under standard conditions. Conversely, the α phase displays the highest total energy across the entire examined volume range, reflecting its considerably lower stability in energetic terms. The γ phase is positioned between these two, being more stable than α but less so than β. Additionally, there are variations in equilibrium volumes among these structures; specifically, the β phase achieves its minimal energy at a slightly larger equilibrium volume compared to the γ phase, pointing to a more expanded crystal lattice structure. These differences in equilibrium volumes highlight variations in atomic packing efficiency and bonding properties among the different polymorphs.The pronounced energy minimum associated with the β phase suggests stronger interatomic interactions and reduced internal energy when contrasted with other phases. Therefore, it can be anticipated that during crystal growth and synthesis at ambient pressure, the β phase will be favored energetically as a polymorph. The energy disparity between β and γ phases is moderate; however, α is significantly less stable overall. This ranking of energies implies that transitions

between the β and γ phases could become feasible under external influences such as changes in pressure or temperature, while the spontaneous formation of α is highly unlikely due to its substantially higher total energy.

Table1. Structural parameters: lattice parameters (*a),* bulk modulüs (*B*), pressure derivatives of the bulk modulus ($B^{'}$), and total energies for the α-, β-, and γ-phases for LiBaAs, and other literature values

Materials	Reference	a=b=c (Å)	Vol Å^3	B (GPa)	$B^{'}$	Etot(ev/atom)
α-phase	This study	7.41	101.69	23.23	3.96	-9.42
β-phase	This study	7.34	98.769	28.15	4.02	-10.96
γ-phase	This study	6.92	82.695	34.107	4.351	-10.73

The optimized structural parameters of the α-, β-, and γ-phases of LiBaAs, including the equilibrium lattice constant (a), unit cell volume (V), bulk modulus (B), pressure derivative of the bulk modulus (B′), and total energy (Etot), are shown in Table 1. These quantities were obtained by fitting our total energy versus volume data to the Birch–Murnaghan equation of state of the third order as shown in the equation of state. Our results show that the three polymorphs exhibit distinct structural and mechanical properties. The lowest total energy of the three polymorphs is in the β phase (−10.96 eV atom^{-1}), which indicates that it is the most stable polymorph in the environment at the present time. The γ phase is slightly higher (−10.73 eV atom^{-1}) and the most stable (−9.42 eV atom^{-1}) in the other two polymorphs. This result is fully consistent with the energy-volume curves in Fig. 1, where the β phase forms the lowest lattice constant in the global energy landscape. The equilibrium lattice constant decreases in the order α, β, and γ, and the equilibrium volume decreases from 101.69 Å^3 for the α phase to 82.70 Å^3 for the γ phase. Such a decrease indicates that the atoms are packing more and more strongly from α to γ. The bulk modulus is also dropping, but it is only a small effect. The values are calculated as 23.23 GPa for the α phase, 28.15 GPa for the β phase, and 34.11 GPa for the γ phase. Since the bulk modulus is defined as the resistance to uniform compression, we see that the γ phase is the most rigid structure and the α phase is the most compressible. While the γ phase has the strongest bulk modulus, it is not the most stable polymorph since the thermodynamic stability is determined by total energy rather than mechanical stiffness. The β phase has a very high bulk modulus and the lowest internal energy. It is the most compact but also the most favorable in terms of bonding interactions. The pressure derivative of the bulk modulus B′ varies only slightly between the three phases (3.96–4.35), and so the compressibility of the three different phases is equal under external pressure. The values are close to 4, which is typical for many covalent and semiconducting compounds and provides a

physically reasonable fit to the equation of state. The structural parameters in this paper show that the β phase is the ground-state structure of LiBaAs, while the γ phase is most resistant to compression due to the smaller structure of the crystal. The differences in structural stability can be attributed to the atomic packing efficiency and chemical bonding among the three polymorphs. The lower overall energy of the β phase implies that its crystal geometry is more favorable in terms of electrostatic and orbital hybridization interactions and thus minimizes internal energy. The higher bulk modulus of the γ phase is due to its smaller equilibrium volume and shorter average bond lengths, making it more resistant to volume deformation.

3.3 Electronic Properties

The half-Heusler compound LiBaAs is a material of significant interest due to its electronic characteristics, particularly its behavior as a semiconductor and its potential applications. This section will concentrate on the band structure analysis of LiBaAs, along with its conductivity, insulating properties, and overall semiconductor behavior. The band structure of LiBaAs is a key determinant of the material's electronic properties. Preliminary calculations suggest that it demonstrates semiconducting characteristics. Analyzing the band structure is essential for understanding energy level transitions and the energy gaps in this compound. Notably, during the beta phase, a narrow band gap is observed, which correlates with improved electrical conductivity. Furthermore, band structure calculations are vital for assessing the future applications of LiBaAs.

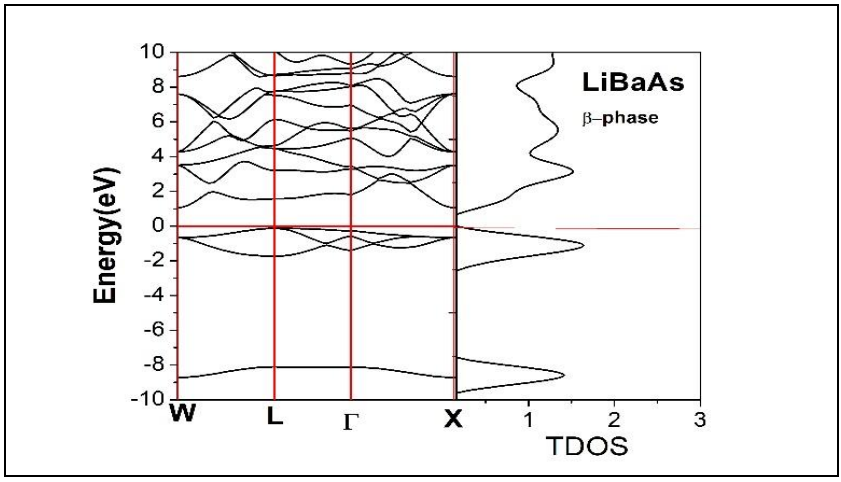


Figure 3. Electronic band structures and total DOS for LiBaAs

The electronic band structure and total density of states (TDOS) for β-LiBaAs are illustrated in Fig. 3. The calculations for the band structure were performed along the high-symmetry paths W–L–Γ–X within the first Brillouin zone. The Fermi level is positioned at 0 eV, denoted by a horizontal red line. As depicted in Fig. 3, there are no electronic bands intersecting the Fermi level throughout the entire Brillouin zone, indicating that β-LiBaAs behaves as a semiconductor. The existence of a distinct forbidden energy region near the Fermi level further validates the presence of an electronic band gap. Furthermore, the significant distance between the valence band maximum (VBM) and conduction band minimum (CBM) from the Fermi level suggests a clear separation between occupied and unoccupied electronic states. This indicates that the material is electronically stable and has a negligible intrinsic carrier concentration at low temperatures. The dispersion of both the valence and conduction bands provides a glimpse of the charge transport of the material. The upper valence bands are fairly non-dispersive, and the conduction bands are more dispersive in a few symmetry directions. This dispersion is associated with lower carrier effective masses and hence high carrier mobility. Hence, β-LiBaAs should have good electron transport properties as compared to materials with flatter conduction bands. The TDOS calculated also supports the semiconducting nature of the compound. As shown in Fig. 3, the density of electronic states disappears around the Fermi level, which is a characteristic of semiconductors. The valence-band states are concentrated mainly around -3 eV and 0 eV, and the conduction-band states begin from the band-gap region and continue to higher energies. The sharp DOS peaks at high energies are caused by localized electronic states in the relatively weakly dispersive bands. On the other hand, the smooth DOS profile near the band edges indicates more dispersive electronic states, which can be used to transport carriers. The relatively broad conduction bands, as well as the finite DOS just above the conduction-band edge, indicate that electrons can be excited by external conditions such as temperature or photon absorption. This property is attractive for electronic transport, optoelectronic devices, and photovoltaic energy conversion. The absence of mid-gap states implies that the intrinsic crystal defects are very low in our theoretical model and that the electronic quality of the crystal structure is good.

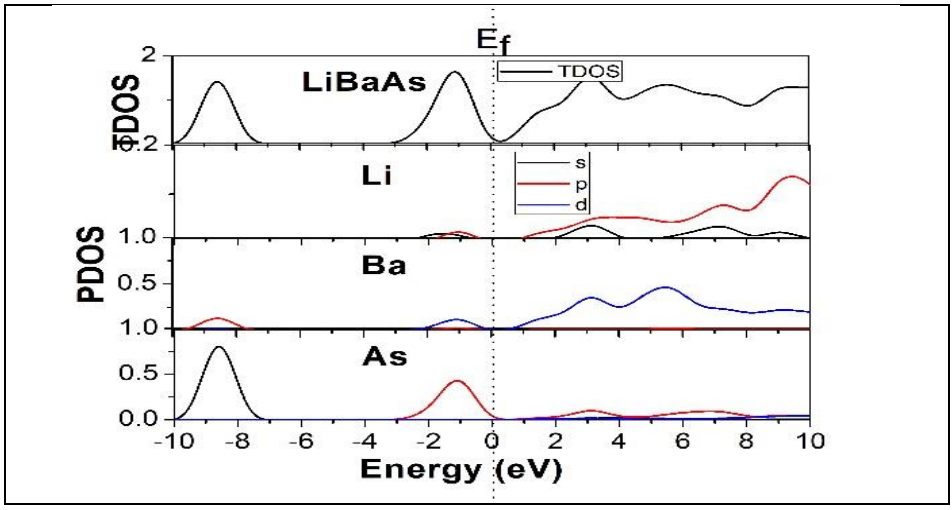


Figure 4. Total and partial density of states for LiBaAs

In Figure- 4 illustrates the total density of states (TDOS) alongside the atom- and orbital-resolved partial density of states (PDOS) for β-LiBaAs. The Fermi level (\(E_F\)) is positioned at 0 eV, denoted by a vertical dashed line. The lack of electronic states at this level unequivocally verifies the semiconducting characteristics of β-LiBaAs, which aligns well with the computed electronic band structure.The valence band primarily spans approximately from −10 to 0 eV and can be categorized into two separate energy regions. Deep valence states near −9 eV are predominantly attributed to As-s orbitals, highlighting their strong localization. A second region extends from roughly −3 eV up to the valence band maximum (VBM), consisting mainly of As-p states along with minor contributions from Ba-p orbitals. These findings indicate that p orbitals belonging to arsenic atoms play a crucial role in determining electronic properties close to the VBM.

Conversely, within the conduction band—ranging from its minimum (CBM) up to around 10 eV—the influence is chiefly due to Ba-d orbitals, while Li's contribution remains relatively minimal across all energy levels. The prominent presence of Ba-d near CBM suggests that these lowest conduction state energies stem largely from barium atoms' influence; meanwhile, lithium plays a more passive role through slight involvement via s and p orbitals as an electron donor rather than actively shaping electronic configurations at or around band edges.The distinct separation between both bands—the As-p enriched valence region and Ba-d dominated conduction area—indicates that interactions between p and d orbitals principally account for creating an electronic gap. Furthermore, negligible density-of-states values at \(E_F\) combined with an absence of

impurity-related features within this gap reinforce β-LiBaAs's classification as an intrinsic semiconductor

3.4 Elastic Properties

Elastic constants govern mechanical stability and inform on stiffness, brittleness versus ductility, bonding character, and anisotropy. The calculated elastic constants and the derived polycrystalline mechanical parameters of β-LiBaAs are listed in Table 3. For cubic crystals, the Born mechanical stability criteria require that

$$C_{11}-C_{12}>0\ ,\ C_{11}+2C_{12}>0, \text{ and } C_{44}>0 \quad (1)$$

The calculated elastic constants (C_{11}=73.5 GPa, C_{12}=15.8 GPa, and C_{44}=1.5GPa) satisfy all these conditions, confirming that β-LiBaAs is mechanically stable under ambient conditions.

Table 3. Elastic properties for β-LiBaAs

Materials	C_{11} (GPa)	C_{12} (GPa)	C_{44} (GPa)	G (GPa)	E (GPa)	v	B/G	θ_D
β-LiBaAs	73.5	15.8	1.5	7.4	20.8	0.4	4.72	144.6

Among the three independent elastic constants, C_{11} is the largest and indicates that the crystal has very high resistance to axial compression along the major crystallographic directions. The very small value of C_{44} shows that the crystal is very weak in terms of shear deformation. The large difference between longitudinal and shear stiffness indicates a very strong elastic anisotropy in the mechanical response and suggests that shear deformation is the lowest mechanical resistance of the crystal. The bulk modulus B ≈ 35.0 GPa obtained from the elastic constants is also very small, thus β-LiBaAs is relatively compressible compared with conventional covalent semiconductors such as Si, GaAs, and many half-Heusler compounds whose bulk moduli are above 60-100 GPa. The low bulk modulus indicates that the average interatomic bonding of the crystal is weak. We calculate the shear modulus and Young's modulus as 7.4 GPa and 20.8 GPa, respectively. Both are much smaller than the bulk modulus. That is the material is much softer under shear and tensile loading than under hydrostatic compression. The very small elastic moduli indicate that β-LiBaAs is relatively less rigid and can be very elastic in the absence of mechanical failure. The Poisson's ratio of 0.40 implies that a large transverse strain response is

expected in the case of uniaxial loading. Values above about 0.33 are typical in materials with a large ionic contribution to chemical bonding, and lower values are more common in very directional covalent solids. So, the present result shows that the bonding in β-LiBaAs is mainly ionic and covalent hybridized, and it is a result of the electronic structure analysis with strong As-p and Ba-d interaction. The ductile or brittle nature of the material can be evaluated according to Pugh's criterion. The ratio of 4.72 B/G is much higher than 1.75, which indicates ductile behavior, and this is also supported by the large Poisson's ratio, which shows that β-LiBaAs is able to take a lot of plastic deformation before fracture. This mechanical behavior could be advantageous in crystal growth, thin film deposition, and device fabrication because ductile materials are less prone to catastrophic cracking. The Debye temperature is measured as 144.6 K, which is relatively low compared to many inorganic semiconductors. A low Debye temperature is associated with weaker interatomic bonding, lower average phonon frequencies, and softer lattice vibrations. This, in turn, is also consistent with the phonon dispersion calculated, in which the optical modes are relatively low in frequency due to the presence of the heavy Ba atom and the lighter Li atom. The low Debye temperature may also contribute to the thermal conductivity of the lattice to reduce phonon scattering. This could be useful in thermoelectric applications. The mechanical properties are closely related to the electronic structure. The relatively weak shear resistance is due to the moderate bonding strength around the conduction-band edge (Ba-d states dominate), while the mixed ionic-covalent bonding (PDOS) contributes to the large Poisson's ratio and ductile behavior. Moreover, the low Debye temperature obtained from the elastic constants is consistent with the phonon calculations, suggesting low-energy lattice vibrations and soft interatomic interactions.

3.5 Vibrational Properties

Phonon dispersion relations illustrate the relationship between vibrational frequencies and wave vectors, playing a crucial role in evaluating dynamic stability, thermal conductivity, phase transitions, and electron-phonon interactions. We employed PHONOPY to compute the phonon bands and phonon density of states (PDOS) utilizing a 2×2×2 supercell alongside Density Functional Perturbation Theory (DFPT). Each compound exhibits nine distinct phonon modes: three acoustic and three optical. For dynamical stability to be confirmed, it is essential that all phonon frequencies remain non-imaginary (positive) across the entirety of the Brillouin zone. The computed phononic dispersion curves along with projected PDOS for β-LiBaAs are illustrated in Fig. 5. The analysis was conducted along the high-symmetry path Γ-X-K-Γ-L-X-W-

L to evaluate the dynamic stability of the optimized crystal structure.As depicted in Fig. 5, every branch within this spectrum maintains positive frequencies throughout the full Brillouin zone without any occurrence of imaginary (negative) modes; their absence signifies that β-LiBaAs demonstrates dynamical stability under ambient pressure conditions—suggesting that this optimized crystal configuration represents a genuine minimum on its potential energy landscape. This finding aligns well with mechanical stability as determined by elastic constants. The range of observed phonons extends up to 5.5 THz and can be categorized into low-frequency, intermediate-frequency, and high-frequency sections. Notably, each of these three acoustic branches begins at zero frequency at point Γ indicating adherence to translational invariance requirements which affirms reliability in our calculations regarding phono dynamics. Additionally, distinctly defined optical branches exist above these acoustic modes due primarily to multi-atomic characteristics inherent within primitive unit cells.The projected phonon density of states gives us a view of the atomic origin of the vibrational modes. The low-frequency (below approximately 2 THz) part is dominated by Ba vibrations. Since barium has the largest atomic mass among the constituent atoms, the vibrational frequencies are shifted towards lower energies in terms of the inverse square root of the frequency of lattice vibration of the atoms. The intermediate frequency region (about 2–4 THz) is dominated by As and Li atoms, which means that these atoms have a larger role to play in lattice vibrations for the chemical bonds. The strongest optical modes (above approximately 4 THz) are dominated by Li vibrations, since the atomic mass of lithium is low, and so it can vibrate with a higher frequency than Ba and As, hence the high frequency peaks observed in the PDOS. The partial overlap in the Li, As, and Ba contributions in the intermediate frequency range indicates a vibrational coupling of the atoms. If the phonon-phonon interactions are efficient in the crystal lattice, the phonon scattering process can be more efficient and, therefore, the lattice thermal conductivity may be affected. The absence of a large phonon band gap between the acoustic and optical branches also indicates that acoustic and optical phonons are partly coupled. This coupling might improve the phonon-phonon scattering process, shorten the lifetimes of phonons, and decrease the thermal conductivity of the crystal lattice, which is favorable for thermoelectric applications when the electronic transport properties are preserved. Such vibrational properties are typical of semiconducting ternary compounds with heavy and light constituent elements in common.

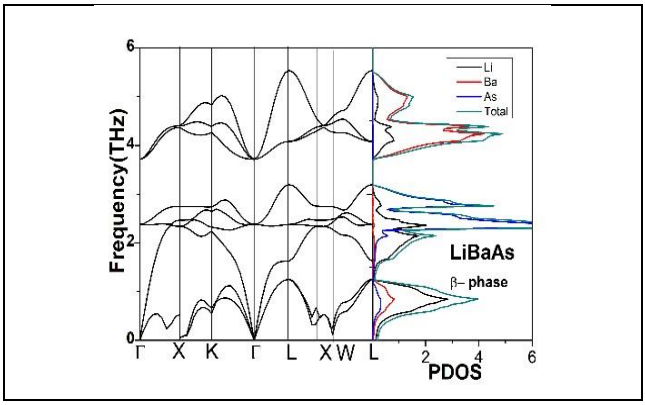


Figure 5. Phonon dispersion curves and phonon partial DOS for LiBaAs

3.6 Optical Properties

The optical characteristics of β-LiBaAs were evaluated through the complex dielectric function, refractive index, and extinction coefficient, as illustrated in Fig. 6. These optical attributes provide critical insights into how electromagnetic radiation interacts with the electronic structure of the material. The real component of the dielectric function $\varepsilon_1(\omega)$ characterizes the crystal's polarization when subjected to an external electromagnetic field. As depicted in Fig. 6(a), within the low energy spectrum, the static dielectric constant $\varepsilon_1(\omega)$ is notably elevated, suggesting significant electronic polarizability. This response diminishes as photon energy increases and turns negative over a specific energy interval. The observed negative values of ε_1 between 7 and 10 eV imply that β-LiBaAs functions as a metallic reflector in ultraviolet light conditions; during this phase, electromagnetic waves struggle to propagate effectively through the crystal due to polarization opposing that from an external electric field. However, at higher photon energies, there is a return to positive ε_1 values which indicates a restoration of typical dielectric behavior beyond plasma resonance effects.The imaginary part, $\varepsilon_2(\omega)$, is the light absorption caused by the inter-band electronic transitions. As shown in Fig. 6(b), β-LiBaAs exhibits strong absorption starting just above the band gap energy. The peak of absorption is in the 2-5 eV range, which corresponds to the transition from the occupied As-p states to the unoccupied Ba-d states in the electronic density of states. The second band of absorption is weaker in the range of 15-16 eV and is associated with the transition to deeper valence states. The agreement of the ε_2 spectrum with PDOS further suggests that the optical transitions are dominated by the As-p → Ba-d electronic excitations.

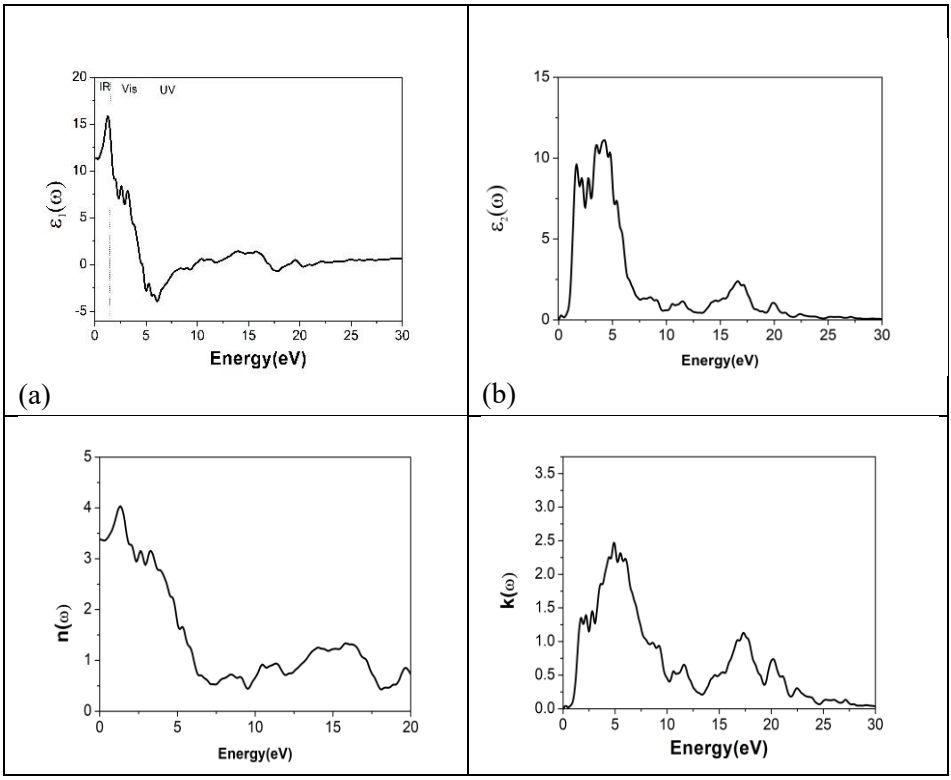


Figure 6. (a) Real and (b) Imaginen dielectric constans c) refractive index and (d) extinction coefficient

The refractive index is calculated in Fig. 6(c). The static refractive index is about 4, and it indicates a relatively high optical density. Such a large refractive index means that β-LiBaAs can effectively slow down the propagation of visible light and is attractive for photonic and optoelectronic applications. As the photon energy increases, the refractive index decreases continuously because of the normal optical dispersion. As the refractive index is very high for the visible and near UV regions, beyond 7-8 eV, it becomes close to unity, which indicates that the interaction between photons and crystal is progressively weaker at higher energies. The very high refractive index in the visible and near UV region is also in accordance with the moderate electronic band gap and large electronic polarizability as predicted from the dielectric function. The extinction coefficient is shown in Fig. 6(d), which describes the loss of electromagnetic waves inside the material. The extinction coefficient is very small in the low-energy region, indicating that β-LiBaAs is almost transparent to photons with energies below the onset of a significant interband transition. The maximum is observed between 3 and 5 eV, which is the strongest peak in $\varepsilon_2(\omega)$. This indicates that optical

absorption is dominated by electronic transition over the band gap. After that, the extinction coefficient decreases gradually, and a weak peak is found around 15-16 eV, which is the second absorption feature appearing in the dielectric spectrum. The excellent correspondence between the values of $\varepsilon_2(\omega)$ and $k(\omega)$ shows that both of them result from the same process of inter-band excitation. The optical spectra are in good agreement with the electronic structure of the previous work. The semiconducting band structure leads to very small optical absorption below the band gap energy, and the expected density of states indicates that the peak in the valence band is dominated by As-p orbitals and the minimum in the conduction band by Ba-d orbitals. Therefore, the dominant optical transitions are due to As-p → Ba-d excitations, which lead to high absorption peaks in the visible and UV regions. The large static dielectric constant and refractive index also indicate very high electronic polarization. The negative value of ε_1 in the UV region indicates plasma-like behavior and higher reflectivity. The reflectivity spectrum $R(\omega)$ and the electron energy loss function $L(\omega)$ of β-LiBaAs are illustrated in Fig. 7. These optical parameters yield critical insights into how electromagnetic radiation interacts with a crystalline material, thereby aiding in assessing its potential applications within the optical and optoelectronic domains. As depicted in Fig. 7(a), β-LiBaAs demonstrates moderate reflectivity across the examined photon energy range, with static reflectivity measured at approximately 30%. Specifically, over one-third of incident light is reflected off the crystal's surface at lower photon energies.

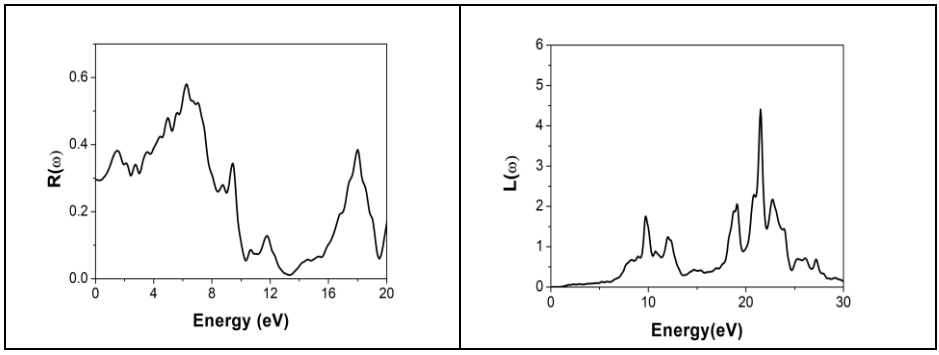


Figure 7 (a) Reflectivity spectrum and (b) energy loss functions for LiBaAs

With an increase in photon energy, there is a gradual rise in reflectivity that peaks between ~55-60% within the 5-7 eV range; this corresponds to significant optical transitions observed in the imaginary component of the dielectric function, indicating enhanced excitation levels among electronic states responsible for elevated reflectivity. Following this peak, there is a rapid decline

leading to minimum values around 11-13 eV due to diminished real part contributions from the dielectric function and redistribution effects on oscillator strength following primary interband transitions. A secondary broad maximum appears near 17-18 eV linked to higher-energy interband transitions involving deeper electronic states.Overall, throughout all investigated spectral ranges, total reflectivity remains below 60%, suggesting that β-LiBaAs does not behave as a highly reflective metallic substance but rather displays characteristic properties typical of semiconductor materials. The electron energy loss function is shown in Fig. 7(b) and represents the energy lost by fast electrons as they pass through the material. The spectrum has several weak loss peaks below 15 eV and a sharp and broad one around 20 eV. This dominant peak corresponds to the bulk plasma resonance (plasma frequency) where the collective oscillation of valence electrons occurs. At this energy, the real part of the dielectric function becomes zero while the imaginary part is still small, and the loss function is so strong that it is resonant. Beyond the plasma frequency, the intensity of the loss function decreases rapidly, and the collective electronic oscillations become weaker. The position of the principal loss peak is consistent with the energy region where the real part of the dielectric function changes sign and where the reflectivity begins to decrease significantly. This fact indicates the internal consistency of the calculated optical constants. The optical response of β-LiBaAs is closely related to the electronic band structure and density of states. The absence of electronic states at the Fermi level inhibits optical absorption at very low photon energies, while the strong interband transitions between As-p and Ba-d conduction states give rise to the strong reflectivity and dielectric properties of the ultraviolet region. The plasma resonance near 20 eV is due to the collective excitation of valence electrons and marks the transition from dielectric behavior to a regime in which electromagnetic waves are strongly screened by free-electron-like oscillations. Such behavior is more common in semiconductors with relatively high valence-electron densities. It is then obvious that the electronic band structure, density of states projected by our model, phonon dispersion, dielectric function, reflectivity, and energy loss function show that β-LiBaAs is a dynamically stable semiconductor characterized by strong dielectric properties (i.e., strong ultraviolet optical activity) and a plasma response that is well defined. These properties make β-LiBaAs a promising candidate in the field of optoelectronics, ultraviolet photonic, and dielectric coatings.

4. CONCLUSIONS

In this study, we investigated the structural, mechanical, electronic, vibrational, and optical characteristics of LiBaAs polymorphs through first-principles calculations. Our energy-volume analysis indicates that the β phase is the most energetically favorable polymorph among α, β, and γ phases. The stability hierarchy established is as follows: β > γ > α. Furthermore, the elastic constants examined in this research adhere to all Born criteria for mechanical stability; thus confirming that β-LiBaAs exhibits mechanical robustness. Its comparatively low elastic moduli imply that it behaves as a mechanically soft material with moderate hydrostatic compression resistance but limited shear deformation resilience. The high Pugh ratio (B/G = 4.72) alongside Poisson's ratio (0.40) reflects significant ductility properties; conversely, a lower Debye temperature (144.6 K) points toward weak lattice stiffness coupled with relatively modest phonon frequencies characteristic of its structure. Additionally, our evaluation of the electronic band structure reveals that β-LiBaAs functions as a semiconductor characterized by a narrow band gap. Analysis of projected density states indicates that As-p orbitals predominantly contribute to forming the valence-band edge while Ba-d states primarily influence conduction-band edges. Phonon dispersion curves reveal no imaginary frequencies across the Brillouin zone further affirming the remarkable stability of this phase; moreover,the phonon density states illustrate dominance by Ba atoms at low-frequency vibrations while As contributes significantly at intermediate frequencies and Li governs high-frequency optical modes. Calculated optical attributes show an appreciable static dielectric response combined with an elevated refractive index along with robust ultraviolet absorption capabilities and moderate reflectivity—featuring distinct plasma resonance observed at higher photon energies.The primary optical transitions correlate closely to electronic state distribution near band edges identified in our density-of-states analysis. The strong correlation between structural integrity and various physical properties substantiate both reliability in our first-principles computations and provide comprehensive insights intoβ-LiBaAs’s behavior under varied conditions.Hence,it emerges as an auspicious candidate for future applications within optoelectronics ,ultraviolet photonics,and semiconductor devices.Furthermore,this work lays down solid theoretical groundwork facilitating subsequent investigations on carrier transport mechanisms , thermoelectric performance evaluations ,pressure-dependent behaviors,and experimental synthesis endeavors centered around LiBaAs-based materials .

Acknowledgement: All calculations were performed at TÜBİTAK ULAKBİM, High Performance and Grid Computing Center (TRUBA resources).

REFERENCES

[1] Sztekler K, Wojciechowski K, Komorowski. The thermoelectric generators are used for waste heat utilization from a conventional power plant. Energy and Fuels. E3S Web of Conferences 2017;14(01032):1-8

[2] World Energy Resources. 2016; http://www.worldenergy.org/

[3]Kardasz P, Wróbel R, Doskocz J, Wiejkut P. The energy harvesting from waste heat. World Scientific News. 2016;48(133):53-68.

[4] Patowary R, and Baruah DC. International Journal of Energy Research. 2018;42(8), 2595-2614.

[5] Zhan T, Yamato R, Hashimoto S, Tomita M, Oba S, Himeda Y et al. Miniaturized planar Si-nanowire micro-thermoelectric generator using exuded thermal field for power generation. Science and Technology of Advanced Materials. 2018 Dec 31;19(1):443453.

[6] Venkatasubramanian R, Siivola E, Colpitts T, O'Quinn B. Thin-film thermoelectric devices with high room-temperature figures of merit. Nature. 2001;413(6856):597-602.

[7] Heremans JP, Jovovic V, Toberer ES, Saramat A, Kurosaki K, Charoenphakdee A, Yamanaka S, Snyder GJ. Enhancement of thermoelectric efficiency in PbTe by distortion of the electronic density of states. Science. 2008 Jul 25;321(5888):554-7.

[8] Gatti C, Bertini L, Blake NP, and Iversen BB. Chemistry. 2003;9(18): 4556–68.

[9] Yin Y, Tudu B, and Tiwari A. Recent advances in oxide thermoelectric materials and modules. Vacuum 2017;146:356–374.

[10] Rogl G, and Rogl P. Skutterudites, a most promising group of thermoelectric materials. Current Opinion in Green and Sustainable Chemistry. 2017;4:50–57.

[11] Huang L, Zhang Q, Yuan B, Lai X, Yan X, and Ren Z. Recent progress in half-Heusler thermoelectric materials. Materials Research Bulletin 2016;76:107–112

[12] He J, Naghavi S S, Hegde V I, Amsler M, and Wolverton C. Designing and Discovering a New Family of Semiconducting Quaternary Heusler Compounds Based on the 18-Electron Rule. Chemistry of Materials 2018;30(15), 4978–4985.

[13] Grytsiv A, Romaka V V, Watson N, Rogl G, Michor H, Hinterleitner B, Rogl P. Thermoelectric Half-Heusler compounds TaFeSb and Ta1-xTixFeSb ($0 \leq x \leq 0.11$): Formation and physical properties. Intermetallics 2019; 111: 106468. doi:10.1016/j.intermet.2019.04.011.

[14] Anand S, Xia K I, Hegde V, Aydemir U, Kocevski V, Zhu T, and Snyder G J. A valence balanced rule for the discovery of 18-electron half-Heuslers with defects. Energy and Environmental Science 2018;11(6): 1480–1488. doi:10.1039/c8ee00306h.
[15] 1. Offernes, L., Ravindran, P., Seim, C.W., Kjekshus, A.: Prediction of composition for stable half-Heusler phases from electronicband-structure analyses. J. Alloys Compd. **458**, 47–60 (2008)
[16] Ameri, M., Touia, A., Khenata, R., Al-Douri, Y., Baltache, H.: Structural and optoelectronic properties of NiTiX and CoVX (X = Sb and Sn) half-Heusler compounds: An ab initio study. Optik - Int. J. Light Electron Optics. **124**, 570–574 (2013)
[17] Safavi, M., Moradi, M., Rostami, M.: Structural, electronic and magnetic properties of NaKZ (Z = N, P, As, and Sb) half-Heusler compounds: a First-Principles study. J. Supercond. Novel Magn. **30**, 989–997 (2017)
[18] Mehmood, N., Ahmad, R.: Structural, electronic, magnetic and optical investigations of half-Heusler compounds YZSb (Z = Cr, Mn): FP-LAPW Method. J. Supercond. Novel Magn. **31**, 879–888 (2018)
[19] Shrivastava, D., Sanyal, S.P.: Theoretical study of structural, electronic, phonon and thermoelectric properties of KScX (X=Sn and Pb) and KYX (X=Si and Ge) half-Heusler compounds with 8 valence electrons count. J. Alloy. Compd. **784**, 319–329 (2019)
[20] Chami, N., Arbouche, O., Chibani, S., Driss Khodja, F.-Z., Amara, K., Ameri, M., Al-Douri, Y., Adjdir, M.: Computational prediction of structural, electronic, elastic, and thermoelectric properties of FeVX (X = As, P) half-Heusler compounds. J. Electron. Mater. **49**, 4916–4922 (2020)
[21] Surucu, G., Isik, M., Candan, A., Wang, X., Gullu, H.H.: Investigation of structural, electronic, magnetic and lattice dynamical properties for XCoBi (X: Ti, Zr, Hf) half-Heusler compounds. Physica B Phys. Condens. Matter. **587**, 412146 (2020)
[22] Shrivastava, D., Sanyal, S.P.: Structural phase transition, electronic and lattice dynamical properties of half-Heusler compound CaAuBi. J. Alloys Compd. **745**, 240–246 (2018)
[23] Nanda, B.R.K., Dasgupta, I.: Electronic structure and magnetism in half-Heusler compounds. J. Phys. Condens. Matter. **15**, 7307–7323 (2003)c
[24 Kresse, G., and J. Furthmüller. 1996. “Efficient Iterative Schemes for *Ab Initio* Total-Energy Calculations Using a Plane-Wave Basis Set.” *Physical Review B* 54(16): 11169–86.
[25] Perdew, John P., Kieron Burke, and Matthias Ernzerhof. 1996. “Generalized

Gradient Approximation Made Simple." *Physical Review Letters* 77(18): 3865–68.

[26] Togo, Atsushi, and Isao Tanaka. 2015. "First Principles Phonon Calculations in Materials Science." *Scripta Materialia* 108: 1–5.

[27] Page, Yvon Le, and Paul Saxe. 2002. "Symmetry-General Least-Squares Extraction of Elastic Data for Strained Materials from Ab Initio Calculations of Stress." 65: 1–14.

Chapter 26

Hydrogen Storage, Mechanic, Electronic, and Vibrtional Properties of Novel TI2XH4 (X=LI, SC, NI) Hydrides

Yasemin O. CIFTCI [1]

Abstract

We employed density functional theory (DFT) to explore the structural, mechanical, electronic, vibrational, and hydrogen-storage characteristics of Ti2XH4 (X = Li, Sc, Ni) hydrides. Phonon spectra and negative formation enthalpies indicate thermodynamic and dynamical stability for these hyrides. Electronic-structure results reveal metallic behaviour for Ti_2XH_4. The Born stability criteria are fulfilled, confirming mechanical stability. Additional elastic metrics, including Pugh's ratio, Poisson's ratio, and the Zener anisotropy factor, were evaluated to infer tendencies toward brittleness or ductility and isotropic versus anisotropic elastic response. Despite some indicators of ductility, Pugh's ratio and the Cauchy pressure point toward potential brittleness. For hydrogen storage, the computed gravimetric capacities (and estimated desorption temperatures) are: 3.78 wt% at 246.14 K, 3.22 wt% at 254.14 K, and 3.05 wt% at 267.09 K for Ti_2XH_4 with X = Li, Sc, and Ni, respectively. Therefore, Ti_2LiH_4 emerges as a promising candidate for moderate hydrogen storage at relatively low desorption temperatures. The results summarize the fundamental physical properties of the examined compounds and include recommendations for further study.

Keywords: DFT, Hydrogen storage, Perovskite, Mechanic, Phonon

[1] Department of Physics, Faculty of Science, Gazi University, 06500 Ankara, Turkey,
ORCID: 0000-0003-1796-0270

1. Introduction

Rapid population growth, deteriorating air quality, and the progressive depletion of conventional energy sources have intensified the need for cleaner, more efficient, and sustainable energy technologies. Rising energy demand and population pressures present urgent challenges for policymakers, governments, and researchers. Problems such as dwindling oil reserves, price volatility, and environmental damage associated with extraction and use require accelerated development and investment in alternative energy solutions. Hydrogen energy stands out as a viable, promising option: it can function as an energy carrier for stationary power plants, fuel cells, and portable devices [1]. Identifying efficient hydrogen-storage materials is fundamental for realizing a future low-carbon energy infrastructure. The increasing deployment of pure and hybrid electric vehicles offers a potential route to address these challenges, although their broader adoption depends on advances and cost reductions in battery technology. Nickel–metal hydride (NiMH) rechargeable batteries remain an important long-term storage technology for vehicles because of their tolerance to overcharge/overdischarge, high current capability, good energy density, long cycle life, and environmental advantages [2–5].

Hydrogen obtained from renewable sources has gained attention as a carbon-free carrier. While hydrogen may be stored as a gas, liquid, or solid, each form has trade-offs in cost, safety, pressure requirements, and energy density. Solid-surface adsorption and solid-state storage are preferred for safety, reliability, and capacity, especially for transport applications. For vehicular use, storage materials must be lightweight, possess high hydrogen density, and exhibit practical adsorption–desorption temperatures [6]. Metal hydrides, in particular, can reach hydrogen storage capacities in the range of 5–8 wt% [7], offering safe, controllable storage at low pressures and compact volumes [8]. Both simple and complex metal hydrides, valued for their high hydrogen densities and safety, have been extensively investigated in the context of material-based solid-state hydrogen storage. Nevertheless, the integration of hydrogen production, storage, and utilization technologies in vehicles remains an active research topic.

Atomic hydrogen accommodated in intermetallic compounds can achieve higher volumetric densities than molecular hydrogen. A practical hydrogen storage system based on metal hydrides (MH) requires two main attributes: rapid, reversible hydrogen exchange under moderate conditions, and low cost. Ti_2LiH_4 is a hydride species that can form by reacting Li with TiH_2 and holds promise for energy storage applications. Detailed studies probe structural and phase transitions in such compounds by tracking crystallographic changes during lithiation and varying hydrogen content. Lithiation profiles and X-ray diffraction

(XRD) data show structural evolution with lithium concentration and potential. For instance, a reduction in the fcc-$Ti_{0.3}V_{0.7}H_2$ phase at low potentials and the appearance of a bct-$Ti_{0.3}V_{0.7}Hz$ phase with variable hydrogen contents indicate a lithiation-driven phase change. During this process, the fcc lattice parameter remains essentially constant, whereas bct lattice parameters decrease notably with lithiation. Abrupt changes in the bct lattice parameter have been linked to the formation of two distinct hydride phases (β1 and β2) with different hydrogen stoichiometries in the V–H system. Reports indicate that, as lithiation proceeds, the tetragonal distortion in the BCC phase lessens and lattice metrics evolve toward the parent BCC $Ti_{0.3}V_{0.7}$ alloy and LiH; however, direct identification of LiH is hindered by low electron density of its components. Moreover, lithiation reactions in TiH_2 and related compounds often show limited reversibility—likely due to kinetic and interfacial constraints. Prior work indicates the initial lithiation of TiH_2 at room temperature leads to irreversible transformations, although reversibility can be partially restored by heating, using Ti–LiH composites, or embedding TiH_2 within nanostructured Mg/LiH matrices [9].

Progress in predicting and understanding low-hydrogen phases in the Ti–Li–H system, such as Ti2LiH4, has been driven by evolutionary crystal-structure prediction methods. The USPEX approach of Oganov et al. [10] pioneered automatic identification of stable phases under pressure via genetic evolution of random populations. The CALYPSO framework by Wang and Chen [11] offered a complementary search based on particle-swarm optimization and has been widely adopted, particularly for light-element hydrides. These approaches enabled systematic screening of the Li–Ti–H phase diagram under high pressure, predicting both high-hydrogen-content superhydrides and lower-stoichiometry phases (e.g., Ti_2LiH_4). Subsequent investigations assessed electronic properties and potential superconductivity—Liu et al., for instance, reported superconducting tendencies in Li_2TiH_{16} around 40 K at ~200 GPa due to intermediate-range electron–phonon coupling [12]. Comprehensive computational screening followed by detailed electronic and thermodynamic analyses suggests that low-hydrogen Ti_2LiH_4-like phases could be experimentally accessible. Thus, a structured research pipeline has emerged: computational structure prediction followed by in-depth property analyses.

Computational materials science provides three essential capabilities: atomistic understanding, predictive modeling, and consistent explanation of observed physical and chemical phenomena [13, 14]. The rise of computational power enables increasingly complex simulations and a detailed characterization of material properties through DFT. Thermodynamic properties follow from comparing energies of ideal and strained crystals, while vibrational and phonon

behaviors are obtained by evaluating forces on displaced atoms [15, 16]. This framework allows accurate, cost-effective assessment of candidate hydrogen-storage materials, covering structural, elastic, electronic, and vibrational properties, without immediate experimental expense. For example, Bortz et al. [17] synthesized Rb_2ZnH_4 and Cs_2ZnH_4 by reacting stoichiometric hydrides with zinc powder at elevated temperature and pressure, finding these compounds isotypic with K_2ZnH_4. Solid-state hydrogen storage is critical for net-zero systems because it can provide intrinsic retention and safety when thermodynamic and kinetic parameters are optimized to maximize volumetric and gravimetric densities. Complex metal hydrides stand out for tunable stability via coordination chemistry, cation/anion substitution, and lattice engineering. Within this class, $A_2T H_4$ (A = alkali metal, T = transition metal) compounds are notable because d^8 Pd(II)/Pt(II) centers stabilize square-planar $[TH_4]^{2-}$ units in ionic lattices. Na_2PtH_4 and related K- and Pd-analogs adopt tetragonal I4/mmm structures hosting essentially isolated planar $[PtH_4]^{2-}$/$[PdH_4]^{2-}$ complexes, as revealed by combined diffraction and electronic-structure studies; these prototypes serve as references for bonding, lattice dynamics, and de(hydrogenation) thermodynamics in complex hydrides [18–20].

Ahmed et al. [18] reported that Cs2CaH4 and Rb2CaH4 possess stable tetragonal lattices, favorable electronic properties, and competitive hydrogen capacities, making them promising practical candidates. Yamicier studied tetragonal X_2MgH_4 (X = K, Rb, Cs) via DFT and found all three satisfy Born stability criteria and show dynamical stability, with gravimetric capacities of 3.8 wt% (K_2MgH_4), 2.02 wt% (Rb_2MgH_4), and 1.37 wt% (Cs_2MgH_4). Rehman et al. examined X_2ZnH_4 (X = K, Rb, Cs) from first principles and found favorable structural, electronic, thermal, and mechanical properties, reporting capacities of 2.7 wt% (K_2ZnH_4), 1.6 wt% (Rb_2ZnH_4), and 1.2 wt% (Cs_2ZnH_4) [21]. Recently, Candan et al. [20] provided a comprehensive DFT study of K_2XH_4 (X = Mg, Ca), evaluating structural, thermodynamic, mechanical, electronic, optical, and vibrational aspects and finding gravimetric capacities of 3.80 wt% (K_2MgH_4) and 3.30 wt% (K_2CaH_4), with desorption temperatures of 207.87 K and 254.88 K, respectively.

Given the expense and scarcity of noble metals, it is natural to ask whether 3D analogues of these structures could present similar structural and electronic traits. Notably, Ti_2XH_4 (X = Li, Sc, Ni) has not been previously explored. Here, we systematically probe the ground-state structures (lattice parameters, elastic stability), electronic properties (band structure, bonding, PDOS), vibrational behavior (phonon dispersions, dynamical stability), and hydrogen-storage characteristics (formation/dissociation enthalpies and estimated desorption

temperatures under realistic chemical potentials) using VASP-based DFT simulations.

2.Method

We performed first-principles (ab initio) computations on Ti_2XH_4 (X = Li, Sc, Ni) to evaluate their structural, electronic, elastic, vibrational properties. The hydrides were modeled in a tetragonal phase with space group I4/mmm. All simulations used the VASP package [22] within the Generalized Gradient Approximation (GGA) using the Perdew–Burke–Ernzerhof (PBE) functional [23]. A plane-wave cutoff energy of 700 eV ensured total-energy convergence better than 10−8 eV. Valence configurations used were Ti($3d^3$ $4s^1$), Li($2s^1$ $2p^0$), Ni($3d^9$ $4s^1$), Sc($3d^2$ $4s^1$), and H($1s^1$) to achieve reliable electronic-property results. Phonon calculations employed a 2×2×2 supercell of Ti_2XH_4; force constants were extracted using VASP and the phonon dispersions were obtained via the PHONOPY package [24]. Elastic constants were computed using the stress–strain approach [25].

3. Results and Discussion

3.1. Structural Properties

Ti_2XH_4 (X = Li, Sc, Ni) adopt the tetragonal I4/mmm (No. 139) structure with Z = 2. As illustrated in Fig. 1, the unit cell places the X atoms at the (0, 0, 0) Wyckoff site, forming the structural backbone. Hydrogen occupies two inequivalent positions: H1 at (0.18, 0.18, 0) and H2 at (0.68, 0.31, 0.5). K atoms appear at (0.0, 0.5, 0.25). The lattice contains isolated square-planar $[XH_4]^{2-}$ units embedded in a matrix of Ti cations. The X(II) centers are d^8 and diamagnetic. Square-planar X–H bond lengths reported in the literature are typically around 1.6–1.7 Å [26]. To determine the ground-state geometry, we optimized atomic coordinates and unit-cell volumes for Ti_2XH_4 (X = Li, Sc, Ni) by minimizing residual forces. Total energies as a function of volume were fit to the Murnaghan equation of state to extract equilibrium lattice constants, bulk moduli, and the pressure derivative of the bulk modulus (B′), summarized in Table 1. As commonly observed with GGA, lattice parameters are slightly overestimated, reflecting a slight volume overestimation.

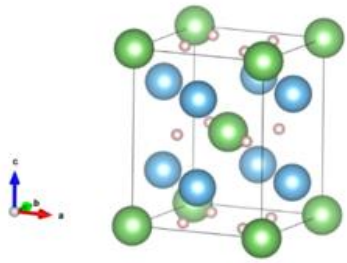


Figure 1. Unit cell of Ti_2XH_4 (X = Li, Sc, and Ni)

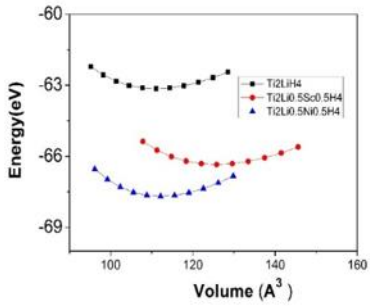


Figure 2. Energy-volume curves for Ti_2XH_4 (X = Li, Sc, and Ni)

The calculated lattice parameters for Ti2XH4 (X = Li, Sc, Ni) are consistent with available literature data. From the energy–volume curves (Fig. 2), the $Ti_2Li_{0.5}Ni_{0.5}H4$ composition exhibits the lowest total energy and is therefore thermodynamically preferred among the studied configurations. Table 1 lists B and B′ values: 111.007, 125.773, 112.138 GPa, and 3.89, 3.76, 4.03, respectively. The relatively small bulk modulus for Ti2LiH4 suggests it can be compressed more readily.

Table1. Structural parameters: lattice parameters (*a, c),* bulk modulüs (*B*), pressure derivatives of the bulk modulus ($B^{'}$), and formation enthalpies (ΔE_f) for Ti_2XH_4 (X = Li, Sc, and Ni) and other literature values

Materials	Reference	a=b (Å)	c (Å)	Vol Å^3	B (GPa)	$B^{'}$	Ef(ev/atom)
Ti_2LiH_4	This study	4.441	5.631	111.007	103.479	3.898	-0.334
$Ti_2Li_{0.5}Sc_{0.5}H_4$	This study	4.774	5.518	125.773	95.492	3.767	-0.344
$Ti_2Li_{0.5}Sc_{0.5}H_4$	This study	4.415	5.754	112.138	125.040	4.03	-0.362

3.2 Hydrogen Storage Properties

To assess the hydrogen-storage potential of Ti_2XH_4, we calculated gravimetric capacities (Cwt, %) using the standard relation [26], with results presented in Table 2:

$$C_{wt\%} = \left(\frac{(\frac{H}{M})M_H}{M_{Host}+(\frac{H}{M})M_H} x100 \right)\% \qquad (2)$$

$D_v = ym_{H2}/V_{tot}$

Here m_H denotes the molar mass of hydrogen and m_{Host} is the molar mass of the host compound; H/M gives the hydrogen-to-metal atom ratio. The gravimetric hydrogen capacities for Ti_2XH_4 (X = Li, Sc, Ni) are 3.78%, 3.22%, and 3.05%, respectively. Given their comparable average Cwt% values, these hydrides merit consideration as hydrogen-storage candidates. Although they do not yet meet the U.S. DOE 2025 ultimate gravimetric target of 5.5 wt% [27], they are within the promising range for lightweight solid-state hydrides. Among the series, pristine Ti_2LiH_4 displays the highest gravimetric capacity (3.78 wt%), the largest volumetric hydrogen density (60.359 g H_2/L), and the lowest desorption temperature (246.14 K). Partial replacement of Li by Sc or Ni lowers gravimetric capacity to 3.22 and 3.05 wt%, respectively, primarily because heavier Sc and Ni atoms raise the host molar mass without changing hydrogen content.

Table 2. The gravimetric (C_{wt})and volumetric (ρ_{vol}) hydrogen storage capacities, and desorption temperatures (T_{des}) for Ti_2XH_4 (X = Li, Sc, and Ni) hydrides

Material	C_{wt}(%)	$\rho_{vol\ (g.H2/L)}$	T_{des} (K)	References
Ti_2LiH_4	3.78	60.359	246.14	This work
$Ti_2Li_{0.5}Sc_{0.5}H_4$	3.22	53.263	254.14	This work
$Ti_2Li_{0.5}Ni_{0.5}H_4$	3.05	59.733	267.091	This work

Volumetric hydrogen storage capacity (ρ_{vol}) expresses how much hydrogen a material can store per unit volume and is defined by the following general formula [29]:

$$\rho_{vol} = \left(\frac{NH\ M_H}{VL\ NA} \right) \qquad (3)$$

where NH is the number of absorbed hydrogen atoms, m_H the hydrogen molar mass, V (L) the total absorbed hydrogen volume, and NA Avogadro's number. Table 2 shows that Sc substitution significantly reduces volumetric hydrogen density to 53.263 g H_2/L, while Ni substitution yields 59.733 g H_2/L, close to the

pristine Ti_2LiH_4 value. Consequently, $Ti_2Li_{0.5}Ni_{0.5}H_4$ offers superior volumetric performance compared with the Sc-substituted system, despite its lower gravimetric capacity. All computed volumetric values exceed the DOE 2025 target of 40 g H_2/L, supporting these materials' potential for practical hydrogen storage.

Beyond gravimetric capacity, desorption temperature (T_{des}) is crucial for application relevance. Thermodynamic behavior can be described via the Gibbs free energy:

$$\Delta G = \Delta H - T\mathrm{des} \,.\, \Delta S \tag{4}$$

where ΔG is Gibbs free energy, ΔH the formation enthalpy, and ΔS the entropy change; for hydrogen ΔS(H2) ≈ 130.7 J mol^{-1} K^{-1} [29]. The desorption temperature corresponds to ΔG = 0 and can be estimated as [30]:

$$T\mathrm{des} = -\Delta H_f / \Delta S \tag{5}$$

Using this relation, Tdes increases from 246.14 K (Ti_2LiH_4) to 254.14 K ($Ti_2Li_{0.5}Sc_{0.5}H_4$) and 267.091 K ($Ti_2Li_{0.5}Ni_{0.5}H_4$), all within the favorable 233–333 K operating window for practical storage [31]. The rise in desorption temperature upon substitution signals increased hydride thermodynamic stability, with Ni producing the strongest stabilization. Therefore, Ti_2LiH_4 favors hydrogen release at lower temperatures, while $Ti_2Li_{0.5}Ni_{0.5}H_4$ offers a balance between volumetric capacity and enhanced stability.

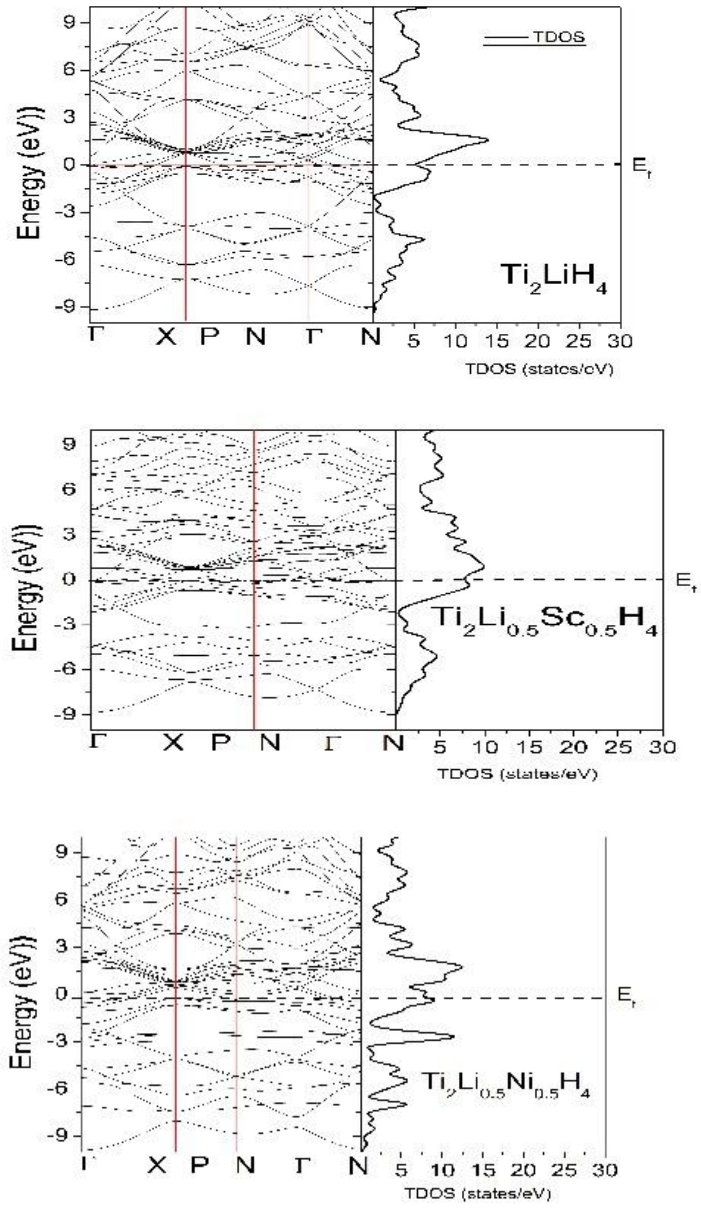
3.3 Electronic Properties

We computed electronic band structures and density of states (DOS) for Ti_2XH_4 (X = Li, Sc, Ni) along high-symmetry paths Γ–X–P–N–Γ–N in the Brillouin zone. Band structures and total DOS (TDOS) were plotted with the Fermi level (EF) set to 0 eV. Orbital-resolved contributions above and below EF were analyzed via projected DOS (PDOS). The calculated band diagrams are shown in Figure 3.

In all three hydrides, several bands cross the Fermi level and the TDOS is finite at E_F, signaling metallic behavior. Pristine Ti_2LiH_4 shows relatively dispersive bands near EF and a moderate DOS. Partial Sc substitution preserves the metallic nature but slightly alters band dispersion and reduces TDOS around EF, suggesting Sc reduces electronic states contributing at the Fermi level and may lower electrical conductivity. In contrast, $Ti_2Li_{0.5}Ni_{0.5}H_4$ exhibits more flat bands near E_F and distinct TDOS peaks due to localized Ni 3d states, indicating

stronger d-state contributions and enhanced orbital hybridization; consequently, its conductivity and electronic localization are increased relative to the Sc-substituted compound.

Overall, substituting Li with transition-metal species does not change the metallic character of Ti_2LiH_4 but modifies the electronic structure near E_F: Sc slightly suppresses the DOS at E_F, whereas Ni enhances localized d-state contributions, consistent with the observed rise in desorption temperature, implying stronger metal–hydrogen interactions and improved thermodynamic stability for the Ni-substituted material.



©

Figure 3. Electronic band structures and total DOS for Ti_2XH_4 (X = Li, Sc, and Ni) hydrides

The DOS, representing available electronic states across energy, strongly influences electrical and optical properties. TDOS and atom/ orbital-resolved PDOS for Ti_2XH_4 (X = Li, Sc, Ni) are presented with EF marked by a dashed line. Figure 4 shows TDOS and PDOS for Ti_2LiH_4, $Ti_2Li_{0.5}Sc_{0.5}H_4$, and $Ti_2Li_{0.5}Ni_{0.5}H_4$. In every case, TDOS is finite at E_F, confirming metallicity consistent with the bands. For pristine Ti_2LiH_4, states near EF are dominated by Ti-3d orbitals; Li and H contribute negligibly around EF. Hydrogen 1s states appear mainly between −7 and −3 eV, reflecting strong Ti–H bonding well below E_F.

With partial Sc substitution, the electronic structure remains metallic and Ti-3d contributions continue to dominate near E_F; Sc-3d participation is minor. The TDOS near E_F is slightly reduced and broadened, indicating Sc redistributes Ti-derived states without eliminating metallic character. Ni substitution modifies the electronic structure more substantially: Ni-3d states occur mainly below EF and hybridize strongly with Ti-3d in the valence region, shifting d-electron states to lower energies and lowering TDOS at E_F relative to pristine Ti_2LiH_4. This stronger Ti–Ni hybridization correlates with increased hydride stability and higher desorption temperature observed for $Ti_2Li_{0.5}Ni_{0.5}H_4$.

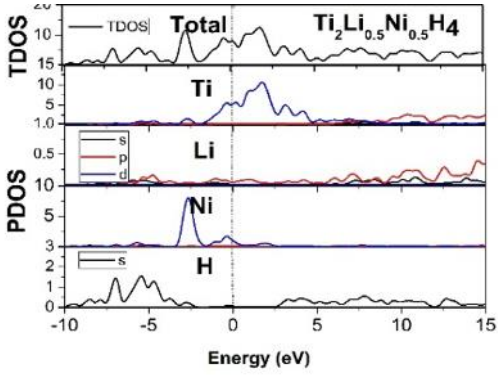


Figure 4. Total and partial density of states for Ti_2XH_4 (X = Li, Sc, and Ni) hydrides

3.4 Elastic Properties

Elastic constants govern mechanical stability and inform on stiffness, brittleness versus ductility, bonding character, and anisotropy. In a tetragonal crystal there are six independent elastic constants: C_{11}, C_{33}, C_{44}, C_{66}, C_{12}, and C_{13}. Table 3 compiles the computed Cij values for Ti_2XH4 (X = Li, Sc, Ni) to assess mechanical stability and bonding.

The Born stability criteria for tetragonal crystals require:

$$C_{11} > 0 , C_{33} > 0, C_{44} > 0, C_{66} > 0$$
$$C_{11}-C_{12}>0, (C_{11}+C_{33}-2C_{13})>0 \quad (6)$$
$$(2C_{11}+C_{33}+2C_{12}+4C_{13})>0$$

All independent elastic constants are positive, and the compounds satisfy Born's conditions, confirming mechanical stability under small elastic deformations. For Ti_2LiH_4, C_{11}, C_{33}, C_{44}, and C_{66} are 165.3, 249.0, 42.4, and 46.1 GPa, respectively. The much larger C_{33} relative to C_{11} indicates greater resistance to uniaxial compression along c versus a. The shear modulus (G) and Young's modulus (E) are 52.2 and 133.0 GPa, respectively, indicating moderate rigidity. The B/G ratio of 1.88 slightly exceeds Pugh's critical value of 1.75, implying moderately ductile behavior.

Poisson's ratio ν provides insight into bond directionality and the relative importance of central forces; systems with higher ionic character tend to show larger ν. Typical ranges are ν ≈ 0.10–0.25 for covalent-dominated systems and ν ≈ 0.25–0.50 for ionic or central-force-dominated materials [38]. The computed ν ≈ 0.27–0.28 here indicates mixed ionic–covalent bonding typical of complex hydrides; ν = 0.27 also supports intermediate bonding and some ductility.Li → Sc substitution reduces C_{11} and C_{33} to 150.8 and 183.4 GPa, respectively, lowering axial-compression resistance, while C_{44} rises from 42.4 to 59.4 GPa—indicating increased shear resistance for that mode. C_{66} drops to 24.1 GPa, revealing marked shear anisotropy. $Ti_2Li_{0.5}Sc_{0.5}H_4$ shows the highest isotropic-averaged shear modulus and Young's modulus (56.5 and 139.2 GPa), making it the stiffest among the trio. However, its B/G = 1.53 and ν = 0.23 indicate a shift toward brittleness relative to the pristine compound.

Ni substitution yields a different mechanical trend. $Ti_2Li_{0.5}Ni_{0.5}H_4$ has C_{11} = 162.7 GPa and C_{33} = 224.0 GPa—lower than pristine but higher than the Sc-substituted variant. Larger C_{12} = 77.6 GPa and C_{13} = 80.8 GPa values indicate stronger coupling of normal strains along distinct crystallographic directions. Its shear modulus and Young's modulus drop to 42.4 and 113.1 GPa, respectively, indicating a softer lattice that can accommodate deformation more readily. The B/G ratio increases substantially to 2.66, and Poisson's ratio rises to 0.33, both signifying a marked gain in ductility. Therefore, Sc substitution yields the stiffest yet most brittle compound, whereas Ni substitution softens the material and enhances ductility, an advantageous trait for hydrogen-storage cycling, where repeated absorption/desorption induces internal stress, volume change, and potential microcracking.

Table 3 Elastic properties for Ti_2XH_4 (X = Li, Sc, and Ni) hydrides

Materials	C_{11} (GPa)	C_{12} (GPa)	C_{44} (GPa)	C_{33} (GPa)	C_{13} (GPa)	C_{66} (GPa)	G (GPa)	E (GPa)	v	B/G
Ti_2LiH_4	165.3	39.4	42.4	249.0	63.2	46.1	52.2	133.0	0.27	1.88
$Ti_2Li_{0.5}Sc_{0.5}H_4$	150.8	28.9	59.4	183.4	63.2	24.1	56.5	139.2	0.23	1.53
$Ti_2Li_{0.5}Ni_{.5}H_4$	162.7	77.6	46.3	224.0	80.8	25.2	42.4	113.1	0.33	2.66

We next estimate mean sound velocities to derive the Debye temperature θ_D [32]. The Debye temperature depends on Planck's constant (h), Boltzmann's constant (kB), the number of atoms per cell (n), Avogadro's number (NA), molecular mass (M), density (ρ), and the average isotropic sound velocity (Vm), where Vm is given by:

$$\theta_D = \frac{h}{k_B}\left[\frac{3n}{4\pi}\left(\frac{N_A\rho}{M}\right)\right]^{1/3} V_m \tag{7}$$

$$V_m = \left[\frac{1}{3}\left(\frac{1}{V_l^3} + \frac{2}{V_t^3}\right)\right]^{-1/3} \tag{8}$$

Here, the longitudinal V_l and transverse V_t sound velocities can be obtained as follows.

$$V_l = \sqrt{\frac{3B+4G}{3\rho}} \tag{9}$$

$$V_t = \sqrt{\frac{G}{\rho}} \tag{10}$$

Calculated θ_D, v_l, v_t, and v_m results are reported in Table 4. The longitudinal, transverse, and average sound velocities reflect elastic-wave propagation and lattice stiffness. Pristine Ti_2LiH_4 has the largest longitudinal velocity (v_l = 7552 m/s) and a high average velocity (v_m = 4501 m/s), consistent with a relatively stiff lattice. Sc substitution modestly alters lattice dynamics: vl decreases slightly while vt and v_m increase to 4126 m/s and 4571 m/s, matching the elevated shear modulus for $Ti_2Li_{0.5}Sc_{0.5}H_4$. Ni substitution lowers vl, vt, and v_m to 6570, 3287, and 3687 m/s, respectively, signaling a softer lattice and reduced phonon velocities.

Debye temperature θ_D correlates with bonding strength and characteristic phonon frequencies; higher θ_D implies stronger interatomic forces and stiffer lattices. Table 4 shows θ_D = 671.8 K for Ti_2LiH_4 (highest), θ_D = 654.5 K for $Ti_2Li_{0.5}Sc_{0.5}H_4$ (slight reduction), and θ_D = 548.5 K for $Ti_2Li_{0.5}Ni_{0.5}H_4$ (notable decrease), reflecting progressively softer lattice dynamics with Ni substitution.

A rough estimate of melting temperature Tm for hexagonal and tetragonal structures uses $C_{ii} = (2C_{11} + C_{33})/3$ and the empirical relation of Fine et al. [33]:

$$T_m = 354 + 4.5\ C_{ii} \quad (11)$$

Table 4 presents the estimated melting temperatures (T_m) for the Ti_2XH_4 compounds. As shown in Table 4, Ti_2LiH_4 exhibits the highest melting point at 1223.4 K, reflecting strong thermal stability. Substituting part of the composition with Sc lowers the melting temperature to 1081.5 K, indicating a slight reduction in thermal stability. Although the Debye temperature decreases, the melting temperature remains relatively high at 1178.1 K. This suggests that Ni substitution significantly diminishes phonon transport without greatly compromising the crystal's overall thermal stability.

Table 4. Debye temperature (θ_D), Melting temperature (T_m), Sound velocities (m/s), *(Vm, V_l, V_t)* , and lattice thermal conductivity (Kl) for K2XH4 (X=Ni, Pt, Pd)

	v_l	v_t	v_m	θ_D (K)	K_l(at 300K) W/mK	T_m(K)
Ti_2LiH_4	7552	4042	4501	671.8	21.16	1223.4
$Ti_2Li_{0.5}Sc_{0.5}H_4$	6987	4126	4571	654.5	24.05	1081.5
$Ti_2Li_{0.5}Ni_{.5}H_4$	6570	3287	3687	548.5	9.339	1178.1

Thermal conductivity K_l reflects heat transport efficiency. For acoustic-phonon-dominated heat conduction, the Slack model can estimate lattice thermal conductivity. The Grüneisen parameter γ can be approximated from Poisson's ratio ν [34]:

$$\gamma = \frac{3(1+\nu)}{2(2-3\nu)}. \quad (12)$$

The Slack equation [35] gives the lattice thermal conductivity as below:

$$\kappa_l = A\frac{\bar{M}\theta_D^3\delta}{\gamma^2 Tn^{2/3}}, \tag{13}$$

The average atomic weight is denoted by M, and absolute temperature by T. Concurrently, θ_D denotes the Debye temperature, and for the unit cell, δ signifies the cube root of the mean volume per atom, and n is the number of atoms. The definition of A as a coefficient as a function of γ [36] is given by the following equation,

$$A(\gamma) = \frac{5.720x0.849x10^7}{\left[1-\left(\frac{0.514}{\gamma}\right)+\left(\frac{0.228}{\gamma^2}\right)\right]}. \tag{14}$$

Low thermal conductivity is generally associated with reduced phonon group velocities and enhanced phonon–phonon scattering processes. In complex hydrides such as Ti_2XH_4, this behavior can be attributed to several factors, including the presence of heavy transition-metal atoms, mass fluctuations among different atomic species, and a complex crystal structure that enhances anharmonic lattice vibrations. The calculated lattice thermal conductivities at 300 K are 21.16, 24.05, and 9.339 W/mK for Ti_2LiH_4, $Ti_2Li_{0.5}Sc_{0.5}H4$, and $Ti_2Li_{0.5}Ni_{0.5}H_4$, respectively. The results reveal that partial substitution of Li by Sc slightly enhances the lattice thermal conductivity, whereas Ni substitution causes a substantial suppression of phonon-mediated heat transport.

Pristine Ti_2LiH_4 exhibits a relatively high lattice thermal conductivity of 21.16 W/mK. This behavior is consistent with its high longitudinal and average sound velocities and its large Debye temperature of 671.8 K. These parameters indicate a relatively stiff lattice, strong interatomic interactions, and efficient propagation of acoustic phonons. For $Ti_2Li_{0.5}Sc_{0.5}H4$, the lattice thermal conductivity increases to 24.05 W /mK, corresponding to an enhancement of approximately 13.7% relative to pristine Ti_2LiH_4. Although the Debye temperature decreases slightly to 654.5 K, the transverse and average sound velocities increase to 4126 and 4571 m /s, respectively. The increased average phonon propagation velocity, together with the relatively large shear modulus, appears to compensate for the moderate reduction in Debye temperature and results in more efficient lattice heat transport. In contrast, $Ti_2Li_{0.5}Ni_{0.5}H_4$ exhibits a markedly lower lattice thermal conductivity of 9.339 W /mK. This value is approximately 55.9% lower than that of pristine Ti_2LiH_4 and 61.2% lower than that of the Sc-substituted compound. The strong reduction is consistent with the decreases in longitudinal, transverse, and average sound velocities and with

the substantially lower Debye temperature of 548.5 K. These results indicate a softer lattice and reduced phonon group velocities.

The pronounced suppression of κ_L in the Ni-substituted compound can also be associated with enhanced phonon scattering caused by mass fluctuation and local structural distortion. The large atomic-mass contrast between Li and Ni introduces mass disorder, while changes in local bonding and force constants may further shorten the phonon mean free path. Consequently, both reduced phonon velocities and enhanced phonon scattering contribute to the low lattice thermal conductivity of $Ti_2Li_{0.5}Ni_{0.5}H_4$.

3.5 Vibrational Properties

Phonon dispersion relations describe how vibrational frequencies vary with wavevector and are central to assessing dynamical stability, thermal transport, phase transitions, and electron–phonon coupling. We calculated phonon bands and phonon densities of states (PDOS) using PHONOPY in a 2×2×2 supercell with DFPT. With 14 atoms per unit cell, each compound has 42 phonon modes: 3 acoustic and 39 optical. Dynamical stability requires non-imaginary (positive) phonon frequencies throughout the Brillouin zone.

Figure 5 shows phonon dispersions and atom-projected PDOS for Ti_2LiH_4, $Ti_2Li_{0.5}Sc_{0.5}H_4$, and $Ti_2Li_{0.5}Ni_{0.5}H_4$. No imaginary frequencies are present in any case, confirming dynamical stability at ambient pressure and that optimized structures correspond to stable minima. For Ti_2LiH_4, acoustic branches occupy the low-frequency region (below ≈8–10 THz) and are dominated by Ti vibrations due to its larger mass. Mid-frequency optical modes stem from coupled Ti–Li motion, while the highest-frequency optical branches are H-derived, concentrated above ≈20 THz—reflecting hydrogen's low mass and strong Ti–H bonding.

Sc substitution slightly modifies the phonon spectrum: intermediate optical bands become somewhat more dispersed and Sc-related PDOS appears mainly between ≈5 and 20 THz, overlapping Ti vibrations and indicating Ti–Sc coupling. H-dominated high-frequency modes remain nearly unchanged, suggesting Sc weakly perturbs Ti–H interactions. Ni substitution produces more notable changes: Ni-related phonon states populate the low- and mid-frequency ranges and hybridize strongly with Ti vibrations, increasing the PDOS below ≈20 THz and broadening optical bands. Yet, high-frequency H modes persist, indicating that hydrogen vibrations are largely preserved despite transition-metal substitution.

These phonon trends dovetail with thermal-transport findings: $Ti_2Li_{0.5}Sc_{0.5}H_4$ shows the highest K_l (24.05 W m^{-1} K^{-1}) consistent with robust acoustic branches, while $Ti_2Li_{0.5}Ni_{0.5}H_4$ exhibits the lowest K_l (9.339 W m^{-1} K^{-1}) due to increased low-frequency phonon scattering from Ni-induced hybridization and mass disorder that

reduces phonon mean free paths. Overall, transition-metal substitution preserves dynamical stability but substantially reshapes lattice vibrations: Sc leads to moderate phonon-spectrum changes while maintaining efficient acoustic propagation; Ni enhances low-frequency hybridization and phonon scattering, diminishing lattice thermal conductivity.

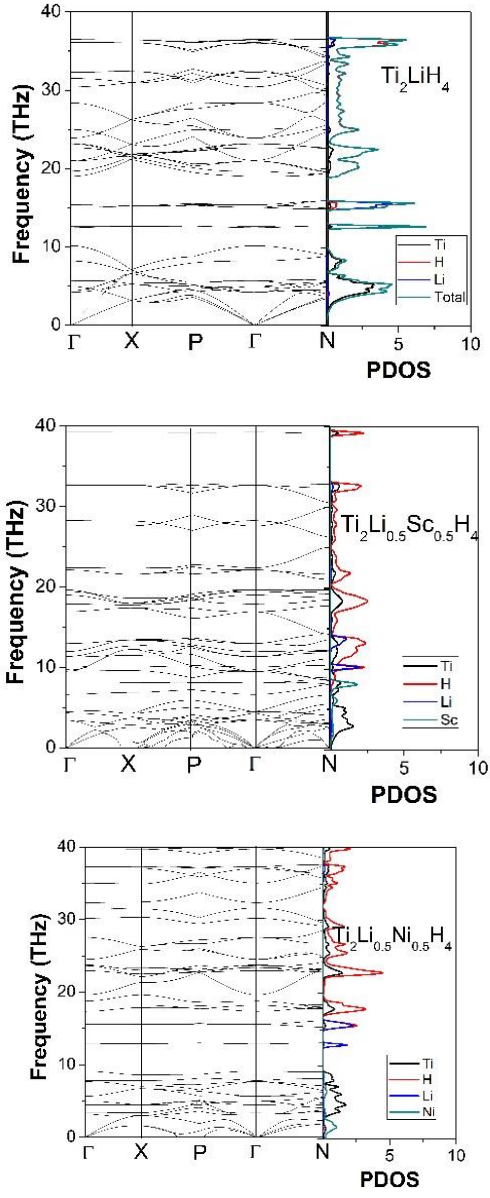


Figure 5. Phonon dispersion curves and phonon partial DOS for Ti_2XH_4 (X = Li, Sc, and Ni) hydrides

4. Conlusions

We performed an in-depth DFT study of structural, electronic, elastic, vibrational, and hydrogen-storage properties for Ti_2XH_4 (X = Li, Sc, Ni) hydrides. Phonon dispersions show no imaginary modes, confirming dynamical stability, while negative formation enthalpies indicate thermodynamic favorability. Electronic-structure calculations classify these materials as metallic with no band gaps; transition-metal substitution substantially alters the electronic states near the Fermi level. Computed elastic constants satisfy Born stability conditions, demonstrating mechanical stability. Mechanical descriptors, Pugh's ratio, Poisson's ratio, Cauchy pressure, and Zener anisotropy factor, suggest a tendency toward brittle mechanical behavior with moderate elastic anisotropy in some compositions. Hydrogen-storage analysis reveals that pristine Ti_2LiH_4 has the highest gravimetric capacity (3.78 wt%), the largest volumetric hydrogen density (60.359 g H_2 L^{-1}), and the lowest desorption temperature (246.14 K), making it the most promising for low-temperature hydrogen release. Substituting Li with Sc or Ni reduces gravimetric capacity due to increased molar mass, while increasing desorption temperatures to 254.14 K and 267.09 K, respectively, indicating greater hydride thermodynamic stability. Sc substitution reduces volumetric hydrogen density substantially, whereas $Ti_2Li_{0.5}Ni_{0.5}H_4$ maintains volumetric capacity close to the pristine compound and gains considerable mechanical ductility and thermodynamic stabilization. In summary, this work elucidates key physical properties of Ti_2XH_4 hydrides and demonstrates that transition-metal alloying is an effective strategy for tuning hydrogen storage, thermal, and mechanical performance. The contrasting roles of Sc and Ni substitutions illustrate how alloying can balance hydrogen capacity, thermal management, and structural reliability, offering guidance for designing Ti-based complex hydrides for next-generation solid-state hydrogen storage.

Acknowledgement:

All numerical calculations in this study were performed at the TÜBİTAK ULAKBİM, High Performance and Grid Computing Center (TRUBA resources).

REFERENCES

[1] Al, Selgin, Cihan Kurkcu, and Cagatay Yamcicier. 2020. "High Pressure Phase Transitions and Physical Properties of Li2MgH4; Implications for Hydrogen Storage." *International Journal of Hydrogen Energy* 45(7): 4720–30. https://doi.org/10.1016/j.ijhydene.2019.12.005.

[2] Ovshinsky, S R, M A Fetcenko, and J Ross. 1993. "Published by : American Association for the Advancement of Science A Nickel Metal Hydride Battery for Electric Vehicles." *Science* 260(5105): 176–81.

[3] Liu, L. 2010. "Introduction to the Welding and Joining of Magnesium." *Welding and Joining of Magnesium Alloys*: 3–8.

[4] Liu, Yongfeng, Hongge Pan, Mingxia Gao, and Qidong Wang. 2011. "Advanced Hydrogen Storage Alloys for Ni/MH Rechargeable Batteries." *Journal of Materials Chemistry* 21(13): 4743–55.

[5] Cao, Zhijie et al. 2015. "Enhanced Discharge Capacity and Cycling Properties in High-Samarium, Praseodymium/Neodymium-Free, and Low-Cobalt A2B7 Electrode Materials for Nickel-Metal Hydride Battery." *International Journal of Hydrogen Energy* 40(1): 451–55. http://dx.doi.org/10.1016/j.ijhydene.2014.11.016.

[6] Møller, Kasper T. et al. 2017. "Complex Metal Hydrides for Hydrogen, Thermal and Electrochemical Energy Storage." *Energies* 10(10).

[7] Bronger, Welf, and Gudrun Auffermann. 1998. "New Ternary Alkali-Metal-Transition-Metal Hydrides Synthesized at High Pressures: Characterization and Properties." *Chemistry of Materials* 10(10): 2723–32.

[8] Schlapbach, Louis, and Andreas Züttel. 2001. "For Mobile Applications." *Nature* 414(November): 353–58.

[9] F. Cuevas, B. Laïk, J. Zhang, M. Mateos, J.-P. Pereira-Ramos ve M. Michel, "Mechanochemical synthesis of pseudobinary Ti-V hydrides and their conversion reaction with Li and Na," cond-mat.mtrl-sci, https://arxiv.org/abs/2211.01550

[10] H. Ohno, S. Aoki, S. Ejiri, K. Kanaya, Y. Maezawa, H. Saito, T. Umeda ve WHOT-QCD Collaboration, "Charmonium spectral functions with the variational method in zero and finite temperature lattice QCD," hep-lat, https://arxiv.org/abs/1104.3384

[11] F. Ferrari, "Emergent Space and the Example of AdS_5XS^5," hep-th, arXiv:1207.0886, 2012. https://arxiv.org/abs/1207.0886

[12] B. Ali, H. Xu, D. Chetty, R. T. Sang, I. V. Litvinyuk ve M. Rybachuk, "Laser-Induced Graphitisation of Diamond Under 30 fs Laser Pulse Irradiation," physics.chem-ph, cond-mat.mtrl-sci, physics.app-ph, arXiv:2203.15505, 2022. https://arxiv.org/abs/2203.15505

[13] Zhao, Chenyang, Chi Fai Cheung, and Peng Xu. 2020. "High-Efficiency Sub-Microscale Uncertainty Measurement Method Using Pattern Recognition." *ISA Transactions* 101: 503–14. https://doi.org/10.1016/j.isatra.2020.01.038.

[14] Yang, Ming et al. 2023. "Binocular Vision-Based Method Used for Determining the Static and Dynamic Parameters of the Long-Stroke Shakers in Low-Frequency Vibration Calibration." *IEEE Transactions on Industrial Electronics* 70(8): 8537–45.

[15] Jia, Li-Chuan et al. 2023. "Self-Standing Boron Nitride Bulks Enabled by Liquid Metals for Thermal Management." *Mater. Horiz.* 10(12): 5656–65. http://dx.doi.org/10.1039/D3MH01359F.

[16] Kuang, Wangwang et al. 2018. "Application of the Thermodynamic Extremal Principle to Diffusion-Controlled Phase Transformations in Fe-C-X Alloys: Modeling and Applications." *Acta Materialia* 159: 16–30. http://dx.doi.org/10.1016/j.actamat.2018.08.008.

[17] Bortz, M, A Hewat, and K Yvon. 1997. "Synthesis and Structure Determination of Complex Zinc Hydrides." *Journal of Alloys and Compounds* 253–254(Ii): 13–16.

[18] B. Ahmed, M.B. Tahir, A. Dahshan, M. Sagir, Advanced computational screening of X2CaH4 (X =Rb and Cs) for hydrogen storage applications, Int. J. Hydrogen Energy 89 (2024) 48–55, https://doi.org/10.1016/j.ijhydene.2024.09.321.

[19] Ç. Yamçıçıer, Exploring the structural, elastic, phonon, optoelectronics, and thermoelectric properties of tetragonal complex metal hydride X2MgH4 (X =K, Rb, and Cs) compounds for hydrogen storage applications, Int. J. Hydrogen Energy 48 (2023) 39930–39943, https://doi.org/10.1016/j.

[20] Candan A, Akbudak S, 2026, First- principles study of K2XH4(X= Mg, Ca) hydrides: structural, mechanical, optoelectronic aspects for hydrogen storage applications, Vacuum, 243, (2026) 114841.

[21] Rehman, Hafeez Ur et al. 2024. "The Investigation of Structural, Electronic, Thermal, and Elastic Properties of X2ZnH4 (X = K, Rb and Cs) for Hydrogen Storage Applications: DFT Study." *Optical and Quantum Electronics* 56(4): 1–19. https://doi.org/10.1007/s11082-024-06308-8.

[22] Kresse, G., and J. Furthmüller. 1996. "Efficient Iterative Schemes for *Ab Initio* Total-Energy Calculations Using a Plane-Wave Basis Set." *Physical Review B* 54(16): 11169–86.

[23] Perdew, John P., Kieron Burke, and Matthias Ernzerhof. 1996. "Generalized Gradient Approximation Made Simple." *Physical Review Letters* 77(18): 3865–68.

[24] Togo, Atsushi, and Isao Tanaka. 2015. "First Principles Phonon Calculations in Materials Science." *Scripta Materialia* 108: 1–5.

[25] Page, Yvon Le, and Paul Saxe. 2002. "Symmetry-General Least-Squares Extraction of Elastic Data for Strained Materials from Ab Initio Calculations of Stress." 65: 1–14.

[26] A. Ayyaz, M.A. Ullah, M. Zaman, N.D. Alkhaldi, Q. Mahmood, I. Boukhris, M. S. Al-Buriahi, M.M. Al-Anazy, Investigation of hydrogen storage and energy harvesting potential of double perovskite hydrides A2LiCuH6 (A =Be/Mg/Ca/Sr): a DFT approach, Int. J. Hydrogen Energy 102 (2025) 1329–1339, https://doi. org/10.1016/j.ijhydene.2025.01.117.

[27] A. Candan, A. Erkisi, B. Yildiz, Revealing the potential of double perovskite hydrides A2SiH6 (A =Li, Na) for solid-state hydrogen storage applications, J. Energy Storage 132 (2025) 117957, https://doi.org/10.1016/j. est.2025.117957.

[28] S. Bahou, H. Labrim, M. Lakhal, M. Bhihi, B. Hartiti, H. Ez-Zahraouy, Magnesium vacancies and hydrogen doping in MgH2 for improving gravimetric capacity and desorption temperature, Int. J. Hydrogen Energy 46 (2021) 2322–2329, https:// doi.org/10.1016/j.ijhydene.2020.10.078.

[29] A. Arharbi, H. Jebari, H. Ez-Zahraouy, New insights from DFT analysis: mg vacancies and hydrogen doping in enhancing thermodynamic properties and hydrogen storage performance of Li2BeMgH6, J. Energy Storage 106 (2025) 114903, https://doi.org/10.1016/j.est.2024.114903.

[30] A. Quader, M. Kiran, A. Bakar, M. Ahmed, Y. Khairy, Density functional analysis of structural, mechanical, electronic, and hydrogen storage properties of thermodynamically stable lead-free hydrides XGeH3 (X =Cs, Fr): a perspective of clean energy and fuel, Int. J. Hydrogen Energy 85 (2024) 652–660, https://doi. org/10.1016/j.ijhydene.2024.08.399.

[31] R.A. Alabdulhadi, S. Khan, A. Khan, L.T. Alfuhaid, M.Y. Khan, M. Usman, A. Helal, Potential use of reticular materials (MOFs, ZIFs, and COFs) for hydrogen storage, ACS Appl. Energy Mater. 8 (2025) 1397–1413, https://doi.org/10.1021/ acsaem.4c02317

[32] B. Ahmed, M.B. Tahir, A. Dahshan, M. Sagir, Advanced computational screening of X2CaH4 (X =Rb and Cs) for hydrogen storage applications, Int. J. Hydrogen Energy 89 (2024) 48–55, https://doi.org/10.1016/j.ijhydene.2024.09.321.

[33] Fine, M.E., Brown, L.D., Marcus, H.L. "Elastic constant versus melting temperature in metals", Scripta Metalurgica, 18, 951-956, 1984.

[34] C Kittel *Introduction to Solid State Physics* (USA: John Wiley&Sons) 156 (2004)

[35] V N Belomestnykh and E P Tesleva Technical Physics 49 1098 (2004)

[36] C L Julian Physical Review 137 A128 (1965)